Mohan Lal Kolhe
Pawan Kumar Labhasetwar
H. M. Suryawanshi   *Editors*

Smart Technologies for Energy, Environment and Sustainable Development

Select Proceedings of ICSTEESD 2018

Springer

Lecture Notes on Multidisciplinary Industrial Engineering

Series Editor

J. Paulo Davim, Department of Mechanical Engineering, University of Aveiro, Aveiro, Portugal

"Lecture Notes on Multidisciplinary Industrial Engineering" publishes special volumes of conferences, workshops and symposia in interdisciplinary topics of interest. Disciplines such as materials science, nanosciences, sustainability science, management sciences, computational sciences, mechanical engineering, industrial engineering, manufacturing, mechatronics, electrical engineering, environmental and civil engineering, chemical engineering, systems engineering and biomedical engineering are covered. Selected and peer-reviewed papers from events in these fields can be considered for publication in this series.

More information about this series at http://www.springer.com/series/15734

Mohan Lal Kolhe · Pawan Kumar Labhasetwar ·
H. M. Suryawanshi
Editors

Smart Technologies
for Energy, Environment
and Sustainable Development

Select Proceedings of ICSTEESD 2018

🐎 Springer

Editors
Mohan Lal Kolhe
Electrical Power Engineering
(Smart Grid and Renewable Energy)
Faculty of Engineering and Science
University of Agder
Kristiansand, Norway

Pawan Kumar Labhasetwar
Water Technology and Management
National Environmental Engineering
Research Institute (NEERI)
Council of Scientific and Industrial Research
Nagpur, India

H. M. Suryawanshi
Department of Electrical Engineering
Visvesvaraya National Institute
of Technology
Nagpur, Maharashtra, India

Preface

We are delighted to be editor(s) of the proceedings of the "International Conference on Smart Technologies for Energy, Environment and Sustainable Development, 2018 (ICSTEESD 2018)," which is published by Springer Nature in 'Lecture Notes on Multidisciplinary Industrial Engineering', ISSN 2522–5022. ICSTEESD 2018 is a major multidisciplinary engineering conference organized with the objective of bringing academicians, industry practitioners and engineering graduates to analyze scientific studies focusing on clean energy technologies, environmental sustainability and smart city concepts, and to integrate the relationship among them. ICSTEESD 2018 was organized at G.H. Raisoni College of Engineering (GHRCE), Nagpur, on July 28–29, 2018.

ICSTEESD 2018 intends to integrate the research and innovation activities for sustainable development focusing on the opportunities of increasing penetration of clean energy technologies with energy efficiency and environmental management as central topics. Most of the time, the industrial energy efficiency has focused on efficiency improvements, but the adequate attention has not been given to the energy balance with the integration of renewable energy sources. ICSTEESD 2018 provides a common platform to academicians, industry practitioners, policy makers and engineering graduates to share their innovation, research and ideas with a special focus on recent trends and advances in smart technologies for sustainable development.

The purpose of this book is the identification of appropriate smart technologies for renewable energy implementation, environmental management and policies for making a transition to more sustainable societies. The peer-reviewed research papers of ICSTEESD 2018 have been categorized into three sections (i) sustainable electrical energy systems, (ii) environmental management and sustainable development and (iii) industrial engineering with a focus on sustainable development.

As editor(s) of this proceedings of ICSTEESD 2018, we wish to express our sincere appreciation to the authors, plenary speakers, participants, supporters, reviewers, technical committee members as well as supporting staff members of G. H. Raisoni College of Engineering, Nagpur (India), who have actively contributed to the success of ICSTEESD 2018 and in the publication process.

We would extend our sincere gratitude to Shri Sunil Gyanchandji Raisoni, Chairperson of the Raisoni Group of Institutions; Dr. Preeti Bajaj, Director, G.H. Raisoni College of Engineering (GHRCE), Nagpur; Dr. Prema Daigavane, Dr. Pramod V. Walke and Dr. P. Y. Pawade, Chairs of ICSTEESD 2018 for successfully organizing this conference.

Kristiansand, Norway   Mohan Lal Kolhe
Nagpur, India   Pawan Kumar Labhasetwar
Nagpur, India   H. M. Suryawanshi

Contents

Environmental Management & Sustainable Development

Contents

Industrial Engineering for Sustainable Development

About the Editors

Dr. Mohan Lal Kolhe is a full Professor of Electrical Power Engineering (Smart Grid and Renewable Energy) in the Faculty of Engineering and Science of the University of Agder, Norway. He has more than three decades of academic experience at international level on electrical and renewable energy systems. He is a leading renewable energy technologist and has previously held academic positions at the world's prestigious universities i.e. University College London (UK/Australia); University of Dundee (UK); University of Jyvaskyla (Finland); and Hydrogen Research Institute, QC (Canada), etc. He was a member of the Government of South Australia's first Renewable Energy Board (2009–2011) and worked on developing renewable energy policies. His academic work ranges from the smart grid, grid integration of renewable energy systems, electric vehicles, energy storage, integrated renewable energy systems for hydrogen production, techno-economics of energy systems, solar and wind energy engineering, development of business models for distributed generation.

Dr. Pawan Kumar Labhasetwar is the Head and Senior Principal Scientist in the Department of Water Technology and Management Division at National Environmental Engineering Research Institute (NEERI), Nagpur. He holds a Ph.D. in Environmental Engineering from Nagpur University. He has published more than 40 papers in various national and international journals. His research interest includes water resource management, water quality monitoring, water safety plan, grey water treatment reuse, and environmental sanitation. Dr. Labhasetwar is a member of the International Water Association (IWA), and a life member of Institution of Engineers (India), Institution of Chemical Engineers, Indian Association for Environmental Management, Indian Water Works Association, and Honorary Secretary, Indian Water Works Association, Nagpur Centre.

Dr. H. M. Suryawanshi is a Professor at the Visvesvaraya National Institute of Technology, Nagpur. He obtained his Ph.D. in Electrical Engineering from Nagpur University. He has over 150 publications in international journals and conferences.

His areas of interest include power electronics, drives, resonant converters, FACTS, multilevel inverters, and renewable energy systems. Dr. Suryawanshi is a recipient of the IETE—Bimal Bose Award and IETE—Biman Behari Sen Memorial Award for distinguished achievements. He is also a Fellow and Chair Professor of Indian National Academy of Engineering.

Part I
Sustainable Electrical Energy Systems

Dr. P. M. Daigavane Conference Organizing Chair

Introduction

In all over the world, electrical energy systems are undertaking a major revolution due to energy transition for increasing penetration of environment friendly energy technologies. It involves massive technological upgradation in the power system network in the power generation, distribution and utilization. This change creates enormous engineering challenges and demands for research, innovation and education of highly skilled and motivated young engineers, professional engineers, researchers and to implement new energy policies and techniques for smart electrical energy system operation and planning.

In the "International conference on Smart Technologies for Energy, Environment and Sustainable Development, 2018 (ICSTEESD 2018)", two technical sessions have been organized for addressing the technical challenges, opportunities, and research innovation related to sustainable electrical energy systems. Both sessions have been chaired by Prof. Dr. Mohan Lal Kolhe of University of Agder (Norway), who has specialization in grid integration of renewable energy systems and smart grid with three decades international experience in the world's prestigious universities.

The research papers of this section have highlighted various technical issues related to solar photovoltaic system engineering, techno-economic sizing of integrated renewable energy systems, power quality challenges due to integration of intermittent renewable energy sources, micro-grid for promotion of distributed energy systems, analysis of power conditioning devices required for smart electrical energy systems, etc.

www.ghrce.raisoni.net

Dr. P. M. Daigavane, Conference Organizing Chair,
International Conference on Smart Technologies for Energy,
Environment and Sustainable Development, 2018 (ICSTEESD 2018);
Head of the Electrical Engineering Department,
G.H. Raisoni College of Engineering, Nagpur, Maharashtra, India

Solar Power Plant at Shradha Park and Optimal Solution to Improve the Advancement in Technology—A Case Study

Devesh U. Sarkar and Manish J. Katira

Abstract The intensity from the sun is the most abundant, infinite, and clean of all the non-conventional energy assets at present. Photovoltaic technology is the optimal ways to absorb the solar power. In this paper, we study the solar power plant which is mounted at Shradha park which is having the installed capacity of 172.5 kW by using polycrystalline module and giving the optimal solution to increase the performance of plants in the form of modern devices like modern transformerless inverter & advanced reverse meter.

Keywords Solar PV module · 3-phase inverter · Transformer · 11 kV transmission line · HT panels

1 Introduction

RGI 172.5 KW solar power plant is divided into two parts: one is G H Raisoni Academy of Engineering and Technology whose installed capacity is 112.5 KW and another one is G H Raisoni polytechnique whose installed capacity is 60 KW. The combination of both solar PV plant generates power. But this is ON-Grid system here solar generation feeding to MSEB substation by 11KV transmission line. So the overall generation is directly feeding to MSEB substation through reverse meter due to ON-Grid system. So, that energy/generation will be reduces from monthly electricity bill.

Location and Area: Shradha Park, Hariganga campus
Latitude: 21.12501476015897°
Longitude: 79.00256752967836°

D. U. Sarkar · M. J. Katira (✉)
Department of Electrical Engineering, G H Raisoni Institute
of Engineering & Technology, Nagpur, India
e-mail: manish.katira@raisoni.net

D. U. Sarkar
e-mail: sarkardevesh@gmail.com; devesh.sarkar@raisoni.net
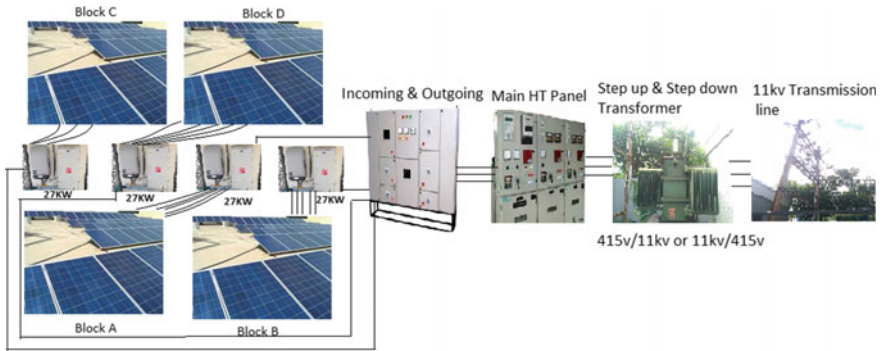
Fig. 1 Systematic block diagram of the system

Area is 1642.1836 m^2
Land: G H Raisoni Polytechnic
Location and Area: Shradha Park, Hariganga campus
21.1238462° Latitude
79.0021815° Longitude
Area is 3354 m^2
Land: G H Raisoni Academy of Engg. & Tech.
Installed By: Amplus Solar Power Private Limited, New Delhi (Fig. 1).

2 System Diagram

Details Specification with Ratings (GHRP):
Solar Photovoltaic Module:
Company: TrinaSolar
Rated Peak Power (0 ~+4.99 wp)(Pmpp): 300 W
Voc: 45.3 V
Isc: 8.60 A
Rated Voltage (Vmpp): 36.9 V
Rated Current (Impp): 8.13 A
Efficiency (%): 15.53%
Maximum series Fuse: 15 A
Maximum System Operating Voltage: DC1000 V
Irradiation: 1000 w/m^2
Cell Temperature: 25 °C.

Designing:
3-ph Inverter: 3 nos
Modules: 200 nos
Strings: 12 nos

17Module: 1 String
3-ph Inverter 1no. or 2no. or 3no.: 4 Strings
Installed capacity: 200×300 W $= 60$ KW

Costing:
1 W $= 53$ Rs.
1 Module $= 300$ W $= 300 \times 53 = 15,900/-$
200 Module $= 200 \times 15,900 = 31,80,000/-$
1 Three phase string Inverter $= 400,000/-$
3 Three phase string inverter $= 12,00,000/-$
Total $= 43,80,000/-$

Details Specification With Ratings (GHRAET):
Solar Photovoltaic Module:
Company: Vikramsolar
Rated Peak Power (0 ~+4.99wp)(Pmp): 250 W
Voc: 37.45 V
Isc: 8.70 A
Rated potential (Vmp): 30.58 V
Rated Current (Imp): 8.18 A
Fill Factor (FF): 76.77%
Efficiency (%): 15.53%
Maximum System Operating Voltage: 1000 V (IEC)
Dimension: $1639 \times 982 \times 36$ mm
Power Specification Is Measured At Standard Test Condition. Insolation: 1000 W/m^2
Cell Temperature: 25 °C.

3 Operation and Working

In Raisoni Group of Institution (RGI) at Hariganga campus, Nagpur, there is the installation of two solar plants [1] GHRAET whose installed capacity is 112.5 KW & [2] GHRPN whose installed capacity is 60 KW, and they both generate power. There is huge amount of power generation happened nearly about 300 units per day from overall solar plant and at the same time that generation would go to MSCB by reverse meter because it is purely ON gird centralized system. So at the time of monthly billing, those amounts of generation happened from solar power plant would be minus from total monthly bill. As per the policy, Amplus solar company, Delhi who installed this solar power plant takes the generation charges from the college authority up to some years, and then, they will be handover this solar power plant to the college authority.

Working:
Photons are coming in the form of radiation, and then, it will penetrate the solar cell. Solar cell is having two layer viz. upper/front layer which is called as N-type &

lower layer/back side layer which is called as P-Type. So when photons came from sun and penetrate at solar cell's upper portion/N-type layer then the electrons may produce but due to the nature of semiconductor (silicon is a bad conductor of heat) electrons cannot flow. So thats why we placed metal finger in it. Metal finger take 15% of area. Also metal finger is a very good conductor of heat due to this electron flows easily and due to the flow of electrons currents may generates.

4 Improvement and Advancement in Technology

(1) Advanced micro-grid: To improve the efficiency due to create saving of energy and to provide grid support to local utilities.
(2) Facility of O&M for proper maintenance and take care of plant; due to this; it is easy to monitor the overall system.
(3) Vaccine Refrigerators.

4.1 Plant Layout

See Figs. 2 and 3.

5 Conclusion

Thus, it is to conclude that the performance of solar photovoltaic power plant is good and the efficiency is also maintaining very well because of daily washing of solar modules and further due to weekly maintenance of solar module and by checking the inverter performance; due to modern technology, its power factor is also better nearly 0.985 PF.

6 Future Scope

(1) The Efficiency of Solar PV cell is low in order to increase the efficiency certain techniques may be employed like MPPT. In the future, lots of works will be done on efficiency of Solar PV cell.
(2) Change the solar panel with new technology solar panel for increasing the solar module efficiency.
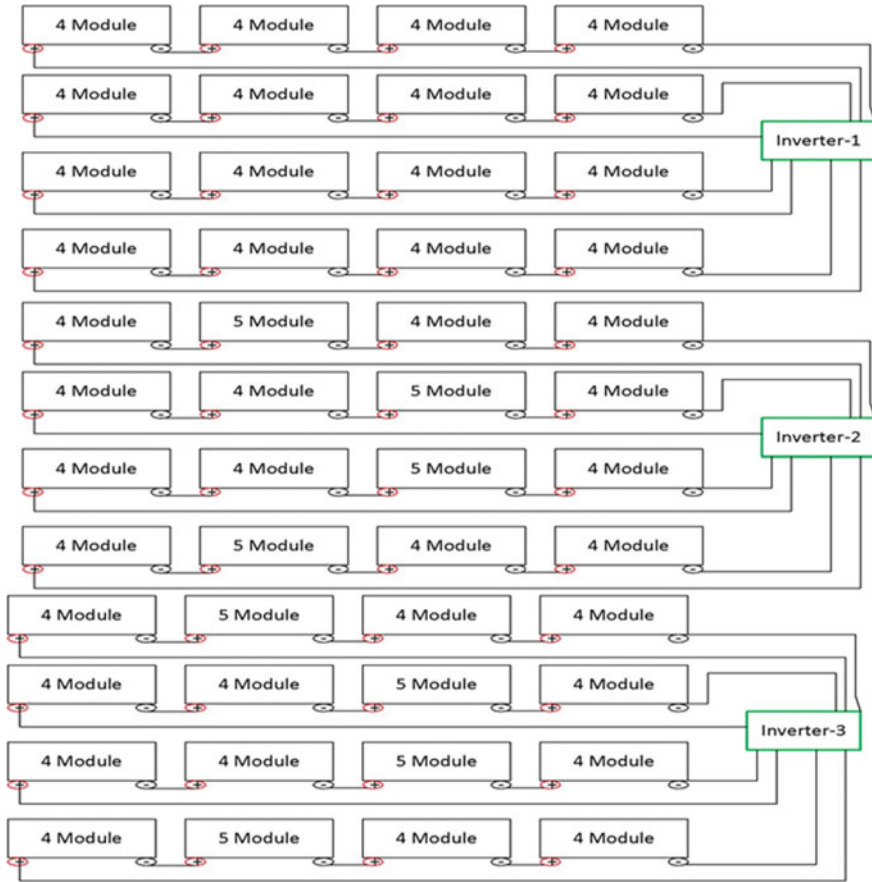
Fig. 2 GHRP plant layout

(3) To increase the plant efficiency, Micro-Inverter technology will be adopted for preventing plant breakdown and overload also to prevent the damage of solar module.

(4) Dual axis technique will be adopted for getting maximum time irradiation from sun.

(5) For voltage stability, we will also use devices like STATCOM, which is very much effective and compensate the voltage.
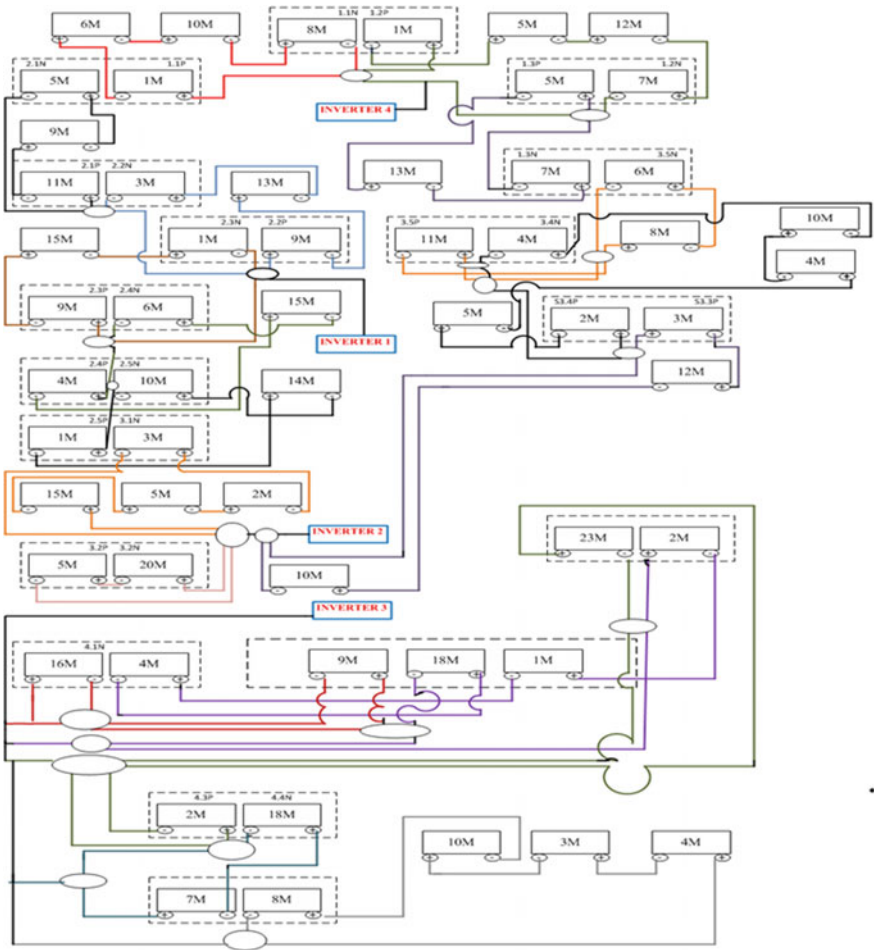
Fig. 3 GHRAET plant layout

References

1. Sangwongwanich, Ariya, Yang, Yongheng, Blaabjerg, Frede: High-performance constant power generation in grid-connected PV systems. IEEE Trans. Power Electron. **31**(3), 1822–1825 (2016)
2. Wandhare, Rupesh G., Agarwal, Vivek: Reactive power capacity enhancement of a PV-grid system to increase PV penetration level in smart grid scenario. IEEE Trans. Smart Grid **5**(4), 1845–1853 (2014)
3. Liserre, Marco, Teodorescu, Remus, Blaabjerg, Frede: Stability of photovoltaic and wind turbine grid-connected inverters for a large set of grid impedance values. IEEE Trans. Power Electron. **21**(1), 263–272 (2006)
4. Tamimi, Behnam, Cañizares, Claudio, Bhattacharya, Kankar: System stability impact of large-scale and distributed solar photovoltaic generation: the case of Ontario, Canada. IEEE Trans.

Sustainable Energy **4**(3), 680–688 (2013)

5. Rajiv, K.V., Rahman, S.A., Vanderheide, T.: New control of PV solar farm as STATCOM (PV-STATCOM) for increasing grid power transmission limits during night and day. IEEE Trans. Power Delivery **30**(2), 755–763 (2015)

6. Wandhare, Rupesh G., Agarwal, Vivek: Novel stability enhancing control strategy for centralized PV-Grid systems for smart grid applications. IEEE Trans. Smart Grid **5**(3), 1389–1396 (2014)

7. Bellia, H., Youcef, R., Fatima, M.: A detailed modelling of photovoltaic module using MATLAB. NRIAG J. Astron. Geophys. 53–61 (2014)

8. Swarna Kumary, S.V., Arangarajan Aman Maung Than Oo, V., Shafiullah, G.M., Stojcevski, A.: Modeling and power quality analysis of a grid connected solar PV system. In: Australasian Universities Power Engineering Conference, (pp. 1–6). AUPEC 2014, Curtin University, Perth, Australia, 28 September—1 October 2014

9. Jain, C., Singh, B.: Solar energy used for grid connection: a detailed assessment including frequency response and algorithm comparisons for an energy conversion system. IEEE Ind. Appl. Soc. **23**(2), 37–50 (2016)

10. Deepak, G., Reddy, M.J.B., Mohanta, D.K.: Hardware implementation of grid connected PV system with energy management scheme. IEEE, Environ. Electr. Eng. (EEEIC) (2014)

11. Fakhfakh, M.A., Ayadi, M., Neji, R.: Implementation of photovoltaic system into microcontroller. IEEE, Renewable Energies and Vehicular Technology (REVET), May (2012)

12. Adhikari, N., Singh, B., Vyas, A.L., Chandra, A., Al-Haddad, K.: Analysis and design of isolated solar-PV energy generating system. In: IEEE, Industry Applications Society Annual Meeting (IAS), pp. 1–6. November (2011)

13. Lakshmanan, S.A., Rajpourhit, B.S., Jain, A.: Modeling and analysis of 3-phase VSI using SPWM technique for grid connected solar PV system. IEEE, Electrical, Electronics and Computer Science (SCEECS), (pp. 1–6). April (2014)

Implementation of Single-Phase SRF (*d-q*) Theory for Control Technique in DVR Restoring Voltage Sag in Sensitive Nonlinear Load

D. N. Katole, M. B. Daigavane and P. M. Daigavane

Abstract In three-phase power system with the presence of nonlinear sensitive load, the complexity of control design for dynamic voltage restorer (DVR) becomes serious issue for unbalance sag mitigation. Restoration of pre-sag value of load voltage requires freezing of phase lock loop (PLL) at the point of initiation of fault. The already in existent single-phase and/or three-phase synchronous reference theory (SRT) utilized for the design of control system for DVR shows poor response in restoration of unbalance voltage sag and harmonics in nonlinear load. Therefore, the ultimate objective of paper concentrates on design of robust controller based on single-phase SRT for DVR mitigating sag in sensitive nonlinear load. Hence, a new control concept has been suggested which incorporates fundamental component extraction required for nonlinear load. The suggested control scheme is phasor based which utilizes pre-sag mitigation technique by single-phase SRT. It operates on forward control strategy for better transient response. The proposed controller for DVR illustrates its effective performance carried out in MATLAB in the obtained results.

Keywords Power quality enhancement by DVR · Voltage sag · Single phase SR theory · Phasor control · Nonlinear load

1 Introduction

The quality issue in power transfer has increasing impact on sensitive modern industrial and utility end. The main issue in quality power is unbalance sag in three-phase system [1]. Industrial and sensitive load needs constant and balance voltage mag-

D. N. Katole (✉)
Department of Electrical Engineering, G. H. Raisoni College of Engineering, Nagpur, Maharashtra, India
e-mail: dn_katole@rediffmail.com

M. B. Daigavane · P. M. Daigavane
G. H. Raisoni Institute of Engineering & Technology, Nagpur, Maharashtra, India
e-mail: mdai@rediffmail.com

nitude at fixed frequency system. Disturbances like unsymmetrical fault in line, variation in load and starting of motor load generates issue of voltage sag [2] resulting in improper operation of sensitive load. Various FACTS devices play effective role in mitigation of power quality issues especially in transmission line [3]. One such custom equipment installed in series with the distribution line before a sensitive load named as dynamic voltage restorer (DVR) is an effective power electronic converter device, utilize to protect from sag voltage [4, 5]. DVR used in series with the distribution line penetrates voltage in series with line voltage and restore the line voltage on load side required by various types of consumers. However, majority of voltage sags are unbalance in nature with the occurrence of phase change. For mitigating unbalance voltage sag, various control techniques have been suggested for DVR in [6–8]. Basically the controller in DVR is mostly based on synchronous reference theory (SRT). Although the unbalance in sag is compensated effectively by aforementioned theory-based controller, it requires freezing of phase lock loop (PLL) to obtain desired pre-sag load voltage [9, 10]. Moreover, the conventional three-phase SRT used in detection and correction of unbalance voltage sag shows poor performance in nonlinear load. Such controllers have more switching losses in bridge inverter so it must be effective in large voltage variation with phase shift and should give fast response. Hence, the design of controller for DVR considering all this issues is not straightforward.

Hence, this paper focuses on two main points. Firstly, to restore the desired load voltage in unbalance sag without freezing the PLL. Secondly, extraction of fundamental component of supply voltage. The overall analysis focuses on mitigation of voltage sag with reduction in switching losses in the presence of nonlinear load. Hence, a single-phase synchronous reference theory-based proposed phasor controller is completely examined and afterword designed without locking the PLL so as to restore the desired nonlinear load voltage during sag time.

2 Operation of DVR

To supply high quality and reliable power at the utility end, one important custom power device known as DVR plays major role in the medium distribution voltage line. In general, DVR consists of energy storage device (ESD), voltage source inverter (VSI), filters, and coupling transformer.

Figure 1 illustrates that during the instant of balance fault, sudden change in voltage of supply V_s with phase jump can be observed, if DVR is connected it penetrates controlled voltage V_{inj} dynamically through a coupling transformer in series with line voltage maintaining the desired pre-fault load voltage at the utility end. However, voltage insertion at proper phase needs active power along with reactive power requirement. DVR is capable of reactive power generation but for active power it needs ESD [11]. In controller design if voltage injected V_{inj} is in phase with V_s, actual load voltage can be obtained with less magnitude of inserted voltage but at the cost of higher active power required by the load [12]. When the compensated voltage V_{inj}

Fig. 1 The configuration of DVR consisting four MOSFET switches based voltage source H-bridge inverter with DC link in series with supply line through transformer
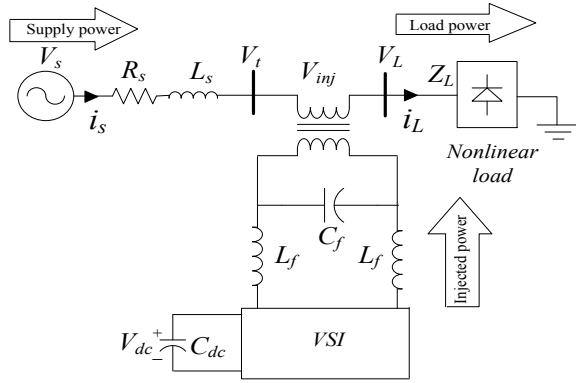
maintains phase with pre-sag voltage (steady state phase of V_s) then required pre-fault load voltage is possible at higher magnitude of compensated voltage, however, can be achieved at low value of active power.

2.1 Different Control Methods for DVR

In-phase Compensation. This method deals in restoration of magnitude of load voltage which requires minimum voltage injection [13] as illustrated in Fig. 2. The restored load voltage follows the post-sag voltage phase. But most of sag happens with change in phase. Therefore, such strategy creates distortions in compensated load voltage which leads to transients. Moreover, presence of nonlinearity in load leads to improper restoration. To realize in-phase compensation, phase lock loop (PLL) must be in synchronization with supply voltage without its locking at sag initiation point.

   Pre-sag Compensation. Exact correction of load voltage in magnitude and phase (steady-state value), during sag in supply voltage at PCC, is possible by this prominent method where no phase change occurs during the compensation time. Hence, this method creates less distortion minimizing transient at the load end. This is achieved at the cost of large value of voltage insertion through the DVR. The value of injected voltage depends on the value of phase change. Moreover, large injected voltage results in minimum extraction of DC energy from inverter link as compared to previous method. Injection of voltage in proper phase results in requirement of active power, whereas the reactive power requirement is itself fulfill by the DVR. To achieve this, synchronization of PLL with terminal voltage is essential and it should be instantly locked at sag initiation point to restore the load voltage to its initial phase [13].

   Energy Optimized Compensation. In this compensation, as given in Fig. 3 in SRF *dq* frame, compensated voltage maintains quadrature nature with the load current, i.e., DVR provides only reactive power which leads to no active power require-
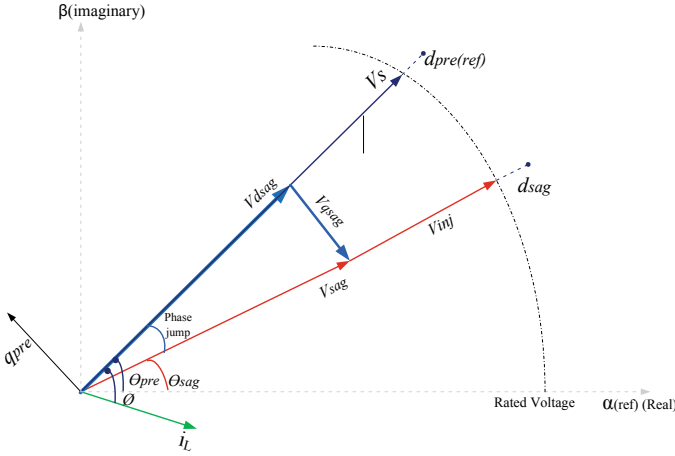
Fig. 2 In-Phase compensation strategy for DVR through SRF dq Theory $V_{d\text{pre}}$: pre-sag voltage along d axis, $V_{s\text{ag}}$: sag voltage, $V_{d\text{sag}}$ and $V_{q\text{sag}}$: sag voltage along dq axis, V_{inj}: injected voltage
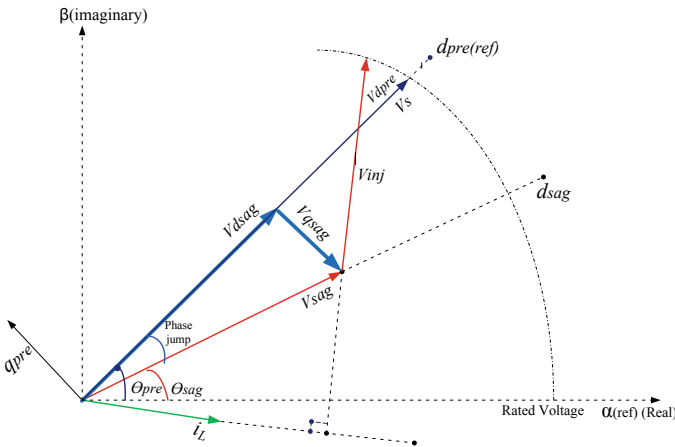
Fig. 3 Energy optimized compensation strategy for DVR through SRF dq Theory. $V_{d\text{pre}}$: pre-sag voltage along d axis, $V_{d\text{sag}}$ and $V_{q\text{sag}}$: sag voltage along dq axis, V_{inj}: injected voltage

ment from the DC link. This method draws complete active power from the grid. This method is only suitable for shallow voltage sag as dip sag needs large injected voltage resulting in requirement of large rating capacitor, besides large compensation time [13]. The magnitude of active and reactive power insertion is finalized by the phase difference between inserted voltage V_{inj} and line current i_{L}. If no phase difference between V_{inj} and i_{L}, then only active power is sheared with the line. And if phase is in quadrature, then only reactive power of DVR is sheared with the line.

Through overall analysis, pre-sag mitigation technique is the most dominant method for improvement of dynamic performance of DVR.

3 Control System

Generally instantaneous reactive power (*p-q*) (IRP) theory [14], mostly applicable to for three-phase system and originally developed by Akagi et al. [15] also its modified *p-q-r* theory used in controlling the voltage profile at load end but this theories gives imperfect information of phase at the point of initiation of sag. Also single-phase IRP (*p-q*) theory is less reported in the literature. The control methods available are based on IRP theory which mostly applied in shunt connected VSI but not reported in series connected VSI through coupling transformer. Whereas three-phase SRT is mostly reported in various literatures as compared to single phase SRT *d-q* theory. Hence, this paper deals with single-phase synchronous *d-q* theory applied in controller of DVR for sag mitigation for nonlinear type load.

The main controller concentrates on feed-forward control technique for fast sag detection and improvement in transient response. The charged DC link capacitor is considered as energy dissipates during compensation of voltage sag with reduced V_{dc} voltage. For desired load voltage restoration, required active power is supplied by ESD resulting in decrease in V_{dc}. Also reduces value of V_{dc} indicates power loss in VSI switches, passive filter, and coupling transformer. The $\pi(L - C - L)$ filter minimizes the higher order harmonics in restored voltage. The primary aim of controller is fast recognition of sag initiation and reference voltage generation which ultimately restores the load voltage without phase jump.

3.1 Single-Phase Synchronous d-q Components Generation

In design process of DVR control part, α phase is considered and quarter cycle delayed phase, obtained by time delay method, which is orthogonal to α phase is named as β phase. This complete transformation process validates Clarke's transformation in three-phase SRT. Then, these instantaneous α–β values with utilization of PLL are converted into *d-q* variables as depicted in Fig. 4. This variable *d-q* component represents dc value which is actually active and reactive power components in linear load. But in nonlinear case, the *d-q* variables of voltage no more remains constant representing the harmonic contents present in it. Hence, to obtain fundamental component of supply voltage, variation in d-axis value is suppressed to minimum level by the use of moving average (MA) filter as shown in Fig. 5.
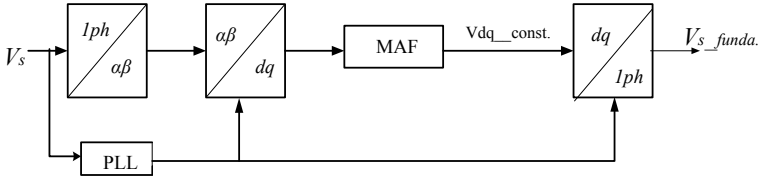
Fig. 4 Fundamental component extraction of supply voltage
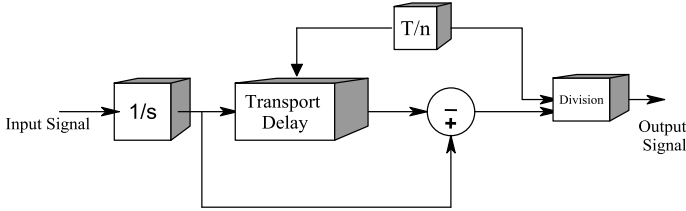
Fig. 5 Block of moving average (MA) filter

3.2 Voltage Sag Detection

The SRF *d-q* value of supply voltage at PCC is used for detection of sag. The rms value of error is utilized to detect symmetrical and asymmetrical sags. The instant of sag detection is given by $|V_{dq\_error}| > V_{Threshold}$. The threshold value of supply voltage is kept 95% for effective detection and correction of voltage sag.

3.3 Reference Voltage Generation

The fundamental component of voltage at load has restored completely where the control action of DVR is based on phasor analysis of inserted voltage. However, this phasor analysis follows pre-sag mitigation method. The complete phasor in *d-q* reference frame is depicted in Fig. 6. With the assumption of sinusoidal supply voltage in healthy condition, only *d*-axis component of voltage (V_{dpre}) is present. At fault instant, sag occur in supply voltage with phase jump (V_{sag}) which restores the load voltage to its desire value by injecting V_{inj} at an angle α. The phasor-based controller incorporating *d-q* theory on single phase is shown in Fig. 7. This controller works on feed-forward control for fast detection and improvement in transient response. In feed-forward control technique, both magnitude and phase angle are decoupled with each other. The controller mainly needs measurement of two parameters, viz. instantaneous supply voltage at the PCC and dc link voltage. The extraction of fundamental component of supply voltage obtained through MAF, as discussed before, is compared with the reference voltage. In the comparison, decoupled magnitude (V_{inj1}) and angle error (θ_{inj1}) signals are obtained. (θ_{inj1}) represents angle after sag event,
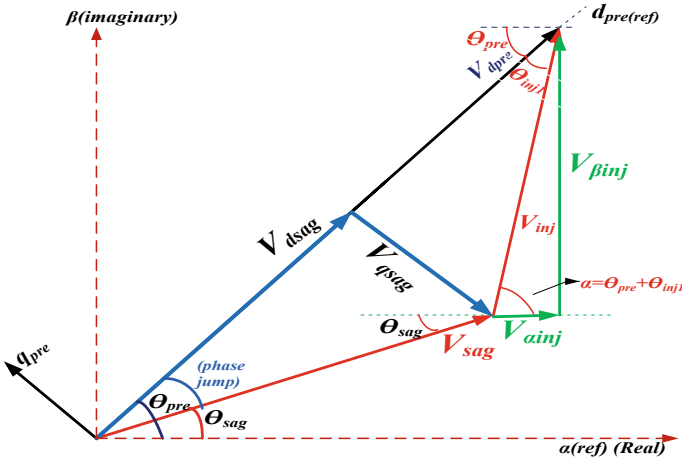
Fig. 6 Pre-sag compensation strategy for DVR through SRF *dq* theory. $V_{d\text{pre}}$: pre-sag voltage along *d* axis, V_{sag}: sag voltage, $V_{d\text{sag}}$ and $V_{q\text{sag}}$: sag voltage along *dq* axis, V_{inj}: injected voltage
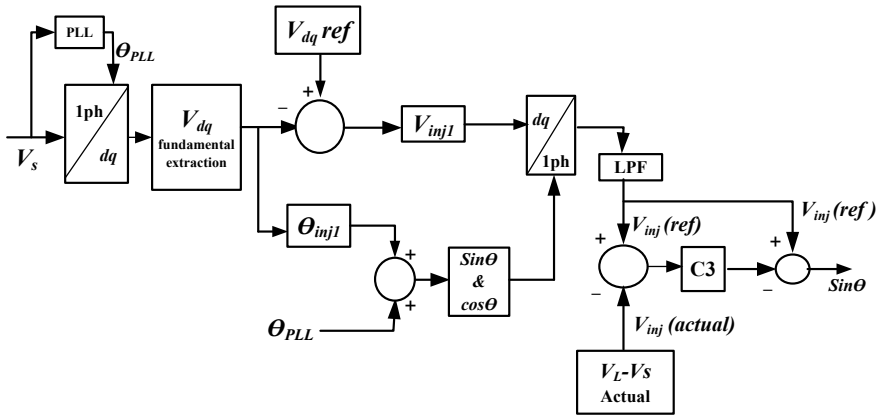
Fig. 7 Control block of phasor-based analysis of injected voltage

i.e., phase jump angle. The magnitude and phase of inserted voltage ($V_{\text{inj}1}$, $\theta_{\text{inj}1}$) are obtained by forward loop in *d-q* frame. Hence, to restore the pre-sag value, initial phase of steady-state condition (θ_{PLL}) must be added with the $\theta_{\text{inj}1}$. After inverse transformation of SRFT, low-pass filter is used to remove higher order harmonics from reference injected voltage. To avoid saturation of transformer, a proportional integral (PI) controller (C3) is used to minimize the error obtained from comparison of actual and reference injected voltage to avoid saturation of transformer. Its value is set by trial and error method. The minimized error is again compared with the reference injected voltage giving sinusoidal signal. After comparing this signal with triangular carrier signal required switching pulses for inverter can be obtained.
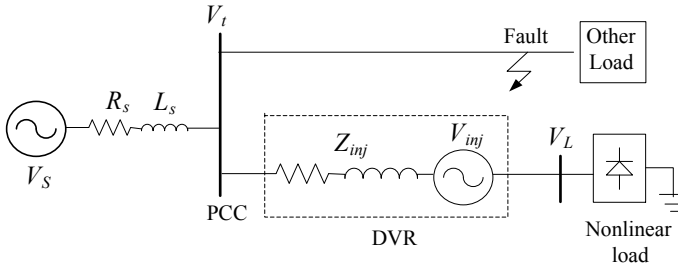
Fig. 8 System for analysis

4 Simulation Outcomes

The system for simulation consists of a source connected at PCC where two parallel loads are present as depicted in Fig. 8. LG fault at one load indicates voltage sag at supply terminal. The DVR in front of the load utilized with phasor controller based on *d-q* theory has been simulated in MATLAB. The simulated results in case of linear load are shown in Figs. 9 and 10 and for nonlinear load are shown in Figs. 11 and 12. With fault at one load, supply bus indicates sag of 60% between period 0.06 and 0.30 s which covers around 5–6 oscillations as indicated in Fig. 9a. It can be commented from Fig. 9b, c that the DVR mitigates the load voltage at its fundamental value. It can be clearly noted that the controller delays by one cycle in its operation due to delay in β phase generation. Also load voltage is kept at reference value without much change in dc voltage reference value validated by Fig. 10a. $\alpha\beta$ Components of linear current are depicted in Fig. 10b, c.

Similar testing has been done for nonlinear load keeping all parameters identical to linear load case. The nonlinear current can be seen in Fig. 12b. And its $\alpha\beta$ component generation has been validated in Fig. 12c. Similar voltage sag is created for nonlinear load shown in Fig. 11a. With the operation of phasor-based control, result obtained for inserted voltage and load voltage is presented in Fig. 11b, c. During compensation time, DC voltage remains constant as shown in Fig. 12a. An important point noticeable is that no delay and transients are found in mitigated voltage. Also hardware results are depicted in Fig. 13.

5 Conclusion

Correction of voltage sag in nonlinear system is the main task in the design of controller for DVR. Initially phasor analysis of the unlock PLL-based various methods has been carried out. And its implementation is based on instantaneous single phase to synchronous *d-q* theory. The generalized synchronous *d-q* theory based-controller for DVR has been analyzed through simulation in MATLAB for two types of load.
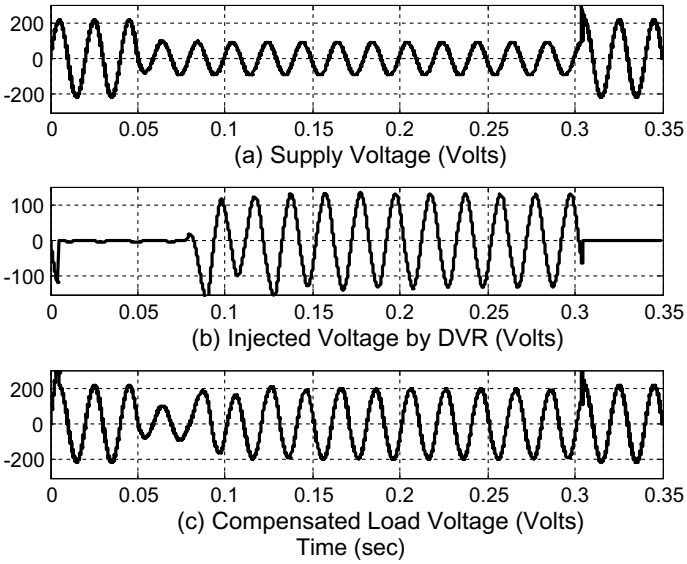
Fig. 9 Linear load system performance by phasor-based control in DVR
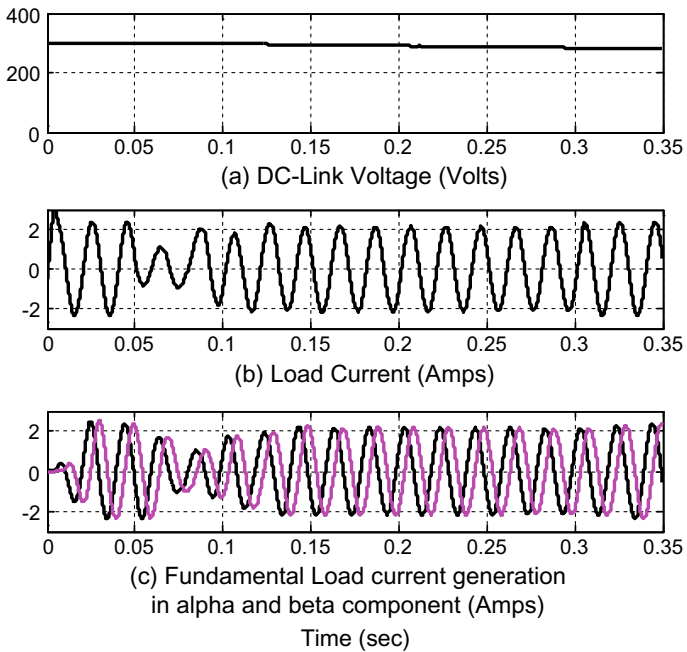
Fig. 10 Inverter dc voltage, linear load current, and its alpha beta component

(a) Supply Voltage (Volt)

(b) Injected Voltage by DVR (volt)

(c) Compensated Load Voltage (Volt)

Time (sec)
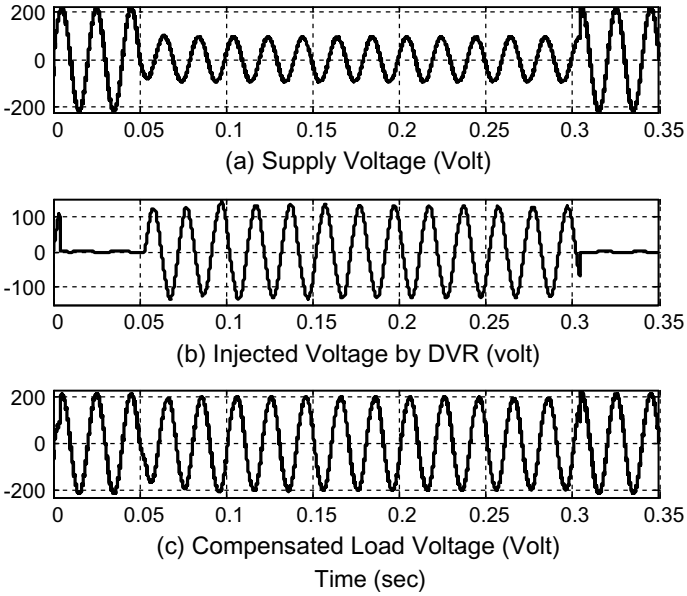
Fig. 11 Nonlinear load system performance by phasor-based control in DVR

(a) DC-Link Voltage (Volt)

(b) Load current (Amp)

(c) Fundamental Load current generation
in alpha and beta components (Amp)

Time (sec)
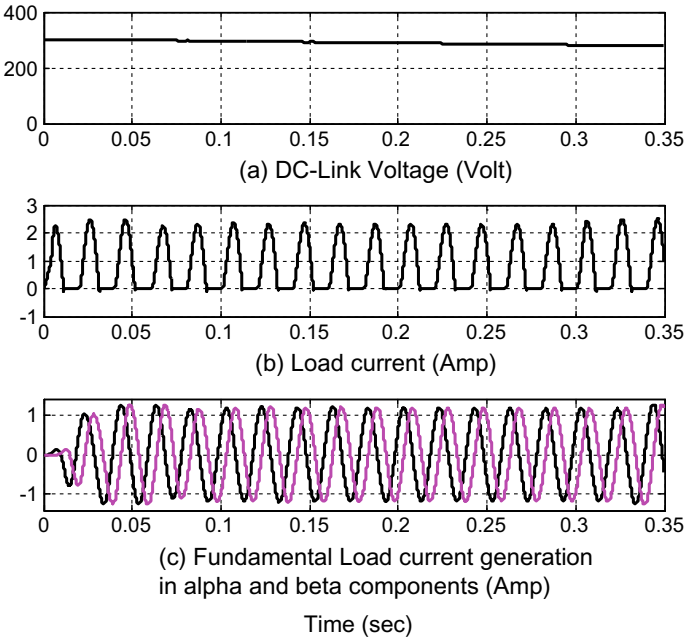
Fig. 12 Inverter dc voltage, nonlinear load current, and its alpha beta component
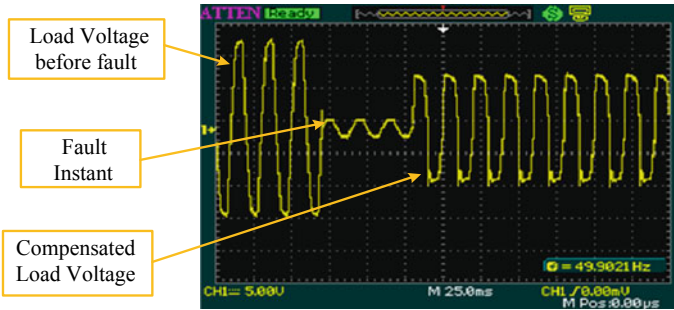
Fig. 13 DVR performance in compensation of voltage

Unfreezing of PLL results in reduction in complexity in the performance of controller. The results illustrates that the proposed controller can be advantageous in following points.

- The single-phase SRF theory-based controller can be effectively applied to n phase system if sequence is properly tracked by the PLL.
- It regulates all sequence components in considerably short time (7 ms) with zero steady error.
- As it is single phase based, it can energize only one phase which reduces the switching losses and increases the time of compensation.

Decoupled control of magnitude and angle of injected voltage reduces dc link error. This limits the modulation index resulting in less distortion in injected voltage.

References

1. Bollen, M.H.J.: Understanding Power Quality Problems—Voltage Sags and Interruptions. IEEE Press, Piscataway (2000)
2. Bollen, M.: The influence of motor reacceleration on voltage sags. IEEE Trans. Ind. Appl. **31**(3), 667–674 (1995)
3. Hingorani, N.G., Gyugyi, L.: Understanding FACTS: Concepts and Technology of Flexible AC Transmission Systems, 1st edn. The Institute of Electrical and Electronics Engineer (2000)
4. Jurado, M.V.: Voltage correction by dynamic voltage restorer based on fuzzy logic controller. IEEE Trans. Ind. Electron. (2003)
5. Haque, M.H.: Compensation of distribution system voltage sag by DVR and DSTATCOM. In: Power Tech Proceedings, 2001 IEEE Porto, vol. 1, 5p, 10–13 Sept 2001
6. Singh, B., Jayaprakash, P., Kothari, D.P., Chandra, A., Kamal-Al-Haddad.: New control algorithm for capacitor supported dynamic voltage restorer. J. Electromagn. Anal. Appl. (2011)
7. Zhan, C., Ramachandaramurthy, V.K.: Dynamic voltage restorer based on voltage-space-vector PWM control. IEEE Trans. Ind. Appl. **37**(6) (2001)
8. Marei, M.I., El-Saadany, E.F.: A new approach to control DVR based on symmetrical components estimation. IEEE Trans. Power Delivery **22**(4) (2007)
9. Choi, S.S., Li, B.H., Vilathgamuwa, D.M.: Dynamic voltage restoration with minimum energy injection. IEEE Trans. Power Syst. **15**, 51–57 (2000)

10. Haque, M.H.: Voltage sag correction by dynamic voltage restorer with minimum power injection. In: IEEE Explorer (2001)
11. Samineni, S., Johnson, B.K.: Modeling and analysis of a flywheel energy storage system for voltage sag correction. IEEE Trans. Ind. Appl. **42**(1) (2006)
12. Weissbach, R.S., Karady, G.G., Farmer, R.G.: Dynamic voltage compensation on distribution feeders using flywheel energy storage. IEEE Trans. Delivery **14**(2) (1999)
13. Meyer, C., De Doncker, R.W., Li, Y.W., Blaabjerg, F.: Optimized control strategy for a medium-voltage DVR—theoretical investigations and experimental results. IEEE Trans. Power Electron. **23**(6) (2008)
14. Peng, F.Z., Lai, J.S.: Generalized instantaneous reactive power theory for three phase power system. IEEE Trans. Instrum. Meas. **45**(1), 293–297 (1996)
15. Akagi, H., Kanazawad, Y., Nabae, A.: Instantaneous reactive power compensators comprising switching devices without energy storage components. IEEE Trans. Ind. Appl. **20**(3), 625–630 (1984)

Performance Degradation of Discrete PID Controller for Digital Excitation Control System Due to Variation of Sampling Time

Deepak M. Sajnekar, Sadanand B. Deshpande, Mohan Lal Kolhe and N. Patidar

Abstract Modern digital AVR are consisting PID controller in forward path ensures fast response in the event of disturbance. Digital keypad is used for setting PID gains to improve performance of the system. Digital PID controller reads the error signal at regular interval unlike analog controller that reads the error signal continuously. Regular interval at which digital processor reads error signal is called sampling time that has substantial effect on the performance of the controller and consequently affects the stability of the power system where synchronous generator using digital excitation system is connected in parallel. This paper addresses the issues of variation of sampling time on the performance of digital excitation control system. Analysis is carried out using model of excitation control system, and result is duly validated using industrial controller board by using hardware in the loop experimentation.

Keywords Automatic voltage regulator (AVR) · Digital PID controller ·
Excitation control system (ECS) · Brushless synchronous generator

1 Introduction

The time constant of the exciter is used to select sampling time of the identified digital excitation control system [1, 2]. There are rules to have sampling time that can

---

D. M. Sajnekar (✉)
Yeshwantrao Chavan College of Engineering, Nagpur, Maharashtra, India
e-mail: sajnekar@yahoo.co.in

S. B. Deshpande
Priyadarshini Institute of Engineering & Technology, Nagpur, Maharashtra, India

M. L. Kolhe
Faculty of Engineering and Science, University of Agder, PO Box 422,
Kristiansand 4604, Norway

N. Patidar
Electrical Engineering Department, M.A. National Institute of Technology,
Bhopal, Madhya Pradesh 462007, India

keep the performance indices such as rise time 't_r', settling time 't_s' and percentage overshoot '$\%M_P$' to a optimum value [3]. These rules estimate the value of sampling time for identified values of PID controller coefficients KP, KI, and KD for a excitation control system [4]. Analog controller-based excitation control systems allow a lot of setting flexibility to the operator to achieve an optimum generator terminal voltage response, and hence, these are still a choice of the industry due to greater reliability, faster response, simplicity, and robustness [5]. However, due to the advancement in 'embedded system technology', the trend of upgrading the analog to a digital excitation control system is in progress that offers a more easy setting flexibility to the operator. A comparison of the popular existing PID controller tuning method as in Kim and Schaefer [6] explains the advantage and disadvantage of each method and implements the digital PID controller using the Pole zero cancelation method. The ECS plays very important role to ensure optimum performance of the generator in terms of maintaining the parameters of the controller at the adequate level, so that dynamic behavior in generator terminal voltage, reactive power, and the power factor can keep the system stable. The industrial standard guidelines to the designer for design of ECS are provided in the documents [7–10]. Design of nonlinear controller for the excitation system to ensure adequate dynamic behavior has been noticed [11, 12]. Currently, the developers of the control strategy are making use of a complex model of the excitation control system that excludes the use of a standard model. The approach to use an intelligent control system provides a method to solve the stability problem of the system, but is difficult to establish as a model by traditional equations. For example, the excitation control system is established by a neural network that is rained by the back-stepping algorithm, which improves the dynamic response in comparison with the conventional PID controller [13]. Moreover, precise data of the system are required to design a neural network to avoid a dangerous transient response at the initial point. Loop shaping trade-off for fractional order PID controllers has been proposed [14] that uses H2 and H∞ norms for optimizing the fractional PID parameters. With the help of precise data of the system in all these cases, optimum performance is observed. However, in the absence of precise data, the initial requirements such as initial weight for the neural network, trails in ant colony algorithms [15], norms in multiobjective optimization, population size in swarm optimization [16], and rules in fuzzy technique are not precisely set, and therefore, the control process fails. In order to calculate the analog controller parameters for excitation systems, and to operate it within protection limits, a method is proposed in Saavedra-Montes et al. [17] to make the performance indexes of the designed controller to comply with the industrial standard but this method is only suitable for analog controllers. PID controllers for the modern excitation control system are used in the forward path. For example, the digital excitation control system as in Kim et al. [18] uses the conventional method for PID gain calculation. Such a design results in optimum performance even in the absence of precise data of the system. However, in this method, saturation data of the generator are used for calculating PID gains and the sampling time of the processor needed for implementing the digital PID controller is very small thus increasing labor and the cost of hardware. The unwanted effect caused due to sampling of error signal on the performance of the

PID controller is in Laskawski and Wcislik [19]. This paper presents the impact of changes in sampling time on the performance of discrete PID controller to be used in the digital excitation control system of a synchronous generator.

2 Impact of Sampling Rate on Digital ECS

In digital ECS model, the generator, exciter machine is of continuous nature and AVR is of discrete nature consists discrete PID controller as its component. The digital PID controller is implemented on a computer chip by the discretization of an integral and derivative block, and the computer chip reads the continuous error signal at regular time intervals that are referred to as sampling time. The analog PID controller in Fig. 3 can be discretized by the use of Forward Euler, Backward Euler method but as reported in [19]. Forward Euler method of integration is very sensitive and makes system unstable; therefore, trapezoidal integration method is used for accumulation of error signal. This method replacing an integral term '$1/s$' with '$T \cdot (1 + z - 1)/2 \cdot (1 - z - 1)$' and a first difference method replaces derivative term 's' with $(1 - z - 1)/T$, where T is the sampling time. In the proposed tuning method of the discrete PID controller, the analog gains calculated and are used with an assumption that 'Behavior of the discrete PID controller is similar to continuous when the sampling time is very small'.

However, if the gains calculated by the analog method are directly used to implement the discrete PID controller, then the system becomes unstable as described by the step response of a typical excitation control system in Fig. 1. It is noted that for different values of sampling time, performance of ECS changes. Table 1 presents the performance of the discrete PID controller used in ECS for different values of sampling time when a typical value of forward loop gain is $K_G = 1$, from this table it is noted that the best performance is achieved when 'T_s' $= 0.15$ s. which means sampling time is twice shorter than lowest exciter time constant 't_e' $= 0.3$ s but overshoot is very high and the system becomes unstable due to negative gain and Phase margin.

3 Application Example and Results

The rotary excitation system of 500 KVA, 440 V, and a 50 Hz brushless synchronous generator can have either PI or PID Controller. The disadvantage of the PI controller is an integral gain that decreases system dynamics and increases phase delay thus decreases system stability. The proposed controller for this system is the PID controller whose derivative element compensates systems deceleration caused by an integral element. Analog PID controller gains are used and gains $K_P = 52$, $K_I = 21$, and $K_D = 14$. It is observed that system gives fast response with rise time less than 1 s and almost no overshoots that ensures stable operation of the generator. When
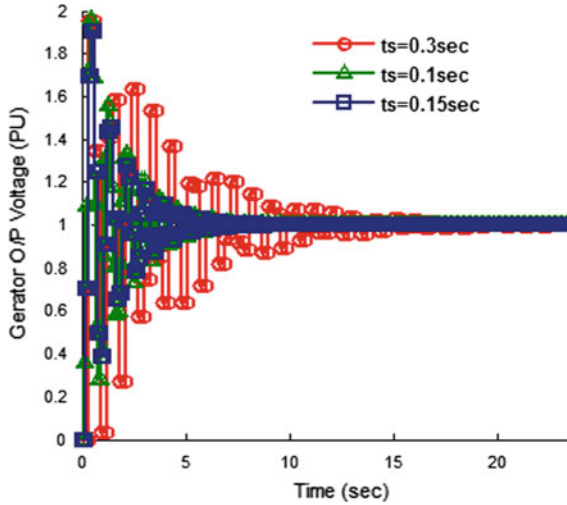
Fig. 1 Comparison of 10% step increment response of a typical discrete closed loop ECS with different sampling time

Table 1 Time response of the discrete PID in ECS with the sampling time is varying

Sampling time 'T_s' in sec	% Peak overshoot	Settling time 't_s' in sec	Rise time 't_r' in sec
0.003	System unstable		
0.1	95.9	6.7	0.1
0.15	90.6	6.15	0.15
0.2	98.7	7.8	0
0.3	95.4	16.2	0
0.4	183	24	0
0.5	System unstable		
0.8	System unstable		

these gains are used to design a discrete PID controller of digital ECS with sampling time $t_s = 0.15$ s calculated so that 't_s' twice shorter than the lowest exciter time constant te. The response of the generator terminal voltage is oscillatory and has 5% overshoot.

The step increment and decrement response of the same system is shown in Figs. 2 and 3 that shows 10% overshoot and undershoot. Though the design of PID controller with adjustment of forward gain gives acceptable range of overshoot, rise time, and settling time, but oscillatory response with discrete PID controller can make the system unstable. Discrete PID controller is then implemented in hardware d-space 1104 controller board to validate the result.

Fig. 2 Step response of generator O/P terminal voltage with 10% step increment at $t = 30$ s
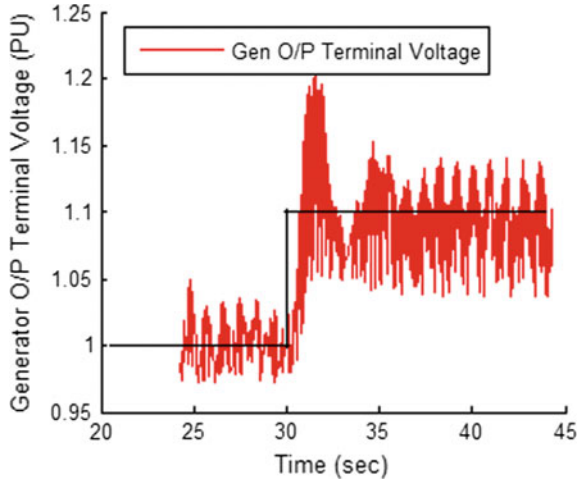
Fig. 3 Step response of generator O/P terminal voltage with 10% step decrement at $t = 30$ s
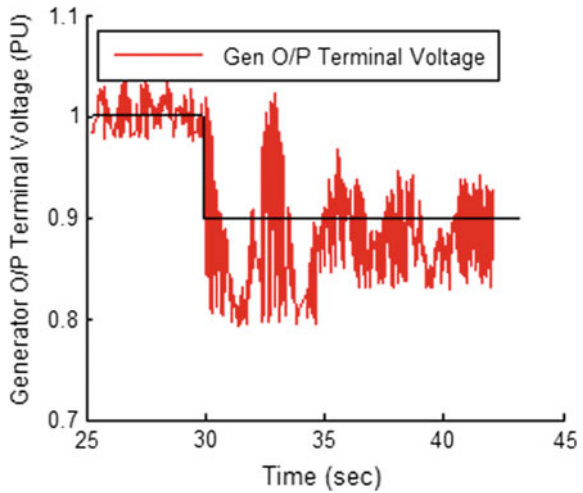
4 Conclusion

The analog PID controller is designed by canceling zeros by the poles method and ensures the desired rise time, and almost a negligible overshoot in the output terminal voltage of a synchronous generator.

The use of a calculated analog PID gains when used for the design of discrete PID controller the system becomes unstable. An investigation shows that the variation of sampling time affects the performance of the PID controller and consequently the performance of ECS. However, the design can be brought to acceptable range by precise adjustment of the forward gain but terminal voltage response remains oscillatory increases risk of systems stability.

References

1. Åström, K.J., Wittenmark, B.: Computer Controlled Systems. Prentice-Hall Information and System Sciences Series. DA Information Services, p. 1 (1984)
2. R. E. Kalman, J. E. Bertram. General synthesis procedure for computer control of single-loop and multi-loop systems. AIEE Trans, 1958
3. Isermann, R.: Digital Control Systems. Springer, Berlin (1981)
4. Godhwani, A., Basler, M.J.: A digital excitation control system for use on brushless excited synchronous generators. IEEE Trans. Energy Convers. **11**(3), 616–620
5. BonFiglio, A., Delfino, F., Invernizzi, M., Perfumo, A., Procopio, R.: A feedback linearization scheme for the control of synchronous generators. Elect Power Components and Systems **40**(16), 1842–1869 (2012)
6. Kim, K., Schaefer, R.C.: Tuning a PID controller for a digital excitation control system. IEEE Trans. Ind. Appl. **41**(2), 485–492 (2005)
7. IEEE Guide for Identification, Testing, and Evaluation of the Dynamic Performance of Excitation Control Systems, IEEE Std 421.2-1990
8. IEEE Guide For Preparation of Specification For Excitation Systems, IEEE Std 421.4 1990
9. IEEE Recommended Practice for Excitation System Models for Power System Stability Studies, IEEE Std 421.5-2005
10. IEEE Standard Definitions for Excitation Systems for Synchronous Machines. IEEE Std 421.1™-2007
11. Hasan, A.R., Sadrul Ula, A.H.M.: Design and implementation of a fuzzy controller based automatic voltage regulator for a synchronous generator. IEEE Trans. Energy Convers. **9**(3), pp. 550–557 (1994)
12. Gunes, M., Dogru, N.: Fuzzy control of brushless excitation system for steam turbogenerators. IEEE Trans. Energy Convers. **25**(3), 844–852 (2010)
13. Xu, L., Wei, J., Peng, C.: Backstepping Control of Digital Excitation Systems Based on Neural Network, pp. 1–5. ISBN 978-1-4244-1706-3/08/2008. IEEE
14. Das, S., Pan, I.: On the mixed H2/H∞ loop shaping trade-offs in fractional order control of the AVR system. IEEE Trans. Industr. Inf. **10**(4), 1982–1991 (2014)
15. Jiang, H., Yin, X., Chen, Y., Li, D.: Optimal excitation control of synchronous generator based on adaptive ants colony algorithm. In: Third International Conference on Natural Computation, vol. 3, pp. 3–7. IEEE
16. Yan, C., Venayagamoorthy, G.K., Corzine, K.: AIS-based coordinated and adaptive control of generator excitation systems for an electric ship. IEEE Trans. Ind. Electron. **59**(8), 3102–3112
17. Saavedra-Montes, A.J., Ramos-Paja, C.A., Orozco-Gutierrez, M.L., Cifuentes, W.A., Ramirez-Scarpetta, J.M.: Calculation of excitation system controllers to fulfill IEEE standard performance indexes. Electr. Power Syst. Res. **89**, 196–203 (2012)
18. Kim, K., Rao, P., Burnworth, J.A.: Self-tuning of the PID controller for a digital excitation control system. IEEE Trans. Ind. Appl. **46**(4), 1518–1524
19. Laskawski, M., Wcislik, M.: Sampling rate impact on the tuning of PID controller parameters. Int. J. Electron. Telecommun. **62**(1), 43–48

Bidirectional Voltage Source Converter for Microgrid

Meghana Khobragade, Harshit S. Dalvi and Prashant Jagtap

Abstract Microgrid is a small-scale power supply network associated with Distributed Energy Resources. Nowadays DC microgrid has become a new subject of research due to addition of renewable energy sources and electric vehicles for small buildings and residential. In this paper, we have taken review of previous published work and based on that we proposed solar-based bidirectional VSC-based Battery Storage System for microgrid applications using flyback converters. To done so, we have make DC bus which takes DC voltage from solar panel stored in battery and given to dc load similarly generated dc power given to AC grid by using Inverter. A bidirectional AC-DC/DC-AC converter has also been designed to allow bidirectional power flow. With a flexible transmission of power in AC and DC grid with a proper battery backup protection, the converter will perform the inverter as well as rectifier operation properly. These modes of operation of voltage source converter (VSC) are controlled by microcontroller according to changing load condition. Both models are simulated on MATLAB, and result shows validity of proposed system.

Keywords Voltage source converter (VSC) · Flyback converter · DC microgrid · Bidirectional AC-DC/DC-AC converter

1 Introduction

A microgrid consists with various distributed energy sources, power electronics converter, energy storage system, and local supply network that can operate independently but also collaborate with main grid. To the grid DERs, the smaller power

M. Khobragade · H. S. Dalvi · P. Jagtap (✉)
Department of Electrical Engineering, G.H. Raisoni College of Engineering, Nagpur, India
e-mail: prashant.jagtap@raisoni.net

M. Khobragade
e-mail: meghnak72@gmail.com

H. S. Dalvi
e-mail: harshit.dalvi@raisoni.net

sources serve individually or combinely, have lead the way for a bidirectional flow of energy and permitted the alliance of new, and hook up technologies for power generation. And for efficient power transmission, the integration of renewable energy sources with power electronics it is the more useful way. The rapid development in power electronics technology, the larger adoption and improvement of renewable energy sources, and cost reduction of energy storage systems, have been proposed for large-scale power integration. Microgrids' pivotal aspect in the present situation consist of integration of DC such as renewable and AC Grid generation, and after that manage loads at both side as per the availability of sources and also isolating with the central grid whenever necessary. The technological advancement requires electronic sensors, control logic systems and controllers, and cost reduction in order to make power system more feasible. Adoption of renewable energy sources expanding awareness of energy saving parts provides attainable market growth for microgrid. Microgrid able to serve power to the offices and homes will achieve efficiencies. Industries, educational institutions, hospitals adopted to DC-to-DC systems in which they get direct supply from the solar panels and feed electronic and lightning and also feed the power to the central grid efficiently which gives rise to the concept of net metering. So, they are in large demand but microgrid market suppress due to the large installation cost of converters. This introduces the concept of bidirectional converter, which reduces the cost of converters because they performed both rectifier and inverter operation. The advancement in power electronics devices and control techniques made the microgrid operation efficient and helps in cost reduction.

Solar Panel

- Solar panel is module contain PV cells made by silicon that convert incoming sunlight into electricity.
- Solar PV cells consist of a positive and a negative silicon film placed under a thin slice of glass. The sunlight when beat down these cells, they push the electrons.

The paper surveys of the bidirectional converter on some of the best papers are done from [1–9]. Considering this survey, some of problems regarding bidirectional power flow are identified and to overview that problem some techniques are introduced in this paper. These design properties are as follows: bidirectional VSC, design topology, and design flow control.

In [1], the author presents bidirectional multiple winding converters, which provide power in all directions. Author gives us a system which is capable for safe converter switching and also controls power flux. They also provide new topology of bidirectional converter which works in discontinuous conductions mode (DCM). In [2], the author presented dc-dc Converter which has high gain and fewer ripples current. Presented system uses P&O MPPT algorithm which is used to extract the compensation of the reactive power, load balancing, and mitigation of current harmonics generated by non-linear loads at unity power factor.

In [3], the author presented a bidirectional DC-to-DC converter and applied in hybrid electric vehicles and AC/DC microgrid system which has capability of bidirectional power flow conversion and inters source power sharing. Presented system can be used for both equal and unequal voltage sources. To achieve high coupled inductor

is used. Also three operating modes of charge and discharged of ultra capacitor are discussed. In [4], the author proposed a system which uses two flyback converters, for each half-cycle of the grid voltage which avoid the usual diode bridge rectifier for load drives and providing a bidirectional power flow. Presented system will behave as an inverter during daytime and PV panel generated power injected in the grid and during the absence of sunlight, it will work as a rectifier in order to supply to the load. In [5], the proposed system maintain the voltage at the load terminals within a tolerance band to do so author suggests to use both VSC and the EH in a coordinated manner. In [6], the author presented flyback converter which integrates the combined functions of uninterruptible power supply (UPS) and switch-mode power supply (SMPS). This has high-voltage main power input and a low-voltage backup battery input. During normal operation, DC output is obtained via a flyback converter and whenever input power fail system uses another flyback converter. In [7], this paper proposes an excitation system designed with a voltage source converter where the excitation controller developed by an integrated model using digital signal processor. The VSC excitation system has to reach the mainly with terminal voltage, field current, field voltage, and generator capacity efficiently. A system consists of three phase VSC, a step down transformer, coordination of excitation controller, and a H-bridge chopper which able to enhance the transient stability and steady-state stability both.

In [8], the author presented a power factor correction (PFC) rectifier which configures isolated single stage and utilizes bidirectional switch to handle both positive and negative input voltage without bridge diodes. The rectifiers can be derived by modifying switch and output winding of conventional DC/DC converter while not increasing the part count of magnetic component. In [9], the author presented instantaneous symmetrical components theory to control the microgrid side voltage–source converter.

The bidirectional converter is simple AC-DC/DC-AC converter designed for two way power exchange. The operation of VSC is based on the flyback converter topology, which performed both the functions and controlled by microcontroller. So, there will be two operation modes: on the one hand, during sun hours when the PV cell is on full generation mode and will generate excess of power, so the converter will act as an inverter, injecting in the AC grid, at the same time the PV panel charges the battery and also drives the DC loads. On the other hand, during the absence of sunlight, it will behave as a rectifier in order to supply the DC grid. The proposed topology is based on the integration of two flyback converters, one for each half-cycle of the grid voltage, avoiding the usual diode bridge rectifier, thus providing a bidirectional power flow. Figure 1 shows the schematic of flyback converter. The flyback converter is a buck-boost converter with the inductor split to form a transformer. Figure 2 shows configuration of flyback converter, in on state, the energy is transferred from the input voltage source to the transformer. In off state, the energy is transferred from the transformer to the output load.
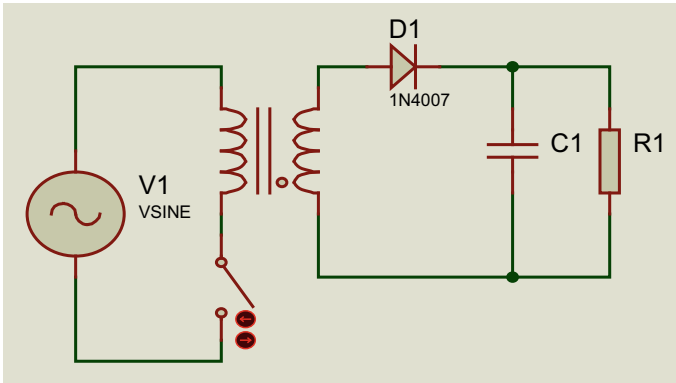
Fig. 1 Flyback converter
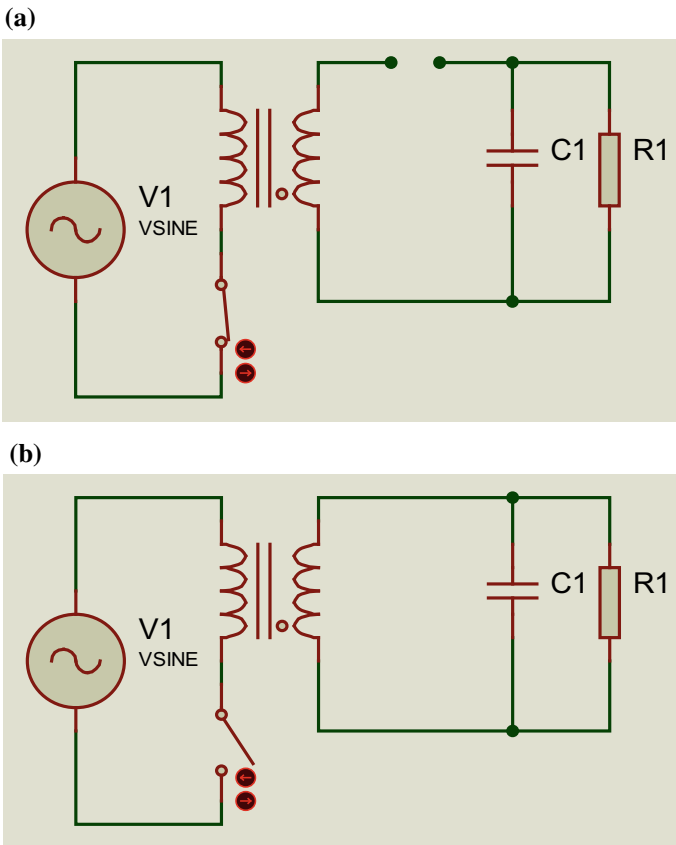
Fig. 2 Configuration of flyback converter **a** ON state, **b** OFF state
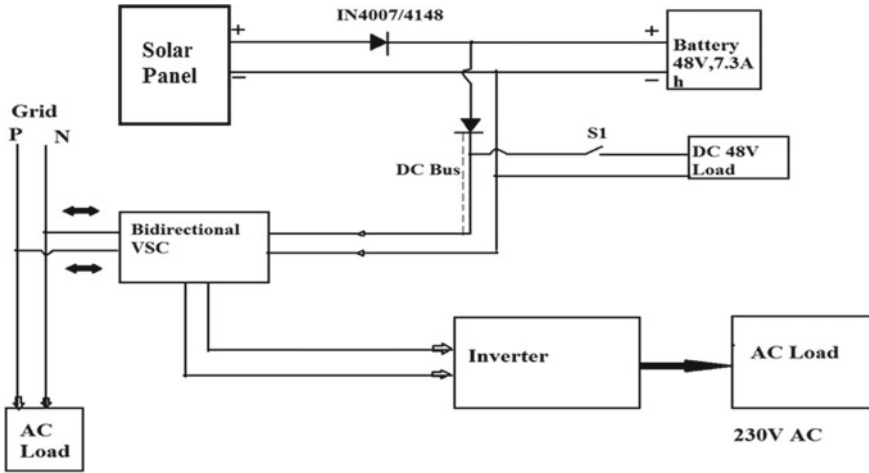
Fig. 3 Block diagram of proposed system

2 System Description, Modeling, and Control

The proposed system design implements bidirectional VSC with flyback topology as shown in Fig. 3. The microgrid rated at 48 V. Solar panel convert light energy to electrical energy by using photo voltaic (PV) cells and given to 48 V battery which store energy. The PN diode (1N4007) is used as switch and connected between solar panel and battery which give forward bias operation only so that reverse voltage should not flow. DC bus line is created between bidirectional voltage control unit and battery which has forward bias operation. DC load is connected to the DC bus which is operated by using switch S1 as shown in Fig. 2. The purpose of switch S1 is that if the system will overloaded, then it will be off. Otherwise it is always on. DC power is given to AC grid by using Inverter which converts DC power to AC power. The bidirectionl VSC, i.e., Voltage source converter have been made which operated in rectifier and inverter mode. The bidirectional VSC working normally as, after the fulfillment of DC load the remaining DC power feed to AC grid through the bidirectional VSC and vice versa. Figure 4 shows operating waveforms of bidirectional voltage source converter in rectifier mode and inverter mode. Controlling of all section is done by microcontroller.

The microgrid consists of DC grid which having a solar panel as a supply source, and it works at 48 V. The solar panel charges the battery through diode which gives forward biasing condition to the battery, it is for backup protection so its creates the DC bus, which again consist of diode for forward biasing condition. Through DC bus drives the DC load will operate through switch S1. The purpose of switch S1 is that if the system will overloaded, then it will be off. Otherwise it will always on. The bidirectional VSC, i.e., voltage source converter is between AC grid and DC bus.
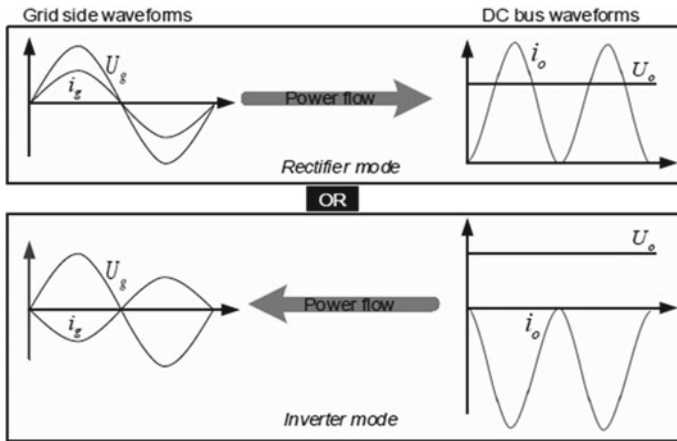
Fig. 4 Bidirectional VSC operation

The bidirectional VSC working normally as after the fulfillment of DC load the remaining DC power feed the power to AC grid through the bidirectional VSC and vice versa. If the dc bus is insufficient to drive the load at dc side, then the bidirectional VSC feed the DC power through AC grid.

2.1 Microcontroller (AT89S52)

The AT89S52 is a low-power 8-bit microcontroller made by Atmel. Microcontroller programmed in Embedded C language. Having useful Features like,

- Operating Frequency: 0 Hz to 33 MHz
- I/O Ports: Ports A, B, C, D
- Timers: Three 16-bit Timer/Counters
- Serial Communications: UART
- RAM: 256 × 8-bit Internal RAM
- 8 K Bytes of In-System Programmable (ISP) Flash Memory.

MATLAB simulation of bidirectional voltage source converter for microgrid has been presented. Figure 5 shows complete model simulation in which we have shown all used component. Bidirectional VSC using flyback converter is made, and gate pulse mode of operation is shown in Fig. 6. Switch S1 and S2 is close and other switch kept open when AC power is transfer to DC grid similarly switch SA and SB is close and other switch kept open when DC power is transfer to AC grid as shown in Fig. 7. Figures 8 and 9 show output waveforms of rectifier and inverter mode, respectively.
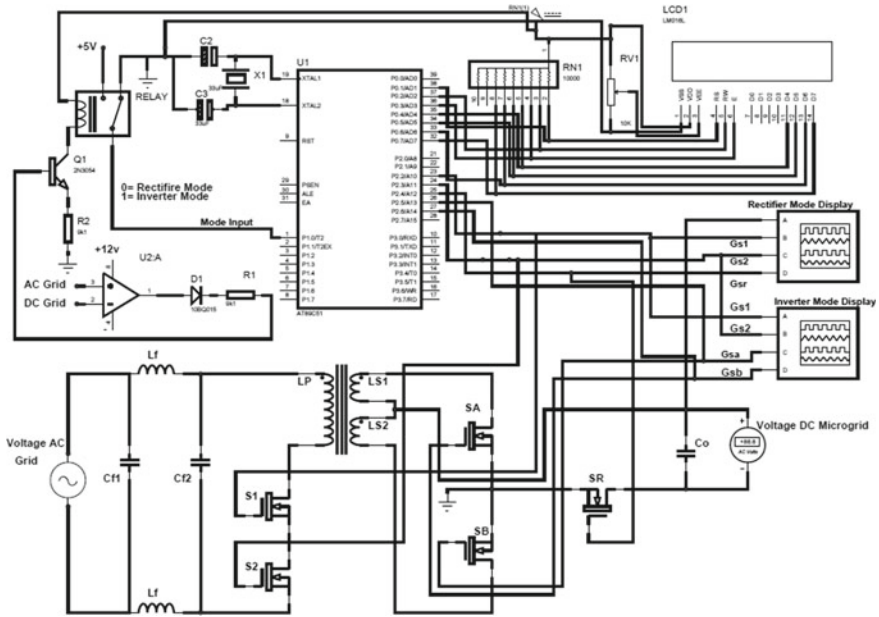
Fig. 5 Mode control and gate pulse system through microcontroller 89C51
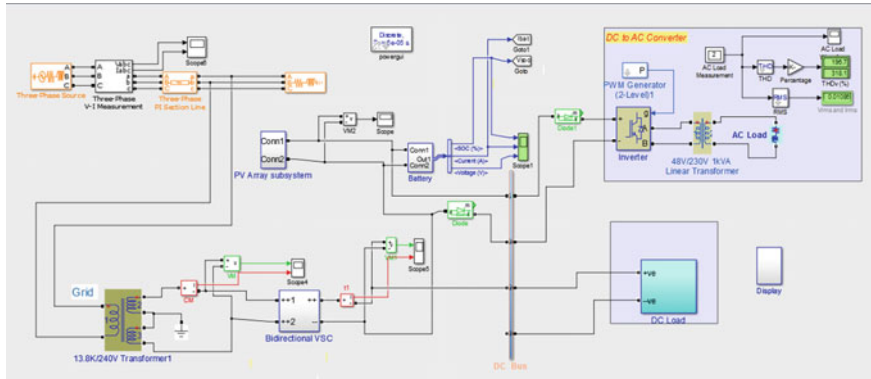
Fig. 6 Complete model

The hardware model of bidirectional VSC for microgrid is shown in Fig. 9. At DC grid side, there is solar panel and a diode is between them so that current cannot flow in reverse direction, solar panel that charges the four batteries are each of 12 V connected in series with each other and a DC load connected at DC bus. At AC grid side, there is a rectifier circuit which gives 5 V DC supply for microcontroller and 12 V DC supply for operational amplifier. The μC provides gate pulses to the bidirectional converters according to the operating mode of converter which is
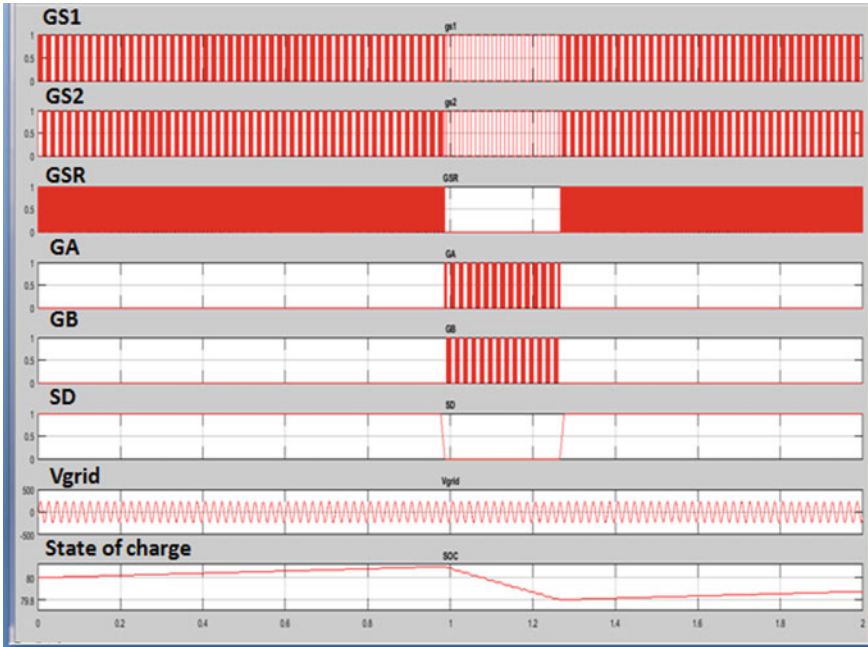
Fig. 7 Gate pulses given by microcontroller
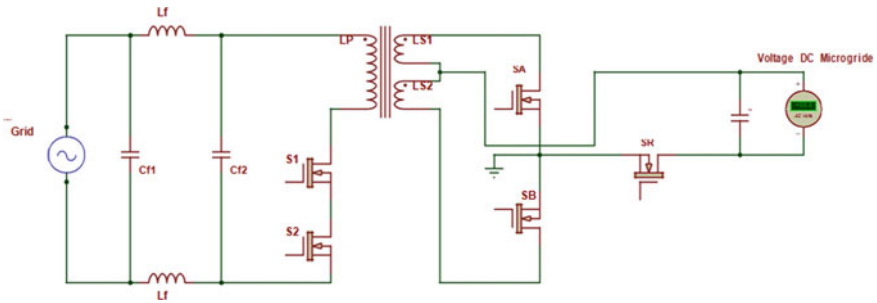
Fig. 8 Flyback converter operation

decided by the microcontroller. The control strategy of bidirectional VSC is shown in Fig. 5. The operating mode decided by the microcontroller is fully based on value given by the operational amplifier. It works as a comparator in a circuit where the comparison of current rating of both AC and DC grid, respectively. The circuit for op-amp is as shown in Fig. 10.
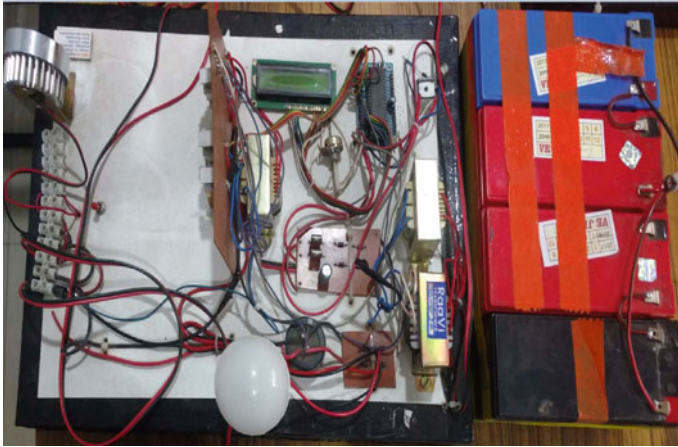
Fig. 9 Experimental setup
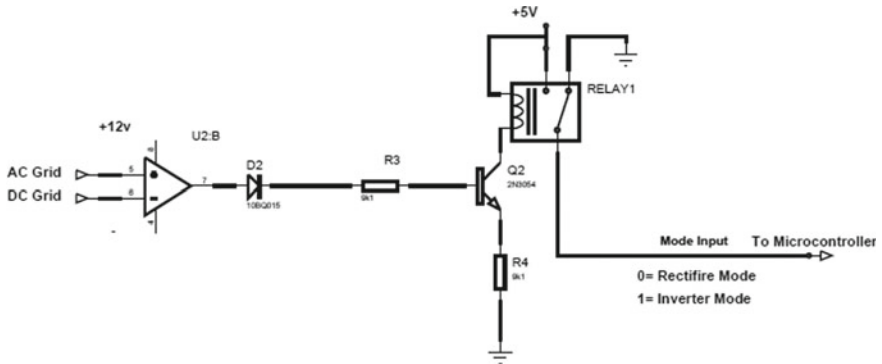
Fig. 10 Comparator circuit

3 Results

From the experimental results of bidirectional VSC, the two cases are investigated (Fig. 11).

(1) Case I: DC and AC load demand at microgrid when DC power is less.
(2) Case II: DC and AC load demand at microgrid when DC Power is greater.
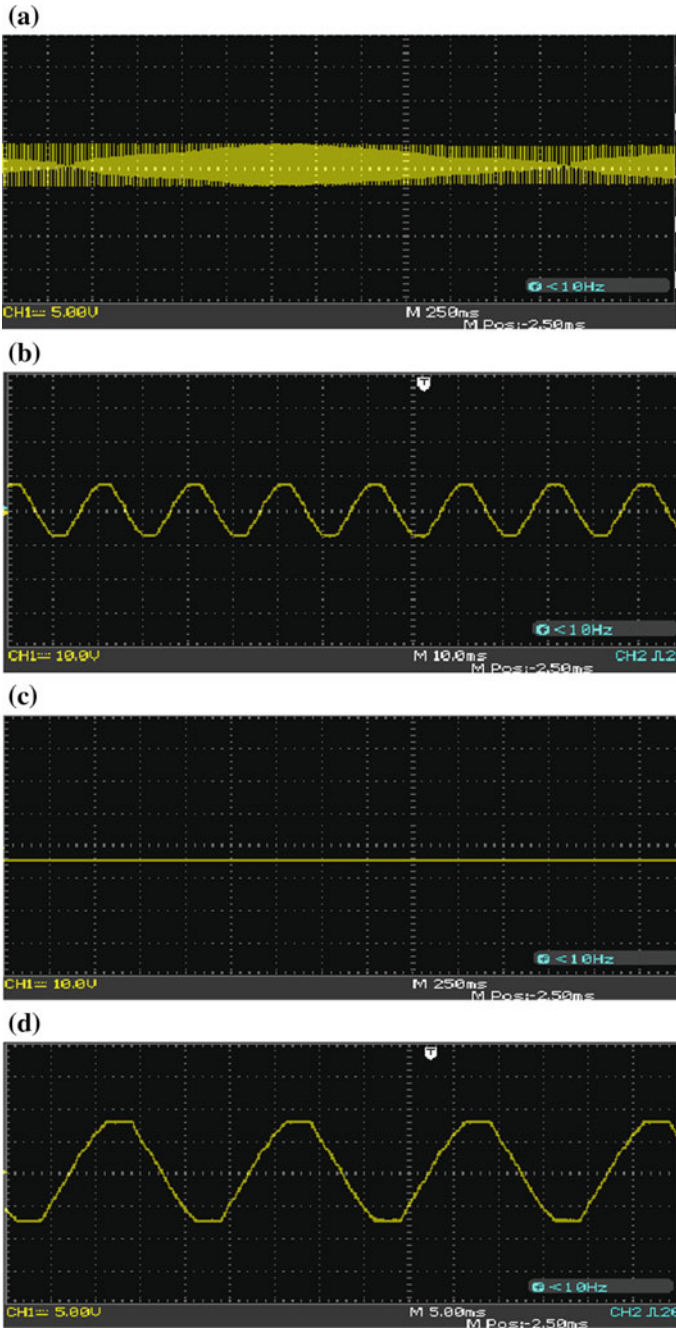
Fig. 11 Experimental results. **a** Rectifier operation across DC load. **b** Rectifier operation across AC load. **c** Inverter operation across DC load. **d** Inverter operation across AC load

4 Conclusion

The proposed solar power microcontroller-based micro grid model is simulated in MATLAB Simulink environment and flyback converter results are shown. A bidirectional VSC is designed for microgrid with the help of flyback converter topology through simple controlled strategy with the help of microcontroller. As the VSC is performed inverter and rectifier operation instantly whenever there is a change in the current rating at DC grid or AC grid. The operations of converters are more flexible with changeover at both sides. And the topology is the more efficient way to transfer two-way power and compatible than the other lengthy algorithms. Also high conversion efficiency is achieved in normal, backup, and charging modes. Simulation and hardware results are presented to validate the proposed voltage control algorithm.

References

1. de Campos, A.S.C., Gomes, A.C., de Morais, A.S.: Multi-winding bidirectional flyback converter. IEEE (2017)
2. Tummuru, N.R., Mishra, M.K., Srinivas, S.: Multifunctional VSC controlled microgrid using instantaneous symmetrical components theory. IEEE (2001)
3. Arif, M., Majid, A., Saleem, J., Khan, F., Abbass, Q., Khan, N., Mahmood, Z: A novel high gain bidirectional multiport DC-DC converter to interface PV, battery, and ultracapacitor with microgrid system. **In:** 2017 International Conference on Frontiers of Information Technology (2017)
4. Dr. Gopalakrishnan, V., Dharani, S.: Implementation of bidirectional flyback converter in lighting integrated system. J. Inform. Knowl. Res. Electrical Eng. (2015)
5. Mudaliyar, S., Mishra, S.: Coordinated voltage control of a grid connected ring DC microgrid with energy hub. IEEE (2017)
6. Ma, K., Lee, Y.: An integrated flyback converter for DC unintruptable power supply. LEEE Trans. Power Electron. **11**(2) (1996)
7. Chen, Z., Mao, C., Wang, D., Lu, J., Zhou, Y.: Design and implementation of voltage source converter excitation system to improve power system stability. IEEE Trans. Ind. Appl. https://doi.org/10.1109/tia.2016
8. Shin, J.-W., Baek, J.-B., Cho, B.-H.: Bridgeless isolated PFC rectifier using bidirectional switch and dual output windings. IEEE (2011)
9. Tummuru, N.R., Mishra, M.K.: Multifunctional VSC controlled microgrid using instantaneous symmetrical components theory. IEEE Trans. Sustain. Energy **5**(1) (2014)
10. Raghupatruni, S., Khanam, S.: VSC based bidirectional converter and battery energy storage system for microgrid application. In: 2015 International Conference on Computation of Power, Energy, Information and Communication (2015)
11. Rather, Z.H., Chen, Z., Thogersen, P., Lund, P.: Dynamic reactive power compensation of large scale wind integrated power system. IEEE Trans. Power Syst. **1** (2014)
12. Aigner, T., Jaehnert, S., Doorman, G.L., Gjengedal, T.: The effect of large-scale wind power on system balancing in Northern Europe. IEEE Trans. Sustain. Energy **3**(4), 751–759 (2012)
13. Baharizadeh, M., Karshenas, H.R., Guerrero, J.M.: Control strategy of interlinking converters as the key segment of hybrid AC-DC microgrids. IET Gener. Transm. Distrib. **10**(7), 1671–1681 (2016)

14. Verma, A.K., Singh, B., Shahani, D.T.: Electric vehicle and grid interface with modified PWM VSC and DC-DC converter with power decoupling and unity power factor. In: 2012 IEEE 5th International Conference on Power Electronics, India, pp. 1–6 (2012)
15. Ron Hui, S.Y., Chung, H.S., Yip, S.C.: A bidirectional AC-DC power converter with power factor correction. IEEE Trans. Power Electron. **15**, 942–948 (2000)

Smart HVAC System Using Fuzzy Logic

Aditya Ghulghule and Harshal Khandekar

Abstract Every building nowadays requires air-conditioning system which consumes very large part of their electrical energy consumption. It is found that locations like theaters, stadium, and corporate offices consume very large amount of energy which is about 45% of their total energy intake. Homes and offices are also the major consumer of energy through air-conditioning system. Hence, it is a need of hour to reduce the power consumption in every possible manner. Automation of air conditioning system is necessary for the user in order to reduce energy consumption and provide comfortable environment. In this paper, FUZZY logics are used in accordance with compact controllers to maintain the temperature close to the comfortable temperature. This paper proposes the idea to minimize user interface with the air-condition system and encourages use of different input methods directly from the surrounding. This system can save 16–25% of total energy consumed by the air-conditioners.

Keywords Control system · Air conditioner · Energy consumption · Energy saving · Fuzzy logic

1 Introduction

1.1 FUZZY Logic

Automation is the key for future processing systems. Usage of different automation system will lead to efficient, consistent, and quality results [1] in respect to rapidly

A. Ghulghule (✉) · H. Khandekar
G.H. Raisoni College of Engineering, Nagpur, India
e-mail: adityaghulghule7@gmail.com

H. Khandekar
e-mail: HarshalDhirajKhandekar@gmail.com

changing technology automation has played an important role for ease and cost cutting life.

The fuzzy system is one of the major keys of automation world. Technologies for controlling different devices and systems are made automatic these days for better performance [2]. Fuzzy logic is the most efficient and easy way of handling and management of different devices and systems [3]. Considering the complex situational data is the main role of fuzzy logic, and fuzzy set also called as fuzzy rules are considered as the base of fuzzy control system [4]. Mamdani-type interface is being considered to build a fuzzy set in this controller system. While one more type of fussy input can be considered which is known as Sugeno-type [5]. Mamdani-type gives a very detailed control over the system and has variety of input patterns [6].

Different types of fuzzy algorithms are used depending upon the complexity of the input, amount of data to be processed, and the number of rules through which the data are to be processed. In order to deal with an HVAC system, certain parameters are to be considered which are explained in depth [7]. The design for fuzzy logic control-based HVAC system has basic two elements as: Outdoor temperature and set point that gives the basic control over heating and cooling. The data are taken into consideration continuously to get accurate control over the HVAC system [8]. A lot of work is done on the air-conditioning systems by different researchers and writers. Air-conditioning systems based on the fuzzy logic controllers are proposed in [8–11]. Papers [8, 9] propose use of one fuzzifier and defuzzifier along with input constraints as temperature and humidity. These papers have designed 25 rules for the data to pass through. This paper considers set point outdoor temperature and human presence as fuzzifiers. Human presence is the new fuzzifier introduced as human body is also a source of heat while use of air-conditioning system is needed in human presence only. Here, human presence will give better performance in the proposed system. With the help of FUZZY logic controller, speed of compressor in air-conditioning system could be controlled detecting very small changes in surrounding temperature.

1.2 Data Collection

ASHRAE is an American organization which is working for finding the comfortable atmosphere for human survival and found that the temperature of most of air conditioners varies in steps which could not actually give the most appropriate temperature output. The desired temperature should vary in continuous form rather than in steps for achieving best possible temperature in addition to economizing the energy constraint (Table 1).

For designing any software which is to be used in real world, it is necessary to study the data from the real world. Hence, with the help of Accuweather, the most trusted online weather forecast site, the data for yearly temperature variation have been collected, studied, and taken into consideration for designing of software . The data for outdoor temperature are considered for Nagpur city only. But due to its

Table 1 Comfortable temperature for humans by ASHRAE standards	Air temperature	
	°F	°C
	67.3	19.6
	75	23.9
	78.2	25.7
	70.2	21.2
	74.5	23.6
	80.2	26.8
	82.2	27.9
	76.5	24.7

Table 2 Temperature data of Nagpur city	Month	High/low (°C)
	Jan	29/13
	Feb	32/16
	March	37/19
	April	40/23
	May	43/28
	June	37/26
	July	32/24
	Aug	31/24
	Sept	32/23
	Oct	33/20
	Nov	31/16
	Dec	29/13

diversity in range of temperature ranging from 7 to 47 °C, the data can be considered to be nearly universal where human beings can survive (Table 2).

2 Design Procedure

2.1 Input Constraints

Three input parameters are designed based on the data collected from different weather apps, ASHRAE standards, and research work by many intellectual scholars.
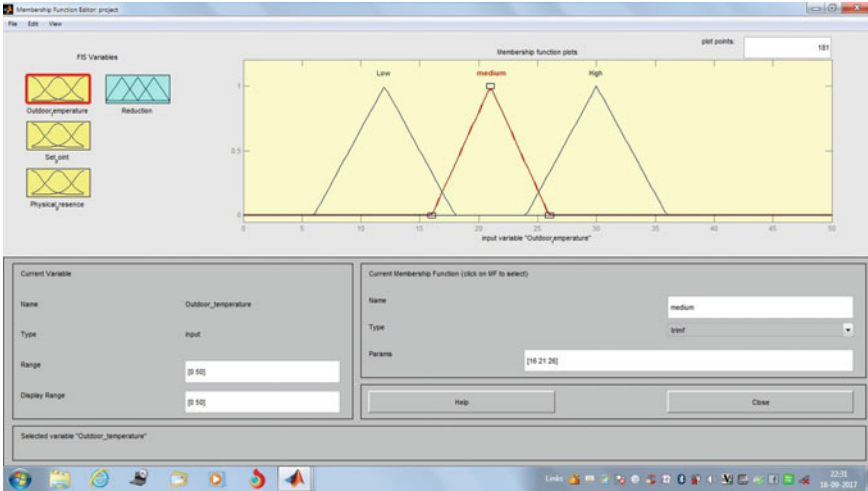
Fig. 1 Input constraint for set point temperature

Following constraints are taken into consideration for programming a controller to optimize energy usage by HVAC system.

- **Set Point Temperature**

  High—20–22 °C
  Medium—18–20 °C
  Low—16–18 °C (Fig. 1).

- **Outdoor Temperature**

  High—26–48 °C
  Medium—18–26 °C
  Low—6–18 °C (Fig. 2).

- **Physical Presence**

  Present
  Absent (Fig. 3).

The result will depend on the input placed in between specified range of membership functions. In FUZZY logic system, the output is also required to be specified for a definite input range. Hence, it is necessary to give a range for output depending upon the input received from sensors. This output is a multiplying factor for the set point temperature which will give the final temperature in degree Celsius by the air-conditioning system.

Also, it can be said that it is the level of control signal given out by controller to control the speed of compressor to optimize energy consumption. The output constraint is considered as a multiplying factor because the temperature cannot be
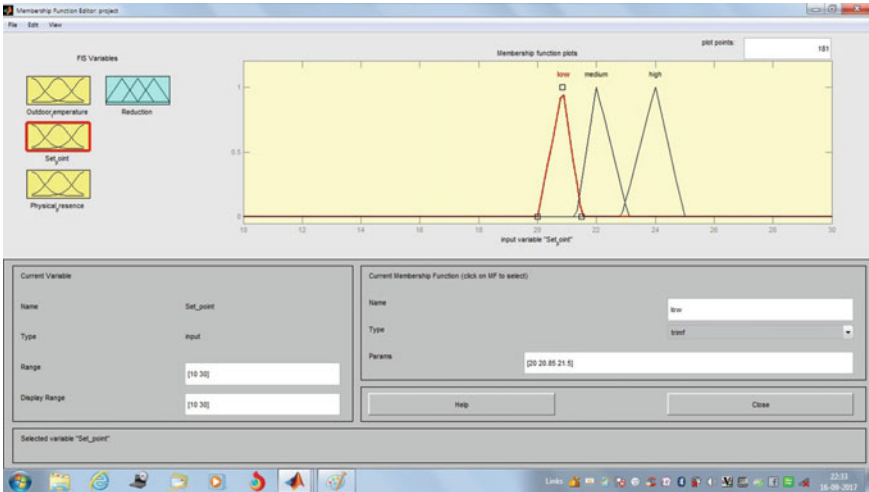
Fig. 2 Input constraint for outdoor temperature
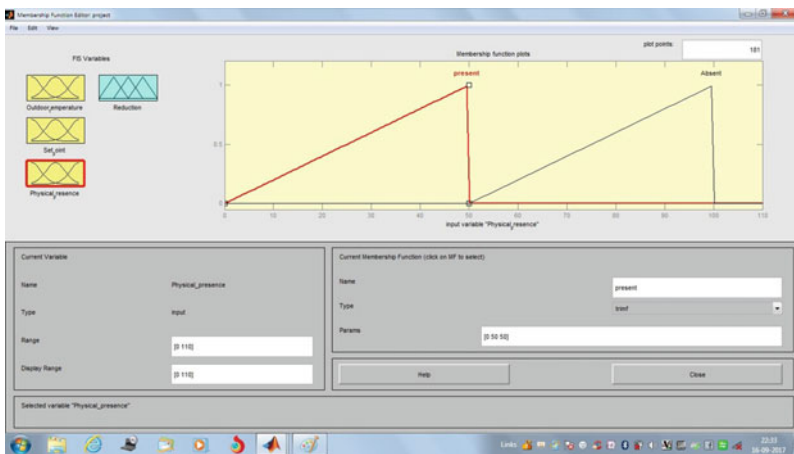
Fig. 3 Input constraint for physical presence

directly decided by the designer, and we are taking the input data from surrounding which could vary from time to time and place to place. Hence, it is necessary to make the controller acceptable under any environmental circumstances.

- Output multiplying factor

  High—0.134–0.25
  Medium—0.021–0.137
  Low—−0.1 to 0.024 (Fig. 4).
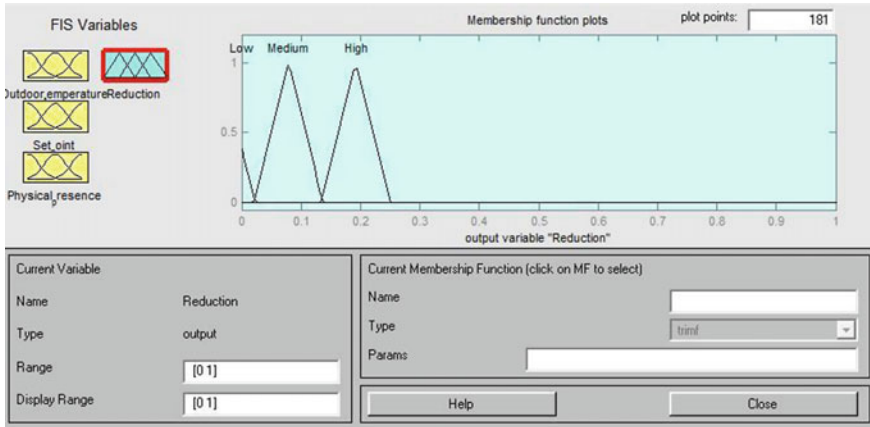
Fig. 4 Output constraint (multiplying factor)

The above described input constraints can be expressed as membership functions to execute a mathematical expression. Also, comparison is necessary between the input data required to get the multiplying factor from the output membership function. This comparison can be achieved by designing the conditions or rules in the FUZZY logic programmer, where every input factor is compared with all the other input factors individually. Also, output multiplying factor is specified for every input comparison.

These comparisons are known as rules in FUZZY language. The rules guide the controller to make proper correction in the data received from the surrounding and decide whether to reduce or increase the room temperature. The lesser the amount of multiplying factor the lesser work has to be done by the compressor of the system, and more is the amount energy saving. A set of 18 rules is prepared in order to guide controller to make air-conditioning system work in most efficient manner.

2.2 MATLAB Designing of the Controller

It is necessary to verify whether the designed set of rules and software will be compatible to the controller as well as what output we can achieve from them. As designing hardware will be TDS method and cost more if the software is not compatible to selected hardware.

Hence, we would first verify the software with MATLAB tool by designing a block diagram on MATLAB M-file. By giving input values as a source and adding a FUZZY logic controller which could read the rules designed in the program and give the multiplying factor as output.

3 Testing and Summary of Results

3.1 Formula Derivation

A formula has been derived which could set the comfortable temperature depending upon the input data, and the above-mentioned output membership function is perfectly compatible to the derived formula which could provide the comfortable temperature maintaining ASHRAE standards.

Let x be the value of set point temperature in °C.

And y, z be the value of outdoor temperature and physical presence, respectively. By the rules designed in the FUZZY logic platform gives a multiplying factor by comparing x, y, z. Let that multiplying factor be w.

$$\therefore \text{Permissible temperature which could be increased above set point} = x \times w = p \tag{1}$$

$$\therefore \text{Comfortable temperature} = \text{Permissible temperature} + \text{set point temperature}$$
$$= p + x$$
$$= c \tag{2}$$

where c is the comfortable temperature that could be provided in the room considering other factors affecting the room temperature.

Also, the percentage saving in energy could be found out which could help us in providing the statistics while explaining the benefits of smart HVAC controller.

$$\text{Percentage saving} = (p \div c) \times 100 \tag{3}$$

This percentage saving can also be used to calculate wattage saving of AC system and number of units saved depending on the time of use of HVAC system.

3.2 Performance and Energy Saving

As the values received from Fig. 5, we can perform theoretical calculations in order to find out the comfortable temperature. The necessary requirement is that the temperature should remain under the standards mentioned by ASHRAE.

We consider three input parameters, i.e., set point, human presence, and outdoor temperature as shown below

- So, the set point by user is 20.2 °C
- Other input sensors show that human presence is available
- And outdoor temperature is 30.5 °C.
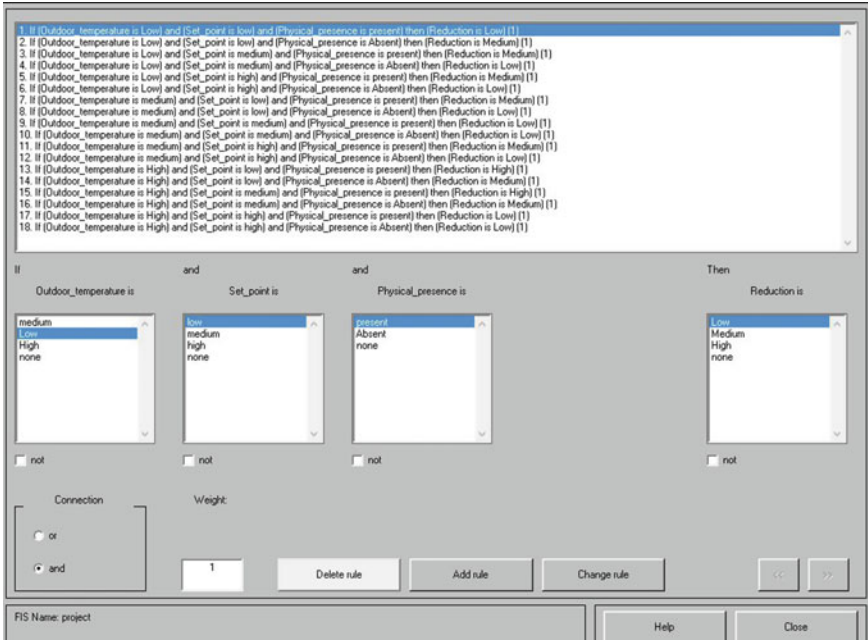
Fig. 5 Set of rules to guide controller
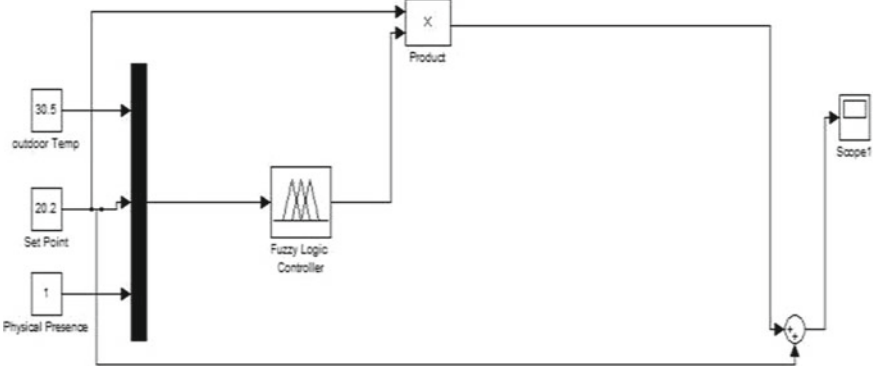
Fig. 6 MATLAB simulation for controller

By comparing these values from the designed rules, we get multiplying factor to be 0.192.

So, from Eq. (1)

$$\text{Set point} \times \text{multiplying factor} = 20.2 \times 0.192$$
$$= \mathbf{3.8784}$$

$$\text{Comfortable temperature} = 3.8784 + 20.2$$
$$= \mathbf{24.0784\,^{\circ}C}$$

The achieved comfortable temperature is found to be 24.0784 °C rather than the set point of 20.2 °C by the user. As the comfortable temperature is higher than the set point, we could save some energy by reducing the load on the compressor. Let us find the percentage of energy saved by this controller (Fig. 6).

So, the set point was 20.2 °C and comfortable temperature found to is 24.0784 °C, their difference is found by the multiplying factor which is 3.8784

$$\text{Percentage saving} = (3.8784/24.0784) \times 100$$
$$= \mathbf{16.10\%}$$

So, we have saved 16.10% load on compressor. Now the compressor is of 1000 W which rated for medium-sized AC system.

$$\text{Saving in watts of HVAC system} = (16.10 \times 1000)/100$$
$$= \mathbf{161\,W}$$

For residential locations, the AC system might operate for say 10 h.

So, the watt hour saving is around **1.610 KW**.

Also, MATLAB simulated result of the above example is obtained and perfectly tallies the mathematically calculated results. Therefore, by getting such results we can state that an optimized alternative for existing HVAC system is found which energy efficient, compact, and accurate (Fig. 7).

4 Conclusion

This paper represents a smart air-condition system designed with help of FUZZY Logic which is explained and tested by the MATLAB simulated results. The simulated results presented are shown by taking a certain range of temperature. This system is effective as human presence taken into consideration for setting for the comfortable temperature. This design is deficient of complication which makes it scalable across multiple industries. It saves around 16–25% of total energy consump-
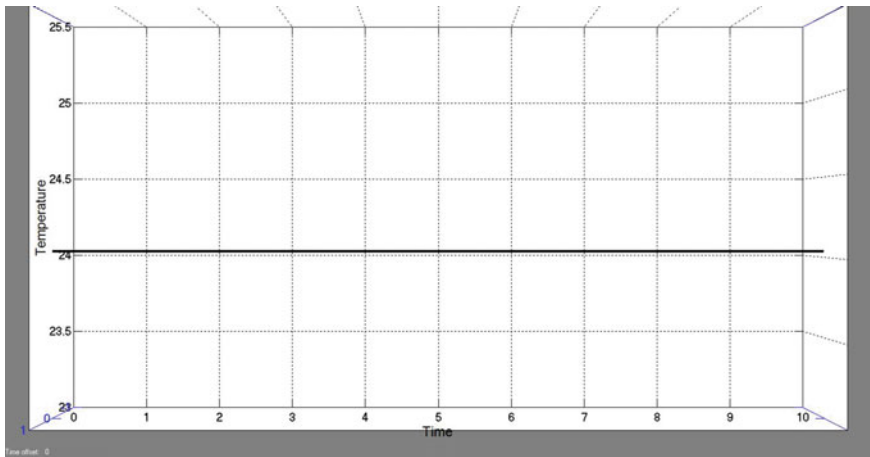
Fig. 7 Output of MATLAB simulation

tion by air-conditioning system. This proposed system is verified with the simulation results and later could be implemented in different industrial applications with the help of different hardware controllers.

References

1. Frias-Martinez, E., Magoulas, G., Chen, S., Macredie, R.: Modeling human behavior in user-adaptive systems: recent advances using soft computing techniques. Expert Syst. Appl. **29**(2), 320–329 (2005)
2. Perkowitz, M., Etzioni, O.: Adaptive web sites. Commun. ACM **43**(8), 152–158 (2000)
3. Sharma, M.L., Atri, S.L.: Fuzzy rule based automatic braking system in train using VHDL. Int. J. Comput. Sci. Technol. (IJCST) **2**(2) (2011)
4. Zimmermann, H.J.: Fuzzy Set and Its Applications, 3rd edn. Kluwer Academic Publishers, Norwell (1996)
5. Fuzzy Logic Toolbox in MATLAB
6. Iancu, I.: Mamdani FLC with various implications. In: 11th International Symposium on Symbolic and Numeric Algorithms for Scientific Computing (SYNASC 09), pp. 368–375 (2009)
7. Hassan, M.Y., Waleed Sharif, F.: Design of FPGA based PID-like fuzzy controller for industrial applications. In: IAENG Int. J. Comput. Sci. **34**(2) (2005)
8. Sarker, M.S.Z., Leng, C.Y., Bhuyan, M.S., Islam, M.S., Othman, M.: A proposed air-conditioning system using fuzzy algorithm for industrial application. IEEE TENCON **2005**, 1–6 (2005)
9. Islam, M.S., Sarker, M.S.Z., Ahmed Rafi, K.A., Othman, M.: Development of a fuzzy logic controller algorithm for air conditioning system. In: IEEE International Conference on Semiconductor Electronics (ICSE '06), pp. 830–834 (2006)

10. Cai, D.L., Chen, W.: Knowledge-based air quality management study by Fuzzy Logic principle. In: International Conference on Machine Learning and Cybernetics, vol. 5, pp. 3064–3069 (2009)
11. Yordanova, S., Merazchiev, D., Jain, L.: A two-variable fuzzy control design with application to an air-conditioning system. IEEE Trans. Fuzzy Syst. **99**, 1, 2

Analysis and Optimization Technique of Secure Smart Grid Communication Network for Sustainable Development

Devendra Singh Kushwaha, Ruchi Jain, Mohan Lal Kolhe and Vikash Kumar Singh

Abstract The smart network includes many sub-frameworks, for example, the Home Area Network (HAN), which are at risk and prone to be attacked remotely. A smart grid communication is meant to design a mutual authentication scheme and a key management protocol. This study is aimed with an efficient arrangement for HAN that analyzes a framework set-up for HAN. In this paper, we have analyzed three cases: First, we show the normal execution then execution along with attackers. Using mutual authentication, we overcome attacks. It has introduced a number of routing schemes for grid networks in recent years, and they provide different level of privacy protection at different cost. First, an unspecified key establishment process is performed to construct secret session keys. By using NS-2, the performance analysis such as energy, bandwidth is simulated. In this work, our primary concern is to identify the attacks in HAN.

Keywords Authentication · Confidentiality · Security · Smart grid · Routing

D. S. Kushwaha (✉) · R. Jain
Faculty of Computronics, Indira Gandhi National Tribal University, Amarkantak, India
e-mail: devendra2904@gmail.com

R. Jain
e-mail: jain.ruchi25@gmail.com

M. L. Kolhe
Faculty of Engineering and Science,
University of Agder, Kristiansand, Norway
e-mail: mohan.l.kolhe@uia.no

V. K. Singh
Faculty of Computronics and Head Department of Computer Science,
Indira Gandhi National Tribal University, Amarkantak, India
e-mail: drvksingh76@gmail.com

1 Introduction

It is expected that the smart network should be secure. Smart Grid is a mix of various frameworks and subsystems and different assault that may make distinctive levels of damages the gadgets and even to the general public on the loose. A fundamental issue connected with orchestrating is security and assurance. Security protection of Grid organize is more asking for than wired frameworks in view of the open nature and versatility of remote media, the aggressor needs an appropriate handset to get remote banner without being recognized. In wired frameworks, contraptions like work territories are static and do not move to begin with one place then onto the following [1].

The purpose is to make imaginative, tried, and true and quality responses for the utilities and system makers with advancement choices to pass on traditionalist and supportable imperativeness to clients. The key structure is one of the requisite surveillance necessities to achieve data characterization and genuineness in master-mind structure. The framework sholud give clients strong, workable, and safe electric essentialness. Surveillance in the Grid sort out is not only requisite to tie down the new trades and structures on the Internet yet despite ensuring prosperity and trustworthiness for the requisite utility of force. Issuing an approval plot and providing key organization traditions are the required starting strides of sketching out and executing network security in orchestrating [2]. This engages private correspondences between clients while making it harder for adversaries to focus their attack; an answer that gives more grounded anonymity properties while handling a part of the efficiency issues.

2 Related Research Work

In this section, we suggest the mechanism for detecting the wormhole ambushes. It alters the received bundle and the delivered bundle, if there is a match by then rejects that bundle. If the packet is timeout, increment the failure tally for the node. And if the tally exceeds the limit, then node will misbehave. If a node can receive a message from a node at time, then node could instead have received a message from node at the time will implement the watchdog [3]. It maintain a buffer of recently sent packets and compares each overheard packet with the packet in the buffer, when forwards a packet from to with the help of, can overhear transmission and capable of verifying that has attempted to pass the packet towards. But this approach has some limitations and it is not detect the misbehaving node during ambiguous collisions, receiver collisions, false misbehaviour and collusion [4].

It uses the method directional receiving wire to perceive and keep the wormhole assault. It acknowledges the technique that hubs keep up exact courses of action of their neighbors, an aggressor cannot execute a wormhole assault if the wormhole transmitter sees the wormhole transmitter fake neighbor and its communication is

disregarded. It doesn't require even the amassing of any unusual information since it uses directing data that is starting at now available to a hub the key idea following this technique remains in how the relative repeat of any association is of the wormhole burrow, will be superior than previous common links [5].

To evaluate the course of received flag and end of arriving of a banner, it needs directional transmission lines. This method works just if two hubs are communicating with one another, and they get action at the backward edge. However, this arrangement is dropped just if the attacker made wormholes passing between two directional antennas [6].

3 Proposed Activity for Securing Smart Grid Communication

We have shown out the diversion of the suggested scenario in helpful profitability of the system; the environmental criterion images are same as accepted in legitimate showing.

Stage 1. Generate a number amidst zero to most outrageous number of hubs.
Stage 2. Make the node with the same number as transmitter hub.
Stage3. Make the route from picked transmitting center to any objective center point with demonstrated ordinary course length.
Stage 4. Send bundle as indicated by picked objective and start clock to count jumps and deferral.
Stage 5. Rehash the system and store courses and their bounces and postponement.
Stage 6. By and by if the jump tally a particular course decreases abruptly for ordinary bounce tally then no not exactly one center point in the course ought to be assailant.
Stage 7. By and by check the deferral of each and every past course which incorporates any hub of the suspicious course. By and by the hub not encounter as of now should be pernicious let there are N such hubs.
Stage 8. In $N = 1$ then it is the attacker, else sit tight for future progressions which shows deviation and incorporate figuratively speaking one of N hubs.
Stage 9. These hubs are boycotted by the hubs; hence, they are not locked in with future courses.
Stage 10. Whole process (from step 1 to stage 9) is repeated until the point that the moment we did not get the predefined objective.

- To get the complete rundown of noxious nodes.
- To continue functioning for the determined time.
- To continue functioning for the particular number of packets etc.

4 Implementation and Testing

In this tradition, both control bundles and information parcels look subjective and unreliable from sham parcels for outside adversaries. Generous center points can perceive directing parcels and information bundles from the sham action with sensible symmetric crypto. The impulse behind the recommended scenario is that if a center can develop a key with each one of its acquaintances, by then it can use such an indicator to scramble the whole bundle for a looking at an acquaintance. The tolerant neighbor can perceive whether it requests the different bundle for itself by primer unscrambling. With an ultimate aim to enable both to discuss and Unicast, a social occasion key and a couple quick code are recommended. In like manner, grid arrange incorporates two phases: obscure trust establishment and imperceptible course identification [7].

4.1 Topology Formation and Anonymous Key Foundation

Constructing project design in NS2 should takes place. In this phase, every node in the ad hoc network communicates with its direct neighbours within its radio range for anonymous key establishment. Each node employs anonymous key establishment to anonymously construct a set of session keys with each of its neighbours [8]. Fig. 2 shows topology formation & anonymous key establishment.

4.2 Security Preserving Route Analysis

This stage is a security sparing course disclosure process considering the codes set up in past stage. Like normal course divulgence process, our disclosure method also includes course demand and course answer. Under protecting these term enters the fundamental stage, the source hub can begin the course exposure process to discover a course to the target hub (Fig. 1).

5 Simulation and Result Analysis

This proposed routing protocol allows been actualized by the Network Simulator. The Network Simulator is, for the most part, spent to execute the routing protocols in the arrangements administration inquire about. The Main focal objective of our research is security and preservation. The reenactment comes about is expressed as follows (Figs. 2, 3, 4 and 5).
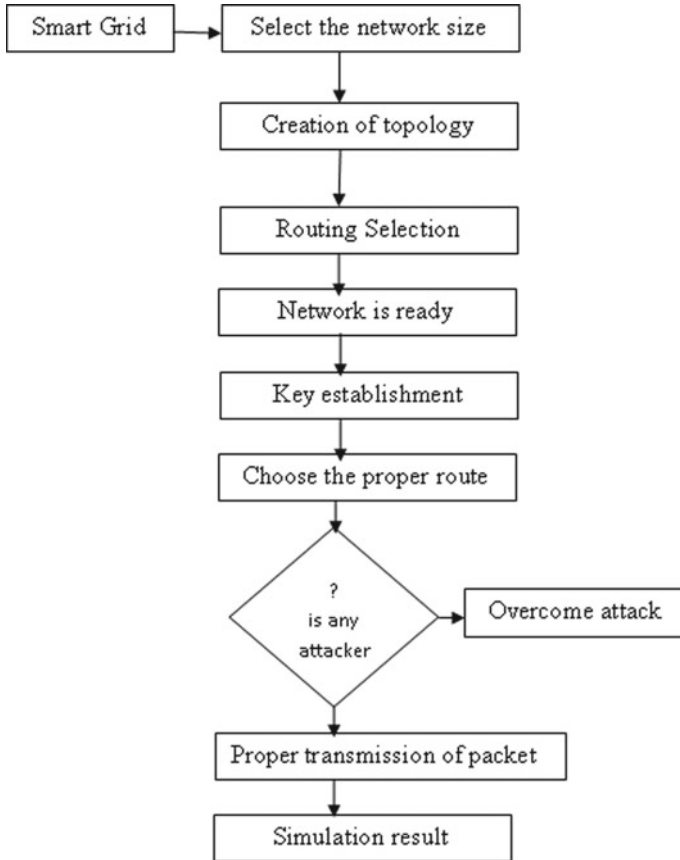
Fig. 1 Architecture of system design

6 Grid Network Application

6.1 Advanced Metering Framework

Build-up two-path interchanges between cutting edge meters and utility business frameworks [9].

6.2 Cyber Security

Guarantee the secrecy, uprightness, and accessibility of the electronic data.
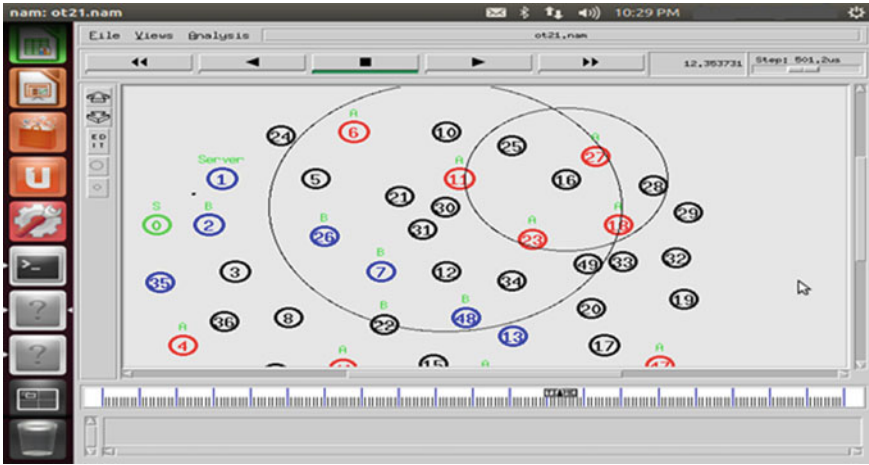
Fig. 2 Topology formation and anonymous key establishment
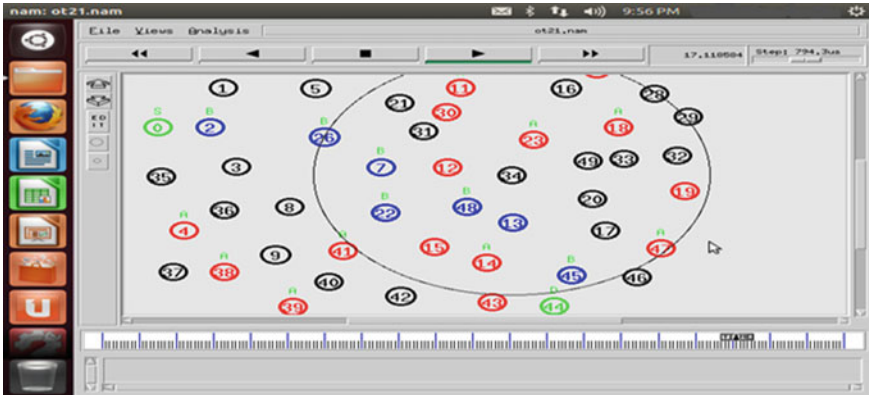
Fig. 3 Privacy-preserving route discovery

6.3 Demand Reaction and Purchaser Vitality Effectiveness:

Give components and motivators to clients to cut vitality use amid times of pinnacle request.

6.4 Distribution Grid Administration:

Amplify the execution of feeders, transformers and different parts of appropriation frameworks.
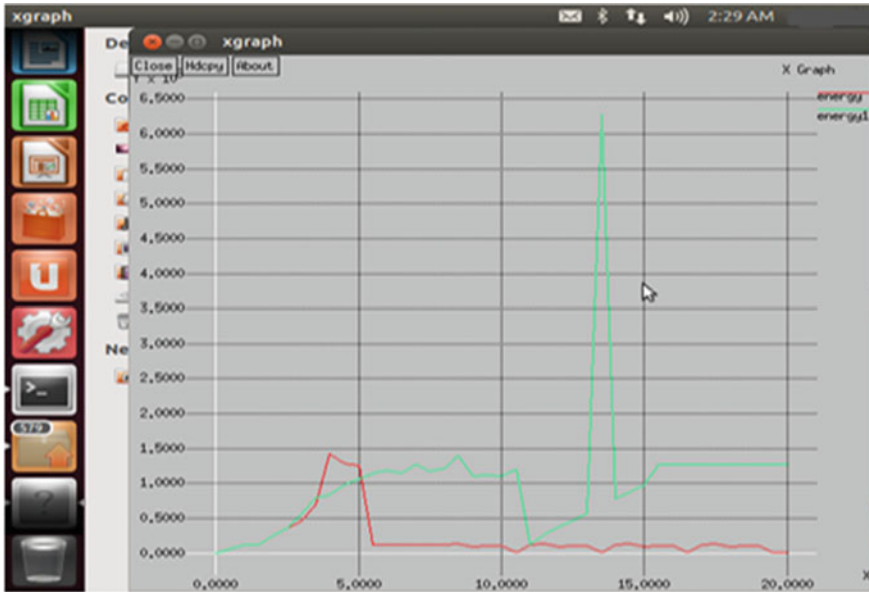
Fig. 4 Maximum throughput
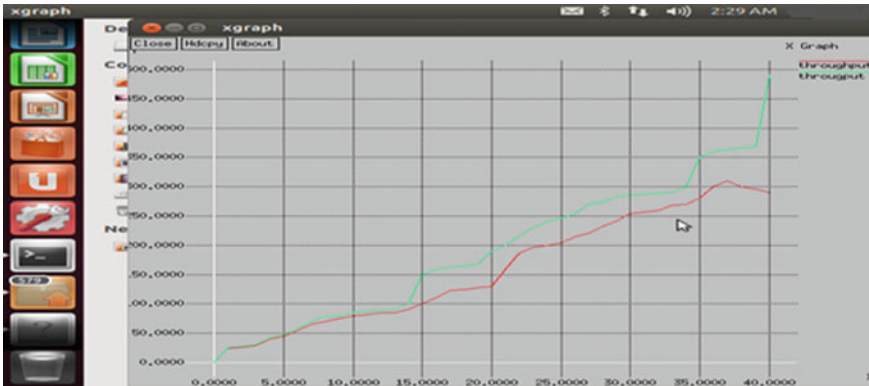
Fig. 5 Minimum energy

6.5 *Electric Transportation:*

Empower substantial scale incorporation of module electric vehicles.

6.6   Energy Stockpiling:

Give the way to store vitality.

6.7   Network Interchanges:

Distinguish execution measurements and center operational necessities of different grid organize applications.

6.8   Wide-Territory Situational Mindfulness:

Observing and show of intensity framework parts over extensive geographic territories in close continuous to upgrade administration of framework segments and execution and react to issues before interruptions emerge.

7   Conclusion

In this paper, every hub in the grid arranges gets through with its immediate neighbors inside its length for an obscure key establishment. Each hub uses baffling key establishment to build up a method of hearing codes with each one of its acquaintances. This strategy is Topology Formation and Anonymous Key system. Again, moreover, a security shielding course disclosure process considering the keys set up in the past stage. Like a run of the mill course exposure process, our disclosure method in like manner incorporates course demand and course answer. Under protecting these term introduces the requisite stage, the source n node can begin the course revelation process to discover a hub to the objective hub. This procedure is Privacy-Preserving Route Discovery. We implemented the protocol on ns2 and examined performance of HAN, which shows that protocol has satisfactory performance in terms of packet delivery ratio, latency and normalized control bytes.

References

1. Wang, J., Leung, V.: A survey of technical requirements and Consumer application standards for IP-based Grid networkAMI network. In: Proceedings of ICOIN, pp. 114–119 (2011)
2. Nicanfar, H., Jokar, P., Leung, V.: Grid network authentication and key management for unicast and multicast communications. In: Proceedings of IEEE PES ISGT, pp. 1–8 (2011)
3. Cooper, D., Santesson, S., Farrell, S., Boeyen, S., Housley, R., Polk, W.: Internet X. 509 Public Key Infrastructure Certificate and Certificate Revocation List (CRL) Profile. Internet Engineering Task Force, Fremont, CA, USA (2008)
4. Amin, M.: Challenges in reliability, security, efficiency, and resilience of energy infrastructure: toward smart self-healing electric power grid. In: Power and Energy Society General Meeting Conversion and Delivery of Electrical Energy in the 21st Century, pp. 1–5. IEEE (2008)
5. Fan, Z., Kulkarni, P., Gormus, S., Efthymiou, C., Kalogridis, G., Sooriyabandara, M., Zhu, Z., Lambotharan, S., Chin, W.H.: Grid network communications: Overview of research challenges, solutions, and standardization activities. IEEE Commun. Surveys Tuts. **15**(1), 21–38 (2013)
6. Metke, A., Ekl, R.: Security technology for smart grid networks. IEEE Trans. Smart Grid **1**(1), 99–107 (2010)
7. Fadlullah, Z., Kato, N., Lu, R., Shen, X., Nozaki, Y.: Towards secure targeted broadcast in smart grid. IEEE Commun. Mag. **50**(5), 150–156 (2012). [Online]. Available: http://bbcr.uwaterloo.ca/h8liang/sg/Papesgcommx.pdf
8. Kushwaha, D.S., Khare, A., Dr. Rana, J.L.: Improved trustful routing protocol to detect wormhole attack in MANET. Int. J. Comput. Appl. (IJCA) **62**(7), 21–25 (2013)
9. Xia, J., Wang, Y.: Secure key distribution for the smart grid. IEEE Trans. Smart Grid **3**(3), 1437–1443 (2012)

Issues Regarding Stability Aspects When SCIG and DFIG Are Interacting with Grid with FACTS Devices

Harshit S. Dalvi and Vinod K. Chandrakar

Abstract This paper focused on stability studies when many generators are integrated with induction generator (IG) and doubly fed induction generator (DFIG). As power system is a complex phenomena and reactive power compensation is a global issue, it needs to be addressed specially during transient conditions. The FACTS devices are best suited for compensation of reactive power. The focus is on multimachine system which is considered for analysis purpose. During transients, the performance of SVC and STATCOM was analyzed using robust PI controller. SVC with PI controller was found to be more reliable as compared to STATCOM when 3-Phase fault is created in simulation environment near the BUS 1 of generator, which is shown in system model. The performance evaluation of controller was studied and compared with SVC and STATCOM.

Keywords Static compensators STATCOM · Static VAr compensators · SVC · Voltage source convertor · VSC PI · Proportional-Integrator PEC · Point of common coupling FACTS · Flexible AC transmission system · SCIG · Squirrel cage induction generator · WRIG · Wound rotor induction generators · Synchronous generator S.G

1 Introduction

Wind is a naturally available phenomenon and normally is developed when low-pressure wind tries to flow toward high-pressure wind area. Wind has huge pressure to rotate the turbine and finally results in generation of active power. The generation of active power is not possible without the help of reactive power. The induction type of wind generator will take the reactive power from the grid. FACTS devices like STATCOM and SVC can enhance the stability of entire power system when

H. S. Dalvi (✉) · V. K. Chandrakar
Department of Electrical Engineering, G. H. Raisoni College of Engineering, Nagpur, India
e-mail: harshitdalvi1974@gmail.com

severe network is subjected to disturbances occurring in the power system. The compensation of reactive power is possible with the help of FACTS devices

This paper specifically deals with Shunt FACTS devices (SVC). The multimachine system is considered having PI controller, and the system can be replaced by robust fuzzy controller, to increase the transient stability of the system.

As trend for coal-/fuel-based power plants is depleting day by day and integration of non-conventional energy sources is increasing, the integration of wind energy is most viable solution as one of the sources for clean energy and also regarding energy conversion in any form. DFIG has many advantages compared to induction generators (IG) when interacted with the grid. The salient advantages of DFIG are that it minimizes peak voltage fluctuations and harmonics and grid interactive system, compared to SCIG and WRIG.

DFIG has gained popularity in wind industry and is available as single unit in wide ranges up to 1.5 MW and more. The limitation of squirrel cage induction generator (SCIG) is during variations in wind speed it causes torque pulsation which finally results in spaces on the drive train and also undesired fluctuation in the grid. The fluctuations will increase during wind gusts; hence, wound rotor induction generators (WRIGs) are preferred where wind variation is large in nature. Wound rotor induction generator can operate with certain range of wind variations; hence, they can be a viable option where wind variation is large in nature. This paper focused on rotor angle issues during transients and behavior of shunt FACTS devices along with PI controllers. The ability to maintain terminal voltage is remarkable ability which STATCOM possess. When 3-Phase faults are generated near the generator, the comparison of rotor angle is shown along with comparative analysis of implementation of SVC and STATCOM in the multimachine system model.

2 System Model

Multimachine system having four generators is interconnected as shown in Fig. 1. IG and DFIG are also injecting active power, which is connected near BUS1. For enhancing the performance of the system, the effect of SVC and STATCOM, shunt FACTS devices which are normally connected near IG and DFIG are shown along with rotor angle swells and settling time. The comparative analysis was made, and inferences regarding controller performance were studied in simulation environment.

3 Case Studies

Comparative analysis of SVC and STATCOM was studied on simulation environment and is presented below

CASE-I: When induction generator is connected to the multimachine system and is subjected to disturbances, comparative analysis of settling time of rotor angle is
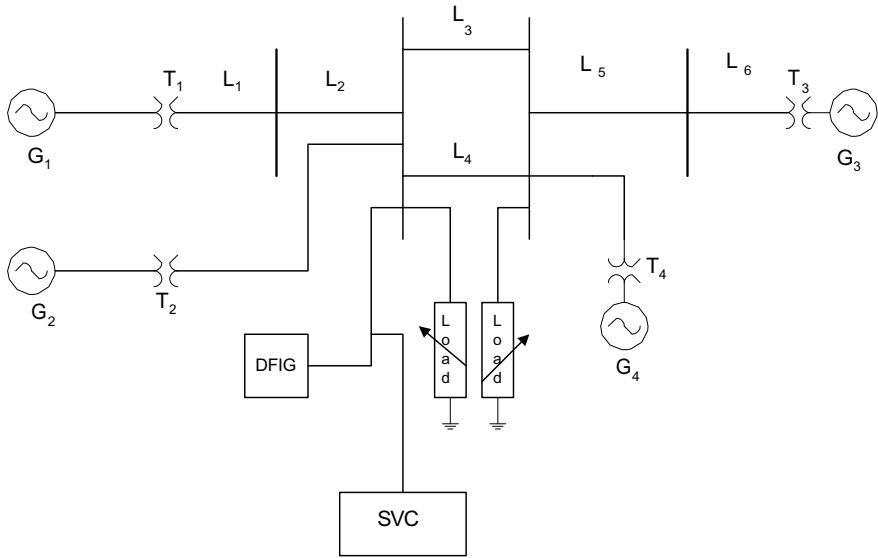
Fig. 1 Multimachine system with DFIG and SVC

Fig. 2 Rotor angle with and without STATCOM
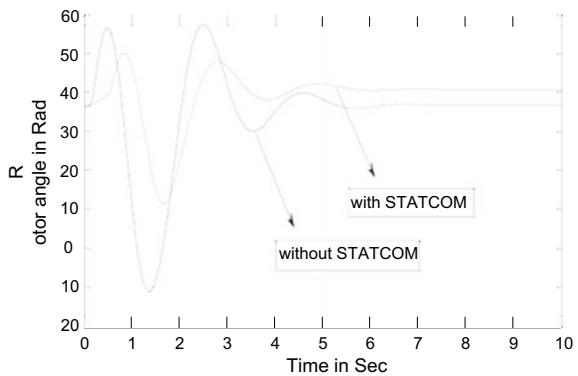
shown in Fig. 2. Without STATCOM, the system will have more peaks, and with the effect of STATCOM, the swells in the rotor angle will be reduced and system will settle with reduced time.

Figure 3 shows the comparison of SVC and STATCOM individually when they are connected independently during transient conditions in the multimachine system. The effect of SVC is more dominant compared to STATCOM during transient condition, regarding peak angle, and also system settling down.

Figure 4 focuses on comparison of only SVC and STATCOM; after implementation, the SVC is more preferred as compared to STATCOM, during active power transfer to the load. When SVC is connected in the system the rotor angle.

Fig. 3 Rotor angle with and without SVC and STATCOM
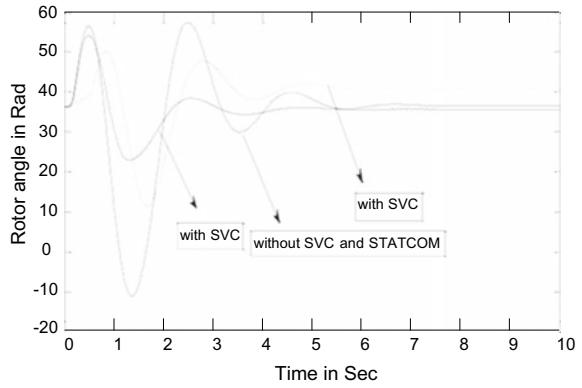
Fig. 4 Rotor angle with SVC and STATCOM
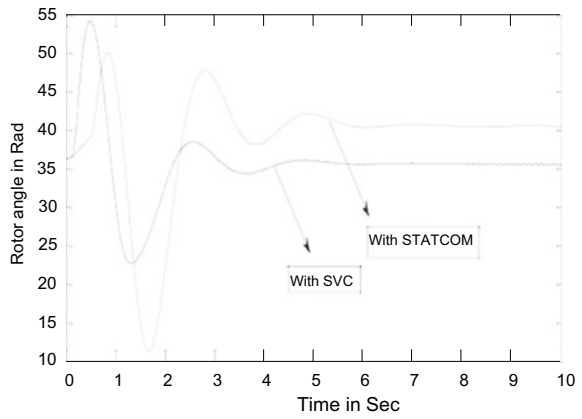
Fig. 5 Rotor angle with and without STATCOM
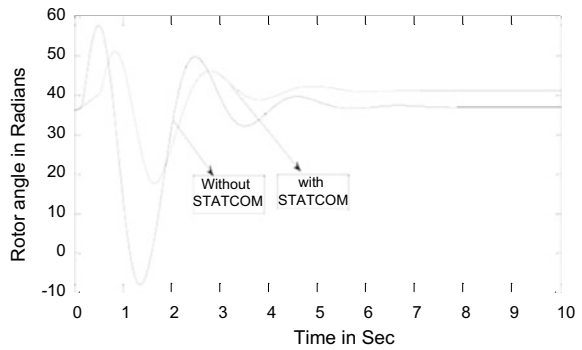
CASE-II: When DFIG is connected in the system, the effect of PI controller using SVC and STATCOM, along with the angle variation is from 20 to 50 radians, as shown in Fig. 5.

Fig. 6 Rotor angle with and Without STATCOM and SVC
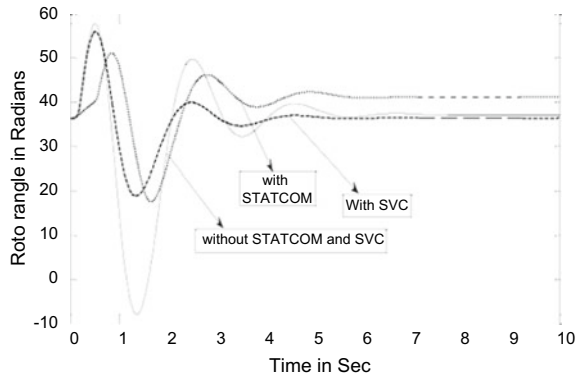
Figure 5 shows comparative analysis of STATCOM, SVC and when both are not connected independently, the effect of SVC was found better than STATCOM during rotor angle settlement during transient conditions. All the figures show comparative analysis of SVC and STATCOM along with their controllers. The transient response was observed by creating deliberate fault on the system, and during faulty conditions, the action of STATCOM and SVC PI based controller was observed.

Figure 6 shows comparative analysis of SVC and STATCOM, when connected with the multimachine system.

4   Validation Using Hardware Model

An experimental set-up for steady-state conditions was tested on STACOM when connected with wind generator. Results were observed during different loading conditions (Tables 1, 2, 3, 4, 5 and 6).

Table 1 Sending end parameters resistive loading

Voltage (V)	Load angle (LA)	Current (A)	Resistance (Ω)
$V_R = 79$	-19	$I_R = 1.5$	50
$V_Y = 83$	-21	$I_Y = 1.5$	50
$V_B = 81$	-23	$I_B = 1.5$	50

Table 2 Receiving end parameters resistive loading

Voltage (V)	Load angle (LA)	Current (A)	Resistance (Ω)
$V_r = 57$	$+1$	$I_R = 1.2$	50
$V_y = 58$	$+2$	$I_Y = 1.2$	50
$V_y = 58$	$+2$	$I_B = 1.2$	50

Table 3 During compensation for resistive loading

Voltage	Load angle (LA)	Current (A)	Resistance (Ω)
$V_R = 69$ V	−17	$I_R = 1.2$	50
$V_Y = 73$ V	−18	$I_Y = 1.4$	50
$V_B = 71$ V	−21	$I_B = 1.4$	50

Table 4 Sending end parameters R-L loading

Voltage (V)	Load angle (LA)	Current (A)	Resistance (Ω)	Inductance (mH)
$V_R = 75$	−40	$I_R = 0.9$A	50	60
$V_Y = 81$	−47	$I_Y = 1$A	50	60
$V_B = 75$	−46	$I_B = 1.1$A	50	60

Table 5 Receiving end parameters R-L loading

Voltage (V)	Load angle (LA)	Current (A)	Resistance (Ω)	Inductance (mH)
$V_R = 75$ V	−29	$I_R = 0.9$	50	60
$V_Y = 62$ V	−34	$I_Y = 0.8$	50	60
$V_B = 54$ V	−33	$I_B = 0.9$	50	60

Table 6 During compensation for R-L loading

Voltage (V)	Load angle (LA)	Current (A)	Resistance (Ω)	Inductance (mH)
$V_R = 91$	−12	$I_R = 1.1$	50	60
$V_Y = 96$	−12	$I_Y = 1.1$	50	60
$V_B = 90$	−19	$I_B = 1.3$	50	60

5   Results

A STATCOM can control voltage magnitude to a small extend and phase angle for a very short time. This is the main reason for improving the damping as well as voltage profile of the system. Comparative analysis of STATCOM and SVC along with simulation results is shown above. The hardware model results also support the simulation results. FACTS devices are most suitable for improving the voltage profile of the overall system when interacted with wind generators.

6   Conclusion

SVC along with PI controller is more robust as compared to STATCOM controller when multimachine system is connected with IG and DFIG. DFIG is more grid interactive and should be preferred for wind integration along with synchronous

generator. VSC operates in four quadrants to control subsynchronous and super synchronous speed of DFIG as the rotor operates by directional power flow. DFIG a strong contestant among all induction generators can operate at variable speed and can produce power while maintaining power factor as unity. Shunt FACTS devices are always preferred for reactive power compensation

References

1. Simoes, M.G., Bose, B.K., Spiegel, R.J.: Fuzzy logic based intelligent control of a variable speed cage machine wind generation system. IEEE Trans. Power Electron. **12**(1), pp. 87–95 (1997)
2. Li, S., Wunsch, D., Hair, E.A.O., Giesselmann, M.G.: Using neural networks to estimate wind turbine power generation. IEEE Trans. Energy Convers. **16**(3), 276–282 (2003)
3. Muyeen, S.M., Hasan Ali, M., Takahashi, R., Murata, T., Tamura, J.: Transient stability enhancement of wind generator by a new logical pitch controller. IEEE Trans. Power Electron. **126**(8), 742–752 (2006)
4. Tabesh, A., Iravani, R.: Small-signal dynamic model and analysis of a fixed-speed wind farm—a frequency response approach. IEEE Trans. Power Delivery **21**(02), 778–787 (2006)
5. Arulampalam, A., Barnes, M., Jenkins, N., Ekanayake, J.B.: Power quality and stability improvement of a wind farm using STATCOM supported with hybrid battery energy storage. In: IEEE Proc. Gener. Transmission Distrib. **153**(06), 701–710 (2006)
6. Gaztanaga, H., Etxeberria-Otadui, I., Oenasu, D., Bacha, S.: Real-time analysis of the transient response improvement of fixed-speed wind farms by using a reduced-scale STATCOM prototype. IEEE Trans. Power Syst. **22**(02), 658–666 (2007)
7. Ko, H.-S., Juri, J.: Power quality control of wind-hybrid power generation system using fuzzy-LQR controller. IEEE Trans. Energy Convers. **22**(2), 516–527 (2007)
8. Chandrakar, V.K., Kothari, A.G.: Fuzzy logic based unified power flow controllers (UPFC) for improving transient stability. Int. J. Power Energy Syst. **28**(01), 784–791
9. Muyeen, S.M., Hasan Ali, M., Takahashi, R., Murata, T., Tamura, J.: Transient stability augmentation of power system including wind farms by using ECS. IEEE Trans. Power Syst. **23**(3), 1179–1187 (2008)

Techno-economical and Feasibility Analysis of Hybrid PV–Wind System–Case Study

Jyoti B. Fulzele, M. B. Daigavane and P. M. Daigavane

Abstract The main aim of this paper was to describe designing, modeling, and optimization of photovoltaic–wind hybrid energy system that can generate and provide techno-economical and reliable electricity to the rural areas of country with constraints renewable energy fraction and minimizing excess energy. The minimum excess energy generation with maximum renewable fraction is considered as the main constraints in this research work while optimizing the size of the components. This work has been devoted to design optimal hybrid renewable energy system for a community of 256 household of a small village of Vidharbha region named Dudhgaon near Arab Bori, Yavatmal district, Maharashtra, India. For optimization procedure, daily load profile, solar irradiance, wind velocity, and scientific requirement of all components have been collected and used as input data. The main objective to design the system is to minimize net present cost of the system by considering the parameters like capacity shortage, renewable fraction, cost of energy, and excess energy. The research tools iHOGA have been used for the optimum design of hybrid photovoltaic–wind system. The residential, commercial, and community load has been considered for electricity demand calculation. The results show that the hybrid renewable energy projects are a good investment for Dudhgaon village which provide the minimum cost of energy to the consumers with reliable power supply.

Keywords Cost of energy · iHOGA · Optimization · Photovoltaic · Wind · Modeling

J. B. Fulzele (✉) · P. M. Daigavane
GHRCE, Nagpur, India
e-mail: bhongade10@gmail.com

P. M. Daigavane
e-mail: prema.daigavane@raisoni.net

M. B. Daigavane
GHRIET, Nagpur, India
e-mail: mdai@rediffmail.com

1 Introduction

Since the world energy demand goes on increasing day by day and is mainly driven because of increasing population rate of developing countries in the world, the different world energy generation projects are launched for 2004–2030; and tentatively it will reach 30.36 trillion KWh in the year 2030 [1]. In 2012, world total primary energy supply was around 155,505 TW h while the world final energy consumption was 104,426 TW h, about 32% less than the total supply [2]. In 2013, world electricity generation was about 23,322 TW h which are about 18% less than the world energy consumption [3]. The present electricity generation mostly depends on coal thermal power plant which leads to challenging issues such as climate change and global warming. The renewable energy power generation has provided an alternative solution to overcome this dilemma and provided access to electricity to many billion people who are living in remote villages where grid is not connected. Even though grid is connected, it does not have reliable electricity [4, 5].

The Indian energy scenario showed that, India had an installed capacity of 314.66 GW as on Jan 31, 2017. Out of this, 68.3% of energy generation are from fossil fuel, mostly the coal, and only 29.9% from renewable resources. Since rapid increase in electricity utilization and the coal stock are incessantly decreasing, the Government of India has taken an initiative to fulfill this energy deficiency. In request to deal with the shortage of ample electricity available to all the individuals in country by March 2019, the Government of India launched a plan called "Power for All" [6]. This plan will make sure uninterrupted power to all household, industries, and commercials.

Due to rapid development in renewable energy sector, now hybrid energy system is the option to meet power demand in the remote area where grid extension is difficult and not reliable. Hybrid energy system is used as an alternative solution to the traditional systems, which typically based on a single fossil fuel source. On design point of view, the optimization of the size of hybrid energy system is very important. Designing of hybrid energy system would require correct component selection and sizing with appropriate operation strategy. Optimally sizing the works is not sufficient to get the most recital of the hybrid as the troubles get difficult when energy abounding by the renewable becomes not capable to assemble the load demand.

Hence, proper design of hybrid energy systems is a very essential and challenging task for the designer to meet coordination between available energy resources and other system components. So, in view of the key objectives of optimization of hybrid energy system of power reliability and cost and without disturbing the environmental planning, system modeling shall be carried out. This paper presents design, modeling, and optimization of hybrid renewable system consist of photovoltaic/wind/battery and converter. The research tool used for the hybrid system design is iHOGA.

2   Research Methodology

In this paper, research methodology used for design of hybrid renewable energy system that includes selection of study area, data collection, and analysis of renewable energy resource potential, electricity demand estimation, control strategy, and objective function of hybrid renewable energy system.

2.1   Study Area

The site which has been selected for case study was Dudhgaon village, near Arab Bori, Darwha Taluka, Yavatmal District, Maharashtra, India. The existing living pattern of the people in this area depends on agriculture. The people living in this village use kerosene, fire wood, cow dung, and agriculture waste for all household activities.

The grid is available in this area, but the supply of power is not reliable and suffered from load shedding (blackouts and brownouts) of five to six hours. The people living in this have been suffering from several problems which include loss of agriculture output due to shortfall of rain, shortage of electricity, load shedding, that immobilized them from irrigating crop on time, harassments by money lenders, lack of health, education, and medical facilities. They are still waiting for reliable electricity, proper healthcare system, education facilities, and employment in rural parts. The renewable energy potential is available there in adequate amount. The area has recorded an average annual temperature from 25 to 27.5 °C. This indicates it has giant solar potential. The study area has rainy season starting from the mid of June to September. There has been a short fall of rain during last three years. This area has no source of water flowing which can be valuable for use of energy production. The energy demand for this area basically includes domestic service, community service area such as schools, health center, irrigation, and commercial use like shops.

2.2   Resource Input

The reserve inputs for the selected site are solar and wind. Solar irradiance data for latitude 20° 24′N and longitude 78° 8′E are serene from [7]. The average daily solar radiation for this site is 5.312 KWh/m^2/day. Similarly, the average monthly wind velocity data are serene from [8], and it is found that yearly average wind velocity is 3.22 m/s. Figure 1 shows the details resource input data, i.e., monthly solar radiation on horizontal surface, clearness index, and monthly wind speed of Dudhgaon village. These are the long-term data obtained from NASA based on satellite estimate and according to standard conventions.
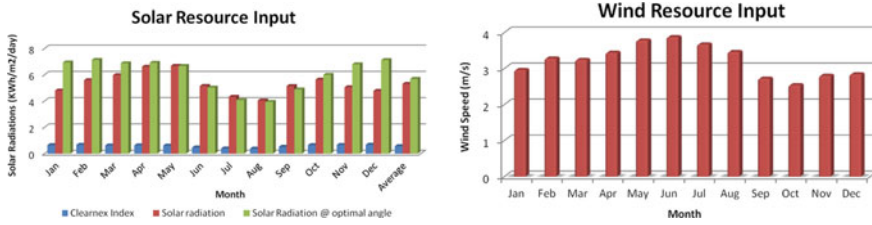
Fig. 1 Resource input data

2.3 Electricity Demand Estimation

The electrical energy demand evaluation has been calculated for four loads, i.e., household, commercial, community, and irrigation load [9].

The household load includes lighting load, TV, and Fan. The individual house is assumed to use maximum 4 units of 11 W compact florescent lamp, three units for residential room lighting and one unit for outdoor lighting, single color TV (36 cm) of 90 W and four units of fan of 55 W. The commercial load includes lighting load of shops and flour mill load. The community load includes load of primary health center, school, and street lights. The electrical load required for irrigation system is used to drive electric motor for water pumping to pump water to the farm land. In this study, it is assumed that twenty five units of 1.49 KW (2 HP) pumps having discharge capacity of 45 L/min which delivers 43.2 m^3 per day is considered for calculation. By considering all this and with the use of power investor tools, each day average electricity demand of Dudhgaon can be reduced to 725.13 KWh/day and peak load can be reduced to 183.80 KW peak [9]. The details of total electrical load for three different seasons are shown in Table 1.

3 Design of Hybrid Energy System

In this study, the structure model consists of photovoltaic generator, wind generator, batteries, and converter shown in Fig. 2. In this study, the main criteria for the selection of hybrid system components depend on the cost of components. The structure has been designed, modeling and optimized by using iHOGA invented by Department of Electric Engineering, University of Zaragoza (Spain). The hybrid system is designed for 300 V DC and 230 V AC. The technical specifications of all components used for system design are shown in Table 2. The selection of different product of the stated company given in Table 2 is based on low cost carried out by market survey. The other input parameters which used for simulation and optimization contain economic parameter such as project life time is consider as 25 years, inflation rate is taken as 7.38%, and discount rate is 6.50%. The fixed capital cost, fixed operation and maintenance cost, and capacity shortage penalty is taken as zero.

Table 1 Details of load demand of village

Time	Electric load (KW h)					Commercial load	
	Household load						
	Lighting load (11 W)	T.V. (90 W)	Fan (55 W)			Lights for shops (20 W)	Flour mill (2.23 KW = 3 HP)
			Summer	Winter	Rainy		
0:0–1:0	5.63	0	28.16	0	0	0	0
1:0–2:0	5.63	0	28.16	0	0	0	0
2:0–3:0	5.63	0	28.16	0	0	0	0
3:0–4:0	5.63	0	28.16	0	0	0	0
4:0–5:0	5.63	0	28.16	0	0	0	0
5:0–6:0	0	0	0	0	0	0	0
6:0–7:0	0	0	0	0	0	0	0
7:0–8:0	0	23.04	0	0	0	0	0
8:0–9:0	0	23.04	0	0	0	0	0
9:0–10:0	0	0	0	0	0	0	0
10:0–11:0	0	0	0	0	0	0	0
11:0–12:0	0	0	56.32	28.16	28.16	0	2.23
12:0–13:0	0	23.04	56.32	28.16	28.16	0	2.23
13:0–14:0	0	23.04	56.32	28.16	28.16	0	0
14:0–15:0	0	0	56.32	28.16	28.16	0	0
15:0–16:0	0	0	56.32	28.16	28.16	0	2.23
16:0–17:0	0	0	56.32	0	0	0	2.23
17:0–18:0	0	23.04	56.32	0	0	0.06	2.23

(continued)

Table 1 (continued)

Time	Electric load (KW h)						
	Household load					Commercial load	
	Lighting load (11 W)	T.V. (90 W)	Fan (55 W)			Lights for shops (20 W)	Flour mill (2.23 KW = 3 HP)
			Summer	Winter	Rainy		
18:0–19:0	11.26	23.04	56.32	28.16	28.16	0.06	0
19:0–20:0	11.26	23.04	56.32	28.16	28.16	0.06	0
20:0–21.0	11.26	23.04	56.32	0	0	0.06	0
21:00–22:0	5.63	0	56.32	0	0	0	0
22:0–23:00	5.63	0	0	0	0	0	0
23:00–24.0	0	0	0	0	0	0	0

Average load (KW h/day) = 725.13

Time	Electric load (KW h)									
	Community load			Irrigation load			Total electric load/h		
	Primary Health Centre (20 W)	Street lights (20 W)	School lights (20 W)	Pump (1.49 KW = 2 HP)			Summer	Winter	Rainy
				Summer	Winter	Rainy			
0:0–1:0	0	1.04	0	0	0	0	34.83	6.67	6.67
1:0–2:0	0	1.04	0	0	0	0	34.83	6.67	6.67
2:0–3:0	0	1.04	0	0	0	0	34.83	6.67	6.67
3:0–4:0	0	1.04	0	0	0	0	34.83	6.67	6.67
4:0–5:0	0	1.04	0	0	0	0	34.83	6.67	6.67
5:0–6:0	0	0	0	22.35	22.35	0	22.35	22.35	0
6:0–7:0	0	0	0	22.35	22.35	0	22.35	22.35	0
7:0–8:0	0	0	0	22.35	0	0	45.39	23.04	23.04

(continued)

Table 1 (continued)

Time	Electric load (KW h)			Irrigation load			Total electric load/h		
	Community load			Pump (1.49 KW = 2 HP)			Summer	Winter	Rainy
	Primary Health Centre (20 W)	Street lights (20 W)	School lights (20 W)	Summer	Winter	Rainy			
8:0–9:0	0.08	0	3.2	0	0	0	26.32	26.32	26.32
9:0–10:0	0.08	0	3.2	0	0	0	3.28	3.28	3.28
10:0–11:0	0.08	0	3.2	0	0	0	3.28	3.28	3.28
11:0–12:0	0.08	0	3.2	0	0	0	61.83	33.67	43.94
12:0–13:0	0.08	0	3.2	0	0	0	84.87	56.71	66.98
13:0–14:0	0	0	0	0	0	0	79.36	51.2	51.2
14:0–15:0	0	0	0	0	0	0	56.32	28.16	28.16
15:0–16:0	0	0	0	0	0	0	58.55	30.39	40.66
16:0–17:0	0	0	0	0	0	0	58.55	2.23	12.5
17:0–18:0	0.08	1.04	0	22.35	22.35	0	105.12	48.8	36.72
18:0–19:0	0.08	1.04	0	22.35	22.35	0	114.15	85.99	63.64
19:0–20:0	0.08	1.04	0	22.35	0	0	114.15	63.64	63.64
20:0–21:0	0.08	1.04	0	0	0	0	91.8	35.48	35.48
21:00–22:0	0	1.04	0	0	0	0	62.99	6.67	6.67
22:0–23:00	0	1.04	0	0	0	0	6.67	6.67	6.67
23:00–24:0	0	1.04	0	0	0	0	1.04	1.04	1.04
Average load (KW h/day) = 725.13									
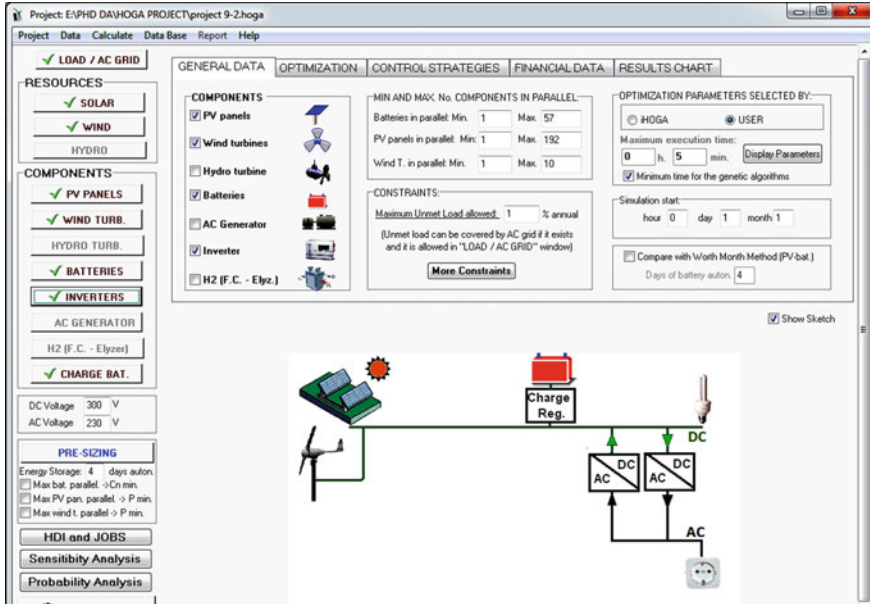
Fig. 2 iHOGA simulated model of hybrid system

Table 2 Scientific requirement and other inputs

PV array		Wind generator	
Nominal voltage (V)	24	Technology	Hummer HWP50
Short circuit current (A)	5.24	Power (W)	50,000
Nominal power (Wp)	190	Hub height	22 m
Capital cost ($)	255.6	Capital cost ($)	7,6700
Replacement cost ($)	255.6	Replacement cost ($)	62,400
O & M cost ($)	2.55	O & M cost ($)	1534
Life time	25 year	Life time	20
Tracking system	No tracking		
Battery		Converter	
Technology	Trojan 12 V 27TMH	Capacity (VA)	150,000
Voltage (V)	12 v	Capital cost ($)	69,820.7
Amp hour (AH)	106	Replacement cost ($)	69,820.7
Capital cost ($)	253.5	Efficiency	90%
Replacement cost ($)	253.5	Vdc (V)	300
O & M cost ($)	2.53	Life time	10 year
Efficiency	80%	Battery Charger	OK
Life time	10196 KWh		

Gen.	Total Cost (NPC)($)	Emission (kgCO2/yr)	Unmet(kWh/yr)	Unmet(%)	D.aut	Cn(Ah)/(Ipv+Iw)(A)	Ren(%)	Cost E.($/kWh)	Simulate	Report	
8	1007881.2	15828	2245.6	0.8	1	2.2	99.2	0.15	SIMULATE..	REPORT...	I
9	1007881.2	15828	2245.6	0.8	1	2.2	99.2	0.15	SIMULATE..	REPORT...	I
10	1004215.4	15832	2494.8	0.9	1	2.2	99.1	0.15	SIMULATE..	REPORT...	I
11	1002330.9	15822	2621.8	1	1	2.2	99	0.15	SIMULATE..	REPORT...	I
12	1002330.9	15822	2621.8	1	1	2.2	99	0.15	SIMULATE..	REPORT...	I
13	1002330.9	15822	2621.8	1	1	2.2	99	0.15	SIMULATE..	REPORT...	I
14	1002330.9	15822	2621.8	1	1	2.2	99	0.15	SIMULATE..	REPORT...	I
15	1002330.9	15822	2621.8	1	1	2.2	99	0.15	SIMULATE..	REPORT...	I

COMPONENTS: PV panels suntech 190W (190 Wp): 13s. x 203p. (slope 30°) // Batteries Trojan12V:J185P (189 A·h): 25s. x 18p. // 2 Wind Turb. DC Hummer: HWP-50 (72477 W at 14 m/s) // Inverter Generic: 150K CARG of 150000 VA // PV batt. charge controller included in bi-di inverter // Unmet load = 1 % // Total Cost (NPC) = 1002330 $ (0.15 $/kWh)

STRATEGY: LOAD FOLLOWING. SOC min.: 10 %.

Fig. 3 iHOGA optimized result of hybrid system

4 Results and Discussion

By considering all this, structure has been computerized generated by using iHOGA. The research tool produce number of simulation results of hybrid energy system based on most favorable solution of system structure and control strategy by genetic algorithm. The system study includes mono-objective function that is to minimize total net present cost for the constraint such as nominal capacity of the batteries bank, minimum number of reserve days, maximum unmeet load allowed, maximum renewable fraction, and minimum cost of energy. The control policy of the system uses both the load following and the cycle charging. The simulated optimized results of hybrid energy system are shown in Fig. 3.

So as to choose techno-economical and reliable result of the system, for the desired parameters such as load of 725.13 KWh/day, peak capacity shortage of 1, and 0% renewable energy fraction. Figure 3 shows the different optimum solution of hybrid photovoltaic–wind energy system with minimum net present cost is 1,002,331$ and corresponding cost of energy equal to 0.15$/KWh. This result is considerable as least because after 15 iteration; with the same parameters, no other better result has been given by iHOGA. The optimum system design of hybrid photovoltaic–wind energy system consists of photovoltic panels of 13 series × 203 parallel with power of 190 Wp, 25 batteries series × 18 parallel with voltage 12 V,189 Ah, two wind turbine with 72477 W at 14 m/s, bidirectional inverter of 150 KVA, photovoltaic battery charge controller built-in in inverter unit. The optimum control strategy selected by iHOGA is load following.

4.1 Technical Feasibility of Optimum Hybrid System

The monthly average electric production by the optimize system is shown in Fig. 4. Solar radiation potential is high in seven months from October, November, December, February, March, April, and May, while it is low in June, July, and August. The
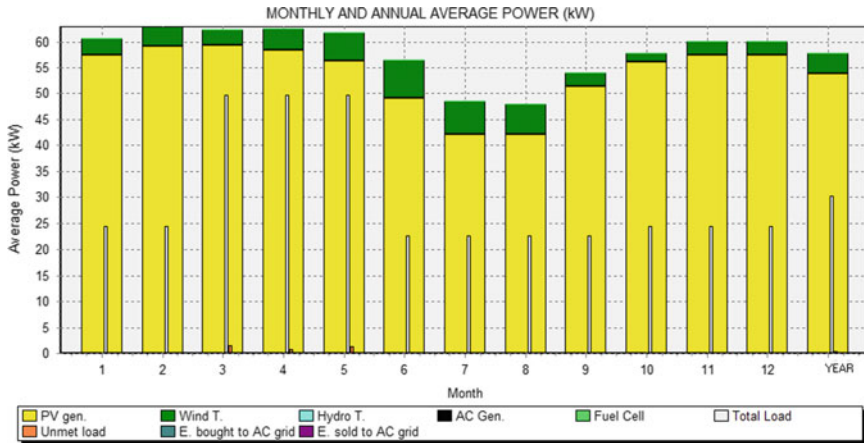
Fig. 4 Monthly average electric production
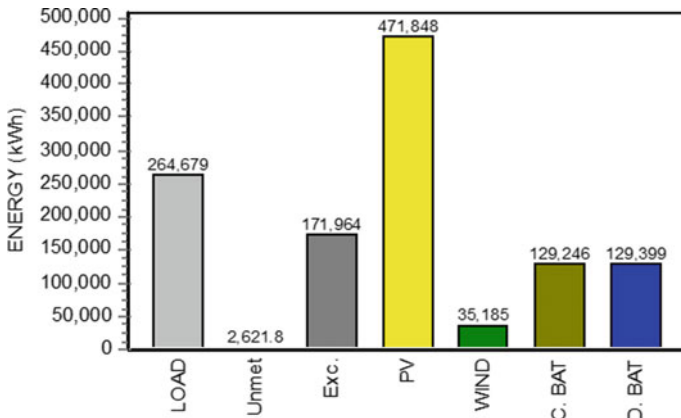
Fig. 5 Share of energy generation and consumption

energy consumption and energy generated by individual units of the hybrid system are shown in Fig. 5. The yearly energy production is 507,035 KWh/year out of which photovoltaic contributes 471,849 KWh/year nearly equal to 93.06% while wind system contributes 35186 KWh/year approximately equal to 6.93%. The energy generated from solar source is higher than any other source; hence, it is considered as the base load of the hybrid system. Figure 5 shows that the energy demands are almost fulfilled by the system in all the periods of the year except 2621.7 KWh/year of energy, i.e., only 0.99% of demand is not fulfilled by the system which is considerable. The excess energy generated by system is 171965 KWh/year nearly equal to 33.91%.

Table 3 Cost summery

S. no.	Components	Cost ($)
1.	PV generator	372,459
2.	Wind turbine	194,460
3.	Battery bank	241,147
4.	Inverter & auxiliary	172,280
5.	Total system	980,346

4.2 Cost Summery of Optimal System

Table 3 shows the cash flow summery of optimal system given by iHOGA. The initial investment cost of the system is about 980,346$, which includes the cost of PV, wind generator, battery storage, and converter. Total net present cost of the hybrid system is 1,002,331$, where the highest share cost is contributed by PV about 372,459$ nearly equal to 38%. The second highest cost is contributed by battery is 241,147$ equal to 25% while wind turbine and inverter contribute to about 20 and 17%.

5 Conclusion

By considering the aim of rural electrification of Vidharbha region of Maharashtra State, this paper provides the techno-economic analysis of hybrid energy system for the Dudhgaon village. This study uses renewable energy assessment tools iHOGA. The detail simulation and optimization results given by iHOGA are discussed. The optimal hybrid renewable power system configuration which consists of photovoltaic system of 501 KW (13 Series × 203 Parallel), two wind turbine (150 KW), 150KW of converter and 450 (25 Series × 18 Parallel) battery configuration that gives the lowest net present cost of 1,002,330.9$ with cost of energy 0.15$ for a period of 25 years is the technical and economically feasible solution for the given study.

References

1. Nath, B.: Experience of policy instruments used to promote renewable energy—case study of Maharashtra, India. Masters Research Thesis, Lund University, Lund, (2008)
2. IEA.: Key world energy statistics. [Online] Available www.iea.org, 5 May 2014
3. IEA.: Key world energy statistics. [Online] Available www.iea.org, 13 Mar 2015
4. Takada, M., Charles, N.A.: Energizing poverty reduction: a review of the energy-poverty nexus in poverty reduction strategy papers. In: United National Development Program, New York (2007)
5. Bhattacharjee, C.R.: Wanted an aggressive outlook on renewable energy. Quart. Electron. Newslett. Renew. Energy Environ. 1–17 (2005)
6. https://enwikipedia.org/wiki/electricity_sector_in_India

7. https://rredc.nrel.gov/solar
8. http://eosweb.larc.nasa.gov/cgi-bin/sse/grid.cgi
9. Fulzele, J.B., Daigavane, M.B., Daigavane, P.M.: Design of hybrid PV-wind stand alone hybrid renewable energy system: case study. J. Inform. Optim. Sci. https://doi.org/10.1080/02522667.2017.1374744

Design and Simulation of Photovoltaic Water Pumping System

Sachin Wadhankar and Bhagyashri Charjan

Abstract The use of the electrical energy increases nowadays. This energy generated by using the fossil fuel that causes the carbon content, which is responsible for the pollution and increase the global warming. So this problem can be solved by using the solar energy, which is the renewable energy source. There are two main types of photovoltaic energy system, i.e., grid-connected PV energy system and standalone PV energy system. This paper presents the stand-alone photovoltaic solar energy system. Because this can be used in remote areas, rural area, where the national grid system is not available. In solar energy system, DC–DC conversion is an important step but due to this, the system will become more complex and increase the price of the system also reduces the efficiency of the system. So here, the single stage conversion of the solar energy uses such as PV panel, Inverter, and pump. The simulation is executed in the MATLAB SIMULINK Software.

Keywords PV panel · Inverter · Induction motor · IGBT · SPWM technique · MPPT technique

1 Introduction

The non-renewable energy sources such as fossil fuels are mostly used for generating the electricity in the whole world. However, this energy generation is responsible for the increasing the carbon content in the environment. Due to the huge amount of the carbon content in the environment, increase the global warming, pollution, and unwanted change in the environment [1].

The shortage of electricity is the big problem in the development of India. Grid-connected energy system of India is under progress. The use PV energy system and

S. Wadhankar · B. Charjan (✉)
G.H. Raisoni Institute of Engineering and Technology, Nagpur, India
e-mail: bhagyashricharjan24@gmail.com

S. Wadhankar
e-mail: Sachin.wadhankar@raisoni.net

the other renewable energy systems are the solutions for this problem. Because many sunny days are accessible in India from beginning to end of the year [2]. There are two main types of the solar energy system first, grid-connected PV energy system, and second standalone PV energy system [3].

The standalone PV solar energy system has the number of applications in the rural area and remote areas where the grid system is not available. One of the most important used of the standalone solar photovoltaic systems is for the water pumping, especially in the rural areas that have a lot of amount of solar radiation and very far from the national grid. So in rural and remote areas, solar photovoltaic water pumping system can be used for the supply of water. Particularly an efficient solution must assure that the solar generators run at the maximum power point (MPP) and the pump, which is driven by the single-phase induction motor run at the high efficiency and give the maximum output [4].

Solar energy-based pump has recently received the more attention due to the development of the materials and the technology of the photovoltaic cell. PV pump based on the DC motor is used in the several parts of the world [5]. Because the output power obtained from the solar panel is the DC power. However, DC machine-based pump suffers from the maintenances problem because the brushes and commutator are present in the DC machines. The induction motor-based water pumps are not facing these types of the problem. Hence the induction motor-based pump maintains free operation, more reliable, and generally used in the day-to-day life because the price of the induction motor is lower and the availability of the AC power.

In the photovoltaic water pumping system, essential input is the solar radiation and the output is the water discharge. However, the water discharge depends on the solar radiation because they are not constant throughout the day. High-intensity solar radiations are obtained at the afternoon time, and intensity of the solar radiation is less in the morning and evening time. To solve this problem, MPP tracking (MPPT) technique is used. MPPT technique will force the PV panel to operate at its maximum point. There are number of types of the MPPT technique like Perturb and Observe technique, incremental conductance technique, constant voltage technique, fuzzy logic technique. The P&O technique has commonly used the method because it is the easy method among all the other methods. This method has an easy algorithm and fast-tracking of MPP.

In this paper, the incremental conductance technique is used because it is more accurate than P&O method. The MPPT technique is commonly used for the off-grid system like standalone solar energy system. In single stage conversion of the PV panel, single phase inverter, and pump. The battery will be used at nighttime and on cloudy days.

2 System Description

The solar panel will absorb the solar radiation from the sun and convert it into electricity. The MPPT algorithm used to exact the maximum power from the PV
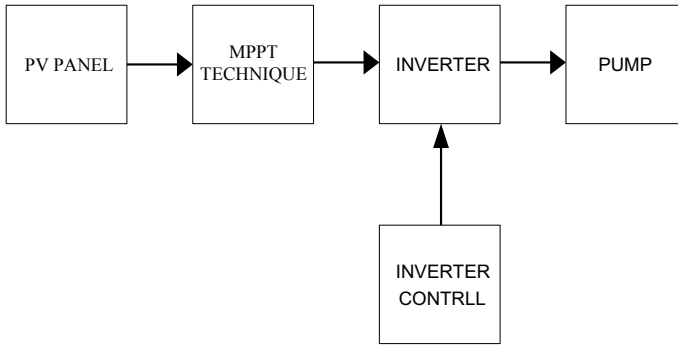
Fig. 1 Block diagram of PV-based water pumping system

array. The output of the solar panel is the DC quantity; hence, the inverter will use the conversion of DC-AC. The pulses for the inverter switches are generated by using the sinusoidal pulse width modulation technique. The AC output of the inverter will be used to driving the Induction motor-based water pump. The block diagram is shown in Fig. 1.

2.1 Solar Panel

The important element of the PV system is the solar cell, which converts the radiation from the sun into electricity. Solar cells are manufactured in two different types, i.e., crystalline and thin film. The thin film solar cell is cheaper but less efficient hence crystalline solar cell is used in most of the applications because of high efficiency.

   When the solar radiation increases, the current and voltage also increase. When a temperature of the cell increases, the voltage decreases but current increases slightly. In the PV array, PV cells and PV panels are connected in parallel connections and in series connection to getting the required current and voltage. Figure 2 shows the diagram of solar array.

2.2 Inverter

The voltage source inverters are used to convert the DC quantities into the AC quantities which have variable magnitude and fixed frequency and suitable for AC load applications. The diagram for single-phase voltage sources inverter is shown in Fig. 3.

   In the single-phase voltage sources inverter, IGBTs are used as the switches. Here, the sinusoidal pulse width modulation technique (SPWM) is used to generate the gate pules for turn-on the inverter switches. The SPWM technique will reduce the har-

monic content in the system and allow the controlling of frequency and magnitude of the output voltage. In SPWM technique, the sinusoidal modulation waves are compared to the high-frequency carrier wave. The SPWM technique has two operating modes: first unipolar and second bipolar. Here, unipolar mode of operation is used because it gives fewer ripples in the input current. The pulses obtained from the SPWM technique are shown in Fig. 4.

2.3 Incremental Conductance Technique

In this technique, the controller measures incremental changes in photovoltaic array voltage and current to guess the effect of a changing voltage. The incremental conductance technique needed more calculation in the controller, but can track changing conditions rapidly than the perturb and observe technique. Same as the P&O algorithm, it can produce oscillations in power output. This technique utilizes the incremental conductance (dI/dV) of the PV module to compute the sign of the change in power with respect to voltage (dP/dV).
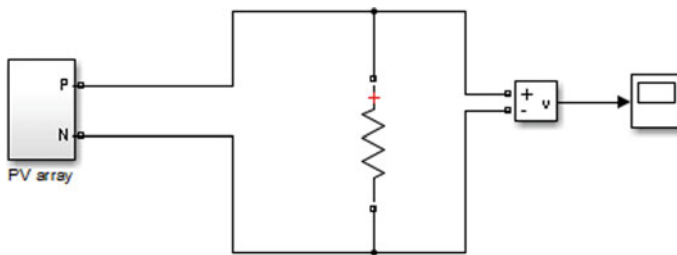
Fig. 2 PV array
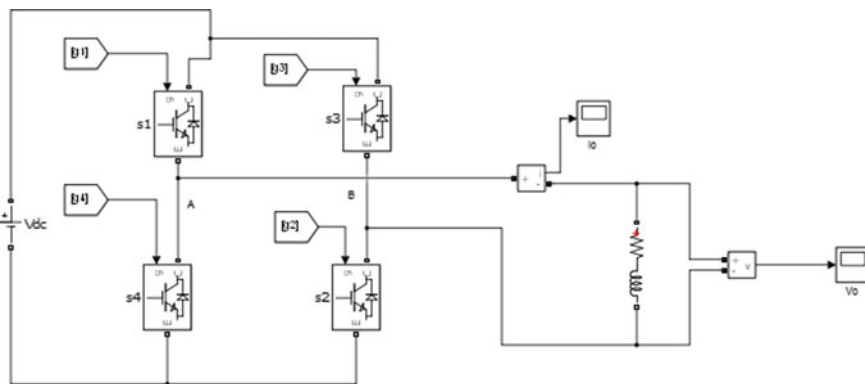
Fig. 3 Single-phase voltage source inverter
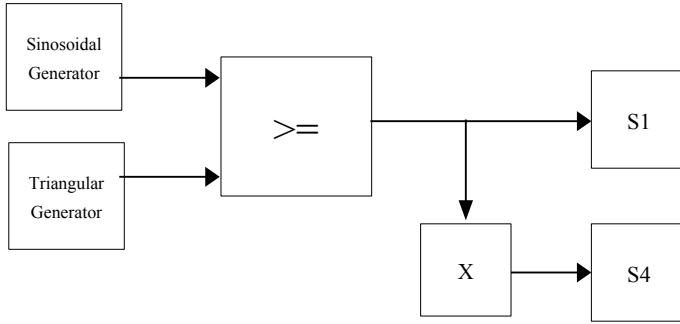
Fig. 4 Pulse generation using SPWM technique

The incremental conductance technique calculates the MPP by comparing incremental conductance (I_Δ/V_Δ) to the array conductance (I/V). When they are the same ($I/V = I_\Delta/V_\Delta$), the output voltage is the MPP voltage. This voltage is managed by controller until the irradiation changes and the process is repeated.

$$dP/dV = 0,$$

and $P = IV$. The current from the array can be expressed is a function of the voltage: $P = I(V)$ V.

Therefore,

$$dP/dV = V dI/dV + I(V).$$
$$dI/dV = -I(V)/V.$$

Therefore, the MPPT technique condition is obtained when the incremental conductance is same as the negative of the instantaneous conductance (Fig. 5).

Where

V_{pv}, I_{pv}—Preasent sample
V_{pv0}, I_{pv0}—Previous sample
dV_{pv}, dI_{pv}—Incremental PV voltage and current.

2.4 Load

Here, the single-phase induction motor-based pump will be used. Single-phase induction motors are widely used today than the other types of motor. Because it is least expensive, it is the lowest maintenance type motor. This type of motor has only one stator winding (main winding) and operates with a single-phase power supply. The stator of this type of motor is provided with single-phase supply; then, alternating
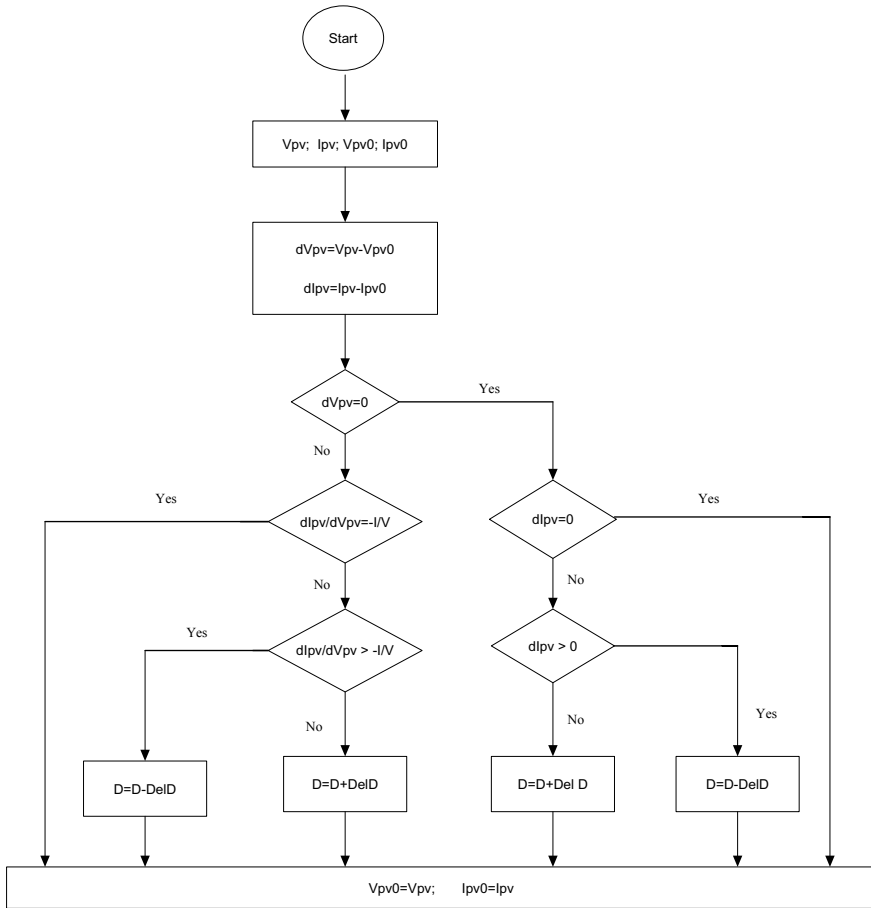
Fig. 5 Flowchart for incremental conductance MPPT technique

flux will produce in the stator winding. The ac current flows through stator winding, due to this current will produce in the rotor bars according to Faraday's law of electromagnetic induction. This induced current in the rotor bars will also produce alternating flux. Even after both alternating fluxes are set up, the motor fails to start. However, if the rotor is given an initial start by external force in either direction, then motor accelerates to its final speed and keeps running with its rated speed.

3   Simulation Result

This simulation is executed in the MATLAB SIMULATION software, and the results are shown here. The output voltage of the solar panel under changing atmospheric
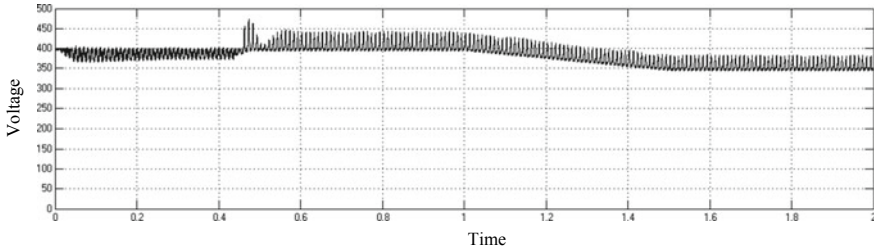
Fig. 6 Output voltage of PV array
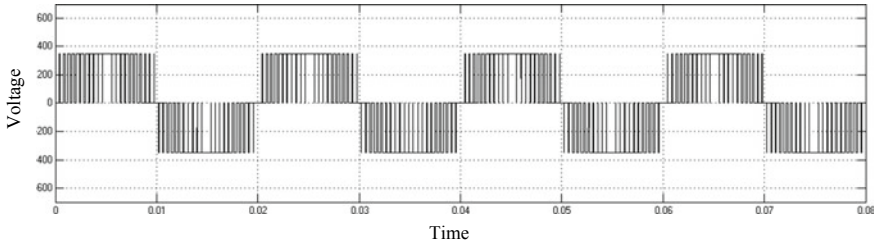
Fig. 7 Voltage output of the single-phase voltage source inverter
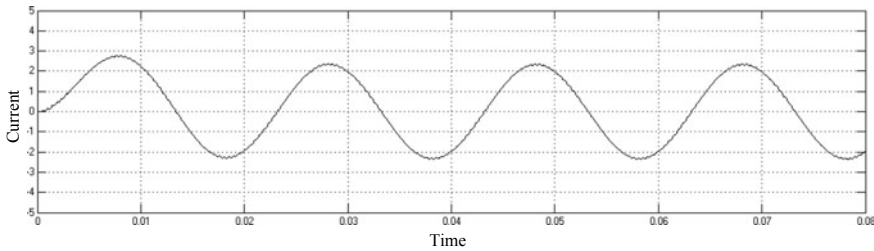
Fig. 8 Output current of single-phase voltage source inverter

condition is shown in Fig. 6. In the open loop system, it operates on the constant input and output parameters, the output voltage, and current of an inverter are shown in Figs. 7 and 8.

Figures 9, 10 and 11 show the output voltage, current, and speed of single-phase induction motor-based pump, respectively, under when the carrier frequency is 1 kHz. On X-axis output voltage, current and speed of single-phase induction motor with respect to time

Figures 12, 13 and 14 show the output voltage, current, and speed of single-phase induction motor-based pump, respectively, when the carrier frequency is 2 kHz. On X-axis output voltage, current, and speed of single-phase induction motor with respect to time.
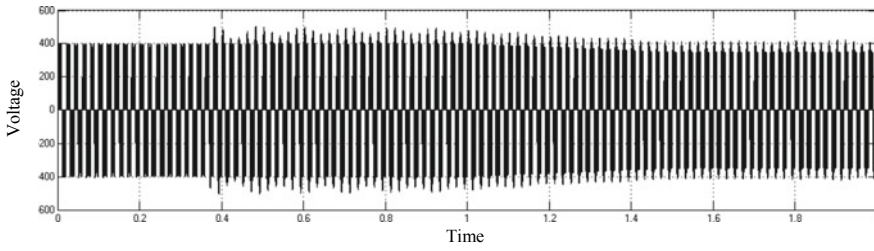
Fig. 9 Output voltage of single-phase induction motor
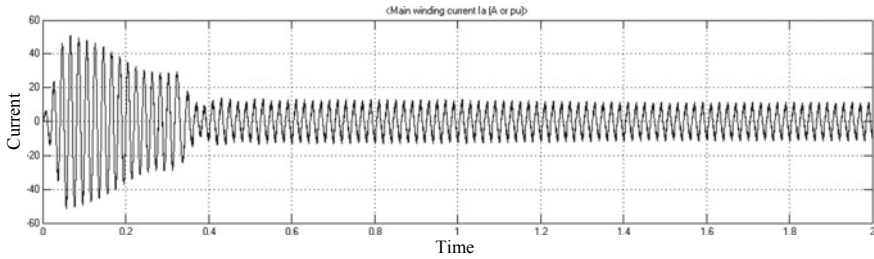
Fig. 10 Output current of single-phase induction motor
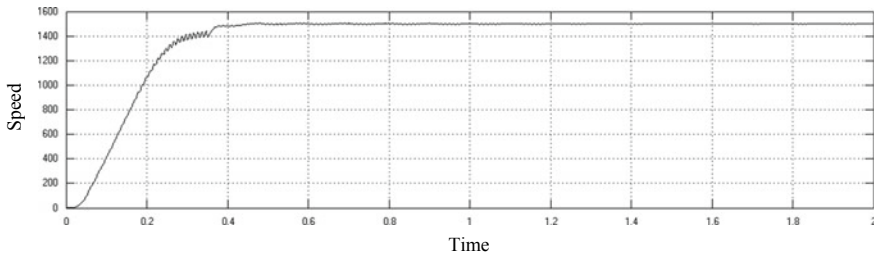
Fig. 11 Speed of single-phase induction motor
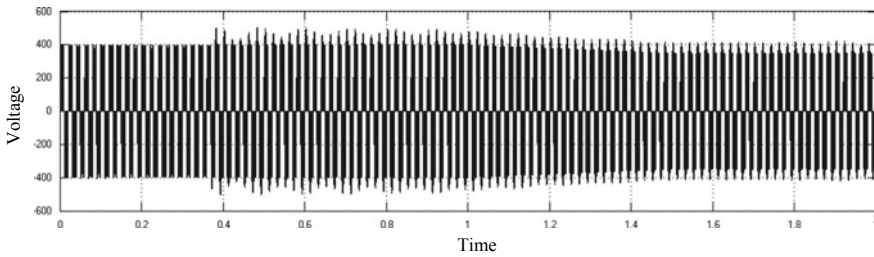
Fig. 12 Output current of single-phase induction motor
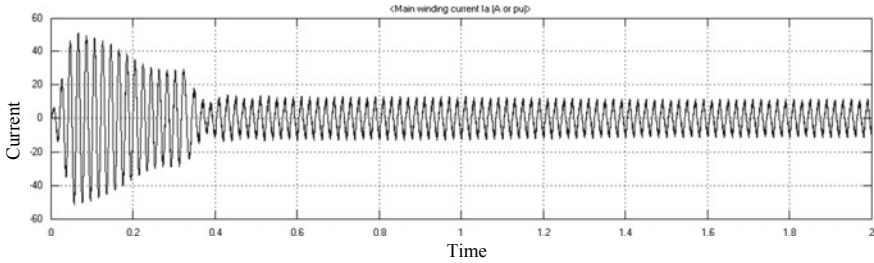
Fig. 13 Output current of single-phase induction motor
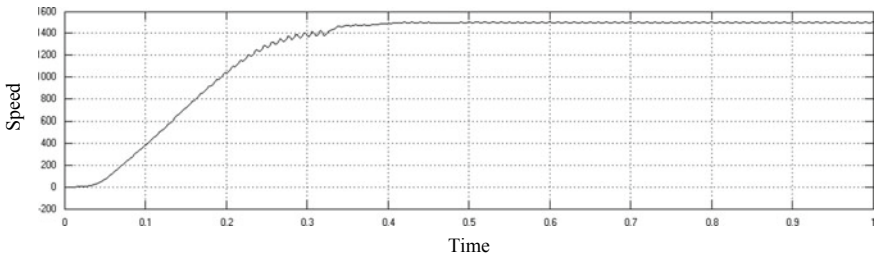
Fig. 14 Speed of single-phase induction motor

4 Conclusion

The output current and voltage of the solar panel is changed due to the change in the atmospheric condition. Hence, the output of the pump is also changed. By using MPPT technique, the changing output of the solar panel can be controlled. By using the solar energy system, the use of the non-renewable sources will reduce. The photovoltaic-based water pumping system has been simulating using the MATLAB SIMULINK Software presented.

References

1. Dubey, K., Shaha, M.T.: Design and simulation of solar PV system. In: International Conference on Automatic Control and Dynamic Optimization Techniques (ICACDOT) International Institute of Information Technology, Pune, pp. 568–573, 16 Mar 2017
2. Malla, S.G., Bhende, C.N., Mishra, S.: Photovoltaic based water pumping system. In: International Conference on Energy, Automation and Signal (ICEAS), Bhubaneswar, 28 Dec 2018
3. Lukhwareni, T., Dobzhanskyi, O., Gouws, R.: Solar power pumping system for domestic appliances. In: IEEE Conferences of Domestic use of Energy (DUE), South Africa, 9 June 2014
4. Charjan, B., Wadhankar, S.: Design of solar power based water pumping system. Int. J. Sci. Res. Sci. Eng. Technol. **4** (2018)

5. Bhat, S.R., Pittet, A., Sonde, B.S.: Performance optimization of induction motor-pump system using photovoltaic energy source. IEEE Trans. Ind. Appl. **IA-23**(6) (1987)
6. Kumar, R., Singh, B.: Single stage solar PV fed brushless DC motor driven water pump. IEEE J. Emerg. Select. Topics Power Electron. **5**, 1377–185 (2017)
7. Esram, T., Chapman, P.L.: Comparison of photovoltaic array maximum power point tracking techniques. IEEE Trans. Energy Convers. **22**(2), 439–449 (2007)
8. Sera, D., Teodorescu, R., Hantschel, J., Knoll, M.: Optimized maximum power point tracker for fast-changing environment conditions. IEEE Trans. Ind. Electron. **55**(7), 2629–2631 (2008)
9. Priyanka, D., Pradnya, H., Dnyaneshwari, S., Kamboj, A.: PV based solar water pumping system. Int. Eng. Res. J. (IERJ) **2**, 744–746 (2016)
10. Sharma, U., Kumar, S., Singh, B.: Solar array fed water pumping system using induction motor drive. In: IEEE International Conference on Power Electronics, Intelligent Control, and Energy System (ICPEICES), 16 Feb 2017
11. Shaikh, S.R., Jain, A.M.: A literature survey of photovoltaic water pumping system. In: International Conference On Control, Instrumentation, Communication and Computational Technologies (ICCICCT), pp. 511–516, 23 May 2016
12. Bala Raghav, M., Naga Bhavya, K., Suchitra, Y, Srinivasa Rao, G.: Design of solar power based water pumping system. Int. J. Eng. Res. Technol. (IJERT) **2**, 333–339 (2013)
13. Vitorino, M.A., Correa, M.B.R.: High-performance photovoltaic pumping system using induction motor. In: Power Electronics Conference, Brazil, pp. 797–804, 27 Sept 2009

Maximum Power Point Tracker for Standalone PV System Using Neural Networks

K. M. S. Y. Konara, Mohan Lal Kolhe, M. A. N. Sanjeewa, W. T. V. S. Fernando, G. M. N. Priyashantha and J. W. G. S. Weerasinghe

Abstract In this work, designing and implementation of a maximum power point tracker (MPPT) based on an artificial neural network is proposed. The output voltage of the selected photovoltaic array is controlled by a DC to DC boost converter in a way that the PV array generates the available possible maximum power correspond to the available solar irradiance and temperature. The neural network (NN) is capable of forecasting the required terminal voltage of the PV array in order to generate the possible maximum power. The pulse width modulation (PWM) signal, which drives the boost converter, is generated through a raspberry pi according to the forecasted terminal voltage. The terminal voltage of the PV array is controlled by changing the duty ratio of the PWM signal accordingly. The impact of the implemented NN toward the response time and the accuracy is discussed. NN based MPPT can provide a reliable solution.

Keywords MPPT · Neural network · PV array · Irradiance sensor · Boost converter · Python

1 Introduction

The power output of the PV system depends on the incident solar irradiance and cell temperature of the PV module. Due to these variables, the output current and the output voltage of the PV module changes with the time. For PV systems, the output power can be increased with increase in the incident solar irradiance on the PV module. This can be done by tracking the position of the sun. But, this is not effective

K. M. S. Y. Konara (✉) · M. L. Kolhe
Faculty of Engineering and Science, University of Agder (UiA), 4898 Grimstad, Norway
e-mail: konara@eie.ruh.ac.lk

M. L. Kolhe
e-mail: mohan.l.kolhe@uia.no

M. A. N. Sanjeewa · W. T. V. S. Fernando · G. M. N. Priyashantha · J.W. G. S. Weerasinghe
Faculty of Engineering, University of Ruhuna, Galle, Sri Lanka

enough for Sri Lanka because solar power plants not situated separately. Especially, individuals those who have implemented roof mounted PV systems cannot use this sun tracking technique to increase the output power.

Another effective way of increasing the output power is operating the PV system on its maximum power point (MPP). Maximum power point tracker (MPPT) and techniques to track the MPP came under this concept. By using a MPPT, the optimum power can be supplied from a PV module. Ref [1] explains the terminal voltage of the PV module is set to a desired value for getting the maximum power for different solar irradiance levels and temperatures. Different methods can be used to decide the terminal voltage required to get the maximum output power. In this work, the main target is to use a neural network to find the MPP of a PV system. A Raspberry Pi-based neural network is going to be implemented and trained to track the MPP for different operating conditions.

2 Design and System Implementation

2.1 Assembling of the PV Array and Sensors

In this work, we used a PV array which was manufactured by Xinfa Industrial Baoan, Shezhen, China and having 520 x 330 x 2.0 mm^3 dimensions. Under 1000 W/m^2 irradiance, 25 °C temperature and 1.5 air mass, 30 W rated power is generated by the PV array. Also, this PV array has 21 V open-circuited voltage and 1.8 A short-circuited current. Maximum peak voltage and current of this PV array are 18 V and 1.6 A, respectively. According to the manufacturer's conditions, the operating temperature is −400 to 850 °C.

In addition to that, MAX6675K thermocouple was used as a temperature sensor and ACS712 was used as a current sensor. All these sensors were connected to the Arduino and measured the particular data from devices. The irradiance measurements are taken by irradiance sensor which is developed as a part of this work and it will be discussed later in Sect. 2.3.

2.2 Implementation of the DC–DC Boost Converter

The boost converter of proposed MPPT is designed according to the characteristics of the PV array. Input to the converter is varying within the range of 9–18 V and a constant output of a 24 V is maintained by adjusting the duty ratio of the PWM signal accordingly. At the output, a 2200 μF capacitor has been used in order to reduce the ripples of the output signal. The inductor is designed mainly considering the current through it and its current storage capacity for a switching cycle. The used equation for the converter design is illustrated in equations (1), (2), (3) and (4), respectively [2, 3].

$$\text{Peak current } (I_{pk}) = 2 \times I_{\text{out}} \times (\frac{t_{\text{on}}}{t_{\text{off}}} + 1) \tag{1}$$

$$I_{pk} = 2 \times I_{\text{out}} \times (\frac{D}{1 - D}), \text{ where } D = \frac{t_{on}}{t_{on} + t_{off}} \tag{2}$$

$$\frac{V_o}{V_{\text{in}}} = \frac{D}{1 - D} \tag{3}$$

$$\text{Critical value of inductor } L_{\min} = \frac{V_{\text{in,min}}}{I_{pk}} \tag{4}$$

Since the required inductor (4 mH) is not available on the market, it also has to be designed. Number of turns and the coil length are calculated using the equation (4). The inductor is designed for a iron core.

The converter is capable of handling 32 W of maximum power and boosting up the varying terminal voltage of the PV array. When the PWM signal is given to the MOSFET, which operates as the high-frequency switch of this converter, it controls the terminal voltage of the PV array and the converter output. Developed boost converter for this work is shown in Fig. 1.

2.3 Implementation of the Solar Irradiance Sensor

An experimental setup was required for the calibration process of the proposed irradiance sensor, arranged with the EDIBON$^{\text{TM}}$ solar trainer kit. And the required irradiance variation was generated through the SCADA software of the EDIBON solar trainer kit and the intensity of the halogen flashlights was adjusted accordingly. The generated output voltage of the proposed sensor was measured against known irradiance level, which was measured using the irradiance sensor of the trainer kit, for each and every position and irradiance level [4].
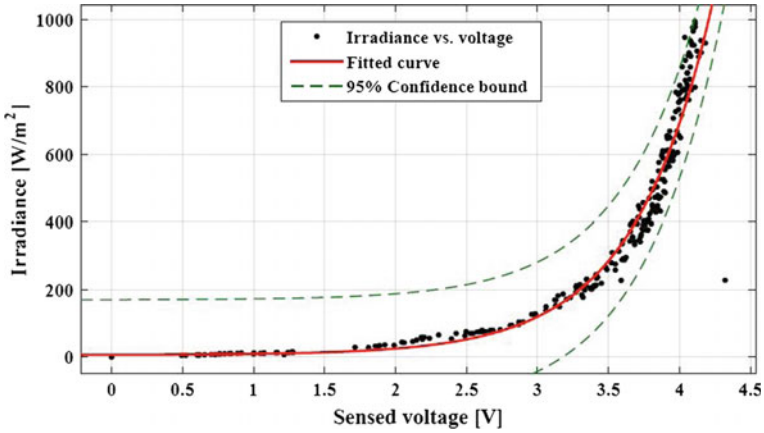
Fig. 2 Fitted curve for irradiance vs voltage

From the experimental data, a 95% of confidence bound can be obtained and have been illustrated in Fig. 2.

The function of the curve and the calculated values of the constants using the MATLAB curve fitting tool are shown below.

$$Y = ae^{(-bX)} + c \tag{5}$$

$$Y = \text{Irradiance (W/m}^2) \tag{6}$$

$$X = \text{Sensed voltage (v)} \tag{7}$$

$$a = 0.5098(0.1731, 0.8465)$$
$$b = -1.801(-1.961, -1.641)$$
$$c = 6.874(-16.33, 30.08)$$

The obtained function from the data set is implemented on the Arduino board, where it calculates the available irradiance. Whenever the irradiance is available on the sensor (PV array), the output voltage sends to the Arduino as the X value of the obtained function. This calculated irradiance can be directly used as the input irradiance for the MPPT device. The flowchart of the function of solar irradiance sensor is shown in Fig. 3.

Fig. 3 Flow chart for solar irradiance sensor
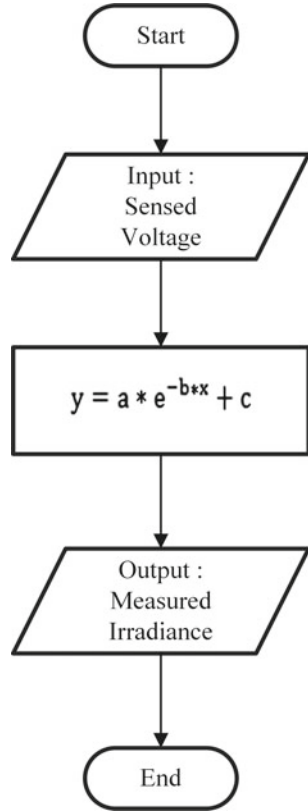
3 Neural Network

3.1 Operation of the Neural Network

In this work, the ultimate target is to absorb the available maximum power from the PV system. As previously discussed, we have to find the V_{MPP} value for the available irradiance level and temperature of the PV system surface. Structure of the neural network is the first important part and it may differ according to the purpose of use. But the main component and the arrangement of a neural network is same in most scenarios. As previously discussed, the inputs to the neural network are solar irradiance and the temperature of the solar panel surface. In this work, the output from the neural network is the voltage, which is corresponding to the MPP for the given conditions. There are two neurons in the input layer and one neuron in the output layer. Here we have used three neurons for the hidden layer. The structure of the implemented neural network is shown in Fig. 4.
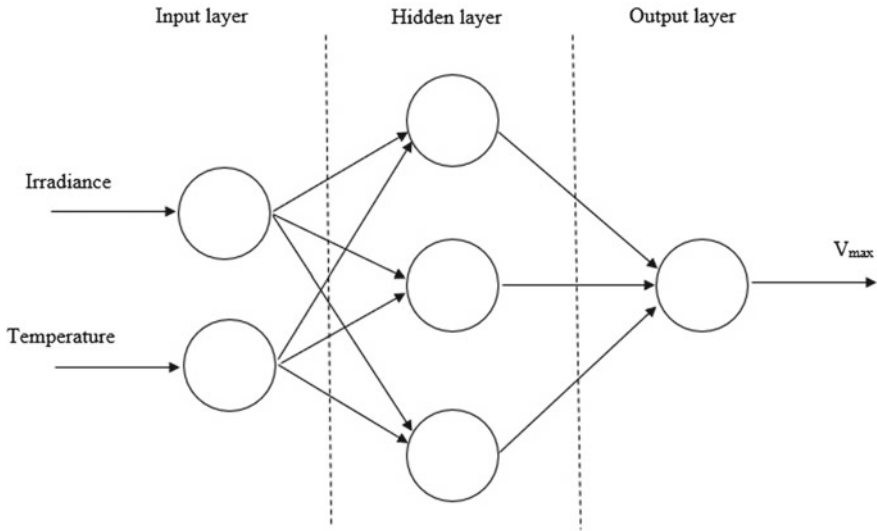
Fig. 4 The structure of the proposed neural network

Since the data processing is done using the Raspberry Pi, the coding of the neural network also done using Python, which is compatible with Raspberry Pi.

3.2 Designing and Developing Techniques of the Neural Network

We have to use several techniques to achieve the desired output from the NN. The accuracy and the response time is totally depending on the techniques used in the network. In this work, a regression problem is going to be solved. An output value is predicted according to given inputs through the knowledge of training. The first important thing is the way of selecting inputs to the neural network. As discussed previously, the inputs to the implemented NN are irradiance on the solar panel and the temperature of the PV panel surface. The voltage value which gives the maximum power from the solar panel is the output of the system. The units of inputs and output are W/m^2 , °C and V. Since the units are different, it is better to scale our data. Therefore all the data sets are divided from their maximum value and converted to a value between 0 and 1. Then the scaled input data forward to the NN as a matrix, since it is easy to handle throughout the process [5].

The next important thing is the process of the each neuron. As previously discussed, neurons use an activation function for its process. For complex problems, a nonlinear activation function should be used in order to get the best output. Therefore, the sigmoid activation function is used for this NN. The sigmoid function is

Fig. 5 The graph of error with the number of iterations
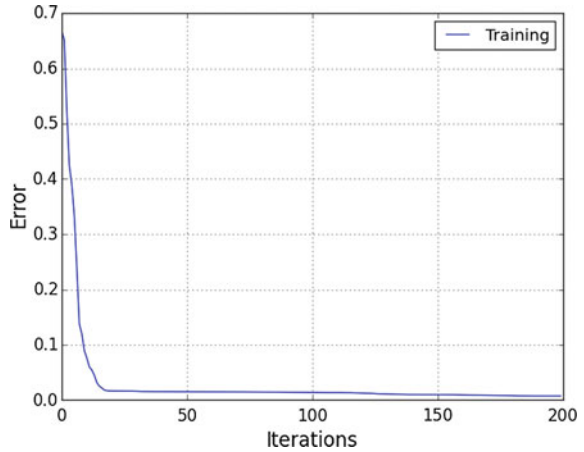
expressed using the equation $1/(1 + e^{-t})$. Initially, some random weights are used and the NN predicts a value based on inputs and those random weights [5]. The output from the network and the desired output, there is an error. The error should be minimized as small as possible. For this purpose, the technique called gradient descent is used with back propagation algorithm, the weights are adjusted to have a better solution. The output space totally depends according to the training data set, and there is a risk of having a over-fitting and not fit for the real-world application. To avoid the over-fitting, a large data set is used for the training and also it uses a regularization parameter.

3.3 Training the Neural Network

As we discussed previously, the learning process is a very important part of the neural network. The supervised learning method is used in this work, in order to train the network. Large data set is experimentally collected using the Edibon solar trainer kit for various conditions (irradiance and temperature) and those data used to train the network. The error of the prediction of the output varies with the number of iterations. According to the implemented system, the variation of the error with the iterations is shown in Fig. 5.

4 Experimental Results

By changing the DC load connected to the system, the variation of the power is observed by means of output voltage and current from the PV array for a given

Table 1 Table of prediction values from the neural network and actual values

Predicted V_{MPP} Values(V)	Actual V_{MPP} Values(V)	Error(V)	Percentage error(%)
12.2	12.24	−0.04	0.328
12.4	12.11	0.29	2.33
13.5	13.16	0.34	2.518
14.2	14.04	0.16	1.126
13.4	13.96	−0.56	4.179
13.6	13.38	0.22	1.617
16.1	16.34	−0.24	1.49
17.3	17.28	0.22	0.115
15.9	15.50	0.4	2.515
16.5	16.27	0.23	1.393
18.5	18.10	0.4	2.162
19.4	19.61	−0.21	1.082
17.7	17.77	−0.07	0.395
18.8	19.01	−0.21	1.117

irradiance and temperature. At the highest point of the power vs voltage curve, the corresponding voltage is taken as the V_{MPP}. After that, by manually given those inputs to the trained NN and observed the output (V_{MPP}) and compared both values. The validated data set along with the corresponding error percentage is tabulated in Table 1.

A PWM signal is used to drive the MOSFET in order to control the terminal voltage of the PV array. The required PWM signal is generated via the Arduino according to the predicted V_{MPP} Values by the neural network. It is observed that the generated PWM signal and calculated PWM are approximately equal for test results.

5   Conclusions

In this work, neural network-based maximum power point tracking device was proposed and implemented in order to provide a reliable solution for drawbacks of existing conventional maximum power point tracking techniques. When analyzing the output results of the boost converter, which is the driver circuit of this work and the neural network, it proves that the response of the systems is fast and accurate. The error percentage of the system is within an acceptable limit. Observed deviations in losses of this proposed system is occurred due to the low reliability of the solar irradiance sensor used for this device. Hence, the error percentage can be reduced further by increasing the reliability of the irradiance sensor or using an industrial

level irradiance sensor.

By analyzing the results of each and every component separately, the accuracy of the neural network is significantly high. Hence, maximum power point tracking using neural networks seems to be successful and fascinating. With a higher accuracy and fast response, this MPPT system can be integrated to a solar power system where a higher stability and low harmonics level required.

References

1. Pakkiraiah, B., Durga Sukumar, G.: A new modified MPPT controller for solar photovoltaic system. In: IEEE International Conference on Research in Computational Intelligence and Communication Networks (ICRCICN) (2015)
2. Konara, K.M.S.Y., Kolhe, M.L., Nishimura, A.: Grid integration of PEM fuel cell with multiphase switching for maximum power operation. In: IEEE International Conference on Power System Technology (POWERCON) (2016)
3. Konara, K.M.S.Y., Kolhe, M.L.: Charging management of grid integrated battery for overcoming the intermittency of RE sources. In: IEEE International Conference on Information and Automation for Sustainability (ICIAfS) (2016)
4. Computer Controlled Photovoltaic Solar Energy Unit, with SCADA: Engineering and Technical Teaching Equipment, Edibon (EESFC)
5. Elobaid, L.M., Abdelsalam, A.K., Zakzouk, E.E.: Artificial neural network-based photovoltaic maximum power point tracking techniques: a survey. IET Renew. Power Gener. **9**, 1043–1063 (2015)

Industrialized Safekeeping Arrangement With GSM Scheme Using Proteus Software

Rashmi Ashok Panherkar and Prajakta Vaidya

Abstract Sanctuary and computerization is a leading distress hip our regular life. The line of attack to home based and industrialized computerization and sanctuary organization scheme is just about consistent nowadays. In this broadsheet, we have strained to grow these principles through joining innovative proposal procedures and technologically advanced a low-slung price home based and industrialized automated sanctuary systems. All and various desires just before persist by way of greatly as safe as houses for instance possible. The scheme of unassuming hardware circuit allows all operator in the direction of using this wireless home-based sanctuary organization through PIR sensor, gas sensor, smoke sensor, and main fuse failure sensor at home and industrialized.

Keywords Wireless regulator system · GSM module · Microcontroller · High temperature sensor · Electrical energy · Current · Lubricate intensity · Stealing · Electrical load levels · Equal of float

1 Introduction

Safekeeping remains the leading disquiet used for all production. Each and every production industry requirements toward grind in harmless and protected environment that are favorable intended for the employees and particularly aimed at their construction progression around on behalf of rare properties in the production. Everyone manufacturing industries neediness their employees in the direction of possess harmless and safeguarded after innumerable instances resembling coincidences affected

R. A. Panherkar
Department of Electrical Engineering, DMIETR of Engineering, Maharashtra, India
e-mail: panherkarrashmi@gmail.com

P. Vaidya (✉)
Department of Electrical Engineering, G. H. Raisoni College of Engineering, Nagpur, India
e-mail: prajakta.vaidya@raisoni.net

due to LPG gas seepage or accidents in arrears to spirit in their drop or their technology department.

On the way to change to the out-and-out armistice of awareness whether you are by the side of household or out of home based you necessity confirm that your home based is fitted by means of the unspoiled home sanctuary intensive care system. This GSM-based manufacturing sanctuary system container remains cast-off to make available sanctuary system used for residential, industrial, and on behalf of all together imported and profitable purposes using GSM technique. Security systems are certain electronic devices which are used to sense interferences in home based or manufacturing.

2 Proposed Technology

The foremost purpose of this projected development stands toward strategy and contrivance a bendable, lucrative, and prevailing GSM Centered Industrial Automation sanctuary system. A GSM grounded Industrial Automation organization is necessary intended for the tenant's handiness and safety. This scheme benefits you to detect burglary, drippy of injurious gas, smolder produced remaining on the way in the direction of fire and next detecting disbelieving activity, and it sends an alarm missive to the owner number in place offline as sanctuary personnel. The concerned individual tenacity take approximately action, by directing nearly directions toward the microcontroller item complete registered cell phone, and reins the developed strategies over and done with relays.

Industrial automation or mathematical controller is the procedure of controller structures such in place of processors in the direction of controller industrialized technology and processes, tumbling the requirement designed for manpower. The procedure and controller of the recent industrial tools and method requests lots of devices to monitor more than a few restrictions of the systems.

The wished-for scheme takes in GSM modem, microcontroller, several sensors, relays, memory, and LCD display. Uncertainty the user needs in the direction of controller the structure beginning a inaccessible residence, he/she takes in the direction of guide the SMS command beginning his recorded cell phone representative the procedure of the device. The GSM modem surrounded through microcontroller collects the manipulator's command. Rendering in the direction of the customary message, the microcontroller motivation difference ON/OFF the relays (i.e., explicit application) (Fig. 1).

The block figure of the GSM-Based Industrialized Automation arrangement takes exposed in the below diagram. The organization generally involves of three components the GSM MODEM and the boundary circuit that embraces the changed instruments used.

Description in detail:

It mainly consists of following blocks:
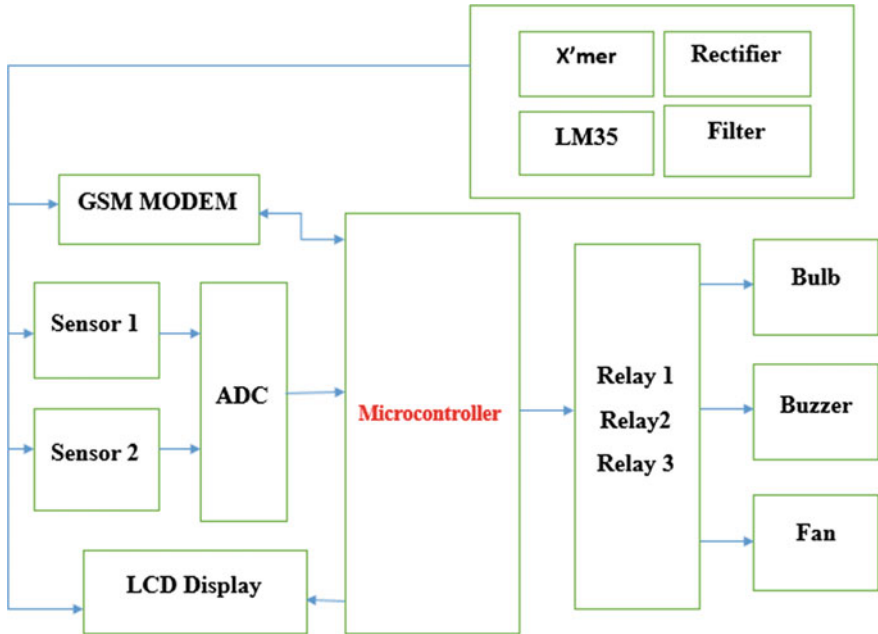
Fig. 1 Block diagram

(1) Microcontroller
(2) Humidity or LPG Gas Sensor
(3) Temperature sensor
(4) GSM Modem (sim900 unit)
(5) LCD Display
(6) Buzzer that beeps for critical conditions.

3 Methodology Simulation

The interface circuit diagram and central power supply relations are certain in the inferior to diagram. The GSM associated in the direction of the user, police station, and fire brigade over done with the mobile cellular network. The purpose of the GSM MODEM be situated the inaccessible communication lined by means of the user terminated and done with cell phone and the controller over and done with the RS232 in arrangement communication standard. The microcontroller is incessantly consideration the produces of the changed expedient and comportment communications done the GSM system up-to-the-minute situation of emergency. The microcontroller be situated in association with the direction of a number of procedures corresponding a smoke detector, motion detector, IR sensor, LDR from side to side relays. An

crossing point path devours stayed intended which take account of the automatic microcontroller and the GSM modem over and done with the consecutive port of the GSM MODEM, the sensors by means of input strategies and persons are associated in the direction of microcontroller and relays (Figs. 2 and 3).

4 Algorithm
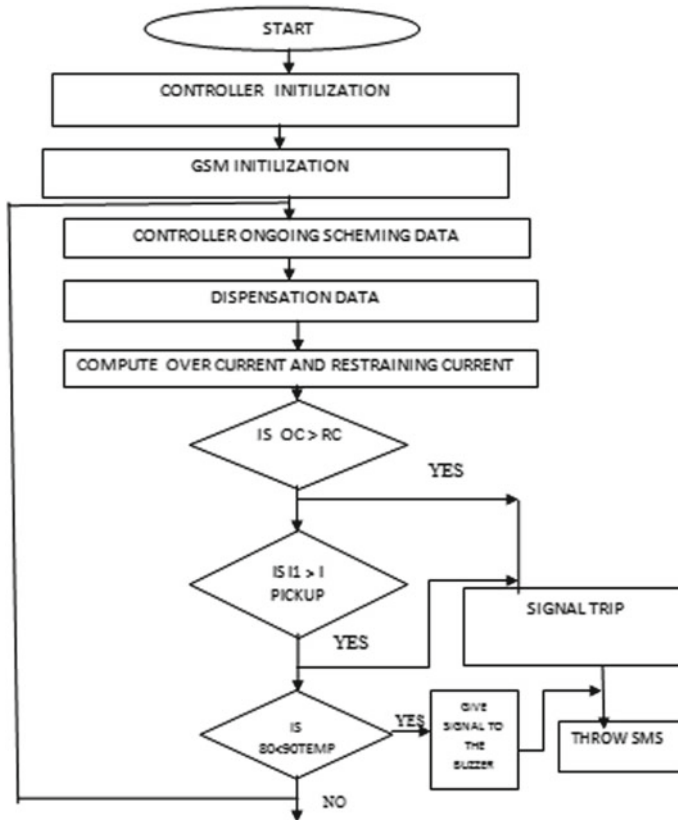
5 Conclusion

This manuscripts grants operator outgoing and low rate home based and developed computerization and safety systems. Subsequently a systematic revision is made of fictions of all the matters that contain home mechanization strategy and wireless networks. A modest system in the direction of advancing the standards is being developed. It is an instantaneous monitor able system scientifically unconventional
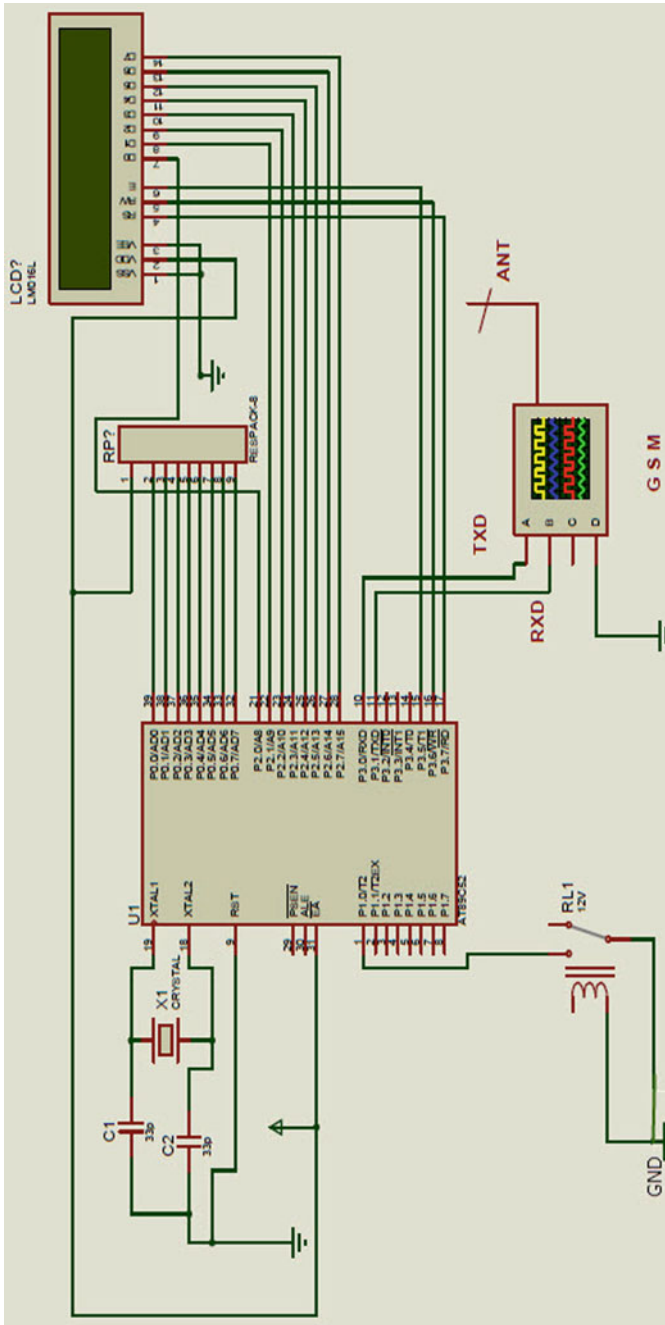
Fig. 2 GSM-based industrial automation
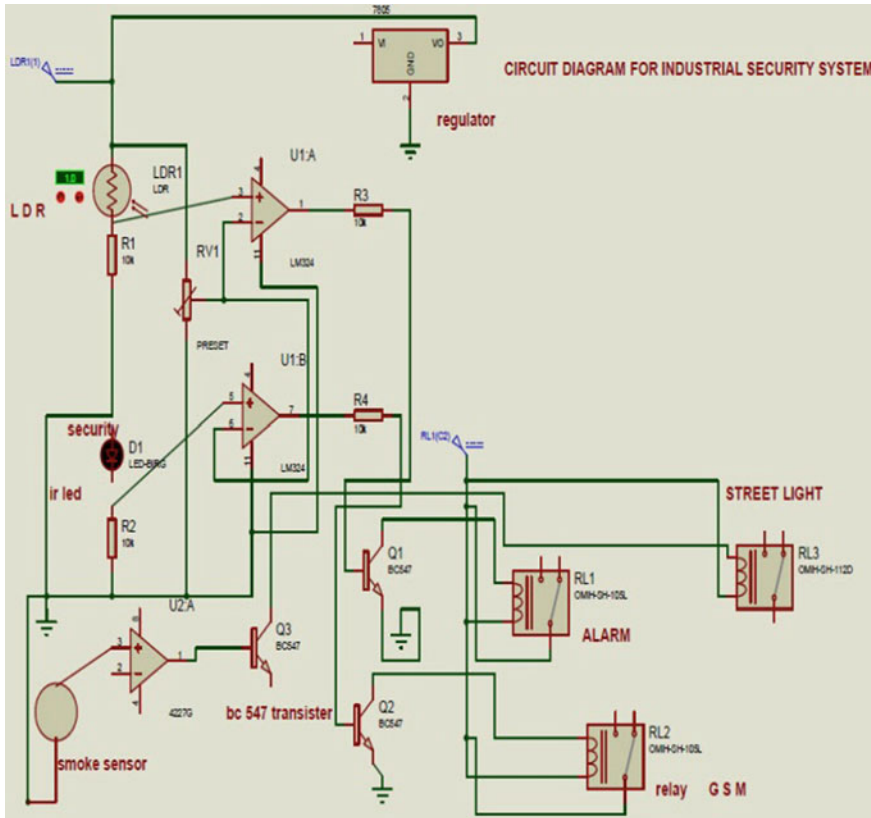
Fig. 3 Main circuit

with simple simulation which makes simpler the opportunity of miscalculation unrestricted sanctuary system. This scheme can be without difficulty instigated through extreme dependability and the high safekeeping with low cost is a special improvement of the present schemes for home security.

6 Applications

This scheme has its leading uses in sanctuary structure or a misfortune evading system for the coal mines or wood cutting industry or cotton industry. A number of strictures scrutinized in this development like LPG gas leakage, wireless regulator system, GSM module, microcontroller, high-temperature Sensor, electrical energy, current, lubricate intensity, stealing, electrical load levels, equal of float are also

designed for industrialized purposes. So this also is used in industrialized purposes as a GSM-based industrial sanctuary system.

7 Advantages

By means of the support of GSM equipment, industry brigadier comes to be remote signal through SMS. So uncertainty the user is not here from industry, employees drive be located intimated about the perilous situations exclusive the house. This is fully automated. So once this system is put in private home-based or industry, then nearby are no needs to activate the structure by way of human. Wetin can with the exception of the life expectancy of person privileged home/industry through the help of this system. In the meantime, the accidents instigated owing in the direction of fire and LPG gas leakage can source life threat.

8 Future Development

We can display and regulate new limitations and devices. Vocal sound broadcast organization can be additional to designate expedient conditions.

References

1. Collesei, S., di Tria, P., Morena, G.: Short message service based applications in the GSM network. In: 5th IEEE International Symposium on Wireless Networks—Catching the Mobile Future, vol. 3, pp. 939–943, 18–23 Sep 1994
2. Al-Ali, A.R., Rousan, M.A., Mohandes, M.: IEEE International Conference on GSM-based Wireless Home Appliances Monitoring & Control System, ISBN: 0-7803-8482-2, pp. 237–238 (2004)
3. Bai, Y.-W., Chen, S.-C., Jen, F.: Design and implementation of home intercom and security control systems for buildings. In: Catholic Univ. Information. Fusion, 2007 10th International Conference on Publication, ISBN: 978-0- 662-45804-3, pp. 1–6 (2007)
4. Zappi, P., Farella, E., Benini, L.: Hydroelectric Infrared Sensors based Distance Estimation. Dept. of Electron, Inf. & Syst., Univ. of Bologna. IEEE Publication, pp. 716–719 (2008)
5. Cheng, X.-H., Wang, Y.: The remote monitoring system of transformer fault based on The internet of Things. In: 2011 International Conference on Computer Science and Network Technology (ICCSNT), vol 1, pp. 84–87, 24–26 Dec 2011
6. Constantin Daniel Oancea, Member, IEEE: GSM infrastructure used for data transmission. In: 2011 7th International Symposium on Advanced Topics in Electrical Engineering (ATEE), pp. 1–4, 12–14 May 2011
7. Wornpuen, A., Charbkaew, N., Bunyagul, T.: Advanced distribution transformer load monitoring. In: 2012 9th International Conference on Electrical Engineering/Electronics, Computer, Telecommunications and Information Technology (ECTI-CON), pp. 1–4, 16–18 May 2012
8. Jayakumar, J., Queen, J.H.J., James, T., Hemalatha, G., Lonappan, N.: Distribution transformer monitoring using GPRS. Int. J. Sci. Eng. Res. **4** (2013)

9. Wang, Q., Shang, Z., Cui, S., Zhang, H., Zeng, P.: Research and application of wireless temperature monitoring for transformer substation. In: 2013 25th Chinese Control and Decision Conference (CCDC), pp. 4010–4015, 25–27 May 2013
10. Reddy, P.A., Sao, A.K., Rajpurohit, B.S.: Advanced monitoring and on-line health diagnosis of single-phase transformers. In 2015 International Conference on Power and Advanced Control Engineering (ICPACE), pp. 308–314, 12–14 Aug 2015

Topology and Control of Hybrid Nine-Level Inverter

Y. Naveen Kumar and P. P. Jagtap

Abstract The requirement of an improved output waveform quality has increased the research in the area of multilevel inverters (MLIs). Active neutral point clamped (ANPC) MLI being one the popular MLI, this paper proposes a new hybrid ANPC topology for nine-level operation. It consists of ANPC leg, an H-bridge, and a floating capacitor (FC) fed H-bridge. The voltage across the FC is regulated using redundant switching states which does not involve complex computations. This balancing can be achieved irrespective of load power factor and modulation index. Extensive simulations are performed to verify the validity of the proposed topology and its control scheme. The corresponding results attesting its merits are presented. Finally, a comprehensive comparison with other classic and latest MLI topologies is presented.

Keywords Floating capacitor · Nine-level inverter · Power quality · Sensorless voltage control

1 Introduction

The advent of multilevel inverters (MLIs) has changed the face of various medium- and high-voltage power electronics applications [1–4]. Some of the most widely used topologies are cascaded H-bridge (CHB), neutral point clamped (NPC) and flying capacitor MLIs [5]. Each of these topologies has advantages and disadvantages. CHB requires several isolated dc sources. Such isolated sources are derived using phase-shifting transformers and diode-bridge rectifiers. Whereas, NPC and flying capacitor require several diodes and capacitors for clamping the voltages and thus exhibit challenge in balancing voltage across them.

Y. Naveen Kumar (✉) · P. P. Jagtap
G. H. Raisoni College of Engineering, Nagpur, India
e-mail: naveen.yejjala@raisoni.net

P. P. Jagtap
e-mail: prashant.jagtap@raisoni.net

To overcome the aforesaid setbacks, researchers have introduced the concept of hybrid MLIs [6]. On this line, several hybrid MLIs are available in literature [7–14]. Active NPC is one such attempt, wherein the clamping diodes are replaced with fully controlled switches. Use of T-type NPC and floating capacitor fed H-bridge (FCHB) without sensing the voltage across FC is presented in [7, 13]. A three-level NPC cascaded with FCHB is presented in [8]. Hybrid ANPCs with reduced number of devices are demonstrated in [10, 14]. Multicell converter is another breed of converter requiring lesser number of FCS [9, 15, 16]. A hybrid-stacked multicell-based topologies for nine-level (9L) operation have been presented in [17, 18].

In this paper, a new ANPC-based hybrid MLI topology is presented. The load is connected across the H-bridge fed from ANPC leg. FCHB is connected in series with the load for level doubling. The operation is explained for 9L, however, higher number of levels by appending additional FCHBs. The methodology for balancing the FC voltage is deliberated in detail. The operation and working concept of the proposed hybrid inverter is verified through simulations, and results are presented. Also, comparisons with other topologies are included.

2 Proposed Hybrid Inverter Power Circuit and its Operation

$$S_{F1} = (C_4 + C_3\bar{C}_4)C_5 + C_1\bar{C}_2\bar{C}_5 \tag{1}$$

$$S_{F2} = \bar{C}_1 + C_4\bar{C}_5 \tag{2}$$

$$S_{F3} = C_1\bar{C}_2 + C_3\bar{C}_4 \tag{3}$$

$$S_{F4} = (C_1\bar{C}_2 + C_2\bar{C}_3 + C_3\bar{C}_4 + C_4)\bar{C}_5 \tag{4}$$

Figure 1 illustrates the proposed hybrid 9L inverter comprising ANPC at front end and an H-bridge at the load end. In addition, a 3L FCHB is also connected. With V_{dc} being the total input voltage, the voltages across FCHB has to be maintained at $V_{dc}/4$. This combination of FC voltage and dc-link capacitor voltage yields in nine unique voltage levels $0, \pm V_{dc}/4, \pm V_{dc}/2, \pm 3V_{dc}/4, \pm V_{dc}$. The switches embodied in the H-bridge operate at 50 Hz and thus has very minimum losses. The switches S_1–S_2 and there complements need to block a voltage $V_{dc}/2$, switches S_3–S_4 and there complements need to block a voltage $V_{dc}/4$ and switches S_5–S_6 and there complements need to block a voltage V_{dc}. The required nine levels of output voltage (only positive half cycle levels) are generated as follows.

1. Mode 0: Two switching states are available for zero level. First, switches $\bar{S}_3, \bar{S}_4, \bar{S}_5, \bar{S}_6$ are ON; load terminals are short-circuited and thus, output voltage $v_0 = 0$ (refer Fig. 2a). Second, switches $\bar{S}_3, \bar{S}_4, S_5, S_6$ are ON; load terminals are short-circuited and thus, output voltage $v_0 = 0$ (refer Fig. 2b).
2. Mode 1: Two switching states are available for $V_{dc}/4$ level. Switches $\bar{S}_3, S_4, \bar{S}_5, \bar{S}_6$ are ON; output voltage $v_0 = V_{cf} = V_{dc}/4$ and the FC discharges (refer Fig. 2c).
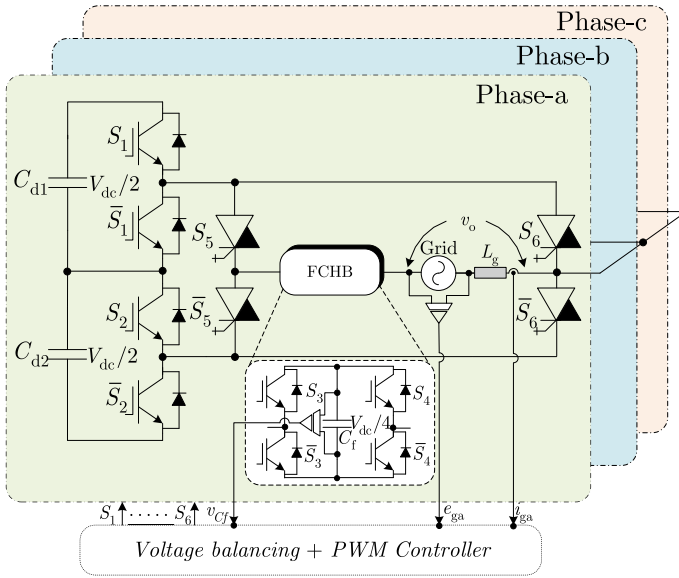
Fig. 1 Proposed hybrid inverter schematic power circuit
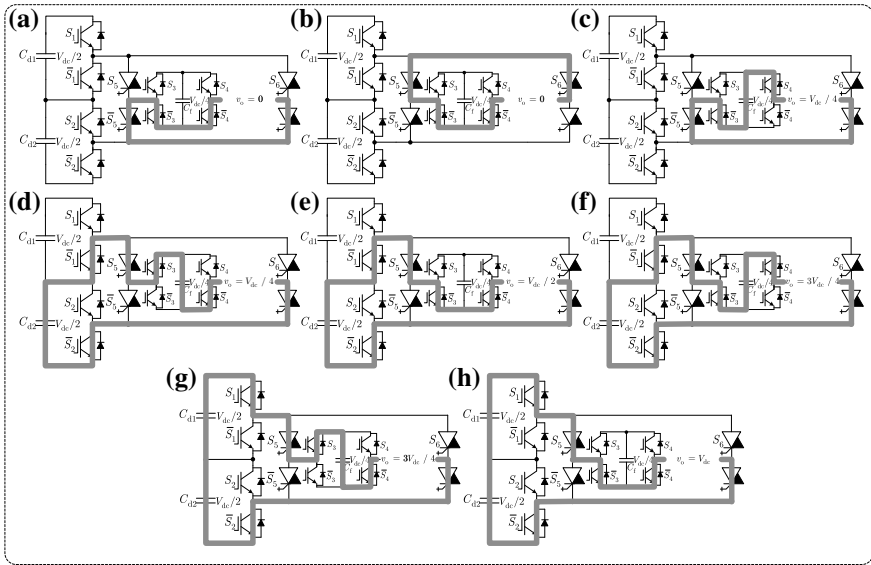
Fig. 2 Operating modes of the proposed hybrid inverter **a–b** $v_0 = 0$. **c–d** $v_0 = V_{dc}/4$. **e** $v_0 = V_{dc}/2$. **f–g** $v_0 = 3V_{dc}/4$. **h** $v_0 = V_{dc}$

Table 1 Switching states and their effect on FC voltage

Voltage levels	S_1	S_2	S_3	S_4	S_5	S_6	FC voltage
V_{dc}	1	0	0	0	1	0	No effect
$3V_{dc}/4$	1	0	1	0	1	0	Charging
$3V_{dc}/4$	0	1	0	1	1	0	Discharging
$V_{dc}/2$	0	0	0	0	1	0	No effect
$V_{dc}/4$	0	0	1	0	1	0	Charging
$V_{dc}/4$	0	1	0	1	1	0	Discharging
0	0/1	1/0	0	0/1	0	0	No effect
$-V_{dc}/4$	1	0	1	0	0	1	Discharging
$-V_{dc}/4$	0	1	0	1	0	1	Charging
$-V_{dc}/2$	0	0	0	1	0	1	No effect
$-3V_{dc}/4$	1	1	1	0	0	1	Discharging
$-3V_{dc}/4$	1	0	0	1	0	1	Discharging
$-V_{dc}$	0	1	0	0	0	1	No effect

Switches $\bar{S}_1$, $\bar{S}_2$, S_3, $\bar{S}_4$, S_5, $\bar{S}_6$ are ON; output voltage $v_0 = V_{dc}/2 - V_{cf} = V_{dc}/4$ and the FC charges (refer Fig. 2d).

3. Mode 2: Switches $\bar{S}_1$, $\bar{S}_2$, S_3, S_4, S_5, $\bar{S}_6$ are ON; output voltage $v_0 = V_{dc}/2$ and no impact on the FC voltage (refer Fig. 2e).

4. Mode 3: Two switching states are available for $V_{dc}/4$ level. Switches $\bar{S}_3$, S_4, S_5, $\bar{S}_6$ are ON; output voltage $v_0 = V_{dc}/2 + V_{cf} = 3V_{dc}/4$ and the FC discharges (refer Fig. 2f). Switches S_1, $\bar{S}_2$, S_3, $\bar{S}_4$, S_5, $\bar{S}_6$ are ON; output voltage $v_0 = V_{dc} - V_{cf} = 3V_{dc}/4$ and the FC charges (refer Fig. 2g).

5. Mode 4: Switches S_1, $\bar{S}_2$, S_3, S_4, S_5, $\bar{S}_6$ are ON; output voltage $v_0 = V_{dc}$ and no impact on the FC voltage (refer Fig. 2h).

The switching states for generation of each of the output voltage levels are enlisted in Table 1.

3 Active Voltage Balancing of FC

As evident from Table 1, the redundant switching states have a disparate effect on the FC voltage while the remaining states do not affect the voltage across FC. Thus, these redundant states can be used to regulate the voltage across FC. For efficient voltage regulation, it is imperative to know whether the FC is overcharged or undercharged and also it is vital to determine the direction of the load current. For this, voltage sensor and current sensors are employed. The FC voltage is sensed and regulated around a hysteresis band.

For example, if the level of the output voltage to be generated is $3V_{dc}/4$, two switching states are available. If at the sampling instance, the FC is found to be undercharged and direction of the current is positive, then the switching state [1 0 1 0 1 0] is applied during the next sampling interval. If the FC is overcharged, then [0 1 0 1 1 0] is applied such that by the next sampling interval, the FC voltage is maintained around the reference value.

The implementation complexity of the above-mentioned active voltage balancing is very minimal and is independent of load power factor. A single carrier with four reference signals-based pulse width modulation [19] is applied.

4 Simulation Study and Results

To demonstrate the performance of proposed inverter and its control strategy, simulations are performed using MATLAB/Simulink. A standard $d - q$ reference frame controller is used to regulate the active and reactive power injections. Table 2 enlists the system parameters employed for the simulation. The system is subjected to three test conditions in order to visualize its performance under the steady state and dynamic conditions as discussed under:

1. Step change in active power: Firstly, at $t = 1$ s, a step change in active power is applied. As a response, the magnitudes of injected grid currents are increased and reaches a value corresponding to the new reference power, validating the fast and satisfactory performance of the controller (see Fig. 3a). Despite such perturbation, the voltage across the various capacitors remain intact validating the correctness of the developed voltage-balancing controller. Also, being reactive power set to zero, the injected currents are in phase indicating the unity power factor operation.
2. Step change in dc-link voltage: Secondly, at $t = 1$ s, the dc-link voltage is stepped up from 4 to 5 kV. The system response to the preceding event is shown in Fig. 3b. It is evident from the plots that the developed voltage-balancing scheme proves to be robust in regulating the capacitor voltages under all possible external

Table 2 Simulation parameters

Parameter	Value
dc-link voltage, V	5000
Grid voltage (line-to-line), V	2300
Fundamental output voltage frequency, Hz	50
Capacitance of FC, μF	2200
Capacitance of dc-link capacitor, μF	1200
Switching frequency of the inverter (f_{sw}), kHz	2.5
Grid inductance, mH	3.3
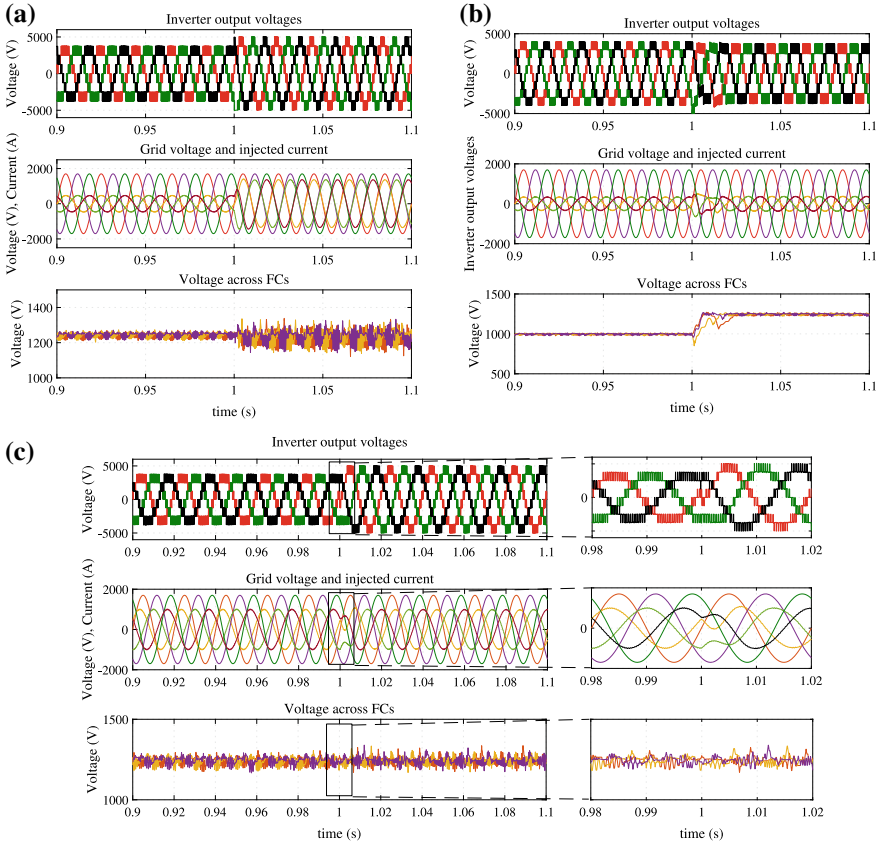
Fig. 3 Simulation results. **a** Step change in reference grid current. **b** Step change in dc-link voltage. **c** Step change in operating power factor

perturbations. Besides, except for a small initial deviation, the injected active power is held constant since the value of reference active power is kept unaltered.

3. Step change in power factor: Lastly, a grid-connected distributed generation system is quite often expected to source/sink reactive power in addition to the active power injections from the renewable sources. To verify the reactive power handling capability, initially the power factor is kept lagging and at $t = 1$ s, the power factor is changed to leading. As evident from Fig. 3c, the inverter absorbs/injects reactive power as desired.

5 Comparison with other Inverter Topologies

The proposed topology shown in Fig. 1 is compared with existing 9L topologies in this section. It requires total 36 switches. Out of which, 12 switches operate at 50 Hz and thus have least switching losses. In case of NPC- and FC-based MLIs, many clamping diodes and flying capacitors are required. Also, they require complex voltage-balancing schemes. In the proposed structure with only three FCs, their voltage can be balanced irrespective of load current power factor and modulation index. Unlike, many isolated dc sources required for a CHB MLI, it requires only three such sources. As compared to the recent MLI topology in [18], though the proposed topology uses same number of switches, it requires only one FC unlike three. Another important feature of the proposed topology is that if any of the switches in FCHB fails, still it can operate as five-level inverter.

6 Conclusion

In this paper, a new ANPC-based hybrid MLI topology was presented. The configuration was derived by connecting ANPC leg at front end and an H-bridge at the back end. In addition, FCHB was connected to double the number of voltage levels. A vital feature of this topology is that if the FCHB fails, the inverter can still operate at lower number of levels. The operating modes were explained in detail. The operating principle and feasibility were verified by considering a grid-connected operation. The corresponding results presented proved the effectiveness of the proposed configuration.

References

1. Rodriguez, J., Lai, J.-S., Peng, F.Z.: Multilevel inverters: a survey of topologies, controls, and applications. IEEE Trans. Ind. Electron. **49**(4), 724–738 (2002)
2. Isalāma, M.R., Guo, Y., Zhu, J.: Power Converters for Medium Voltage Networks. Springer, New York (2014)
3. Chen, Z., Guerrero, J.M., Blaabjerg, F.: A review of the state of the art of power electronics for wind turbines. IEEE Trans. Power Electron. **24**(8), 1859–1875 (2009)
4. Blaabjerg, F., Chen, Z., Kjaer, S.B.: Power electronics as efficient interface in dispersed power generation systems. IEEE Trans. Power Electron. **19**(5), 1184–1194 (2004)
5. Kouro, S., Malinowski, M., Gopakumar, K., Pou, J., Franquelo, L.G., Wu, B., Rodriguez, J., Pérez, M.A., Leon, J.I.: Recent advances and industrial applications of multilevel converters. IEEE Trans. Ind. Electron. **57**(8), 2553–2580 (2010)
6. Manjrekar, M.D., Steimer, P.K., Lipo, T.A.: Hybrid multilevel power conversion system: a competitive solution for high-power applications. IEEE Trans. Ind. Appl. **36**(3), 834–841 (2000)
7. Sandeep, N., Udaykumar, R.Y.: Design and implementation of a sensorless multilevel inverter with reduced part count. IEEE Trans. Power Electron. **32**(9), 6677–6683 (2017)
8. Sandeep, N., Yaragatti, U.R.: Operation and control of an improved hybrid nine-level inverter. IEEE Trans. Ind. Appl. **53**(6), 5676–5686 (2017)

9. Gateau, G., Meynard, T., Foch, H.: Stacked multicell converter (smc): properties and design. In: Power Electronics Specialists Conference, : PESC. 2001 IEEE 32nd Annual, vol. 3. IEEE **2001**, 1583–1588 (2001)

10. Sandeep, N., Udaykumar, R.Y.: Operation and control of a nine-level modified anpc inverter topology with reduced part count for grid-connected applications. IEEE Trans. Ind. Electron. **65**(6), 4810–4818 (2018)

11. Li, J., Bhattacharya, S., Huang, A.Q.: A new nine-level active npc (ANPC) converter for grid connection of large wind turbines for distributed generation. IEEE Trans. Power Electron. **26**(3), 961–972 (2011)

12. Lezana, P., Aceiton, R.: Hybrid multicell converter Topology and modulation. IEEE Trans. Ind. Electron. **58**(9), 3938–3945 (2011)

13. Sandeep, N., Yaragatti, U.R.: A switched-capacitor-based multilevel inverter topology with reduced components. IEEE Trans. Power Electron. **33**(7), 5538–5542 (2018)

14. Sandeep, N., Udaykumar, R.Y.: Design and implementation of active neutral-point-clamped nine-level reduced device count inverter: an application to grid integrated renewable energy sources. IET Power Electron. **11**(1), 82–91 (2018)

15. Sadigh, A.K., Hosseini, S.H., Sabahi, M., Gharehpetian, G.B.: Double flying capacitor multicell converter based on modified phase-shifted pulsewidth modulation. IEEE Trans. on Power Electron. **25**(6), 1517–1526 (2010)

16. Ebrahimi, J., Karshenas, H.R.: A new reduced-component hybrid flying capacitor multicell converter. IEEE Trans. on Ind. Electron. **64**(2), 912–921 (2017)

17. N. Sandeep and U. R. Yaragatti, "Simplified hybrid nine-level stacked multiceli converter with reduced part count for grid-connected applications," in *2017 IEEE PES Asia-Pacific Power and Energy Engineering Conference (APPEEC)*, Nov 2017, pp. 1–6

18. Nair, V., Kaarthik, R.S., Kshirsagar, A., Gopakumar, K., et al.: Generation of higher number of voltage levels by stacking inverters of lower multilevel structures with low voltage devices for drives. IEEE Trans. on Power Electron. **32**(1), 52–59 (2017)

19. Sandeep, N., Salodkar, P., Kulkarni, P.S., A new simplified multilevel inverter topology for grid-connected application. In: IEEE Students' Conference on Electrical, Electronics and Computer Science **2014**, 1–5 (2014)

Leveraging Education Sector Using Cognitive Big Data for the Recruitment Process and Sustainable Development

Ruchi Jain, Devendra Singh Kushwaha, Mohan Lal Kolhe and Vikash Kumar Singh

Abstract Nowadays, we are not confined to traditional education. We are on the verge to make our education system more job oriented by providing various vocational trainings to our students. The various universities and higher education are facing the problem of inadequate placement. Even the job providers have to quell ample amount of time to judge the potential candidates. The right placement is a challenge for both the recruiters and the candidates. The cognitive science and big data can untangle the conundrum. The main goal of this paper proposal can be stated as: To display the appropriate job offer from the job provider, select the perfect profile for the job at the right place at the right time, and connect the perfect profile to the job provider. The outliers must also be suggested with right start-ups.

Keywords Big data · Cognitive science · Feature extraction and recruitment process

1 Introduction

In the present scenario, the entire world is engrossed in plethora of data. These data have been resonating from various devices. Each activity on the networking

R. Jain (✉) · D. S. Kushwaha
Faculty of Computronics, Indira Gandhi National Tribal University, Amarkantak, India
e-mail: jain.ruchi25@gmail.com

D. S. Kushwaha
e-mail: devendra2904@gmail.com

M. L. Kolhe
Faculty of Engineering and Science, University of Agder, PO Box 422, 4604 Kristiansand, Norway
e-mail: mohan.l.kolhe@uia.no

V. K. Singh
Faculty of Computronics, Indira Gandhi National Tribal University, Amarkantak, India
e-mail: drvksingh76@gmail.com

generates big and unstructured data. Then exponential increase of the big data yields the hassle of storage. The process of leveraging data is beyond to our innate human ability. Thus, the system must be developed that can mimic the thinking of human brain. The solution to this problem can be cognitive computing which comprises of data mining, pattern recognition, and natural language processing that initiates self learning systems. These system uses machine learning algorithm that can solve problems without the human assistance.

Big data deals with voluminous, complex, auto-generating datasets with multiple and autonomous sources. HACE theorem can be applied which is used to characterize big data. This even meant to analyze the underlying the arrangements of the data within cluster. HACE stands for heterogeneous, autonomous, complex, and evolving [1].

The concept can be introduced in many sectors including education sector. In this sector, the incorporation of cognitive science on big data can be very beneficial to each one of them who are involved. From the student, faculty, stakeholder perspective, generates data and demands to utilize it at its optimum.

The problem of unemployment and underemployment is the challenging issue for the growth of the developing countries like India (Fig. 1).

Rate of Unemployment in India has been decreased to 4.90% in 2013 from 5.20% in 2012. The rate of unemployment in India can be averaged to 7.32% from 1983 to 2013 touching an all time high of 9.40% in 2009 and a record low of 4.90% in 2013. The economists "Dharmakirti Joshi and Dipti Deshpande" from CRISIL in June 2015 had written for the Financial Express said that even if the Indian government is working for the India's manufacturing and employment capability still they need to consider on improving the measurement of employment and wages so as to enhance the standard of living.

So as to make the standard of living up to the mark, one has to make the present education system, competitive, market friendly, and vocational so as to make the students more capable and can acquire good placement. The various universities and higher education are facing the problem of right placement. Even the job providers have to quell ample amount of time to judge the potential candidates. Most of the candidates are unable to perform at that very time. The judgment of the candidate performance cannot be made at one instance of time. The process must be gradual.

Fig. 1 Empowment rate in India. *Source* Ministry of Labour and Employment, India
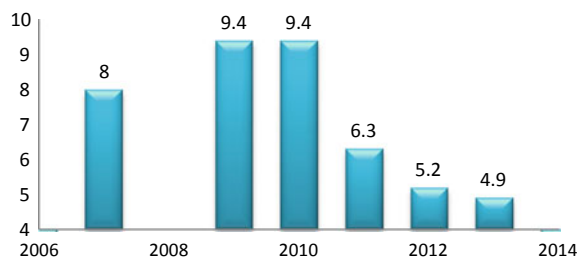
2 Literature Review

Various software have been developed on job recommender system (JRS). This system has been studied from many aspects, which states that it recommends one type of service from one type of users to another type of users where one type of user is applicant and another type is recruiter. Considering from the technical perspective, the JRS have been classified into five categories:

(i) Content-based recommendation: It acquires the content information of the candidate and similarly of the jobs and recommends them after calculating their similarities.

(ii) Collaborative filtering recommendation: It evaluates the similar type of users having the same type of preferences for the job are recommended to the provider.

(iii) Knowledge-based recommendation: The concept of data mining and ontology is incorporated by applying the association rules and concept of decision tree.

(iv) Reciprocal recommendation: It works at the particular instance of time, all the users priorities are considered and must act accordingly at the same instance. This system achieves a win-win situation for the candidates and enhances the efficiency of the recommender system. It works on the concept of bipartite graph.

(iv) Hybrid recommendation: All the above recommended system have some limitations so in order to overcome them, the hybrid of two systems can be made. The seven weights have been evolved: switching, weighted, mixed, cascade, feature combination, feature augmentation, and model.

Different online job recommendation systems have been working on this direction such as PROSPECT, Proactive, eRecruiter, CASPER [2]. SONAR (Sourcing and Automated recruitment) research and development project was introduced by French interministerial single fund in 2013. This project has been developed to aid the recruiters and academicians. Various partners like Wrok4, Multiposting, CNRS-LIMSI, Universitè Paris8-LIASD have been contributed to this project. Even Oracle company has also worked on the same technology to make the recruitments using the same way. These companies judge the candidate's profile using either any other social networking media like Twitter, Facebook, or online profiles. The learning outcomes cannot be judged using these profiles [2].

IBM cognition states that "cognitive systems as being able to extend the capabilities of educators by providing deep domain insights and expert assistance through the provision of information in a timely, natural and usable way. These systems will play the role of an assistant, which is complementary to and not a substitute for the art and craft of teaching. At the heart of cognitive systems are advanced analytic capabilities. In particular, cognitive systems aim to answer the questions: 'What will happen?' and 'What should I do?'" [3].

According to Shengbo Shi [4], three layered technology has been proposed which states that the three layered technology can be introduced for the development of the

recommendation of the job to the college graduates using their persona. Persona includes six aspects of the graduates like basic attributes which includes personal details can be obtained using text analysis, knowledge attributes can be extracted using text analysis from the various examinations conducted during the whole tenure, skill attributes can be derived from the resume which may be specified by the learner, job preference can be evaluated by the log and behavior data using Page Dwell Time, Collection added, etc., Employment Psychological Attributes can be obtained by the previous history mentioned by the candidate, social relationship attributes must also be considered which can be obtained from the resume itself and by the social media surfed.

It has been explained that the different layers in the following way; The lowest layer is data layer which contains basic, behavior, and log data and can be easily obtained by the Persona technology. As the number of the candidates and their respective data is huge, it possesses the characteristics of large data. The middle layer includes feature extraction and recommendation model which constitutes to form the recommendation engine layer. The main motive of the feature extraction is to obtain the learners' profile by analyzing the basic attribute, knowledge attribute, skill attributes, job preference, employment psychological attributes, social relationship attributes, etc., whereas the recommendation model construction incorporates the different recommendation algorithms to assemble the desired recommendation model.

Thus, this research enlightened the persona technology and Apatch Storm Platform for the recommendation model but the accuracy of this model can be improvised for the future [4].

3 Proposed Methodology

The implementation of big data with cognitive science can be termed as cognitive big data which can be used to evaluate the learning capability of the students gradually. The proposed methodology uses hybrid representation of domain knowledge analysis and a temporal prediction model. Textual analysis is required for the semantic classification of job board. On the basis of browser history or clicks, the best job offer can be evaluated using time series analysis module. The profile of the candidate can be obtained from the various social networking sites.

The data can be structured as well as unstructured must be managed using cognitive computing. The fundamental of cognitive computing is Patten Discovery. This concept is capable of deducing the meaning from the unstructured data. The concept of Neural Network and Deep Learning is constituted to form Machine Learning. The Machine Learning is effective for depicting the future and can generate the precedents from the present attributes. The result of the pattern discovery contributes a lot for integrating the unstructured data to structured one. It even determines that which kind of data should be amalgamated with which specific type of data and helps in the process of Cleansing, Extraction, Transformation and Loading, Enrichment and
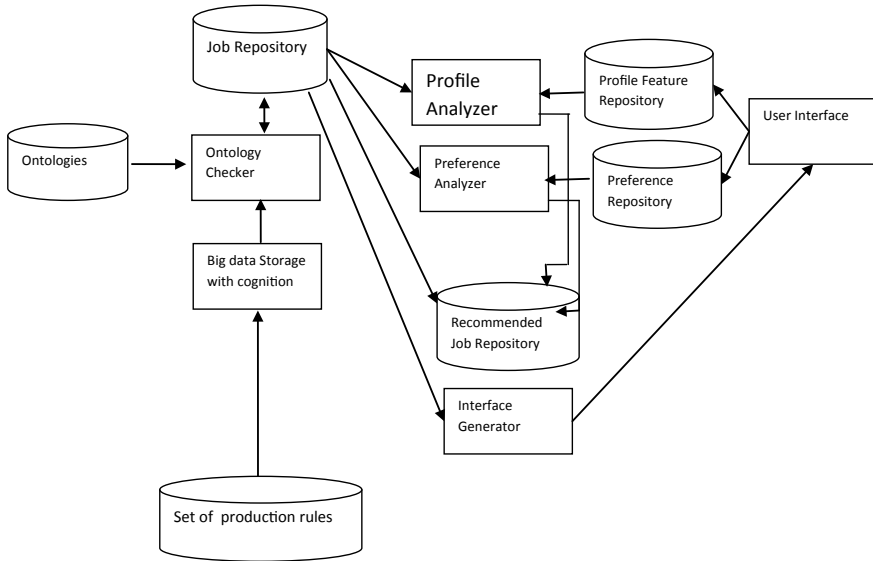
Fig. 2 Job recruitment system

imputation of data. The cognitive computing may excel the process of data discovery and data analytics of the big and huge data [5].

The ontologies can be traced out using the data received from the university and various other sources which incorporate the concept of big data, and the classification algorithm can be applied to classify the various students using data mining approach (Fig. 2).

The profile analyzer is meant to analyze the complete profile of the candidate by analyzing the structured and unstructured data. The feature extraction of the said data can be done as follows:

Step 1: Pattern Discovery is implemented to integrate unstructured with structured data.
Step 2: The Spaces or Tab is used for the purpose of word segmentation.
Step 3: The formation of dictionary and the statistics of frequency of the words and patterns is discovered.
Step 4: The construction of Huffman tree is done on the basis of the occurrence and their probability. The formed categories are placed as leaf nodes.
Step 5: Each leaf node is provided with a binary code.
Step 6: The implementation of the whole tree is done according to the neural network. The leaf nodes are treated as the input layer, and the intermediate nodes works as hidden layer of the neural network. The hidden layer together with the input layer evaluates the classification results. The nodes are in the form of vectors of the specified length.

Step 7: The vectors of the hidden layer are being trained by following the process of classification of the words.

Step 8: The process of Tokenization, Fit, Transform Fit, Inverse Transform (TFIDF) for the keywords used.

Step 9: The keywords and the labels are matched and the sum of the similarity is evaluated by traversing each label.

Step 10: The resultant are the job labels of the utmost similarities.

The whole recruitment recommendation process will be as follows:

Step 1: The complete profile of the candidate is analyzed and the process of text analysis is implemented with the implementation of pattern discovery for the unstructured data.

Step 2: The job providers are searched over the whole web and are sorted according to the classification criterion assigned for the candidates.

Step 3: The candidates are matched to the appropriate jobs avoiding the underemployment problem.

Step 4: The outliers detected must be suggested certain start-ups according to their eligibility or the skills.

The detection of the outliers must be suggested which may be categorized according to the skills possessed by the candidates. There can be various factors considered right from the skills, social background, financial status, demographic area, attitude, etc. for the appropriate start-ups which should not be very common. For this purpose, the concept of data mining must be incorporated. The various classification process can be used to categorize the candidates detected during the process of recruitment process as the outliers. The KNN algorithm can be used integrated with the Genetic algorithm which makes it more efficient to categorize the candidates.

The structured and unstructured data are considered as the input for the considerable outcome of the candidates suggestion for the start-ups. The interface generated in the whole process must include both the options for the job recommendation and the start-ups which have great opportunities with sufficient amount of profit margins. The candidate must not be necessarily convinced for the job recommendation and the start-ups, as it is a mere suggestion for the candidates but recruiters may overcome the problem of inappropriate hiring.

The recommendation of job provider can also be analyzed and can be matched through the following process. The implementation of the said algorithm has increased the performance of the recruitment process. Prior to this implementation, the scenario was as follows [11]. The real-time recommendation based on persona and collaborative filtering is given in Fig. 3. It can be useful for finding relation between start-ups and employment growth rate [12].

Fig. 3 Comparison of the real-time recommendation to the recommendation of the collaborative filtering
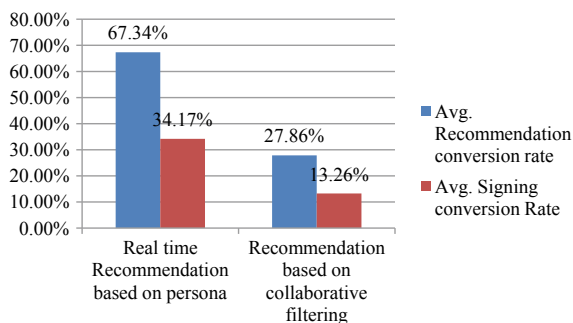
4 Conclusion

This development can help the administrators, funders, educational authorities, learners, and instructors at institutional, regional, and national level. The direct beneficiaries will be the currently enrolled students and the future student will be indirect beneficiaries. Real-time student assessment records the student progress. Cohorts or individuals who are struggling and pattern of underperformance must be addressed regularly. This enables the stakeholders to learn about the student progress periodically in order to attain their goal. It even submits the longitudinal commitment to enhance the student equitability by engaging the desirable faculty and other intake stakeholders and making them capable of handling the obstacles and challenges. Interrogating the students and hence the reported data in delayed posting leads to more general interventions for future student than the context-specific continuous interventions identified in real-time assessment.

References

1. Dinesh, U., et al.: Data mining with big data using Hace theorm. IJSRD—Int. J. Sci. Res. Dev. **4**(5) (2016)
2. Hong, W., et al.: A job recommender system based on user clustering. J. Comput. **8**(8) (2013)
3. Ben, W.: Artificial Intelligence, Cognitive Systems and Biosocial Spaces of Education. Code Acts in Education, May 2017
4. Shi, S.: Real-time job recommendation engine based on college graduates' persona. J. Residuals Sci. Technol. **13**(7) (2016)
5. Aasman, J.: Taming unstructured data with cognitive computing. Datanami, January 2016
6. Peggy, M.L.: Real Time Student Assessment. Stylus Publishing, Sterling, Virginia (2017)
7. Sidahmed, B., et al.: Smart4Job: A big data framework for intelligent job offers broadcasting using time series forecasting and Semantic classification. Big Data Res., 16–30 (2017)

8. Pradit, S.: Big data in the cloud for education institutions. In: The Twelfth International Conference on eLearning for Knowledge-Based Society, Thailand, 11–12 December 2015
9. Zhang, G., et.al.: Research on cloud computing and its application in big data processing of distance higher education. Interact. Comput. Aided Learn. iJET **10**(8) (2015)
10. Woo, B.: Education at the crossroads of big data and cloud. EMC, April 2012
11. Sheetal, et al.: Research analysis using big data. Int. J. Trend Res. Dev. (IJTRD), March 2017
12. About ART-R Tutorial. Carneige Mellon University

Energy Assessment on Double Power Generation System of Building Integrated Photovoltaic and Fuel Cell

Akira Nishimura

Abstract To develop the technology utilizing renewable energy source more, this study proposes a building integrated energy system (photovoltaic (PV) and fuel cell (FC)). The proposed system is evaluated by the energy self-sufficiency rate in the case of seven cities in Tokai region, Japan. This study assumes that the building integrated photovoltaic (BIPV) system provides the electricity to the household user in building and FC provides the electricity to meet the unsatisfied electricity demand. The FC is fueled by the H_2 produced by electrolysis using the surplus power of PV. According to the design study, it has been observed that the monthly power production from BIPV as well as FC system is higher in spring and summer, while it is lower in autumn and winter among considered cities. The self-sufficiency rate of the FC system is higher with deceasing households' number, and it has been clarified that the 16 households are more suitable. It has been revealed that people can predict the performance of proposed BIPV + FC system by the approximate curve of $y = ax^{-b}$ well.

Keywords Smart building · Photovoltaics · H_2 produced by water electrolysis · Polymer electrolyte fuel cell · Self-sufficiency rate

1 Introduction

According to Energy White Paper 2017 in Japan [1], the global consumption of primary energy will increase by annual average of 1.2–1.8% from 2015 to 2030. From the viewpoint of energy type, it is expected that the renewable energy excluding hydro power in 2030 will increase 2.1–3.4 times as large as that in 2015. In Japan, the renewable energy, especially photovoltaic (PV), has been introduced rapidly by feed-in tariff started in 2012. However, the ratio of Japan to the world on introduction amount and quantity of production is decreasing. It is important to develop the low

A. Nishimura (✉)
Mie University, 1577 Kurimamachiya-cho, Tsu, Mie 514-8507, Japan
e-mail: nisimura@mach.mie-u.ac.jp

cost product and to solve the imbalance of power output due to climate and insolation condition for the wide introduction of PV system.

Recently, building integrated photovoltaic (BIPV) attracts attention from the world for the one of PV system introduction procedure [2, 3]. The assessment on power generation characteristics and economy characteristics considering Singapore [4], Malaysia [5], and Brazil [6] and the environmental assessment by Life Cycle Assessment (LCA) [7, 8] were reported. The assessment on power generation characteristics and economy characteristics of the combination of PV and battery for output fluctuation provision was also reported [9]. On the other hand, it was reported that H_2 is superior to battery for large and long storage [10] and it was proved for the combination of PV and H_2 conversion system [11]. However, there is a few study investigating the double power generation system that is a combination of BIPV and fuel cell (FC) system using electrolytic H_2 [12–14]. Especially, there is no study to investigate the feasibility of BIPV and FC system considering the climate condition for actual city and investigation for the optimum size of building to match the electricity demand.

This study has evaluated a proposed BIPV system utilizing electrolytic H_2 through FC. H_2 is assumed to be produced by the surplus power of the BIPV. FC can cover the building electricity demand which is not covered by PV system. This study has clarified the feasibility of BIPV and FC system for seven cities in Tokai region in Japan by the meteorological data "PV300" which was obtained from the Project for Power Stabilization at the Mass Introduction of New Energy. The Ministry of Economy, Trade and Industry in Japan sponsored this project. Using the data base of households' electricity demand [15], this study has optimized how to supply the power in order to meet the electricity demand. In this study, the self-sufficiency ratio of the proposed BIPV system to electricity demand has been estimated. Furthermore, this study has optimized the households' number in the building, i.e., the building size.

2 Analysis Model

2.1 Power Generation of BIPV System

This study has assumed that the building has the following size: width of 10 m, length of 40 m, and height of 40 m (assumed to be 10 stories) [16] where 40 households live [17]. It has assumed that The PV modules are installed on the roof of building, and a FC is operated by H_2 produced by the water electrolyzer using the power of PV which is over the electricity demand. In this study, the power generated by PV system can be estimated as follows [18]:

$$E_{PV} = H \times K \times P \times 1^{-1} \quad (1)$$

where E_{PV} is hourly electric power generated by PV system (kWh), H is hourly solar radiation (kWh $\cdot$ m^{-2}), K is loss factor (-), P is capacity of PV system (kW), 1 is solar radiation under standard condition which is AM1.5, hourly solar radiation of 1 kWh m^{-2}, module temperature of 25 °C (kW m^{-2}). To calculate the hourly electric power generated by PV system, this study refers the solar radiation data by 10 s interval (PV300).

The commercial high-performance PV P250α Plus (produced by Panasonic), whose conversion efficiency and maximum power are 19.5% and 250 W, respectively [19], has been applied to estimate the power production. According to the reference [19], the size of module is 1580 mm × 812 mm × 35 mm. Considering the roof area of the building model, P is set at 75 kW$_p$ (=300 solar modules). K is calculated as follows:

$$K = K_p \times K_m \times K_i \tag{2}$$

where, K_p is power conversion efficiency for the intended power conditioner (-), K_m is correction factor relating module temperature (-), K_i is loss due to interconnecting and grime on module surface (-). In this study, K_p is 0.945 referred from the commercial power conditioning devise VBPC259B3 (produced by Panasonic [20]), and K_i is 0.95. K_m is calculated as follows:

$$K_m = 1 - C(T_m - T_s) \times 100^{-1} \tag{3}$$

where T_m is module temperature (degree Celsius), T_s is standard condition temperature (=25 °C), C is correction factor changing temperature of 0.35 [21] (% degree Celsius^{-1}). T_m is calculated as follows [22]:

$$T_m = T_a + 46H(0.41U_m^{0.8} + 2)^{-1} - 2 \tag{4}$$

where T_a is outside air temperature (degree Celsius), U_m is velocity of wind flowing over module (m s^{-1}). U_m is used for considering the heat transfer between wind and module.

This study has referred from PV300 about the data on solar radiation, the outside air temperature, and wind velocity of some cities in Japan. From the previous study [23], it was revealed that the tilt angle of 0 degree was the best in the case of installing PV module on a roof-top of the building. Therefore, this study has adopted the data of horizontal solar radiation to calculate the power generation from PV system.

2.2 Power Generation of FC System Utilizing Electrolyte H$_2$

In this study, it has been assumed that the power generated from PV system over the electricity demand of households [15] in the building model is applied to electrolyze

H_2. In other words, the power generated from PV system can be stored for long time by conversion into H_2. Since it is important to design the optimum size of BIPV system, this study has changed the households' number by 40, 20, 16, and 12 (=10, 5, 4, and 3 stories of the building). It has been assumed that there is 4 households per floor in building, resulting that the multiple of 4 is basis for the evaluation of this study. This study has assumed that the lowest class building having 12 households is the minimum case, resulting in the lowest limit of stories of 3. The Type-S electrolyzer (produced by IHT [24, 25]) has been adopted. According to the references [24, 25], H_2 production rate is 760 $Nm^3 h^{-1}$ and power consumption is 4.45 $kWh Nm^{-3}$. The electrolytic H_2 is estimated as follows [23]:

$$V_{H2} = E_s \times P_e^{-1} \tag{5}$$

where V_{H2} is produced electrolytic H_2 (Nm^3), E_s is surplus power generated from PV system (kWh), and P_e is power consumption ($kWh Nm^{-3}$).

The H_2 produced by the electrolyzer has been assumed to be provided for power generation by fuel cell system. In this study, polymer electrolyte fuel cell (PEFC) system is adopted. Electricity is generated from H_2 by FC as follows:

$$H_2 + 0.5O_2 = H_2O + \eta_f Q \tag{6}$$
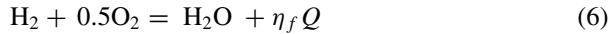
where η_f is power conversion efficiency of leading-edge PEFC stationary system in Japan based on lower heating value (=0.39) [26], Q is 242 ($kJ mol^{-1}$). This study ignores the energy loss of pump operation to preserve and provide gases.

A monthly self-sufficiency ratio of the proposed BIPV and FC system has been investigated for seven cities in Tokai region in Japan which are Nagoya, Toyohashi, Tajimi, Takayama, Ogaki, Hamamatsu, and Shizuoka. This study has investigated the self-sufficiency ratio, which is defined as the power generated by the proposed combined PV and FC system to the electricity demand of the households in the building model. The hourly the self-sufficiency ratio in the day has been calculated for the daily average horizontal solar radiation per month.

3   Results and Discussion

Figure 1 shows the monthly self-sufficiency ratio of FC system in the case of seven cities for 40 and 12 households' cases, respectively. According to this figure, it is seen that the monthly self-sufficiency ratio of FC system falls below 100% through a whole year for 40 households' case, while it is almost over 100% for 12 households' case. In addition, the ratio is inclinable to be higher in spring and summer seasons while it is inclinable to be lower in autumn and winter seasons, which follows the characteristics of PV power generation.
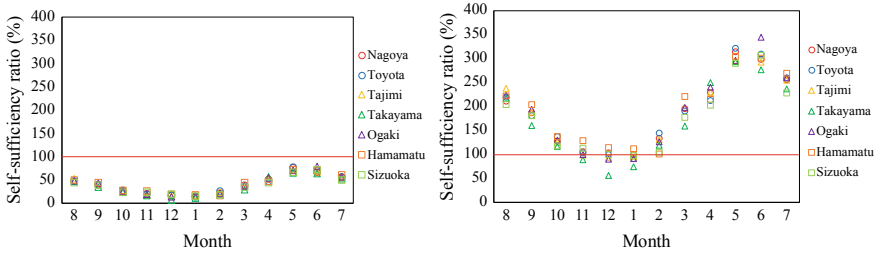
Fig. 1 Characteristics of monthly self-sufficiency ratio of FC system among seven cities (Left: 40 households' case, Right: 12 households' case)

Table 1 Relationship between annual self-sufficiency ratio of FC system and seven cities (unit: %)

City	Households			
	40	20	16	12
Nagoya	38	99	130	182
Toyota	38	99	130	182
Tajimi	38	98	129	180
Takayama	34	87	115	163
Ogaki	39	99	130	183
Hamamatsu	40	102	134	189
Shizuoka	36	92	121	171

Table 1 lists the annual self-sufficiency ratio of FC system in case of seven cities to decide the optimum households' number in the building. From this table, it can be seen that the annual self-sufficiency ratio of FC system increases when the households' number decreases. In addition, it is 100% for 16 and 12 households. Since the power can supply for the larger number of households, 16 households' case is optimum.

Figure 2 shows an example considering the effect of households' number on self-sufficiency ratio of FC system toward solar PV installation area. From this figure, it is clarified that people can predict the performance of the proposed BIPV and FC system by the approximate curve of $y = ax^{-b}$ well. This is confirmed from the other cities cases.

4 Conclusion

According to the investigation of this study, the following conclusions are obtained.

(1) The self-sufficiency ratio of FC system is inclinable to be higher in spring and summer seasons though it is inclinable to be lower in autumn and winter seasons, which follows the characteristics of PV power generation.
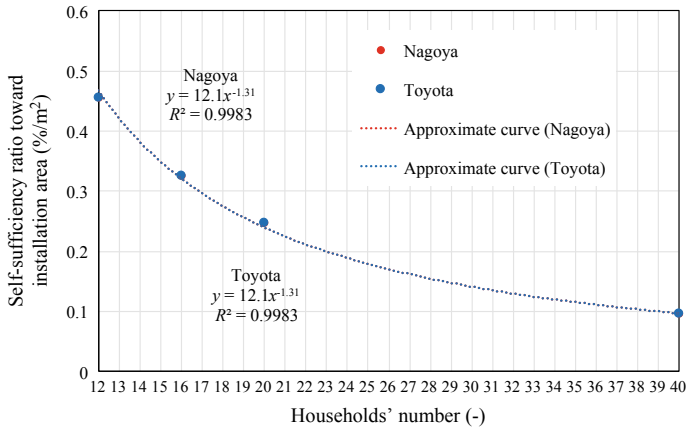
Fig. 2 Effect of households' number on self-sufficiency ratio of FC system toward solar PV installation area for Nagoya and Toyohashi

(2) The annual self-sufficiency ratio of FC system is higher when the households' number decreases. The optimum households' case is 16.

(3) It is revealed that the relationship between the households' number and self-sufficiency ratio of the FC system toward solar PV installation area can be shown by $y = ax^{-b}$ well.

References

1. Agency for Natural Resources and Energy. Energy White Paper 2017. http://www.enecho.meti.go.jp/about/whitepaper/2017pdf/ (2017). Accessed 5 April 2018
2. Jelle BP. Energies. https://doi.org/10.3390/en9010021 (2016)
3. Tripathy, M., Sadhu, P.K., Panda, S.K.: Renew. Sustain. Energy Rev. **61**, 451–465 (2016)
4. Zomer, C., Nobre, A., Reindl, T., Rhther, R.: Energy Build. **121**, 169–164 (2016)
5. Humada, A.M., Hojabri, M., Hamada, H.M., Samsuri, F.B.: Energy Build. **119**, 233–241 (2016)
6. Davi, G.A., Caamano-Martin, E., Ruther, R., Solano, J.: Energy Build. **120**, 19–29 (2016)
7. Burg, B.R., Ruch, P., Paredes, S., Michel, B.: Sol. Energy **147**, 399–405 (2017)
8. Lamnatou, C., Baig, H., Chemisana, D., Mallick, T.K.: Energy Build. **138**, 514–525 (2017)
9. Uddin, K., Gough, R., Radcliffe, J., Marco, J., Jennings, P.: Appl. Energy **121**, 159–164 (2017)
10. Kumagai, H.: Preprints of the 3rd Hydrogen Energy Lecture Meeting of the Japan Society Energy, vol. 24 (2016)
11. Marchenko, O.V., Solomin, S.V.: Int. J. Hydrogen Energy **42**, 9361–9370 (2017)
12. Baumann, L., Boggasch, E.: Int. J. Hydrogen Energy **41**, 740–751 (2016)
13. Khalid, F., Dincer, I., Rosen, M.A.: Int. J. Hydrogen Energy **41**, 7960–7967 (2016)
14. Singh, A., Baredar, P., Gupta, B.: Energy Convers. Manag. **145**, 398–414 (2017)
15. The Society of Heating, Air-Conditioning and Sanitary Engineers of Japan: Plan, Design and Assessment on Co-generation System Sing City Gas. 1st edn, Maruzen (1994)
16. Nishimura, A., Ito, T., Kakita, M., Murata, J., Ando, T., Kamada, Y., Hirota, M., Kolhe, M.: J. Jpn. Inst. Energy **84**, 315–322 (2014)
17. e-Stat.: https://www.e-stat.go.jp/ (2018). Accessed 5 April 2018

18. NEDO.: Guideline on Field Test Project of Photovoltaic Power Generation for Design, Construction and System. http://www.nedo.go.jp/content/100110086.pdf (2018). Accessed 5 April 2018
19. Panasonic.: http://sumai.panasonic.jp/solar/lineup.html (2018). Accessed 5 April 2018
20. Panasonic.: https://sumai.panasonic.jp/solar/need_power_conditioners.html (2018). Accessed 5 April 2018
21. Kawamoto, K., Nakatani, S., Hagihara, R., Nakai, T.: Sanyo Tech. Rev. **34**, 111–117 (2002)
22. Oozeki, T., Izwa, T., Otani, K., Tsuzuki, K., Koike, H., Kurokawa, K.: IEEJ Trans. Power Energy **125**, 1299–1307 (2005)
23. Nishimura, A., Kitagawa, S., Hirota, M., Hu, E.: Smart Grid Renew. Energy **8**, 195–211 (2017)
24. IHT.: http://www.iht.ch/technologie/electrolysis/industry/technical-information-benefits-electrolysers.html (2018). Accessed 5 April 2018
25. Kato, T.: J. Jpn. Inst. Technol. **94**, 7–18 (2015)
26. Panasonic.: https://panasonic.biz/appliance/FC/house_07.html (2018). Accessed 5 April 2018

Analysis of Switched Reluctance Motor for Reduction in the Torque Ripple Without Controller

Megha Chaple, Sanjay Bodkhe and Prema Daigavane

Abstract The switched reluctance motor (SRM) is highly nonlinear machine. As this machine consists of torque ripples in its output characteristic, the main drawback of SRM is torque ripple. Because of this torque ripple, SRM contains vibrations and acquist noise. The SRM requires a controller to reduce the torque ripple. This paper presents the performance of the SRM without current or torque controller.

Keywords Switched reluctance motor · Torque ripples

1 Introduction

A switched reluctance motor (SRM) has simple and robust construction. Nowadays in many industrial application, SRM is preferable as it has low cost, simple, and less copper loess's SRM consists of winding on its stator and rotor contain no winding or coil therefore minimum copper loss. SRM contains no permanent on its rotor; therefore, this is light weight motor SRM can be used for variable speed applications. The SRM is the type of reluctance motor and move by electromagnetic torque produced by stator and rotor poles. Hence, many people find interest in this motor. This motor is popular because of above discussed advantages. But, unfortunately this motor has inherent torque ripples at its output, at high speed.

Because of double salient structure, SRM has torque ripples. Due to the torque ripples in output characteristics, the applications of SRM are limited. Hence in order to increase the application of SRM, it is necessary to reduce or minimize the ripples from SRM. Because of the nonlinear behavior of SRM, it is very difficult to control

M. Chaple (✉) · S. Bodkhe · P. Daigavane
G.H. Raisoni College of Engineering, Nagpur, India
e-mail: chaplemegha@gmail.com

S. Bodkhe
e-mail: s_b_bodkhe@yahoo.co.in

P. Daigavane
e-mail: prema.daigavane@raisoni.net

Fig. 1 Basic block diagram of SRM
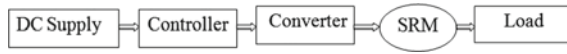
motor parameters and hence torque ripples as machine has saturation effect [1, 2–4]. Various methodologies are developed to improve the performance of SRM [5–7].

The performance of SRM can be improve with (current or torque, speed) controller [8, 9]. The output of SRM with no controller shows torque ripples in its output characteristics. This paper presents the output torque characteristics of SRM with no controlled.

1.1 Block Diagram of SRM

Construction: The SRM consists of stator and rotor both having salient poles. Stator and rotor are laminated in order to reduce the eddy current losses. Stator consists of winding or coil. The rotor has neither winding nor permanent magnet; hence, SRM is cheap and light weight. The block diagram consists of controller, power converter, dc supply as shown in Fig. 1. SRM cannot start directly from dc supply, but it requires power converter to operate.

Working principle: When DC supply is applied, the stator phase becomes electromagnets, reluctance torque is developed, and rotating member has the tendency to come to minimum reluctance position; therefore, stator pulls the rotor pole.

1.2 SRM Description

The four phases 8/6 SRM are presented in this paper. The details of model are as follows:

Phases: Four phase 8/6 SRM Dc voltage: 100 V.
Stator poles: 8
Rotor poles: 6
Stator phase resistance: 3.1 Ω.
Rated speed: 800 rpm.
Rated current:10 A.

Working of SRM: When input DC supply is applied to the stator phase, it becomes electromagnetized and reluctance torque is developed. Stator and rotor poles have tendency to come to minimum reluctance position. When both stator and rotor poles are aligned, the stator phase becomes demagnetized. Then, next pair of stator poles energies and in this way the stator phase is excited sequentially to developed electromagnetic torque and hence rotor start rotating.
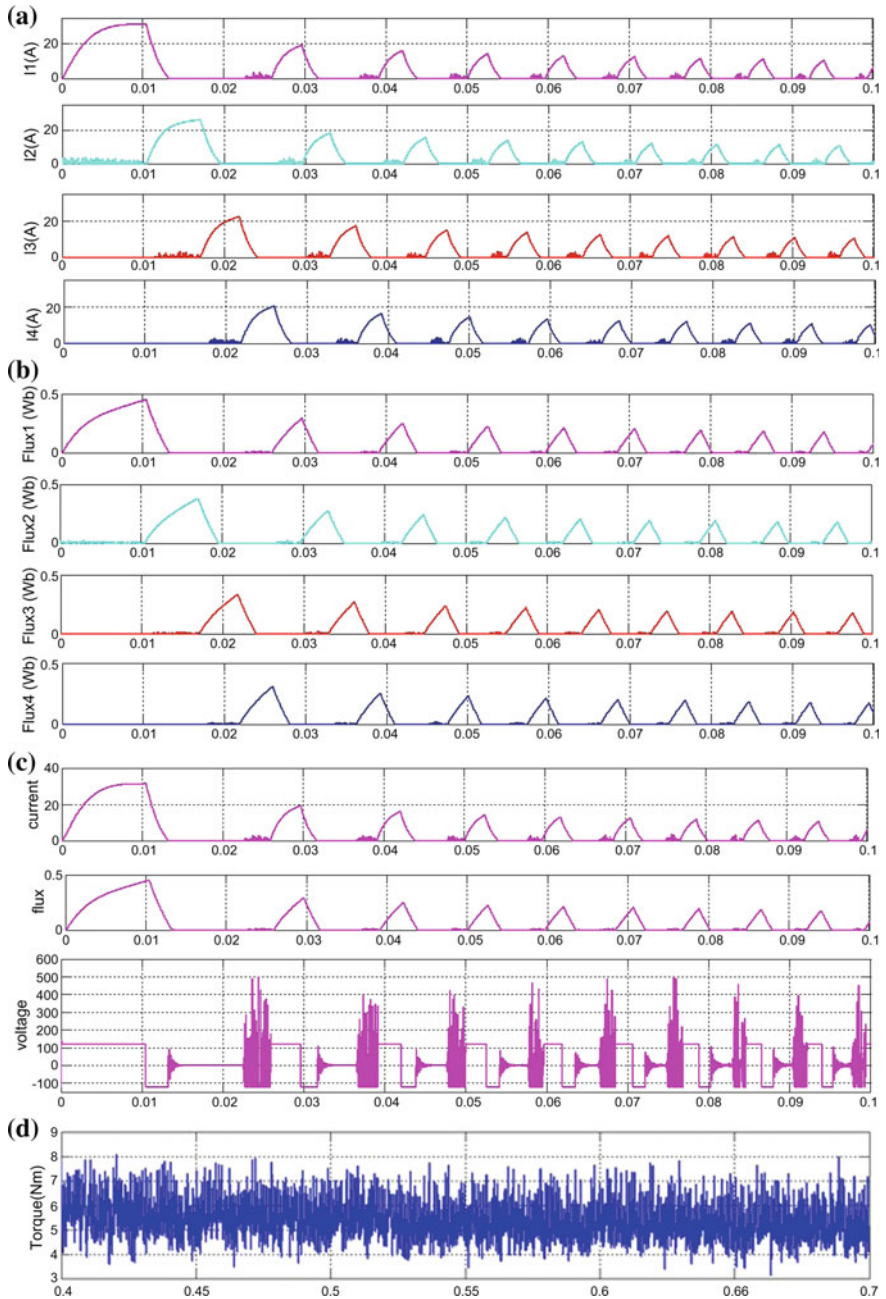
Fig. 2 Simulation results **a** phase currents, **b** phase fluxes, **c** variation of phase current, flux with applied voltage, **d** total output torque of motor

2 Simulation

2.1 Results and Analysis

The four phases 8/6 SRM is modeled. The MALAB/SIMULINK software is used for simulation. Figure 2 shows the simulation results of phase currents, flux, torque when no controller is used. It observed that current in the phase winding is nonlinear which leads to nonlinear phase flux and output torque. The phase current increases when voltage is applied, and it freewheels to the source when negative voltage is applied as shown in Fig. 2a. Similarly, current rise flux also rises, and when current decreases, flux also decreases as shown in Fig. 2b. This shows that phase currents and phase flux are proportional. As voltage applied stator current increases linearly and hence motor flux similarly when negative voltage is applied current and hence flux decrease as shown in Fig. 2c. This shows that as output torque is a function of stator current and flux and both these parameters are nonlinear; therefore, higher ripples present in its output torque characteristic Fig. 2d.

3 Conclusion

The simulation results show that the conventional SRM consists of torque ripples in its output torque characteristics. Hence, to reduce the torque ripple from SRM, controller is necessary. Since torque is controlled by controlling the current and flux, the current, speed, and flux controller are necessary to improve the performance of SRM. So the future work of this paper is to design the controller to control the stator phase current, to minimize the torque ripples in its output torque characteristics.

References

1. Labioda, C., Srairia, K., Mahdada, B., Benchouiab, M.T., Benbouzidc, M.E.H.: Speed control of 8/6 switched reluctance motor with torque ripple reduction taking into ac- count magnetic saturation effects. In: International Conference on Technologies and Materials for Renewable Energy, Environment and Sustainability, Energy Procedia, vol. 74, pp. 112–121 (2015)
2. Pratapgiri, S., Polaki, P., Narsimha, V.: Direct torque control of 4 phase 8/6 switched reluctance motor drive for constant torque load. World J. Modell. Simul. **8**(3), 185–195 (2012)
3. Cheok, A.D., Fukuda, Y.: A new torque and flux control method for switched reluctance motor drives. IEEE Trans. Power Electron. **17**(4), 543–557 (2002)
4. Saha, N., Panda, A.K., Panda, S.: Speed control with torque ripple reduction of switched reluctance motor by many optimizing liaison technique. J. Electr. Syst. Inf. Technol. (2017)
5. Huang, H., Hu, K., Liaw, C.: Switch-mode rectifier fed switched-reluctance motor drive with dynamic commutation shifting using DC-link current. IET Electric Power Appl. **11**(1) (2017)
6. Cho, Y., Bak, Y., Lee, K.: Torque-ripple reduction and fast torque response strategy for predictive torque control of induction motors. IEEE Trans. Power Electron., 1 (2017)

7. Huang, H., Hu, K., Liaw, C.: Switch-mode rectifier fed switched-reluctance motor drive with dynamic commutation shifting using DC-link current. IET Electric Power Appl., 640–650 (2017)
8. Chaple, M., Bodkhe, S.B.: Minimization of the torque ripples of 8/6 switched reluctance motor with PI controller. In: 2nd IEEE International Conference on Recent Trends in Electronics, Information & Communication Technology (RTEICT), pp. 2106–2110 (2017)
9. Chaple, M., Bodkhe, S.: Comparative analysis of 8/6 switched reluctance motor drive with different converter topologies for minimization of torque ripple. In: IJCTA, International Science Press, vol. 10, No. 38, pp. 41–48, ISSN: 0974-5572 (2017)

Overview of the Controllers Used for Mitigation of Harmonics Injected Due to Nonlinear Loads

Kanchan Vipul Narode and Asha Shendge

Abstract The harmonics distortion due to huge non linear loads is always a serious concern of any power system. The harmonics not only increases the distortion in the supply but causes the power factor to be lowered. To improve upon these conditions, various harmonic controllers are used in conjunction with the power system. The researchers and technocrats are working on various aspects to be improved for assured better power quality to be achieved. This paper have presented the comparison of various power controllers to improve the performance of the system. Active and passive both the methods are found suitable for various systems. This paper have tried concluding with the identification of the suitable controlling method of harmonics for PV systems connected to the non linear loads through the power grid. For the countries like India, photovoltaic will be the most contributing electricity source in coming future. This paper have presented the system with consideration of the filter requirement for improving the performance of the PV system in this paper. MATLAB implementation of the system is presented in this paper.

Keywords Harmonics · Mitigation methods · Active and passive controllers · PV system · Etc.

1 Introduction

The numerous power electronics appliances connected to electric system are nonlinear in nature. It may affect the performance of the power system such as harmonic

K. V. Narode (✉)
Electrical Power System, Department of Electrical Engineering, G. H. Raisoni
Institute of Engineering & Technology, Pune 412207, India
e-mail: dhatkanchan@gmail.com

A. Shendge
Department of Electrical Engineering, G. H. Raisoni Institute of Engineering & Technology,
Pune 412207, India
e-mail: asha.shendge@raisoni.net

lesser power factor and harmonic distortion. To overcome this situation, harmonic mitigation techniques are being used which comprises of active filters, passive filters, and harmonic filters. The filters tries to nullify the harmonics before feeding it to the grid. Authors have presented the various filters for mitigation of the harmonics to improve the performance of the PV system connected to the grid.

The solar energy is being very popular in India during recent years. The government policy supports the renewable energy, mainly solar. In previous days to popularize solar generation, it is being subsidized by the Indian government. Being the easily available source of energy, solar systems are installed widely in India. Corporate and commercial buildings are now a day's coming up with installation of the solar roof top systems for the production of electricity with net metering facility. The clean energy is attracting the industries to earn better and to have the sustainable energy generation. The solar systems in India are now modernized as far as the performance is concerned. The cost of the setup has also been reduced in recent years and hence the system is becoming popular day by day. The flexibility and the quality power is the requirement of any electrical system. The power drawn from PV system when connected to the grid faces the issues with the harmonics distortion. Consistent performance without disturbance of the electrical supply makes any power system a reliable and trustworthy.

The boost converter connected to the PV with MTTP and controller to optimize the performance of the system. The filters are incorporated in the solar system helps in reducing the harmonics. It also helps in improving the power factor and reduction of inter harmonics or triplen harmonics. The developed system is found to be useful as simulated model along with hardware shows the improve in performance and enhanced control (Fig. 1).
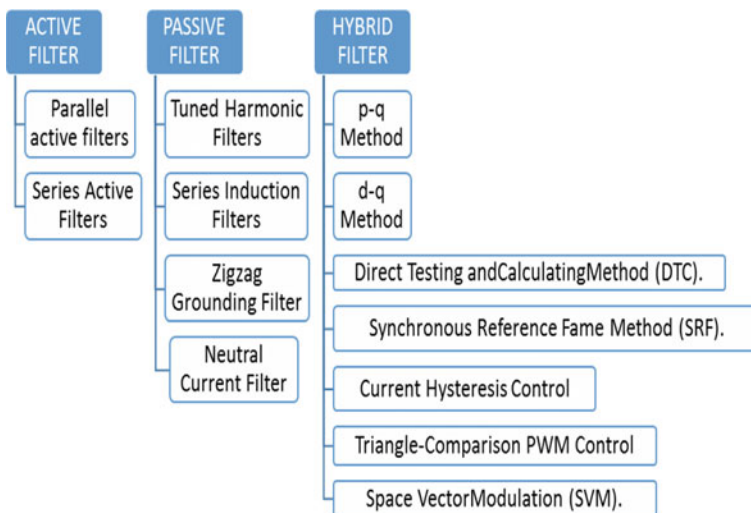
Fig. 1 Classification of filter technologies

1.1 Filter Technologies

2 Passive Harmonic Mitigation Techniques

Various passive filtering techniques are available for reduction in level of harmonics in electrical system which may incorporate higher pulse converter circuits, e.g., 12 pulse, 18 pulse, and 24 pulse. In all passive filtering technique undesirable current distortion is being blocked from flowing into grid is either by using high series inductance or diverting the flow if harmonic current by means of a low impedance parallel path. New era of harmonic filters focuses on the improvement of power factor as well. Utility companies across the globe have put a limit on the permissible power factor for various loads. (e.g., <0.8 leading and >0.75 lagging). In many countries and few states of India there is a limitation on the current harmonic produced. Generally it is being expressed in terms of total harmonic distortion or odd multiples of fundamental component. Harmonic laws are current applied to keep current and voltage harmonic at check for utility and consumer both (Fig. 2).

3 Active Filter

In this technique active Alteration of the harmonics, the improvement in power quality is achieved by injecting equal and opposite current or voltage into electrical network thus canceling a original distortion. Active harmonics filters generally uses an insulated gate bipolar transistors (IGBT's) for production of output current of the required shape when injected into AC lines and it abandons the original load generated harmonics. The control strategies play very important role in deciding the quality of filtering. The active harmonic technique uses fourier transform technique for calculation of the phase angle and amplitude. Another method is based on the cancelation of the full spectrum which the full current waveform is used by the controller of the filter which nullifies the effect of fundamental component and orders a filter to inject a equal and opposite of remaining waveform (Fig. 3).
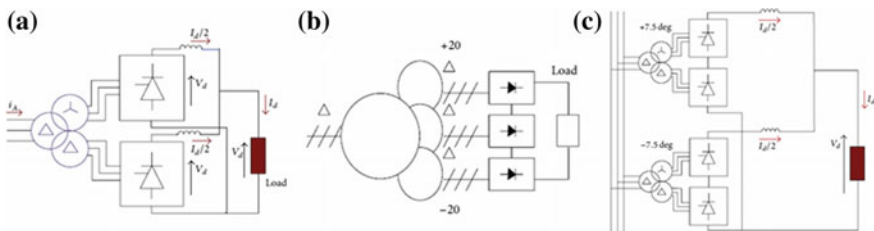
Fig. 2 **a** 12 pulse converter system **b** 18 pulse converter system **c** 24 pulse converter system
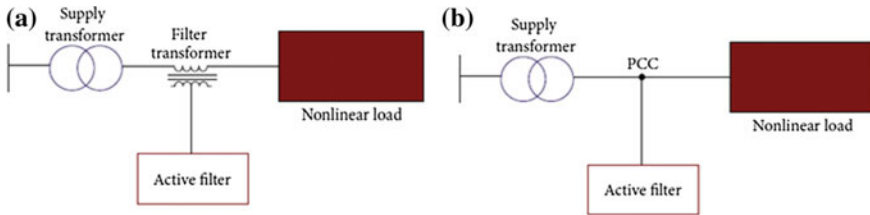
Fig. 3 a Series active filter **b** Parallel active filter

4 Hybrid Filters

The combination of the active filter and passive filter is used for further enhancement of the results for the harmonic filter. The passive filter are used in fixed characteristics and in many of the cases it is observed that is not efficient to mitigate the current harmonics. Hence in addition to passive filter, active filter is also employed to overcome the drawback of the passive harmonic filter. Active harmonic filter uses switching mode power converter for performing the harmonic current elimination. However the limitation is that, the construction cost of active harmonic filter. The power rating required for the active harmonic filter is very large. These limits the application of active harmonic filters in practical. This problem attracted attention of many researchers and then altogether new era of hybrid harmonic filter began. Passive filter has an low cost that is why it is used in hybrid harmonic filter. Hybrid harmonic filter has an advantages of passive and active harmonic filter, hence rating of active harmonic filter comes drastically lesser making it affordable to implement (Fig. 4).

5 Simulation Design

Following diagram shows the developed MATLAB model for the main system developed for improvement of the quality of the power supply. The developed system consists of the controller, power tracking, filters, and the basic elements of the PV. The converters with control are also the part of the system (Fig. 5).

The model for the PV system developed in MATLAB as shown below. The grid connected systems consisting of voltage, current, and power control with the converters to control. The power electronics circuits are very important from the point of view of controlling the power (Figs. 6 and 7)
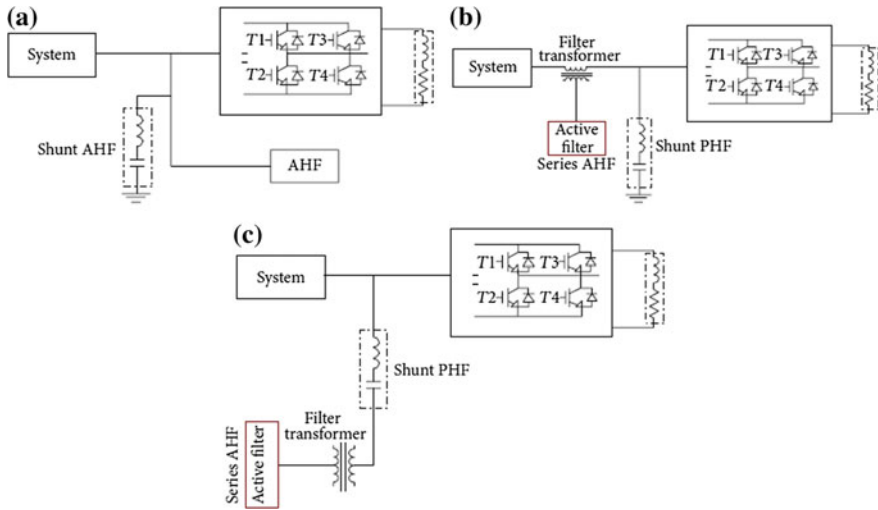
Fig. 4 Various configuration of various hybrid filters
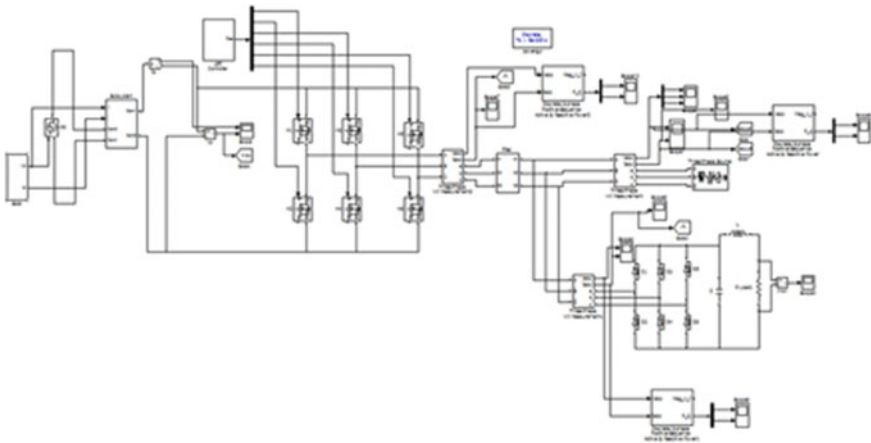
Fig. 5 Main simulation

6 Simulation Results

The results of the simulated circuit to verify the expected results have been shown below (Figs. 8, 9, 10, 11 and 12)

The table below shows the percent THD for various configurations and it can be easily observed that the harmonic distortion has been reduced with the implemented module of PV-Hybrid controller (Table 1).
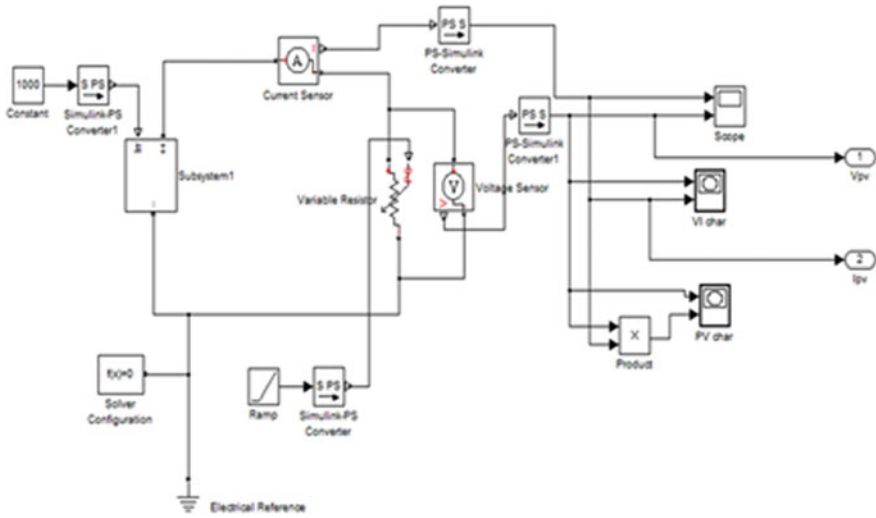
Fig. 6 PV unit system
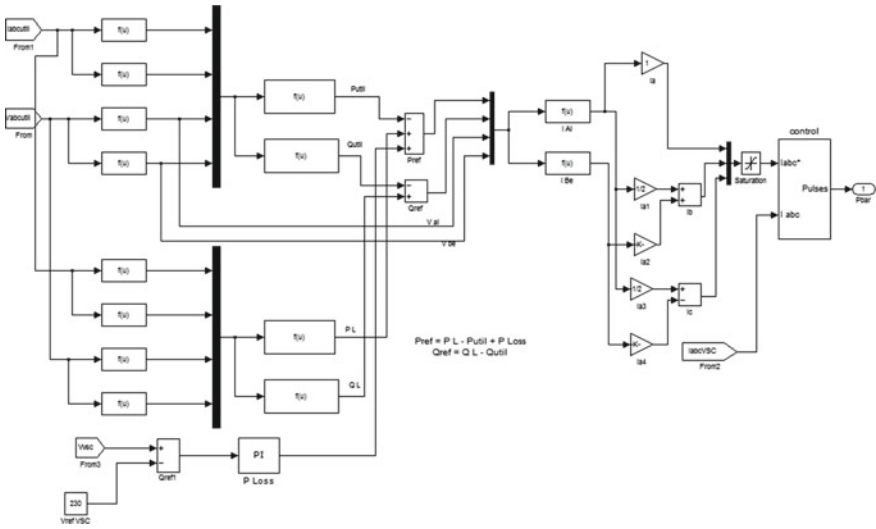
Fig. 7 PV-APF controller

Table 1 Comparison of THD with various filters

Sources	THD (%)
Without filter	61.30
Active power filter	14.64
Hybrid power filter	5.78
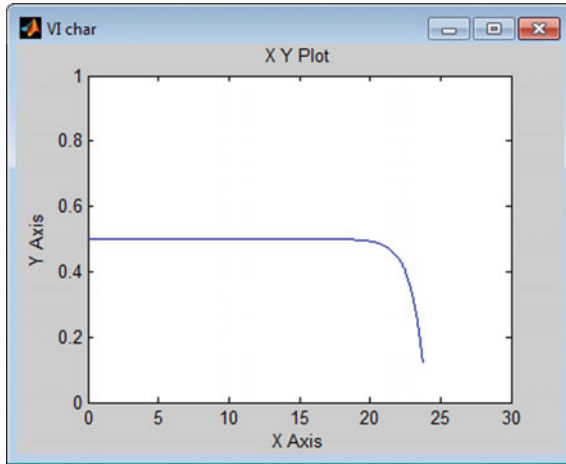
Fig. 8 VI characteristics
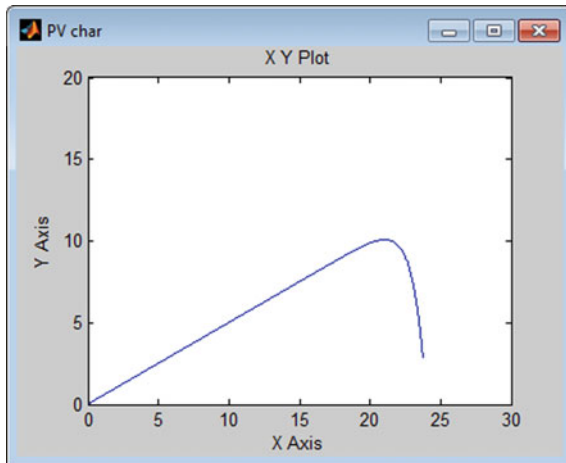
Fig. 9 PV characteristics

The harmonics reduction being the primary target of the model development for the non-linear load has been achieved through the software results. The MAT-LAB/SIMULINK model shows that the hybrid power filter works completely to fulfill the objectives.
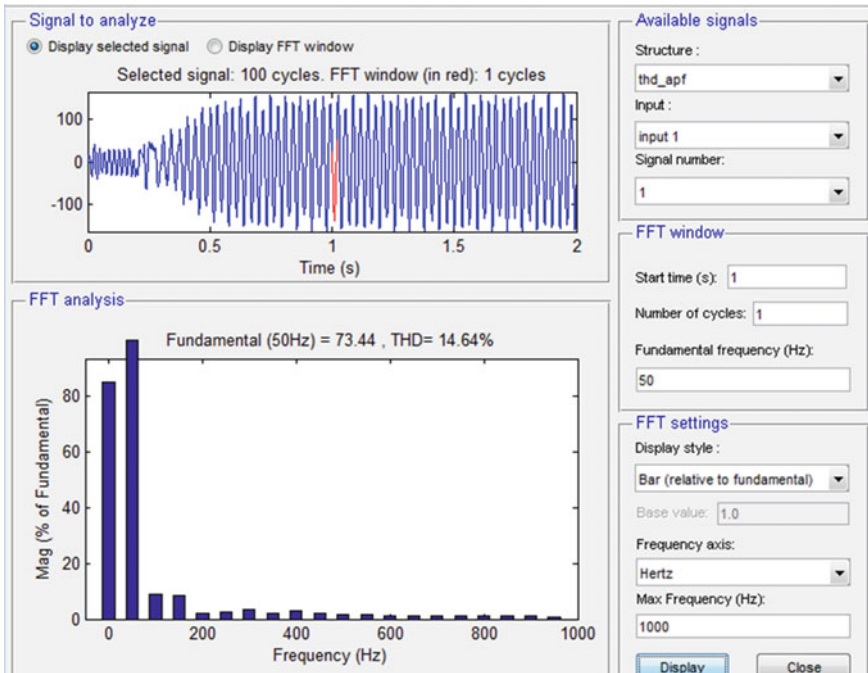
Fig. 10 THD for APF
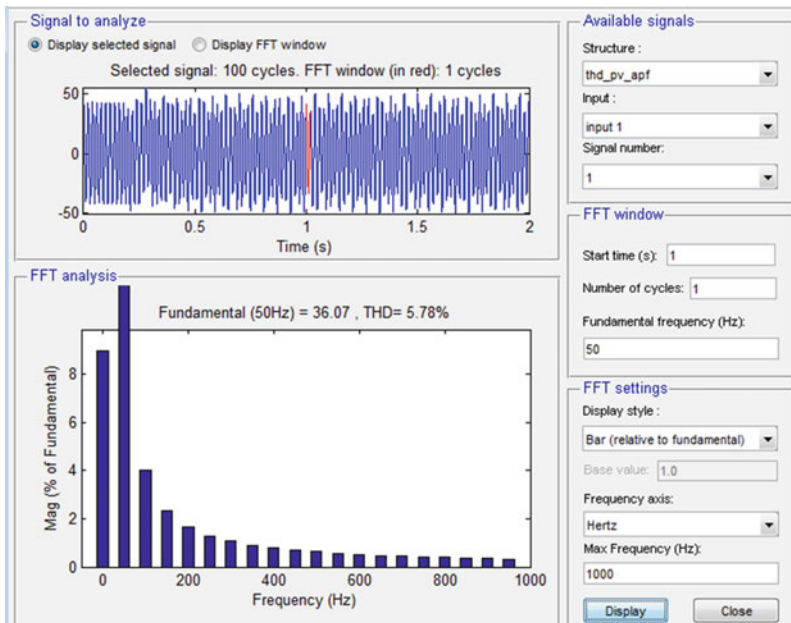
Fig. 11 THD for PV-APF
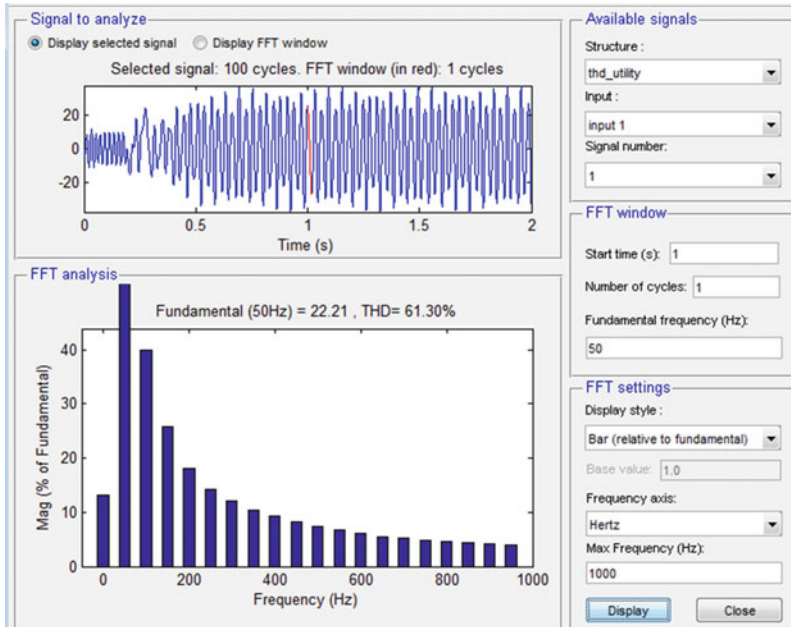
Fig. 12 THD for utility

7 Conclusion

The non-linear loads are always connected to every electrical system. The problems with such load are the harmonic distortion and hence to improve the harmonics performance of the system various controllers are to be used. This paper have presented the brief information about the various controllers available to address this problem and concluded that the Hybrid Power Filters using P-Q method are found suitable for the PV system.

References

1. Zha, X., Chen, Y.: The iterative learning and control strategy for hybrid active power filter in dampen harmonics resonance in industrial power system. In: IEEE International Symposium on Industrial electronics, vol. 2, pp. 848–853 (2003)
2. Hamrouni, N., Jraidi, M., Cherif, A.: New control strategy for 2-stage grid connected photo-voltaic power system. Renew. Energy **33**(10), 2212–2221 (2008)
3. Villalva, M.G., Gazoli, J.R., Filho, E.R.: Comprehensive approach to modeling and simulation of photovoltaic arrays. IEEE Trans. Power Electron. **24**(5), 1198–1208 (2009)
4. Zhou, K., Lv, Z., Luo, A., Liu, L.: Control strategy of shunt hybrid active power filter in distribution network containing distributed power. In: China International Conference on Electricity distribution, pp. 1–10 (2010)

5. Houssamo, I., Locment, F., Sechilariu, M.: Experimental analysis of impact of MPPT methods on energy efficiency for photovoltaic power systems. Int. J. Elect. Power Energy Syst. **46**, 98–107 (2013)
6. de Brito, M.A.G., Sampaio, L.P., Luigi, G., e Melo, G.A., Canesin, C.A.: Comparative analysis of MPPT techniques for PV applications. In: Proceedings of the International Conference of Clean Electric Power (ICCEP), pp. 99–104, Jun 2011
7. El-Habrouk, M., Darwish, M.K., Mehta, P.: Active power filters: a review. Proceedings of the IEEE Electric Power Applications, vol. 147, no. 5, pp. 403–413, Sept 2000
8. Akagi, H., Kanagawa, Y., Nabae, A.: Generalized theory of the instantaneous reactive power in three-phase circuits. In: Proceedings of the International Conference Power Electron. Tokyo, Japan, pp. 1375–1386 (1983)
9. Li, Y.W., He, J.: Distribution system harmonic compensation methods: an overview of DG-interfacing inverters. IEEE Ind. Electron. Mag. **8**(4), 18-31 (2014)
10. Kim, S., Yoo, G., Song, J.: A bifunctional utility connected photovoltaic system with power factor correction and UPS facility. In: Proceedings of the Conference Rec. 25th IEEE Photo volt. Specialists Conf., pp. 1363–1368, May 1996
11. Komatsu, Y.: Application of the extension pq theory to a mains-coupled photovoltaic system. In Proceedings of the Power Convers. Conf. (PCC), vol. 2, pp. 816–821. Osaka, Japan (2002)
12. Cheng, L., Cheung, R., Leung, K.H., Advanced photovoltaic inverter with additional active power line conditioning capability. In: Proceedings of the IEEE Power Electron. Specialists Conference, vol. 1, pp. 279–283, Jun 1997
13. Aredes, M., Monteiro, L.F.C., Miguel, J.M.: Control strategies for series and shunt active filters. In: IEEE Borlogna Power Tech Conference, pp. 1–6, June 2003
14. Chen, D.H., Xie, S.J.: Review of control strategies applied to active power filter. In: IEEE International Conference on Electrical Utility Deregulation, Restructuring & Power Technologies, Hong Kong, pp. 666–670 (2004)
15. Chen, X., Fu, Q., Yu, S., Zhou, L.: United control of photovoltaic grid-connection and power quality managements. In: Proceedings of the Workshop Power Electron. Intel. Transport System (PEITS), pp. 360–365, Aug 2008
16. Khalid, S., Tripthi, A.: Comparison of sinusoidal current control strategies and synchronous rotating frame strategy for total harmonics reduction for power electronics converters in air craft system under different load conditions.Int. J. Adv. Res. Electrical Electron. Instrum. Eng. **1**(4), 305–313 (2012)
17. Norooziana, R., Gharehpetianb, G.B.: An investigation on combined operation of active power fillter with photovoltaic arrays. Int. J. Elect. Power Energy Syst. **46**, 392–399 (2013)

Part II
Environmental Management & Sustainable Development

Dr. Prashant Pawade Conference Organizing Chair

Introduction

The main aim of this theme of conference is to bring together academics and other professionals for the presentation and exchange of their thoughts and experiences on concepts, trends and practices in civil, transportation and environment fields. The conference was intended to offer a stimulating environment to encourage discussion and exchange of ideas leading to the advanced as well as sustainable construction technology.

In the "International conference on Smart Technologies for Energy, Environment and Sustainable Development, 2018 (ICSTEESD-18)", three technical sessions have been organized for addressing the technical challenges, opportunities, and research innovation related to Environmental Management & Sustainable Development. First session was chaired by Dr. Pawan Kumar Labhasetwar, Senior Principal Scientist (Water Technology and Management), NEERI, Nagpur which includes papers related to Environmental Engineering. Second session was chaired by Dr. L. M. Gupta, Professor, VNIT, Nagpur which includes papers on Sustainable development in Structural as well as material engineering. The final session was chaired by Prof. Nitin Mishra, Graphic Era University, Deharadun which includes papers on Remote sensing & GIS Applications, Geotechnical Engg. as well Transportation Engg.

This proceeding comprised the selected papers from the subject areas of Civil Engineering and Structural Engineering, Architecture Environment and Sustainable Resources and Development, Materials and Applications, Transportation Engineering, Environmental Protection and Planning. All the papers in the con-

ference proceedings have been checked for plagiarism by ithenticate and undergone the intensive review process performed by the Review committee, and only accepted papers were included. The total number of submitted papers in this theme were 82 and 39 are accepted.

www.ghrce.raisoni.net

Study of Properties of Coal Bottom Ash and Waste Foundry Sand and its Use in Concrete

Aasif Baig and Valsson Varghese

Abstract India produces abundant of industrial waste like bottom ash (CBA) and waste foundry sand (WFS) whose productive use or recycling and reuse is the best option available to reduce the threat caused by their disposal on environment. This research work aimed to find possibility of using both these waste materials in concrete for which study of characteristics of the materials is important. It is found that CBA needs to be processed before using in concrete. The results of Grounded CBA & WFS resemble within its permissible limit, and thus, these waste materials can be used as a substitute of cement and sand, respectively. Experiments are conducted on concrete containing CBA & WFS in the proportion of 10 and 6%, respectively. Through the experiment, we concluded that processed CBA & WFS can be partially replaced for cement and sand, respectively.

Keywords Physical properties · Chemical properties · Mechanical properties · Coal bottom ash · Waste foundry sand

1 Introduction

The developing construction industry needs concrete as a basic construction material for its development. Hence, subsequently the requirement of natural aggregates is increasing day by day due to its ever increasing consumption as a constituent of concrete which has further lead to increase in its economic value. These problems make us find an alternative option to the natural resources by utilizing some waste products which otherwise if dumped pose environmental threat. Among all waste products, the large production of coal bottom ash and waste foundry sand (WFS)

A. Baig (✉)
TGPCET, Wardha Road, Mohgaon, Nagpur, India
e-mail: aasif.civil@gmail.com

V. Varghese
KDK College of Engineering, Great Nag Road, Nandanvan, Nagpur, India
e-mail: valsson_v@yahoo.com

which is generated from the industries causes various environmental hazards and hence use of these wastes as construction materials would help to reduce burden on environment. Foundry sand, being a by-product of ferrous and nonferrous metal casting industries, is considered as good quality silica sand not having varied physical characteristics [1]. Foundry sand is obtained after repetitively recycling and reusing sand many times by the foundries. The casting process and the industry from which foundry sand originates govern its physical and chemical characteristics [2]. On an average India produces around 7.8 million tons of WFS every year. Basically foundry sand is available in two forms, green sand also termed as molding sand wherein clay acts as binding agent, and chemically bonded sand in which polymers are used for binding grains of sand together. First form of sand consists of primarily silica as 85–95%, 0–12% clay, 2–10% carbonaceous additives like sea coal and 2–5% of water. This sand also contains chemicals like MgO, K_2O, and TiO_2 in a small amount. Second type, i.e., chemically bonded sand consists of 93–99% silica and 1–3% chemical binder [3]. Physical test on this sand indicates that the physical properties are nearly equivalent to the natural sand, and also there is no harmful chemical in it due to which if used is considered as non-hazardous to concrete [3]. In view of protection of environment, the industries generating power, specifically coal-based power plants, are highly affected. Coal bottom ash (CBA) produced by power plants is now major concern in view of economic and environmental aspect and needs various recycling options rather than the regular land filling as the current recycling rate is very less [4]. Bottom ash is collected in hopper at bottom of the furnace wherein it is quenched with water and crushed to clinkers which and conveyed to the storage site. CBA basically is available either in coarse or fine gravel size grain structure and its use till date is limited only to low cost replacement materials in field of construction sector. However, though its recycling options are studied, there is still quite scope of research on the overall properties and characteristics of CBA and WFS. Hence, this research work aimed to study the physical, chemical, and mechanical properties of coal bottom ash and waste foundry sand. Various physical properties like particle size distribution, dry density, specific gravity, moisture content, soundness, fineness, and chemical composition of materials are tested to predict the performance as compared to cement and natural fine aggregates, respectively, and also determine its possible application in concrete.

2 Literature Review

Many researches have been done to study the effective use of materials like fly ash in concrete and its detail material properties but materials CBA and WFS are not yet fully explored. For reducing the carbon content in obtained sample of CBA, treatment method of crushing and subsequently screening was found to be more effective than other methods of heavy medium separation and electrostatic separation [4]. Ramzi and Shahidan (2016) studied the physical as well as chemical properties of coal bottom ash (CBA) and found that there is much variation between properties of natural

fine aggregate and CBA but yet recommended to be used as partial replacement of sand in concrete [5]. Amritkar and Chandak (2015) experimented on effect of waste foundry sand (WFS) on concrete by replacing it with the fine aggregate partially and found that as the amount of WFS was increased in percentages in concrete the compressive strength of concrete also increased correspondingly [6]. Pathariya Saraswati also observed the increase in compressive strength of concrete with increasing percentage of sand and also suggested as economical and application for preparing low cost concrete [7]. Antonio and Zarco (2007) determined the engineering properties of calaca batangas bottom ash and found that bottom ash is light weight, non-plastic. Gurpreet Singh found that WFS has lesser values of physical properties and also has less unit weight [8]. It was found by Haldun Kurama that CBA had comparatively clear mineralogical nature with minerals like alumina, glass, and also different percentage of crystalline phases of quartz, ferrite spinel, and calcite. Bottom ash seemed to have pozzolanic effect wherein the silica in bottom ash reacted with the available lime in the paste and formed calcium silicate hydrates which not only improved the later strength but also it was found to be very high than Ordinary Portland Cement [9]. It is observed that mortar prepared from unprocessed bottom ash required more amount of water than that required for cement mortar, whereas contradict to it mortar prepared from grounded bottom ash required less amount of water than cement mortar. Hence, it is recommended not to use bottom ash without processing as a partial replacement to cement, though grounded bottom ash grinded to be retained by less than 5% on 325 sieve showed positive effect for partial replacement in cement [10].

3 Research Significance

Waste foundry sand and Coal Bottom ash are abundantly available waste materials which pose environmental threat. There use in concrete can only be studied when their behavior as a material is studied in detail, and feasibility of using these materials is checked for partial substitute to fine aggregate and cement. Many researchers have studied the feasibility of using coal bottom ash as a partial replacement of natural sand in concrete but its possible utilization as a pozzolanic material, i.e., as a partial substitute of cement is yet not much looked into. The research aimed to check feasibility of use of waste foundry sand as partial substitute for natural sand and partial substitution of Coal bottom ash to cement is hence studied. The data obtained in this investigation will be used to predict about the material properties of WFS and CBA and to suggest the possible recycling option so that they can be effectively used in concrete.

4   Experimental Materials and Methods

The waste materials undertaken for the research work are Coal Bottom ash (CBA) and Waste foundry sand (WFS).

Coal Bottom Ash
The coal bottom ash samples were procured from Koradi Thermal Power Plant; Nagpur wherein approximately 28,744 T/M of bottom ash generated is disposed in ash pond. The power plant produced type 'F' fly ash and bottom ash with general percentage of fly ash and bottom ash as 80 and 20 percent, respectively. The bottom ash initially collected was in the form of wet material. Hence, CBA was sundried for about 2–3 days on open terrace till it is fully dried.

Waste Foundry Sand Source
Waste foundry sand was procured from local Industry.
   Testing Method and Results

4.1   Physical Properties

(a) *Fineness and Fineness modulus*:
   This test is simple in procedure and was practiced by using IS 4031 part I-1996. Fineness of CBA is measured by sieving it on standard sieve. A 100 g of CBA sample obtained from sampling was placed on IS sieve of 90μ and sieved. The percentage passing is determined as fineness of cement and was determined as 14.5% for CBA [11]. Hence, there was need to process CBA and hence it was grounded further and then the fineness of grounded CBA was found to be 9.52%.
   The grain size nature of waste foundry sand was calculated by using IS 2386 part I (1963). Fineness modulus of WFS was found to be 3.852. The foundry sand was conformed to be from zone III.

(b) *Specific Gravity*
   The specific gravity of coal bottom ash and waste foundry sand is determined using IS Code 4031-1(1996). Specific gravity of CBA & WFS was measured using a pycnometer. From the analysis, as expected the specific gravity of CBA was much less than the Portland cement as shown in Table 1. The values are 1.6 and 2.64 of CBA & WFS, respectively. The specific gravity of Portland cement is generally around 3.15.

(c) *Water Absorption, dry density*
   WFS used for the test was initially oven dried for 24 h, and then, water absorption and dry density were evaluated as per the procedures provided in IS 2386-3(1963) [12]. In WFS, water absorption is found to be 20.89 which is found to be more than the natural sand.

Table 1 Result of physical properties of CBA and WFS

SR. NO.	Tests performed	Results			
		CBA	Standard values of cement	WFS	Fine aggregate
1.	Specific gravity	1.63	3.15	2.64	2.45
2.	Water absorption (%)	–	–	20.89	1.0
3.	Dry density (kg/lit.)	0.56	1.44	0.66	2.0
4.	Bulking of sand (%)	–		4.16	3.2

Table 2 Result of Chemical Properties of CBA and WFS

Sample	Na_2O	MgO	SiO_2	Al_2O_3	Fe_2O_3	TiO_2	CaO	K_2O	P_2O_5	MnO_2	CeO_2
CBA	0.19	0.78	65.33	20.57	4.93	1.37	1.79	1.51	0.07	0.07	0.04
WFS	0.84	0.91	83.83	5.12	3.72	0.39	0.69	0.12	0.08	0.05	–

Table 3 XRF scan of CBA and WFS

Sample	NiO	CuO	SrO	SO_3	BaO	Cl	ZrO_2	Cr_2O_3	Tb_4O_7
CBA	0.01	0.01	0.01	0.16	0.03	0.05	0.05	0.04	0.01
WFS	0.007	0.009	–	0.13	–	0.08	0.01	0.03	–

(d) *Bulking of Sand*

Bulking of WFS was evaluated as per IS 2386-3(1963). Bulking of WFS was found as 4.16.

4.2 Chemical Properties

Chemical composition of CBA and WFS was studied using X-ray fluorescence (XRF). Also pH [13], electrical resistivity, soluble chloride content, and soluble sulfate content were evaluated. All these tests were performed at Indian Bureau of Mines laboratory at Nagpur (M.S) [14]. Results indicate that the oxides composition of cement and coal bottom ash can be identified, and the total composition of SiO_2 + Al_2O_3 + Fe_2O_3 is found to be 90.83, while in waste foundry sand, the total composition was 92.67 as shown in Table 2. As per IS 3812, SiO_2 should be minimum 35, MgO should be less than 5, Na_2O and SO_3 should be less than 1.5 and 3, respectively, and all the values are within these permissible limits.

The chemical composition of coal bottom ash and waste foundry sand was found by using X-ray Fluorescence Scan (XRF Scan), and various other tests were performed as shown in Tables 3 and 4.

Table 4 pH, electrical
conductivity, soluble chloride,
and soluble sulfate test

Parameters	CBA	WFS
pH (10% Solution)	6.58	7.10
Electrical Conductivity(Micro Siemens/cm)	182.1	153.5
Soluble chloride (%)	0.014	0.003
Soluble sulfate (%)	0.053	0.078

Table 5 Mechanical
properties of CBA and WFS

Sr. No.	Test Performed	Results			
		CBA	Cement	WFS	Fine Aggregate
1.	OMC (%)	–	–	6	2
2.	MDD (%)	–	–	12.3	2.5
3.	Soundness (%)	8.0	4.3	9.56	–

4.3 Mechanical Properties

The optimum moisture content and maximum dry density was calculated using IS
2386-3(1963). Soundness of CBA was found by using IS 2386-5(1963).

Three sets of soundness tests were conducted. After 5 cycles of immersion and
drying, the measured losses were 8 and 9.56% for CBA and WFS, respectively, as
shown in Table 5.

Water Absorption

The output of water absorption tests are given on the basis of accelerated curing
conditions and concrete types [15]. The highest water absorption value was obtained
from conventional concrete, i.e., 12.6%, which reduced to 2.26% for concrete with
WFS (6% replacement) while the lowest water absorption value from concrete having
CBA (10% replacement) and WFS (6% replacement), i.e., 1.74%.

Initial Surface Absorption

The test results of initial surface absorption are on the basis of oven drying method.
The highest initial water absorption value was obtained from conventional concrete,
i.e., 5.6%, which further reduced to 2.42% while the lowest initial surface absorption
value was obtained as 1.84%.

4.4 Mix Design

Control concrete mixtures were designed as per guidelines given in BIS 10262-
1982 to achieve 28-day compressive strength of 31.6 N/mm^2. Concrete was made
with River sand conforming to grading Zone III of BIS: 383-1970 [16] and having
fineness modulus of 2.17.

Table 6 Mix proportions of control concrete mixtures

Sand conforms to grading zone as per 383-1970	Water–Cement ratio	Cement (kg/m^3)	Sand (kg/m^3)	Aggregate (kg/m^3)	Water liters
III	0.55	358.18	642.39	1214.95	197

Table 7 Compressive strength for M20 grade of concrete mix with different percentage of WFS

Sr. No.	Mix proportion	Test results (N/mm^2)		
		7 days	14 days	28 days
1.	B0	24.73	25.47	27.85
2.	B2	25.32	26.42	29.86
3.	B4	26.89	27.94	32.2
4.	B6	28.24	30.22	34.5
5.	B8	27.9	29.4	32.9
6.	B10	27.1	28.6	31.12
7.	B12	26.8	27.92	29.42
8.	B14	26.37	26.88	28.5
9.	B16	24.58	25.32	26.2

- 28 day Compressive strength $= 20$ N/mm^2
- Degree of quality control $=$ Good
- Maximum size of coarse aggregate $= 20$ mm
- Degree of workability (Slump) $= 100$ mm
- Type of Exposure $=$ Mild
- Target 28 day compressive strength $= 31.6$ N/mm^2
- Minimum cement content—250 kg/m^3
- Maximum water cement ratio—0.55
- Maximum cement content—340 kg/m^3

A detail of mix proportions is mentioned in Table 6.

4.5 Compressive Strength Test Results for WFS

The optimum percentage replacement of WFS with fine aggregate in terms of compressive strength was obtained as 6%, and then, with the constant 6% replacement of WFS, cement was replaced partially with CBA from 0 to 18%.

In B2 Mix, B represents the Mix and 2 represents the replacement percentage of waste foundry sand with fine aggregate as shown in Table 7.
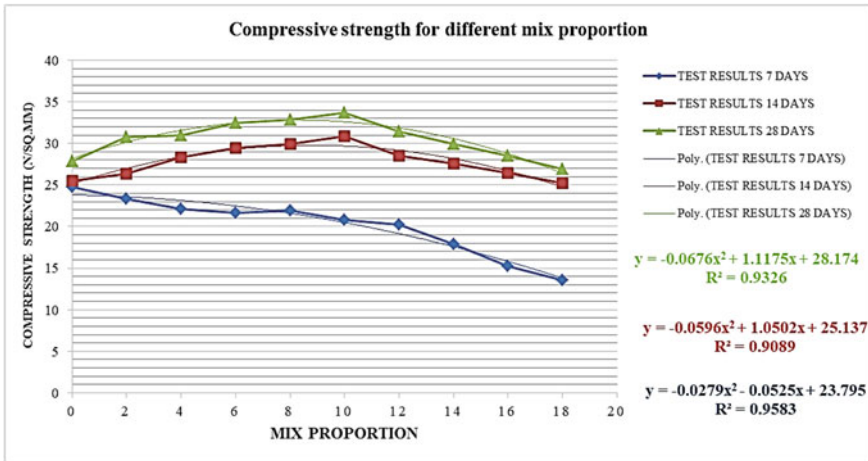
Fig. 1 Graph representing compressive strength for different mix proportion with only replacement of WFS

Table 8 Compressive strength for M20 grade of concrete mix with 6% of WFS and different percentage of CBA

SR.NO.	Mix proportion	Test results (N/mm^2)		
		7 days	14 days	28 days
1.	B0	24.73	25.47	27.85
2.	C2	23.3	26.36	30.8
3.	C4	22.1	28.29	31
4.	C6	21.62	29.42	32.47
5.	C8	21.9	29.88	32.81
6.	C10	20.8	30.85	33.67
7.	C12	20.27	28.47	31.4
8.	C14	17.86	27.6	29.88
9.	C16	15.2	26.4	28.5
10.	C18	13.59	25.2	26.89

Figure 1 shows the relationship of compressive strength with mix proportions when replaced by WFS only (Table 8).

The equation showing the relationships between compressive strength, and mix proportions together with the coefficients of determination R2 derived is given in Figs. 1 and 2. Higher value of coefficient of determination indicates good relevance between the data points and curve.
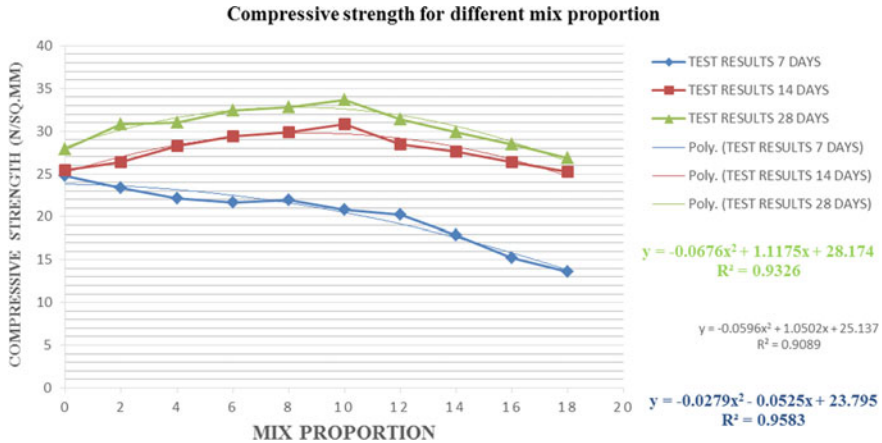
Fig. 2 Graph representing compressive strength for different mix proportion with replacement of WFS and CBA

5 Discussion

Specific gravity of CBA is lower than the normal range of cement, i.e., 3.15 and WFS are very much in range of 2.63–2.67 that indicate the strength of concrete will be good. Water absorption of WFS is at greater extent to its limits which resembles the workability of concrete will be reduced by using WFS. As low-density aggregates have relatively high absorption capacity, a careful mix proportion has to be chosen for such type of sand. Dry Density of CBA and WFS is lower than its permissible limits, i.e., up to 1.44 kg/lit for cement and 1.6 kg/lit for sand which shows that the weight of concrete can be reduced and can also affect the elastic modulus which can be tested and verified. OMC and MDD of WFS are just within its permissible limits.

Fineness of CBA is not in permissible limit, and it indicates the size limits for ash as granular base material. As the fineness was not in limits so material has to be processed before use and hence CBA was crushed. After crushing, the processed CBA was again tested. Fineness of processed CBA is within its permissible limits, and hence, it can be replaced by cement after processing. Fineness modulus of sand range from 2.0 to 4.0 and hence fineness modulus of WFS is within range. Bulking of WFS is within its permissible limits as the grain size is larger. It is observed that pH of CBA and WFS is within its permissible limits and is in contrast to cement which is alkaline. This indicates that the concrete will behave as neutral. Soluble chlorine of CBA and WFS is much within their permissible limit that denotes the concrete will resist the chemical attacks. Soluble Sulfate of CBA and WFS is also well within its permissible limits that indicate the concrete will resist the sulfate attacks.

Soundness of CBA was found to be 8% which is less than 10% which shows that the durability of concrete will be good.

More amount of silica in CBA and WFS will impart more strength to concrete but may prolong the setting time of cement. Sulfur and magnesia in CBA and WFS is very much less than the maximum limit.

It can be deduced that the 7, 14, and 28 days of compressive strength of the concrete increases gradually from 0 to 6% replacement of fine aggregate with waste foundry sand. Then, the compressive strength of concrete goes on decreasing but it is still more than the conventional concrete till 14% of replacement. The 7, 14, and 28 days o strength of the concrete at 6% replacement is 28.24, 30.22, and 34.50 N/mm^2 which is more than compared to that of conventional concrete. The compressive strength of concrete is less than the conventional concrete at 16% replacement of sand with WFS.

It can be deduced that the 14 and 28 days of compressive strength of the concrete with 6% waste foundry sand and up to 16% coal bottom ash increases gradually from 0 to 10% replacement of cement with CBA. Then, the compressive strength of concrete goes on decreasing but 28 days of strength is still more than the conventional concrete up to 16%. The 7-day strength of the concrete at all replacement is found to be less than conventional concrete.

6   Conclusion

The physical chemical and mechanical properties of CBA and WFS are estimated and studied in comparison with Cement and Sand.

- The results of CBA and WFS resemble within its permissible limit and thus these waste materials can be used as a substitute of cement and sand, respectively.
- As waste by-products from industries causes various environmental hazards. Uses of these in building materials would help in reduction of stresses on environment.
- Maximum compressive strength of concrete is obtained at 6% replacement of sand with WFS, and percentage increase is found to be 14.19, 18.64, and 23.87% at 7, 14, and 28 days, respectively.
- Optimum ratio of replacement of CBA with cement along with fixed 6% replacement of WFS with sand is obtained at 10% though CBA can be replaced till 16% as the compressive strength of concrete is more than conventional concrete.
- Maximum increase in strength of concrete is 21.12 and 20.89% than conventional concrete for placement of 6%WFS and 10% CBA at 14 and 28 days, respectively. The 7-day compressive strength of concrete decreases by 15.89% than conventional concrete which indicates that CBA delays the early rate of gain of strength though its long-term rate of gain is more.

Curing conditions can greatly affect the water absorption of concrete. As the concrete was exposed to air curing, it exhibited low water absorption. Also it can be interpreted that surface water absorption was higher than internal water absorption and does not depend on curing conditions. As a whole, surface water absorption can

be applied to predict some performance of concrete, including compressive strength, permeability, resistance to sulfate attack, and chloride ion diffusion.

Thus, the use of WFS and processed CBA is strongly recommended in concrete as the results are favorable as compared to conventional concrete and would eventually save the environment from land filling of these waste materials. Also its utilization will help the industry to follow the government norms of reusing the industry waste coal bottom ash.

References

1. Baig, A.M., Varghese, V.: Waste foundry sand as fine aggregate in concrete for resistance to sulfuric acid attack. In: IJERMCE, vol. 2, issue 3, pp. 269–273 (2017)
2. Siddique, R., de Schutter, G., Noumowe, A.: Effect of used-foundry sand on the mechanical properties of concrete. Constr. Build. Mater. **23**, 976–980 (2009)
3. Attar, I.M., Gupta, A.K.: Application of foundry sand in civil construction. IOSR J. Mech. Civil Eng. (IOSR-JMCE), 38–42, ISSN: 2278-1684
4. Kurama, H., Kaya, M.: Usage of coal combustion bottom ash in concrete mixture. Constr. Build. Mater. **22**, 1922–1928 (2008)
5. Ramzi, S.S., Mand, M.Z., Ali, N.: Physical and chemical properties of coal bottom ash (CBA) from Tanjung Bin Power Plant, IRIS, IOP Conference Series (2016)
6. Amritkar, S., Chandak, S.P., Jadhav, R.: Effect of waste foundry sand (WFS) on the mechanical properties of concrete with artificial sand as fine aggregate. In: IJERT, vol. 14. ISSN: 2278_0181 (2015)
7. Pathariya, C., Rana, K., Shah, A., Mehta, G., Patel, A.: Application of waste foundry sand for evolution of low-cost concrete. In: IJETT, vol. 4 (2013)
8. Singh, G., Siddique, R.: Effect of waste foundry sand (WFS) as partial replacement of sand on the strength, ultrasonic pulse velocity and permeability of concrete. Constr. Build. Mater. **26**, 416–422 (2012)
9. Olubajo, O., Osha, A., Nafaty, U., Adamu, H.: Effect of water-cement ratio on the mechanical properties of blended cement containing bottom ash and limestone. Civil and Environmental Research www.iiste.org. ISSN 2224-5790 (Paper) ISSN 2225-0514 (Online) vol. 6, no. 12 (2014)
10. Jaturapitakkul, C., Cheerarot, R.: Development of bottom ash as pozzolanic material. J. Mater. Civil Eng., 48–53 (2003)
11. IS 4031(part 2): 1996. Methods of physical tests on hydraulic cement, determination of fineness by dry sieving
12. IS 2386 (part 3): 1963. Methods of test for aggregates for concrete, specific gravity, density, voids, absorption and bulking
13. IS 9103: 1999. pH of Coal bottom ash and Waste foundry sand
14. Indian Bureau of Mines: Chemical tests
15. IS 383: 1970. Specification for coarse and fine aggregates from natural sources for concrete
16. IS 2185 (part1): 2005. Procedure of water absorption & initial surface absorption

Assessment of Biogas Production from Energy Crop Using Animal Manure as Co-substrate Through Portable Reactor

Harshal Warade, Ramesh Daryapurkar and P. B. Nagarnaik

Abstract The study is based on production of Biomethane by using Napier grass along with co-substrate as a cow dung. The lignocellulosic content in Napier species increases with development of the grass. The principal cut gives more Biomethane potential than the later cuts since water-dissolvable sugars are higher in previous case coming about higher methane potential. The parameters like pH, moisture content, total solids, volatile and fixed solids, chemical composition, TSS, and TDS were measured. An economical bioreactor having 35 L working volume was designed for evaluating the biogas potential of above substrates and was operated at ambient temperature range 20–32 °C. The outcomes revealed that there was a continuous reduction in pH level, i.e., up to 4.6 during initial fifteen days since beginning of slurry feeding. The average gas production of continuous mode biogas digester and Batch mode digester containing of slurry feed gave a result of 0.43 and 0.34 m^3/kg VS added, respectively, at an average temperature of 29.91 °C. The Napier grass test unit showed 88.38% VS removal during the studies and the chemical composition for the Yeshwant specie of Napier grass showed lignin, cellulose, hemicellulose, and ash content as 32.2, 35.9, 40.1, and 3.2%, respectively.

Keywords Biogas production · Napier grass · Co-substrate · Hydrolysis · Anaerobic digestion

H. Warade (✉)
Ph.D Scholar GHRCE, Nagpur, India
e-mail: harshalwarade@gmail.com

R. Daryapurkar
Lars Enviro Pvt. Ltd., Nagpur, India

P. B. Nagarnaik
G.H. Raisoni College Of Engineering, Nagpur, India

1   Introduction

Energy is a standout among the most vital elements to worldwide thriving. In the present energy requesting way of life, the requirement for investigating and abusing new wellsprings of energy which are inexhaustible, manageable, and also eco-friendly is unavoidable; accordingly, bioenergy has turned out to be as of late prominent. Grass biomethanation is a good source of biogas due to the organic matter present in it. Biomethanation, i.e., anaerobic digestion is the degradation of organic materials by microorganisms in the absence of oxygen [1, 2]. It is a multi-step biological process where the organic carbon is mainly converted to carbon dioxide and methane [3]. All biomass and agricultural wastes provide energy in different forms. Biomass having high energy yield per hectare is called as energy crop [4]. Napier grass commonly known as *Pennisetum purpureum* is a hybrid variety of Bajra, and its species are grown primarily for grazing. Napier grass improves soil fertility and protects arid land from soil erosion [5]. However, the remains of the Napier grass represent a category of surplus lignocellulosic biomass [6]. Napier grass has high composition of organic substances including carbohydrates, fats, and proteins which would be used in anaerobic fermentation process to adjust balance between foods and microorganism within the system [7, 8].

2   Characteristics of Napier Grass

It is a bury particular mixture of Bajra and consolidates high caliber and quicker development of Bajra with the profound root system. It is generally developed in sub-tropical locale of Asia, Africa, Southern Europe, and America [9]. Crossover Napier is better in quality than Napier grass and contains around 10.2% crude protein and 30.5% unrefined fiber [10]. It is triploid grass and consequently does not deliver any seed but rather it creates high number of tillers and various takes off [11]. The fast development of grass is up to 4 m tallness and has around 7-year life. Napier grass creates not very many seeds with high profitability up to 350 ton/hector around 7 harvest every year and is for the most part spread vegetatively through stem cuttings comprising of no less than 3 nodes, 2 of which are covered in columns (Table 1).

Cellulose, hemicellulose, and lignin are the three principle kinds of polymers that constitute lignocellulosic materials like grass [12]. Cellulose and hemicellulose are macromolecules comprising of the same or distinctive starch units. The chemical composition of grass changes as the plant develops, e.g., the lignin content begins expanding with plant development and developing season [13, 14].

In hydrolysis, cellulose is changed over into the simple sugar glucose [15]. Hydrolysis decides the scope of stacking and operational measures of the digester, as it holds a basic and rate restricting part in the anaerobic absorption of lignocellulosic substrate [16] (Fig. 1).

Table 1 Chemical composition of grass

Cellulose (%)	25–40
Hemicellulose	15–50
Lignin	10–30
Ash	1.5
C	49.93
N	2.05
K	1.51
Ca	1.91
Mg	0.26

Fig. 1 Continuous batch feed digester

3 Operational Procedure

3.1 Bio-digester Design

The bio-digester PVC tank having 35 L volume was used for the experiment. The digester was equipped with inlet and outlet ports for feeding and effluent discharge as shown in Fig. 2. The second digester has setup with batch feeding mode having various ratios of cow dung with Napier grass as shown in Fig. 3.

A plastic tube with 2-L. capacity bladder is connected to digester for gas collection The digester was maintained at mesophilic temperature range (30 ± 2 °C). All

Fig. 2 Batch feed Digester

Fig. 3 Cut pieces with cow dung slurry

perforations were properly sealed with rubber tubes and adhesives to make the whole bio-digester system airtight.

3.2 Material Preparation

3.2.1 Cultivation and Harvesting of Napier Grass

Toward the start of development clearing of the shrubberies, evacuation of thistles, weeds, and so on must be finished. Hybrid Napier requires a deep, careful, weed-free, and conservative seed bed. One plate furrowing might be trailed by a few fork ploughing, leveling, and evacuation of clods [17]. Planting is finished with the beginning of monsoon or whenever, if irrigation facility is accessible [18]. Being a

sterile hybrid, the grass is planted by established slips or by stem cuttings. Cuttings with 2 hubs from the center segment of modestly developed stems (3–4 months old) are favored. The principal cut gathering is taken from 60 to 75 days after planting. Resulting cuts are taken following 30–45 days or when the plants achieve a tallness of 1½ m.

3.2.2 Materials

The following materials were used for the purpose of this hydrolysis work: plastic bucket bio-digester, weighing balance, pH meter, connecting tubes, measuring bladders, plastic jar for silaging, and fresh cow dung.

3.2.3 Chemical Characterization

Slag, lignin, cellulose, and hemicellulose substance of biomass were dictated by taking four examples of air-dried grass 0.7 g each were overflowed with 5 mL of 72% w/w H_2SO_4 answer for 4.5 h keeping in mind the end goal to hydrolyze the cellulose and hemicellulose. The suspension staying after the above treatment was filtered through a cauldron and the strong deposit dried at 105 °C for 24 h and measured (W1). The deposit was then exchanged to a pre-measured dry porcelain cauldron and warmed at 600 °C for 5 h. After cooling down, it was measured (W2) and cinder content (%) was resolved. Corrosive insoluble lignin was then figured by the difference (W1–W2). The filtrate from the H_2SO_4 treatment that contained the sugars discharged from cellulose and hemicellulose was altogether blended and homogenized. Glucose (C1) and lessening sugar (C2) fixations in the filtrate were resolved by a glucose oxidase–peroxidase test unit (Biosis TM, Athens, Greece) and the DNS technique (Miller 1959), individually.

3.3 Analytical Methodology

3.3.1 Substrate Ratio and Preparation

The first growth harvested Napier grass used for this study was collected from nearby educational institute farm. Average height of grass is 250 cm. The cow dung was procured from cattle of same institute. For the hydrolysis process, fresh grass was cut into 4-mm to 8-mm pieces. The ratio decided on the basis of volume of digester. Cut pieces were thoroughly mixed in a cow dung: water slurry made in a ratio of 0.5:0.5 kg in a separate bucket as shown in Fig. 4.

The slurry (1 L. Volume) in the bucket is fed daily in bio-digester. This enabled the reactor to operate under anaerobic conditions. Manual mixing was ensured daily

Fig. 4 Silaging of grass

for effective degradation of organic matter in reactor. The bladders were made flat to ensure no air remains inside prior to biogas collection for measurement.

The routine parameters were analyzed continuously every day. Moisture content, total solids, volatile solids, fixed solids, pH, TSS, and TDS were measured. Chemical characterization like lignin, cellulose, and hemicellulose content was done intermittently with standard methods.

For another observation, Napier grass was silaged in 5.20-L airtight jar having height 27 and 15.5 cm diameter. Cut pieces of grass were ensiled in cylindrical jar with compaction and manual pressure as shown in Fig. 4. Which shows effect of silaging on ensiling characteristics and nutritive value of Napier grass.

4 Results and Discussion

4.1 Silage Position of Napier Grass

The dry matter content was very low due to lowest temperature at harvesting and cutting in cold season. After 80 days of airtight storage, the grass volume reduce from 5.20 to 1.793 L.

Fig. 5 pH variations
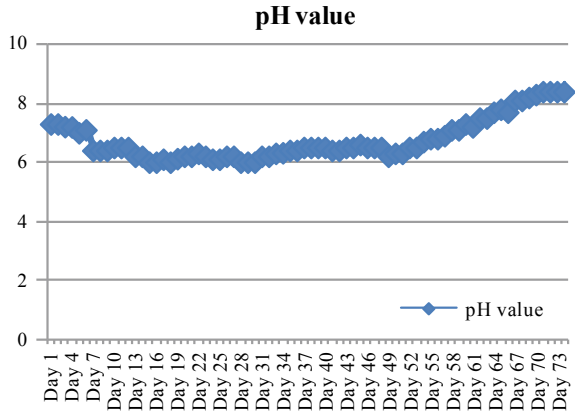
4.2 Analysis of Grass Characteristics

The sample of Napier grass species Yeshwant (RBN-9) was analyzed by mentioned methods.

4.3 Evolution of Parameters

The results of the experiment carried out for the 40 days indicated that blending of Napier grass with cow dung affected the biogas yield. The temporal variations in pH, volatile solids, and fixed solids are presented.

The pH is regarded as the key indicator of operational stability. Above graph shows the pH of initial days 6.5–7.3 which is suitable of microorganism (Fig. 5). Due to VFAs production of acidogenic bacteria during the start up phase as well carbonic acid associated with the high concentration of carbon dioxide gas, pH values of reactor were decreased up to 6. It was again increased since the protein-containing hard biodegradable fraction began to hydrolyze after some days of the beginning of the digestion process [19] (Fig. 6).

The above graph shows the moisture content and solids variations in grass. A known value of 4-, 6-, and 8-mm cut pieces were analyzed at initial cut level (Fig. 7).

The above graph shows the moisture content and solids variations on grass after silaging about 10 days. A known value of 4-, 6-, and 8-mm cut pieces were analyzed, whereas moisture content slightly decrease up to 5–7%. Same difference was found in remaining solids also (Fig. 8).

The above graphical comparison shows the biogas production in batch scale (1:1) and continuous mode digester.

The horizontal axis depicts the number of readings taken randomly, and the vertical axis denotes the average biogas production in both batch scale (1:1) and continuous

Fig. 6 Variation in solid
content (during cut)
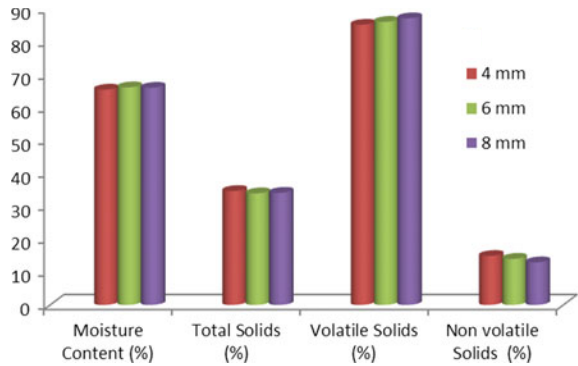
Fig. 7 Variation in solid
content (after 10 days)
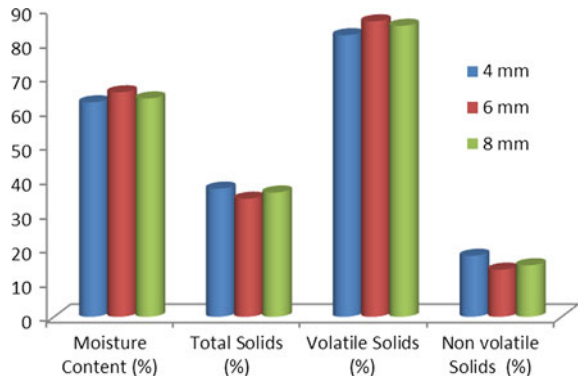
Fig. 8 Comparison of
biogas produce (m^3/kg) in
different digester
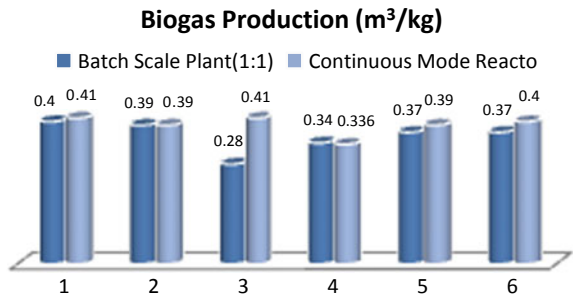
mode digesters in m^3/kg simultaneously. On an average considering the corresponding readings taken, the results can be evaluated as the average biogas production found in batch scale digester (1:1) is comparatively little greater than that of continuous mode digester.

5   Conclusion

Considering the overall results of anaerobic digestion of Napier grass with animal manure could be enhanced significantly. The amount of average gas production in batch scale digester unit of ratio 1:1 is calculated to be 0.34 m^3/kg VS and average gas produced in continuous mode digester unit arrived as 0.44 m^3/kg VS. In the batch scale digester unit of ratio 1:1, the resulting inlet slurry's VS was found to be 83.12%, that of outlet slurry was 75.85% and the final VS reduction can be estimated as 7.3%. Production of biogas from Napier grass seen best approach to agricultural and bioenergy sector.

References

1. Smyth, B.M., Smyth, H.: Can grass biomethane be an economically viable biofuel for the farmer and the consumer. Published Online In Wiley Interscience 10.1002/Bbb.238 (2010)
2. Jha, A.K., et al.: Comparison Between wet and dry anaerobic digestion of cow dung under mesophilic and thermophilic conditions. Adv. Water Resour. Prot **1**(2), 29–38 (2002)
3. Ganiyu, O.T., Oloke, J.K.: Effects of Organic Nitrogen and Carbon Supplementation on Biomethanation of Rice Bran. Fountain J. Nat. Appl. Sci. 25–30 (2012)
4. Ahn, H.K., Smith, M.C.: Biogas production potential from switch grass-animal manure mixture using dry anaerobic digestion. J. Environ. Manage. **50**(1), 5–25 (2008)
5. Riordan, K.O., McEniry, J.: Grass for biogas production—anaerobic methane production from five common grassland species at sequential stages of maturity. Int. J. Environ. Sci **1**, 383–388 (2013)
6. Rekha, B.N., Aniruddha, B.P.: Performance enhancement of batch anaerobic digestion of Napier grass by alkali pre-treatment. Int. J. Chem. Tech. Res. **5**(2), 558–564 (2013)
7. Xie, S.: Evaluation of biogas production from anaerobic digestion of pig manure and grass silage. National University of Ireland (2012)
8. Vogel, T., Ahlhaus, M., Barz, M.: Optimisation of biogas production from grass by dry-wet Fermentation. Jelgava (2009)
9. Uzodinma, E.O., Ofoefule, A.U.: Biogas production from blends of field grass (panicum maximum) with some animal wastes (2009)
10. Prabhudessai, V., Ganguly, A.: Biochemical methane potential of agro wastes. Hindawi Publishing Corporation J. Energy. **1**, Article ID 350731, 7 p (2013)
11. Mallick, J., Narayana, K.L., Khuntia, S., Singh, D., Barik, R.: Biogas generation from leafy biomass and vegetable wastes by application of ultrasound. In: Institute of Minerals and Materials Technology (CSIR) Bhubaneswar, Orissa
12. Perez, J., Munoz-Dorado, J., De-la-Rubia, T., Martınez, J.: Biodegradation and biological treatments of cellulose, hemicellulose and lignin: an overview. Int. Microbiol. **5**(2), 53–63 (2002)
13. Carpita, N.C.: Structure and biogenesis of the cell walls of grasses. Annu. Rev. Plant Physiol. Plant Mol. Biol **47**(1), 445–476 (1996)
14. Esposito, Giovanni, et al.: Bio-methane potential tests to measure the biogas production from the digestion and co-digestion of complex organic substrates. Open Environ. Eng. J. **5**, 1–8 (2012)
15. Murphy, J.D., McCarthy, K.: Ethanol production from energy crops and wastes for use as a transport fuel in Ireland. Appl. Energy **82**(2), 148–166 (2005)
16. Lynd, L.R., Weimer, P.J., van Zyl, W.H., Pretorius, I.S.: Microbial cellulose utilization: fundamentals and biotechnology. Microbiol. Mol. Biol. Rev. **66**(4), 506–577 (2002)

17. Ranade, D.R., Nagarwala, N.N., Dudhbhate, J.A., Gadare, R.V., Godbole, S.H.: Production of biogas at different total solid content in cattle dung. Indian J. Environ. Health **32**(1), 63–65 (1990)
18. Hobson, P.N., Bousfield, S., Summers, R.: Methane Production From Agricultural And Domestic Waste, pp. 181–217, Applied Science Publication Ltd., Microbiology Department, Rowett Research Institute UK
19. Nijami, A.S., Korres, N.E., Murphy, J.D.: Review of the integrated process for the production of grass biomethane. Environ. Sci. Technol. (2009)

Land Use/Land Cover Change Analysis of Doon Valley Using ArcGIS Tools

Nitin Mishra, Sanjeev Kumar and Bhaskar R. Nikam

Abstract One of the main starling issues for the country is the quick progress of urbanization. The stakeholders should take this factor in interest for the efficient and intensified urban improvement of the nation. Distinctive variations have been observed in land use/land cover due to the significant preferment of the urban sector. Land cover is a physical substance at the surface of the earth. In recent years, the employment of remotely sensed data and geographical information system (GIS) has been broadly adopted for the consequence of spatial data technologies. The present study aimed to investigate and examine the urban growth and extension in association with land use/land cover of Doon Valley, Uttrakhand, India, using IRS satellite data for the period of 20 years (1995, 2005, and 2015). The three satellite images of 1995–2015, path row 146/39, were procured from the USGS domain. The ISO cluster unsupervised classification method has been opted to classify the satellite images. The several bands pertaining to multiple land use were distinguished from remotely sensed data through GIS platform. After the processing of the data set, the analysis results that there is a radical hike in the urban area, agriculture, and barren land, but the green cover and water bodies within the study area are reduced.

Keywords Urban · Land use/land cover · Change detection · Remote sensing · Geographical information system

1 Introduction

The land is the most pressing common resource as all the activities are assigned to it. The intensive hike in the population and human exercises is not limited to concerns with regard to the land as a resource [1–3]. The agribusiness, woodland,

N. Mishra (✉) · S. Kumar
Graphic Era (Deemed to Be University), Dehradun 248001, India
e-mail: nitinuag@gmail.com

B. R. Nikam
Indian Institute of Remote Sensing, Dehradun 248001, India

urban, and modern area employment can be the indebtedness of the assets [4–6]. The variations in the usage of land are quite critical, and it is demanding that the proper sequencing, controlling and to the scheduling of the land as a resource, with respect to utilization is the present and future need [6–8]. Most of the lands are now operated and administered at discrete magnitudes, depending on its habit and the demand of the man. The world as a whole should have satisfactory knowledge over its resources, especially natural. This knowledge demands integral aspects of its exercises for better judgment. The swift hike of the population in the civic areas has concluded as the primary change for the region's land use/land cover. Furthermore, it busted to the worsening of the urban habitat. Therefore, environmental researchers with immense zest have considered the land use/land cover alterations as a chief assignment to interpret. Subsequently, measuring and distinguishing the magnitude and spatial dispersion of land use/land cover alteration furnishes a detracting attention to the critique of environmental modifications at discrete computations, and this variety of evaluation presents a decent medium to amplify the work rate of land cover and area change and to settle inconsistent socio-environmental fallout labeled with land use/land cover.

Urbanization is a vital element of the up-to-date world, but it is also playing a sideways influence of economic growth of any country. In India, being a developing country, urbanization makes a major contribution to its economic growth. In India, all the towns and cities have developed at a slow rate during the nineteenth and the twentieth centuries. Urbanization is rated as an inexorable process due to rapidly growing population and economic expansion [9, 10]. Encroachment into metropolitan principalities endowed on agricultural lands may confer ruinous impressions, dreadful forms, and desertification of land [11]. The brisk extension of the population in the new years is implied to ascertain essentially around metropolitan and new cities.

Land cover proffers weight in detail to its characteristics and exhibits several basics in global facade concealed with the conventional structure. Remote sensing classification method has its attribute of dividing whatever applied or not applied, masking the objects on the surface. Restoration exercises that human opts various biological and technological measures to manage and administer the land timely relying on economic and social constraints which have made land use to affirm further on land's characteristics with respect to the social environment. Hence, land employment is affirmed as a manner of transfiguring communal ecology into natural ecology [12].

For reliable and effective socio-economic functioning and devising, the knowledge of land use/land cover is a must. The knowledge engulfed about land use/land cover allows an evaluated understanding of the land usage and its attitude toward cropping patterns, fallow lands, forest, wastelands, and surface water bodies, by virtue of which detailed and efficient planning is possible [13, 14]. One such research was initiated, with an objective to process and value the use of various satellite data to signify built-up area progress in urban regions of Udupi Taluk. The research was based on variations of the region for about ten years (2000–2010) by using geoinformation technology. The effort was made for the analysis of change in land cover classes for

urbanization development which effects temperature variations. The results of the study reveal that there is a remarkable change in agricultural and cultivable lands mainly due to the interchange of cultivable land into a residential area. The analysis also revealed that the residential land was increased by almost 320 sq.km, and due to increase in built-up area and other urban development activities, there is a rise in temperature over several regions confined in the study area [15].

A study was conducted, questioning the rapid population growth and anthropogenic activities to determine and identify variations in land use/land cover for a period of 15 years (1990–2005), specifically in forest regions. The object was to restrain Mahananda Catchment's forest from degeneration and deforestation. From the map application of multispectral remotely sensed data (TM and Etm+), and MAXLIK and MINPAR, and use of automated classification technique, i.e., supervised classification as well as change detection techniques, the study was able to mark and outline the alterations in several varieties of forests. The study was able to find out that there is an undulating shift in forest cover as the stretch comprising obtuse forests diminished from 58 to 33% from 1990 to 2000, respectively, but somehow raised in 2005 from 33 to 39% [16].

2 Materials and Methods

2.1 Study Area

Doon Valley, a unique micro-geomorphic unit, is engulfed in the north by lesser Himalaya and in the south by Shiwalik, in the northwest by River Yamuna and in the southeast by River Ganga. The co-ordinates lie between latitudes 29°55′ and 38°30′ N and longitudes 77° 35′ and 78°28′ E, masking an area of 3070.99 sq.km. Its elevation ranges from 315 to 2500 m, while the gradient varies between 7 and 10 m/km. This synclinal formation receives 210 cm annual rainfalls, and annual temperature in summer season varies between 38 and 41 °C, while the winter temperature varies between 15 and 50 °C.

As per the Census report, the population of Dehradun in 2016 is 655,356. The figure of the professional population in Dehradun city is 463,791, which comprises 251,832 males and 211,959 females. The ordinary literacy rate of Dehradun city is 89.32%, in which male literacy rates is 92.65 and female literacy rate is 85.66 percent, sequentially. The study area comprises of alluvium parent matter derived from lesser Himalayas and comprises of sedimentary and meta-sedimentary rocks. The area is composed of gravels, pebbles, cobbles, and boulders, mainly of quartzite with fine sandy and silt matrix and also fragments of shale, slate, limestone, sandstone, etc. (Fig. 1).
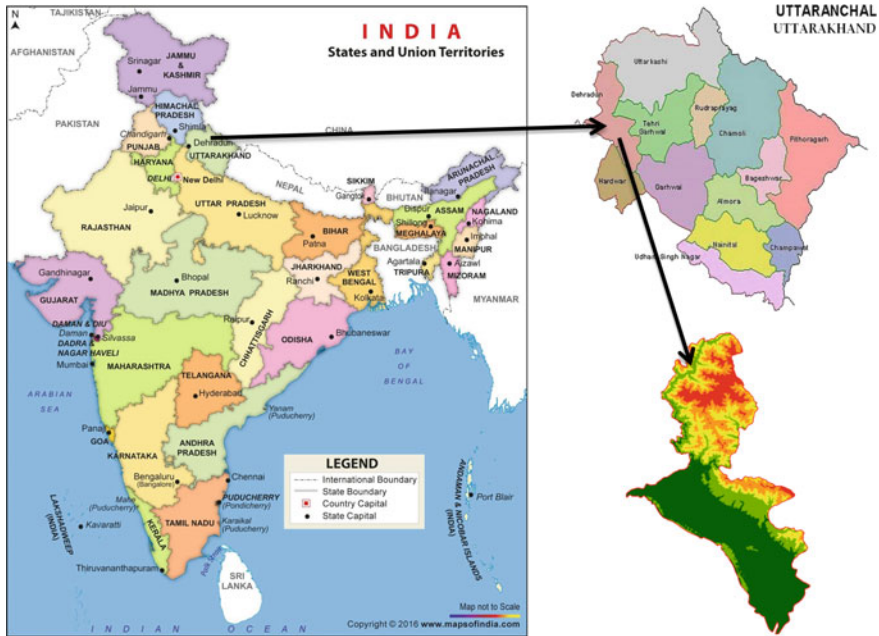
Fig. 1 Study area showing Doon Valley

2.2 Land Use Classification

The two basic operations have been derived for land use classifications, namely unsupervised and supervised classification techniques. Land use classification by their relative spectral agreement may be done through an unsupervised approach or via a supervised approach depending upon agreement of the asset of already defined classes which are delineated spectrally. In the current study, an unsupervised method of classification is adopted, also called live classification. This approach of classification gives an accurate and precise classified image. The land use/cover map was procured through the satellite images of the years 2000, 2005, and 2015 and processed them in ERDAS IMAGINE (version 9.2). The resolution of digital land cover classification is to have a significant information class value that will be able to grade and examine the landscape accurately. Land cover is a term which attributes to the cover in addition to vegetation, urban development, water, barren land, etc. Land cover is a basic and crude element that influences directly socio-environmental relationships. Therefore, land cover is mainly altered by human interventions and exercises when compared to natural activities. For the present-time scenario, the most influencing factor for land use/land cover change is drastic population hike which resolves into different factors such as agriculture inflation, exploitation of forest as a resource, and nevertheless, advancement in urbanization. Simultaneously, such modifications may have out-and-out outcomes on the catchment of study area reason being varying

Fig. 2 DEM of the study area
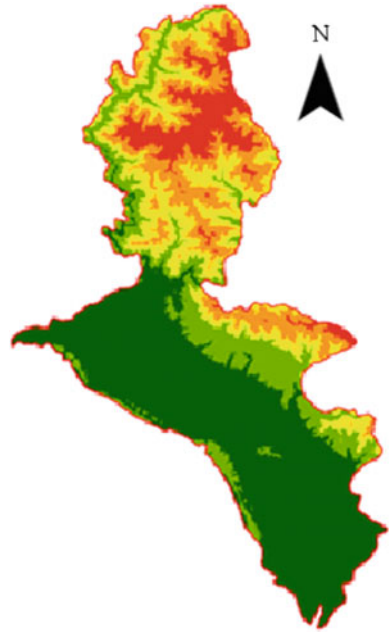
hydrological procedures which include infiltration, groundwater recharge, etc. For efficient and effective socio-economic growth and sustainable environment, land use variation should be taken up as a factor, and it should be prioritized by stakeholders and country planners.

2.3 Preparation of DEM

The digital elevation model (DEM) for the Doon Valley was taken up with the help of ArcGIS software, version 10.3, using elevation data of 30-m interval of the study area, as shown in Fig. 2. The interpolation zone between two contours is represented by different colored region. The accuracy attained is the function of current topography of contours and resolution. Interval was found to be satisfactory when a resolution of 30 × 30 m was opted for DEM preparation. A lot of information regarding the morphology of land via algorithms in raster processing systems can be derived by application of DEM and neighborhood procedures. One can generate flow direction, drainage network, slope aspect, and drainage density map and contour map with the help of information that DEM provides. The variation in elevation can be represented with the help of slope map, as shown in Fig. 3.

Fig. 3 Slope map of the
study area
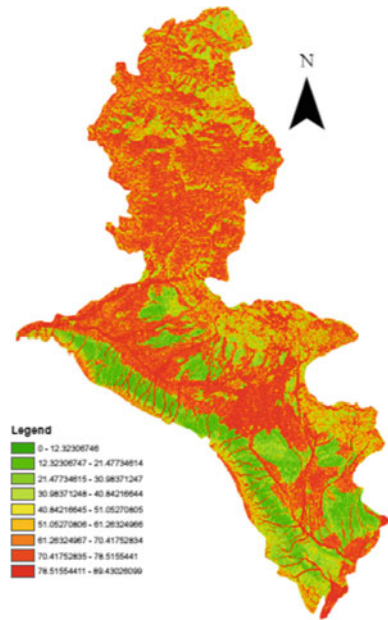
Table 1 Details of data
acquired

S. no.	Date of acquisition	Data	Resolution (m)
1	9th September 1995	Land sat data	30
2	21st September 2005	Land sat data	30
3	7th April 2015	Land sat data	30

3 Results and Discussions

The satellite images corresponding to the path and row 146/39 for different years were
taken and processed, as listed in Table 1 with their data procurement and resolution
for study. Classified images are shown below:

To dilute concerns regarding loss of ecosystems, biodiversity, environmental dete-
rioration, the decline in agricultural lands, reduced water bodies, wildlife environ-
ment, and information about the land use/land cover elements is the clear explication
[17, 18]. The current study area, Doon Valley, has Dehradun city in between the study
area limit, which is one of the fast advancing and progressing cities in North India.
During the past few decades, the city has captivated a commendable rise in popu-
lation, economic development, and industrialization. On the basis of land use/land
cover basics, the study area has been classified into five classes which constitute

Table 2 Land use/land cover statistics of Doon Valley (in sq. km)

Class	1995		2005		2015	
	Area (%)	Area (km^2)	Area (%)	Area (km^2)	Area (%)	Area (km^2)
Urban	16.59	509.51	22.60	694.01	39.25	1205.37
Water	5.12	157.23	4.02	123.45	1.69	52.01
Vegetation	12.82	393.77	10.54	323.77	8.90	273.34
Agriculture	43.14	1324.88	41.53	1275.43	33.12	1016.98
Barren land	22.33	685.59	21.31	654.33	17.04	523.29

urban area, water bodies, vegetation, agriculture land, and barren land, as shown in Fig. 4a, b, c. This has been done with the help of remote sensing imagery and actual study area statuses. The study area is about 3070.99 km^2, and the time period was taken as 20 years (1995–2015). The analytical evaluations of land use/land cover variations are given in Table 2 below. It is evident from Table 2 that mainly urban class has changed over the two decades.

Correlating the land use/land cover in 1995, 2005, and 2015 opted from satellite imagery interpretation signifies that urban area, consisting human habitation advanced for non-agricultural applications such as building, transport, recreation, etc., hiked from 16.59 to 39.25%, i.e., urban area has increased from 509.51 to 1205.37 km^2. This is because the study area during the study period had undergone a population increase which directly resulted in urban advancement and industrialization. When taking into consideration the agriculture land for the study period, the change in this very class is from 43.14 to 33.12%, i.e., agriculture sector has decreased from 1324.88 to 1016.98 km^2, as some parts of agriculture and vegetation have been settled into urban development exercises. Furthermore, the study area experienced significant variation in water bodies and vegetation cover. The water bodies have decided from 5.12 to 1.69%, i.e., the area under water body has decreased from 157.23 to 52.01 km^2. Also, vegetative cover has been declined approximately from 12.82 to 8.90%, i.e., vegetative cover has decreased from 393.77 to 273.34 km^2. This is mainly attributed to human involvement and settlements along the region.

We wish that this work can bring attention to the present scenario of Doon Valley with respect to land use/land cover variations and assist the up-gradation of concern that consequently symbolizes the pressure of the land resource. By selecting fundamental administration techniques with appropriate application of knowledge, a lot could be accomplished to organize the land resource, and sustainable environment will be the outcome.
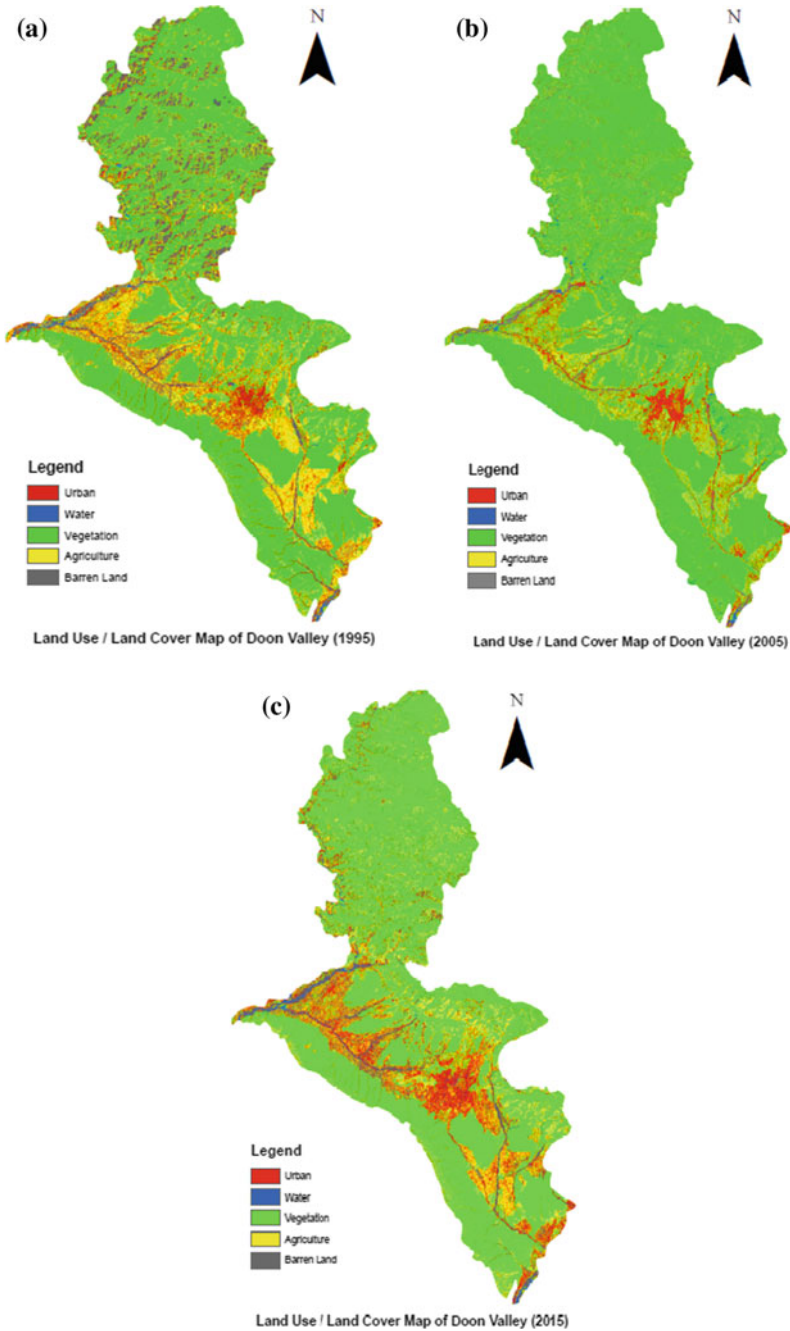
Fig. 4 **a**. Land use/land cover map for 1995 of the study area **b**. Land use/land cover map for 2005 of the study area **c**. Land use/land cover map for 2015 of the study area

4 Conclusion

The results of the present study stand as scientific symbolization and also the source of knowledge for accomplice operating for the planning of supportive and embellished land use/land cover management operations. Although the land use/land cover as a subject is in its prior stages when compared to other resource studies, it is suggested that land use/land cover study should be taken throughout for useful, elevated, and embellished functioning of socio-environment constituents. The deviations in land use/land cover necessitate the adoption of technical management modes. The need for administering and controlling of these management procedures will lower the rate of the effect of unusual population growth and rapid industrialization.

References

1. Frimpong, A.: Application of Remote Sensing and GIS for Forest Cover Change Detection, Kwame Nkrumah University of Science and Technology (Knust) Kumasi, Ghana (2011)
2. Bhandari, A., Bela, N., Mishra, N., Gupta, S.: Change Detection of Land use Land Cover using GIS & Remote Sensing for Doon Valley, SRG Int. J. Civil Eng. (SSRG-IJCE). **3**(7), 77–78 (2016) (36)
3. Chaudhary, B.S., et al.: Human induced land use/land cover changes in northern part of Gurgaon district, Haryana, India: natural resources census concept. J. Hum. Ecol. **23**(3), 243–252 (2008)
4. Dunno, R.M.W., Glenn, A.: Riparian vegetation mapping and hopi indian reservation, Arizona image processing techniques. Photogram. Eng. 8r Remote Sens. 179–186 (2001)
5. Gautam, N.C., Narayanan, E.R.: Satellite remote sensing techniques for natural resources survey, In: Singh, L.R., Singh, S., Tiwari, R.C, Srivastava, R.P. (eds.) Environmental Management, Allahabad geophysical society, 177–181 (1983)
6. Harish, N., Rao, K.C., Venkateswarlu, K., Reddy, B.G., Siddiq, M.A., Rajarajeswari, P., Sai, M.K.: Land use land cover change mapping using remote sensing and gis: a case study of Gudur Mandal, SPSR Nellore District, Andhra Pradesh. Int. Res. J. Eng. Technol. (IRJET). **03**(02) (2016)
7. Mallupattu, P.K., Reddy, J., Reddy, S.: Analysis of land use/land cover changes using remote sensing data and GIS at an Urban area. Tirupati India Sci. World J. Article ID 268623 (2013)
8. Nishkalank, R.A.R., Gurugnanam, B., Land use and land cover change detection using remote sensing. SSRG Int. J. Geo Inform. Geol. Sci. (SSRG-IJGGS). **1**(2) (2014)
9. Farooq, S., Ahmad, S.: Urban sprawl development around Aligarh city: a study aided satellite remote sensing and GIS. J. Indian Soc. Remote Sens. **36**, 77–78 (2008)
10. Mishra, N., Khare, D., Shukla, R., Singh, L., Change detection of land use/land cover in upper Ganga canal command. India using Arc-GIS tools J. Remote Sens. GIS. **36**, 77–78 (2013), ISSN: 2230-7990
11. Shalaby, A., Aboel Ghar, M., Tateishi, R.: Desertification impact assessment in Egypt using low resolution satellite data and GIS. Int. J. Environ. Stud. **61**(4), 375–384 (2004)
12. Swapan, K.D., Rajiv K.N.: Land use/cover classification—an introduction review and comparison. Global J. Res. Eng. **12**(1) (2012)
13. Suneela, T., Mamatha, G.: Detection of land use and land cover changes using remote sensing and geographical information system (Gis) techniques. Int. J. Electr. Electron. Data Commun. **4**(12) (2016)
14. Sreenivasulu, V., Bhaskar, P.U., et al.: Change detection in landuse and landcover using remote sensing and gis techniques. Int. J. Eng. Sci. Technol. **2**(12), 7758–7762 (2010). (2007)

15. Usha, N., Thukaram, M., Mohandas, C., Naveenchandra, B.: Urbanization study with land use/land cover change detection for the environmental impact on climate change using remote sensing and GIS technology (A case study of Udupi Taluk, Karnataka State, India). Int. J. Geoinf. (2014)
16. Kiran, V.S.S.: Change detection in landuse/landcover using remote sensing and G.I.S techniques: a case study of Mahananda catchment. West Bengal. Int. J. Res. Manage. Stud. (IJRMS). **2**(2) (2013)
17. Lin, Y.P., Hongb, N.M., Wu, P.J., Wu, C.F., Verburg, P.H.: Impacts of land use change scenarios on hydrology and land use patterns in the Wu-Tu watershed in Northern Taiwan. Landscape Urban Plann. 111–126 (2007)
18. Shrestha, D.P., Zinck, J.A.: Land use classification in mountainous areas integration of image processing degital elevation data and field knowledge. Int. Inst. Aerosp. Surv. Earth. **3** (2001)

Change Detection of Land Use/Land Cover of Sardar Sorovar Command Area, India, Using Arc-Gis Tools

Shahid Shuja Shafai, Nitin Mishra, Sanjeev Kumar and Murari Kumar

Abstract The accelerated advancement of urbanization in India is one of the prime alarming concerns for the country. For the better and promising urban development of the nation, this cause is taken into consideration by the town planners. The relentless advancement of the urban sector has inferred in acute variations land use/land cover. Focus on the wide use of remotely sensed data and geographical information systems (GIS) has commenced along with the initiation of land use/land cover variations. The current study examines the built-up growth and headway in Sardar Sarovar Singh Command Area, Gujarat, utilizing data from IRS satellite for the years 1992, 2000, 2008 and 2016. The four satellite images of 15 April 1992 to 1 April 2016, path row 148/44, were acquired from the USGS website. The technique applied to classify the land use/land cover was unsupervised classification method. The several layers pertaining to various land uses recognized from remotely sensed data were adopted through GIS. After the review and analysis of the data, it is resolved that there is a rigorous hike in the urban division and the green cover within the study area extent is abbreviated.

Keywords Urban · Land use/land cover · Change detection · Remote sensing · Geographical information system

1 Introduction

The land is numerously lowering resource even though all the ecological activities are based on it. The agribusiness, woodland, urban and modern area employments are advancing due to the increment in the growth rate of population, thereby pressurizing the constrained land. To regularize the utilization of before-mentioned resources, it

S. S. Shafai (✉) · N. Mishra · S. Kumar
Graphic Era (Deemed to Be University), Dehradun 248001, India
e-mail: shahidshafai@gmail.com

M. Kumar
Lovely Professional University, Punjab 144411, India

should be obligatory that the erudition of the scale and variety of variations in the exertion of area resource should be appropriately sorted, consistently conducted [1]. Also, grading and acknowledging the severity and spatial configuration of land use/land cover is a significant undertone to the review of environmental modification at several extents. Furthermore, this sort of analysis identifies and offers to model a relevant tool and heightens the turnout of land cover and area applicability and to flinch the abrogating environmental and societal holdings. Land use intimates to man's employment and numerous pertinence that are conducted aground, for example, farming, industrialization, urbanization and so on. The land cover features to the material permanence, e.g. vegetation, water bodies, soil and diversity arising due to area variations. Even though land use can be figured out by taking the cover into reflection, however, both of the integrities land use and land cover are parallel in connection and are interchangeable [2]. In relation to land use/land change interpretation, it has been perceived that the superior and most controlling factor for land use/land cover transition is the accession of the population, which heads to urbanization.

For the modern world, urbanization plays a vital role as it dominates the economic growth and development of any country. India, being the fastest developing country in the world, it can be judged that the industrial extension in the country is affected by urbanization. However, fewer than one-third of the country's population dwell in urban stretches but these aggregate more than two-thirds of country's GDP. Furthermore, more than 85% of government revenues are accounted by the urban regions. In past two decades, changes over urbanization have been observed and are remarked as strange in the history. It has been seen that the built-up area in the country, considering all town and cities, has been on a slow hike all the way through the nineteenth and twentieth century. In the primitive times, the population stabilized along the river ledges, religious cores and agricultural centres, the object signifying the facile and elementary availability of water for various social and domestic uses. However, in the recent years, the metropolitan and new cities have mainly resolute the advancement in the population.

Therefore, there has held a shift in the trend of land use/land cover and thereby one of the considerations for landscape ecological plans is change detection. Change detection can be circumscribed with the help of planning landscape characteristics maps [3].

The land is remaking into a limited resource due to extensive agricultural and demographic exercises. Thus, knowledge of land use/land cover and credible upshots for their absolute distinction is indispensable to the assortment, devising and regulation of land use strategies to match the accreting demands for requisite human necessities and well-being cover modifications likewise involve the arrangement either linear or radical of typical habitats and their impact on the environment of the stretch. Therefore, a meticulous effort was made by [4], to generate land use/land cover classification plot for Hyderabad district. The research was done for a duration of six years (2013–2016) employing multi-temporal satellite imagery. The study region was incorporated into four groups, namely water bodies, built-up area, barren land and vegetation region. Through the study, it was resolved that the land

use/land cover alterations of the subject area are a consequence of both natural and socioeconomic components and their application by the man in time and space.

Farming practices, mechanical sand winning procedures and the allocation of land to recommended contractors encompassing the catchments boundary of the Owabi Dam, which is the study area. These practices have driven the forest cover and the lifespan of the dam vulnerable to peril. The purpose of this examination was to dissolve and identify the alteration of land cover target the forest cover in the study region, utilizing Geographic Information System (GIS) integrated methods and multi-temporal Remote Sensing (RS) data for a time interval of 22 years (1986–2007). The images were processed, and land use/land cover maps were recognized and acquired from inclusive eight classes, namely water, barren land, built-up area, wetlands, forest, croplands, high-density forest and grasslands, based on land use/land cover identification. The study resolved that the forest cover had dwindled to 39%. The analysis inferred that the reduction in the region was due to the human exercises and population growth rate within the catchment area [5].

2   Materials and Methods

2.1   Study Area

Narmada command (Gujarat state, India) has been divided into 13 homogenous agro-climatic zones, based upon important physical characteristics such as rainfall, land irritability class, groundwater quality and quantity and drainage condition (Operational Research Group, Narmada Project, 1981–1982), the present study area is one of these of Narmada project command, namely having geographical area of 295,700 ha out of which 70% land is cultivable, i.e. 206,990 ha is cultivable command area. Extending from 72°35′ to 73°20′E longitude and 22°40′–23°10′N latitude, it covers nine talukas of state within its boundaries, River Sabarmati and River Shedi serve as two hydraulic boundaries to this triangle-shaped basin on two sides. A lined canal runs along the third side (Fig. 1).

2.2   Land Use Classification

The association of abiotic and biotic components on the covering of the earth can also be expressed as land cover, and it is unique amidst the most significant possession of the framework of the earth. The land cover consolidates snow, water bodies, exposed soil, forests and grasslands. Land use comprises a built-up area, farming area, particular engagements county also called recreational land, wildlife zone, etc. Therefore, land use is related to the manly activities while the land cover related to natural and human prospectus like built-up area, farms, forest, lakes, etc. present
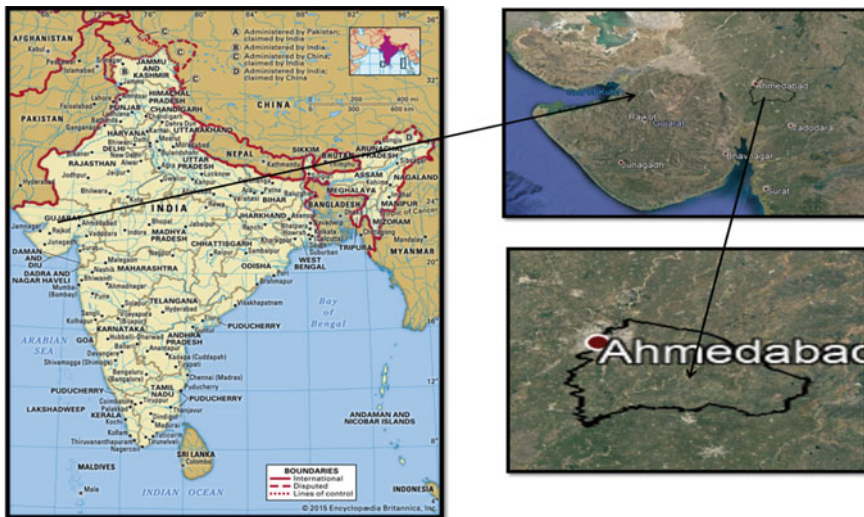
Fig. 1 Study area showing Sardar Sarovar command area region-V

on the face of the earth. Nowadays, the main exercises that constitute land cover changes are agriculture expansion, burning activities or fuel wood consumption, deforestation, some construction works and urbanization.

The satellite images of the year 1992, 2000, 2008 and 2016 were processed in ERDAS IMAGINE (version 9.2), which is powerful image processing software, and a land use/land cover map was adopted. The resolution of the digital land cover categorization is to have a significant data class content, which can estimate the landscape in an absolute manner [6]. Mainly land use classification is done in two methods, namely unsupervised and supervised classification. An unsupervised method is used when the group's cases have their relative spectral similarity, and the other method being supervised method of classification is centred on the relationship of the state to an asset of pre-fixed classes which have been distinguished spectrally. In this study, an unsupervised method of classification has been opted, which resulted in accurate and precise classification.

2.3 Preparation of DEM

The Digital Elevation Model (DEM) for the study area was generated by using ArcGIS software, as shown in Fig. 2. The elevation data used for generating DEM map were of the range of 30-m interval. The several coloured sections epitomize the zone of interpolation amid two contours, and the different colours describe diverse zones of interpolation. The recent topography of contours and resolution is the function of the accuracy of results obtained. 30×30 m resolution was taken for DEM generation,

Fig. 2 DEM of the study area
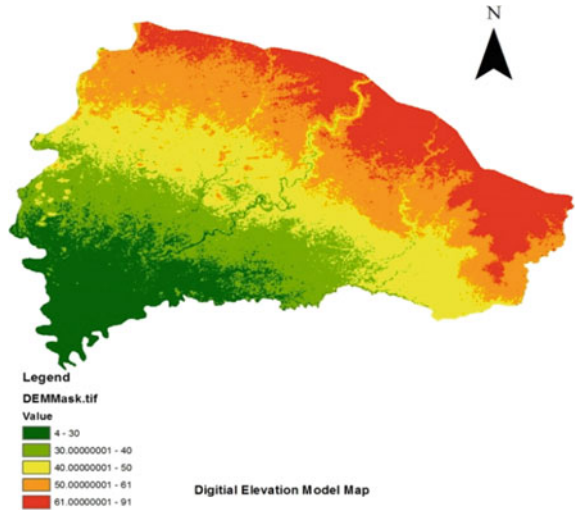
Fig. 3 Slope map of the study area
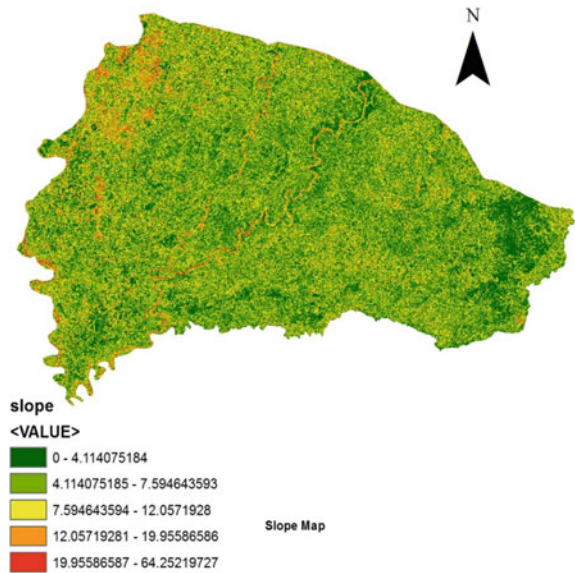
and the interval was found to be satisfactory. A mass of knowledge regarding the morphology of land surface by virtue of algorithms in raster processing operations can be selected using DEM and other side operations. The information it provides can be made useful to prepare flow direction, drainage network, slope aspect and drainage density map, contour map. Slope map indicates the change in elevation, as shown in Fig. 3.

3   Results and Discussions

The processed images of the path and row 148/44 for different years are used as listed in Table 1 with their data acquisition and resolution for study. Classified images are shown below:

In this era, it is desirable to have the knowledge of land use/land cover constituents prior hand, so that the issues related to loss of dynamic ecosystems, biodiversity, environmental degradation, fall of agricultural lands, reduced water bodies, etc. can be noticed, marked and eventually stopped. LU/LC changes involve rapid advancement in population as one of its prime and foremost cause [7, 8]. The current study area, Sardar Sarovar Command Area Region-V, has a part of Ahmadabad city engulfed within boundary limit, which is one of the rapidly growing and developing towns in the country as being the largest city of the country. As being the industrial hub and important economic element of the state, during the past few decades, the city has absorbed the significant hike in population, economic advancement and industrialization. Consequently, land use/land cover reckoning and analysis were executed to acquire the land use/land cover map for the study area by the arbitration of several data sets, remote sensing and GIS [9, 10]. With the help of remote sensing imagery and present study area statuses, we have divided the study area into five classes, namely, urban area, water bodies, vegetation, agriculture land and barren land, as shown in Fig. 4. The area to be examined for the analysis is approximately 2373.1 km^2, and land use/land cover alterations were analysed for a period of 24 years (1992–2016). Table 1 shows the statistics of land use/land cover shifts. It is manifest from Table 2, that the land use/land cover variations were principally in urban and agriculture class from 1992 to 2016.

Correlating the land use/land cover in 1992 and 2016 opted from satellite imagery interpretation signifies that urban area, consisting human habitation advanced for non-agricultural applications like building, transport, recreation, etc. hiked from 20.96 to 61.39%, i.e. urban area has increased from 496.72 to 1456.88 km^2. This is because the study area during the study period had undergone population increase which directly resulted in urban advancement and industrialization. When taking into consideration the agriculture land for the study period, the change in this very

Table 1 Detail of data acquired

S. no.	Date of acquisition	Data	Resolution (m)
1	14 April 1992	Land sat data	30
2	21 April 2000	Land sat data	30
3	27 April 2008	Land sat data	30
4	1 April 2016	Land sat data	30
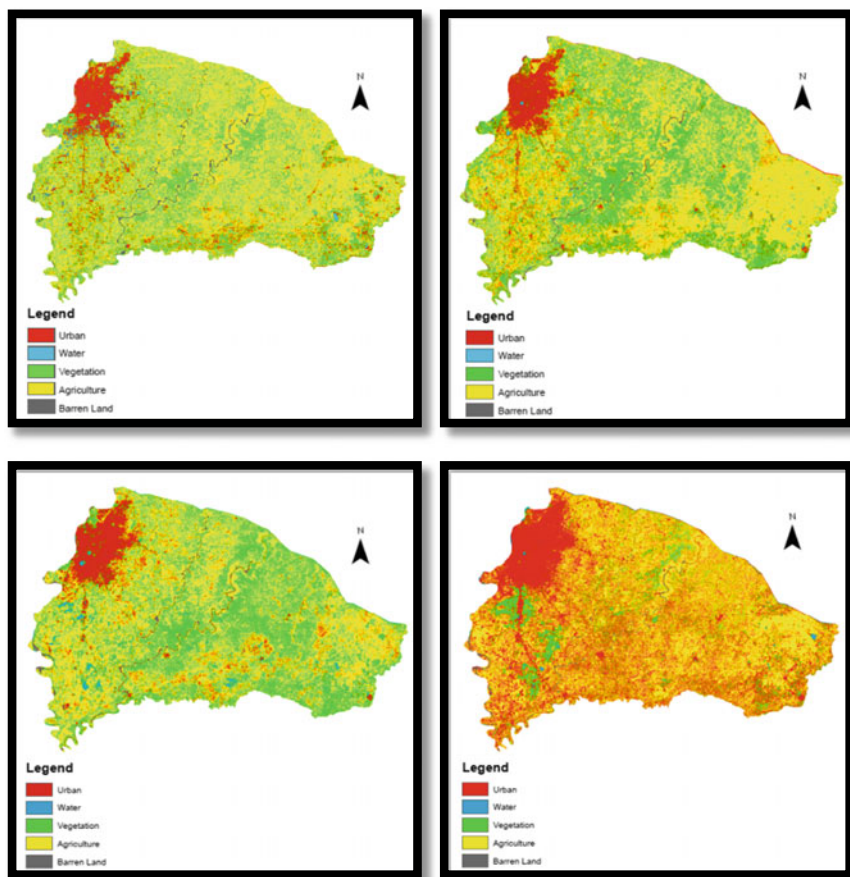
Fig. 4 Land use/land cover map of the study area

Table 2 Land use and land cover statistics of Sardar Sarovar Command area (in sq. km)

Class	1992		2000		2008		2016	
	Area (%)	Area (km^2)	Area (%)	Area (km^2)	Area (%)	Area (km^2)	Area (%)	Area (km^2)
Urban	20.93	496.72	22.47	533.31	53.47	1268.89	61.39	1456.88
Water	4.18	99.13	2.40	57.05	1.53	36.31	0.93	22.04
Vegetation	60.35	1432.08	62.19	1475.82	24.23	575.01	12.27	291.18
Agriculture	9.57	227.11	10.20	242.15	18.74	444.72	24.07	571.21
Barren land	4.97	118.05	2.73	64.76	2.03	48.17	1.34	31.79

class is from 9.57 to 24.07%, as it has increased from 227.11 to 571.21 km^2. This is due to the enhanced irrigation facility which has been provided through canals, sub-canals of Narmada Waters. Even though there is an increase in agriculture sector but, however, some part of agriculture and vegetation has been settled into urban development exercises [11, 12]. Furthermore, the study area experienced significant variation in water bodies and vegetation cover. The water bodies have decided from 4.18 to 0.93%, which computes to a decrease in area from 99.1 to 22.04 km^2. Also, vegetative cover has been declined from approximately 60–12%, indicating a variation of 1432.08–291.18 km^2. This is mainly attributed to human involvement and settlements along the region and an increase in agricultural activities.

We wish that this work can bring attention about the present scenario of land use/land cover change of the Sardar Sarovar Command Area Region-V and benefit the promotion of issue that certainly represents crisis of the land as a resource. Adopting basic management exercises in addition to proper use of knowledge, a lot could be achieved to regulate the decent and appropriate use of land as a resource and in turn result in sustainable environment.

4   Conclusion

The results of the current study act as both as a scientific characterization and as an origin of information for associates functioning for the formation of favourable and enhanced land use/land cover management strategy [13, 14]. Since land use/land cover study is in its inception stage when recognizing the country and numerous other study perspectives, it is proposed that land use/land cover knowledge should be conveyed all the way for proper, efficient and enhanced working of social-environment elements. The variations in land use/land cover bring forth the necessity of use of management techniques for land as a resource. The need of applying and adopting these management techniques is probable from the increasing and unplanned population growth and unprecedented industrialization. The importance of land as a resource should be made a priority and operations over the resource should be executed accordingly.

References

1. Gautam, N.C., Narayanan, E.R.: Satellite remote sensing techniques for natural resources survey. In: Singh, L.R., Singh, S., Tiwari, R.C., Srivastava, R.P. (eds.) Environmental Management, pp. 177–181. Allahabad geophysical society (1983)
2. Chaudhary, B.S., et al.: Human induced land use/land cover changes in northern part of Gurgaon district, Haryana, India: natural resources census concept. J. Hum. Ecol. **23**(3), 243–252 (2008)
3. Sreenivasulu, V., Bhaskar, P.U., et al.: Change detection in landuse and landcover using remote sensing and Gis techniques. Int. J. Eng. Sci. Technol. **2**(12), 7758–7762 (2010). (2007)

4. Suneela, T., Mamatha, G.: Detection of land use and land cover changes using remote sensing and geographical information system (Gis) techniques. Int. J. Electr. Electron. Data Commun. **4**(12) (2016)
5. Frimpong, A.: Application of remote sensing and GIS for forest cover change detection. Kwame Nkrumah University of Science and Technology (Knust) Kumasi, Ghana (2011)
6. Dunno, R.M.W., Glenn, A.: Riparian vegetation mapping and hopi Indian reservation, Arizona image processing techniques. Photogram. Eng. 8r Remote Sens, 179–186 (2001)
7. Bhandari, A., Bela, N., Mishra, N., Gupta, S.: Change detection of land use land cover using GIS and remote sensing for Doon Valley. SRG Int. J. Civil Eng **3**(7), 77–78 (2015). 36, July 2016
8. Farooq, S., Ahmad, S.: Urban sprawl development around Aligarh city: a study aided satellite remote sensing and GIS. J. Indian Soc. Remote Sens. **36**, 77–78 (2008)
9. Harish, N., Rao, K.C., Venkateswarlu, K., Reddy, B.G., Siddiq, M.A., Rajarajeswari, P., Sai, M.K., Land use land cover change mapping using remote sensing and GIS: a case study of Gudur Mandal, SPSR Nellore District, Andhra Pradesh. Int. Res. J. Eng. Technology (IRJET). **3**(2) (2016)
10. Mishra, N., Khare, D., Shukla, R., Singh, L.: Change detection of land use/land cover in upper Ganga canal command. Using Arc-GIS Tools, J. Remote Sens. GIS **36**, 77–78. ISSN: 2230-7990
11. Mallupattu, P.K., Reddy, J., Reddy, S.: Analysis of land use/land cover changes using remote sensing data and GIS at an Urban Area, Tirupati, India. Sci. World J. Article ID 268623 (2013)
12. Nishkalank, R.A.R., Gurugnanam, B.: Land use and land cover change detection using remote sensing. SSRG Int. J. Geo Inf. Geol. Sci. (SSRG-IJGGS), **1**(2) (2014)
13. Lin, Y.P., Hongb, N.M., Wu, P.J., Wu, C.F., Verburg, P.H.: Impacts of land use change scenarios on hydrology and land use patterns in the Wu-Tu watershed in Northern Taiwan. Landscape. Urban Plan. 111–126 (2007)
14. Shrestha, D.P., Zinck, J.A.: Land use classification in mountainous areas integration of image processing digital elevation data and field knowledge. Int. Inst. Aerosp. Surv. Earth **3** (2001)

Environmental Impact of Fly Ash Brick in Comparison with Traditional Brick

Amit Kumar Sharma, Sanjeev Kumar and Nitin Mishra

Abstract The conventional burnt clay bricks are usually employed for constructional purposes. However, there is another type of bricks called fly ash bricks that can also be broadly employed in all such works. When compared on the basis of weight and substantiality, this variety of brick is relatively better than the conventional bricks. Its application as chief crude material in the brick manufacturing will formulate adequate possibilities for its strait-laced and beneficial disposal and additionally support in environmental deterioration check to a vaster scope in the neighbouring regions of power manufactories as fly ash is being stockpiled as a rubbish element in great abundance around such power manufactories and producing severe environmental deterioration predicaments. The severe predicaments posed by brick manufacturers inflate unwanted outcomes such as soil erosion, deforestation, unwanted gas exhaustion, etc. As per statistics, 5000 acres of the uppermost cover of soil which formulate around 340 billion tones of clay is emptied out for bricks production, and annually we are able to employ 180 billion tonnes of conventional bricks. Therefore, such environmental predicaments can be subdued to a certain degree if fly ash bricks are employed for constructional purposes in place of conventional bricks and a lot of top covers can be conserved. This study aimed to interpret knowledge concerning about fly ash as a raw material in brick manufacturing and thereby establish and characterize its performances in an usual economical manner.

Keywords Fly ash · Gypsum · Cement and sand

1 Introduction

Due to coal kindling, the gases arrive towards the smokestacks of thermal power manufactories in extremely high amounts and are accumulated by the mechanical or electrostatic precipitator (ESP). This accumulated produce is termed as fly ash. The

A. K. Sharma (✉) · S. Kumar · N. Mishra
Graphic Era (Deemed to Be University), Dehradun 248001, India
e-mail: amitsharma812010@gmail.com

fly ash comprises notable quantities of oxides of aluminium, silicon, magnesium, calcium and iron. In addition to these oxides, fly ash is compounded by some trace components such as cadmium, selenium, chromium, mercury, lead, arsenic, nickel, antimony and zinc [1]. However, the composition may differ if there is variation in the standard of coal used and the burner introduced. The name fly ash is given so because the elements are accumulated at the exhaust of power manufactories as they try to fly away from it. On chemical grounds, when lime (calcium hydroxide) is infused with fly ash, it forms a cementitious union; therefore, it is classified as a pozzolan [2].

The basic environmental elements which are air, water and soil can be directly affected by fly ash if it is kept as the copious element and therefore it can aggregate environmental perils. As far as biotic well being is taken into consideration, the area where the fly ash gets disintegrate and decomposed can cause adverse and severe effects as it has few volumes of toxic metals as one of the constituents. One of the subjects in relation to the socio-economic environmental aspects is the disposing of this rubbish substance. The sustained and remunerative use of this element has remained one of the subjects of research over a considerable amount of time. The alternatives of ash utilization involving the ash-based materials are in the growing frame and demand to be addressed further eco-friendly [3].

2 Materials and Methods

The following test was performed on fly ash and clay bricks both being the subjects in the present study [4–8].

2.1 Tolerance Test

The tolerance test for fly ash bricks and clay bricks of stack comprising 10 bricks each (Tables 1, 2):-

Table 1 Tolerance test for fly ash bricks

	Length (mm)	Width (mm)	Height (mm)
Fly ash (stack A)	2326	1113	713
Fly ash (stack B)	2323	1116	716
Mean	232.45	111.45	71.45
Tolerance	±2.45	±1.45	±1.45

Table 2 Tolerance test for clay bricks

	Length (mm)	Width (mm)	Height (mm)
Clay bricks (stack A)	2327	1116	714
Clay bricks(stack B)	2325	1117	715
Mean	232.6	111.65	71.45
Tolerance	±2.6	±1.65	±1.45

2.2 Water Absorption Test

The water absorption test on the subjects was done for a time period of 28 days with period interval being 7 days. The water absorption test is given by the formula,

$$\text{Water Absorption} = \frac{M2 - M1}{M1} \times 100$$

2.3 Compressive Strength Test

The compressive test on the subjects was done for a time period of 28 days with period interval being 7 days and is calculated with the help of the formula given below,

$$\text{Compressive Strength} = \frac{(\text{Maximum load at failure (N)})}{(\text{Avg.area of bed face}(\text{mm}^2))}$$

3 Results and Discussions

Water Absorption Test: The water absorption test on the fly ash bricks was done for a time period of 28 days with period interval being 7 days (Table 3 and Fig. 1).

Table 3 Water Absorption test for fly ash

Fly ash (%)	7 days (%)	14 days (%)	21 days (%)	28 days (%)
35	14. 96	13.2	12.61	12.22
40	13.15	12.525	11.86	11.18
45	11.729	11.73	10.51	10.15
50	10. 65	9.702	9.115	8.23
55	9.72	9.17	8.49	7.9
60	8.5	7.825	7.06	6.68
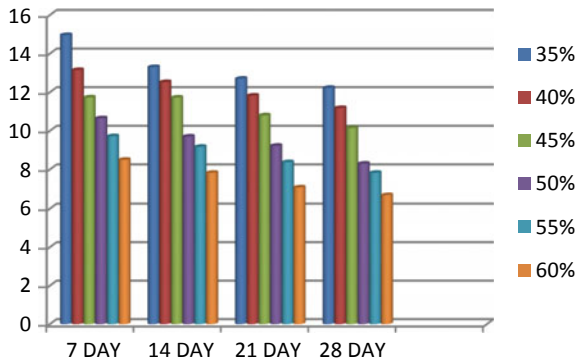
Fig. 1 Water absorption in %

Table 4 Compressive strength test for fly ash

Fly ash (%)	7 days (MPa)	14 days (MPa)	21 days (MPa)	28 days (MPa)
35	5.11	5.414	5.85	6.29
40	5.35	6.04	6.57	7.26
45	5.78	6.13	7.14	7.29
50	6.37	6.95	7.66	8.36
55	6.91	6.79	7.18	7.66
60	5.76	6.3	7.04	7.53

Fig. 2 Compressive strength in MPa for fly ash bricks
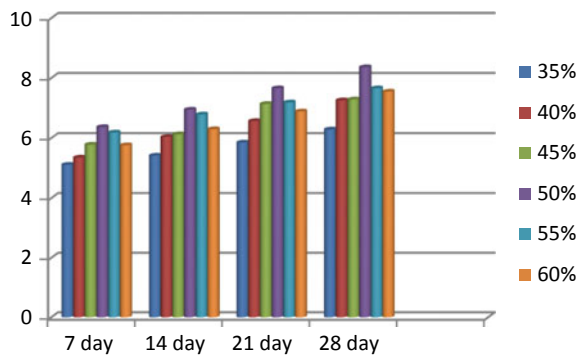
Compressive Strength test: The compressive strength test for fly ash bricks was done for a time period of 28 days with period interval being 7 days (Table 4 and Fig. 2).

Efflorescence test for fly ash bricks with different percentage (Table 5).

Water Absorption Test: The water absorption test on the clay brick was done for a time period of 28 days with interval being 7 days (Table 6 and Fig. 3).

Table 5 Efflorescence for fly ash bricks

Specimen (%)	Efflorescence
Fly ash 35	Moderate
Fly ash 40	Moderate
Fly ash45	Slight
Fly ash 50	Slight
Fly ash 55	Slight
Fly ash 60	Nil

Table 6 Water absorption for traditional clay bricks

Days	Result (%)
7	18.72
14	14.652
21	12.44
28	11.31

Fig. 3 Water absorption of clay bricks
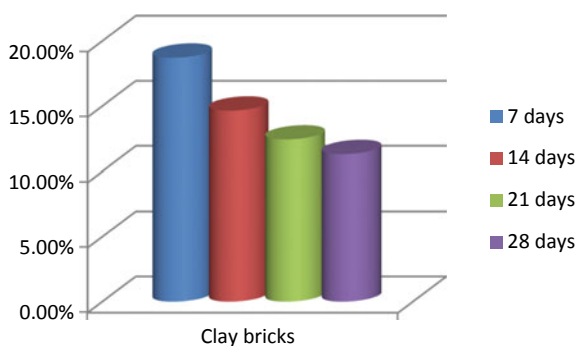
Table 7 Compressive strength test for traditional clay bricks

Days	Result (MPa)
7	5.227
14	5.226
21	5.225
28	5.224

Compressive Strength Test: The compressive strength test on the clay brick was done for a time period of 28 days with interval being 7 days (Table 7 and Fig. 4).

Fig. 4 Compressive strength
test of clay bricks
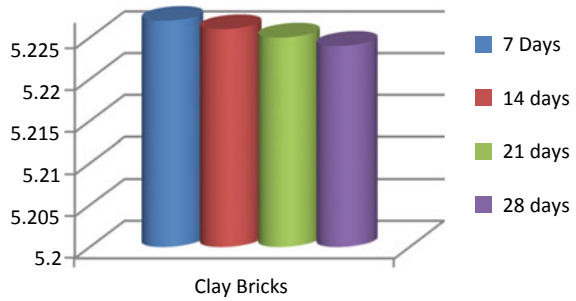
4   Conclusion

In our country, the consumption of fly ash has achieved around 30% mark through
the prior five-year span and demands some more time to attain the position of whole
utilization. As per statistics, annually there around 160 million tonnes of fly ash is
produced but, however, we are not able to put forward more than 50% of fly ash
for all potential purposes and applications. To employ such a tremendous volume
of ash, assured actions from administration front and the nongovernment front both
should be taken with respect to the application of fly ash. On the basis of various test
performed and analysis done on fly ash brick, the compressive strength is found out
to be 54.25 kg/cm^2 and water absorption percentage is 19.26%.

The study concludes when compared to conventional clay bricks, fly ash bricks
are extra secure, cost-effective and possess greater strength. Both the test subjects are
compared, and the relative differences with respect to properties have been tabulated
and shown in the table below (Table 8).

Some additional advantages of fly ash bricks are listed below:

- Environmental friendly
- Economical
- More compressive strength
- Light weight
- Use of wastage
- Saving of fertile land, pure water.

In addition to the engineering characteristics, fly ash brick releases 50% less radon
gas as compared to usual bricks. Fly ash bricks can assimilate carbon dioxide from the
atmosphere in a chemical manner called "Carbonation." This process induces carbon
sequestration, diminishing the CO_2 in the atmosphere, which assists to moderate
global warming.

Table 8 Comparison of fly ash bricks and ordinary red clay bricks [9]

Properties	Red bricks	Fly ash bricks	Remarks (for fly ash bricks)
Colour	Vary	Uniform	Good appearance
Density	1600–1750 kg/m^3	1700–1850 kg/m^3	Higher load bearing
Compressive strength	6.93 MPa	8.36 MPa	Higher load bearing
Water absorption	15–25%	10–14%	Less dampness
Dimensional stability	Very low tolerance	High tolerance	Saving in mortar up to 25%
Wastage during	Up to 10%	Less than 2%	Saving in cost up to 8%
Transit plastering	Thickness vary on the both sides of walls	Even on both sides of walls	Saving in plaster up to 15%
Environmental advantage	Nil	Absorbs CO_2 from atmosphere	Eco-friendly

Source https://theconstructor.org/building/fly-ash-bricks

References

1. Bhanumathidas, N., Kalidas, N.: Fly ash: the resource for construction industry. Indian Concr. J. pp. 997–1004 (2003)
2. Dhadse, S., Kumari, P., Bhagia, L.J.: Fly ash characterization, utilization and government initiatives in India—a review. J. Sci. Ind. Res. **67**, 11–18 (2008)
3. Malaviya, S.K., Chatterjee, B., Singh, K.K.: Fly ash—an emerging alternative building material. Nat. Metall. Lab. Jamshedpur, 59–67 (2013)
4. Fly ash bricks masonry: an experimental study. Nat. Conf. Recent Trends Eng. Technol (2014)
5. IS 3495: Method of Testing of Burnt Clay Building Bricks (Part 1): Determination of Compressive Strength (Part 2): 1992 Determination of Water Absorption (Part 3):1992 Determination of Effloration (1992)

Indian Standard Referred

6. IS 12894: Pulverised fuel ash-lime bricks—specification (first Revision) (2002)
7. IS 3812: Pulverised fuel ash—specification (Part 1): for use as pozzolana in cement, Cement Mortar and Concrete, (Part 2): 2003 For use as Admixture in Cement Mortar and Concrete (2003)
8. IS 456: Plain And Reinforced Concrete—Code Of Practice (Fourth Revision) (2000)
9. https://theconstructor.org/building/fly-ash-bricks/5330/

Land Cover/Land Use Change and Fragmentation in Uttarakhand, the Western Himalaya Based on GlobeLand30 Datasets

A. Arun Kumar, Tanvi Gaur, Sujata Upgupta, K. Ramesh and Sanjeev Kumar

Abstract Globally, a widespread decline of the forest ecosystems and increasing fragmentation has been reported, yet there is no comprehensive assessment of degradation across the country. In this study, land cover change and fragmentation from 2000 to 2010 were analyzed for the state of Uttarakhand, using GlobeLand30 datasets at 30-m spatial resolution (GlobeLand30) developed by the National Geomatics Center of China (NGCC). Further, spatial patterns were analyzed, focusing on forest loss and patch matrices. The results show that during the last decade, vegetation cover has reduced by 523 km^2, whereas the artificial surface has increased by 103 km^2. Also, the fragmentation analyses show that the intact forests have reduced about 105 km^2 resulting in more open and patchy forests. The paper also highlights the effectiveness of using global land cover datasets and digital techniques for monitoring the forest structure spanning over vast areas and to see the effectiveness of management policies in the long run.

Keywords Deforestation · Fragmentation · Uttarakhand · Landscape fragmentation tool · Himalaya

1 Introduction

Land use/land cover (LULC) change is a dynamic process that takes place over space and time and is of enormous importance in natural resource management studies. Land cover is the characteristic of the earth's surface that spatially captures the distribution of vegetation, water, barren land, and ice, and it also includes the man-made structures such as settlement [1]. Land use is the management and modification of land, to exploit the land cover and captures the distribution of human activities includ-

A. Arun Kumar (✉) · T. Gaur · S. Upgupta · K. Ramesh
Landscape Ecology and Visualization Laboratory, Wildlife Institute of India, Dehradun, India
e-mail: arunkumar.gis@gmail.com

S. Kumar
Department of Civil Engineering, Graphic Era University, Dehradun, India

ing industrial zones, residential zones, agricultural fields, grazing, logging, mining, and many others [2]. Information on land cover/use is important for the selection, planning, and implementation of management policies to meet the increasing human needs as well as the wildlife conservation.

Changes in land use and cover do not essentially indicate degradation of the land. However, human activities cause shifting land use patterns that result in land cover changes that affects ecosystems and biodiversity [3]. Land conversion results in habitat loss and is the single greatest cause of extinction of species [4, 5]. Use of satellite imagery along with fragmentation analysis is becoming a valuable technique for assessing the temporal changes in the land cover and its effect on various ecosystem [6–10].

Forest degradation is the conversion of forest to some other land use, and forest fragmentation is breaking down of a large forest into a smaller patch of forest habitat [11]. The forest fragmentation in general is a consequence of increasing agricultural practices; logging and deforestation; development projects. Forest deforestation and fragmentation not only modify the natural landscapes, but also will lead to loss of habitat and biodiversity, and ecosystem functioning [12–16]. The single most significant factor for biodiversity loss is forest fragmentation [17]. Habitat fragmentations have forced many species to become highly vulnerable [18]. Evaluation of landscape indices has been recognized as the most effective way to quantify forest fragmentation [19–22]. Contrary to the availability of a large number of deforestation studies from the tropical forest, there are very few studies that report deforestation and fragmentation of the tropical forests [23].

Numerous studies have documented the adverse effects of anthropogenic drivers on the biodiversity, habitat loss, and fragmentation in the Hindu Kush Himalaya [24–28], and forest fragmentation studies are still patchy and are not adequate to make any management intervention at the landscape levels. In this study, we have addressed the landscape dynamics in the state of Uttarakhand, in view to detect the integrity of forest ecosystems and the changes that has taken place between 2000 and 2010 using geospatial techniques. Specifically, we aimed (i) to identify and delineate LULC changes in Uttarakhand between 2000 and 2010, (ii) to determine the shift in LULC classes, and (iii) to determine the extent of forest fragmentation as a potential indicator for forest degradation.

2 Materials and Methods

2.1 Study Area

Uttarakhand state is located in the northern part of India and shares North Western boundary with Himachal Pradesh, North and North Eastern boundary with Tibet, Eastern boundary with Nepal, and Southern boundary with plains of Uttar Pradesh (Fig. 1). Uttarakhand has an area of 51954.76 km^2 (Survey of India) and lies between
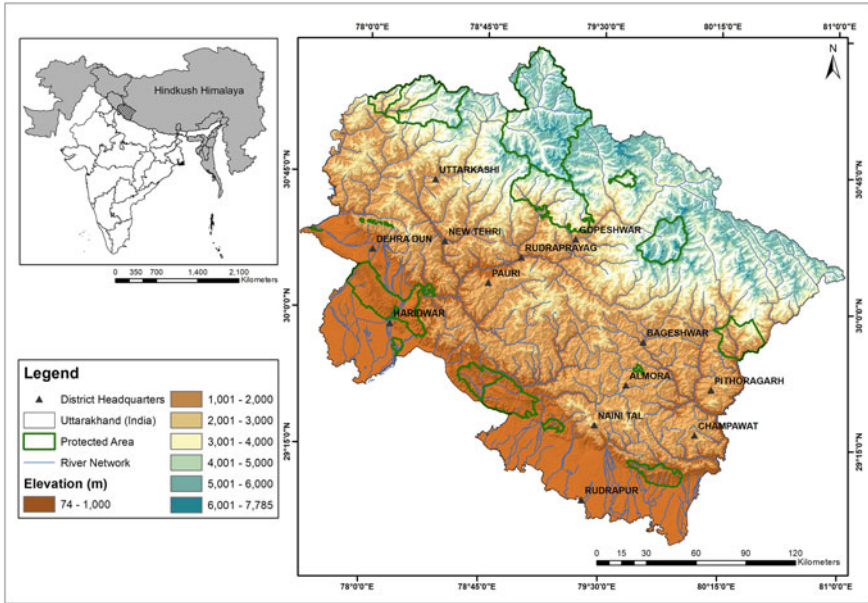
Fig. 1 Map showing the study area, the Uttarakhand

28° 43′N and 31° 27′N latitude and 77° 34′E to 81° 02′E longitude. The recorded forest area in the state is 24,240 km² [29], which constitute 46.65% of total geographical area covered by the state. The state lies in the western part of the Indian Himalaya region, with glaciers at the highest and tropical forests at the lowest elevation. The state experiences a wide range of climate and has different vegetation type changing with elevation.

Physiographically, the state can be divided into three parallel zones: the Himalayas, the Shiwaliks, and the Terai region, with temperate climate in higher elevation and tropical climate in plains, with temperatures ranging from sub-zero in the higher regions to >40 °C in the plains.

The state experiences an average annual rainfall of 1432.2 mm with a range varying between 328 and 3673 mm. Some of the major forest types in the state include Tropical Moist Deciduous, Tropical Dry Deciduous, Subtropical Pine, Himalayan Moist Temperate, Himalayan Dry Temperate, Sub-Alpine, and Alpine forests [29, 30].

2.2 Dataset

Information on temporal changes in the land cover is vital for any environmental research needs and for the sustainable development planning [2, 3, 31–33]. Since

Fig. 2 GlobeLand30 data for the Uttarakhand
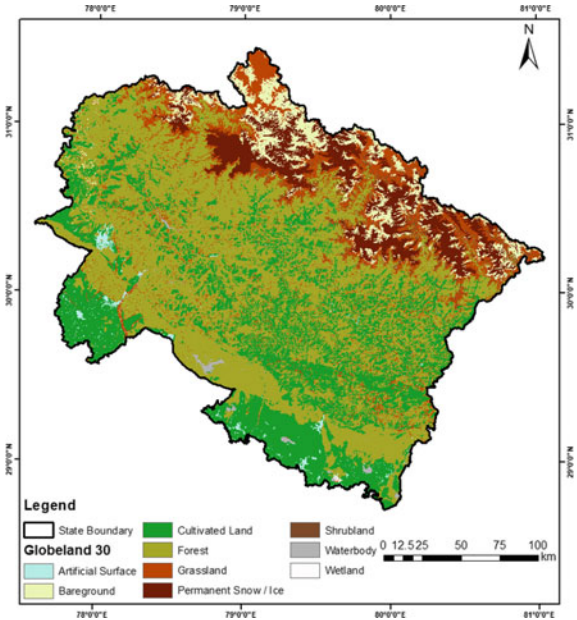
satellite-based remote sensing has long been a standard tool for broad-scale land cover mapping [34], a number of global land cover datasets have been developed with resolution ranging from 300 m to 1 km, using low-resolution satellite imagery such as the Advanced Very High-Resolution Radiometer (AVHRR), MODISModerate Resolution Imaging Spectroradiometer (MODIS), and MEdium Resolution Imaging Spectrometer (MERIS) [7, 33–35]. Although researchers have highlighted the shortfalls of these GLC datasets due to its poor resolution, these data products are still being widely used in various research [36–38].

The GlobeLand30 dataset was developed by the National Geomatics Centre of China (NGCC), which provides global land cover data at 30-m resolution (Fig. 2.). The accuracy assessment per class analyses reveals that classes 20 (Forest) and 90 (Bare ground) has an accuracy of 75 and 60%, respectively, while 60 (Water body), 10 (Cultivated land), and 30 (Grassland) have the highest accuracy above 85%, and class 50 (Wetland) is the lowest with 8.3%. The overall accuracy is 78%, which falls into "substantial" category [39]. Covering a decade from 2000 to 2010, the GlobeLand30 dataset is derived from over 10,000 images from Landsat Thematic Mapper (TM), Enhanced Thematic Mapper plus (ETMþ), and the HJ-1 (Chinese Environmental Disaster Alleviation Satellite).

Apart from a few recent studies [40, 41], these data are still not exploited effectively, regardless of being a potential source of understanding the landscape and land cover change. In the present study area, 4 tiles for each period (N43 25 2000 LC 030; N43 30 2000 LC 030; N44 25 2000 LC 030; N44 30 2000 LC 030; N43 25 2010 LC 030; N43 30 2010 LC0 30; N44 25 2010 LC 030; N44 30 2010 LC 030) of Glo-

beLand30 were used; this dataset is available in raster format with WGS84 (World Geodetic System 1984) reference system and UTM (Universal Transverse Mercator) projection. The GlobeLand30 dataset classifies land cover into ten categories, viz. artificial surfaces, bare ground, cultivated land, forests, grassland, shrubland, wetlands, water bodies, tundra, and permanent snow/ice.

2.3 Land cover Change Analyses

Tabulate Area Tool in ArcGIS 10.5 was used to quantify land use and land cover change (LULC) [42]. The results highlight the changes in the LULC classes, and these changes were compared to quantify the gains and losses between 2000 and 2010. The gain and loss were calculated by subtracting the persistence from the column total and the row total, respectively.

2.4 Fragmentation Analyses

The Landscape Fragmentation Tool (LFT v2.0) was developed by Center for Land Use Education and Research, University of Connecticut [28]. The land cover maps for the years 2000 and 2010 were reclassified into forest and non-forest classes. The fragmentation tool classifies forest class into four main categories: patch, edge, perforated, and core [28]. We have considered 100 m as an edge width, as it is a default value used in general purpose analyses [28, 43]. The forest areas were classified into: (i) "intact" forest—the forest that is relatively distant from the non-forest boundary; (ii) "patch" forest—small forest area surrounded by non-forested area; (iii) "perforated" forest—transition zone between the intact forest and perforations; (iv) "edge" forest—transition zone between the intact forest and large non-forest land; and (v) "non-forest" [28].

2.5 LULC and Forest Fragmentation Change Analyses

The annual rate of change was calculated by comparing the area of different classes (land cover and fragmentation) at two different periods. The annual rate of change was derived from the formula [44].

$$r = \frac{1}{(t_2 - t_1)} X \ln\left(\frac{a_2}{a_1}\right) \tag{1}$$

where r is the annual rate of change (percentage per year); a_1 and a_2 are the estimates at time t_1 and t_2, respectively.

3 Results

3.1 Land cover Changes

The land use pattern of Uttarakhand is governed by its characteristic topography. There are steep variations in the gradient of the land surface while moving from south to north, starting from the Gangetic plains to the mountainous snow-covered peaks. The study result shows that in both the time period (2000 and 2010), the forest class occupies the majority of the state with 46.47% (24141.55 km^2) and 45.46% (23617.93 km^2), respectively, followed by cultivated land with 26.31% (13667.28 km^2) and 26.22% (13624.13 km^2) (Fig. 3.).

Table 1 shows both positive and negative changes occurred in the land use/cover pattern in the state. Over the decade period from 2000 to 2010, the forests have reduced from 24141.55 to 23617.93 km^2 that equates to 523.61 km^2 and 1.01% of the total area of the state. The cultivated lands have reduced from 13667.28 to 13624.13 km^2 that equates to 43.15 km^2. Interestingly, the grasslands have increased from 5322.61 to 5832.38 km^2, which is an increase of 509.77 km^2. The artificial surfaces have increased from 257.81 to 360.74 km^2, which is 102.93 km^2. The water body has also increased from 246.08 to 274.23 km^2. Figure 4 illustrates the magnitude of change in different land categories. A total of 1638.80 km^2 of the forest area have been converted into other land cover classes (Table 2). Table 3 shows a total of 1115.20 km^2 of other land cover types converted to forest. Between 2000 and 2010,
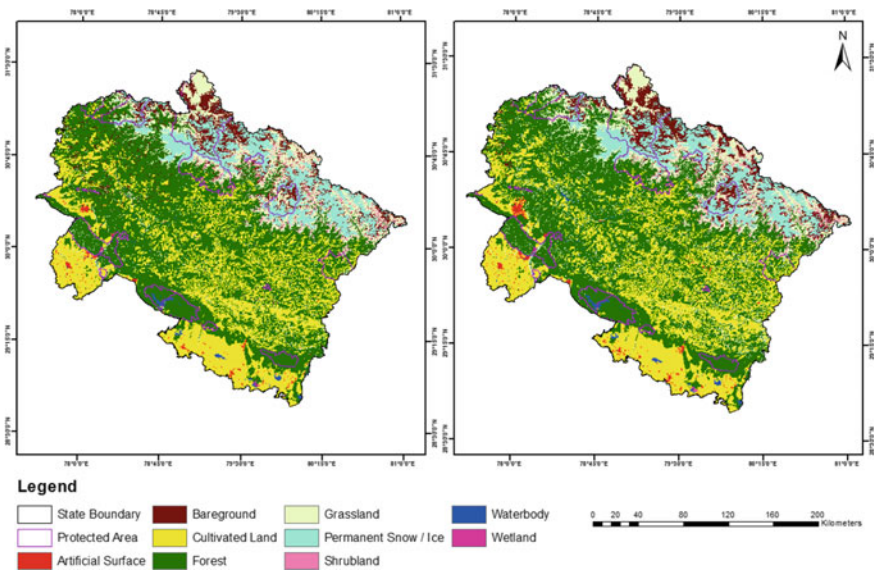
Fig. 3 Land use status of Uttarakhand (A. 2000; B. 2010)

Table 1 Area of different land cover units in Uttarakhand

Land use/land cover type	Area in 2000		Area in 2010		Change
	km²	%	km²	%	km²
Cultivated land	13667.28	26.31	13624.13	26.22	−43.15
Forest	24141.55	46.47	23617.93	45.46	−523.61
Grassland	5322.61	10.24	5832.38	11.23	509.77
Shrub land	750.39	1.44	749.36	1.44	−1.03
Wetland	13.74	0.03	13.77	0.03	0.03
Water body	246.08	0.47	274.23	0.53	28.14
Artificial surface	257.81	0.50	360.74	0.69	102.93
Bare ground	3029.67	5.83	3017.33	5.81	−12.34
Permanent snow/Ice	4525.64	8.71	4464.89	8.59	−60.75
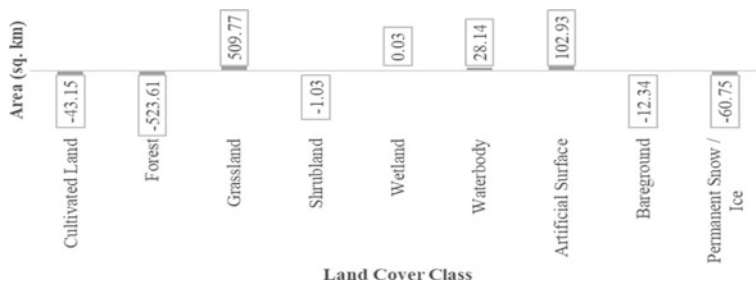
Fig. 4 Magnitude of land use change between 2000 to 2010

Table 2 Land use/cover in deforested areas

S.no	Cover type	Area (km²)	%
1	Grassland	1130.29	68.97
2	Cultivated land	342.60	20.91
3	Shrub land	76.85	4.69
4	Bare ground	41.44	2.53
5	Water body	36.68	2.24
6	Others	10.95	0.67
	Total	1638.80	

the percentage change of forest is −1.01% with a net annual deforestation rate(r) of 0.0022%.

Table 3 Other land use/cover areas converted to forest

S.no	Cover type	Area (km^2)	%
1	Grassland	428.51	38.42
2	Cultivated land	302.65	27.14
3	Bare ground	278.46	24.97
4	Shrubland	84.63	7.59
5	Water body	20.03	1.80
6	Others	0.93	0.09
	Total	1115.20	
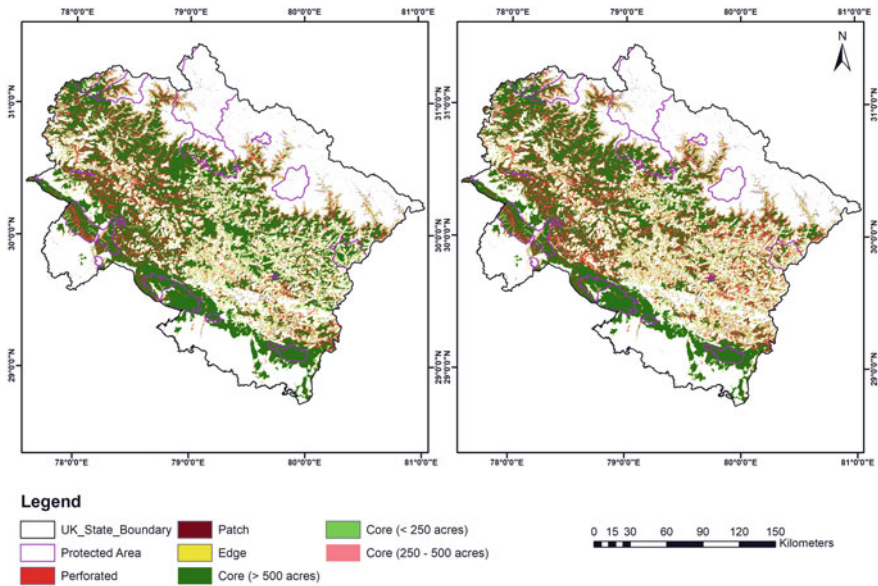
Fig. 5 Fragmentation status of Uttarakhand (A. 2000; B. 2010)

3.2 Fragmentation Status

Forest fragmentation analyses revealed a significant decrease in the large intact patch area (>500 acres). In 2000, the large intact patches were dominant, covering 63.41% of the total forest area, but got reduced to 55.25% in 2010 (Fig. 5), followed by edge (15.57%), perforated area (15.09%), small intact (2.84%), patch area (1.86%), and medium intact (1.23%) (Table 4).

However, the edge (16.93%), perforated area (19.92%), small intact (4.07%), patch area (2.27%), and medium intact (1.59%) have increased in 2010. Between 2000 and 2010, the percentage change of the large intact patch was −4.35% with a

Table 4 Forest fragmentation in area and percentage

Fragmentation class	Area 2000		Area 2010	
	km^2	%	km^2	%
Patch	449.55	1.86	536.85	2.27
Edge	3760.01	15.57	3998.44	16.93
Perforated	3642.03	15.09	4704.58	19.92
Intact (<250 acres)	686.35	2.84	960.27	4.07
Intact (250–500 acres)	297.17	1.23	376.32	1.59
Intact (>500 acres)	15309.20	63.41	13049.21	55.25

net annual reduction rate (r) of 0.016%. And the percentage change of perforated area was 2.05% with a net annual increase rate (r) of 0.026%.

4 Discussion

The changes in land cover/land use provide a useful understanding for the landscape pattern and processes. In the present context, it was possible to deduce that the rate of deforestation across space and time is minimal (0.0022%). But the fragmentation process is affecting the intact forests, and there is a significant increase in edge and forest perforation, reflecting that the landscape integrity is suffering. The GlobeLand30 dataset has been recognized as an essential geospatial database by the United Nations Committee of Experts on Global Geospatial Information Management, United Nations Environment Programme, and Global Observation for Forest Cover and Land Dynamics.

This study was to examine the suitability of using GlobeLand30 dataset for mapping large landscapes in the countries with inadequate National and regional land cover maps. The study illustrates the change in the land cover classes and also quantified the changes in the forest class and fragmentation over large landscapes. The results demonstrate that there are minimal changes occurring in different land use/cover type with a very low annual rate of change as compared to studies from other parts of the world [9]. The land cover change analysis shows that there is a decline in the forest (523.61 km^2), agriculture area (43.15 km^2), and permanent snow (60.75 km^2), whereas grassland (509.77 km^2), artificial surface (102.93 km^2), and water body (28.14 km^2) have increased. Also, the results show a reduction in the forest area (1.01%) to be less compared to other similar studies [8, 18, 21, 23], but there is a serious fragmentation happening in the state's forests. A total of 2259.99 km^2 (4.35%) area of large core forest (>500 acre) have been lost, whereas perforations have increased by 1062.55 km^2 (2.05%) in the forested areas between 2000 and 2010. This information is essential for national and state-level policy making to tackle deforestation and habitat protection. Most global land cover datasets suffer at

details due to their coarser spatial resolution (300 m–1 km) and has limited usability in research and policy deliberation [39, 40, 45]. Given the free availability of GlobeLand30 data with 30-m resolution, the dataset provides more details on land cover patterns and its change over time. This can bring in better understanding of landscape heterogeneities and also will increase the performance of landscape level modeling and predictive simulations.

5 Conclusion

This study conducted in one of the states of the Indian Himalayan Region (IHR) advocates that importance of multi-temporal and regional datasets in detecting the landscape changes rapidly and accurately. The results of our study demonstrate that there is no considerable forest decline in the state of Uttarakhand but the visible fragmentation events in the forests are of significant importance. Although the state is covered with 45.47% of forests, only 55% of the total forest fall into a large intact patch (>500 acre) and the remaining 45% falls into other fragmentation classes indicating clear and persistent degradation happening in the Uttarakhand's forests. The integrity and intactness of the forests are of high importance value to the species inhabiting those areas. Perforations in the forests can often lead to isolated patches that can completely lose its connections with the main forest areas and will further be completely lost leading to species extinction. Prioritizing the target areas where maximum changes and forest decline have taken place will aid in better conservation and management practices within the area. Even though this work has shown the present state of forests in Uttarakhand, more detailed analyses on patch metrics will be required to identify the factors that have resulted in the present spatial pattern of the forest.

References

1. Vogt, P., Riitters, K.H., Estreguil, C., Kozak, J., Wade, T.G., Wickham, J.D.: Mapping spatial patterns with morphological image processing. Landscape Ecol. **22**(2), 171–177 (2007)
2. Hansen, M.C., Potapov, P.V., Moore, R., Hancher, M., Turubanova, S., Tyukavina, A., Thau, D., Stehman, S.V., Goetz, S.J., Loveland, T.R., Kommareddy, A., Egorov, A., Chini, L., Justice, C.O., Townshend, J.R.G.: High-resolution global maps of 21st-century forest cover change. Science **342**, 850–853 (2013)

3. Herold, M., Mayaux, P., Woodcock, C.E., Baccini, A., Schmullius, C.: Some challenges in global land cover mapping: An assessment of agreement and accuracy in existing 1 km datasets. Remote Sens. Environ. **112**(5), 2538–2556 (2008)

4. Foley, J.A., DeFries, R., Asner, G.P., Barford, C., Bonan, G., Carpenter, S.R., Chapin, F.S., Coe, M.T., Daily, G.C., Gibbs, H.K., Helkowski, J.H.: Global consequences of land use. Science **309**(5734), 570–574 (2005)

5. Bustamante, R.O., Serey, I.A. Pickett, S.T.A.: Forest fragmentation, plant regeneration and invasion processes across edges in central Chile. Bradshaw, G.A. and Marquet, P.A.: How landscapes change, pp. 145–160. Springer Berlin Heidelberg (2003)

6. Zanella, L., Borém, R.A.T., Souza, C.G., Alves, H.M.R., Borém, F.M.: Atlantic forest fragmentation analysis and landscape restoration management scenarios. Natureza & Conservação **10**(1), 57–63 (2012)

7. Echeverría, C., Newton, A., Nahuelhual, L., Coomes, D., Rey-Benayas, J.M.: How landscapes change: integration of spatial patterns and human processes in temperate landscapes of southern Chile. Appl. Geogr. **32**(2), 822–831 (2012)

8. Sundriyal, R.C., Sharma, D.: Anthropogenic pressure on tree structure and biomass in the temperate forest of Mamlay watershed in Sikkim. For. Ecol. Manage. **81**(1), 113–134 (1996)

9. Lavreniuk, M., Kussul, N., Skakun, S., Shelestov, A., Yailymov, B.: Regional retrospective high resolution land cover for Ukraine. In: Serpico, S.B., Pascazio, V. (eds.) Geoscience and Remote Sensing Symposium (IGARSS), IEEE International, pp. 3965–3968, July (2015)

10. Arsanjani, J.J., Tayyebi, A., Vaz, E.: GlobeLand30 as an alternative fine-scale global land cover map: Challenges, possibilities, and implications for developing countries. Habitat Int. **55**, 25–31 (2016)

11. Collingham, Y.C., Huntley, B.: Impacts of habitat fragmentation and patch size upon migration rates. Ecol. Appl. **10**(1), 131–144 (2000)

12. Armenteras, D., Gast, F., Villareal, H.: Andean forest fragmentation and the representativeness of protected natural areas in the eastern Andes, Colombia. Biol. Conserv. **113**(2), 245–256 (2003)

13. Lele, N., Joshi, P.K.: Analyzing deforestation rates, spatial forest cover changes and identifying critical areas of forest cover changes in North–East India during 1972–1999. Environ. Monit. Assess. **156**(1), 159–170 (2009)

14. Fahrig, L.: Effects of habitat fragmentation on biodiversity. Annu. Rev. Ecol. Evol. Syst. **34**(1), 487–515 (2003)

15. FSI: State of the forest report. Forest Survey of India, Ministry of Environment and Forest, Govt. of India, Dehradun (2009)

16. Cihlar, J.: Land cover mapping of large areas from satellites: status and research priorities. Int. J. Remote Sens. **21**(6–7), 1093–1114 (2000)

17. Leal, I.R., Filgueiras, B.K., Gomes, J.P., Iannuzzi, L., Andersen, A.N.: Effects of habitat fragmentation on ant richness and functional composition in Brazilian Atlantic forest. Biodivers. Conserv. **21**(7), 1687–1701 (2012)

18. Imbernon, J., Branthomme, A.: Characterization of landscape patterns of deforestation in tropical rain forests. Int. J. Remote Sens. **22**(9), 1753–1765 (2001)

19. Skole, D., Tucker, C.: Tropical deforestation and habitat fragmentation in the Amazon: satellite data from 1978 to 1988. Science **260**, 1905–1909 (1993)

20. Defourny, P., Vancutsem, C., Bicheron, P., Brockmann, C., Nino, F., Schouten, L. and Leroy, M.: Globcover: a 300 m global land cover product for 2005 using ENVISAT MERIS time series. In: ISPRS Commission VII mid-term Symposium: Remote Sensing: from pixels to processes, pp. 376–382. ISPRS, Enschede (The Netherlands), May (2006)

21. Loveland, T.R., Reed, B.C., Brown, J.F., Ohlen, D.O., Zhu, Z., Yang, L.W.M.J., Merchant, J.W.: Development of a global land cover characteristics database and IGBP DISCover from 1 km AVHRR data. Int. J. Remote Sens. **21**(6–7), 1303–1330 (2000)

22. Brovelli, M.A., Molinari, M.E., Hussein, E., Chen, J., Li, R.: The first comprehensive accuracy assessment of GlobeLand30 at a national level: Methodology and results. Remote Sens. **7**(4), 4191–4212 (2015)

23. Perez, J.M., Kobayashi, H., Matsumura, I.: Analysis of land use change in Comayagua County, Honduras, based on remote sensing and field survey data. J. Japan. Agric. Syst. Soc. **21**(3), 199–208 (2005)
24. Lambin, E.F., Geist, H.J., Lepers, E.: Dynamics of land-use and land-cover change in tropical regions. Annu. Rev. Environ. Resour. **28**(1), 205–241 (2003)
25. Foley, J.A., Ramankutty, N., Brauman, K.A., Cassidy, E.S., Gerber, J.S., Johnston, M., Mueller, N.D., O'Connell, C., Ray, D.K., West, P.C., Balzer, C.: Solutions for a cultivated planet. Nature **478**(7369), 337–342 (2011)
26. Luque, S.S.: Evaluating temporal changes using Multi-Spectral Scanner and Thematic Mapper data on the landscape of a natural reserve: the New Jersey Pine Barrens, a case study. Int. J. Remote Sens. **21**(13–14), 2589–2610 (2000)
27. Parent, J.: Landscape Fragmentation Analysis. University of Connecticut Press, USA (2009)
28. Puyravaud, J.P.: Standardizing the calculation of the annual rate of deforestation. For. Ecol. Manage. **177**(1), 593–596 (2003)
29. Munsi, M., Areendran, G., Ghosh, A., Joshi, P.K.: Landscape characterisation of the forests of Himalayan foothills. J. Indian Soc. Remote Sens. **38**(3), 441–452 (2010)
30. Li, M., Huang, C., Zhu, Z., Shi, H., Lu, H., Peng, S.: Assessing rates of forest change and fragmentation in Alabama, USA, using the vegetation change tracker model. For. Ecol. Manage. **257**(6), 1480–1488 (2009)
31. Rogan, J., Chen, D.: Remote sensing technology for mapping and monitoring land-cover and land-use change. Prog. Plann. **61**(4), 301–325 (2004)
32. Fischer, J., Lindenmayer, D.B.: Landscape modification and habitat fragmentation: a synthesis. Glob. Ecol. Biogeogr. **16**(3), 265–280 (2007)
33. Staus, N.L., Strittholt, J.R., DellaSala, D.A., Robinson, R.: Rate and pattern of forest disturbance in the Klamath-Siskiyou ecoregion, USA between 1972 and 1992. Landscape Ecol. **17**(5), 455–470 (2002)
34. Hansen, M.C., DeFries, R.S., Townshend, J.R., Sohlberg, R.: Global land cover classification at 1 km spatial resolution using a classification tree approach. Int. J. Remote Sens. **21**(6–7), 1331–1364 (2000)
35. Garcia, S., Saura, S.: February. Estimating landscape fragmentation indices from satellite images: the effect of sensor spatial resolution. In: Owe, M., Urso, G., Moreno, J.F., Calera, F (eds.) Remote Sensing for Agriculture, Ecosystems, and Hydrology V, vol. 5232, pp. 668–676. International Society for Optics and Photonics, USA (2004)
36. Biswas, S., Khan, D.K.: Habitat fragmentation and nutrient dynamics in tropical dry deciduous forests of West Bengal, India. ARPN J. Sci. Technol. **2**, 109–119 (2011). (2011)
37. Bawa, K.S., Joseph, G., Setty, S.: Poverty, biodiversity and institutions in forest-agriculture ecotones in the Western Ghats and Eastern Himalaya ranges of India. Agr. Ecosyst. Environ. **121**(3), 287–295 (2007)
38. Chettri, N., Sharma, E., Deb, D.C., Sundriyal, R.C.: Impact of firewood extraction on tree structure, regeneration and woody biomass productivity in a trekking corridor of the Sikkim Himalaya. Mt. Res. Dev. **22**(2), 150–158 (2002)
39. Riebsame, W.E., Meyer, W.B., Turner, B.L.: Modeling land use and cover as part of global environmental change. Clim. Change **28**(1–2), 45–64 (1994)
40. Bartholomé, E., Belward, A.S.: GLC2000: a new approach to global land cover mapping from earth observation data. Int. J. Remote Sens. **26**(9), 1959–1977 (2005)
41. FSI: State of the forest report. Forest Survey of India, Ministry of Environment and Forest, Govt. of India, Dehradun (2015)
42. Coppin, P., Lambin, E., Jonckheere, I. and Muys, B., 2002. Digital change detection methods in natural ecosystem monitoring: A review. In: Bovolo, F., Ferraioli, G., Celik, T. (eds.) Analysis of multi-temporal remote sensing images, World Scientific, 3–36 (2002)
43. Friedl, M.A., McIver, D.K., Hodges, J.C., Zhang, X.Y., Muchoney, D., Strahler, A.H., Woodcock, C.E., Gopal, S., Schneider, A., Cooper, A., Baccini, A.: Global land cover mapping from MODIS: algorithms and early results. Remote Sens. Environ. **83**(1), 287–302 (2002)

44. He, C., Okada, N., Zhang, Q., Shi, P., Zhang, J.: Modeling urban expansion scenarios by coupling cellular automata model and system dynamic model in Beijing, China. Appl. Geogr. **26**(3), 323–345 (2006)
45. Adnan, M., Tariq, A., Shinwari, Z.K.: Effects of human proximity and nomadic grazing on the diversity of medicinal plants in temperate Hindukush. Pak. J. Bot. **47**(1), 149–157 (2015)

Marine Debris in India: Quantifying Type and Abundance of Beach Litter Along Chennai, East Coast of India

A. Arun Kumar, R. Sivakumar, Y. Sai Rutwik, T. Nishanth, V. Revanth and Sanjeev Kumar

Abstract Though numerous studies on marine debris are conducted with an emphasis on analyzing the composition, quantification, and distribution on beaches around the globe, studies are still restricted to some areas of the coast, and the quantities and the spatiotemporal patterns are unknown for the Indian Coastline. NOAA Marine Debris Program methodology was used to collect and quantify various debris along the two beaches in Chennai, East coast of India. On four occasions, debris were collected and were categorized according to the type, quantity, and source. The results demonstrate that the shoreline and recreational activities to be the major source of beach debris. Also, the results show a strong correlation between coastal activities and debris type, and this difference in debris sources explain the importance of framing different management and prevention strategies at different beaches. The study highlights the requirement to establish long-term monitoring protocols, to address the existing knowledge gap on marine debris impacts on the Indian coastline.

Keywords Marine debris · Chennai · Plastic pollution · Beach litter

1 Introduction

Any manufactured or processed solid material that is and directly or indirectly, intentionally or unintentionally, disposed of or abandoned into the marine environment constitutes to the marine debris [1, 2]. To understand the type and composition of marine debris, beach surveys are conducted around the globe [3–11]. There are a large number of studies reporting the presence of marine debris from coastal areas,

A. Arun Kumar (✉)
Landscape Ecology and Visualization Laboratory, Wildlife Institute of India, Dehradun, India
e-mail: arunkumar.gis@gmail.com

R. Sivakumar · Y. Sai Rutwik · T. Nishanth · V. Revanth
Department of Civil Engineering, SRM Institute of Technology, Kancheepuram, India

S. Kumar
Department of Civil Engineering, Graphic Era University, Dehradun, India

sea floor, and oceanic gyres [5, 12–17]. The effects of marine debris on the wildlife are well-documented, and the results are disturbing. Entanglement of marine species in marine debris causing laceration and/or death [18–21]. Ingestion of plastic debris leading to starvation, laceration and death [22–25]. Heavy debris can damage the shallow coral substrate [26]. Drifting debris also act as a vector for alien and potentially harmful, invasive organisms, and can harbor toxic chemicals [27–29]. The economy of many coastal communities is also impacted due to 'ghost fishing' by derelict fishing gear and other debris [30]. Marine debris adversely affects tourism, shipping, and commercial fishing revenue [31, 32].

Although India has a coastline of about 7,500 km, its marine debris research is still at infancy compared to USA, UK, Brazil, Indonesia, Australia, etc. Of the few studies conducted, none of them follow a consistent methodology so as to make meaningful comparisons between the Indian beaches. The presence of plastics along the Caranzalem beach of Goa reported in 1982 was the first account of marine debris from the Indian coastline [33]. In 2003, large amounts of debris were reported around the Great Nicobar Island [34]. Different polymer groups were identified from accumulated debris originating from ship breaking along the Gulf of Cambay in 2006 [35]. A study conducted in five sandy beaches of Karnataka [36] revealed that the southwest coast of India is polluted mostly with the recreational use plastics. A 2011 study concluded that the most common debris in the ecologically sensitive Gulf of Mannar were plastic [37]. The coastal activities along the Veraval, Mumbai, Mangalore, Kochi, Tuticorin, Mandapam, Chennai, and Vishakapatnam were studied to quantify the debris generated by different activities [38]. In 2013, the seasonal fluctuations in the debris load along the recreational beaches in Mumbai were reported [39]. The marine debris occurring at the Marina beach, Chennai, was quantified based on NOAA Marine Debris program protocol in 2016 [10]. The number of microfibers isolated from beaches around the Indian Ocean found to be more than those found in other countries [40]. Veerasingam et al. [41] have studied the change in abundance of microplastic pellets along the Chennai coast before and after 2015 flooding and discussed the impacts of microplastics in the marine system [42].

The numerous input and output pathways makes the debris science complex and adding to it are the other factors such as (i) massiveness of the ocean, (ii) patchy distribution of debris, (iii) inconsistency in space and time, and (iv) intricate life cycle of the debris itself [16]. The lack of reliable monitoring protocol for the marine debris is obstructing our understanding of the source, composition, distribution, abundance, pathway, and their impact on a local, national, and global scale [43]. In this paper, we compared the marine debris load at two beaches along the Chennai coastline. The objectives of the study were (1) to estimate the quantities and composition of debris on both the beaches; (2) to relate the debris composition between the beaches; (3) and to categorize the possible origins of the debris at each site.

2 Methodology

2.1 Study Area

Chennai located on the East Coast of India is the capital of the Indian state of Tamil Nadu. The city is the one of the largest metropolis, and the coast is a typical example for uncontrolled disposal of domestic and industrial waste [10]. The estuarine ecosystem of river Coovum and Adyar harbors migratory birds, Neelankarai beach at the south of the Adyar river mouth is a nesting site for turtles. These same rivers traversing the city also act as the source of domestic sewage and industrial effluents into the Bay of Bengal [44]. Coastal pollution in Tamil Nadu is seriously affecting the economic, ecological resources, and the overall integrity of the marine and coastal ecosystems [10].

In this study, two sites were surveyed for the quantification and comparison of marine litter; these sites were decided based on the use of the beach (Fig. 1). The Marina beach at the North is one of the longest beaches and is a major tourist attraction of the city. In the South, abutting the Adayar river is the Srinivasapuram, a fishermen's settlement built by government [45].

For this study, 50 × 100 m segment of the beach between 13° 03′36.56″N; 80° 17′12.72″E and 13° 03′38.26″N and 80° 17′13.13″E in the Marina beach (Site A) and an area between 13° 01′17.87″N; 80° 16′43.27″E and 13° 01′19.49″N; 80° 16′43.52″E in the Srinivasapuram beach (Site B) were considered (Fig. 1). NOAA Marine Debris Program [1, 46] methodology was employed to carry out the transect survey. The coastline is flat with an average elevation around 6.7 m (22 ft.).
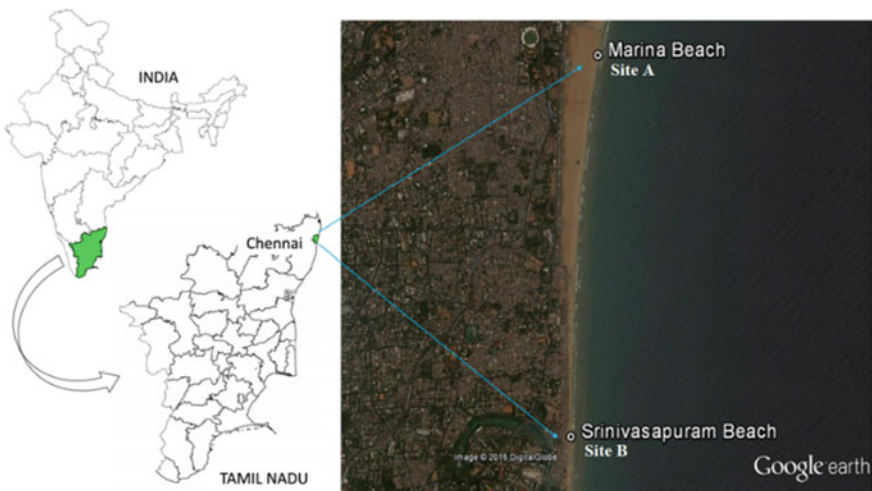
Fig. 1 Map showing the study area and sampling locations
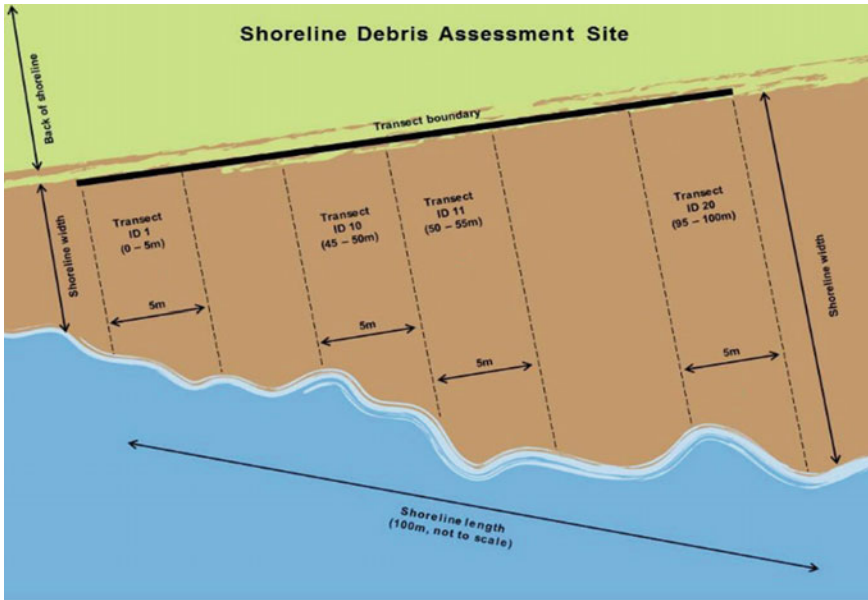
Fig. 2 Shoreline section (100 m) showing transects [46]

2.2 Debris Collection

The surveys were carried out bimonthly between March 2015 and April 2015 in Marina Beach (Site A) and between June 2015 and July 2015 in Srinivasapuram (Site B). Five-m-wide and 100-m-long transects were laid as per the NOAA Marine Debris Program methodology from the HTL toward the backshore encompassing an area of 5000 m^2 (Fig. 2). The accumulated debris on the beach were removed at the end of February 2015 at Site A and mid of May 2015 at Site B, so as to eliminate bias due to the accumulation during the past months. Only the debris on the beach surface were removed and collected in labeled plastic bags; no buried items were removed other than those protruding through the surface.

2.3 Debris Quantification and Classification

The data were recorded on the NOAA Marine Debris program data sheet. Accumulation survey method is used, where we have removed debris from the beach and then conducted regular surveys to record and remove the debris; over time, the collected data have provided an estimate of the change of debris in the shoreline (#items/m^2/time) [46]. The data sheets comprise of seven broad classes based on the type of material, viz. plastics, metal, glass, rubber, wood/paper, cloth/fiber, and

others. In turn, these seven classes were further categorized into 46 different types of debris like food wrappers, beverage bottles, aerosol cans, flip-flops, paper bags, ropes, etc. The Ocean Conservancy's methodology [47] categorizes the debris types into five classes of origin (i) shoreline and recreational, (ii) ocean and waterway, (iii) smoking related, (iv) dumping, and (v) medical and personal hygiene activities. The items that are not identifiable were categorized as 'others'. Concentration of debris along the beach was calculated using

$$C = n/(w * l) \tag{1}$$

C = Concentration of debris; n = Total debris; w = width of the transect; l = length of the transect.

3 Results

3.1 Quantities of Collected Debris

Table 1 shows the total debris quantity and the weight at both the sites. At site A, the average number of the debris item is 171.8 counts/100 m, and the average weight is 3.24 kg/100 m, whereas at site B, the average number of the debris item is 140.1 counts/100 m and the average weight is 5.72 kg/100 m. The number of items recorded at Site A was higher than Site B, whereas the weight of the debris was higher at Site B as compared to Site A.

The debris concentration at both the sites (A and B) were found to be 1.37 items/m^2 and 1.12 items/m^2, respectively. These values are smaller compared to the other regional and global studies and could be accredited to the patchy distribution of the debris [4, 7, 9, 48–50].

3.2 Beach Debris Composition

The plastics form the majority of the beach debris with an average of 44.89% at Site A and 56.42% at Site B (Fig. 3). Lumber 28.94% and others 16.42% forms the second major debris item at site A and site B, respectively. Plastic bags (33.26% at Site A and 26.57% at Site B) were the most common plastic debris found at both the sites, followed by food wrappers (17.50%) and plastic cups (15.92%) at site A and plastic cups (14.61%) and thermocol/styrofoam (12.21%) at Site B. With 29.95% of the total weight, corn stalk and food waste (others) constitute the most debris followed by plastics (19.58%) and rubber (20.53%) at site A. And at Site B, plastics were the most abundant with 41.18% of total weight, followed by glass (29.28%) and corn stalk and food waste (others) with 9.59%. In terms of number of

Table 1 Debris collected during sampling period

Date	Plastic	Metal	Glass	Rubber	Lumber	Cloth	Others	Total
Marine debris—abundance (At site A)								
14th Mar	751	26	21	24	497	11	132	1462
29th Mar	507	26	26	22	415	22	343	1361
12th Apr	656	62	28	27	526	19	436	1754
28th Apr	1171	48	17	37	551	19	452	2295
Tot	3085	162	92	110	1989	71	1363	6872
Avg	771.3	40.5	23	27.5	497.3	17.75	340.8	1718
S. Dev	284.8	17.69	4.97	6.66	59.11	4.72	147.2	419.2
Occ%	44.89	2.36	1.34	1.6	28.94	1.03	19.83	100
Marine debris—weight (At site A)								
14th Mar	6.89	0.68	1.82	4.34	5.05	2.82	5.04	26.64
29th Mar	3.61	0.97	0.93	6.12	4.26	3.43	9.63	28.95
12th Apr	4.97	1.03	1.1	6.82	5.2	2.2	11.1	32.42
28th Apr	9.93	0.46	2.3	9.34	4.77	1.8	13.06	41.66
Tot	25.4	3.14	6.15	26.62	19.28	10.25	38.83	129.7
Avg	6.35	0.79	1.54	6.66	4.82	2.56	9.71	32.42
S. Dev	2.74	0.27	0.64	2.07	0.41	0.71	3.41	6.6
wt%	19.58	2.42	4.74	20.53	14.87	7.9	29.95	100
Marine debris–abundance (At site B)								
01st Jun	875	30	70	17	262	14	260	1528
16th Jun	695	52	62	18	249	17	172	1265
02nd Jul	711	56	105	19	141	22	228	1282
17th Jul	881	38	83	23	223	21	260	1529
Tot	3162	176	320	77	875	74	920	5604
Avg	790.5	44	80	19.25	218.8	18.5	230	1401
S. Dev	101.3	12.11	18.78	2.63	54.31	3.7	41.51	147.4
Occ%	56.42	3.14	5.71	1.37	15.61	1.32	16.42	100
Marine debris—weight (At site B)								
01st Jun	25.86	0.46	14.6	4.1	3.46	2.36	6.42	57.26
16th Jun	23.25	0.69	13.59	3.72	2.92	1.95	4.23	50.35
02nd Jul	21.39	2.04	22.1	3.95	1.59	3.12	5.79	59.98
17th Jul	23.73	0.98	16.71	9.32	2.32	2.7	5.5	61.26
Tot	94.23	4.17	67	21.09	10.29	10.13	21.94	228.9
Avg	23.56	1.04	16.75	5.27	2.57	2.53	5.49	57.21
S. Dev	1.84	0.7	3.8	2.7	0.8	0.5	0.92	4.87
wt%	41.18	1.82	29.28	9.22	4.5	4.43	9.59	100
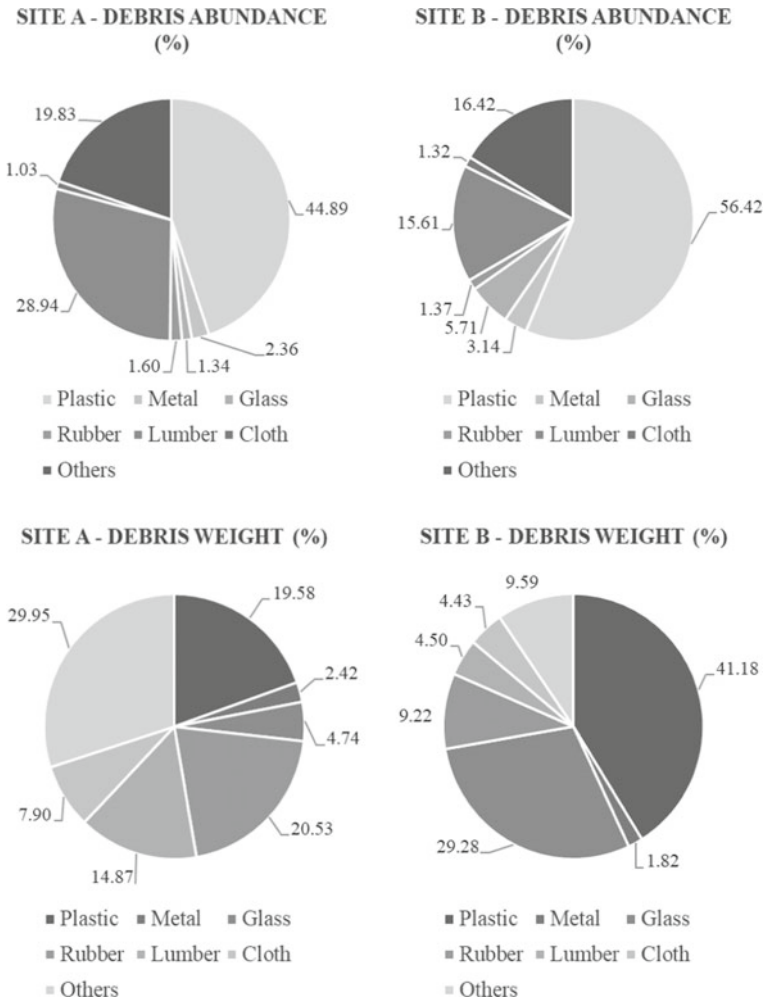
Fig. 3 Fragmentation status of Uttarakhand (A. 2000; B. 2010)

item, the food wastes are the most abundant debris item on both the survey beaches (Table 2), comprising 19.44% (Site A) and 15.76% (Site B) of the total number, followed by paper (15.22%), plastic bags (14.93%), paper bags (12.21%), and food wrappers (7.86%) at Site A. Subsequent to the corn stalk and food waste, plastic bags (14.99%), paper (9.87%), plastic cups (8.24%), thermocol (6.89%) were the most abundant debris at Site B.

For more than 5 decades, the production and consumption of plastics have continued to rise. Each year, about 20 million tons of plastic enters the oceans [51] and in 2015, 5.25 trillion plastic particles weighing 268,940 ton was estimated to be floating

Table 2 Abundance of 10 major debris

Debris at site A	Nos.	Occ %	Debris at site B	Nos.	Occ %
Food waste	1336	19.44	Food waste	883	15.76
Paper	1046	15.22	Plastic bags	840	14.99
Plastic bags	1026	14.93	Paper	553	9.87
Paper bags	839	12.21	Plastic cups	462	8.24
Food wrappers	540	7.86	Thermocol	386	6.89
Plastic cups	491	7.14	Food wrappers	342	6.10
Metal fragments	135	1.96	Plastic rope/net	335	5.98
Flip flop	98	1.43	Paper bags	268	4.78
Building materials	89	1.30	Plastic utensils	188	3.35
Glass fragments	71	1.03	Glass fragments	171	3.05

Table 3 Summary of plastic debris collected [10]

S.No	Plastic Debris Type	At Site A		At Site B	
		Count	Occ %	Count	Occ %
1	Food wrappers	540	17.50	342	10.82
2	Beverage bottles	16	0.52	75	2.37
3	Containers	30	0.97	44	1.39
4	Bottle and caps	233	7.55	164	5.19
5	Cigar tips	167	5.41	119	3.76
6	Cigarettes	7	0.23	30	0.95
7	Cig. lighters	0	0.00	1	0.03
9	Bags	1026	33.26	840	26.57
10	Plastic rope/Net	28	0.91	335	10.59
12	Fishing line	8	0.26	1	0.03
13	Cups	491	15.92	462	14.61
14	Utensils	45	1.46	188	5.95
15	Straws	206	6.68	89	2.81
16	Balloons	199	6.45	17	0.54
17	Thermocol/styrofoam	57	1.85	386	12.21
18	Personal care products	9	0.29	15	0.47
19	Other	23	0.75	54	1.71
Total		3085		3162	

in all of the oceans [52]. In this study, of the 12,476 debris items collected, 50.07% (6247) were plastics weighing about 61 kg (Table 3).

Although the abundance of plastic debris items from both beaches was not significantly different, the composition shows the difference in the use of these beaches.

SOURCES OF BEACH DEBRIS (ICC METHOD)

	Occ % at A	Occ % at Site B
Others	0.51	1.62
Medical / Personal Hygiene	0.04	0.09
Dumping Activities	21.07	0.29
Ocean / Waterways Activities	1.38	27.71
Smoking - Related Activities	2.53	2.68
Shoreline / Recreational Activities	74.46	67.61

■ Occ % at A ■ Occ % at Site B
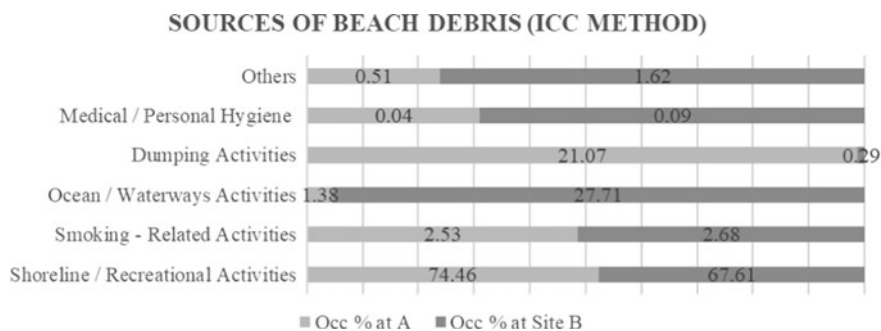
Fig. 4 Source of marine debris at both sites

At both the sites, the plastic bags were the most abundant with 1026 at site A and 840 at site B, followed by food wrappers (540), cups (491) and bottle and caps (233) at site A and cups (462), thermocol/styrofoam (386) and food wrappers (342) at site B. The composition of these plastic debris demarcates the source activities of the debris. At site A, the debris contamination is majorly due to littering by visitors and illegal dumping activities, wherein at site B, the debris composition suggests that most debris arise due to the fishing activities which includes plastic ropes, nets, thermocol, and styrofoam. Further studies are required to associate the debris with the sources so as to develop appropriate prevention and mitigation efforts. The impacts of debris on marine flora and fauna in the Indian coastline remain unknown and should be investigated.

3.3 Sources of Marine Debris

As prescribed in the Ocean Conservancy's Methodology [47], the debris were grouped into (i) shoreline and recreational, (ii) ocean and waterway, (iii) smoking related, (iv) dumping, and (v) medical and personal hygiene activities (Fig. 4). Shoreline/recreational activities were the largest source of debris (74.46%) at Site A and (67.61%) Site B which included corn stalks, plastic bags, paper bags, food wrappers, plastic cups, etc.

Cardboard, glass, and metal fragments are categorized into dumping activities and constitutes the second major source of debris (21.07%) at Site A. At Site B, the second major source of debris is ocean/waterway activities (27.71%) which includes buoys/floats, fishing line, fishing nets, rope, etc, which clearly indicates the difference in the use of the beaches.

4 Discussion

Only few studies have been reported from India in spite of marine debris being a worldwide problem and posing serious threats for both ecology and economy. A comprehensive monitoring protocol needs to be developed to recognize the impacts of marine debris along the Indian coastline, which must also allow the results to be comparable with local and global scale. The debris accumulation rates, quantity, and sources differ from site to site with changing wind and tidal characteristics [53, 54]. The littering behavior and high usage of plastics by the beachgoers contribute to the debris along the beaches in developing countries [39].

Marina beach (Site A) has meaner total density of marine debris than Srinivasapuram beach (Site B). This is attributed by the fact that Marina beach being a recreational beach. On the other hand, at Srinivasapuram beach (Site B) debris items related to fishing activities were found in large number, this can be attributed to the local fishing activities. This clear difference in the type of debris pattern calls for the implementation of suitable management plans based on the local activities. The debris concentration shows a strong temporal trend between two months; the increase in the debris concentration in Marina beach during April month can be explained by the onset of summer vacation in the state, where a large number of tourists visit the beach (Fig. 5). The fluctuation in the debris concentration at Srinivasapuram beach can be attributed to rainfall and runoff into the sea, as June–Sep is usually the monsoon months. The Ocean Conservancy methodology is the widely used approach to categorize the sources of debris. This method has proven to be successful, as it allows the comparison of other debris study results around the globe [55].

Shoreline and Recreational activities (71.36%) form the major source of debris, followed by Ocean and Waterways activities (13.21%) and Dumping activities (11.73%). The quantity of debris originating from shoreline and recreational activity in Chennai is much higher in comparison with the international reports [47, 56]. In general, all the debris studies conducted globally including this study showed the plastics to be predominant [3, 6, 19, 37, 39, 57].

We hope that this work will bring awareness about the present situation of marine debris along the Chennai coastline and help publicizing the hazard of the debris issue. Practicing simple management practices, including the use of reusable and recyclable plastics, careful handling at industrial site, bans and fees for using plastic bags, systematic beach cleanup activities and regulating debris load from shipping and sea-based activities, can help reduce the litter load entering the oceans [43]. In addition, use of modern imaging technologies, including UAV and satellite remote sensing, should also be used in surveying coastal areas for understanding the source and pathway of these debris.
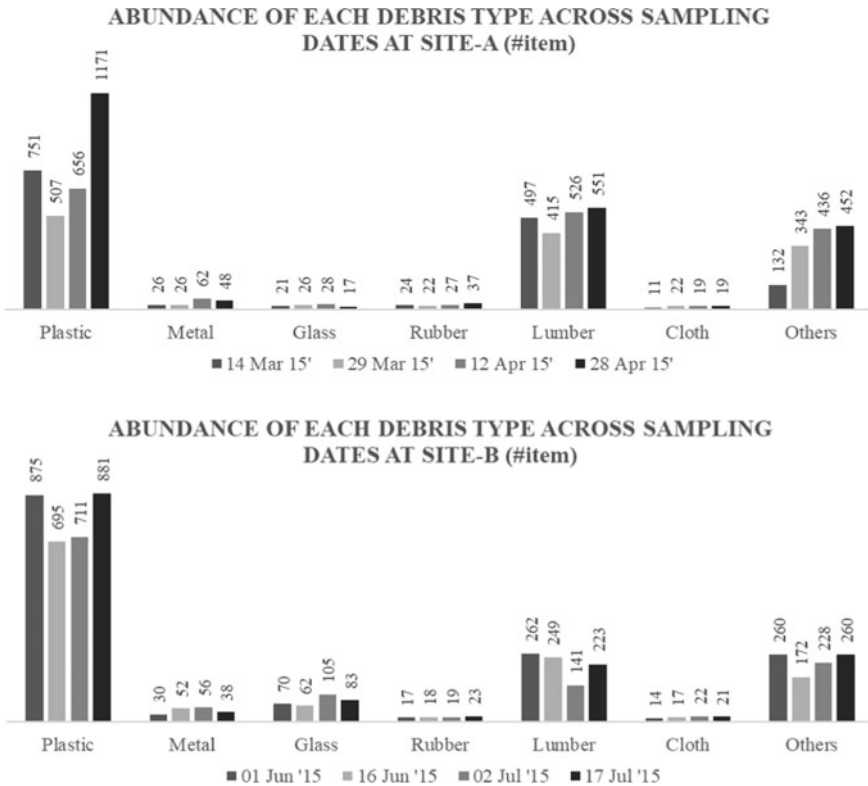
Fig. 5 Composition of marine debris collected

5 Conclusion

This study documents the first account of debris pollution along Chennai coast and provides information for stakeholders working on waste management plans. As marine debris study is in its infancy in the country, quantification and accumulation rate of the debris is an essential research topic that can provide insights about health of the coastline. Diverse management strategies should be adopted at different beaches owing to the variability in the debris sources. Apart from management plans, actions aiming at creating awareness should be implemented at all the beaches and should be prioritized not only for recreational users, but also for hawker and the fishermen, who are a part of the coastal ecosystem.

References

1. NOAA Marine Debris Program.: Information on marine debris. Office of Response and Restoratio: NOAA's National Ocean Service, USA (2011)
2. Sheavly, S.B.: National marine debris monitoring program: final program report, data analysis and summary. US Environmental Protection Agency by Ocean Conservancy, USA (2007)
3. Golik, A., Gertner, Y.: Litter on the Israeli coastline. Mar. Environ. Res. **33**(1), 1–15 (1992)
4. Kusui, T., Noda, M.: International survey on the distribution of stranded and buried litter on beaches along the Sea of Japan. Mar. Pollut. Bull. **47**(1), 175–179 (2003)
5. Martinez-Ribes, L., Basterretxea, G., Palmer, M., Tintoré, J.: Origin and abundance of beach debris in the Balearic Islands. Sci. Mar. **71**(2), 305–314 (2007)
6. Santos, I.R., Friedrich, A.C., Do Sul, J.A.I.: Marine debris contamination along undeveloped tropical beaches from northeast Brazil. Environ. Monit. Assess. **148**(1), 455–462 (2009)
7. Moore, C.J., Lattin, G.L., Zellers, A.F.: Quantity and type of plastic debris flowing from two urban rivers to coastal waters and beaches of Southern California. J. Integr. Coast. Zone Manage. **11**(1), 65–73 (2011)
8. Hong, S., Lee, J., Jang, Y.C., Kim, Y.J., Kim, H.J., Han, D., Hong, S.H., Kang, D., Shim, W.J.: Impacts of marine debris on wild animals in the coastal area of Korea. Mar. Pollut. Bull. **66**(1), 117–124 (2013)
9. Duhec, A.V., Jeanne, R.F., Maximenko, N., Hafner, J.: Composition and potential origin of marine debris stranded in the Western Indian Ocean on remote Alphonse Island, Seychelles. Mar. Pollut. Bull. **96**(1), 76–86 (2015)
10. Kumar, A.A., Sivakumar, R., Reddy, Y.S.R., Raja, M.B., Nishanth, T., Revanth, V.: Preliminary study on marine debris pollution along Marina beach, Chennai, India. Reg. Stud. Mar. Sci. **5**, 34–40 (2016)
11. Moore, S.L., Allen, M.J.: Distribution of anthropogenic and natural debris on the mainland shelf of the Southern California Bight. Mar. Pollut. Bull. **40**(1), 83–88 (2000)
12. Moore, S.L., Gregorio, D., Carreon, M., Weisberg, S.B., Leecaster, M.K.: Composition and distribution of beach debris in Orange County, California. Mar. Pollut. Bull. **42**(3), 241–245 (2001)
13. Convey, P., Barnes, D., Morton, A.: Debris accumulation on oceanic island shores of the Scotia Arc, Antarctica. Polar Biol. **25**(8), 612–617 (2002)
14. Barnes, D.K., Milner, P.: Drifting plastic and its consequences for sessile organism dispersal in the Atlantic Ocean. Mar. Pollut. Bull. **146**(4), 815–825 (2005)
15. Kei, K.A.: Beach litter in Amami Islands, Japan. South Pac. Stud. **26**, 15–24 (2005)
16. Ryan, P.G., Moore, C.J., Van Franeker, J.A., Moloney, C.L.: Monitoring the abundance of plastic debris in the marine environment. Philos. Trans. R. Soc. Lond. B Biol. Sci. **364**(1526), 1999–2012 (2009)
17. Law, K.L., Morét-Ferguson, S., Maximenko, N.A., Proskurowski, G., Peacock, E.E., Hafner, J., Reddy, C.M.: Plastic accumulation in the North Atlantic subtropical gyre. Science **329**(5996), 1185–1188 (2010)
18. Boerger, C.M., Lattin, G.L., Moore, S.L., Moore, C.J.: Plastic ingestion by planktivorous fishes in the North Pacific Central Gyre. Mar. Pollut. Bull. **60**(12), 2275–2278 (2010)
19. Derraik, J.G.: The pollution of the marine environment by plastic debris: a review. Mar. Pollut. Bull. **44**(9), 842–852 (2002)
20. Gregory, M.R.: Environmental implications of plastic debris in marine settings-entanglement, ingestion, smothering, hangers-on, hitch-hiking and alien invasions. Philos. Trans. R. Soc. Lond. B Biol. Sci. **364**(1526), 2013–2025 (2009)
21. Murray, F., Cowie, P.R.: Plastic contamination in the decapod crustacean Nephrops norvegicus (Linnaeus, 1758). Mar. Pollut. Bull. **62**(6), 1207–1217 (2011)
22. Gregory, M.R.: The hazards of persistent marine pollution: drift plastics and conservation islands. J. R. Soc. N. Z **21**(2), 83–100 (1991)
23. Azzarello, M.Y., Van Vleet, E.S.: Marine birds and plastic pollution. Mar. Ecol. Prog. Ser. **37**, 295–303 (1987)

24. Nevins, H., Hyrenbach, D., Keiper, C., Stock, J., Hester, M., Harvey, J.: Seabirds as indicators of plastic pollution in the North Pacific. Paper for Plastic Debris Rivers to the Sea Conference, September (2005)
25. Barnes, D.K., Galgani, F., Thompson, R.C., Barlaz, M.: Accumulation and fragmentation of plastic debris in global environments. Philos. Trans. R. Soc. Lond. B Biol. Sci. **364**(1526), 1985–1998 (2009)
26. Abu-Hilal, A.H., Al-Najjar, T.: Litter pollution on the Jordanian shores of the Gulf of Aqaba (Red Sea). Mar. Environ. Res. **58**(1), 39–63 (2004)
27. Barnes, D.K.: Biodiversity: invasions by marine life on plastic debris. Nature **416**(6883), 808–809 (2002)
28. Barnes, D.K., Fraser, K.P.: Rafting by five phyla on man-made flotsam in the Southern Ocean. Mar. Ecol. Prog. Ser. **262**, 289–291 (2003)
29. Engler, R.E.: The complex interaction between marine debris and toxic chemicals in the ocean. Environ. Sci. Technol. **46**(22), 12302–12315 (2012)
30. Newman, S., Watkins, E., Farmer, A., ten Brink, P., Schweitzer, J.P.: The economics of marine litter. In: Marine Anthropogenic Litter, Springer International Publishing. 367–394 (2015)
31. Sheavly, S.B., Register, K.M.: Marine debris and plastics: environmental concerns, sources, impacts and solutions. J. Polym. Environ. **15**(4), 301–305 (2007)
32. Secretariat of the convention on biological diversity (SCBD) and the scientific and technical advisory panel—GEF, Impacts of Marine Debris on Biodiversity: Current Status and Potential Solutions. Technical Series No. 67, 61 (2012)
33. Nigam, R.: Plastic pellets on the Caranzalem Beach sands, Goa, India. Mahasagar **15**(2), 125–127 (1982)
34. Dharani, G., Nazar, A.K.A., Venkatesan, R., Ravindran, M.: Marine debris in Great Nicobar. Curr. Sci. **85**, 574–575 (2003)
35. Reddy, M.S., Basha, S., Adimurthy, A., Ramachandraiah, G.: Description of the small plastics fragments in marine sediments along the Alang-Sosiya shipbreaking yard India. Estuar. Coast. Shelf Sci **68**(3), 656–660 (2006)
36. Sridhar, K.R., Deviprasad, B., Karamchand, K.S., Bhat, R.: Plastic debris along the Beaches of Karnataka, Southwest Coast of India. Asian J. Water Environ. Pollut. **6**(2), 87–93 (2007)
37. Ganesapandian, S., Manikandan, S., Kumaraguru, A.K.: Marine litter in the northern part of Gulf of Mannar, southeast coast of India. Res. J. Environ. Sci. **5**(5), 471–478 (2011)
38. Kaladharan, P., Vijayakumaran, K., Singh, V.V., Asha, P.S., Sulochanan, Bindu, Asokan, P.K., Valsala, K.K., Veena, S., Jayasankaran, L., Bhint, H.M.: Assessment of certain Anthropogenic Interventions and their Impacts along the Indian Coastline. Fishery Technology, **49**, 32–37 (2012)
39. Jayasiri, H.B., Purushothaman, C.S., Vennila, A.: Quantitative analysis of plastic debris on recreational beaches in Mumbai. India. Mar. Pollut. Bull. **77**(1), 107–112 (2013)
40. Balasubramaniam, M., Phillott, A.D.: Preliminary observations of microplastics from beaches in the Indian ocean. Indian Ocean Turtle Newsletter, 13–16 (2016)
41. Veerasingam, S., Mugilarasan, M., Venkatachalapathy, R., Vethamony, P.: Influence of 2015 flood on the distribution and occurrence of microplastic pellets along the Chennai coast, India. Mar. Pollut. Bull. **109**(1), 196–204 (2016)
42. Veerasingam, S., Saha, M., Suneel, V., Vethamony, P.: Microplastic pollution: a serious threat to the marine ecosystem. Blue Waters Newslett. Mar. Environ. Prot. **18**, 6–9 (2017)
43. Kumar, A.A., Sivakumar, R.: Marine debris—the global problem least studied in India. Curr. Sci. **110**(7), 1153–1154 (2016)
44. Mishra, P., Panda, U.S., Pradhan, U., Kumar, C.S., Naik, S., Begum, M., Ishwarya, J.: Coastal water quality monitoring and modelling off Chennai City. Procedia Eng. **116**, 955–962 (2015)
45. Rademacher, A.M., Sivaramakrishnan, K.: Ecologies of Urbanism in India: Metropolitan Civility and Sustainability. Hong Kong University Press, Hong Kong (2013)
46. Lippiatt, S., Opfer, S., Arthur, C.: Marine Debris Monitoring and Assessment. NOAA Technical Memorandum NOS-OR&R-46, USA (2013)

47. Ocean Conservancy.: Turning the Tide on Trash. Accessed through: http://www.oceanconservancy.org/our-work/marine-debris/icc-data-2014.pdf (2014)
48. Rees, G., Pond, K.: Marine litter monitoring programmes—a review of methods with special reference to national surveys. Mar. Pollut. Bull. **30**(2), 103–108 (1995)
49. Edyvane, K.S., Dalgetty, A., Hone, P.W., Higman, J.S., Wace, N.M.: Long-term marine litter monitoring in the remote Great Australian Bight, South Australia. Mar. Pollut. Bull. **48**, 1060–1075 (2004)
50. Oigman-Pszczol, S.S., Creed, J.C.: Quantification and classification of marine litter on beaches along Armacao dos Buzios, Rio de Janeiro. Brazil. J. Coast. Res. **23**(2), 421–428 (2007)
51. Gourmelon, G.: Global plastic production rises-recycling lags. New world watch Institute analysis explores trends in global plastic consumption and recycling. Available from: http://www.worldwatch.org. Accessed: 04 March 2016 (2015)
52. Eriksen, M., Lebreton, L.C., Carson, H.S., Thiel, M., Moore, C.J., Borerro, J.C., Galgani, F., Ryan, P.G., Reisser, J.: Plastic pollution in the world's oceans: more than 5 trillion plastic pieces weighing over 250,000 tons afloat at sea. PLoS ONE **9**(12), e111913 (2014)
53. Coe, J.M. and Rogers, D.: Marine Debris: Sources, Impacts, and Solutions. Springer Science & Business Media (2012)
54. Ribic, C.A., Sheavly, S.B., Rugg, D.J., Erdmann, E.S.: Trends in marine debris along the US Pacific Coast and Hawai'i 1998–2007. Mar. Pollut. Bull **64**(5), 994–1004 (2012)
55. Cheshire, A., Adler, E., Barbière, J., Cohen, Y., Evans, S., Jarayabhand, S., Jeftic, L., Jung, R.T., Kinsey, S., Kusui, E.T., Lavine, I.: UNEP/IOC Guidelines on survey and monitoring of marine litter (2009)
56. Ocean Conservancy.: International coastal cleanup. 2009 report. A rising tide of ocean debris. Ocean Conservancy, USA (2009)
57. Madzena, A., Lasiak, T.: Spatial and temporal variations in beach litter on the Transkei coast of South Africa. Mar. Pollut. Bull. **34**(11), 900–907 (1997)

Self-curing Possibilities of Polygel in Ordinary Concrete

Nagesh T. Suryawanshi and Sunil B. Takare

Abstract The super absorbent polymer (SAP) absorbs the water and forms gel results in increase in the volume proportionally. The gel form will act as a source for self-curing after final setting of concrete. In this study, poly acrylic acid (PAA) has been tried as self-curing agents and its effect on ordinary concrete was examined. This report is an experimental investigation in which PAA mixed with ordinary concrete in varying percentages. Poly acrylic acid available in crystal and powder form mixed separately with ordinary concrete, and its effect on properties of concrete was examined. Powder form of PAA was found to be more effective than crystal form. This may be because of crystal form of PAA provides additional void in the concrete mass. The concrete strength may get reduced because of porous nature in a concrete.

Keywords Super absorbent polymers · Poly gel · Poly acrylic acid · SEM

1 Introduction

Superabsorbent polymers were effectively used for curing concrete internally. Internal water curing is the process in which self-curing agents mixed with concrete, which helps to keep the concrete moist as it hardens. Internal curing has been used for decades to encourage hydration of cement; it also helps to restraint cracks likely to occur in hardening process. From the literature reviewed, only saturated light weight aggregate was tried as self-curing agents. But there are some key issues associated with the use of lightweight aggregates, includes difficulty in concrete workability, reduction in strength and elastic modulus. To reduce or overcome these problems, the super absorbent polymers are the best alternative [1]. Super absorbent polymers

N. T. Suryawanshi (✉) · S. B. Takare
JSPM's RSCOE, Savitribai Phule Pune University, Tathwade, Pune, Maharashtra, India
e-mail: nt.Suryawanshi@gmail.com

S. B. Takare
e-mail: prof_sbthakare@rediffmail.com

releases the hold water during hydration process act as internal water reservoir. Since many years, public healthcare industry was effectively utilizing SAPs in production of various items. It was found that SAPs can absorb water up to 5000 times of its weight [2, 3]. There are various types of polymers known for water absorption ability. Poly acrylic acid is one of most widely used polymers as its water absorption ratio is higher than any other polymers. Bi-functional molecules cause formation of cross-linked polymers [4].

The objective of this study was to examine water retention ability of PAA in different forms. It also includes finalizing of optimum dose of PAA that would improve mechanical properties.

1.1 Properties of PAA

Chemical and physical properties of PAA provided by manufacturer are as follows

1.1.1 Chemical Properties

Poly acrylic acid is prepared from monomer acrylic acids by free radical polymerization reaction. The presence of carbonyl group causes high reactivity of acrylic acid leads to the addition of versatile nucleophiles. PAA is white, colorless, and fluffy powder at room temperature. It is soluble in water, and pH of solution ranges between 3 and 5. The empirical formula of PAA is $C_3H_4O_2$.

1.1.2 Physical Properties

Sr. no.	Physical parameter	Values
1	Molecular weight	Avg. 1200–100,000
2	Melting point	13.5 °C
3	Density	1.23 g/cm^3 @ 20 °C
4	Boiling point	116 °C

Fig. 1 PAA in dry state

1.1.3 Poly Acrylic Acid (Powder Form)

This powder form of acid is completely dissolved in water at room temperature. After dissolving, there is formation of colorless solution and there is no evolution of heat. Powder is passing through 90 μ and retain on 75 μ (Fig. 1). There is no hazard during handling of this powder. In this study, we completely dissolve the powder in water as per design (% by weight of cement), and this water is added in dry mixed material (sand, cement, aggregate).

1.1.4 Poly Acrylic Acid (Crystal Form)

This crystal of acid is passing through 150 μ and retain on 90 μ. These crystals absorb water up to 100–110 times of its weight, Fig. 2 shows swelling of crystals, and we can make ball of PAA as shown in Fig. 3. No water will be absorbed beyond this limit, and the addition of water beyond this limit results in formation of colorless slurry. Figure 4 shows the scanning electron microscopy images (SEM) represents the structure and various elements present in it.

Fig. 2 PAA in swollen state

Fig. 3 Ball formation of PAA

Fig. 4 SEM image of PAA
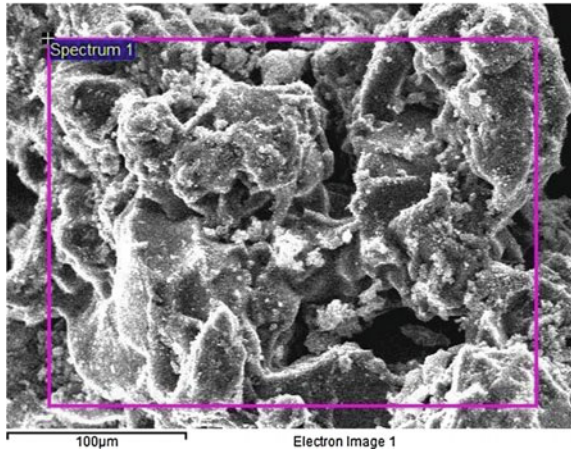
2 Experimental Procedure

Ordinary Concrete mix design of M20 grade was prepared as per IS 10262:1982. Concrete was prepared in horizontal pan mixer. Initially all the ingredients mixed for two minutes in dry state. Half of the mixing water was added little by little with PAA. PAA added in varying percentages from 0.2, 0.4, 0.6, 0.8, and 1.0% by the weight of cement. All the constituents mixed thoroughly in mixer for 2 min to produce homogeneous mass. After mixing, three types of specimens, namely cubes (150 mm × 150 mm × 150 mm), beams (100 mm × 100 mm × 500 mm), and cylinders (Ø100 mm, length 200 mm), were cast by using steel moulds. The casted specimens demolded after 24 h and kept in dry air in laboratory for 28 days. Every day weight loss was observed, tabulated, and represented graphically in figures. Compressive strength, splitting tensile strength, and flexure strength were measured by conducting tests on cubes, cylinders, and beams, respectively, at the end of 28 days (Figs. 5 and 6).

3 Results and Discussion

3.1 Weight Loss

Weight loss observations were made of Powder form of PAA every day, and the weight loss observed is tabulated and also represented graphically in Figs. 7, 8, 9, 10 and 11. It was found that the weight loss increases as PAA addition increases, and it is up to 2%. Weight loss observed was found nearly equal up to 0.6% addition of PAA. Weight loss observations were made of Crystal form of PAA every day, and it was found that the weight loss increases as PAA addition increases, and it is up to 4%.

3.2　Compressive Strength

Compressive strength obtained of Powder form PAA is tabulated and represented graphically by Figs. 5 and 6. Compressive strength obtained for 0.2–0.6% addition of PAA is found to be nearly equal to control mix, and it is up to 27 N/mm^2. Compressive strength obtained for all variations of PAA crystal form is up to 15 N/mm^2, and it was not up to the mark.

Relation between compressive strength and PAA % is mathematically expressed by equation

$$Y = -4.232\,x^2 - 2.929\,x + 29.04 \text{ with degree of Confidence } 0.889.$$

■ Series1	0	0.2	0.4	0.6	0.8	1
	29.32	28.4	25.6	27.7	24.3	21.46
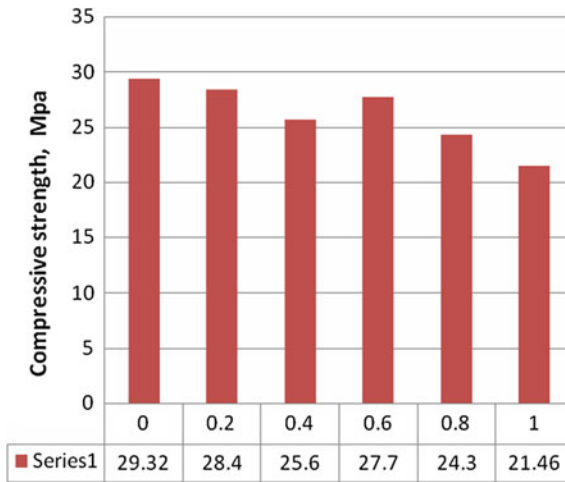
Fig. 5 Compressive Strength of PAA (powder form)

$y = -4.232x^2 - 2.929x + 29.04$
$R^2 = 0.889$
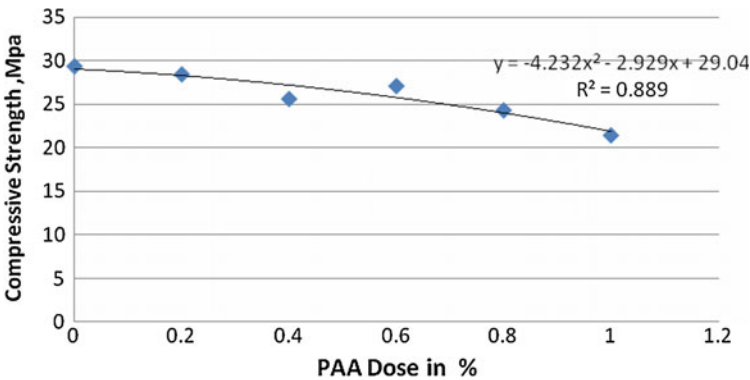
Fig. 6 Curve fitting (compressive strength versus %PAA)
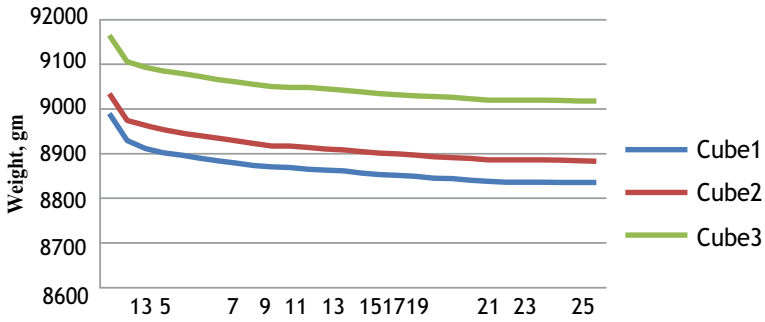
Fig. 7 Weight loss of control mix M20 without PAA
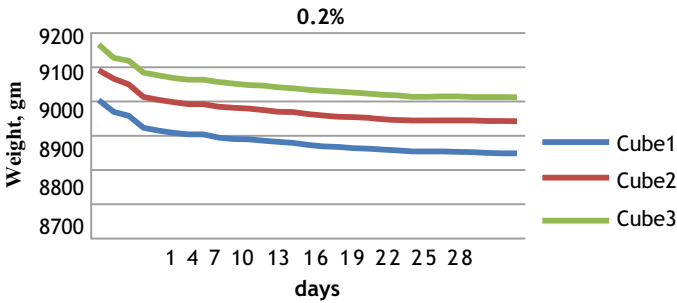
Fig. 8 Weight loss for 0.2% PAA by weight of cement
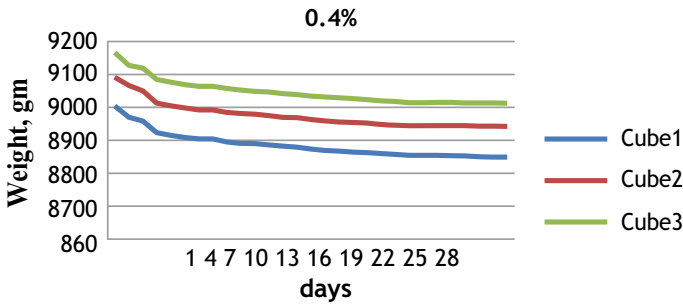
Fig. 9 Weight loss for 0.4% PAA by weight of cement

3.3 Split Tensile Strength

Test conducted on cylinders and results show that split tensile strength found of concrete with powder form of PAA is up to 10% of control mix, and of crystal PAA is up to 7% of Control mix.
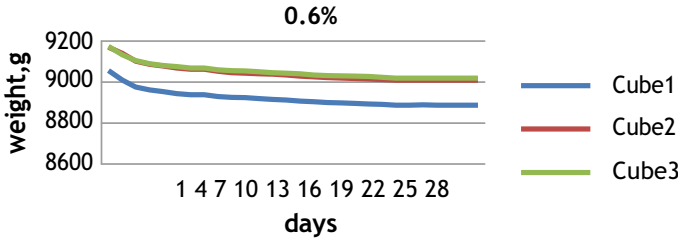
Fig. 10 Weight loss for 0.6% PAA by weight of cement

Fig. 11 Weight loss for 0.8% PAA by weight of cement
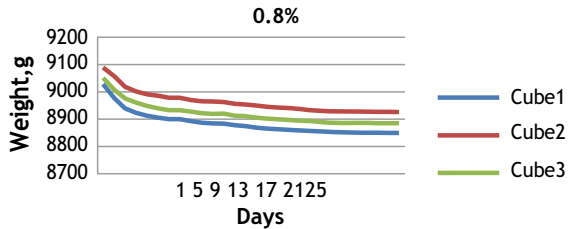
3.4 Flexural Strength

Flexural strength obtained of concrete added with powder as well as crystal PAA is almost Zero. No flexural strength has been observed for all variations.

4 Conclusion

  i. Ordinary concrete of grade M20 mixed with powder form of PAA shows nearly same weight loss up to 0.6% addition, thereafter there was increase the weight loss would affect on strength of concrete.
 ii. The crystal form PAA addition from 0.2 to 1% in concrete results in increase in weight loss and produce brittle concrete of lower density.
iii. The optimum dose of PAA powder form is found to be 0.6%. It would provide compressive strength nearly equal to the compressive strength of control mix.
 iv. The crystal form of PAA produce compressive strength which is very less than the strength of control mix.
  v. Split tensile strength of PAA crystal form and of powder form found is about 7 and 10% of strength of control mix resp.
 vi. Flexural strength for both forms of PAA is found to be Zero.
vii. Powder form of PAA is more suitable to use in ordinary concrete than crystal form of PAA.

References

1. Jensen, M.: Use of superabsorbent polymers in concrete. Concr. Int. **35**(1), 48–52 (2013)
2. Jensen, O.M., Hansen, P.F.: Water-entrained cement-based materials I.: principles and theoretical background. Cem. Concr. Res. Heft **31**, 647–654 (2001)
3. Jensen, O.M., Hansen, P.F.: Water entrained cement based materials II. Exp. Obs. Cem. Concr. Res. Heft **32**, 973–978 (2002)
4. Buchholz, F.L., Graham A.T.: Modern Superabsorbent Polymer Technology, Wiley, ISBN-0-471-19411-5 (1998)
5. RILEM: Internal Curing of Concrete—State- of-the-Art Report of RILEM Technical Committee 196-ICC. State of the Art Report, RILEM Publications SARL (2007)

Light Transmitting Concrete—Litracon

Ashish B. Ugale, Rushikesh R. Badnakhe and Prathmesh P. Nanhe

Abstract Due to the increasing population in world and excessive use of energy, there can occur condition where all energy generating resources can be depleted. As mainly energy is generated by nonrenewable energy resources and to save these resources, there is need to make alternative energy generating as well as energy saving material. In this paper, one such construction material is reviewed which can be also called as energy saving construction material named as light transmitting concrete—Litracon. Also its manufacturing, uses, its different properties, and its effect on power consumption are reviewed. In this paper, it is conclude that, various additives and replacement in material in manufacturing of Litracon which increases its efficiency and make it more effective.

Keywords Concrete technology · Light transmitting concrete · Litracon · Power consumption

1 Introduction

Advanced growth in the infrastructure globally has made concrete the most widely and ordinarily utilized construction material all through the world. Growing demand of infrastructure has created huge pressure on the concrete industry to produce large quantum of concrete. The cost of concrete production primarily depends on the cost of its constituent raw materials, namely cement, aggregates (coarse and fine), and water. Among the raw materials of concrete, the Natural River sand which forms around 35% of the concrete volume plays an important role in deciding the cost

A. B. Ugale (✉) · R. R. Badnakhe · P. P. Nanhe
P.R.M.C.E.A.M, Badnera, Amravati, India
e-mail: abugale@rediffmail.com

R. R. Badnakhe
e-mail: rushikeshbadnakhe@gmail.com

P. P. Nanhe
e-mail: prathnanhe500@gmail.com

of concrete. As concrete is most ordinarily used material for construction and used on large scale, researchers have tried to make a smart type of concrete named it as Litracon. In this material, optical fiber will be embedded in concrete and will make it translucent. This paper focused on "Litracon" concept, having a relation with energy consumption and architectural look. It also describes the role of Litracon in energy saving and making of cities smart [1].

2 Motivation

The city is a government unit which is growing increasingly larger, complex, and important as the population ranks of urban areas. By 2050, this number is expected to increase. With the rapid increase in the urban population worldwide, it faces a variety of risks concerns and problems. The unprecedented rate of urban growth creates urgency to finding smarter ways to manage the accompanying challenges. Researchers has recognized gap in developing the concept of energy consumption, its saving, and its smarter alternatives. Considering the gap, some of the points are focused and under study such as

1. The reason for excessive use of energy
2. Aspect to look toward the issue
3. Smarter material for saving energy
4. The construction material which enhances in world due to its good esthetic appearance and energy saving property.

This paper gives an idea about the inquiries, fill the research gap, and conceptualize Litracon and its effect on world [2].

3 Literature Review

Aron Losonczi (2002) has invented LTCM, and named it as Litracon. The product was blocks of polished prefabricated fiber concrete, and its composition was 96% concrete and 4% fiber. The maximum dimension of blocks was 600 mm × 300 mm, and the colors of them were gray, black, or white. The compressive and flexural strength were 50 and 7 N/mm^2, respectively. These products have been used in Hungary, America, France, Belgium, Germany, and Japan. Vitreous optical fibers with diameters of 0.2 mm were used in Litracon.

Annual report of 2011–12 on working of state power and utility and electricity department and Energy statistics 2017 twenty-fourth issue report explained us the energy sources in India also tells about current condition of energy generation and energy generating fuels. According to both report, energy is consumed on large scale by commercial and industrial sectors in India thus indirectly our energy generating

fuels are coming toward depletion so preventive measures as well as alternative should be find out is concluded in these reports.

Al-Kurdi, Architect [3] has used Litracon project in an official building of Jordan city and found that this construction material is highly energy saving if we used in external wall of frame structure, according to research there is direct saving of artificial light consumption for 8–10 h in official building which is great thing. It was found that 80% of light is passing through optical fiber from one end to another, and 20% is loss due to impurities by light transmitting test on Litracon.

Juan and Zhi [4] has discussed the development of smart transparent concrete with the use of optical fiber, which will reduces the power consumption of illumination. And also this will be used for an architectural purpose for good esthetical view of the building. It can be used where the light cannot reach with appropriate intensity. It has some disadvantages, such as it requires skilled supervision and also its cost is very high due to the optical fibers used in it.

Demirel [5] has investigated the effects of using waste marble dust (WMD) as a fine material on the mechanical properties of the concrete. For this purpose, four different series specimen of size $100 \times 100 \times 100$ mm were prepared by replacing the fine sand (passing 0.25 mm sieve) with WMD at proportions of 0, 25, 50, and 100% by weight. Relative to the reference sample, the 28-day compressive strength and dynamic modulus of elasticity of the 100% replacement samples were increased by 10 and 25%, respectively, and the porosity decreased by 8%.

Belachia and Hebhoub [6] had studied the use of waste marble aggregates in concrete production. They prepared mixtures in which natural sand (NS) is substituted by the recycled sand (RS) at 25, 50, 75%, and 100%. The compressive strength was conducted on cylinder of size 16×32 cm. The highest compressive strength was achieved at the 25% substitution ratio maintaining the ratio at 0.45 w/c, they found that the samples not containing waste marble have a compressive strength of 33 N/mm^2, whereas in samples containing 25% waste marble, the compressive strength increased to approximately 36 N/mm^2. These researchers concluded that waste marble is a suitable alternative material to natural aggregates.

Li et al. [7] had discussed about compressive test and flexural test on Litracon beam after 28 days of curing, beam was of size 4 cm $\times$ 4 cm $\times$ 16 cm with variation in optical fiber diameter from 0.5 to 1 mm with different volume fraction of optical fiber; according to them, maximum compressive strength was of block in which 0.5 diameter optical fiber were used at volume fraction 0.25% which was 70.1 and 9.1 N/mm^2 they said that strength of Litracon will be decreased as we increase volume fraction of optical fiber and light transmitting capacity will increase.

Basma and Bashbash [8] have prepared 50 mm $\times$ 50 mm $\times$ 50 mm cubes with plastic optical fiber 4% with diameters of fiber as 1, 2, 3, 4 mm. Weight of cube specimen cement is 500 g and water 250 g. Fine aggregate is 1350 g. The compressive strength for 1-, 2-, 3-, 4-mm optical fiber diameter was observed as 21.5, 22, 23, and 23.5 N/mm^2. They observed that for the same percentage of fiber, the larger diameter fiber concrete has higher strength.

Amlan Kumar Sahoo, Sachin Sahu, Aman Kumar Singhal, Kuramana Stephen, Tamo Talom, Subham Saroj Tripathy, Sidhant Das, in January 2017 examined the

solid examples by strengthening optical strands and contrasting it and the customary cement. The solid examples were subjected to various tests, for example, compressive quality test, light transmission test, and so on. The compressive quality outcomes acquired for the translucent solid examples was relatively same as that of the customary solid example. The aftereffects of the transmission test were tasteful as the POF hold its productivity. Consequently, it is apparent that the straightforwardness of the solid structures can be presented with the inclusion of optical strands without trading off the quality, which is a stage forward to the desire of accomplishing some new feet in current.

According to Author H.B Valambyia in January 2017 Light Transmitting concrete, otherwise called translucent cement. Light transmitting properties because of installed light optical components. Light is directed through the solid square starting with one end then onto the next. Hence, strands need to experience the entire question, with a specific end goal to accomplish most extreme entrance of light. It create distinctive light example at first glance, contingent upon the fiber structure, their course of action, and the span of filaments utilized. This paper portrays chronicled improvement of light transmitting concrete and different strategies to create and given light transmitting solid board, likewise examined around two contextual analyses on light transmitting solid board or square made undertaking by Litracon and Italcementi Groups. These two organizations made light transmitting solid board or square in various ways.

4 Materials and Methods

To achieve the objectives of this experimental study, an extensive experimental program was planned by researchers, which included study of concrete prepared with substitution of fine aggregates with quarry dust/marble dust (varying the percentage of marble dust) and replacing coarse aggregates with marble aggregates. Out of these different ratios, the best possible ratios are selected on the basis of strength, permeability, dynamic modulus of elasticity, porosity, and thereafter light transmitting concrete is prepared which is further evaluated for compressive strength, durability, and finding out the light transmittance characteristics of light transmitting concrete.

4.1 Material Used

4.1.1 Cement

Portland Pozzolana cement conforming to IS: 8112-1989 was used, tested according to IS: 4031-1988 having uniform color, i.e., gray with light greenish shade.

4.1.2 Quarry and Marble Dust

Quarry dust has been sieved from IS 2.36 mm sieve, not containing any impurities such as vegetable matters, organic matter, lumps, etc.

4.1.3 Coarse and Marble Aggregate

The maximum nominal size of aggregate used was 10 mm.

4.1.4 Water

It is used for mixing and curing, must be clean potable and free from injurious amounts of oils, acids, alkalis, salt, sugar, organic materials, or other substances having PH value of the water was 7.6.

4.1.5 Plastic Optical Fiber

An optical fiber is an adaptable, straightforward fiber made of expelled glass, its capacity as a wave guide, or "light pipe,", to transmit light between the two finishes of the fiber. The exploratory program was partitioned into two sections by the specialists. The initial segment was committed to look at the impact of substitution of fine totals with quarry dust (QD)/marble dust (MD) and coarse totals (CA) with marble totals (MA). The examples were tried for compressive quality, flexural quality, penetrability, and ultrasonic heartbeat speed. The impacts of these properties were inspected by fluctuating the rate supplanting of quarry dust with squander marble dust. The second piece of the exploratory program concentrated on the improvement of the chose configuration blend.

From there on, light transmitting concrete is set up for the chose configuration blend to think about the light transmittance qualities and strength viewpoints.

4.1.6 Proportions for Nominal Mix Concrete

According to IS 456:2000, the blend extents will be chosen to achieve the satisfactory functionality of the crisp cement, and when concrete is solidified, it will have the required quality, sturdiness, and wrap up. The assurance of the extents of bond, totals, and water to guarantee the required quality will be made as takes after:-

1. By planning the solid blend configuration blend concrete.
2. By embracing ostensible blend concrete.

Table 1 Quantity of aggregates and water for various concrete mixes with respect to 50 kg of cement

Grade of concrete	Total quantity of Dry aggregate by mass per 50 kg of cement	Proportion of fine aggregate to coarse aggregate (by mass)	Quantity of Water per 50 kg of cement Max
M5	800	Generally 1:2 but subject to an upper limit of 1:1 and lower limit 1:2	55
M7.5	620		40
M10	470		30
M15	320		28
M20	240		25

Ostensible blend concrete is utilized for cement of M20 or lower. The extents of materials for ostensible blend concrete will be as per IS 456:2000 which is mentioned below in Table 1.

4.2 Preparation of Concrete Specimen

Distinctive blocks of cement were set up according to previously mentioned proportions. The quality required for light transmitting cement to be utilized as a part of load bearing dividers is 10MPA. In request to fulfill the above, prerequisite M10 review is chosen for exploratory investigation.

Writing said the more will be the compressive quality can be accomplished if sand is supplanted by marbel dust up to 100% and coarse total is supplanted by marbel total up to 100% that is the reason in this examination for best outcomes distinctive shapes where made of.

1. Concrete sand coarse total
2. Concrete marble dust marble total.

Readiness of light transmitting concrete specimen, during the time spent making light transmitting concrete, the initial step included is planning of shape. The shape required for the model can be made with various materials which can be of either tin or wood. Wooden molds of various sizes were set up with the punctured wooden sheets. Wooden sheets which are utilized for electrical switchboards were utilized. Punctured wooden sheets with differing number of bored gaps were joined in the molds, for planning 3D shapes of fluctuating level of P.O.F. The distance across and dividing of the openings relied upon the level of fiber in the 3D square. Reason for sheet is to empower the arrangement of P.O.F appropriately in the solid.

4.3 Testing on Light Transmitting Concrete

4.3.1 Test for Light Transmittance Property

Light transmittance test was performed to ponder the light transmittance attributes. It is the most imperative test to be performed, as fundamental motivation behind translucent cement is to transmit light. For concentrate light controlling property of light transmitting solid, examples of P.O.F volume of 4% for each sort were thrown. The transmittance was estimated by photometer (or lux meter) that measures force of light in lumens, having scope of 0.1–100,000 lx. The glowing light with light force of 1100 lx was picked as light source. A wooden box with light source fitted on one face, photometer was appended on other face in the container, to such an extent that all light transmitted from the example falls in the crate of photometer.

Readings of transmitted light were noted with photometer. Safeguard was taken to see that the case of photometer was accurately joined and all transmitted light fall in the crate. Results for light transmitting are mention in Table 3.

4.3.2 Compressive Strength Test on Light Transmitting Concrete

3D squares of 4% plastic optical fiber proportion were readied. Three examples of each POF rate and blend extent were set up as indicated by system said above. The 3D shape examples were thrown and unmolded following 24 h. In the wake of throwing blocks, curing was improved the situation 7 days. The 3D shapes were tried for multiday compressive quality on compression testing machine. The results for compressive strength test are mention in Table 2.

5 Results

5.1 Compressive Strength Result

See Table 2.

Table 2 Compressive strength result with varying diameter and percentage of optical fiber

Type of concrete	Diameter of optical fiber in (mm)	Percentage of optical fiber (%)	Compressive strength In (N/mm^2)	
			7 days	28 days
Cement- sand -CA	0.75	4	8.00	13.22
Cement-marbel dust	0.75	4	10.13	16.98

Table 3 Light transmitting tests result for CA and MA concrete type

Concrete type	Diameter of optical fiber in (mm)	Percentage of optical fiber by volume of concrete cube (%)	Light transmittance (lux)
Cement- sand CA	0.75	4	121
Cement- marbel dust MA	0.75	4	149

5.2 Result on Light Transmittance

See Table 3.

From the above table, it can be seen light transmittance increments with increment in substitution of waste marble dust. It is expanded for blend arranged with marble residue and marble totals when contrasted with control blend (arranged with regular coarse total). At the point when light is episode on the 3D shapes (arranged with marble dust as fine total and marble as coarse totals), it gets reflected and brings about more light to go through optical strands and when light is occurrence on the 3D squares (arranged with quarry dust as fine total and ordinary coarse total), it retains all the light and does not reflect. Subsequently, it can be reasoned that joining of marble as total has enhanced the light transmittance and enhanced outcome is the result from least ingestion of light and most extreme impression of light by marble because of its white shading and the greatest assimilation of light and least reflection by the customary coarse total in the control blend example.

6 Summary and Discussion

In this paper by writing and a few outcomes, it is discovered that a savvy vitality sparing and great tasteful material Litracon. The light transmitting concrete has numerous ideal physical and compound properties contrasted with conventional cement. It is up to 15 times more grounded than conventional cement with high sturdiness while it is 30% lighter. It is 100% waterproof, bolsters high temperatures. The translucency can be direct from the season of make; it permits the section of 80% of the light along these lines it is vitality sparing through lessening lighting and cooling costs. Light transmitting cement can suit an assortment of building outlines. Is worked in various sorts of complete, can be pigmented with an extensive variety of hues and appropriate for both inside and outside. It has numerous points of interest; it opposes assault salts, extraordinary cohesiveness, and it gives a chance to plan component with bring down thicknesses (for their high mechanical properties). Be that as it may, light transmitting solid expands expenses of devastation since it is pulverization safe cement is extremely troublesome. This solid is 15–20% more costly. At last, on account of its high level of straightforwardness, the inner structures of the building are noticeable,

which sooner or later might be unattractive; yet, on account of mechanical advances, structural designing is searching for approaches to that with a decent complete, the iron segments and different materials, might please to the eye to acquire a level of regular and exceptionally natural appearance. It can be utilized for development of roof of bigger workplaces or business building which can diminish cost of lighting amid sunshine hour. At the point when embedded in front entryway of house, it can likewise use as safety efforts with the end goal that inhabitant can be see when there is individual remaining outside, utilized as a part of deck section surface lighting up from beneath. Litracon can be utilized as a part of section, floor, or divider as enlivening material and furthermore utilized as a part of indoor stairwell.

For considering vitality sparing outcomes, get from straightforward case of authority assembling an official building having 8 rooms +2 toilets on ground floor, and has 3 stories up. Its day by day working hour is of 14 h from 8 am to 10 pm. Think about 4(55 W) tube light is utilized as a part of each room as fake lighting and 3(100 W) knob in latrine. Presently as probably am aware 55 W tube light takes around 18 h to consume 1 unit of power and 100 W globule takes 10 h. Every day working hour of office is 14 h in which 10 h we have daylight. So day by day utilization will be as per the following, If 4 lights are utilized for 10 h, around 2 units are scorched and if 3 knobs are singed for 10 h 3 units are singed. If 8 rooms having 4 tubes light each and to toilets having 3 knobs every so add up to unit devoured in 10 h by one story is 22 unit and by 4 stories it will be 88 units. Month to month it will expend 2728 units and yearly 32,736 units. Presently on the off chance that utilized Litracon board or block as outside divider or parcel divider it will maintain a strategic distance from the unreasonable utilization of power straightforwardly by utilizing normal daylight. The main most essential factor is that cost of Litracon will be 15% to 20% higher than basic development; however, it will influence it to up after vitality sparing and will fill in as manageable development material. Add up to cost required for utilizing of Litracon will be recuperated in 1.5–2 years roughly as it will spare power exorbitant utilize.

7 Conclusions

From think about the accompanying closing comment has been drawn.

1. As because of better way of life region is being stuffed, because of which most extreme use of land is finished by building multi-storied structure. This made living territory denser step by step. Along these lines issue of determining regular light inside working because of impediment close-by structure can be comprehended by applying Litracon board in outline structure.
2. It will likewise spare fake light need in day hours because of which power will likewise get spared in all business and private areas. In a roundabout way, it will spare vitality producing assets.
3. It will likewise give great tasteful appearance to building.

4. The quality of Litracon diminish with increment in volume portion of optical fiber and light passing limit expanded.

5. The compressive quality increments with increment in rate supplanting of fine total with marble powder.

6. Maximum compressive quality is discovered when blend is utilized with 100% substitution of fine total with marble powder and coarse total with marble.

7. The light transmittance proportion up to 12% was accomplished by utilizing 4% plastic optical fiber proportion.

8. Thus, it demonstrates that light transmitting cement can be productively utilized as a part of green structures. On the off chance that looking toward vitality sparing on the off chance that we consider a case it will guarantee regular daylight inside the structures for the duration of the day. It will diminish reliance on counterfeit wellsprings of vitality. Starting venture will be high of Litracon yet further will diminish after investigation and will and compelling item in showcase.

References

1. Annual report on working of state power and utility and electricity department (2011–12)
2. Energy statistics 3017 twenty fourth issue report
3. Al-Kurdi, N., Abdel-Aziz, D., Alshboul, A.: Department of Architecture, The University of Jordan, Amman (1942)
4. Juan, S., Zhi, Z.: Some progress on smart transparent concrete. Pacific Sci. Rev. **15**(1) (2013)
5. Demirel, B.: The effect of the using waste marble dust as fine sand on the mechanical properties of the concrete. Int. J. Phys. Sci. **5**(9), 1372–1380 (2010), ISSN: 1992-1950
6. Belachia, M., Hebhoub, H.: Use of marble wastes in the hydraulic concrete. In: 6th International Advanced Technologies Symposium (IATS'11), Elazıg, Turkey, 16–18 May 2011
7. Li, Y., Xu, Z.Y., Gu, Z.W.: Preparation of light transmitting cement-based material with optical fiber embedded by the means of parallel arrange. Adv. Mater. Res. **391–392**, 677–682 (2012)
8. Bashbash, B.F., Hajrus, R.M., Wafi, D.F., Alqedra, M.: Basics of Light Transmitting Concrete. Glob. Adv. Res. J. Eng. Technol. Innovation. **2**(3), 076–083 (2013), (ISSN: 2315-5124)
9. Roye, A., Barle, M., Janetzko, S., Gries, T.: Faser-und textilbasierte Lichtleitung in Betonbauteilen-Lichtleitender Beton. Beton- und Stahlbetonbau **104**(2), 121–126 (2009)
10. Li, Y., Xu, Z.Y., Gu, Z.W.: Research on the light transmitting cement mortar. Adv. Mater. Res. **450–451**, 397–401 (2012)
11. Zareeia, S.A., Ameri, F., Dorostkar, F., Ahmadi, M.: Rice husk ash as a partial replacement of cement in high strength concrete containing micro silica: Evaluating durability and mechanical properties
12. Krishna, R.N., Admixtures, K.C.C.: India, rice husk ash—an ideal admixture for concrete in aggressive environments. In: 37th conference on our world in concrete and structures. Singapore The Impact of Using Light Transmitting Concrete on Energy Saving in Office Buildings-Case of Jordan, 29–31 August 2012
13. Department of Architectural Engineering, Al-Zaytoonah University, Jordan
14. Li, Y., Li, J., Wan, Y., Xu, Z.: Construction and building material, experimental study of light transmitting concrete cement-based material (ltcm)
15. Chawla, A.: Impact of use of marble waste on properties of light transmitting concrete (2016)
16. Chawala, A.: Impact of use of marble waste on the properties of light transmitting concrete. National Institute of Technology, 2014PSC5364 (2016)

17. Ahuja, A., Mosalam, K.M., Zohdi, T.I.: Computational modeling of translucent concrete panels. https://doi.org/10.1061/(asce)ae.1943-5568.0000167. © 2014 American Society of Civil Engineers (2014)
18. Sahoo, A.K., Sahu, S., Singhal, A.K., Stephen, K., Talom, T., Tripathy, S.S., Das, S.: Experimental study of light transmitting concrete using optical fiber. Department of Civil Engineering, National Institute of Technology, Rourkela (2017)
19. Valambhiya, H.B., Tuvar, T.J., Rayjada, P.V.: History and case study on light transmitting concrete. J. Emerg. Technol. Innovative Res. (JETIR). **4**(1) 2017

Interlinking of Dams to Transfer Water Under Gravity

Asmita A. Naitam, Rupesh B. Satpute and A. D. Vasudeo

Abstract India is honored with abundant of water assets; however, its colossal populace development has brought about poor per capita accessibility. Additionally in India, precipitation/Monsoon is not uniform at each place. A few zones are surplus with water then again some are shortfall with water. Around the same time, there is surge in one region and dry season in another. In the event that this water from surplus territory can be exchanged to water deficiency zone, then this issue can be dealt with to substantially more noteworthy degree. In the Nagpur region which is the examination region in the present work, it is observed that all stations have recorded normal yearly precipitation inside the scope of region typical yearly precipitation aside from at Hingni, Narkhed, and Kalameshwar where it is not exactly even an average. Thus, the water availability in the dam in water deficiency territory can be upgraded by moving water in it from dam with nearly greater limit by giving canal interlink between them two. A suitable interlink for connecting these dams has been suggested so that the water transfer will be by gravity.

Keywords Interlinking · Water transfer · ArcGIS

1 Introduction

1.1 General

Water is unquestionably the most vital regular resource on the planet, as it supports all parts of life in a way that no other asset can. According to the National Water Policy, water is a prime common asset for people, and henceforth a valuable national resource. Nowadays, it is elusive freshwater because of development in populace, horticultural and mechanical exercises, and defilement of water assets. The fast devel-

A. A. Naitam (✉) · R. B. Satpute · A. D. Vasudeo
Department of Water Resources Engineering, Visvesvaraya National Institute of Technology, Nagpur 440010, India
e-mail: asmita.naitam22@gmail.com
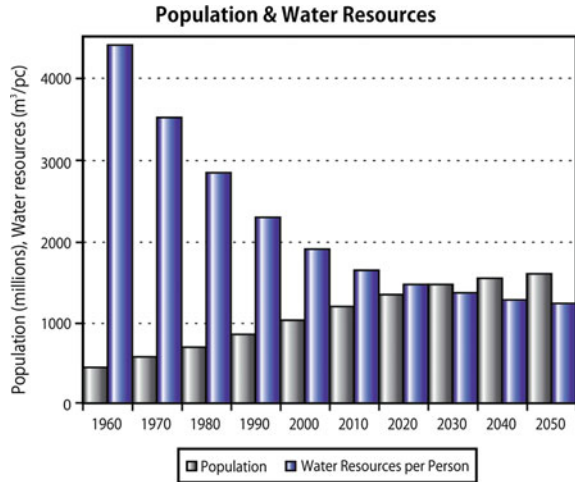
opment in the request of freshwater driven by development in the worldwide populace
and of the economies has prompted this normal asset ending up rare in many parts
of the world. Step-by-step expanding population verses accessible water assets is
demonstrated graphically in Fig. 1. Additionally per capita water accessibility in
world has been appeared in Fig. 2. Therefore, the proportion between the quantity
of individuals and the accessible water asset is compounding step by step. By 2020,
the worldwide populace is anticipated to be in the scope of 7.3–7.9 billion, which is
50% bigger than that in 1990. In view of this quickly developing human populace,
the world may see more than a six overlay increment in the quantity of individuals
living in states of water pressure—from 470 million today to 3 billion of every 2025
[1].

In the worldwide picture, India is recognized as a nation where water scarcity
is relied upon to develop extensively in the coming years as appeared in Fig. 1.
Further, draught conditions coming about because of climatic changeability cause
extensive human enduring in many parts of the nation. This shortage of water is for
both fulfillment of local needs and for crop protection. United Nations agencies and
the World Bank have asserted that these shortcomings will heighten later on, making
major issues for mankind and nature [1]. India needs to adopt a crystal clear water
mission that can help us to use available water resources to fields, villages, towns
and industries round the year, without harming our environment.

The rivers in India are really lifeline of masses as well as for natural life. The rivers
assume a crucial part in the lives of the Indian individuals. The river frameworks help
us in water system, consumable water, cheap transportation, power, and addition-
ally a wellspring of occupation for our regularly expanding populace. "A standout
among the best approaches to expand the water system potential for expanding the
nourishment grain generation, moderate floods and draughts, and diminish regional
irregularity in the accessibility of water is the inter-basin water transfer (IBWT) from

Fig. 2 Per capita water availability in the world. *Source* Home page of International Water Management

Per capita water availability in the world

Population

○ India
○ Other Countries

2.4%

4.6%

Land
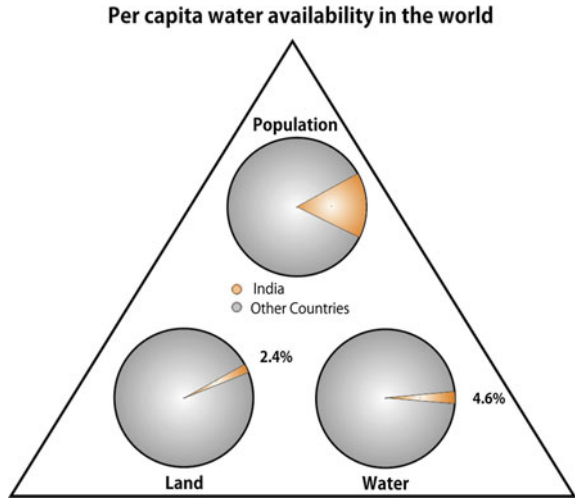
Water

the surplus waterways to shortage zones." In the event that we can construct reservoirs on these rivers and associate them to different parts of the nation, provincial irregular characteristics could be diminished essentially and parcel of advantages by way of additional irrigation, household and industrial water supply, hydropower age, navigational offices, and so forth would gather.

1.2 Objectives of the Study

As a result, in the present study, a limited attempt has been made to analyze some crucial policy issues related to the water scarcity problems in Nagpur district by interlinking of the two dams for the capacity enhancement. In making this analysis, the ongoing shift in the paradigm that is going on in the field of water resource management worldwide has been kept in mind. The project of interlinking rivers initiated by NWDA has been referred. Remedies to the problems have been suggested keeping economy in mind. Thus, the objective of this study is that in spite of Nagpur has endowed with good water resources, some parts of district are facing scarcity due to comparatively less rainfall even for drinking water and to produce required food grains sufficient for growing population. To achieve this objective, it is necessary to implement interlinking of the dams for enhancement of the water availability in the deficit area to fulfill the needs. Thus, here an attempt has been made to interlink the dam in deficit area with the dam in surplus area.

2 Data Acquisition and Methodology

2.1 General

The whole study area has been studied to gather the information about all the features such as geology of the area, hydrogeology, climate and rainfall, temperature, demographics, ground water availability in the area, soil types, and crop types has been studied. All the necessary data are obtained by various sites such as Bhuvan, Indian WRIS, and CGWB, etc. Weather data, ground water data, rainfall records of last few years, DEM, contour maps, river maps are the very useful inputs for this study.

2.2 Digital Elevation Model

Shuttle Radar Topography Mission (SRTM) and digital elevation model (DEM) are used for the study. A digital elevation model, which also called digital terrain model, is a digital representation of surface topography or terrain (Figs. 3, 4 and 5).

Fig. 3 2D DEM of Maharashtra
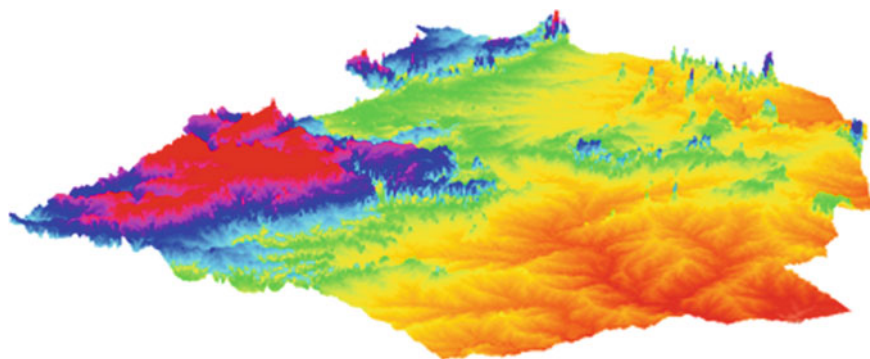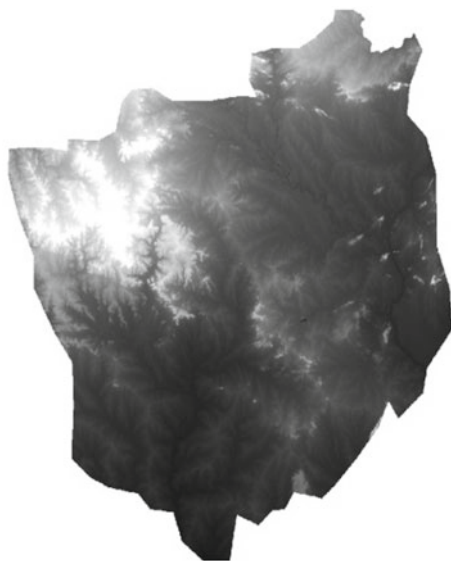
Fig. 5   3D DEM of the Nagpur District

2.3   Contour Map

Contour means line joining points of same elevation. Contour maps are very useful since they provide valuable information about the terrain. Using study area DEM, in ArcGIS contour map has been created with the contour interval of 25 m (Fig. 6).
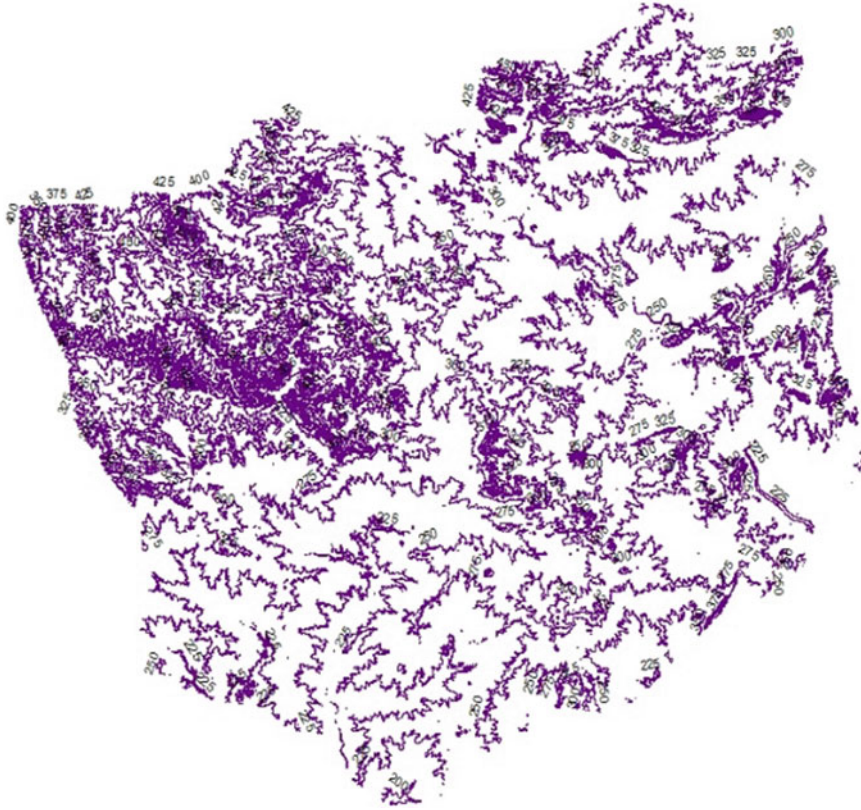
Fig. 6 Contour map of the study area

2.4 Major River Map of India

Major river map of India has been obtained from India WRIS 4.1, and it is used to study the location of dams in the area with respect to the river basins (Fig. 7).

2.5 Methodology

 i. Digital elevation model (DEM) of Maharashtra has been prepared.
 ii. After digitizing map of Maharashtra, study area has been clipped from the map of Maharashtra.
 iii. Using Arcscene 3D DEM of Nagpur district has been prepared. DEM which helps to understand elevation of each point with respect to the mean sea level.

Fig. 7 Major river map of India [2]. *Source* www.india-wris.nrsc.gov.in

- iv. Using this DEM of study area, contour map with the contour interval of 25 m has been prepared in ArcGIS.
- v. All the Dam locations have been plotted on Google Earth and have been saved as KML files.
- vi. Link of major river map of Indian rivers has been taken from India WRIS site, and it is imported in ArcGIS through Add WMTS Server.
- vii. Later on all these maps and files have been imported in ArcGIS and respective study of the whole study area has been done by overlapping them over one another.
- viii. As we have studied the climate data and Taluka-wise annual rainfall distribution of the Nagpur district, it has been noticed that Kalmeshwar, Narkhed, and Hingni are the areas which receive less comparatively rainfall.
- ix. Chandrabhaga dam is the nearest dam to the Kalameshwar. Thus, aim of the study was to increase the capacity of the Chandrabhaga by interlinking it with the another nearby dam having comparatively more capacity, by canal and water transfer should happen by gravity so that to maintain the economy.

x. So the dam positions have been plotted on contour map and major river map of India.

xi. The study of slopes between the dams and their capacities has been done mutually.

xii. Accordingly Jam Dam is interlinked with the Chandrabhaga dam by proposing a canal and the transfer of water will be by gravity. After connecting these two dams, water storage capacity of Chandrabhaga dam will get increased and sufficient quantity of water will be available for irrigation purpose.

3   Results and Discussions

3.1   *Dams to Be Interlinked*

After referring annual rainfall data, it is observed that as all stations have recorded average annual rainfall within the range of district normal annual rainfall except at Hingni, Katol, Narkhed, and Kalameshwar where it is less than average rainfall. The nearest dam and reservoir to the Kalameshwar city is Chandrabhaga Dam. So it is decided to increase the water availability of Chandrabhaga dam by interlinking it with the dam having comparatively higher capacity, and interlinking is done in such a way that water transfer should get possible by gravity so that the project will be economic.

Jam Dam (Latitude: 21.22 N, Longitude: 78.64 E): The dam was built as a feature of water system extends by Government of Maharashtra in the year 1996. It is based on Jam River close Katol in Nagpur District of Maharashtra. The Dam is an earth fill dam. The length of dam is 3460 m. (11,351.71 ft) while the tallness of the dam over the most reduced establishment is 24 m (79 ft). It has catchment territory of 17.1 thousand hectors. Most extreme/gross stockpiling limit is 28.05 MCM. Live capacity limit is 23.55 MCM.

Chandrabhaga Dam (Latitude: 21.27 N, Longitude: 78.76E): It is based on Chandrabhaga River. Closest city to dam is Kalmeshwar in Nagpur District of Maharashtra. The dam is an earth fill dam. The length of dam is 2194 m (7198.163 ft.), while the stature of the dam above most reduced establishment is 21.1 m (69.225 ft.). Dam has catchment territory of 4.845 thousand hectors. Most extreme/Gross stockpiling limit is 8.886 MCM.

3.2   *Alignment of Canal*

The alignment of canal has been found out by tracing of contour gradients and location of route method (Figs. 8 and 9).

Scale: 1 cm = 1.40 km
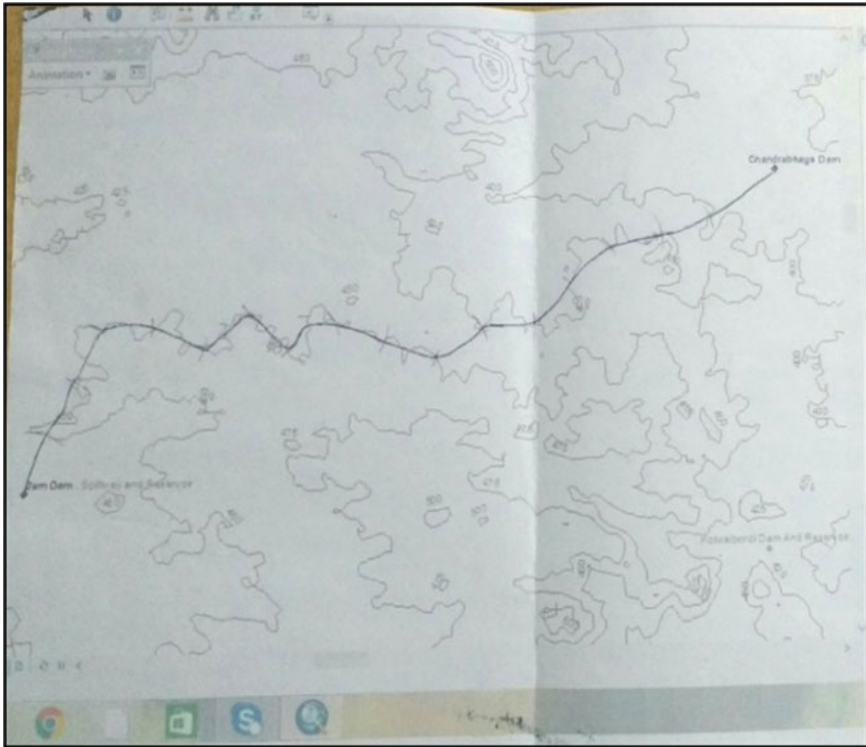
Fig. 8 Interlink between the dams

3.3 : Quantity of Water Transfer to Chandrabhaga Dam from Jam Dam

Capacity of water available in Chandrabhaga dam is 8.886 M cum

Monthly storage capacity of Chandrabhaga dam in the year 2016 is given below (Table 1):

Net difference is 8.886−5.315 = 3.57 M cum.

Direct outlet should be formed from a canal for irrigation and storage of water.

Whenever there is need of requirement of water, then open gated system should be adopted to transfer the water.
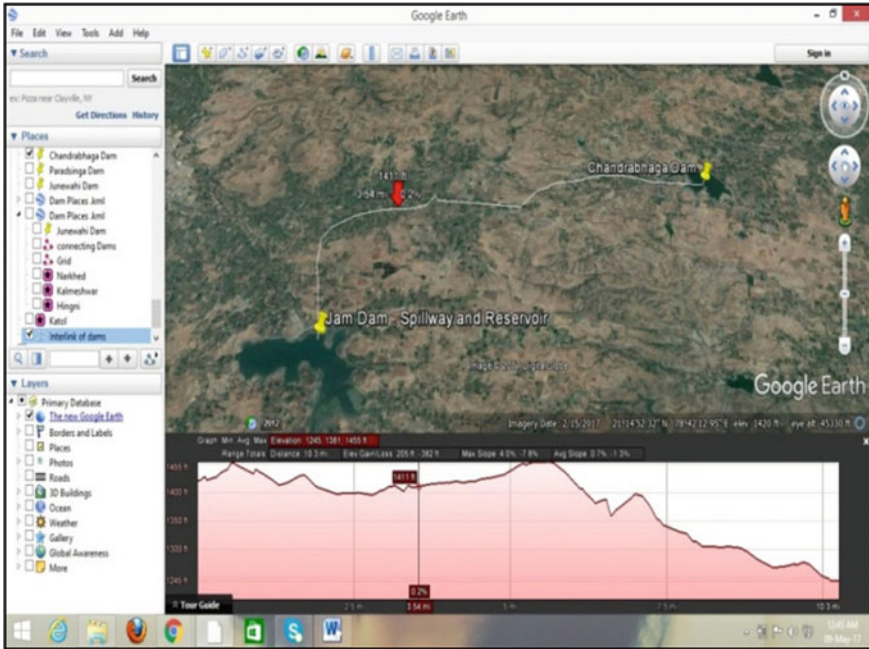
Fig. 9 Elevation pattern of slope between the dams

Table 1 Monthly capacity of water available in Chandrabhaga Dam for year 2016

Month	Capacity (M cum)	Percentage %	Difference (M cum)	Average (M cum)
January	5.454	33.98	5.867	
February	6.987	15.43	7.515	
March	8.048	2.59	8.656	
April	8.048	2.59	8.656	
May	8.129	1.609	8.7431	
June	4.623	44.04	4.973	5.315
July	1.668	79.811	1.794	
August	2.625	67.98	2.8453	
September	2.878	65.165	3.096	
October	3.123	64.854	3.124	
November	3.826	56.943	3.827	
December	4.689	47.231	4.69	

Source Irrigation Department, Nagpur

4 Conclusions and Recommendations

4.1 *Conclusion*

From the present study, following points can be concluded:

1. Detail study of Nagpur region is completed. From this study, water surplus areas and deficit areas are identified.
2. Chandrabhaga, the nearest dam to Kalmeshwar, is in deficit; hence, it is necessary to enhance the capacity of the dam.
3. From the study of DEM obtained from ArcGIS, the height of Jam dam above the lowest foundation is 24 m and height of Chandrabhaga dam is 21.1 m above the lowest foundation.
4. Thus, the natural slope is present from Jam dam to Chandrabhaga dam and water transfer by gravity is possible.
5. The alignment of canal between Jam dam to Chandrabhaga dam is suggested.

4.2 *Recommendations*

- Capacity of dam should be increased so that more quantity of water should be available in deficit areas.
- In the Kalmeshwar and Hingna MIDC regions, the nalas conveying the modern effluents must be lined on a level plane and vertically on the two sides, in order to evade tainting of ground water.
- A sewage treatment plant must deal with all the sewage's getting through the lined nalas before being arranged off in the close-by waterways with legitimate check.

References

1. Mehta, D., Mehta, N.K.: Geo-Eco-Marina 19, Interlinking of rivers in india: issues & challenges (2013)
2. www.india-wris.nrsc.gov.in
3. Porter, M.: Deakin University, Australia, Interlinking of rivers: boon or bane?, TERRAGREEN, December (2013)
4. Sivanappan, R.K.: Inter-Linking of indian rivers-need and importance, J. Indian Water Res. Soc. **32**(3–4) (2012)
5. Current Science, **86**(4) (2004)
6. Naveen, M.J.: National river linking project of India. Hydro Nepal Issue, 12, January (2013)

7. Shah, T., Amarasinghe, U.A., McCornick, P.G.: International Water Management Institute, India International Water Management Institute, Sri Lanka, "India's River Linking Project-The State of the Debate"

8. Amarasinghe, U.A., Shah, T., Singh O.P.: Changing consumption patterns: implications on food and water demand in India. Re-search Report 119. Colombo, Sri Lanka: International Water Man-agement Institute (IWMI) (2007)

Effect of Cow Urine on Municipal Solid Waste: Composition, Leachate Generated and Quality

Shivanand Kamde, P. K. Ghosh and M. K. Gupta

Abstract The objective of this paper is to study the effect of GOMUTRA (A cow urine) on various parametersof municipal solid waste like temperature, pH value, organic carbon, nitrogen, phosphorous, odour, colour after 4–8 weeks withGomutra as stimulator. In the second part of the study, the quality of leachate is studied to analyze the effect of Gomutra on MSW.The results obtained in leachate quality after treating MSW with Gomutra indicate that the use of Gomutra can be an instrumental in efficient treatment of MSW. Gomutra has the potential to produce the fruitful and effective results. Hence, this method is very beneficial to control over the several characteristics of MSW.

Keywords Municipal solid waste · Gomutra · Parameter · Leachate

1 Introduction

In present scenario, the treatment of municipal solid waste is a very essential task. The generation of the municipal solid wasteis increasing in India. The present methods of disposal of MSW are leading to many undesirable results. The most widely used method is to dump the MSW in open space which leads to generation of leachate. Leachate means liquid that seeps through various strata of solid waste or other medium. In the present study, Gomutraas a stimulator has achieved the desirable quality of leachate which can reduce the adverse effects on the ground water table. The many studies have suggested the use of enzymes to treat the MSW to control the leachate quality, but this is not economically viable [1]. The use of Gomutra as

Shivanand Kamde (✉)
Faculty of Civil Engineering Research Scholar, Durg, India
e-mail: shivanandkamde77@gmail.com

P. K. Ghosh
Principal Krishna Engineering College, Bhilai, India

M. K. Gupta
B. I. T. Durg, Durg, India

stimulator has proved to be economically viable and effective. The nitrogen composition of Gomutra will also enhance the soil quality in land fill where nitrogen is deficient. The laboratory analysis of Gomutraexhibits that it comprisesof Nitrogen, Sulphur, iron, chlorine, manganese, silica and minerals (maric, titric, carbon acids). It also contains vitamins A, B, C, D, and E and lactose and enzymes [2].

2   Materials and Methods

The procedure adopted here is similar to actual procedure adopted for sanitary land filling, however the ratio is kept 1:10 to simulate a sanitary landfill having a maximum possible depth of 20 m. The acrylic hollow tube and MS frame was used to construct a model to study the realistic effect of Gomutra and enzymes of the MSW and the leachate quality [3]. To simulate natural conditions of landfill a water spray system was fitted, which has capacity to simulate rain of 20 mm to 200 mm/hr. The thickness of acrylic tube was 5 mm and diameter was 600 mm. The bottom of transparent tube was covered with a 5 mm sieve size mesh. It was then supported with steel stand vertically in such a way that the bottom of tube touches the ground. The MSW is then filled for 5 cm and compacted with a compacter, this was repeated until the depth become 15 cm, and then 2 cm good earth/soillayer was spread and compacted [4]. This process was repeated until the tube was filled for 1.95 m and finally top layer was 6 cm depth good earth Fig. 1. The leachate is developed using de-ionized water in a static exposure and a rainfallsimulation using water flow meter @ 2–20 ml/minutes. Using 9, 5, 10 and 15% of Gomutra in 4 models filled with MSW and all other arrangement are made to produce leachate, continuous monitoring has also been done for 30 days.

3   Result

Today's industrialization and ever changing civilization scenario has led to the increase of the waste which gets produced in cities as well as village to a great extent [5]. The increasing demands and ease of consumer has encouraged the use and throw culture. The one time use or use and throw attitude is budding in today's generation which has made the life easy but at the same time, this clumsy attitude has given air to extreme production of the waste in many folds. The manufacturing of these onetime use products is being supported by the excessive demand and attitude of the user. The products are usually made from non-biodegradable and environmentally unfriendly material [6]. Now, the increasing waste of nature that cannot be biodegraded easily has compelled a scientist to device a system that does not require or require minimal treatment. On the other hand, the rising civilization and population has increased the demand of land [7].
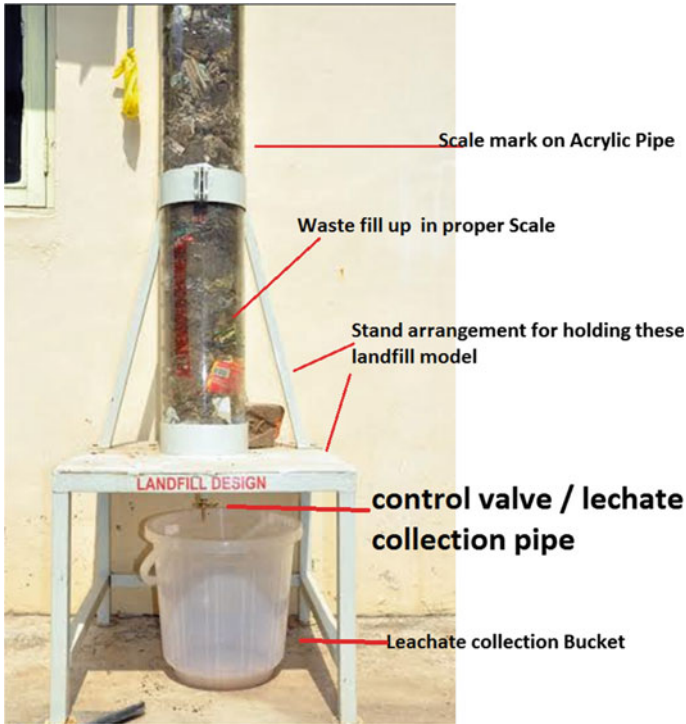
Fig. 1 Model view

3.1 Leachate Management

To fulfill these both demands, the scientists have recommended the landfill system. Landfill is nothing but filling of uneven surface of the lands with the debris, soil and/or now-a-days solid wastes. Again, the time has changed and scientists have gone a step ahead to study the effects of these landfills on the soil strata, ground water and nearby areas. Here, goumutra and enzyme are used as stimulator to leach out pollutants. Following are the parameters areColour, pH, Suspended Solids, Chloride (as Cl), Total Hardness (as CaCO3),Calcium (as Ca), Magnesium (as Mg), Sodium, Acidity, Kjeldahl Nitrogen, Total Phosphorous, Biological Oxygen Demand, Chemical Oxygen Demand, Iron (as Fe), Oil and Grease, Copper (as Cu), Cadmium (as Cd), Lead (as Pb), Total Chromium (as Cr), Zinc (as Zn) studied for the effect of mixing goumutra on the solid waste leachate (Fig. 2).

Lechate Characteristics after Treatment
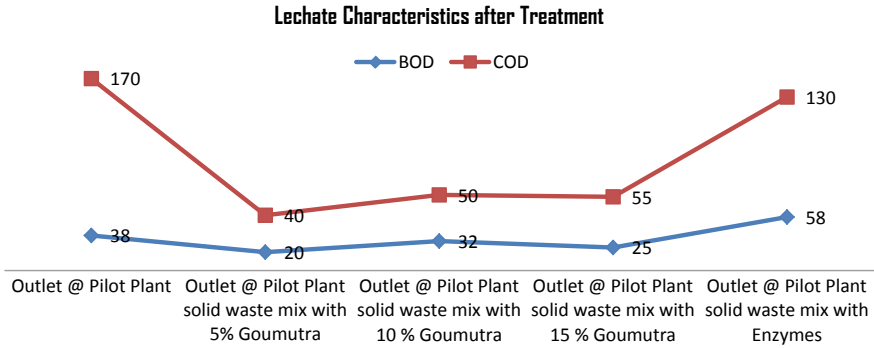
Fig. 2 Graphical representation of lechate characteristics after treatment

3.1.1 Biological Oxygen Demand (BOD)

Biological Oxygen Demand (BOD) is relatively less dependable parameter, but it gives fair idea of pollution level. The leachate from pilot plant without stimulator has shown the BOD of 32 mg/L and leachate from plant with enzyme as stimulator has shown 50 mg/L BOD. The goumutra has been used as stimulator with various concentrations in plants with solid waste mix. The leachate from the plants with 5%, 10% and 15 goumutra as stimulator have recorded 20, 32 and 25 mg/L BOD respectively.

3.1.2 Chemical Oxygen Demand (COD)

Chemical Oxygen Demand (COD) is the most reliable parameter to assess the extent of pollution in any water. The COD also followed the trend of BOD. The goumutra used as stimulator with various concentrations in plants with solid waste mix. The leachate from the plants with 5%, 10% and 15 goumutra as stimulator has recorded 40, 50 and 55 mg/L COD respectively. The leachate from pilot plant without stimulator has shown the COD of 170 mg/L and leachate from plant with enzyme as stimulator has shown 130 mg/L COD.BOD/COD ratios are observed during the treatment are to be 0.22, 0.50, 0.64, 0.45, and 0.45 against the Outlet @ Pilot Plant, Outlet @ Pilot Plant solid waste mix with 5% Goumutra, Outlet @ Pilot Plant solid waste mix with 10% Goumutra, and Outlet @ Pilot Plant solid waste mix with 15% Goumutra (Fig. 3).

3.1.3 Effect on Municipal Solid Waste Management by Gomutra:

In the experiment performed by the scholar using 0, 5, 10, and 15% Gomutra were mixed with 3 kg of municipal solid waste for leachate generated. The moisture
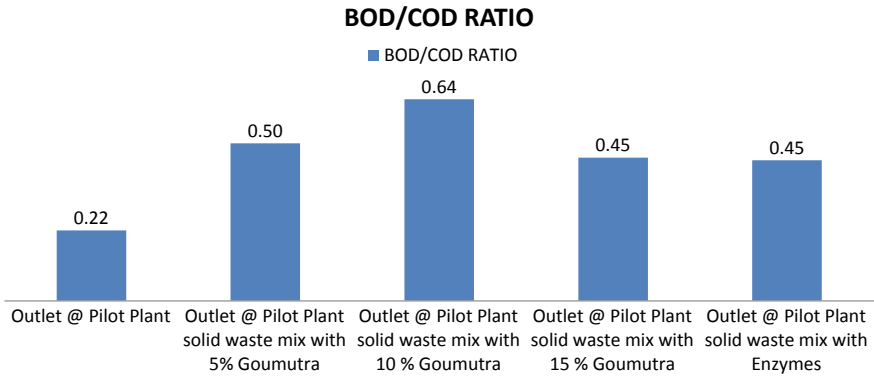
BOD/COD RATIO

Fig. 3 BOD/COD ratio after treatment
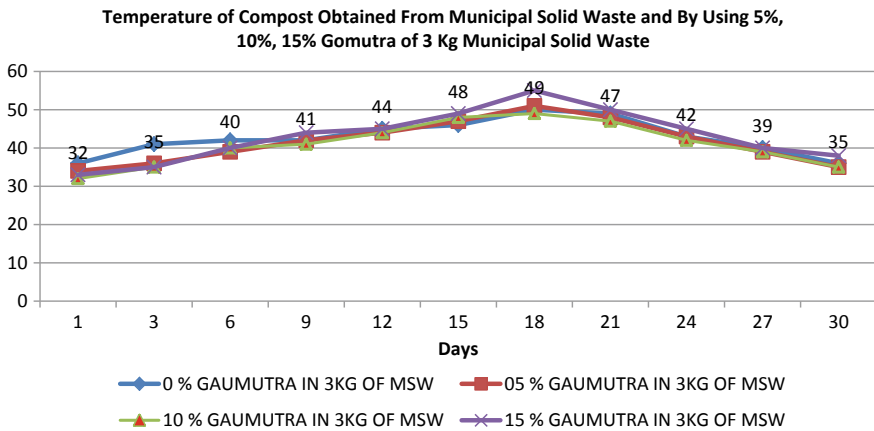
Fig. 4 Temperature study of MSW

content has beenshown to 48.5, 48.5, 54.81 and 53.07% for the pilot plants with 0, 5, 10 and 15% of Gomutra. The temperature decreased by 1 °C and for 10% Gomutra increased by 3 °C (Figs. 4, 5 and 6).

4 Conclusion

The conclusion exhibits that the result of combination of municipal solid waste and 10% of gomutrais effective organic treatment solution andgomutra tends to accelerate the composting process. Reduction of waste by recycling at an affordable cost can be achieved with locally available resources which isa practical approach for waste management policy under the reduction of waste and environmental protection.

Moisture of Compost   Obtained From Municipal Solid Waste and By Using 5%, 10%, 15% Gomutra of 3 Kg Municipal Solid Waste
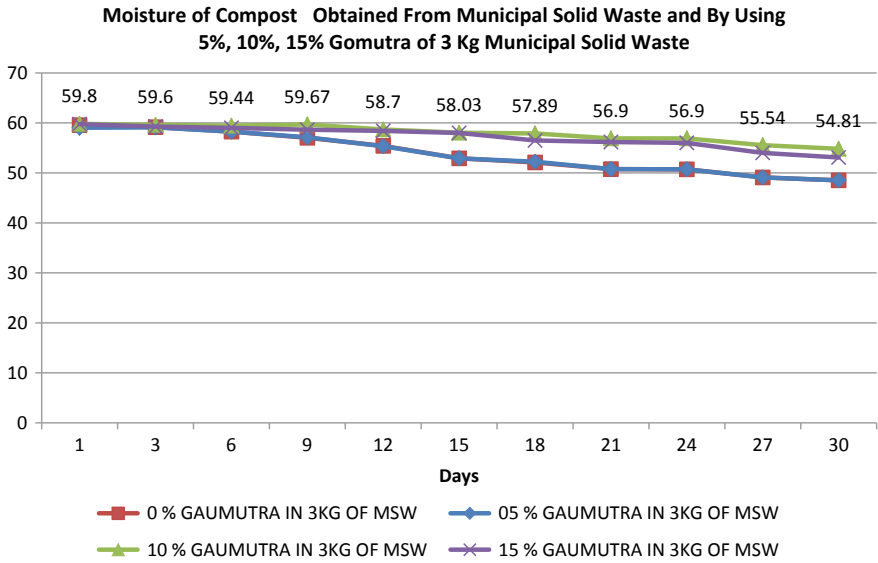
Fig. 5   Moisture study of MSW

pH of Compost   Obtained from Municipal Solid Waste and By Using 5%, 10%, 15% Gomutra of 3 Kg Municipal Solid Waste
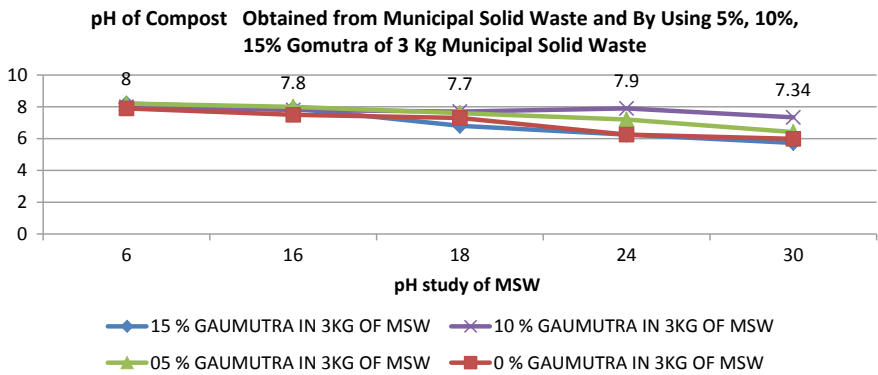
Fig. 6   pH study of MSW

Here, further the leachate can be collected and treated with other available treatment methods effectively and the solids are separated, analyzed and depressed to remove all the water present. The water collected after depressing can be treated along with leachate and cakes of solids can be used as landfill.

References

1. Benson, C.H., Barlaz, M.A., Lane, D.T., Rawe, J.M.: Practice review of five bioreactor/recirculation landfills. Waste Manage. **27**, 13–19 (2007)
2. Eriksen, G., Coale, F., Bollero, G.: Soil nitrogen dynamics and maize production in municipal solid waste amended soil. Agron. J. **91**, 1009–1016 (1999)
3. Vinnerås, B., Palmquist, H., Balmer, P., Jönsson, H.: The characteristics of household wastewater and biodegradable solid waste—a proposal for new Swedish design values. Urban Water Pollut. **3**(1), 119–127 (2006)
4. Jain, P., Powell, J., Townsend, T., Reinhart, D.: Air permeability of waste in a municipal solid waste landfill. J. Environ. Eng. ASCE **131**(11), 1565–1573 (2005)
5. Golvan, Y., Hebe, I.: Methane mass balance at three landfill sites: what is the efficiency of capture by gas collection systems? Waste Manag. **26**(5), 516–525 (2006)
6. Rodhe, L., RichertStintzing, A., SteineckS.: Ammonia emissions after application of human urine to clay soil for barley growth. Nutr. Cycl. Agroecosyst. **68**, 191–198 (2004)
7. Read, A.D., Hudgins, M., Philips, P.: Perpetual landfilling through aeration of the waste mass; lessons from test cells in Georgia (USA). Waste Manag. **21**, 617–629 (2001)
8. Chong, T.L., Matsufuji, Y., Hassan, M.N.: Implementation of the semi aerobic landfill system (Fukuoka method) in developing countries: a Malaysia cost analysis. Waste Manag. **25**, 702–711 (2005)
9. Jain, P., Powell, J., Townsend, T., Reinhart, D.: Estimating the hydraulic conductivity of landfilled municipal solid waste using the borehole permeameter test. J. Environ. Eng. ASCE **132**(6), 645–652 (2006)
10. Schouw, N.L., Danteravanich, S., Mosbaeck, H., Tjell, J.C.: Composition of human excreta—a case study from Southern Thailand. Sci. Total Environ. **286**, 155–166 (2002)
11. Wolkowski, R.: Nitrogen management considerations for land spreading municipal solid resources were a practical approach for waste management waste compost. J. Environ. Qual. **32**, 1844–1850 (2003)
12. Zhong, Z.Y., Zhou, Q.X.: Sanitation landfill technology for refuse. Urban Environ. Urban **4**, 352–367 (1999)

Application of Tube Settlers in Water Treatment Process—A Review

M. P. Bhorkar, A. G. Bhole and P. B. Nagarnaik

Abstract Water is a basic need of human being and requires at every level of life. The widespread importance to the treatment of water is given by many researchers and scientists. But as the advancement in human life and processes because of increase in population, good quality of water requires at every hour of day. Water should meet the desired standards governs by the regulatory agencies and can fulfill the demand. The demand of water for the masses can be provided with the help of advance techniques. The treatment process involves various operations in water treatment plant out of which sedimentation plays very much vital role of removal of solids present in water. The removal of colloidal particles with high rate can be achieved through high rate settling after application of lamella settlers & tube settlers in settling tank. A system of lamella or tube settlers is a feasible solution for drinking water treatment process to increase treatment capacity within small duration. Further it reduces load on treatment units & improves effluent water quality and decrease operating costs at optimum level. Tube settler modules are available in various sizes which can fit on any tank size according to requirement and required designed length of tubes allow varied rate of flows. Year by year, advancement incorporated in the module & simultaneously addition in the extensive knowledge of the water treatment process is done. This paper emphasizes on the work which is carried out & the basic application, advancement in lamella & tube settlers done by various researchers.

Keywords Water treatment · Lamella settlers · Tube settlers · Flow through velocity

1 Introduction

During raining in a catchment area, a runoff gets available and termed as surface water. This runoff flows either into streams or into undrained lakes. It contain certain

M. P. Bhorkar (✉) · A. G. Bhole · P. B. Nagarnaik
Department of Civil Engineering, GHRCE, Nagpur, India
e-mail: mangesh.bhorkar@gmail.com

impurities like dissolved gases, dissolved organic and/or inorganic matter, suspended colloidal, living organisms (micro/macro organisms) etc. Availability of such impurities causes ill effects on human health. The removal of such impurities includes the methods in conventional water treatment plant like aeration coagulation, flocculation processes, sedimentation & filtration. Finally it distributes to the distribution system followed by disinfection process. These are time taken process which leads to the uneconomical issues. The present study is carried out on the sedimentation with coagulation function in which addition of coagulant is done. Coagulation process starts & results in floc formation in flocculation tank. Later the accumulated floc settled and removed in the sedimentation tank which takes 2.5–3 h to settle which is too high. To overcome this issue high rate settlers are used. This paper proposed the study & review of high rate settling model.

1.1 *High Rate Settling (Plate Settler & Tube Settlers)*

Inclined plate settlers/tube settler system acted as shallow settling equipments includes the package of plates of certain thickness/tubes of specific shape and defined material which helps to improve the settling characteristics of sedimentation tank. It is based on the theory that settling depends on the settling area rather than detention time. Although it is used predominantly in water treatment applications, plate and tube settlers are used in waste water treatment plant. The basic function of incline plates/tube settlers is to provide large settling area in laminar flow condition.

To achieve self cleaning of these plates or tubes, these are usually set at an angle between 45°–60° to the horizontal line as shown in Fig. 1. When the angle is increased above 60°, efficiency decreases [1]. There will be chances of sludge accumulation, if inclination is less than 45°. Nominal spacing is about 50 mm (2 inch), with an inclined length of 1–2 m (3–6 ft). High rate settling devices like tube settler improves the settling capacity of sedimentation basin by reducing vertical space through which flocs settle at larger surface. It provides smaller depth to settle a particle as compare to larger depth of conventional clarifier which simultaneously reduces time. Tubes are enough sufficient to trap the fine flocs which escapes from clarification zone below the tubes and emanate the larger flocs to settle down towards the sludge zone of tank in dense form. The agglomerated form of flocs at the tube surface tries to slide down the tube channel under gravity.

The application of tube settlers proves an economical method to upgrade the conventional clarifiers and settling tanks of existing water treatment plant to improve performance. It also helps in reducing the load on further units like filter by trapping most of the solids in sedimentation tank and increases the tank age/footprints for installation of new plant [2]. Over and above the plates settlers were not using after words because of great efficiency from the tubes and hence tubes settlers achieved the prime interest in high rate settling process.
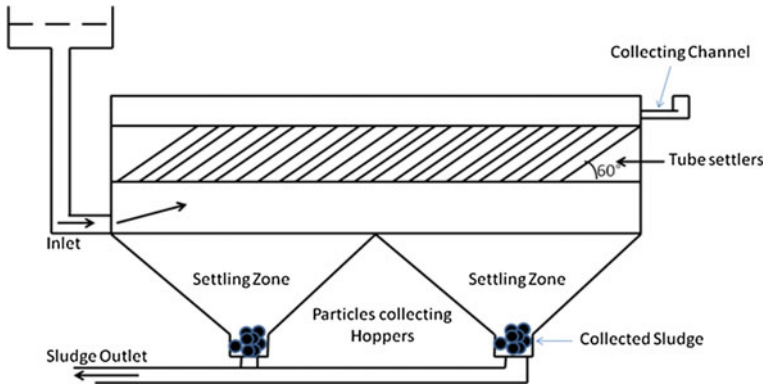
Fig. 1 Inclined tube settlers in tank

1.2 Advantages of Tube Settlers

- Requires less time for settling after installing tube settlers
- Moving parts not involved in the system
- Detention time is less after installing tube settlers
- After installation of tube settlers in settling basin can in improves operation up to 2–4 times to that of normal rate of settling basin without tube settlers.
- Curtailment of coagulant dose up to 50% and maintain lesser turbidity to the further units.
- Because of less turbidity faced by filter unit, operation cost savings can be made.
- This also leads to the sustainability somewhere by saving quantity of water and electricity because of less filter backwashing.
- Capacity of the water treatment plant can be increased after installation of tube settler in sedimentation tank.
- As soon as the particle gets settle at collecting surface of tube, the adhering tendency of particles improves steady sludge formation.

1.3 Limitations of Tube Settlers

- Laminar flow is necessary through the tubes for descent settling of particles at large flow rate, which do not disturb the particles to sweep upward with flow within the tube.
- Each particle should get sufficient time to trap at inner surface inside tube.
- The flow through velocity of tube should not increase at maximum which can disturb settled sludge and can break adhesion. It would lead to failure of treatment option.

1.4 Working of Tube Settlers

Flocculated raw water entered in inlet of sedimentation tank and allows passing through installed set of tube settlers (inclined at certain angle) in upward direction as shown in Fig. 1. Such tube settler modules provide excellent clarification with detention time of 15–20 min or less than that. Horizontal tubes may give the best performance but desludging of the tubes becomes a major constraint. Hence inclined tubes with angle of inclination 40°–60° to horizontal are recommended. Inclination of 60° facilitates simultaneous desludging of tubes in the downward direction while the water travels upward [3].

2 Literature Review

High rate settling in the form of lamella settlers or tube settlers of various cross sections has widespread interest in water treatment as well as waste water treatment for domestic or industrial uses. The prime function of these kinds of settlers is its small depth which is usually of small interval of few centimeters.

Hazen [4] has reported this concept first and later explored by camp in 1945. The circular shape of tubes, diameter varies from 1.3 to 10.2 cm has been applied by Hansen & Culp in [5]. Length of the tube was kept as 2.44 m and found the removal of turbidity up to 90%. Afterwards, many iteration in high rate settling, small diameter tubes had been proven successful in laboratory as well as pilot plant studies and hence chosen for the installations. Later many industries and municipalities applied the high rate settling in their plants and saved time as well as the resources required to run the plant.

Initially Culp and Hansen [6] had described basic arrangement of tube settlers viz. horizontal and inclined. The horizontal tubes were not perfectly horizontal but essentially horizontal kept at 5° inclination to normal flow for the purpose of sliding of sludge in downward direction. But leads towards the problem of filling of tubes with sludge. It requires several backwashing for the clearing of chocking of tubes. The arrangement of inlet, tubes and outlet tank followed by the filter unit was involved in the setup. In steeply inclined tubes at an angle of 45°, this achieves continuous sludge removal & because of inclination no backwashing is required and mechanical arrangement for removal.

Yao [7] had given the design equation based on overflow rate parameter by studying the high rate settlers of certain shapes [7].

$$V_s = S_c \, X(v/(\sin \theta + L \cos \theta)) \tag{1}$$

where

V_s Overflow Rate
V Velocity of water through tubes

S_c The Critical S value (4/3 for Circular Tubes)
θ Inclination Angle of tubes with horizontal
L Relative Length (l/d)
l Length of tube
d Diameter of tubes

Initially when water enters to the tube, it follows transition behavior up to certain length and then transfers to the laminar afterwards, equation for the relative length L'' of the transition zone is give by-

$$L' = 0.058 \, V_d / V \tag{2}$$

where,

V   Kinematic viscosity of suspension medium

Eshwar and Tare [8] analyzed the influence of flow through velocity on the performance of basic tube clarifier systems, and suggested an appropriate design criterion and certain modification in the configurations of basic tube clarifier system. They observed that the flow through velocity in tube settlers would not remain same over the depth of tube settlers if they kept one above the other as assumed in design made by Yao [7]. The upper tubes will carry more discharge than the lower ones. Because of more discharge in upper tubes, detention time will be less which is assumed in design and will results in carryover of flocs. This may create problem in the settling process because of accumulation of particles in upper tubes and less cross sectional area for flow. They also suggested, during design consider actual velocity rather than assumed one to overcome abovementioned problems. Again the opening of all tubes will be at same level then this issue can be overcome stated by authors. The velocity distribution changes the settling operations progresses. The tubes should be designed for the critical velocity distribution for its efficient working.

Badrinath et. al. [9] has determined the settling characteristics of river water and presented the results of column settling test. Results were obtained for designing the settling tank, pre-settler unit and settling of flocculant suspension. The settling of flocculant particles occurs when the flocs have tendency to change its size and shape due to coalescence with other newly formed flocs. Column settling tests helps to determine settling basin design parameters like overflow rate, detention time for specific quality of raw water. In design of pre-settler unit at located water treatment plant, the overflow rate was assumed to be 29 m^3/m^2/day for the removal of 50% discrete particle. From the plain settling test, solids removal efficiency was higher up to certain limit for the given surface overflow rate. The SOR & detention time can be determined from flocculant column settling test for defined solids removal efficiency. Defining of SOR for flocculant settling was by Krishnan's method, which is a usually similar result which is obtained by Eckenfelder Method using Iso-concentration lines. In this research it was also observed that the increase in solid concentration, there is increase in bonding of smaller particles in to larger one helps in increase in solid removal for given SOR.

Fadel et al. [10] invented a new configuration of tube settler module which is useful for tubes design and performance evaluation. Uniformly distributed discharge velocity through the tube is responsible for good efficiency. And due to this the mix flow becomes laminar when it passes the tubes. Laminar flow doesn't allow the particle to hinder here and there and causes settlement. Author developed a model based on above mentioned theory and proven the results through the tests conducted in lab. The prediction of solid agglomeration effect on bottom of essentially horizontal tubes had been done in this model. Lab tests show that predictions are accurate up to 40% of the diameter is used for accumulation storage.

The application of inclined settlers are not limited to treat the potable water only but can be used to treat storm water also. In the study of Shirley Clark et al. [11] has studied the storm water particles settling with the help of inclined plate settle. Storm water runoff contains many impurities including major part of silts and degrades the quality of reservoir. Therefore, removal of some amount of the solid particles (such as all particles above a critical particle size) can minimize conc. of many pollutants. Application of inclined plate settlers can remove the load up to 80%.

Sadataka Shiba prepared a model (mathematical) for the flow simulation required for boundary layer approximation and the clear layer averaged inertia identified as momentum equations. In order to analyze theoretical design & this mathematical modeling is used for operations of plate/tube settlers for water/wastewater treatment.

The flow should be affected to settling phase due to density difference between the clear fluid and prepared suspension for experimental study. In this study the prediction of discharge velocity and layer thickness by analytical solutions has been given on the basis of experimental results identified in batch study to verify the theoretical analysis.

According to the Wheelabrator Engineered Systems, UK, the use of tube settlers removes settable solids with great efficiency. Right from the smaller to the larger sedimentation tank to be working can be increase flow capacity by 50–150% with great quality of clarified water.

The position of the tube settler module shall be at 60° and length shall be 3000 mm long. In view of structural strength the direction of tubes are placed in such a way that it its passageways is alternated.

A typical super settler by A. Tripathi and A. Acrivos, shown in Fig. 2 is being operated at the bottom of the tank from where feeding is done. They prepared the mono disperse suspension of heavy particles & provided in the tank from feeding portion. At the bottom of the tank the Reynolds no is obviously small results in the sediment and slipping of particles in the direction opposite to feeding [12].

The 3 different phases of fluid are shown in Fig. 2 viz. (1) a clear water layer; (2) bulk of the suspension and (3) the sediment layer. The first layer inside the inclined tube contains the clear water and goes upward. The remaining accumulated particles slides down and collects in the feeding tank & can be removed later [13].
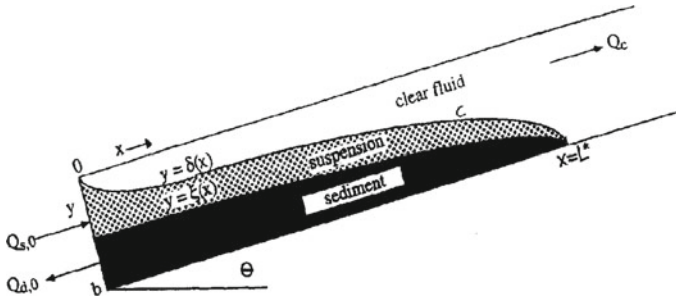
Fig. 2 Cross section of inclined settler showing the variables used in the analysis

3   Identification/Suggestions

The identifications form the review is

1. Tubes are available in various shapes like circular, triangular, square, hexagonal, chevron etc.
2. Inclined tubes/plates provide sludge sliding efficiency at large.
3. Inclination at an angle varies from 45° to 60° gives better efficiency.
4. Solids of various sizes can be removed after flocculation.
5. Tubes provide more removal of sludge as compare to plates.
6. Column settling test is essential to determine the capacity as well as design of pre-settler and sedimentation tank.
7. Installation of tubes leads towards the overall economy of treatment process.
8. Circular tubes form the cusp shape between each other and hence problem of choking may arise.
9. In case of horizontal plates or tubes, the velocity at bottom is less as compare to upper and gives more discharge which results in carryover of flocks.

The suggestions from the review is

1. Provide angle of inclination as 60° to the horizontal which gives better efficiency of solids removal
2. Modification in tubes can give again improved results of settling
3. Stepped high rate settling also a good option in removing flocculants from water
4. Removal of sludge from the bottom should be a regular activity which improves the life of tank and gives clear water in short duration.
5. This kind of equipment can be used in WTP for getting maximum amount of water in short duration.
6. This can be a part of package water treatment plant used in small village or at the fairs etc.

4 Conclusion

From the above review, the tube settlers are very much useful, advantageous, time saving & economic module used in the water/wastewater treatment system. The efficiency depends on the inclination as well as its size & length also. Coagulant plays very much important role in high rate settling. Flocks settles under gravity after agglomeration.

References

1. Gurjar, A., Bhorkar, M., Bhole, A.G., Baitule, P.: Performance study of tube settlers module. Int. J. Eng. Res. Appl. **7**(3), 52–55 (2017)
2. Product News of Wheelabrator Engineered Systems, Filtration & Separation, Nov/Dec UK (1995)
3. Bhole, A.G.: Design of water treatment plant (Indian Water Works Association) (2003)
4. Hazen, A.: On Sedimentation, Transactions, ASCE, **53**, 63 (1904)
5. Hansen, S.P., Culp, G.L.: Applying shallow depth sedimentation theory. J. Am. Water Works Assoc. **59**, 1134 (1967)
6. Culp, G., Hansen, S., Richardson, G.: High rate sedimentation in water treatment works. J. Am. Water Works Assoc. **60**, 218 (1968)
7. Yao, K.M.: Theoretical study of high rate sedimentation. J. Water Pollut. Cont. Fed. **42**, 218 (1970)
8. Eshwar, K., Tare, V.: Role of flow through velocity in tube settlers. J. Indian Water Works Assoc. **XIII**(1), 87–91 (1981)
9. Badrinath, S.D., Deshpande, V.P., Raman, V.: Column settling tests for sabarmati river waters, Ahmedabad. J. Indian Water Works Assoc. **XIII**(3), 263–270 (1981)
10. Fadel, A., Baumann, E.: Tube settler modeling. J. Environ. Eng. **116**(1), 107–124 (1990)
11. Clark, S., Roenning, C., Elligson, J., Mikula, J.: Inclined plate settlers to treat storm-water solids. J. Environ. Eng. **135**(8), 621–626 (2009)
12. Tripathi, A., Acrivos, A.: A new criterion for the continuous operation of supersettlers in the bottom feeding mode. Int. J. Multiphase Flow **22**(2), 353–361 (1996)
13. Shiba, S.: Flow under tilt surface for high rate settling. J. Environ. Eng. **111**(3), 285–303 (1985)

Evaluate Properties of GPC with the Addition of an Alkaline Solution and Different Types of Fly Ash

S. L. Hake, O. D. Waghmare and M. P. Bhorkar

Abstract Cement industry assumes significant part for outflow of greenhouse gasses. Thus, there is requirement for assembling of natural well-disposed cement. Geopolymer solid aides in lessen world-wide change in temperature and in addition fly ash transfer issue. This paper presents think about the impact of kinds of curing, temperature, curing time and rest period. Among all these, one parameter is kept as factor and remaining three kept constant. Well ordered all parameters are worked out. The different strategies for curing broke down by upgrading temperature, changing the rest time frame and for various curing time of GPC. Different curing techniques can be received are Oven curing, accelerated curing, Membrane curing, steam curing, wet curing and curing at room temperature. The Variation in temperature ranges from 60, 90, 120, 150 °C. Once the temperature for kind of curing is fixed at that point continue to curing time i.e. 6, 12, 18 and 24 h. After the curing time frame at given temperature and kind of curing is settle in the wake of testing time of cement. The rest time frame contrasts like 1, 3, 7, 14, 21, 28, 56 days. In this examination these factors are to be break down with the assistance of characteristic compressive strength of geopolymer concrete.

Keywords Geopolymer concrete · Temperature · Fly ash

1 Introduction

For arrangement of GPC, cement is completely supplanted by fly ash debris. As the fly ash has pozzolanic properties which comprise of silica and alumina in substantial sum. To enact fly ash, the soluble activators like NaOH/KOH and Na_2SiO_3 can utilized. Fly ash utilized as waste material of cement. For the framework improvement

S. L. Hake (✉) · O. D. Waghmare
Department of Civil Engineering, DVVP COE Ahmednagar, Ahmednagar, Maharashtra, India
e-mail: drsandeephake@gmail.com

M. P. Bhorkar
Department of Civil Engineering, G.H. Raisoni COE, Nagpur, Maharashtra, India

require immense amount of cement. It is verifiable truth that the creation of cement not just devours noteworthy measure of normal assets and vitality yet in addition discharges gigantic amount of CO_2 to the surrounding environment. Along these lines, it is important to discover other options to make the solid condition well-disposed with thought of regular assets and barometrical contamination.

Every year in excess of 100 million tons of fly ash is created in India. The hectares of land required for dumping of wastage fly slag. Then again, CO_2 emanation causes green-house gasses. The cement industry emanates more CO_2 in surrounding environment. On the off chance that we utilize geopolymer concrete as another option to normal solid which diminish greenhouse gasses too fly ash as transfer issue. In geopolymer, 100% fly ash utilized as restricting material. For polymerization of geopolymer concrete require heat, because of this it is poor to ponder the kinds of curing and temperature variety of geopolymer concrete.

2 Research Review

To upgrade the polymerization, curing of geopolymer concrete by giving heat to concrete in an oven has been proposed by different specialists, while it is very hard to cure GPC on site using oven curing method. With the goal that it is important to complete an exploration on simple techniques for curing which makes GPC cured as ahead of schedule as could reasonably be expected. The oven curing for geopolymer concrete is for the most part utilized. Different scientists did tests by fluctuating curing temperature by utilizing an oven curing the GPC, tragically couple of analysts has done trials on curing strategy by utilizing steam curing, membrane curing. No one does the analyses on accelerated curing alongside correlation between the steam, accelerated, membrane, natural and oven curing. In this way, there is extension on strategy for curing of geopolymer concrete. Additionally, specialists examined for various curing time like 6,12,18,24 and the ideal quality acquired at 18 h. of curing. The temperatures impact saw at 60, 90, 120 and 150 °C. To contemplate and streamline the outcomes, different strategies for curing which can be embraced are viz. Steam curing, Membrane curing, Oven curing and the Accelerated curing [1].

The assess the properties of soluble base actuated geopolymer solid blocks and its durability in which the fly ash remains is fundamental ingredient. For the throwing the samples, sample size to be taken as 200 mm × 200 mm × 400 mm. The block was thrown with fly ash debris to natural river sand, M-sand and eco-sand (silica sand) with the proportion of 1:2.5 by weight. Sodium hydroxide and Sodium silicate arrangement were utilized as the basic activators in geopolymer concrete. The cover arrangement comprises of a blend of NaOH and Na_2SiO_3 arrangement in the proportion of 1:2.5. Absolutely 60 cubes were throwing in this investigation under encompassing curing. The cubes were thrown with various kinds of sand with river sand, M-sand and eco-sand (silica sand). The test comes about got were contrasted and locally accessible Cement Solid Blocks [2].

The strength of GPC in compression is principally relying upon the measure of water to be taken, term of warming GPC. To shape a homogeneous mix of GPC, NaOH arrangement having 13 M molarity is utilized with Na_2SiO_3 arrangement. Na_2SiO_3 arrangement comprise of Na_2O of 16.45%, SiO_2 of 34.35% and H_2O of 49.20%. Geopolymer concrete mix were set up with 0.35 answers for handled fly ash remains proportion. The workability of GPC was measure by using a flow table apparatus. The cube shape having size of 150 mm × 150 mm × 150 mm was threw with the GPC. The temperature of curing was changed as 40, 60, 90, and 120 °C for every time of 8, 12 and 24 long stretches of oven heating and tried after a rest time of 1, 2, 3, 7 and 28 days in the wake of demolding the solid cubes. Test outcomes demonstrate that the amount of water assumes essential part in adjusting usefulness however not impact on quality. While higher temperature requires less term of warming to accomplish wanted quality and the other way around. The researcher conclude that the rest time of 3 days is adequate in the wake of heating at or more 90 °C temperature [3, 4].

Geopolymer concrete is created by cement totally supplanting with took care of fly ash which is started by essential courses of action like Na_2SiO_3 and NaOH. The shape having size of 150 mm × 150 mm × 150 mm was selected with the GPC and for that they take the extent of alkaline solution and fly ash and fixed around 0.35. The NaOH course of action was set up with 16 mol obsessions. The cases were cured in oven at 60, 90 and 120 °C for 6, 12, 16, 20 and 24 h's terms. Test results exhibit that the strength of GPC in compression get increased with increase in time and temperature of oven curing up to 24 h [5].

The extent for alkaline solution increases, the workable properties of mix keeps extending. The test occurs show that the nature of GPC contrasts as we reduce the water to binder ratio. In like manner, by reducing the aggregate to binder ratio. In ongoing the test, the water accepts a basic part in polymerization reaction and in the cementing methodology of GPC. To redesign the polymerization reaction as we increase binder content it will clearly impacts the last quality. Any survey of GPC illustration having greater quality results with weight and strain can made by picking a perfect estimation of stomach settling agent plan i.e. is of 2.5. To tie the essential constituents i.e. sand and coarse aggregates, the fly ash waste is used which outlines the GPC. In like manner, these concretes can be considered as eco-friendly materials [6].

3 Methodology

The geopolymer concrete was plan for its characteristic compressive strength of M30 grade. The proportion mixed for M30 grade [7]. The Pozzo Crete fly ash of P60 grade is utilized to produce GPC by full substitution of OPC. For a wide range of curing techniques, mixed can be set up by choosing answer for fly ash-binder proportion of around 0.35. The soluble base activators proportion i.e. sodium silicate to sodium hydroxide arrangement proportion is 2.5. The rest time frame for GPC is

of 7 days and curing time for solid 18 h. The enhancement of curing time and rest period was likewise think about in this paper. The distinctive sorts of curing were considered oven, steam, membrane, wet, normal daylight and accelerated curing. In this examination, the fresh geopolymer concrete were found by proper mixing of dry ingredients and activators. The Pozzo Crete of P60 review fly ash remains are taken from Dirt India Pvt. Ltd., the form GPC with expansion of fine total, coarse total and basic arrangement. The alkaline liquids are the Sodium hydroxide (NaOH) and Sodium Silicate (Na_2SiO_3). The sodium silicate to sodium hydroxide proportion utilized is 2.5 and the answer for fly ash proportion is 0.35. The pallet type of sodium hydroxide lab grade was acquired from market. The sodium silicate acquired from market in the liquid form. For the preparation of 1 M arrangement 40 grams of sodium hydroxide pellets of solid form were utilized. While we mixed 40 grams' pellets in one-liter arrangement then we get 1 M sodium hydroxide arrangement. In comparative way, we have arranged the arrangement of molarity 16 M for GPC. We have included $16 \times 40 = 640$ g NaOH chips into the consumable water to get 16 M one-liter NaOH solution. The heat revaluation rate is so high at the time of mixing pellets into water. Because of Sodium hydroxide arrangement was prepared one day before the throwing of solid cube.

In the lab, the dry mix of fly powder and aggregates were mixed in pan mixer. At that point, required amount of Sodium Hydroxide liquid and sodium silicate liquid with additional water mixed until the point when homogeneous blend was formed. Subsequent to making the homogeneous mix, workability tested by using a slump cone and compaction factor is found out. At that point, solid shapes of size 150 mm $\times$ 150 mm $\times$ 150 mm were given in three layers a role according to standard process. Enable the GPC to set into the form. These solid cubes were put for curing subsequent to demolding. The different techniques are received for Oven, Steam, Accelerated and Membrane Curing at different temperatures like 60, 90, and 120 °C. These solid cubes were put at room temperature in the wake of curing up to the testing age. The testing age for cube will be accepted as 7 days which was mentioned from previous researcher. The processed and unprocessed form of fly powder analyzed with the pallet and flake type of sodium hydroxide and sodium silicate. In general, silicon and aluminum oxides are the principle substance in the low-calcium fly ash remains which specifically respond with an alkaline solution to produce a geopolymer concrete so it can bind the free coarse aggregates and also fine aggregates with each other and furthermore other un-responded materials together to deliver a very much compacted mass of GPC. The NaOH can be acquired as pallets and flakes. NaOH is an important material in polymerization process as the bond quality of NaOH in pallet shape is more than that of NaOH in flake form [8].

4 Result and Discussion

The underlying parameter for geopolymer concrete were investigate with the type of fly ash and the type of sodium hydroxide activators. The processed and unprocessed

Fig. 1 Concentration effect of sodium hydroxide on compressive strength of GPC
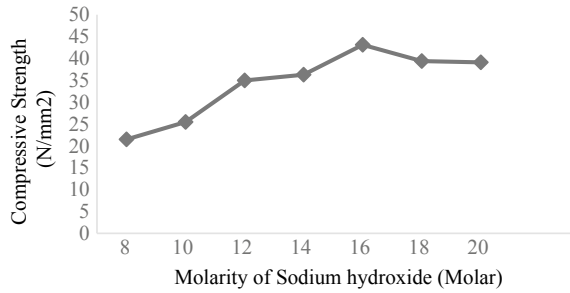
fly ash is optimized with flake and pallet type of sodium hydroxide arrangement [9]. At that point rest period, curing time, temperature and distinctive curing state of concrete was examined. This parameter was upgraded one by one. While considering one parameter other two parameter fixed with reference of previous experimental study. Once the rest time period fixed at that point goes for the curing time. The rest time period and curing time enhance at that point consider for temperature of geopolymer concrete.

4.1 Concentration Effect of Sodium Hydroxide on GPC

The molarity of sodium hydroxide plays a vital role in geopolymer concrete. In this investigation, the temperature (90 °C), curing duration (24 h) and testing age (7 days) are used from past study. The processed fly ash (PF-I) used for further study. It is observed that the concentration of sodium hydroxide is optimized at 16 M. The effect of concentration of sodium hydroxide on geopolymer concrete is shown in Fig. 1.

4.2 Analysis of Fly Ash with Sodium Hydroxide in Form of Pallet and Silicate Solution

Figure 2 demonstrates the compressive strength of prepared fly ash with temperature variety. It is watched that the quality for P100 is substantially higher than other yet the cost of the P100 handled fly ash is significantly higher than other. As we consider for economy the characteristic compressive strength of M30 grade concrete acquired for P60 grade of prepared fly ash, so for the further investigation the P60 review handled fly ash was utilized. Alongside that the natural fly ash was tried in mix of NaOH in pallet shape. The fly slag was obtained from Bhusawal, Nashik and Beed thermal power plant and cured at various temperature 80, 100 and 120 °C in Fig. 2.
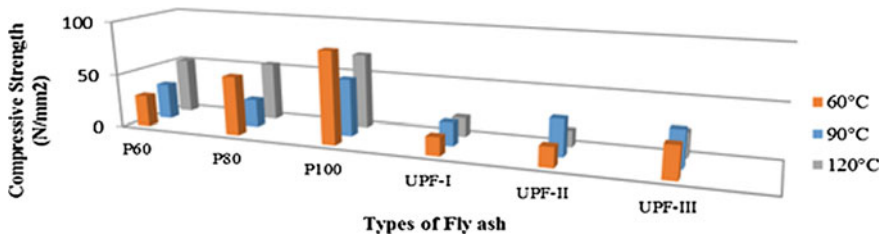
Fig. 2 Compressive strength test after effects of NaOH in pallet form with various types of fly ash
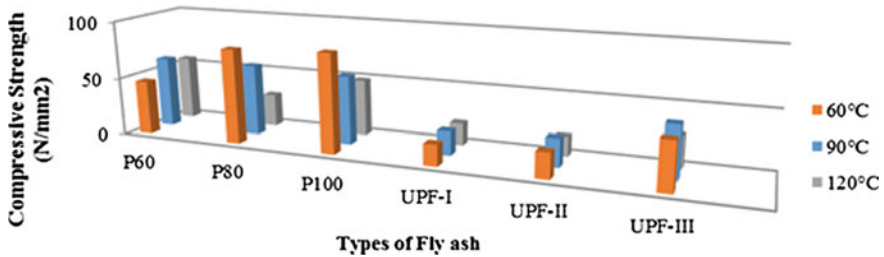
Fig. 3 Compressive strength test consequences of NaOH in flakes form with various fly ash

4.3 Test on Fly Ash with NaOH in Flakes Form and Silicate Na₂SiO₃ Solution

The Fig. 3 demonstrates the characteristic compressive strength consequences of NaOH in flake form with various type of fly ash is investigated. As observed the quality for P100 is higher than the other however the cost of the fly ash is more as contrast with different types of handled fly ash remains with thought of economy the P60 kind of prepared fly powder is less expensive. These fly ashes examined with various temperature like 60, 90 and 120 °C.

4.4 Analyze Result for Rest Period

The investigative correlation is improved the situation the compressive quality of GPC at the rest time frame which is cured by various strategies viz. wet curing, membranecuring, oven curing, accelerated curing, steam curing and natural daylight curing. The rest time period breaks down for 1, 3, 7, 14, 21, 28 and 56 days. The temperature of oven and membrane curing kept up at 90 °C. 90 °C temperature was kept up for accelerated curing technique and 120 °C temperature was kept up for steam curing strategy. The natural daylight curing strategy and additionally regular curing technique was selected for blocks prepared from GPC. As the rest time of solid expands the characteristic compressive strength increases. The compressive
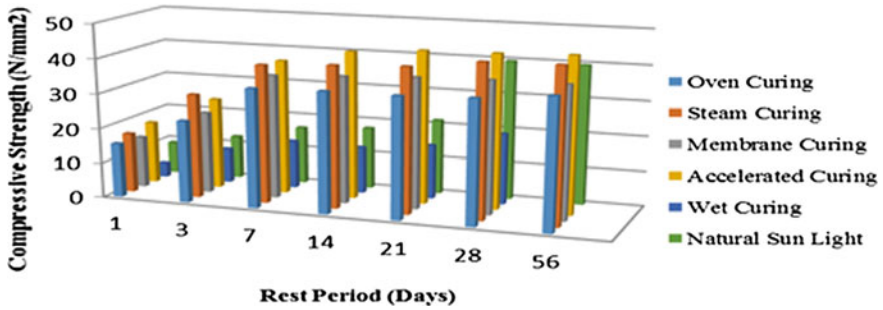
Fig. 4 Compressive strength test comes about for various types of curing and the rest time period
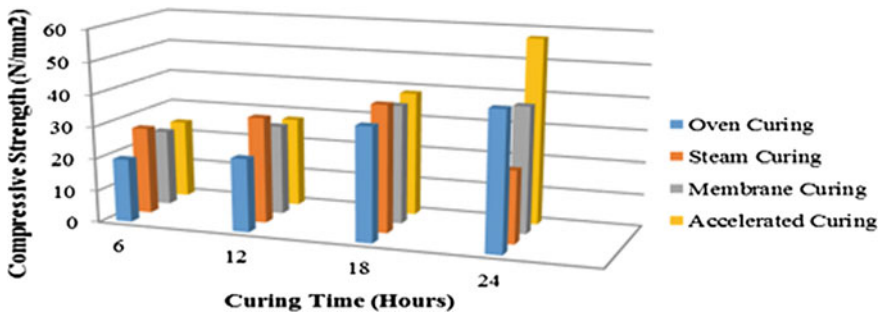
Fig. 5 Compressive strength for various curing and its time

strengthat 28 and 56 days was not taken into account. As we found in diagram 1 the 7 days' rest period gives target strength (Fig. 4).

4.5 *Analyze Result for Curing Time*

Figure 5 demonstrates that the Characteristic Compressive Strength of GPC cured with different strategies for curing and in addition the curing time. Curing period extents to 6–24 h. For higher temperature the curing time lessens. For oven and membrane curing the temperature upgrade at 90 °C. Yet, in the event of steam it was upgrade at 120 °C and for quickened curing it was 90 °C for these temperatures the curing time advance at 18 long hrs. of a wide range of curing.
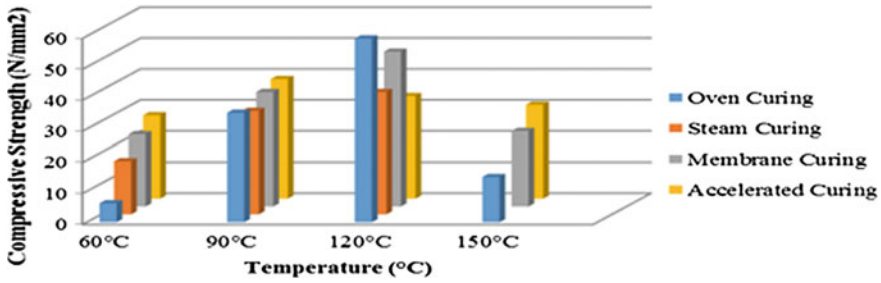
Fig. 6 Compressive strength for temperature variety and curing time

Fig. 7 Effect of split tensile strength on types of curing of geopolymer concrete
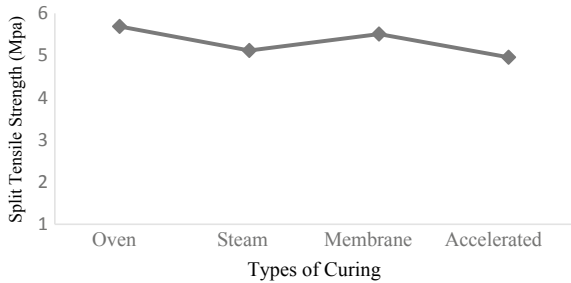
4.6 Analyze Result for Temperature Variation

Figure 6 demonstrates the impact of temperature variety and diverse kind of curing on geopolymer concrete. In oven curing the temperature fluctuates from 60 to 150 °C the ideal outcome we get at 90 °C with thought of vitality for heating.

Accelerated curing the impact of temperature on geopolymer concrete will demonstrate the ideal outcome at 120 °C. Additionally, in membrane curing the impact of temperature changes from 60 to 150 °C the ideal outcome we get at 90 °C. If there should be an occurrence of Steam curing the temperature advance at 120 °C.

4.7 Effect of Split Tensile Strength on Geopolymer Concrete

Spilt tensile strength is analyzed on the different types of curing. The effect of oven, steam, membrane and accelerated type of curing on tensile strength of geopolymer concrete were analyzed. The M30 grade of geopolymer concrete cast with a cylinder of size 300 × 150 × 150 mm. After demoulding they were cured at 90, 100, 90, and 80 °C in an oven, steam, membrane and accelerated type of curing respectively for 18 h, 7 days. The test procedure follow as mention in IS 5816:1999. It is observed that the oven cured cylinder gives better result as compare to other type of curing (Fig. 7).

Fig. 8 Effect of flexural strength on geopolymer concrete
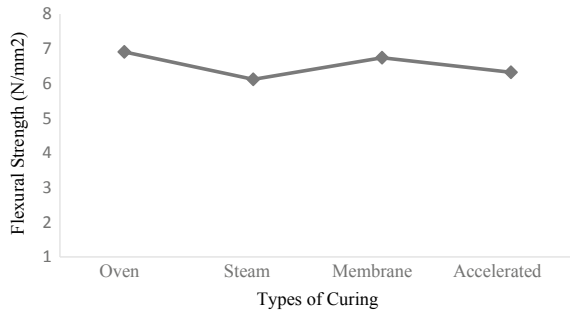
4.8 Effect of Flexural Strength on Geopolymer Concrete

The flexure strength carried out on the beam of M30 grade and of size $500 \times 100 \times 100$ mm. After the casting, it was kept for drying for 24 h at room temperature. After 24 h the beam were de-moulded and cured at 90, 100, 90, and 80 °C for oven, steam, membrane and accelerated curing respectively for 18 h. The cured sample tested after 7 days. The test process confirming IS 515:1959 were used for finding flexure strength of geopolymer concrete. After observing all the result it is concluded that oven and membrane cured average flexure strength of M30 geopolymer concrete is better than the steam and accelerated curing shown in Fig. 8.

5 Conclusion

In light of examination, the accompanying conclusions have been drawn.

1. The analysis is done on effect of different forms of activator NaOH i.e. flakes and pallet form which reacts with different types of fly ash. It is observed that the strength of GPC is dependent on form of NaOH activator.
2. The types of fly ash particularly fineness influences the compressive quality of geopolymer concrete.
3. In geopolymer concrete after 7 days the compressive strength of cement accomplishes their objective quality.
4. It is seen that in natural curing thecharacteristic compressive strength accomplishes at 28 days. And further more wet curing not reasonable for geopolymer concrete.
5. In brief time of curing time i.e. 18 h the polymerization of geopolymer concrete happens and gives characteristic compressive strength.
6. It is watched that; the objective compressive quality of cement accomplishes at 90 °C for oven curing and furthermore after that the quality increments up to 120 °C however at 150 °C the quality of solid misfortunes his compressive quality because of overheating.

7. If there should arise an occurrence of steam curing the characteristic compressive strength accomplished at 100 °C after that the quality increments yet vitality utilization for steam age is all the more so it is enhanced at 100 °C.

8. In instance of Membrane curing the characteristic compressive strength acquired at 90 °C because of utilization of power this parameter enhances at 90 °C while thinking about economy.

References

1. Hake, S.L., Dr Damgir, R.M.: State of art—investigation of method of curing on geopolymer concrete. IOSR J. Mech. Civil Eng. (IOSR-JMCE), **12**(3) Ver. I (2015)

2. Hake, S.L., Dr Damgir, R. M.: Effect of temperature and curing type on geopolymer concrete. International Journal of Advance Research in Science and Engineering, vol. 5, February 2016, ISSN 2319-8354 (Special issue 01)

3. Sayyad, A.S., Patankar, S.V.: Effect of steel fibers and low calcium fly ash on mechanical and elastic properties of geopolymer concrete composites. Indian J. Mater. Sci. Vol Article ID 357563, 8 (2013)

4. Hardjito, D., Rangan, B.V.: Development and properties of low-calcium fly ash-based geopolymer concrete. Research report gc 1 faculty of engineering Curtin university of technology Perth, Australia (2005)

5. Anuradha, R., Sreevidyaa, V., Venkatasubramania, R., Rangan, B.V.: Modified guidelines for geopolymer concrete mix design using Indian standard. Asian J. Civ. Eng. (Building and Housing), **13**(3), 353–364 (2012)

6. Sanni, S.H., Khadiranaikar, R.B.: Performance of Alkaline solutions on grades of geopolymer concrete. Int. J. Res. Eng. Technol. (IJRET), e-ISSN: 2319–1163, pp. 366–371. p-ISSN: 2321–7308 (2013)

7. Patankar, S.V., Jamkar, S.S., Ghugal, Y.M.: Effect of fly ash fineness on workability and compressive strength of geopolymer concrete. Indian Concrete J. (2013)

8. Hake, S.L., Dr Damgir, R.M., Dr Patankar, S.V.: Temperature effect of lime powder-added geopolymer concrete. Advances in Civil Engineering, Hindawi, 2018 Volume, Article ID 6519754

9. Hake, S.L., Dr Damgir, R.M.: Evaluation on types of fly ash and alkaline activators of Gpc. In: International Conference on Innovative Trends in Engineering Research, 2016, pp. 171–176. ISSN: 2394–3696

Removal of Hexavalent Chromium from Aqueous Solution by Alumina-Supported Copper Aluminum Oxide Nanoparticles

Vivek Bhusari, Amit Bansiwal and Sadhana Rayalu

Abstract Chromium is a toxic metal pollutant found in effluent of electroplating and metal finishing industries. Copper aluminum oxide nanoparticles supported on alumina were synthesized and evaluated for the removal of Cr(VI) from water. The CANP-A was characterized by X-ray powder diffraction, scanning electron microscopy, and transmission electron microscopy. The adsorbent was evaluated for the removal of chromium (VI) from water. The effect of adsorption time was studied. The experimental data were fitted to Langmuir and Freundlich adsorption model, and it is found that Langmuir model has maximum adsorption capacity.

Keywords Chromium removal · Alumina · Metal oxide · Nanoparticles

1 Introduction

Chromium is one of the important metals widely used in number of products and processes. About 60% chromium is used in alloys, 20% in electroplating industry and other in steel fabrication, leather tanning, refractory product, fine chemicals, etc. [1]. The contamination of heavy metal ion in surface and ground water is a matter of concern due to increasing the level of metal ion in water and wastewater [2]. The Cr(VI) is more hazardous because of its carcinogenic and mutagenic effect on human [3, 4]. Mainly surface water contains 1 and 10 μg/liter. The recent guideline for drinking water as per WHO standard is 0.05 mg/liter.

Various technologies are available to remove hexavalent chromium from water include chemical precipitation, membrane filtration, solvent extraction, and adsorption. These technologies have limitations such as less removal efficiency and high

V. Bhusari (✉)
G.H. Raisoni College of Engineering, Nagpur 440020, India
e-mail: vnbhusari@gmail.com

A. Bansiwal · S. Rayalu
Environmental Material Division, National Environmental Engineering Research Institute,
Council of Scientific and Industrial Research, Nehru Marg, Nagpur 440020, India

operational cost. Among these methods, adsorption as an effective method for removing chromium from water [5].

The commonly used adsorbents that have been reported for Cr(VI) removal from water include natural adsorbents clay, dolomite, bentonite [6, 7], bio materials and agricultural wastes comprising bark [8], rice bran, wheat bran [9], coconut shell, leaves, algae, saw dust [10], activated alumina [11], activated carbon [12], modified chitosan, hydrocalcite, zero valent iron [13], bimetal oxides [14]. The application of nanomaterials in the removal of heavy metal ions from water, and wastewater has good potential because of higher adsorption capacity at very low dose. Nanomaterials are efficient and viable alternate for the conventionally used adsorbent.

In this study, nanoparticles of CANP-A were synthesized and used for the removal of hexavalent chromium from water. The adsorbent was thoroughly characterized by X-ray diffraction, SEM, TEM, etc. The adsorption capacity of CANP-A was determined adsorption capacity by computing the adsorption isotherms.

2 Experimental

All chemicals used in synthesis and evaluation study were analytical grade of E Merck and Aldrich. CANP-A was prepared by sol gel method using equal concentration of copper salt and aluminum salt in appropriate amount of DI water. The gelating agent was used mono hydrated citric acid. The solution was then heated to 90 °C temperature with constant stirring up to formation of gel. The gel was calcined at 500 °C temperatures for 4 h. After calcinations, material was washed with deionised water and dried in oven for 4 h.

2.1 Characterization of CANP-a

CANP-A was compressively characterized for the X-ray diffraction (Model Rigaku: Miniflex) to identify phase and crystalline nature. The PXRD pattern for the adsorbent was recorded at 2θ range from 10° to 90°. Scanning electron microscopy (SEM)-EDX was carried out to understand the surface morphology and composition of CANP-A. Transmission electron microscopy (TEM) technique was used to confirm the formation of nanoparticles.

2.2 Adsorption Studies

Batch adsorption study was conducted to study optimum dose onto removal of Cr(VI). The efficiency of adsorbent was investigated by varying dose from 1 to 6 gm/l. in aqueous solution of 5 mg/L chromium (VI). The aqueous solution of Cr(VI) was

Fig. 1 Chromium (VI) removal by CANP-A
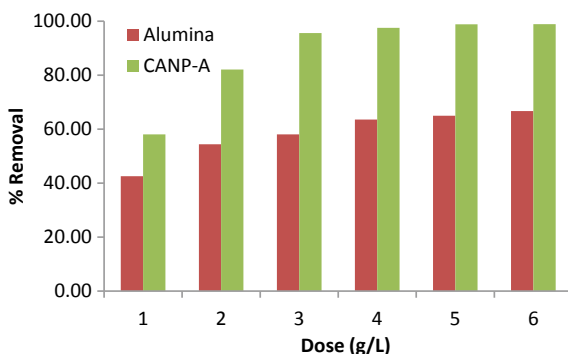
prepared from 1000 mg/L of chromium stock solution. The CANP-A was taken in 250 ml flask kept for shaking in shaker at 150 rpm on room temperature. The pH of sample was maintained 6–6.5. After 24-h shaking time, the flask was taken out from the shaker and centrifuged the sample to decant filtrate. The concentration of residual chromium (VI) in samples was determined by ICP-MS.

The Cr(VI) adsorbed at time t was calculated using following equation:

$$q_1 = \frac{[C_0 - C_t]V}{m} \tag{1}$$

The results of chromium removal using alumina and CANP-A are shown in Fig. 1. It is found that CANP-A has much higher removal efficiency for chromium (VI) than bare alumina. The 98% removal was achieved 4 g/L dose of CANP-A.

3 Results and Discussion

3.1 Characterization of Adsorbent

The PXRD pattern of CANP-A is given in Fig. 2. The major peaks were obtained at $2\theta = 35.4°$ which confirmed the formation of CuO (PDF 89-2529)and next peak at $35.5°$ which shows the presence of Al_2O_3 while the other major peak was obtained at $2\theta = 38.7°$ which confirmed the presence of copper and aluminum oxide phases as per JCPDS database (PDF 752360).

The EDX-SEM of CANP-A was carried out and presented in Fig. 3a which shows the bright nanoparticles of CuO and Al_2O_3 composed on the surface of alumina powder. SEM indicates the surface structure of alumina crystal on which nanoparticles appeared in agglomerate form. The elemental composition of CANP-A is given in EDXA graph (Fig. 4), and the percentage composition of different elements is shown in Table 1.
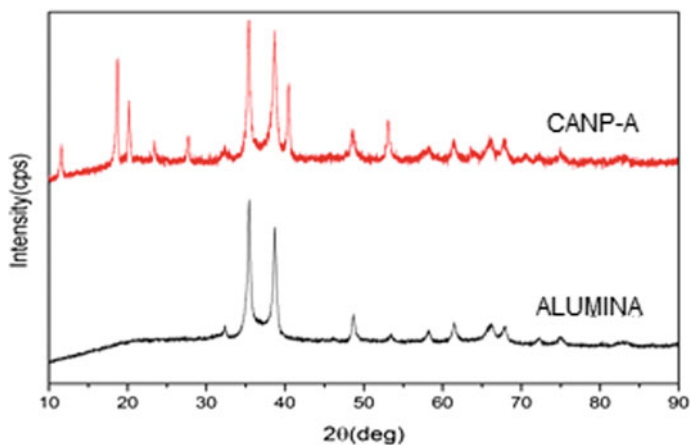
Fig. 2 XRD of CANP-A
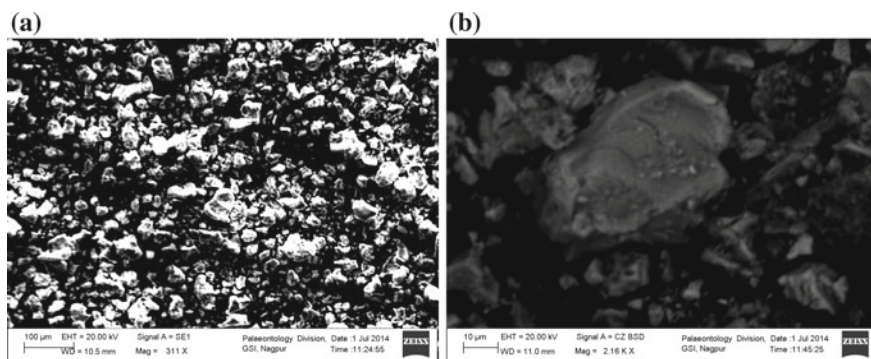
Fig. 3 a, b SEM of CANP-A

Table 1 Composition of CANP-A obtained in EDXA analysis

Element	Intensity	Weight%	Weight%	Atomic%	Compd%	Formula	Number of ions
Al K	0.5062	15.74	1.04	18.09	29.75	Al_2O_3	1.59
Cu K	0.8976	56.12	1.69	27.39	70.25	CuO	2.41
O		28.13	1.51	54.52			4.80
Total		**100.00**	**Anion sum**				**4.80**
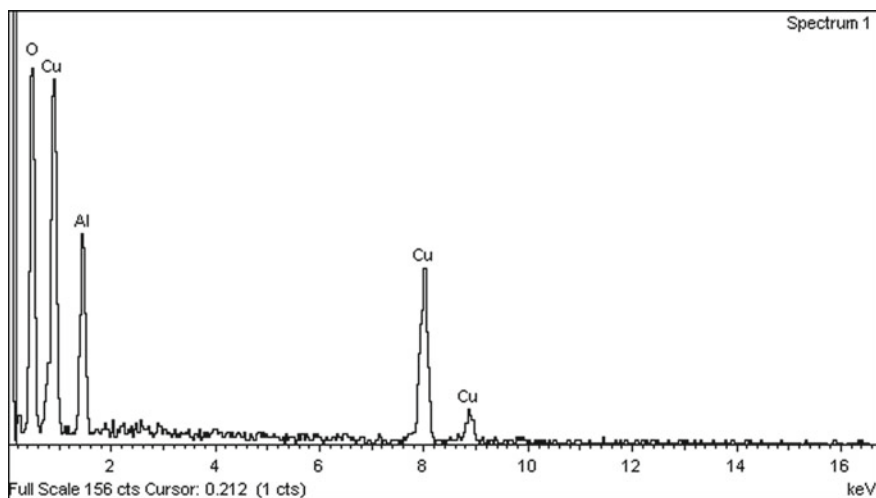
Fig. 4 EDXA of CANP-A
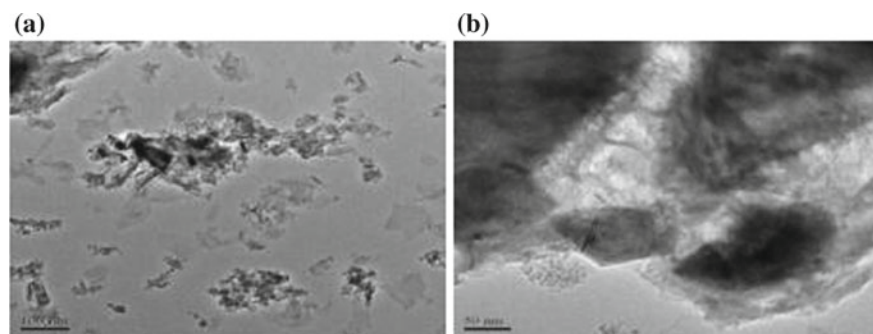
Fig. 5 **a**, **b** TEM of CANP-A

Transmission electron microscopy results of CANP-A are given in Fig. 5a, b. The TEM images show distribution of copper and aluminum oxide nanoparticles, which are highly dispersed on alumina surface. The black dispersed spot in TEM image attributes to the presence of nanoparticles.

3.2 Adsorption Studies

The adsorption isotherm is a fundamental of describing the surface properties and affinity of the adsorbent. To study the mechanism of adsorption, two adsorption parameters, namely Langmuir and Freundlich model, were used [15]. The Langmuir adsorption model can be represented in linear form as follows [15].
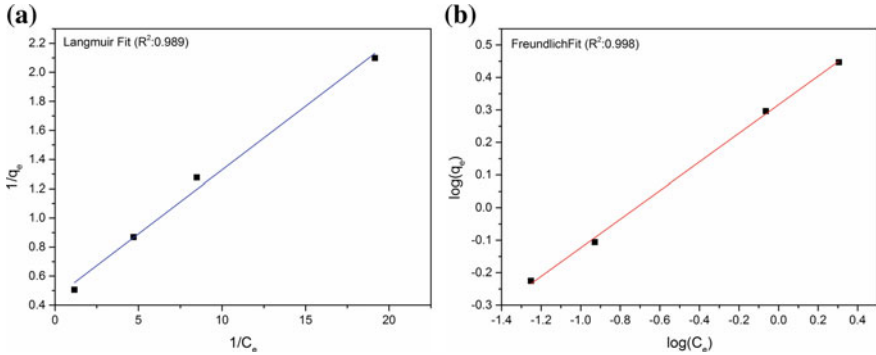
Fig. 6 **a** Langmuir Isotherm **b** Freundlich Isotherm

Table 2 Adsorption isotherm parameters for chromium adsorption onto CANP-A

Langmuir parameters			Freundlich parameters		
q_m mg g^{-1}	K	R^2	Q_f mg g^{-1}	1/n	R^2
2.35	5.25	0.959	1.27	0,406	0.889

$$\frac{1}{q_e} = \frac{1}{q_m K_L C_e} + \frac{1}{q_m} \tag{2}$$

The Freundlich model is an empirical model that indicates heterogeneous adsorptive energies on the adsorbent surface considers multilayer adsorption [16].

$$\log(q_e) = \log k + \frac{1}{n} \log(C_e) \tag{3}$$

On comparison, the equilibrium adsorption of Cr(VI) by CANP-A from the experimental data Langmuir model (Fig. 6a) is well fitted as compared to Freundlich model (Fig. 6b) signifying the monolayer adsorption. The values of higher coefficient of determination obtained for Langmuir model are 2.35 mg/l for Cr(VI) (Table 2).

4   Conclusion

The finding of the study has proved that the CANP-A can be effectively used for the removal of Cr(VI) from water. The experimental data were best fitted to Langmuir model as compared to Freundlich model signifying the monolayer adsorption of Cr(VI) on uniform surface. The values of adsorption capacity by Langmuir model were 2.35 mg/l for Cr(VI). The removal efficiency was 98% for Cr(VI); hence, the adsorbent can be used for removal of hexavalent chromium from water and wastewater.

References

1. Sharma, S.K., Petrusevski, B., Amy, G.: Review paper chromium removal from water : a review (2008)
2. Kumari, V., Sasidharan, M., Bhaumik, A.: Mesoporous BaTiO 3 @SBA-15 derived via solid state reaction and its excellent adsorption efficiency for the removal of hexavalent chromium from water. Dalton Trans. **44**(4), 1924–1932 (2015)
3. Lazaridis, N.K., Bakoyannakis, D.N., Deliyanni, E.A.: Chromium(VI) sorptive removal from aqueous solutions by Nanocrystalline Akaganèite. Chemosphere **58**(1), 65–73 (2015)
4. Li, H.: A novel technology for biosorption and recovery Hexavalent Chromium in wastewater by bio-functional magnetic beads. Biores. Technol. **99**(14), 6271–6279 (2008)
5. Hu, X.J.: Adsorption of Chromium (VI) by Ethylenediamine-modified cross-linked magnetic Chitosan resin: isotherms. Kinetics and Thermodynam ics. J. Hazardous Mater. **185**(1), 306–314 (2011)
6. Bhattacharyya, K. G., Sen Gupta, S.: Adsorption of Chromium(VI) from Water by Clays. Ind. Eng. Chem. Res. **45**(21), 7232–7240 (2006)
7. Jabari, Maher, Aqra, Fathi, Shahin, Safa, Khatib, Awni: The treatment of chromium tanning wastewater using natural Marl. Chem. Speciat. Bioavailab. **21**(3), 185–191 (2009)
8. Netzahuatl-muñoz, A.R., De María Guillén-jiménez, F., Chávez-gómez, B., Villegas-garrido, T.L.: Kinetic Study of the Effect of pH on Hexavalent and Trivalent Chromium Removal from Aqueous Solution by Cupressus Lusitanica Bark. 625–624 (2012)
9. Dakiky, M.U, Khamis, M., Manassra, A., Mer, M.: Selective adsorption of chromium Ž VI/ in industrial wastewater using low-cost abundantly available adsorbents. pp. 533–540 (2002)
10. Baral, S.S., Surendra, N.D., Pradip R.: Hexavalent chromium removal from aqueous solution by adsorption on treated Sawdust. Biochem. Eng. J. **31**(3), 216–222 (2006)
11. Rajurkar, N.S., Gokarn, A.N., Dimya, K.: Adsorption of Chromium(III), Nickel(II), and Copper(II) from aqueous solution by activated Alumina. CLEAN—Soil Air Water **39**(8), 767–773 (2011)
12. Gholipour, M., Hashemipour, H., Mollashahi, M.: Hexavalent chromium removal from aqueous solution via adsorption on granular activated carbon: adsorption, desorption, modeling and simulation studies. Network **6**(9), 10–18 (2011)
13. Liu, T., Zhao, L., Sun, D., Tan, X.: Entrapment of nanoscale zero-valent iron in chitosan beads for hexavalent chromium removal from wastewater. J. Hazard. Mater. **184**(1–3), 724–730 (2010)
14. Xu, K., Li, C., Liu, J., Peng, W.: Study on Chromium (VI) removal from aqueous solution using Fe-Mn Bimetal oxide. Education (2008), 1569–1572 (2011)
15. Langmuir.: The constitution and fundamental properties of solids and liquids, J. Am. 392 Chem. Soc. **38**(1916), 2221–2295 (1996)
16. Freundlich, H.M.F.: Uber die adsorption in losungen, Z. Phys. Chem. (Leipzig) **57A**, 385–470 (1906)

Remote Sensing and Geographic Information System-Based Route Planning

Priyanka Deshmukh, DSP Rao, Rajashree Botale and P. Y. Pwade

Abstract Network analysis is a crucial thing of sorting route problem, shortest path and provide optimal route to daily transport vehicles. With help of proper route planning by network analysis gives quickest way and can sort out problem of longest facility of hospital, petrol centre, police station, etc. Closest facility is the also main factor while performing a network analysis for congested routes. Network analysis can solve single route transportation, and it is also capable of solving the multimodal route transportation. The single route transport means by roads and multimodal route transport means by railroads, roads and waterways. To solve route analysis, it means to find out the shortest route and to find out scenic route depend on the impedance. Impedance can give in the form of time which helps to find out the quickest route. The route has lower impedance value and less cost. Remote sensing and global information system (GIS) are the most useful technologies to take out data regarding network analysis and transportation network data sets. Remote sensing and GIS is related to the satellites information to be collected. Optimization of quickest and optimal route based on satellites data collected through computer and mobile-based app to simplify the critical and longest network facility. ArcGIS is software used worldwide to manage the route network facilities within the city or country. In developing and designing the smart city project, ArcGIS is mostly used for optimization of route planning process and location-routing problem (LRP). With the help of remote sensing and GIS technology, we should look for reduction in travel time and consumption of fuel. Location-based service helps me out to collect data with regard to bus user.

P. Deshmukh (✉)
Transportation Engineering, G. H. Raisoni College of Engineering
Nagpur, Nagpur, Maharashtra, India
e-mail: priyankadeshmukh0123@gmail.com

D. Rao
Regional Remote Sensing Department, RRSC Nagpur, Nagpur, Maharashtra, India

R. Botale
Indian Space Research Organization, ISRO Balanagar, Hyderabad, India

P. Y. Pwade
Civil Engineering, G. H. Raisoni College of Engineering
Nagpur, Nagpur, Maharashtra, India

After gathering all these bus stops data, it would be easy to find out correct location of bus stops. With the help of ArcGIS software, network analysis can be done to get shortest and optimal route for bus which will reduce travelling time and cost of transportation.

Keywords LBS (Location-based Service) · GPS (Global positioning System) · Route planning

1 Introduction

With evolving times, the versatile innovation has changed a considerable measure and over the most recent couple of years we have seen the landing of different new type of devices as Smartphone, camera-telephone, Android and tablet telephones. Actually, the handset business has abandoned straightforward spending handsets to ultra-present day top of the line cell phones. The present gadget is nearly everything—it is in vogue, inventive, engaging, high performing, solid, up-to-date and multi-entrusting. Most recent contraptions can be utilized for different purposes like perusing portable, web, playing amusements, messaging, and blogging, informing, GPS, YouTube, Google look, Gmail and then some. Along this, there has been a blasting business sector for the mixed media cell phones. Present-day contraptions are accompanying worked in cameras with cell phone applications, supposed applications; today are all the more searching for data on the go. This is one region of cell phone innovation upgrade that enables designers and software engineers to offer clients just what they look for under their favoured zone of intrigue. Google's Android is one of the most recent and special development which in a split second has assumed control over the portable market. There are 17,000 area construct fly out applications with respect to the market, and 160 million application good gadgets are possessed around the world—iPhones, Androids, Blackberries and tablet gadgets, for example—the iPad and Motorola. There are applications that can make our voyaging somewhat less demanding, more fun and more important. They let you do anything you can do on the web or with a manual, yet more rapidly and effortlessly and keeping in mind that you are progressing—with maps and GPS to reveal to you where you are and catch awesome recollections. This examination depends on improvement of an easy to use Android-based application called Vehicle Tracker. Vehicle Tracking Solutions or location tracking solution is a main supplier of GPS administration has presented a free downloadable "application" for the Android telephone that communicates with the director's Vehicle Tracking Solutions account Called Silent Traveler. This GPS following Android application offers adaptability and versatility operations administration empowering them to alter settings, get reports all from their advanced mobile phone. We will utilize GPS for finding the position of vehicle. We can track vehicles or track the person location point through android application utilizing GPS to discover a transport vehicle is utilizing a web application which requires login of Vehicle User details. We utilize the Vehicle points of

interest From Vehicle Registration Form, i.e. (Vehicle User Name and Vehicle user Mobile No.). This is the Administrative Activity Form that detail we can track the area of Vehicle, just enlisted vehicles area can track.

2 Related Work

Ding Bing Lin has proposed cell place estimation and monitoring approach for wireless communique structures. The place estimation is based totally at the differences of downlink signal attenuations, which can be used to decide circles composed with the aid of feasible places. Then, the actual area is given by way of the intersection of the circles. The extraordinary advantages of this method are the non-necessity of an acknowledged and correct route loss modelling and the discount of shadowing effect. Furthermore, a cellular monitoring approach through linear optimization using easy genetic set of rules was implementing to improve the places estimation. This paper has proposed a cell vicinity estimation and monitoring technique for GSM structures. The estimation is based totally on the variations of signal attenuations, and its blessings consist of the non-necessity of an excellent direction loss modelling and the discount. The proposed scheme changed into implemented to a realistic GSM system. Although it could perform better in rural environment than in city because of shadowing, encouraging area accuracy is received in urban city. Furthermore, the proposed monitoring method, linear optimization using GA, smooth and corrected the place mistakes. The corresponding values after monitoring are decreased. With the assist of virtual map, machine screen can almost verify which path the cellular user locates.

Pradnya Battin and Dr. S. V. Markande researched on "Location Based Reminder." The telephone has GPS which received signal from GPS receiver. Geo location primarily deals with GPS reading to locate present location of person. Favored locations and responsibilities restored in the form of database. Database will perform contrast of the vicinity which vicinity related to the preferred machine. If the application user is physically present around given vicinity, then reminding alert had given to that person related to the project. If specific responsibilities include places for into the database, then it uses Google Maps. With help of selecting up the favoured location which is displayed on Google maps, user can upload the desired mission into the database. This could be used for putting reminder in LBR (Location Based reminder) utility. It is not always important for the person to bodily gift on the unique location even as entering the reminder within the software.

Rene Hense et al. described Smart CampusAAU—it is an open, extendable platform that helped smooth creation of indoor area-based structures. SmartCampusAAU has given an app and can be used to permit indoor positioning and navigated any building. The SmartCampusAAU app available on all mobile systems (Android, iPhone and Windows Phone) and helps each tool and infrastructure based positioning. SmartCampusAAU additionally given a publicly to be had Data back end that lets in researchers to percentage radio map and vicinity monitoring records. In

this paper provided the SmartCampusAAU software platform designed to facilitate indoor positioning and navigation. SmartCampusAAU overcomes the limitations of current offers via providing help to ubiquitous positioning and navigation for all predominant mobile gadget. SmartCampusAAU depend on crowdsourcing to construct indoor radio maps, graphs and insurance so probably limitless. Mobile platforms, the other most important characteristic made SmartCampusAAU precise that it makes possible to share radio map and area. This opens up further studies opportunities, now not most effective within region fingerprinting and information control, but indeed anywhere, where get admission to indoor vicinity information is needed. The steps worried in facilitating indoor positioning and navigation in a building are given:

(1) Add constructing floors and building.
(2) Made a radio map to permit IP (Indoor Navigation).
(3) Generate features facts for places.
(4) Perform a graph to permit IP (Indoor Navigation).

3 Need of Research

(1) Global Positioning System
    GPS (Global Positioning System) gives clients situating, route and timing administrations. This framework comprises of 3 sections: the space section, the control portion and the client fragment. The space section comprises of an ostensible heavenly body of 24 working satellites that transmit one-way flags that give the current Global Positioning System satellite position and time. The Control Segment tracks the Global Positioning System satellites, transfers refreshed navigational information, keeps up wellbeing and status of the satellite group stars. The client portion comprises of the Global Positioning System collector hardware and transmitted data to compute client's 3-dimensional time and position.
(2) Android
    It is a versatile working framework which deals a bound together way to deal with application improvement. Engineers require to create applications utilizing Android, and these applications can keep running on various diverse gadgets, as long as the gadgets are controlled utilizing Android.
(3) Google Maps
    It gives a guide of an open Google Maps API (Application Programming Interface). Designers can effortlessly connect the Google maps administration application.
(4) Web Client
    The data in the vault overseen and seen utilizing the web customer. The client gets the area data from the web customer on Mobiles.
(5) Map Services

The guide benefit is a specialist based which gives both the portable and the web customer with outline. The guide benefit utilizes Global Positioning System to track the position of companions or relatives. The area data are refreshed to web customer each time by the cell phone.

(6) Data Sharing Centre

Share a module deals with images, documents, details of users and location of users.

(7) PHP—

PHP manage database, DC (Dynamic Content), ST (Session tracking) and it is compiled with various databases. Server side scripting language means PHP, and it is embedded with HTML.

(8) My SQL

My SQL works on various OS (Operating System) along more languages including C++, PHP, JAVA, C, etc. My SQL is fast, easy to use and works with large data sets as well (Fig. 1).

4 Proposed Architecture

The proposed architecture for location-based android mobile app shown the number of technical aspects has been compiled in research. The proposed architecture to developed location-based android mobile app as given below:

- Mobile Client
- Web Client
- Map Service
- Data Sharing Centre (Fig. 2).

Global positioning system used to take a longitude and latitude point of area within an accuracy range. Android-based mobile app for location tracking leads to find out actual position of person. The following icons are given in app, and it compiled below as a serial number:

(a) Check GPS connection
(b) Make a Profile
(c) Capture Photograph
(d) Attributes input
(e) Save the data
(f) Send the data.

The steps to be followed for login/Register to Bhuvan Geotag House for Route Planning app are as follows:

Step 1: GPS connection should be open and accurate. If accuracy is less than 10 m, then to collect location tap on GPS icon. If the accuracy of GPS is accurate, then tap on "OK" otherwise tap on "CANCEL" to cancel the collection of data. Clear sky view is required to collect The GPS.
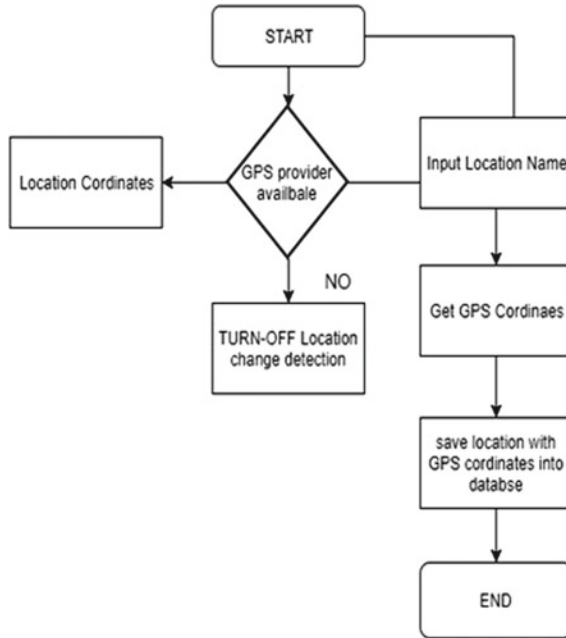
Fig. 1 Architecture proposed framework

Step 2: With the help of this app, photograph can be captured of desired location by tap on the photo icon. Two photographs are necessary to recognize the exact GPS location. Tap on photo icon for first photograph then tap on the second photograph as app provide instruction of second photograph.

Step 3: Attributes are more important to collect the information of particular location. App has been designed with attributes input requirement. The user has to give exact address of their location with pin code and landmark of their location.

Step 4: After all the requirement of data collection has been done, then file will be generated of collected location data. That file has to be sending on Bhuvan Server by clicking send icon. Then User will get the windows of "Data Successfully Uploaded" on screen. But first mobile internet connection must be strong.

Step 5: If internet connectivity is not available, then data can be send later on. The generated location data file will remain on same place. Once user will get good Internet connectivity that time user can follow step 6 to upload the data on Bhuvan Server.

Step 6: Manage icon is given to manage the data later on. This feature will store the data file in the user mobile. While sending the data, user should select data file that needs to be uploaded on the server and tap on Send icon. User will get confirmation message on mobile window "Data Uploaded Successfully."
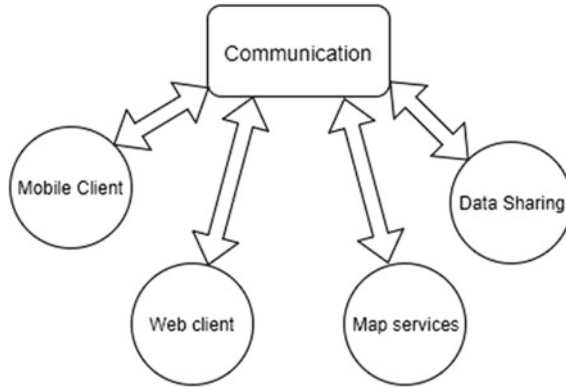
Fig. 2 Communication system between clients

5   Experiment

The experiment of Bhuvan Geotag House Route Planning shows following window after tap on the installed app. At the starting, it will be loaded first to achieve the latitude and longitude of particular area where user will present. This app designed to people location data by fetching GPS latitude–longitude. These data would be helpful to do network analysis in ArcGIS software to find shortest route or quickest route for those people. It will result into reducing travel time of people. The integration of GIS (Global Information System) and GPS (Global Positioning System) is called as LBS (Location-Based System). Location-based system use smart mobile devices to collect information regarding location for optimization of existing route. Network analysis helps to reduce the constraint of route (Fig. 3).

After loading, user will get another window which will consist different icons like GPS, camera, attributes, send and manage, save, exit, profile and help. The user should wait to collect accuracy of GPS more than 10 m. If user will get accuracy below 10 m, then tap on GPS icon to recollect the latitude and longitude point. Once user got longitude and latitude point, then user can switch on profile icon for login registration (Fig. 4).

Once user has done with profile details, then tap on save icon for saving data for further process. Then, user can move through home window for giving attributes input details.

In attributes window, attributes input will ask for a personal details about name of user/student, enrolment number, mobile number, transport facility (Require OR not Require), address type (House address location and Pick-up address location). While giving input to the address details, care should be taken to select house address location and pick-up address location. If user giving input while going to designation place or organization places, the user must choose the pick-up address location at that present time and follow further procedure. If user is going to house or their

Fig. 3 Start Screen of Bhuvan Geotag for Route Planning App

Fig. 4 Icons window and profile window of app

residential place from organization or designation place, then user should choose the house address location after reaching to destination point and follow further procedure (Fig. 5).

In attributes window, attributes input will ask for a personal details about name of user/student, enrolment number, mobile number, transport facility (Require OR not Require), address type (House address location and Pick-up address location). While giving input to the address details, care should be taken to select house address location and pick-up address location. If user giving input while going to designation place or organization places, the user must choose the pick-up address location at that present time and follow further procedure. If user is going to house or their residential place from organization or designation place, then user should choose

Fig. 5 Icons window and attributes activity profile window of app

the house address location after reaching to destination point and follow further procedure.

After filling all these details, user must have to save these data. Data saving will just take a while to save and as the data saved user will get an alert about that data are saved then tap on send icon to share the data with Bhuvan server. These data will be to know starting and destination point of user. To know data about like this, it will be helpful to sort out problem of transportation facility of student or employee of organization (Fig. 6).

Data saving will be done after you have completed with all the user details. Then user can move to manage icon which located on home window of the app. After clicking on manage icon, user will get upload data window. If user did not share the data with Bhuvan server may be because of less connectivity of Internet, then now user can send data by clicking on first string of "upload send later data." Seldom, user uploaded the data but it failed due to some reasons of Internet connectivity. So user can able to send that data by clicking on "Upload sent failed data." Once user will have done with all these steps user may see his/her sent data along with number of data have sent. All these steps lead towards the confirmation message of uploaded data (Fig. 7).

As user will get "uploaded data successfully" confirmation message, then it will show the direction message as well to get exit of current windows by clicking on "OK" and app will be ready to take another location user (Fig. 8).

6 Techniques of Network Analysis

The Line highlight is more vital in the maps, since it speaks to a noteworthy guide highlight. There are numerous GIS programming that gives a Line Feature Specu-

Fig. 6 Profile data saving window

Fig. 7 Upload Data Window and Data Saving Window

lation office. The geometric activities are engaged with this speculation like choice, combine, symbolization, disposal and so forth. Yet, there is no appropriate definition for speculation. In ArcGIS, a point remove instrument utilizes Douglas-Peucker (DP) calculation. This calculation was generally famous calculation, which was utilized as a part of numerous applications like Road, stream, beach front line speculation. The accompanying activities are required to sum up a street organize.

1. Characterization: It distinguishes a question and makes bunches as indicated by properties. For less demanding determination and more precise streets relies upon the great grouping. It limits the many-sided quality. Ex. street width.
2. Determination: Select specific street class at the target scale
3. Elimination: Eliminate shorter street of a certain length.
4. Disentanglement: choose streets can be streamlined to diminish the points of interest. Ex. Expel incidental twists of streets.
5. Exemplification: This is manual altering approach. It lessens the Network thickness and streamlines the dissemination and the example of the system.
6. Symbolization: To speak to highlights on maps, realistic imprints are utilized. Ex. Street Name, Road Number.

There are numerous applications like Google Earth, which can demonstrate the course between two nodes puts by utilizing just significant streets. Additionally these courses try not to consider the impediment like harm of street. To defeat this issue, ArcGIS programming can be utilized. The information gathered from Google Earth and OSM (Open street map) also, spoke to utilizing the ArcGIS application. The application can demonstrate the most limited way between two nodes with all upsides and downsides of those streets. The Circular segment View was utilized to manufacture the topology while playing out the system examination on a line subject. Before utilizing the vector-based pictures in GIS application, it is required to be geo-referenced. In ArcGIS, the geo-database must be made, and this database is further partitioned into data sets. The data sets are subseparated into the component classes which comprise of two classes: a point and streets. Presently the information and pictures are added into the Arc MAP to alter and draw the street organize and to find the focuses. It is moreover conceivable to demonstrate the nearest office from any specific area. The nearest office implies closest healing centre, inn, transport stop and so on. The application can be utilized to demonstrate the city transport courses. In GIS by utilizing Remote detecting high determination IKONOS and security information for making the topical maps were utilized as a part of ArcGIS application. The Arc View was utilized to construct the topology while playing out the system investigation on a line subject. Like all GIS programs, Arc View joins graphical highlights to a database that contain. For the use of GIS in street arrange examination takes the essential information from the study of India (guide of scale 1:2000). After the digitization of essential information, a system investigation undertaking was performed. This was finished by utilizing ArcGIS programming. It helps in the defeat following and likewise in making the most brief way between two or then again more places. In each transport, a GPS collector and GSM modem with microcontroller interface was put and this gadget was utilized to send the message to control station and modem or cell telephone gets and gives the contribution to PC. The application was created in Java to store and process information into a database. At that point, the co-ordinates from database were put on outline utilizing Visual Essential to demonstrate position of each transport on outline quality data.

In another framework, design was isolated into two sections, i.e. Spatial and Non-Spatial information. For spatial information examination, the information was taken

Fig. 8 Data successfully
uploaded confirmation
message
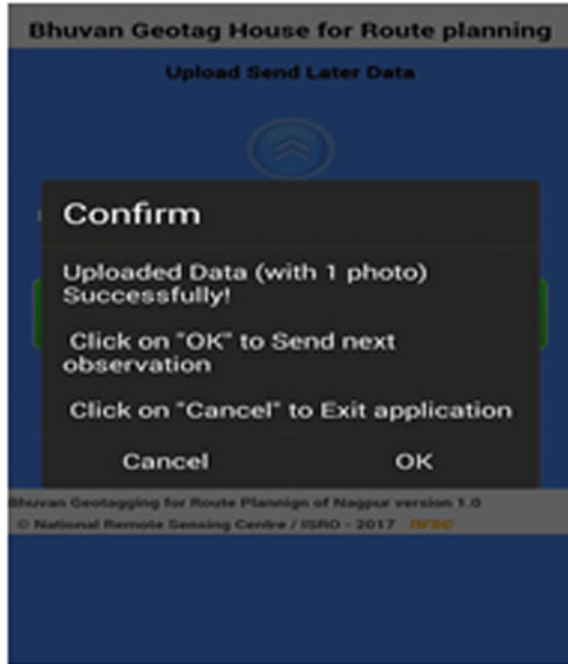
from the Indian Space Research Organization (ISRO Nagpur) and Survey of India
(SOI) maps (1:50,000 scale) as base maps. After digitizing this line information, the
updating was conveyed out on IRS satellites Panchromatic (PAN) and Straight Imaging self-checked sensor (LISS). The Dish information was geo-referenced to study
of India maps. To approve the status of street, the real ground review was performed.
Non-Spatial information ascribes are required to be appended to the spatial information layers. The application was outlined and created by utilizing the Power Builder
as front-end instrument, and for information section and capacity of characteristics,
a MS SQL was utilized as back-end instrument. An ESRI's Circular segment View
was utilized to modify the GIS interface. The ArcGIS9.2 were utilized to geo-amend
the topographic maps and satellite symbolism acquired from the Google Earth. For
digitizing the limit, the polygon was utilized, and for street, the polyline was utilized as a part of ArcGIS. The aggregate length in kilometre and territory in square
kilometre was ascertained in ArcGIS.

7   Analysis of Transportation Network

The Shortest Time Distance (STD) is strategy for assessing the street organize
openness. It alludes to the aggregate time from one hub to different hubs inside the

street organize by most limited time spending course. The lower STD esteem that a hub has demonstrates that the hub's availability is higher. The second strategy is Weighted Average Travel Time (WATT); speaks to the significance of a furthermore, travel time is helpful for state transportation division. The impedance esteems are required at the point when arrange examination is performed on every street in the system. For ideal course assurance, perspective impedance esteem is vital since it gives a need to streets. There are diverse sorts of impedances; however, briefest time perspective speed impedance is more vital. It implies that there is a speed restrict for various sorts of streets. What's more, at the convergence of the streets, the turn impedance is helpful, for example, U turn, right turn, left turn is permitted or not. In Arc GIS, system examination utilizes an impedance esteems to recognize a street compose like one way or two ways. On the off chance that there is another enlisted picture at that point, picture to picture enlistment ought to be performed. Also, if the authoritative limit is there, at that point it should cut the chose region concurring to regulatory limit. Ordinarily our chosen area is not on a solitary top sheet/picture at that point mosaics it. This prompts a determination adjustment to a length of give or takes 5 m. In relatively every field, a yield of remote detecting is an info a GIS. GIS not just take input from RS yet in addition take contribution from filtered maps. There are numerous application territories in RS; furthermore, GIS yet significantly these are arranged in Normal Resource Management, Urbanization, Horticulture and National Security. Be that as it may, in this paper, the approach is worried about as it was urban transport investigation. In first period of approach, the acquisitions of favoured information ought to be finished. The information, for example, topographic sheets like 1:50,000 or satellite pictures with great determination. On the off chance that Top sheets are there, then it ought to be examined with the characterized determination proposed. It ought to be digitized with a characterized zoom level, so all the highlights can be digitized in number of layers. In next stage play out, the GPS overview for most extreme ground control focuses (GCP) of each Region of Interest (AOI) on the known streets/critical stops (Fig. 9).

8   Result and Discussion

1. With the help of ArcGIS software, it could be possible to do network analysis on routes of Nagpur road network. After the network analysis, institution buses got the shortest route for transport the student from their pickup locations to their destination location of GHRCE.

2. The basic work of network analysis is to find out route which reduces distance between origin stop to destination stop by finding the route which can be early reaching to destination stops. ArcGIS sorted out more time-consuming route of transportation of institution buses and obtained the optimal route for transportation.

3. Result showed the optimal route for institution buses without any constraints between so many of stops. There is number of between each buses and network
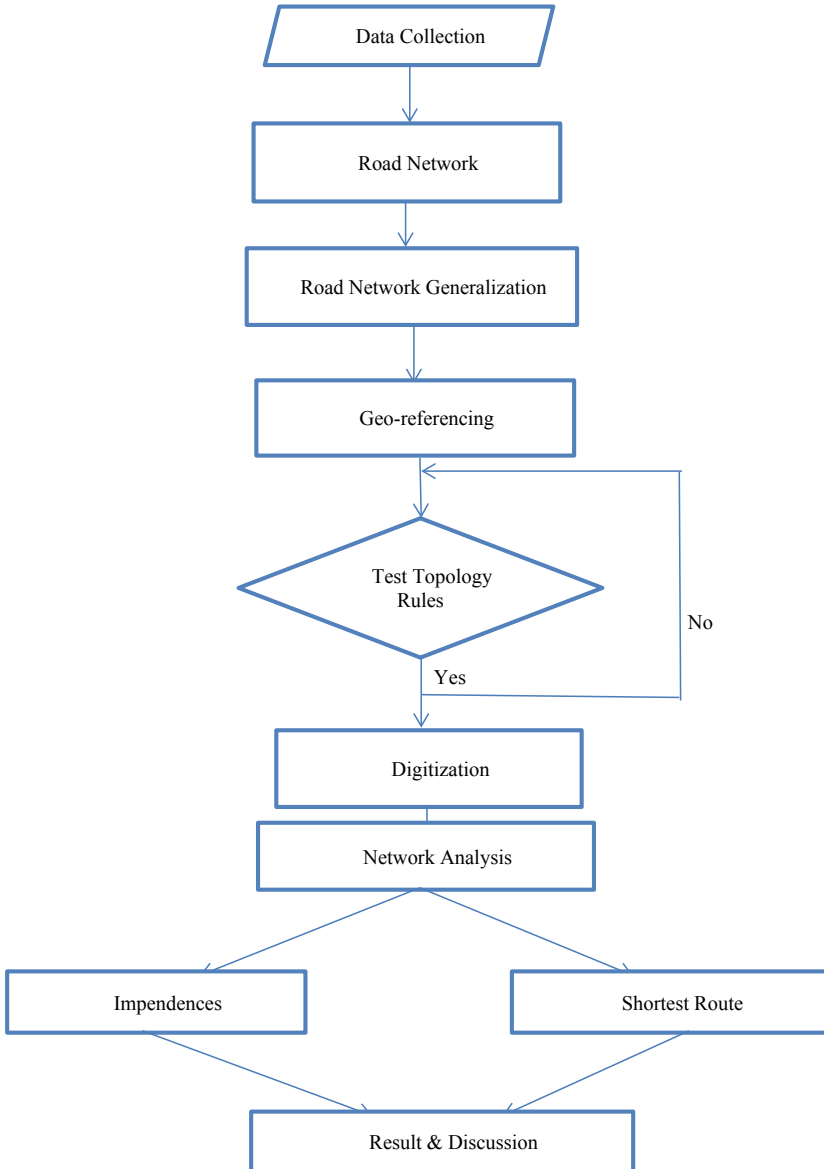
Fig. 9 Flowchart of transportation network analysis

analysis extension given best route by covering all those stops came between the each route of buses.

4. This project has worked on the main two objectives, i.e. reduce travel time of institution buses and reduce cost of transportation. By obtaining the best shortest route for the institution buses which previously consume more time to travel. A shortest route reduces the travel time. Bus will consume less travelling time of transportation.

5. While going through network analysis, impedances are required to get quickest route between numbers of stop. In this number, origins and destinations can be there for finding the routes. Cost of travelling reduced by reducing the length between origin and destination stops of each bus. The quickest path based on the connectivity, flow and rules. Incorporation of direction flow rules helped to determine the lowest cost of transportation of institution buses.

6. To find out the result for number of student is more convenient than find out result for individual student. The result sorted out problem for travelling time and cost of transportation of buses by giving best quickest route for each bus. The final result of network analysis shows the shortest and optimal route for a number of students at one time.

9 Conclusion

To track the location of people to sort out problem of congestive traffic route by providing best shortest route to people, location-based service is a pivot contribution to network analysis. This Bhuvan Geotag for Route Planning app can be used for companies, organization and institutional places to find optimal route for employees, workers and students. The actual aim of this work was to reduce time of travelling, reduce the fuel consumption in travelling and find the best shortest route for people for ease. Nowadays, people facing the congestion problem in wide range. With increasing population of a country, it is necessary to design the beat optimal route for people. By finding the best optimal route by network analysis will be useful to solve the problem of congestive traffic, consuming excessive time to reach destination point and traffic vehicular activity. Compilation of location-based service, Global Positioning System, Network analysis and route planning gives the modified solution over the existing work. Most of the people are using smart technology systems for every query about day-to-day life. The standard of people tries to touch the tangent of smart technologies to get a comfortable life; in such case, this app for location tracking and network analysis is the biggest acceptable technology to make transportation facility without constraint of time. Due to enhance transportation system according to get a destination point in shortest time and to get a shortest route to reach systems for every query about day-to-day life. The standard of people tries to touch the tangent of smart technologies to get a comfortable life; in such case, this app for location tracking and network analysis is the biggest acceptable technology to make transportation facility without constraint of time. Due to enhance

transportation system according to get a destination point in shortest time and to get a shortest route to reach.

References

1. Lin, D.-B., Juang, R.-T., Lin, H.-P.: Mobile location estimation and trracking for GSM. Institute of Computer and Communication, National Taipei University of Technolog, In: IEEE Conference (2004)
2. Battin, P., Dr.Markande, S.D.: Location based reminder android application using Google Maps API, In: International Conference on Automatic Control and Dynamic Optimization Techniques (ICACDOT) International Institute of Information Technology (IIT), Department of Electronics & Telecommunication NBN Sinhgad School of Engineering Ambegaon, Pune (2016)
3. Hansen, R., Thomsen, B., Thomsen, L.L., Adamsen, F.S.: SmartCampusAAU—an open platform enabling indoor positioning and navigation. In: IEEE 14th International Conference on Mobile Data Management. Department of Computer Science, Aalborg University (2013)
4. Sun, N., Han, G., Duan, P., Tan, J.: A global and dynamitic route planning application for smart transportation. In: 2015 First International Conference on Computational Intelligence Theory, Systems and Applications, College of Internet of Things Engineering Hohai University Changzhou, China (2015)

Analysis of Foundations and Soil–Structure Interaction Using FEM—A Review

S. M. Khanapurkar, V. R. Upadhye and M. S. Dixit

Abstract This paper deals with the review of the literature regarding the dynamic and static analysis of foundations resting on different types of soils. This study focuses on the application of various finite element analysis (FEA) methods for the designing and analysis of various foundations rested on different types of soils. The papers studied for the project dealt mainly with the use of FEA software ANSYS for the analysis of foundations and soil–structure interaction. Further, the areas where more research work is still needed are discussed.

1 Introduction

The purpose of the foundation is to make the load of the structure within the safe bearing capacity by distributing the load over a large bearing area, also preventing lateral movement of the supporting material, increasing the stability of the structure as a whole, and securing the firm bed for building operations [1]. Therefore, to prevent the structure from failure, special care should be taken while designing the foundations. The interaction between the soil beneath the structure and the structure is termed as soil–structure interaction. Seismic waves propagating through near-surface soil layer are able to produce ground motions much larger as compared to those at the rock base [2]. And therefore the effect of seismic waves on soil strata is needed to be studied. For the analysis of this type of structures interaction, mathematical modelling methods are adopted. For the analysis, a variety of numerical methods is available, and out of these methods, FEM is one of the most widely used method for solving engineering problems.

S. M. Khanapurkar (✉) · V. R. Upadhye · M. S. Dixit
Civil Engineering Department, Marathwada Institute of Technology, Aurangabad, India
e-mail: sampada.makarand@gmail.com

This study reviewed the literature related to the analysis of soil–structure interaction using FEA software ANSYS. Various authors have reported the analysis of foundations under different magnitudes of earthquakes. The methodology adopted by these authors for the modelling and analysis of structures are considered. Their obtained results are studied as well as compared in this paper. Based on these papers, general conclusions are drawn regarding the modelling of foundations and soil–structure interaction.

2 Methods of Modelling in ANSYS

Various studies regarding the soil–structure interaction have been done by the researchers. Julio A. Garcia [3] studied the influence of soil–structure interaction and fixed base condition on a 6-storey building with the help of ANSYS. On including soil–structure interaction in the dynamic behaviour of the structure, an increase in the vibration period and in the system damping was observed by the authors in comparison with the fixed base model. In the seismic design of the structure, it is observed that the horizontal spectral acceleration values decreased when the SSI was considered. The results show the values of stresses and displacement more accurate when the soil was considered in the analysis.

Gaikwad, Ghogare and Mathada [4] compared the behaviour of the in-filled frame and bare frame with and without soil–structure interaction. The authors considered the columns as fixed at the foundation level. The authors stated that, while considering soil in the analysis of building frame 100% fixity might not be ensured. Due to the settlement of foundation and rotation of foundation, the shear force and bending moment in the superstructure may also get altered. This effect is stated as "soil–structure interaction." From the analysis, it was found that the in-filled frame and the bare frame with SSI gave more displacement, bending moment, and less shear force as compared to the frames without SSI. The authors observed that the in-filled RC frame has excellent strength and stiffness.

Peizhen, Xilin, et al. [5] determined the influence of various parameters like soil property, seismic response, excitation on dynamic characteristics, and the rigidity of the structure. They also found that the interaction effect of the SSI system on soil with viscous boundary has the influence on soil–structure interaction. It was observed by the authors that the natural frequency of SSI system increased with an increase in dynamic shear modulus of soil and the displacement peak value of the structure increases with the decrease in shear modulus of soil.

Abdel, Ahmed and Alazrak [6] analysed a 6-storey and 12-storey building rested on raft foundation for soil–structure interaction. The Egyptian seismic code provisions for analysis were used for the evaluation. For the analysis, ground motion records of seven different earthquakes were used. In the seismic behaviour of a structure, they found that the dynamic SSI plays a significant role and so the SSI should be considered while designing a midrise moment resisting building frame resting on soft soil.

Raghuveeran and Hassan [7] studied the roof displacement, soil settlement, and lateral floor displacement for a building frame of 8, 6, and 4 stories resting on a pile-grid foundation in loose sand and dense sand. The structure was modelled using ANSYS Workbench 14.5. Static as well as the transient analysis was performed for the considered frames. On analysis, it was found that the settlement was more for the loose sand than medium soil and the lateral floor deflection is directly proportional to the increase in floor level, i.e., with the increase in floor level the lateral floor deflection also increases. Also, the soil stiffness and number of stories decreases as the natural frequency of the structure increases

Li and Zhang [8] analysed the soil–pile interaction problem of pile group foundation by FEA software ANSYS along with a parallel computational technique to improve the analysis efficiency. According to them, analysis of bridge pile group foundation design took very long time on one computer and therefore various parallel computational methods such as symmetric multiprocessor (SMP) system, massively parallel processor (MPP) system, distributed sheared memory (DSM) system, and cluster of workstation (COW) was proposed. They adopted the method Cluster of workstation (COW) where a group of linked independent computers connected to each other through fast local area networks were used to run tasks independently or work together closely by commands. From the proposed method of analysis, they concluded that the computational efficiency of solving complicated problems could be improved with the help of computer network COW and corresponding parallel algorithm.

Spyrakos and Xu [9] studied seismic response of massive flexible strip foundations. The foundations were considered to be embedded in the layered soil. In the proposed BEM–FEM formulation by authors, the flexible foundation was modelled using the finite element method (FEM) and the soil strata was modelled using the boundary element method. The seismic response of foundations subjected to S-waves and P-waves was investigated. Numerical examples were presented to assess the effects of foundation stiffness. It was found, in the analysis, that the deeper the foundation embedment, the lower was the natural frequency. The authors also found that when the excitation frequency exceeds the fundamental frequency of the soil foundation system, the response of soft foundations showed the considerable difference from that of stiff foundations.

Shah, Solanki and Desai [10] reviewed the state of art about SSI analysis methods. They discussed various global procedures for dynamic analysis for unbounded domains which included boundary element method, thin-layered method, and scaled boundary finite element method. Also, literature related to various local procedures such as transmitting boundary conditions, infinite elements, and absorbing layers was also discussed. The review revealed that for simple analysis, global procedures are feasible; while for nonlinear analysis, substructure method is effective and simple to apply.

Ceroni, Sica, et al. [11] described the state of the art on SSI and studied the effects of SSI on different structural typologies by means of approaches widely used in the literature. Case studies were presented for masonry palace, masonry bell tower, RC frame with beams and columns and RC frames with shear walls. It was observed

that the influence of soil–structure interaction is more relevant when the period reduces and when the stiffness of the structure increases. The effects of soil–structure interaction could become relevant for also for very deformable buildings.

Lewis, Masoud and Joseph [12] carried out an investigation to study the effects of soil–structure interaction on various structural parameters such as the stresses and displacements in the structure, etc. The investigation was carried out on the soil of a fifty-storey steel frame structure with a concrete mat foundation resting on a deformable soil. A two-dimensional analysis was carried out, and the effects of increasing wind load on the structure were also studied. Linear elastic and elasto-plastic analyses were carried out with the help of FEA software ANSYS and PLAXIS. This research also provided a comparison of two finite element packages: ANSYS, a general-purpose FEA package, and PLAXIS, a package used for geotechnical engineering analysis. The authors found that ANSYS was more beneficial as compared to PLAXIS since it provides a wide variety of options for the analysis of complex structural models and various loading conditions.

Jancy, Rajagopal, et al. [13] modelled SSI using FEA package ANSYS to demonstrate the behaviour of the structure while considering the actual nature of the ground response. Three different cases were considered wherein the first case, a single-storey portal frame fixed at the base was modelled as linear elastic without considering the ground response. In the second case, both the frame and ground were modelled as linearly elastic, and in the third case, the frame was modelled as linear elastic and the soil as nonlinear elastic. From the results, the maximum displacement of the portal frame was found to be higher when the fixed base condition was considered. They concluded that, the ground interaction effect on the portal frame behaviour could be more significant for multistoried buildings, and therefore, the SSI should be accounted for in the structural analysis of important buildings.

Rajasankar, Iyer et al. [14] investigated the seismic soil–structure interaction of a massive concrete structure. The structure was considered to be supported on a raft foundation. The linear transient dynamic analysis was carried out using the FEM. Transmitting boundary conditions at far-field of layered elastic half space were imposed. FEA software LS-DYNA was used for finding out the moments. From the results, the authors found the tensile stresses of considerable magnitude at few locations in the rock–raft interface. Also, typical stress responses at the interface were presented and discussed.

Sunny and Mathai [15] evaluated SSI of buildings founded on Piled Raft Foundation through FEA using ANSYS v17.0. Static analysis was carried out for a 10-storied building, and total deformation and equivalent stresses in the building were evaluated. From the study, the total vertical deformation of the building was found to be a more inflexible base model than in fixed base model and in the model where the soil is considered stress distribution pattern has varied. Average stress developed in the model with soil is observed to be greater than other models.

Yang, Jia and Yan [16] studied the distribution of extra stress and distortion of homogeneous soil supporting a weak foundation of an oil storage tank by using ANSYS. The authors compared the result by using the formula of criterion. And then, several methods on how to deal with foundation were studied. The minimum

compound modulus of elasticity and Poisson's ratio required to control the settlement in some magnitude were found. From the experiment, they proved that the FEA method could be used for analysing extra stress and distortion of the foundation of an oil storage tank and that this method could provide a reference for the analysis of elasticity and plasticity of foundations and dependability for engineering design.

Rizos and Edward [17] presented simplified, soil foundation models for dynamic, and seismic analysis of a bridge model by taking into consideration soil–structure interaction effects. The investigations showed that the significance of SSI effects depends upon the relative rigidity between the superstructure and soil foundation system.

Various methods are available for the modelling of soil strata and foundations in ANSYS. Few most widely used methods for modelling of soil are the direct method, Winkler's method and Boussinesque's model or theory of elastic half space. Authors Ravishankar and Satyam [18] modelled the soil by the direct method. In the **direct method**, foundation system, superstructure. and unbounded soil mass are modelled together with an interface element. Another method proposed by authors was **substructure method**. In this method, foundation system and the superstructure is modelled separately with proper consideration of the load transfer from the superstructure to the foundation system.

Yu, Andrew, et al. [19], George and Lovely [20] and Kalavathi and Murlidhar [21], in their papers, modelled soil using Winkler's approach. In **Winkler's approach,** soil is represented as a system of closely spaced, mutually independent, linearly elastic springs. According to this idealization, the deformation of foundation due to the applied load is confined to loaded regions only. While modelling soil strata using Winkler's approach, the soil has meshed and each node is then attached with a spring which is then fixed at the other end to show the fixity of soil at some point.

Ing. Máleková V. and Ing. Jendželovský [22] modelled soil using the theory of elastic half space. For modelling the soil using the **theory of elastic half space** also called as **Boussinesque's model**, the soil strata below the foundations is considered to be of infinitely large dimensions to show the continuity of the soil. They stated another method of modelling called **Pasternak Model**. While modelling the soil using Pasternak method, all the springs are connected to a single rigid plate that undergoes only transverse shear deformation.

Pasternak proposed this model by assuming the existence of the shear interaction between the spring elements. Sushma and Kumar [23] analysed a high-rise structure supported by pile foundation by considering pile completely embedded in large soil strata fixed at all boundaries.

Shanmugan, Dode and Chore [24] performed a two-dimensional analysis of soil–structure interaction in framed structure. The superstructure and piles were modelled in ANSYS using BEAM188, and the interface between soil and structure was modelled using CONTA175 and TARGE170. The soil was modelled using SOLID185 element. A two-dimensional analysis of piled raft foundation was performed by Srilakshmi and Darshan [25] and Harish and Naidu [26] analysed the free-standing pile group foundation using finite element analysis software ANSYS.

Both the research papers used PLANE82 element for modelling of the pile, raft, and soil and CONTA172 (for soil) and TARGE169 (for pile and raft) at the interface.

Thusoo, Modi, et al. [27] and Mathew, Tomer and Lovely [28] prepared a 3D model of soil foundation system using SOLID45 element for soil and the SOLID65 element for the foundation in ANSYS. R. Gadpande [29] used the element SOLID45 for the modelling of soil, pile, and raft. SOLID45 has plasticity, creep, swelling, stress stiffening, large deflection, and large strain capabilities. The contact pair was modelled using CONTA174 and TARGE170.

3 Conclusion

Various papers related to the analysis of foundations rested on different types of soil were studied. The main aim of the study was to determine the importance of modelling and analysis of foundations with and without considering soil–structure interaction. On reviewing the literature, it was found that the results obtained by considering the SSI while foundation analysis gave more accurate results as compared to the foundations analysed without the consideration of SSI. The analysis method considered was finite element analysis, and the software ANSYS was used for the same. Special attention was also given to the modelling of soil strata in ANSYS, and it was found that the software gives accurate results for the analysis as compared to the numerical methods. It was also seen that various methods are available in ANSYS to model the soil strata and different types of elements are to be used for modelling different structural components.

It can be concluded that the element most suitable for the modelling of soil strata would be element **SOLID185** and to model foundation would be **SOLID65**.

Although a lot of research has been done on each method of modelling individually, the comparative study between the various modelling methods has not yet been done and so, the most suitable type of method for the modelling of soil cannot be concluded.

References

1. Samridhi, S., Faizan A., BanditaPaikaray.: Effects of earthquake on foundations. Int. J. Res. Eng. Technol. **04**(13), 168–176 (2015) e-ISSN:2319-1163/ pISSN:23217308
2. Matinmanesh, H., Asheghabadi, M.S.: Seismic analysis on soil-structure interaction of buildings over sandy soil. In: The Twelfth East AsiaPacific Conference on Structural Engineering and Construction, pp. 1737–1743. (2011)
3. Julio, A.G.: Soil structure interaction in the analysis and seismic design of reinforced concrete frame buildings. In: 14th World Conference on Earthquake Engineering, Beijing, China (2008)
4. Gaikwad, M.V, Ghogare, R.B, et.al.: Finite element analysis of frame with soil structure interaction. Int. J. Res. Eng. Technol., **04**(1) (2015)
5. Peizhen, L, Xilin, L., Chen, B., Chen, Y.: Computer simulation on dynamic soilstructure interaction system. In: 13th World Conference on Earthquake Engineering, Paper No. 3233 (2004)

6. Raheem, S.E.A., Ahmed, M.M., Alazrak, T.M.A.: Evaluation of soil—foundation—structure interaction effects on seismic response demands of multi-story MRF buildings on raft foundations. Int.J. Adv. Struct. Eng. (2014)
7. Raghuveeran, R., Hassan, P.H.: Seismic Soil Structure Interaction Effects on RC Bare Frames Resting on Pile-Grid Foundation. Int. J. Sci. Res. Public. **5**, 1–6 (2015)
8. Fei-ran Li, Zhe Zhang," Numerical Analysis of Settlement of Bridge Pile Group Foundation", EJGE, Vol-14, PP.1–9
9. Spyrakos, C.C., Chaojin, X.: Seismic soil-structure interaction of massive flexible strip foundations embedded in layered soils by hybrid BEM–FEM. pp. 383–389. Elsevier (2003)
10. Shah, S.G., Solanki, C.H., Desai, J.A.: Soil structure interaction analysis methods - State of art-Review. Int. J. Civil Struct. Eng. **2**, 176–204 (2011)
11. Ceroni, F., Sica, S., Pecce, M., Garofano, A.: Effect of Soil-structure Interaction on the Dynamic Behavior of Masonry and RC buildings. In: 13th World Conference on Earthquake Engineering (2012)
12. Lewis, E., MasoudSanayei, Joseph, L.A.: Modeling the Effects of Soil-Structure Interaction on a Tall Building Bearing on a Mat Foundation" (2005)
13. Jancy, F., Rajagopal, A., Umashankar, B., Madhav, M.R.: Finite element modelling of ground structure interaction considering nonlinear response of the ground. In: Indian Geotechnical Conference, Paper No.N-281 (2011)
14. Rajasankar, J, Iyer, N.R., YerrayaSwamy, B ., Gopalkrishnan, N , Chellapandi, P.: SSI analysis of a massive concrete structure based on a novel convolution/deconvolution technique. Sadhana, **32**(3), 215–234 (2007)
15. Sunny, N.A., Dr Mathai, A.: Soil structure interaction analysis of multi storey building. Int. J. Sci.Technol. Eng. **3**
16. Xiujuan, Y., Shanpo, J., Xiangzhen, Y.: Finite Elements Analysis on Weak Foundation Of Oil Storage Tank
17. Dimitris C. Rizos and Edward H. Stehmeyer III, (August 2004),"Simplified Seismic Analysis of Soil- Foundation Structure Systems including SoilStructure Interaction Effects.", 13th World Conference on Earthquake Engineering
18. Ravishankar, P., Dr NeelimaSaatyam, D.: Finite element modelling to study soil structure interaction of asymmetrical tall building. In: 18th International Conference on Soil Mechanics and Geo-technical Engineering, IIIT/TR/2013/-1. Yu Bao, Andrew Rietz and Steven Halewski. Numerical Modeling of Dynamic Soil-Structure Interaction in Bridges with HP Driven Piles, pp.1–8 (2013)
19. George, A., Lovely, K.M.: Analysis of Pile subjected to Lateral Loading in Clay modeled using ANSYS. Int. J. Eng. Develop. Res. **3**, 414–417 (2015)
20. Kalavathi, G.N., Muralidhar, : Behavior of Piles under lateral loading soil structure interaction. J. Mech. Civil Eng. **4**, 68–74 (2015)
21. Ing. Malekova, V., Prof. Ing. Jendzelovsky.: An Analysis of Contact Elements of Foundation Structures, supported by Grant Agency VEGA, project No. 1/0629/12
22. Sushma, P., Kumar, R.P.: Dynamic soil structure interaction analysis of pile supported high rise structures. In: Fifth International Conference on Recent Advances in Geotechnical Earthquake Engineering and Soil Dynamics (2010)
23. Shanmugam, J., Dode, P.A., Chore, H.S.: Analysis of soil structure interaction in framed structure. Int. J.Comput. Appl. 11–15 (2015)
24. Srilakshmi, G., DarshanMoudgalya N.S.: Analysis of piled raft foundation using finite element method. Int. J. Eng. Res. Sci Technol. **2**, 89–96 (2013) (ISSN:2319–5991)
25. Harish, S., Damodar Naidu, Ch.: A Study on soil-structure interaction of free standing pile group foundation using finite element analysis. IJARIIE **3**, 1582–1594 (2017)
26. Thusoo, S., Modi, K., et.al. Response of buildings with soil-structure interaction with varying soil types. Int. J. Civil Struct. Constr. Architect. Eng. **9**(4) (2015)

27. Mathew, A.K., Tomer, S.K., Lovely, K.M.: Effect of soil-structure interaction in seismic analysis of framed structures using Ansys. Int. J. Eng. Develop. Res. **3**, 1–9 (2015)
28. Gadpande, R.R.: Analysis of piled Raft Foundation using ANSYS. Int. J. Innovative Res. Sci. Technol. **3**, 142–146 (2016)

Effect of Floor Diaphragms on Seismic Response of RCC Framed Building—A Review

Akshay Nagpure and S. S. Sanghai

Abstract Diaphragms are required to be designed as part of the seismic force-resisting system of every new building as they distribute lateral forces to the vertical elements of lateral force-resisting system. Concrete diaphragms consist of different element which plays an important role in resisting lateral loads. It can be conventionally reinforced or prestressed and can be cast-in-place concrete, topping slabs on metal deck or precast concrete, or interconnected precast concrete. For analysis of building structure, modeling of floor diaphragm plays important role. Diaphragms acts differently according to the configurations of the building and type of load acting on it. So it will require different methodologies to study their behaviors. This paper is an effort made to review the literatures available for modeling of floor diaphragms.

1 Introduction

Building structure generally consist of vertical elements, horizontal elements, and foundation. The vertical element extends from foundation to the elevated level which provides a load path from elevated levels to the foundation. The horizontal element consists of diaphragms which includes collectors. In a general framed structure, beams act as a collector. These all elements are configured together to resist and support gravity load and different lateral loads. Let us consider a common seismic force-resisting system where these elements play a vital role in resisting and transmitting the lateral loads. Diaphragms carry inertial load and transmit it to the vertical elements of seismic force-resisting system which finally goes to the foundation.

A. Nagpure (✉) · S. S. Sanghai
Department of Civil Engineering, G. H. Raisoni College of Engineering, Nagpur, India
e-mail: akshaynagpure7@gmail.com

S. S. Sanghai
e-mail: sanket.sanghai@raisoni.net

Diaphragms also tie the vertical elements together thereby stabilize and transmit force among the elements during seismic activities. Diaphragms thus play important role in seismic force-resisting system, and hence, design attentions are required by the engineer to ensure the adequacy of structural system performance during seismic activities.

2   Components of Diaphragms

Diaphragms commonly consist of diaphragm slab, chords, collectors (drag struts or distributors), and connections to the vertical elements. A rectangular diaphragm is a beam spanning between two end walls where lateral inertial load is indicated by an arrow at the top as shown in Fig. 1. Diaphragm could be modeled as beam spanning between two supports with reactions. The bending moment (Mu) created by lateral inertial load is resisted by tension (Tu) and compression (Cu) couple as shown in the figure. The components that resist bending moment (Mu) at the diaphragm boundary are known as tension and compression chord as per their action of tension or compression.

The boundaries of the diaphragms have tension and compression chords which resist the moment created due to horizontal load. Equilibrium demands uniform distribution of the shear along the diaphragm depth. Tension and compression elements collect the shear force and transmit it into the vertical members and are known as
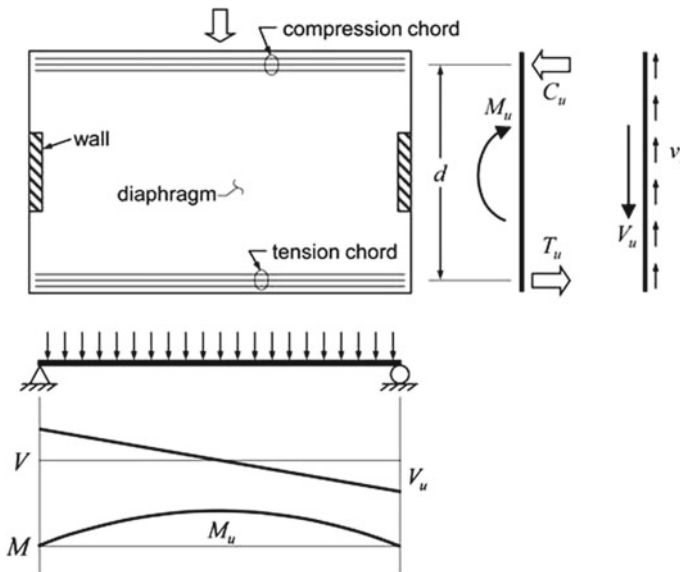
Fig. 1 Tension and compression chord [20]
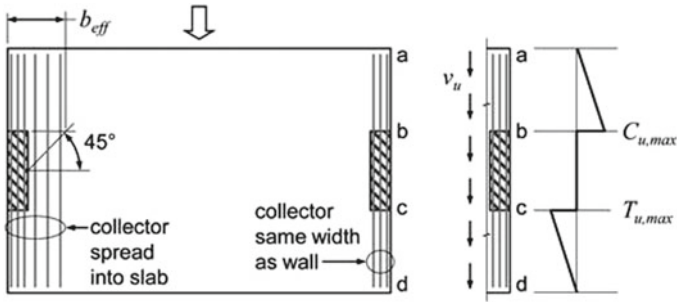
Fig. 2 Collectors [20]

Fig. 3 Distributors [20]
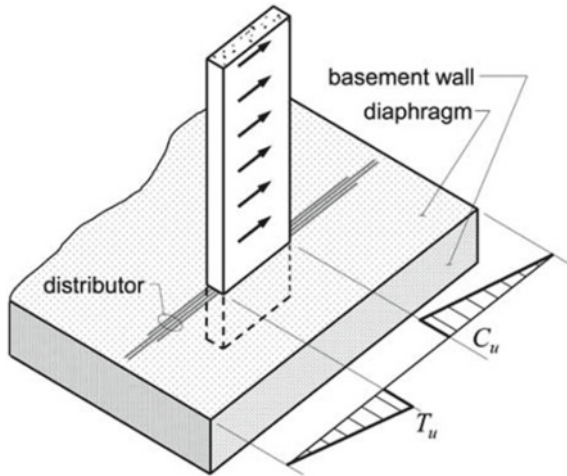
collectors. When force and its resulting accumulation crosses the limit, then the collectors can be spread to the adjacent slab. If the collectors have same width as that of walls, then we can determine tension and compression force. Tension and compression force increases linearly as the shear is transferred into the collector (Fig. 2).

Diaphragms also play an essential role in transferring load among vertical elements of the seismic force-resisting system. A common example is where a vertical members or wall intersects a podium slab in a building with subterranean levels where shear is transferred from vertical elements like walls to the diaphragms and this goes on continuation. The element that transfers force from walls to the diaphragms is a collector but sometimes it is known as distributor. A collectors collects distributed loads from the diaphragms and transfers it to the vertical elements, whereas a distributor (Fig. 3) distributes transferred forces from the vertical elements to the diaphragms.

Fig. 4 Flexible floor
diaphragm [1]

$$\Delta_{middle} > 1.2 \, \Delta_{average}$$
$$\text{Where} \, \Delta = (\Delta_1 + \Delta_2)/2$$
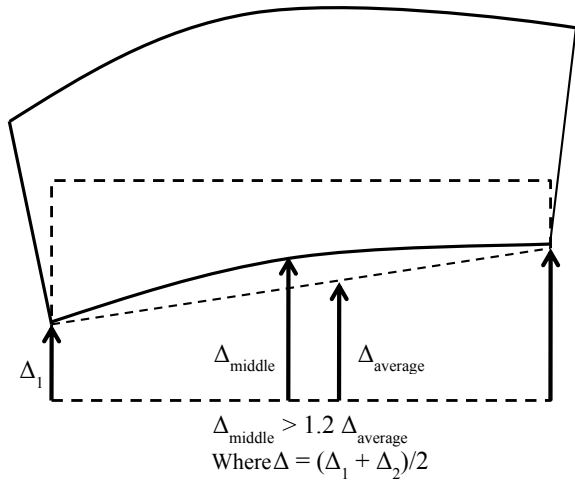
3 Types of Floor Diaphragms

As per IS 1893 (Part 1) 2016, a diaphragm may be classified into following two
types,

1. **Flexible Floor Diaphragm**—A floor diaphragm whose maximum displacement
   at the chord of the deformed shape exceeds 1.2 times the average displacement
   of the diaphragm is known as flexible floor diaphragm [1].
2. **Rigid Floor Diaphragms**—A floor diaphragm whose maximum displacement
   at the chord of the deformed shape does not exceed 1.2 times the average dis-
   placement of the diaphragm is known as rigid floor diaphragm [1]. It is assumed
   that diaphragm does not deform as its stiffness is relatively more than that of
   vertical elements causing the vertical elements to deflect in same amount. It can
   be found out by comparing diaphragm in plane deflection with vertical element
   drift under lateral loads (Fig. 4).

4 Types of Diaphragm Action

The elements of structure acts differently based on their relative stiffness with respect
to other elements. The Diaphragms become Flexible, Rigid, or Semi-Rigid based on
different cases like size of element, height of the floors, span of the floor diaphragm,
materials. The changes in those things affect the stiffness of the elements. The com-
parison of those different cases can be explained by Fig. 5. Let us consider a single
storyshear wall structure as shown in Fig. 5a. By varying the diaphragm span(L) and
wall height(H), it is possible to get different behaviors of diaphragms. The stiffness
of the walls goes on decreasing as the floor height increases similarly the diaphragm

Fig. 5 Different types of
diaphragm actions
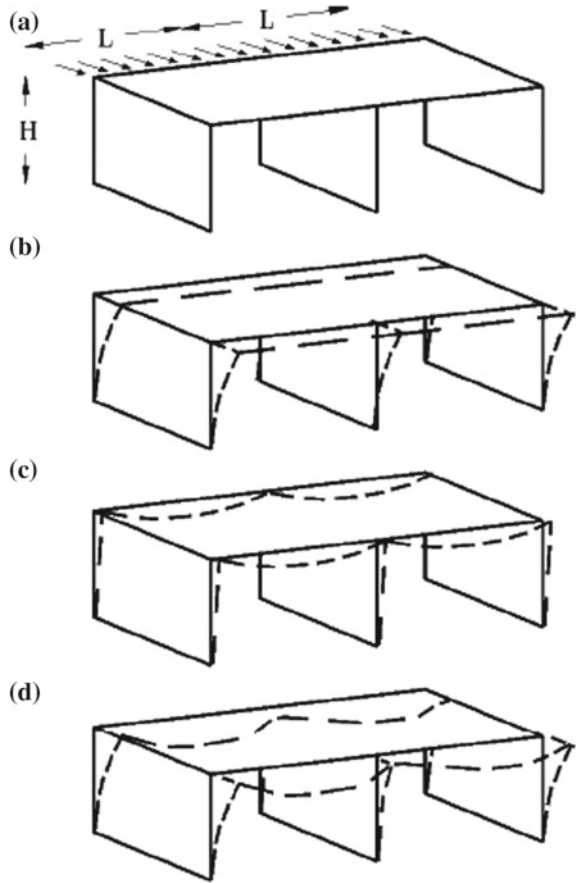
stiffness decreases as the floor height increases. The dashed line in the Fig. 5b shows
the deflection of the system under lateral load when diaphragm stiffness is more
than that of wall. This condition can be achieved by increasing floor height (H) and
decreasing diaphragm span (L) making it relatively stiffer; therefore, diaphragm acts
as rigid element. In this case, it is assumed that the wall stiffness and the applied loads
are symmetric, if this is not the case, along with rigid body translation, diaphragm
will do rigid body rotation. Figure 5c is showing the behavior of the system in terms
of deflection under lateral load when the diaphragm is flexible. This condition is
achieved when the floor height (H) decreases and diaphragm span (L) increases
which make the diaphragm less stiff than walls. In case of the system when the
stiffness of the walls and the floor are of same order, the behavior of the diaphragm
would be semi-rigid as shown in Fig. 5d. In system, both walls and floor contribute
the total system deflection.

5 Modeling Approaches

There are various methods suggested by researcher to model floor diaphragms. Some of those are briefed as below:

5.1 Equivalent Beam Model

In this modeling approach, diaphragm is assumed to act as horizontal beam spanning between two rigid supports. Shear and moments are evaluated by treating as if it were beams. Diagram in Fig. 1 indicates equivalent beam model.

5.2 Equivalent Beam on Springs Model

The equivalent beam on spring model assumes the diaphragms as beams supported on flexible supports. This approach has been found most suitable for single story structure where spring stiffness is readily determined (Fig. 6).

5.3 Corrected Equivalent Beam Model

The corrected equivalent beam model makes approximation on diaphragm action where significant interaction between vertical members of seismic force-resisting system occurs (Fig. 7).

5.4 Finite Element Model

Finite element model can be useful for finding out force transfer among vertical element, addressing force transfer among large openings, assessing the impact of ramps in parking garages and designing irregularly shaped diaphragms. More realistic transfer distributions can be obtained by modeling diaphragm flexibility at the level of irregularity and adjacent floors.

Scope of Work

After studying Diaphragms, some important scopes of this study which have been evaluated are:

1. Diaphragm flexibility study can be useful in determining force transfer through floor elements of different materials. As different materials have different stiff-

Fig. 6 Equivalent beam on spring model [20]
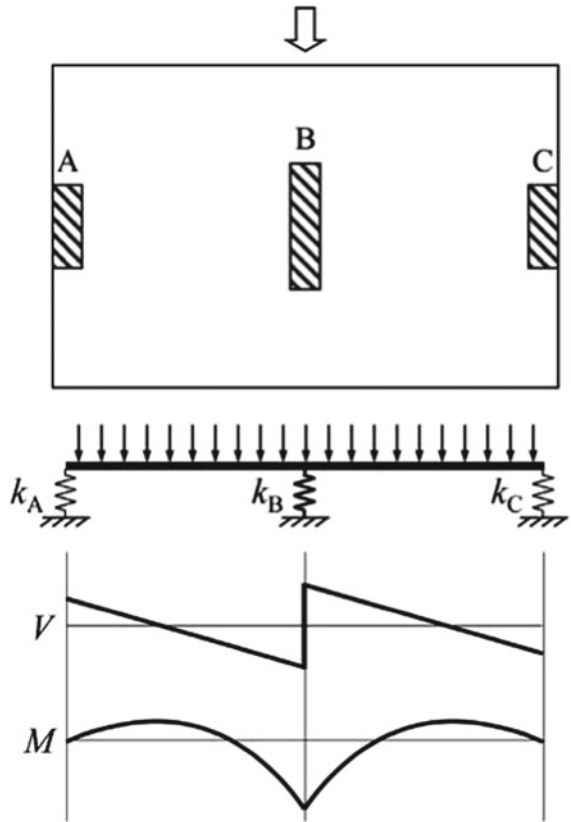
ness values, this study would be helpful for determining responses of structures with different floor properties.

2. Floor diaphragm shows flexibility and rigidity property according to the relative stiffness of vertical members of the structure and floor diaphragm as studied earlier. So this study would be helpful for determining deflection of slabs and vertical elements and their corresponding responses to the same structure.

6 Literatures Available

Various studies, experiments, and researches have been carried out in all over the world to understand the behavior of floor diaphragms. Some of the prominent literatures available on floor diaphragms with analytical approaches have been reviewed briefly as follows.

Fig. 7 Corrected equivalent
beam model [20]
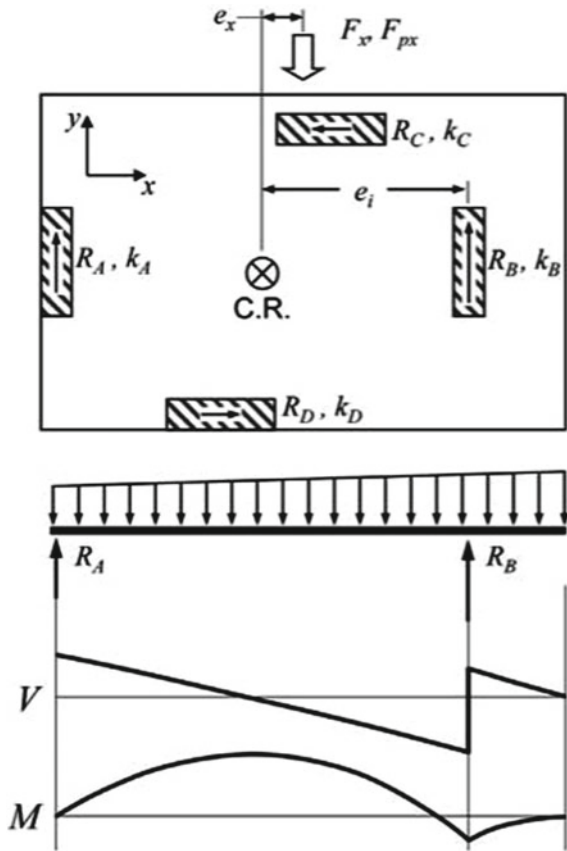
Dolce et al. [2] studied inelastic nonlinear response of building with flexible
diaphragms where they have modeled 330 structures with their floors as a rigid or
alternatively as flexible beam with different stiffness and strength distribution in lat-
eral load resisting system then the elastic design analysis has been carried out on
them. The nonlinear responses of all those structures were studied where deforma-
bility has not produced important effects on linear and nonlinear structural response
when distribution of stiffness of vertical elements is uniform except in case of con-
siderable deformability of floors. Fleischman et al.'s [3] nonlinear transient Seismic
analyses on the perimeter lateral system structures considering flexible diaphragm
gave excessive drifts in the gravity system remote to lateral system elements, and
demanded large unintended ductility on the diaphragm. Basu [4] compared the nature
of mode shapes in the models where they found that rigid floor modes of the flexible
floor model are well agreement with those obtained from the associated rigid floor
model. Simsir et al. [5] studied out of plane response of URM bearing wall attached
to flexible diaphragm and reached to the conclusion that diaphragm flexibility signif-

icantly increased the out of plane displacement response. Eivani et al. [6] conducted elastic dynamic time history analysis where intensities of rigid modes of diaphragm deformation have been reduced but bending and shear dominant deformations have increased. They also concluded that diaphragm flexibility reduces ductility demand. Zahrai et al. [7] studied behavior of composite diaphragms through Finite Element Model where diaphragms were first subjected to lateral seismic load then distribution of the lateral load among the resistant elements were studied using FEM analysis and they got adequate results when rigid diaphragm was considered for stresses of the laterally resisting vertical structural but Kollerathu et al. [8] did a numerical study on the role of diaphragm flexibility modeling considering global seismic performance of existing masonry structures and has examined the effect of diaphragm flexibility on story drifts and floor accelerations where with increasing diaphragm flexibility reduction in peak floor displacements has found, whereas peak floor accelerations have found increasing.

Soeprapto et al. [9] studied effect of longitudinal joint on the shear key of hollow core slab which function as a rigid diaphragm where installation and additional longitudinal reinforcement on the shear key has not gave significant shear strength and longitudinal shear key between HCS with 2 or more longitudinal reinforcement can be used for HCS. Doudoumis et al. [10] proposed a methodology of modeling of the floor diaphragm of multi story building with 2-D finite element and have preferred this method simple in application, fulfilling all design demands and standards of codes and can be effectively used for analytical modeling of floor diaphragms. Goel et al. [11] presented an approach for lateral load analysis of building with asymmetric plan without locating center of rigidity where they combined results obtained from three static analyses which can be implemented directly on computer programs for analysis of multistory buildings but this procedure has also found confusing and cumbersome. Basu et al. [12] also analyzed the asymmetric building with flexible diaphragm and got errors for torsional analysis when diaphragm is treated as rigid.

Hatami et al. [13] did comparison on the horizontal diaphragm in linear behavior of concrete by numerical method to investigate how concrete slab behaves if the slab is modeled as flexible and rigid floor diaphragms where in the shear wall resisted structure the rigid floor assumption has found invalid so flexible floor diaphragms need to be considered but as per Foud et al. [14] if the flexural stiffness of the slab is totally ignored during the presence of shear wall, it is recommended to include adequate flexural stiffness of the slab during analysis of shear wall structures. Moeini et.al's [15] study of a building without shear wall found rigid floor assumption correct. For a building with shear wall, rigid floor and flexible floor analysis differs considerably due to large lateral shear wall stiffness. Scarry et.al [16] developed Truss method as an alternative to the strut and tie method for design and analysis of the diaphragm which allows modeling of the complex diaphragms. Bhuiyan et al. [17] inserted equivalent shell model into a 64 story tall diagrid structure where they got a safer structure while assuming diaphragm as rigid, only the roof acceleration under predicted but appears reasonable for design purposes to use rigid diaphragms except in some special floors (like mechanical floors, etc.). Jain et al. [18] took an example of Y-shaped building where significant difference in the natural periods

and base shear has not found; however, significant difference may come in shear distribution among the transverse frames. Lawson et al. [19] studied behavior of collective chord members on flexible diaphragms where reduction in chord forces and a reduction in horizontal diaphragm deflection have been found.

7 Concluding Remarks

On studying the above literatures, we have reached to the following conclusions,

1. Deformability does not produce important effects on linear and nonlinear structural response when distribution of stiffness of vertical elements is uniform except in case of considerable deformability.
2. Diaphragm flexibility significantly increased the out of plane displacement response, peak floor accelerations, whereas it reduces floor displacements. Diaphragm flexibility reduces ductility demand but structure with highly flexible diaphragm demands large unintended ductility on diaphragm.
3. FEM analysis gives adequate results for stresses of the laterally resisting vertical structural elements when rigid diaphragm is considered while in case of asymmetric building for torsional analysis, considering rigid diaphragm may cause considerable error.
4. In shear wall resisted structure, the rigid floor assumption is not valid so it needs to be considered as flexible floor diaphragms but for a diagrid structure rigid floor diaphragm approach gives safer structure.
5. Truss method as an alternative to the strut and tie method allow modeling of the complex diaphragms.
6. Structure with plan irregularity does not provide significant difference in the natural periods and base shear in the building; however, significant difference may come in shear distribution among the transverse frames.
7. Study of the effect of slab as diaphragm on performance of high rise ductile moment resisting frames under seismic loads considering various parameters like time period, base shear, story drift, member forces must be studied.
8. Comparison of the flexible and rigid floor Diaphragm when diaphragm discontinuity is considered should be done.

References

1. IS1893, B.I.S.: Indian Standard criteria for earthquake resistant design of structures (part 1): general provisions and buildings (sixth revision, Bureau of Indian Standards, New Delhi. Google Scholar (2016)
2. Dolce, M., Lorusso, V.D., Masi, A.: Seismic response of building structures with flexible inelastic diaphragm. Struct. Design Tall Spec. Build. **3**(2), 87–106 (1994)
3. Fleischman, R.B., Farrow, K., Eastman, K.: Seismic performance of perimeter lateral-system structures with highly flexible diaphragms. Earthquake Spectra **18**(2), 251–286 (2002)

4. Basu, D.: Dynamics of a class of horizontal setback buildings with flexible floor diaphragm. J. Struct. Eng. **135**(7), 873–877 (2009)
5. Simsir, C.C., Aschheim, M.A., Abrams, D.P.: Out-of-plane dynamic response of unreinforced masonry bearing walls attached to flexible diaphragms. In: 13th World Conference on Earthquake Engineering. (2004)
6. Eivani, H., et al.: Seismic response of plan-asymmetric structures with diaphragm flexibility. Shock and Vibration (2018)
7. Zahrai, S.M., Sarkissian, L.: In-Plane Rigidity of Laterally Loaded Composite Floor Systems, A Finite Element Approach. 161–181 (2015)
8. Kollerathu, J.A., Menon, A.: Role of diaphragm flexibility modelling in seismic analysis of existing masonry structures. Structures. vol. 11. Elsevier (2017)
9. Soeprapto, G., et al.: Effect of longitudinal joint on the shear-key of hollow core slab which function as an rigid diaphragm. MATEC Web of Conferences. vol. 101. EDP Sciences, (2017)
10. Doudoumis, I.N., Athanatopoulou, A.M.: Code provisions and analytical modelling for the in-plane flexibility of floor diaphragms in building structures. J. Earthquake Eng. **5**(04), 565–594 (2001)
11. Goel, R.K., Chopra, A.K.: Seismic code analysis of buildings without locating centers of rigidity. J. Struct.Eng. **119**(10), 3039–3055 (1993)
12. Basu, D., Jain, S.K.: Seismic analysis of asymmetric buildings with flexible floor diaphragms. J. Struct. Eng. **130**(8), 1169–1176 (2004)
13. Hatami, F., Esmaeili, N.: Evaluation and comparing the behavior of concrete horizontal diaphragms in linear behavior of concrete by numerical method. Life Sci. J. **4**, 9 (2012)
14. Fouad, K., Ali, Z., Mustapha, R.: Strucural analyses with flexiblility effect of the floor slabs. In: Proceedings of the Fifteenth World Conference of Earthquake Engineering, Lisboa, Portugal. (2012)
15. Moeini, M., Rafezy, B., Howson, W.: Investigation into the floor diaphragm flexibility in rectangular reinforced concrete buildings and error formula. In: 14th World Conference on Earthquake Engineering, Beijing, China (2008)
16. Scarry, J.M.: Floor diaphragms–Seismic bulwark or Achilles' heel. In: New Zealand Society for Earthquake Engineering Conference. (2014)
17. Bhuiyan, M.T., Leon, R.T.: Effect of diaphragm flexibility on tall building responses. Structures Congress 2013: Bridging Your Passion with Your Profession. (2013)
18. Jain, S.K., Jain, C.K.: Dynamics of a class of horizontal setback buildings. J. Eng. Mech. **129**(9), 1092–1103 (2003)
19. Lawson, J.W., Yarber, C.N.: Collective chord behavior in large flexible diaphragms. Structures Congress 2013: Bridging Your Passion with Your Profession. (2013)
20. Moehle, J.P., et al.: Seismic design of cast-in-place concrete diaphragms, chords, and collectors. In: Seismic design technical brief, US Department of Commerce, Building and Fire Research Laboratory, National Institute of Standards and Technology (2010)
21. Naeim, F., RaoBoppana, R.: Seismic design of floor diaphragms. The Seismic Design Handbook. pp. 373–407. Springer, Boston, MA, (2001)

A Review on: 'Performance of Friction Damper for Response Control of Buildings Considering Effect of Soil–Structure Interaction'

S. S. Sanghai and P. Y. Pawade

Abstract It is a well-known fact that soil–structure interaction plays vital role in governing the response of building during seismic activities. Also, for better stability of buildings during earthquakes, energy dissipation devices are widely used. This paper is an attempt to gather the work done by researcher to study the influence of soil–structure interaction and friction dampers. From the available literature, it was concluded that friction dampers which are designed and placed based on rigid base hypothesis may not perform same under consideration of soil–structure interaction. So, it is needed to study the performance of friction damper considering soil–structure interaction with suitable assumptions.

Keywords Friction damper · Soil–structure interaction · Energy dissipation

1 Introduction

Earthquakes impart inertial forces in buildings, causing them to vibrate proportional to the input energy. According to energy balance equation, the part of this input energy gets converted into kinetic energy and strain energy while some amount of this energy get dissipated due to inherent damping. To consume maximum amount of this input energy, along with inherent damping, supplemental damping can play important role. Hence, the manner in which this energy is consumed in the structure determines the level of damage.

Using the devices which provide supplemental damping, only the response of superstructure could be improved. But, after some recent earthquakes, it was clear that, response of structure also depends upon soil beneath it along with the performance of superstructure. Because of which many people have studied soil–structure

S. S. Sanghai (✉) · P. Y. Pawade
Department of Civil Engineering, G. H. Raisoni College of Engineering, Nagpur, India
e-mail: sanket.sanghai@raisoni.net

P. Y. Pawade
e-mail: prashant.pawade@raisoni.net

interaction under effect of dynamic loading. From analytical as well as experimental investigations, it was understood that, under the influence of dynamic loading, soil plays vital role in damage of super structure. As composition of soil is very complex, many parameters need to be considered while studying soil–structure interaction.

For controlling seismic response of structure, phenomenon called as 'Energy Dissipation' is very popular all over the world. Energy dissipation devices are broadly classified as 'Active devices' which requires external power supply and 'Passive devices' which work when vibrations start. In many high-rise structures, passive energy dissipation devices such as friction dampers, viscous dampers, visco-elastic dampers, metallic dampers, and isolators have been used to provide supplemental damping. However, soil strata beneath structure which can be used as medium of energy dissipation is totally neglected. Energy dissipation devices are always designed without considering potential benefit of soil–structure interaction in certain situations.

Available literature provides study of seismic response of structure having friction dampers and study of seismic response of structure considering soil–structure interaction. But very few researchers study the seismic response of structure having passive energy dissipation devices considering soil–structure interaction. Also, without considering soil–structure interaction, the stiffness of the structure is overestimated while the damping capacity is underestimated. Underestimation of damping capacity of structure will definitely change design of friction dampers. Also, the change in stiffness and damping of the structure will change location of critical members thereafter changing locations of friction dampers. Hence, the study of response of building having friction dampers and considering soil–structure interaction is necessary.

2   Mechanism of Friction Damper

Friction is one of the types of natural forces which develops between two surfaces in contact when either there is tendency of relative motion or relative motion works between them. According to Coulomb's Law of friction, the magnitude of friction force depends on normal reaction between two surfaces and nature of surfaces. Hence, magnitude of limiting force F_t, is proportional to normal reaction, i.e.,

$$F_t = \mu N \tag{1}$$

where μ is coefficient of friction.

During the friction between two bodies, energy is dissipated due to friction. This benefit of dissipation of energy is utilized in working mechanism of friction damper. According to D'Alembert's principle, in state of dynamic equilibrium along with external force a fictitious force known as inertia force also act on system which gives equation of motion [1].

$$m\ddot{x}(t) + c\dot{x}(t) + kx(t) = -m\ddot{x}_g(t) \tag{2}$$

where m, c, and k are the mass, viscous damping constant, and stiffness of a system, respectively; $x(t)$, $\dot{x}(t)$ and $\ddot{x}(t)$ are the displacement, velocity, and acceleration of the system. To dissipate the energy induced in the system, in addition with the inherent damping supplemental damping can also provided to control the seismic response of building. There are numerous approaches for providing supplemental damping out which friction damping is one of the best methods. Providing friction dampers in system, the equation of motion changes to

$$m\ddot{x}(t) + c\dot{x}(t) + kx(t) + f_d sgn\,\dot{x}(t) = -m\ddot{x}_g(t) \tag{3}$$

f_d is the friction force of a damper, $sgn\,\dot{x}(t)$ is the symbolic function defined as $-1, 0$, and 1, respectively, in case $\dot{x}(t) < 0$, $\dot{x}(t) = 0$ and $\dot{x}(t) > 0$ [1, 2].

Example: Consider a SDOF system with mass 25 kN-sec^2/m, stiffness 100kN/m with $\mu = 0.5$ and friction force as 5 kN. 1 m of initial displacement is given to the system. The response of system will be as shown in Fig. 1.

The plot of friction force versus displacement results in Rectangular Hysteresis loop which indicates energy dissipated due to friction as shown in Fig. 2

Pall et al. [3] conducted static and dynamic tests on simple sliding elements with different surface coating. Using test results, they studied hysteresis loops to find better energy dissipation. Pall and Marsh [4] studied an existing scale model of 9 story steel moment resisting frame modified to include friction damped bracing as part of the lateral load resisting system. It was observed that the friction damped braced frame (FDBF) system had the ability to behave in a nonlinear fashion without demanding inelastic behavior in the frame itself. This implied continued integrity of the structure during and after a seismic event. Filiatrault et al. [5] compared experimental results of three-story friction damped braced frame with results of nonlinear time history

Fig. 1 Response reduction of SDOF using Friction damping
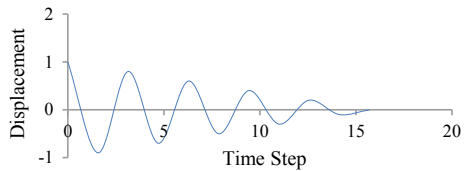
Fig. 2 Rectangular Hysteresis Loop
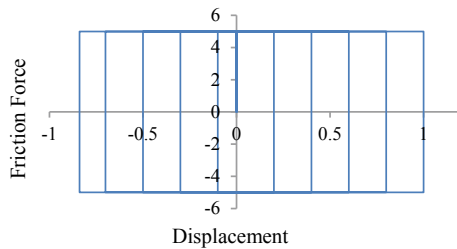
analysis. It was observed that, friction damped system performed better than moment resisting frame system. Aiken et al. [6] investigated the performance analytically as well as experimentally of 9-story steel frame model modified with friction dampers. It was observed that friction damped braced frame behaves in nonlinear fashion without yielding of main structural members. Similarly, various frames equipped with friction dampers in X-bracing, Chevron bracing, single diagonal bracing have been tested by Wen-I et al. [7], Vaseghi et al. [8], Marianchik et al. [9], Colajaani and Papia [10], Hakimi et al. [11]. It was observed that friction damper plays vital role in dissipation of input energy induced in the structure due to earthquakes. Bhaskararao and Jangid [12] studied the response of two adjacent SDOF systems connected with friction damper. The study showed that with selection of appropriate slip load of friction damper, seismic response of adjacent structures with different frequencies can be reduced. They also investigated response of adjacent SDOF systems connected with friction damper under harmonic excitations. It was observed that with optimum slip force in friction damper, peak displacement can be reduced to minimum value. Also, they derived response during the non-slip and slip motion in friction damper [13].

3   Optimized Design of Friction Dampers

During the initial studies, it was observed that the seismic response control using friction dampers can be increased significantly by using appropriate slip load, location, and number of friction dampers. It was observed that, just using more no. of friction dampers does not lead to best response control [2, 14–16]. Hence, researchers started to design friction dampers optimally, based on various parameters. In one of the approaches, Moreschi and Singh [17] discussed the optimal design of yielding metallic dampers and friction dampers. Using genetic algorithm, the optimum slip load and brace stiffness was decided for better response control. Garcia and Eeri [18] used Sequential Search Algorithm method to control the number of different sizes of dampers. The applicability of the method was limited to those cases where the response was linear. Fallah and Honarparast [19] investigated the optimal slip loads of Pall friction dampers. The optimization procedure based on NSGA-II was used to satisfy the objectives. Marianchik et al. [9] suggested two stage iterative procedures: the design of the braces and slip elongations. Amini and Tavassoli [20] proposed a new method for optimizing the control force, the number and location of controllers of a closed–open loop control system. Based on the results obtained by the proposed method, an artificial neural network has been trained for yielding result with the less effort.

4 Mechanism of Soil–Structure Interaction

The performance of structure under influence of ground motion depends on three key factors, i.e., structure, foundation, and soil beneath the foundations. Hence, seismic soil–structure interaction analysis calculates the response of all three elements collectively. Generally, while calculating the response of structure to seismic activities, it is assumed that rigid foundations are supported on rigid soil. Hence, SSI causes the difference between actual response and response of rigid base condition [21].

The soil–structure interaction is classified into three categories as:

4.1 Inertial Interaction

According to D'Alembert's principle, inertia force developed in vibrating structures give rise to base shear and member forces. These developed forces cause displacements and rotations at soil–foundation interface because of flexibility of soil. These displacements dissipate energy via hysteretic soil damping. These effects are referred as inertial interaction effects.

4.2 Kinematic Interaction

When the structure is designed assuming rigid base hypothesis, the free-field motion acts as foundation input motion. But, the stiffness of foundation is very much high as compared to stiffness of soil beneath it which causes deviation in free-field motion. Hence, rigid foundation acts as low-pass filter causing base slab averaging and embedment effect. The effects arising due to wave propagation consideration are called as Kinematic interaction effects.

4.3 Foundation Deformation

As results of forces and displacements applied by superstructure and soil medium, flexural, axial, and shear deformations are developed in foundations. Hence, foundation should be significant enough for these seismic demands.

To study the effect of these interactions, direct and substructure approaches are used. In direct approach, the soil and structure are included within same model and analyzed as complete system; while in substructure approach, the SSI problem is separated into distinct parts that are combined to formulate the complete solution.

Example: Consider a SDOF system with mass 25 kN-sec^2/m, stiffness 100 kN/m and $h = 3$ m subjected to force $F = 100$kN. The response of system is calculated

Case (a)   Case (b)
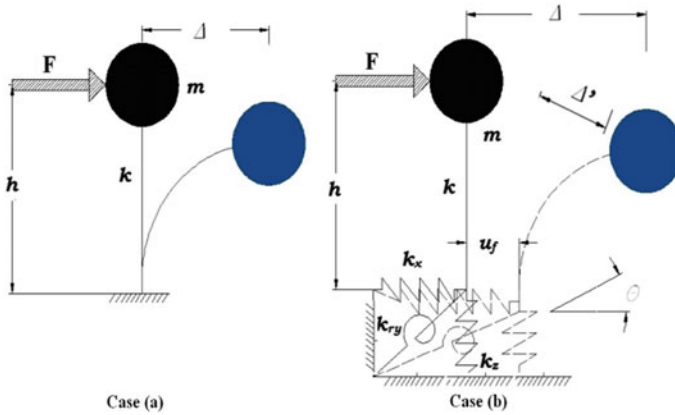
Fig. 3 Soil–structure model [21]

(a) when resting on fixed base (Without SSI) (b) when resting on flexible base (With SSI) (Fig. 3).

For Case (a)

$$\Delta = \frac{F}{k} = 1m$$

$$\omega = \sqrt{\frac{k}{m}} = 2 \text{ rad/s}$$

$$T = 3.14 \text{ s}$$

For Case (b)

Medium soil strata is considered with $N = 6$ which yields $k_x = 1.17 \times 10^5$ kN/m; $k_z = 1.76 \times 10^5$ kN/m and $k_{ry} = 1.87 \times 10^4$ kN/m

$$\Delta = \frac{F}{k} = 1 \text{ m}$$

$$\Delta' = \frac{F}{k} + u_f + \theta.h = \frac{F}{k} + \frac{F}{k_x} + \left\{ \frac{F*h}{k_{ry}} \right\}h = 1.04 \text{ m}$$

$$T'^2 = (2\pi)^2 * m * \left\{ \frac{1}{k} + \frac{1}{k_x} + \frac{h^2}{k_{ry}} \right\} = 10.304$$

$$T' = 3.21 \text{ s}$$

$$\omega' = 1.95 \text{ rad/s}$$

From this example, it is clear that considering SSI increases time period of vibration along with deflection.
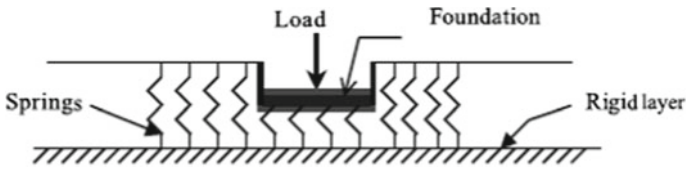
Fig. 4 Winkler Model [22]

5 Effectiveness of Soil-Structure Interaction

In past few years, many authors studied the influence of soil–structure interaction on performance of structure during earthquakes analytically as well as experimentally.

5.1 Analytical Investigation

5.1.1 Winkler Model

In Winkler model, soil medium is modeled using discrete, independent, and linear elastic springs. According to this idealization, deformation of foundation is due to applied load and only restricted to loaded region. The pressure-deflection relation at any point is given by '$p(x, y) = k * w(x, y)$' where k is modulus of subgrade reaction and w is deflection. Hence, calculation of modulus of subgrade reaction plays vital role in modeling of soil media (Fig. 4).

5.1.2 Elastic Continuum Model

Elastic continuum model is conceptual way of modeling of infinite soil media. The basic problem in soil mechanics is boundary conditions and loaded regions to be considered. So, in this model, some continuous function is assumed to represent mechanism of soil strata. This approach is useful in extracting more information on deformations and stresses as it is required to input modulus of elasticity and Poisson's ratio of soil media.

5.1.3 Elasto-Plastic Idealization

Generally, an elasto-plastic element is used to model nonlinear behavior of soil. The behavior of soil medium is linear up to certain stress level. When the behavior is linear, stress in soil is directly proportional to strain which can be represented by ideal reversible spring. For modeling the perfectly plastic behavior, Coulomb unit can be used. St. Venant's unit combined both linear spring and Coulomb unit to model elasto-plastic behavior of soil. This single unit facilitates the transformation of soil medium from elastic zone to plastic zone (Fig. 5).
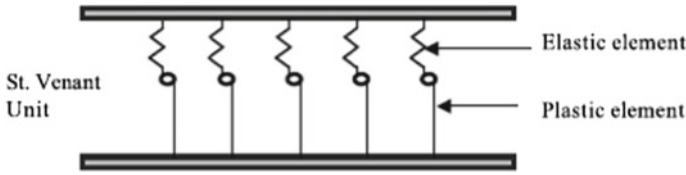
Fig. 5 St. Venant's Unit [23]

5.1.4 Nonlinear Idealization

While modeling soil media, it is necessary to understand that stress strain behavior of soil is always nonlinear. The solution of nonlinear equations can be found out using iterative methods like Conjugate Gradient iteration, GMRES iteration, Newton's method, etc. Also, incremental methods could be also used.

5.1.5 Visco-Elastic Idealization

For modeling of soil strata, visco-elastically, it is necessary to understand damping as well as stiffness properties of soil. Hence, for this type of idealization, generally elastic, plastic, and viscous elements are used. In Maxwell's model, spring and dash-pot system are connected in series while in Kelvin's model they are connected in parallel. These models are useful in predicting shear strain more accurately (Fig. 6).
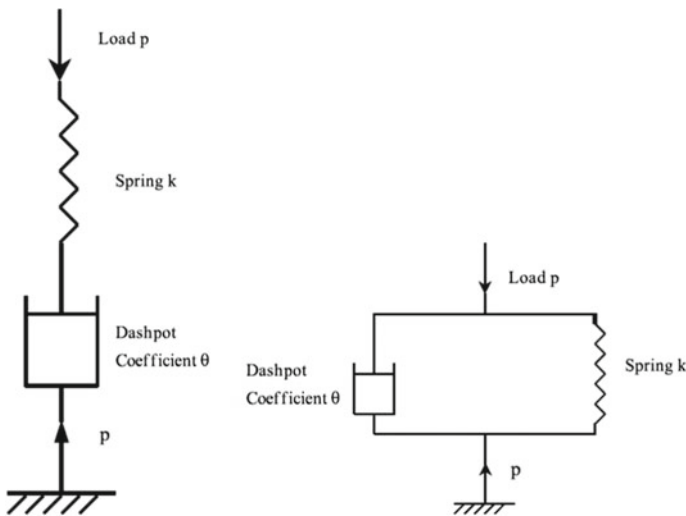
Fig. 6 Maxwell's model & Kelvin's Model [24]

5.1.6 Finite Element Modeling

Nowadays, with the easy availability of high computing facility, finite element method is widely used for modeling of many complex problems. In finite element modeling, soil medium is converted into physical model with assigned material properties and boundary conditions which is then discretized. Assuming displacement functions, stiffness matrix is formulated which is then used for calculating stresses in elements. This method is very useful as it can model the nonlinearity, viscosity, and geometry of soil media.

5.1.7 Available Literature

For simplification of soil modeling, Gazetas [25] presented a set of algebraic formulas and dimensionless charts for calculation of dynamic stiffness and damping coefficients for soil. Ostadan [26] studied damping characteristics of soil media. He presented effective approach to estimate damping for SSI which will help to find realistic response while considering SSI. Roy & Datta [27] studied seismic demand of low-rise structures considering soil flexibility. Datta et al. [28] studied the influence of soil–structure interaction on response of low-rise building under seismic excitations. The study showed that SSI increases response for stiff structural system. In other study, Datta et al. [29] investigated the seismic safety of structures by considering soil flexibility and asymmetry. Celebi et al. [30] used finite element modeling for soil–structure interaction. They considered elasto-plastic Mohr-Coulomb model for prediction of mechanical behavior of soil medium. Wen & Chen [31] developed a simple lumped parameter model having spring and dashpot system connected in parallel to mass for representing vertical, horizontal, and torsional vibrations of rigid foundations.

5.2 Experimental Investigation

Many researchers have studied the influence of soil–structure interaction by constructing scaled model for experimental investigation. Hosseinzadeh et al. [32] studied SSI effects on 5-, 10-, 15-, and 20-story scaled models resting on soft and very soft media using Shake table. He also compared test results with analytical results. Similarly, Hokamabadi et al. [33] investigated response of super structure resting on soft soil and considering soil–pile–structure interaction. Later he compared experimental results with numerical results which showed increase in lateral deflection in flexible base condition. Salajegheh et al. [34] investigated experimentally effect of fault rupture on structure considering soil–structure interaction. From results, they showed that surface fault rupture has been diverted more effectively for strip foundation. Todorovska [35] also studied full scale models of soil–structure interaction. It was concluded that to eliminate problems related to boundary conditions and scaling, it is better to perform full scale studies.

6 Effect of SSI on Performance of Energy Dissipation Devices

Many researchers have studied influence of soil–structure interaction on performance of building structures during seismic activity. Also, many researchers have studied various methods for seismic response control of buildings. But, very few have studied the influence of soil–structure interaction on performance of energy dissipation devices during seismic activity. In one of the few studies, Zhou et al. [36] have analyzed 7-story frame with viscous dampers. They used time stepping solution method to study effect of SSI on performance of viscous damper. It was concluded that, viscous dampers designed on the hypothesis of rigid foundations fail to achieve same effectiveness with consideration of SSI. Kokil & Shrikhande [37], also studied effectiveness of viscous dampers in response control of 10-story building with and without eccentricities. It was found that supplemental damper's effectiveness reduces with increase in irregularity and soil compliances. Wong & Luco [38] studied the effects of soil–structure interaction on structures having active control for vibration reduction. It was concluded that rocking of foundation changes design of active control. Li & Wang [39] tested experimentally a 2-story RCC framed building equipped with MR dampers subjected to various seismic excitations. Armouti [40] investigated response of structure with short time period founded on deep cohesion less soil. It was concluded that, dampers with damping ratio more than 20% help structure to remain in elastic range.

7 Concluding Remarks

This paper presents a review of the studies done on effects of friction dampers, soil–structure interaction on seismic response of building. Also, review of some studies on influence of soil–structure interaction on performance of energy dissipation devices is done. Following are the conclusions:

1. It is a well-known fact that, for controlling the seismic response, passive energy dissipation devices are effective. But, proper design, location, and number of friction dampers lead to better performance of building structures.
2. The design of friction dampers depends upon seismic demand of structure. The slip load of damper is selected such that maximum input energy due to earthquake should be dissipated.
3. After considering influence of soil–structure interaction, the response of structures varies under seismic excitations. It was found that, the response becomes very poor as soil strata become softer.
4. As response of the structure after considering SSI varies, seismic demand of structure also changes.
5. It was found that, energy dissipation devices designed by considering rigid bases fail to achieve performance for same structure with flexible bases.

6. It is necessary to study the effectiveness of passive energy dissipation devices with consideration of soil–structure interaction.

References

1. Chopra, A.K.: Dynamics of Structures: Theory and Applications (2001)
2. Min, K.W., Seong, J.Y., Kim, J.: Simple design procedure of a friction damper for reducing seismic responses of a single-story structure. Eng. Struct. **32**(11), 3539–3547 (2010)
3. Pall, A.S.: Friction joints for seismic control of large panel structures. J. Prestressed Concrete Inst. **25**(6), 38–61 (1980)
4. Pall, A.S., Marsh, Cedric: Response of friction damped braced frames. J. Struct. Eng. **108**(9), 1313–1323 (1982)
5. Filiatrault, A., Cherry, S.; Performance evaluation of friction damped braced steel frames under simulated earthquake loads. Earthquake Spectra **3**(1), 57–78 (1987)
6. Aiken, I.D., Kelly, J.M., Pall, A.S.: Seismic response of a nine-story steel frame with friction damped cross-bracing. In: Proceedings, ninth world conference on earthquake engineering, Tokyo and Kyoto, Japan (1988)
7. Liao, W.I., Mualla, I., Loh, C.-H.: Shaking-table test of a friction-damped frame structure. Struct. Des. Tall Spec.Build. **13**(1), 45–54 (2004)
8. Vaseghi, J., et al.: A parametric assessment of friction damper in eccentric braced frame. World Acad. Sci. Eng. Technol. **58**, 208–212 (2009)
9. Marianchik, E., et al.: Optimal seismic design of friction damped braced frames based on existing earthquake records.In: Proceedings of the 12th World Conference on Earthquake Engineering, Auckland, New Zealand. (2000)
10. Colajanni, P., Papia, M.: Hysteretic behavior characterization of friction-damped braced frames. J. Struct. Eng. **123**(8), 1020–1028 (1997)
11. Hakimi, B.E., Rahnavard, A., Teymour, H.: Seismic design of structures using friction damper bracings. In: 13th world conference on earthquake engineering, Vancouver Google Scholar. (2004)
12. Bhaskararao, A.V., Jangid, R.S.: Seismic analysis of structures connected with friction dampers. Eng. Struct. **28**(5), 690–703 (2006)
13. Bhaskararao, A.V., Jangid, R.S.: Harmonic response of adjacent structures connected with a friction damper. J. Sound Vib. **292**(3–5), 710–725 (2006)
14. Lee, S.-H, et al.: Allocation and slip load of friction dampers for a seismically excited building structure based on storey shear force distribution. Eng. Struct. **30**(4): 930–940
15. Lee, S.-K, et al.: Design of a bracing-friction damper system for seismic retrofitting. Smart Struct. Syst. **4**(5), 685–696 (2008)
16. Sanghai, S.S., Khante, S.N.: Seismic response of unsymmetric building with optimally placed friction dampers. Int. J. Civil Eng. Technol. **8**(2), 72–88 (2017)
17. Moreschi, L.M., Singh, M.P.: Design of yielding metallic and friction dampers for optimal seismic performance. Earthquake Eng. Struct. Dynam. **32**(8), 1291–1311 (2003)
18. Garcia, D.: A simple method for the design of optimal damper configurations in MDOF structures. Earthquake spectra **17**(3), 387–398 (2001)
19. Fallah, N., Honarparast, S.: NSGA-II based multi-objective optimization in design of Pall friction dampers. J. Constr. Steel Res. **89**, 75–85 (2013)
20. Amini, F., Tavassoli, M.R.: Optimal structural active control force, number and placement of controllers. Eng. Struct. **27**(9), 1306–1316 (2005)
21. Venture, NEHRP Consultants Joint. Soil-structure interaction for building structures. NIST GCR 12–917 (2012)
22. Dutta, S.C.: Seismic torsional behaviour of elevated tanks for improved code provisions: elastic behaviour. J. Inst. Eng. India. Civil Eng. Div. 80.FEV, 169–181 (2000)

23. Smolira, M.: Analysis of Tall Buildings by the Force-Displacement Method. McGraw-Hill (1975)
24. Noda, T., Fernando, G.S.K., Asaoka, A.: Delayed failure in soft clay foundations. Soils Found. **40**(1), 85–97 (2000)
25. Gazetas, G.: Formulas and charts for impedances of surface and embedded foundations. J. Geotech. Eng. **117**(9), 1363–1381 (1991)
26. Ostadan, F., Deng, N., Roesset, J.M.: Estimating total system damping for soil-structure interaction systems. In: Third UJNR Workshop on Soil-Structure Interaction, Menlo Park, California (2004)
27. Roy, R., Dutta, S. C.: Inelastic seismic demand of low-rise buildings with soil-flexibility. In. J. Non-Linear Mech. **45**(4 (2010): 419–432
28. Dutta, S.C., Bhattacharya, K and Rana Roy. "Response of low-rise buildings under seismic ground excitation incorporating soil–structure interaction. Soil Dyn. Earthquake Eng. 24(12), 893–914 (2004)
29. Dutta, S.C, et al.: Seismic safety of structures: influence of soil-flexibility, asymmetry and ground motion characteristics. J. Sound Vibr. **307**(3–5), 452–480 (2007)
30. Celebi, E., Göktepe, F., Karahan, N.: Non-linear finite element analysis for prediction of seismic response of buildings considering soil-structure interaction. Nat. Hazards Earth Syst. Sci. **12**(11), 3495–3505 (2012)
31. Wu, W.H., Chen, C.Y.: Simple lumped-parameter models of foundation using mass-spring-dashpot oscillators. J. Chin. Inst. Eng. **24**(6), 681–697 (2001)
32. Hosseinzadeh, N., Davoodi, M., Roknabadi, E.R.: Comparison of soil-structure interaction effects between building code requirements and shake table study. J. Seismolog. Earthquake Eng. **11**(1), 31 (2009)
33. Hokmabadi, A., Fatahi, B., Samali, B.: Seismic Response of Superstructure on Soft Soil Considering Soil-Pile-Structure Interaction. University of Technology Sydney (UTS), Broadway NSW, School of Civil and Environmental Engineering (2007)
34. Salajegheh, A., et al.: Experimental investigation of fault rupture-soil-structure interaction. In: 7th International Conference on Seismology & Earthquake Engineering (2015)
35. Todorovska, M.: Full-scale experimental studies of soil-structure interaction. ISET J. Earthquake Technol. **39**(3), 139–165 (2002)
36. Zhou, Y., Yangzhao G., Yong Z.: Influence of soilstructure interaction effects on the performance of viscous energy dissipation systems. In: Proceedings of the 15 h World Conference on Earthquake Engineering (2012)
37. Kokil, A,S., Shrikhande, M.: Optimal placement of supplemental dampers in seismic design of structures. J. Seismolog. Earthquake Eng. **9**(3), 125 (2007)
38. Wong, H. L., Luco, J.E.: Effects of soil-structure interaction on the seismic response of structures subjected to active control. In: Proceedings of 10th World Conf. on Earthquake Engineering, Madrid, Spain (1992)
39. Li, H., Wang, J.: Experimental investigation of the seismic control of a nonlinear soil-structure system using MR dampers. Smart Mater. Struct. **20**(8), 085026 (2011)
40. Armouti, N.S.: Effect of dampers on seismic demand of short period structures in deep cohesionless sites. Adv. Steel Const. 7(2), 192–205 (2011)

Effects of Temperature Curing on Concrete with Silica

Mohit Manwatkar and P. Y. Pawade

Abstract Steam curing results in gain of early strength of the concrete in comparison with normal curing. If the concrete develops considerable strength in its initial and ultimate stage, then curing plays foremost important role and on the other hand large curing time may lead to excess of cost of structure and sometimes may even lead to unexpected delay. Steam curing is one of important tools due to which erection of the formworks can be done at early age and can be used for other important works. Due to steam curing, the hydration process takes place at rapid rate and the double the strength in comparison with normal curing at 3 days and 7 days can be obtained. In this paper, silica fume has been used as partial replacement in collaboration with cement and also the comparative comparison was made between steam curing results and normal curing result. All the results obtained are for various mixes and are presented in this paper.

1 Introduction

Curing is the process in which it is important to maintain sufficient water content and optimum temperature after the concrete has been placed in the service or on the formwork till its hydration process is reached to its ultimate stage in order that the expected results are obtained at any stage. Curing results in the homogeneity of the concrete as a whole and plays foremost important role in the formation of the Bouge's compound and particularly C_3S which is predominant in its early stage. Due

M. Manwatkar (✉)
Master of Technology (Structural Engineering), G. H. Raisoni College
of Engineering, Nagpur, India
e-mail: mohit.manwatkar@gmail.com

P. Y. Pawade
Department of Civil Engineering, G. H. Raisoni College of Engineering, Nagpur, India
e-mail: hodcivil.ghrce@raisoni.net

to formation of C_3S at very rapid rate, the steam curing results in early rate of gain of strength in comparison with normal curing where all Bouge's compound develop equally and so does early strength is not very high as of steam curing. During steam curing, the constant temperature needs to be maintained so that it does not result in shrinkage cracks. And if early period of concrete hydration is neglected, then it results in irreparable loss.

2 Experimental Programs

Portland pozzolona cement is used for the proposed experimental studies. The Cement conformed to Indian par IS: 8112-1989. Silica fume used has a silica content of more than 90%, and various other constituents are listed in Table 1. Natural sand was used in initial phase having fineness modulus of 2.2 and in later stage silica sand was used having fineness modulus of 2.11 all of which passed through 4.75 mm sieve. The coarse aggregates were having size of 12.5 mm.

The superplasticizer used was Sulphonated Naphthalene formaldehyde Condensate (SNF).

3 Fresh Properties of Concrete

In this research paper, the silica fume was used as partial replacement having composition of various ingredients as shown above. Silica fume was replaced as 10, 12, 14, 16, 18, 20%, and the dosage which gave maximum strength was selected, and silica sand was added to that dosage in proportion 2, 4, 6, 8 ,and 10%. And to this, dosage

Table 1 Shows the various ingredients present in the silica fume

Mineral Name	% present
SiO_2	93
Al_2O_3	2
Fe_2O_3	0.1
MgO	1.6
Na_2O	0.4
K_2O	0.2
CaO	0.6
S	0.2
C	0
Loi	2.6

steel fibres were added in proportion 0.5, 1, 1.5, 2% by weight of dry concrete. And all this research work was done for M30 grade concrete.

4 Compressive Strength

The compressive strength results for various days with conventional curing and steam curing at 60 °C were determined, and the comparison was made between the two results followed by the percentage increase in strength due to steam curing with regard to conventional curing was made. All the testing for compression test was done on $150 \times 150 \times 150$ mm cube specimen.

4.1 Results of Compression Test Strength

While preparing the test results, the 4 samples (cubes) have been prepared for each mix and average those 4 cubes have been listed in all the tables hereafter (Graphs 1 and 2, Table 2).

From Tables 3 and 4, the comparison regarding increase in strength of steam cured concrete in regard to conventional concrete can be made (Table 5).

From Tables 3 and 4, mix M4, i.e., 14% silica fume gives the maximum strength and so is chosen as an optimum dosage for further mixes.

Table 2 Showing variation of silica fume and other materials added into get M30 grade concrete to get 1 m³ of concrete

1	2	3	4	5	6	7	8
Mix1	0	394	787	1082	0	0.4	1.59
Mix2	10	354	787	1082	39	0.4	1.52
Mix3	12	346	787	1082	47	0.4	1.46
Mix4	14	338	787	1082	55	0.4	1.40
Mix5	16	330	787	1082	63	0.4	1.35
Mix6	18	323	787	1082	70	0.4	1.29
Mix7	20	315	787	1082	78	0.4	1.24

Column 1 Mix
Column 2 Silica fume replacement %
Column 3 Cement requirement
Column 4 Natural Sand
Column 5 Coarse Aggregate
Column 6 Silica fume
Column 7 Water-cement ratio
Column 8 Super plasticizer
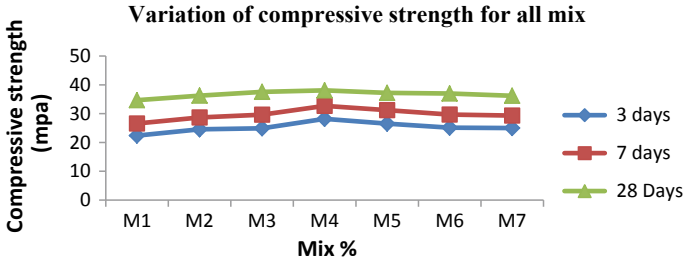
Graph 1 From values obtained from Table 1 the variation of all design is as above
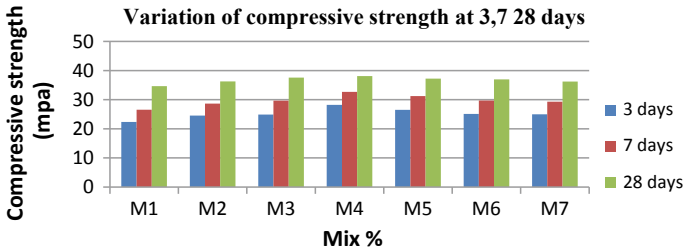
Graph 2 Shows the variation compressive strength at various ages

Table 3 Shows the variation of steam curing results for various ages, respectively

Mix	Slump (mm)	3 days (mpa)	7 days (mpa)	28 days (mpa)
M1	64	22.36	26.58	34.67
M2	52	24.56	28.68	36.25
M3	47	24.90	29.65	37.58
M4	56	28.20	32.69	38.10
M5	78	26.52	31.22	37.22
M6	58	25.12	29.69	36.98
M7	62	24.99	29.32	36.22

M1 Control mix
M2 10% silica fume
M3 12% silica fume
M4 14% silica fume
M5 16% silica fume
M6 18% silica fume
M7 20% silica fume

Table 4 Shows the variation of compressive strength of conventional (normal) cured concrete

Mix	Slump (mm)	3 days (mpa)	7 days (mpa)	28 days (mpa)
M1	60	12.20	18.32	30.56
M2	56	14.36	20.54	31.22
M3	55	14.98	21.58	32.58
M4	47	18.55	24.66	33.87
M5	51	16.47	22.55	32.95
M6	60	16.20	22.40	32.78
M7	63	15.77	21.69	32.01

Table 5 Shows the difference in the gain of strength of concrete between both the curing, which also shows that the steam curing predominates the conventional curing at all early ages. The various results obtained are thus shown in the table

Mix	3 days (mpa)	7 days (mpa)	28 days (mpa)
M1	42.79	30.39	14.32
M2	40.13	33.35	16.54
M3	42.97	31.32	19.58
M4	41.23	29.87	18.54
M5	39.57	28.54	17.02
M6	38.02	27.87	16.54
M7	36.54	25.02	14.21

Furthermore the % of silica fume (14%) is kept constant, and silica sand is added in proportion 2, 4, 6, 8, and 10%, respectively, and are named as M8, M9, M10, M11, M12, respectively.

In the case of silica sand, only steam cured results are shown. All the replacement in case of silica sand was done by weight of cement.

Silica sand is the one which constituents of minerals composed of silicon and oxygen. Silica sand adds to durability and anti-corrosion of the structure. It is very widely used for ceramics sanitary ware which improves the structural integrity of the structure. In fewer cases, silica sand has been used in medium as filtration medium especially in slow sand filters to increase its effectiveness as a whole (Table 6).

As silica sand is finer than the naturally available sand, the particle size of the silica sand used was around 0.3 mm (Graphs 3 and 4).

So 14% silica fume + 4% silica sand is chosen as dosage for steel fibres addition.

Properties of steel fibres

Hooked-shaped fibres are used in the further concrete addition (Table 7).

The steel fibres are added in concrete by dry weight of cementitious material in different proportion as listed below (Graphs 5 and 6; Tables 8 and 9).

Table 6 Shows the variation of rate of gain of strength

Mix	% replacement	3 days	7 days	8 days
M8	2	23.45	27.97	37.20
M9	4	26.69	29.20	38.15
M10	6	25.60	28.30	38.05
M11	8	25.43	28.10	37.96
M12	10	24.60	27.54	37.55

M8 14% silica fume + 2% silica sand
M9 14% silica fume + 4% silica sand
M10 14% silica fume + 6% silica sand
M11 14% silica fume + 8% silica sand
M12 14% silica fume + 10% silica sand
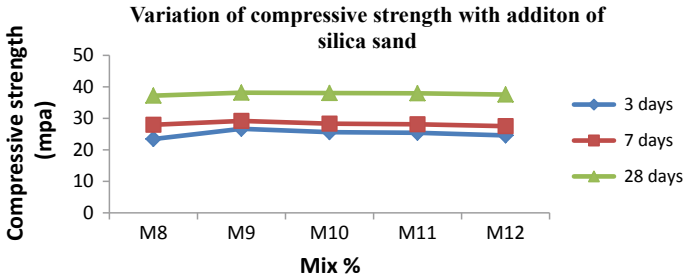
Graph 3 Above graph shows the gain of concrete at different % of addition of silica sand in silica fume
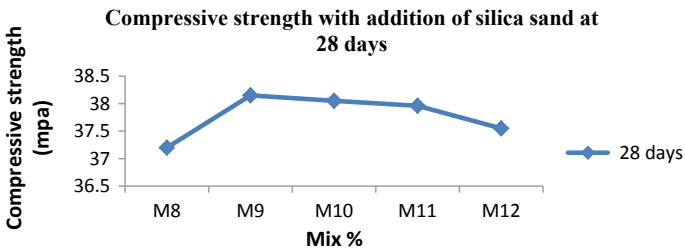
Graph 4 Shows the variation of compressive at 28 days, and from graph, it is quite clear that M9 gives maximum strength and is so selected for steel fibres addition

Table 7 Shows the properties of steel fibres used in concrete

Length (mm)	Diameter (mm)	Aspect ratio
25	0.6	41.67
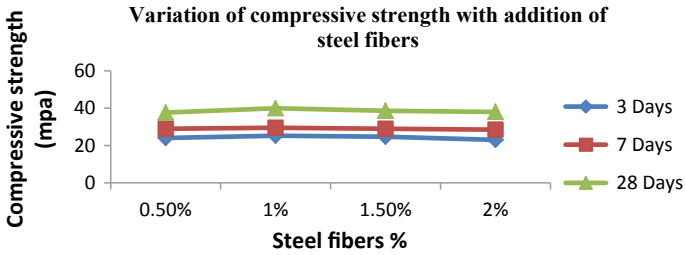
Graph 5 Shows the rate of gain of strength of strength at 3, 7, and 28 days with addition of steel fibres in different %
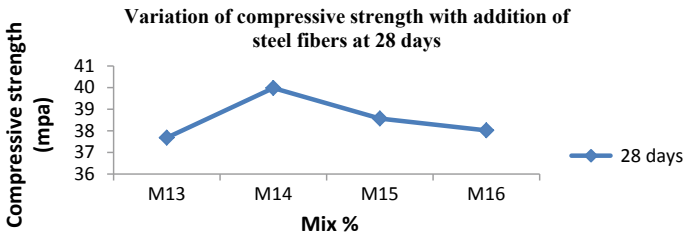
Graph 6 Above graph shows the gain of strength at different ages of curing

Table 8 Shows the % in which steel fibres are added in design mix

Mix designation	% of fibres added
M13	0.5
M14	1.0
M15	1.5
M16	2.0

M13 14% silica fume + 4% silica sand + 0.5% fibres
M14 14% silica fume + 4% silica sand + 1.0% fibres
M15 14% silica fume + 4% silica sand + 1.5% fibres
M16 14% silica fume + 4% silica sand + 2.0% fibres

Table 9 Rate of gain of strength at varying ages(steam curing results)

Sr. no	3 days	7 days	28 days
M13	24.02	28.97	37.68
M14	25.22	29.55	39.98
M15	24.69	29.01	38.57
M16	23.00	28.50	38.02
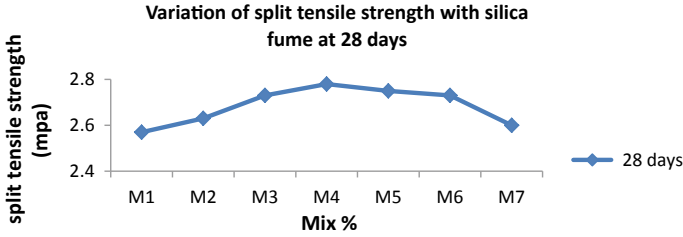
Graph 7 Above graph shows the variation of split tensile strength
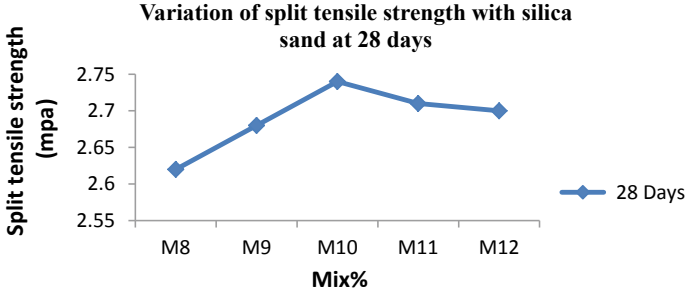
Graph 8 Above graph shows the variation split tensile strength with silica sand
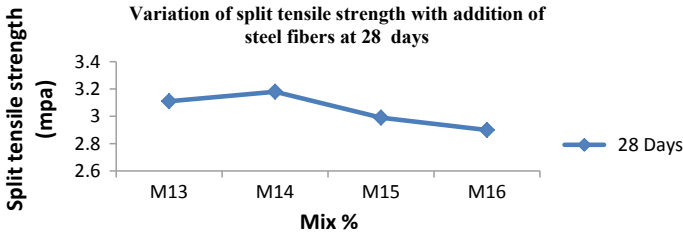
Graph 9 Above graph reflects the variation of split tensile strength at different dosage of steel fibres for 28 days

4.2   Split Tensile Test Results

The graph for split tensile test has been divided into three parts for getting the exact knowledge of the mix and its strength.

The dimensions of the cylinder for split tensile strength were 150 mm diameter and 300 mm length.

The following graph shows the strength (steam cured) at the age of 28 days with addition of silica fume in different % to concrete mix (Graphs 7, 8 and 9).
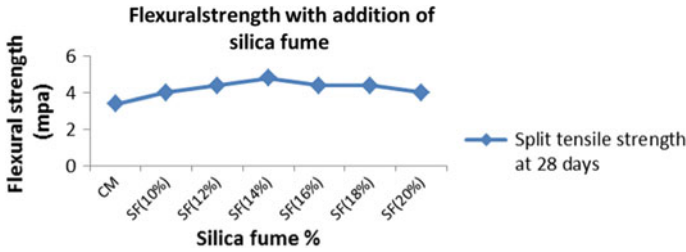
Graph 10 flexural strength with addition of silica fume
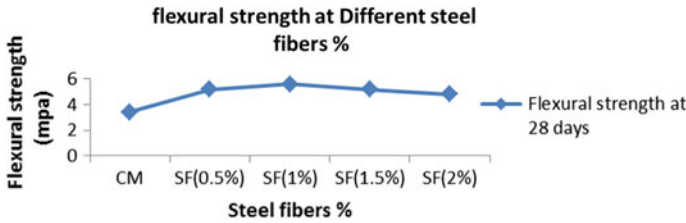
Graph 11 Shows the variation of flexural strength when steel fibres are added in silica fume(14%)

4.3   Flexural Strength Results

CM: Control mix (Graph 10).

And the other results are for silica fume which are added in 10, 12, 14, 16, 18, 20% (Graph 11).

CM: control mix

And other results are for steel fibres which are in 0.5, 1, 1.5, 2% by dry weight of cementitious material.

5   Results

(1) Silica sand resulted in decrease in specific heat and the considerable increase in thermal conductivity in comparison with opposite effects of silica fume.

(2) The steam cured concrete gave 45% more strength in comparison with normal cured concrete at the age of 3 days, and about 33% at the age of 7 days and about 11% at the age of 28 days.

(3) The silicate hydrate reaction was very faster in steam cured concrete in comparison with normal cured concrete, and this was the actual result of high gain of strength of steam cured concrete.

(4) High-temperature steam curing generates higher strength and durability in the case of cement containing a proportionately higher amount of C_3S.

References

1. ACI Committee 234 Report.: "Guide for the Use of Silica Fume in Concrete," ACI Manual of Concrete Practice: Materials and General Properties of Concrete (Part 1): 234R1—234R51. American Concrete Institute. Farmington Hills, MI (1997)
2. Abo-ElEnein, S., Daimon, M., Ohsawa, S., Kondo, R.: Hydration of low porosity slag-lime pastes. Cem. Concr. Res. **4**, 299–312 (1974)
3. Husem, M.: The effects of high temperature on compressive and flexural strengths of ordinary and high-performance concrete. Fire Saf. J. **41**(2), 155–163 (2006)
4. Khoury, G.A.: Compressive strength of concrete at high temperatures: A reassessment. Mag. Concr. Res. **44**(161), 291–309 (1992)
5. William Andrew.: Concrete admixtures handbook, properties, science, and technology, crafts and Hobbies (1995)
6. Dotreppe, J.C., Fransen, J.M., Bruls, A., Baus, R., Vandervelde, P., Minnes, R., van Meurvenburg, D., Lambette, H.: Experimental research on the determination of main parameters affecting the behaviour of reinforced concrete columns under fire conditions. J. Mag. Concr. Res. **49**, 117–127 (1997)
7. Kjellsen, K.O., Wallerik, O.H., Fjallberg, L.: Microstructure and microchemistry of the paste—aggregate interfacial transition zone of High—performance Concrete. J. Adv. Cem. Res. **10**, 33–40 (1998)
8. Felicetti, R., Gambarova, P.G.: Effect of high temperature on the residual compressive strength of high strength siliceous concretes. J. ACI Mater. J. **95**, 395–406 (1998)
9. Calado, C., Camoes, C., Monteiro, E., Helena, P., Barkokebas Jr., B.: Durability indicators comparison for SCC and CC in tropical coastal environments. Materials **8**, 1458–1481 (2015)
10. Farve, R., Charif, H., Jaccoud, J.-P.: Large reduction of deflections due to high performance concrete. In: Malier, Y. (ed.) High performance concrete: From material to structure, pp. 160–185. London, UK, E & FN Spon (1992)
11. Aitcin, P.-C.: Developments in the application of high performance concrete. Constr. Build. Mater. **9**, 13–17 (1995)
12. Ryell, J., Bickley, J.A.: Scotia plaza: High strength concrete for tall buildings. In: Proceedings of the Symposium on Utilization of High Strength Concrete, pp. 641–653 Stavanger, Norway 15–18 June 1987

Review on an Experimental Study on Concrete Strength by Using Sugarcane Bagasse Ash and Steel Fiber

S. S. Solanke and P. Y. Pawade

Abstract Various possible alternatives to OPC are being considered along with their benefits that may occur from these alternatives in order to mitigate the problems mentioned above especially in developed countries. In the development of shelter and other infrastructural facilities, the construction industry depends a lot on cement for its working. It then becomes extremely difficult for majority of the people to own their own houses. Thus, minimizing the global temperature and various pollution, cost of concrete, hence successful implementation under such raw materials plays a very important role and improves concrete. One of major construction materials in the world ordinary Portland cement is been used. Hence, supplementary cement replacement materials are arrived as waste product of the industries. The silica (SiO_2) existing above raw material operates the free lime, and CSH is formed. Factors are responsible for the different properties of the sugarcane bagasse ash. To reduce the solid waste generated due to industrial processes, its utilization is one of the effective ways.

Keywords Sugarcane · Bagasse ash · Cement

1 Introduction

1.1 General

The researchers are finding a substitute for cement by different cement-replacing materials because of the increasing demand of cement in construction and also due to improper waste management. The maximum height of the crop found out to be

S. S. Solanke (✉) · P. Y. Pawade
Department of Civil Engineering, G. H. Raisoni College of Engineering, Nagpur, India
e-mail: shrikant.solanke@raisoni.net

P. Y. Pawade
e-mail: prashant.pawade@raisoni.net

eight to twenty feet tall and in thickness measures 2 cm. Among the 200 sugarcane cultivable countries, Brazil is found to be the highest production all over the world. India ranks two in producing sugarcane. The total numbers of sugarcane mills in India are around 571 producing a large amount of sugar. Sugar production, Falernum, molasses, rum, soda, cachaca, and ethanol for fuel are some of the advantages of sugarcane. As there is production of vast amount of sugarcane and hence due to industrials process, sugarcane bagasse ash is expelled in large amount by sugar mills or industries.

The affordable housing is not possible for the average citizen of the country because of the high cost of the building materials. The eventual cost of the finished ordinary.

Portland cement product is usually very high when other factors such as logistics and high demand are added to the aforementioned. The technique of some local wastes as alternative to conventional material in the construction industry has led.

For identifying optimal level of replacement, SCBA is evaluated for concrete property. Sugarcane bagasse ash is a by-product of sugar factories, and it is produced by burning sugarcane bagasse where it is formed by the extracting all sugar from sugarcane.

The properties like compressive strength and water tightness of concrete and mortar were found to be increased in some percentage of replacement and fineness.

Higher silica content is one of the important factors responsible for this. The silica content may vary considering the ash content and which depends on the burning condition of sugarcane bagasse. Although SCBA is a worthy by-product of agricultural industries because of some of the ingredients which can be use to alter cement. The different reactions formed: first, the hydration reaction which takes place after addition of water in cement to form CH and CSH, and after this, second reaction is pozzolanic reaction which takes place between CH from hydration reaction and SiO_2, a pozzolan from SCBA, and produced second phase of CSH which increase the compressive strength. For making the environment good, the actions are taken all over the world to control and to manage the agricultural waste. Thus, there is necessity of burning the waste material. Variation in burning temperature and duration of burning, size of particle, and chemical composition has been examined. Aim of the study is the evaluation of potential application of SCBA substituting cement. More viscous and plastic binary paste is formed when SCBA is presented as compared to the absence of SCBA. When concentration of SCBA resulted an increased in yield stress linearly, the use of 20% of SCBA was beneficial. SCBA is easily available and cheap waste material of sugar industries. The waste material released from industry is of large amount. Around quarterly SCBA is been produced by effective burning of one ton of sugarcane. SCBA is defined as good so it can be used in place of cement as a mortar. Near-about 5–8% of global CO_2 emission is caused due to manufacturing of Portland cement, and this environmental problem will most likely to be increased due to growing demand of Portland cement. Several research groups are investigating to produce green building material. There are many studies related to use of SCBA. Having low compressive strength, SCBA cannot be effectively utilized in alkali-activated system to produce geopolymer. SCBA produced by burning
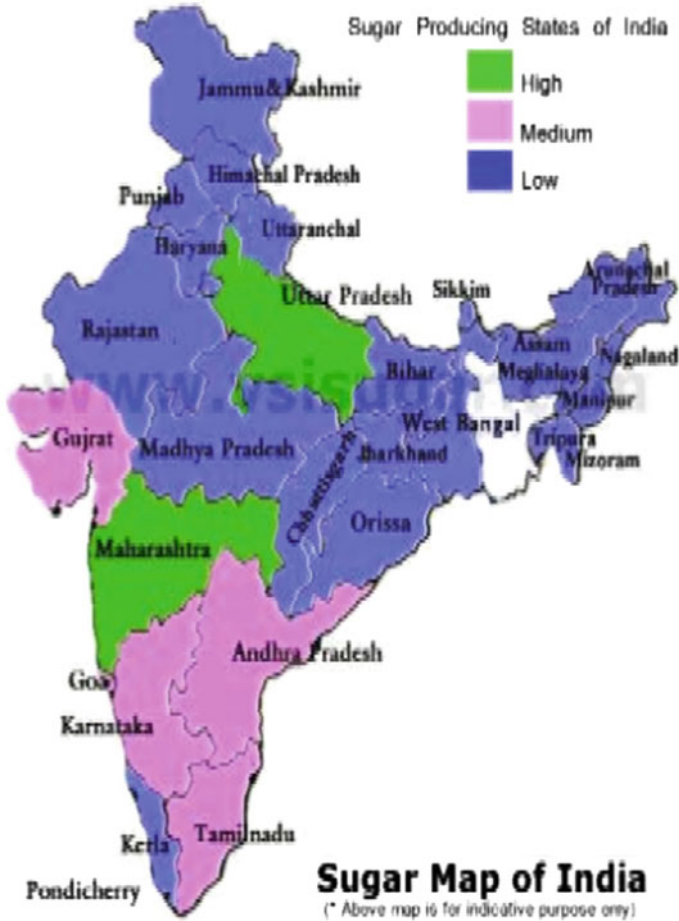
Fig. 1 Sugar map of India

the sugarcane residual as a by-product, and it mainly constitutes silica. The burning process is performed in uncontrolled condition. Thus, the black particles present in the ash are of carbon and crystalline silica (Fig. 1).

2 Literature Review

Nuntachai et al. (2009) (1) [1]

The researchers explained the importance of bagasse ash for development in concrete. Portland cement occupies many places in building construction due to its strength.

Concrete production cost can be effectively reduced with the use of similar material without varying the properties. Un-ground BA is kept in place of PPC. The American Standard Codes of practice were used for determining the physical nature water permeability and heat evolution test. It was found that concrete with bagasse ash in grounded state had 113% more strong than conventional mix.

Srinivasan et al. (2010) (2) [2]

In this study, the researcher worked on utilization of the waste by-product on inline sugarcane industry and bagasse biomass fuel in the electric generation industry. The investigations are performed, the total 180 cubes are prepared of different dimensions, and mix design used was M20 grade. In which the sugarcane bagasse ash is replaced with the varying percentage of cement replacement, and the properties are identified like strength and elastic modulus for different time duration. Thus, plasticizer's use is arrested, and lighter material is produced in the society.

Fairbairn et al. (2010) (3) [3]

Examined that CO_2 emission found to be less when catalyzed by the sugarcane bagasse ash. The study in this topic: The material SCBA was collected from southern region of Brazil. The CDM analysis for the global increase in temperature was checked in the city. The ash was used instead of cement in varying proportions identifying strength and liable characteristics. Near-about 5–8% of global CO_2 emission is caused due to manufacturing of Portland cement, and this environmental problem will most likely to be increased due to growing demand of Portland cement. Several research groups are investigating to produce green building material. The greenhouse effect of the city was studied against CO_2 emission. The literature admires the engineering properties of concrete which can be improved if sugarcane bagasse ash is properly blended with the OPC as it provides a good bond.

Modani et al. (2012) (4) [4]

Optimized the workability and flow ability in which the bagasse ash is partially replaced by different percentages of fine aggregate. In this subject, sugarcane bagasse ash is analyzed chemically by XRF scan test, and test results were found out. Material shows good nature under chemical test, and radicals are found worthy. With the effective replacement of bagasse ash by fine aggregate replaced by 10–20%, an experimental investigation is carried out. All tests were done in accordance with Indian standard.

Kawade et al. (2013) (5) [5]

The author examined the effect of use of SCBA modifying cement in different ratios by weight of SCBA for compressive strength. With the use of similar raw material of same composition by weight of cement without affecting the quality, the cost can be reduced. The maximum percentage of the cement could be effectively replaced with SCBA is not more than 15%. The concrete without SCBA is having lower strength.

Sivakumar et al. (2015) (6)

Analyzed SCBA, 20% cement replacement by the bagasse ash gave higher compressive strength. In this paper, sugarcane bagasse ash is determined chemically. The sugarcane bagasse ash is analyzed chemically by XRF scan test, and the test results are found out. The compressive strength of the different agro-industrial waste material in place of concrete is examined with varying mix designs and duration of curing. The final results found out to be cost reduction occurs when the waste material is utilized forming a cheaper cost of 12%. Also, the problem regarding the waste disposal is also solved.

Aigbodion et al. (2010) (7) [6]

They are studied the chemical and physical characterization of bagasse ash, and they found that there is high percentage of silica and aluminum oxides presence in ash; therefore, it can be used as sand replacement in casting operations.

Sua-iam and Makul (2013) (8) [7]

They are studied the self-compacting concrete which is made by replacing fine aggregate with sugarcane bagasse ash in volume percentage that varies from 10 to 100 and performing fresh and hardened concrete test and their analysis says replacement up to 20% bagasse ash effectively enhanced properties of self-compacting concrete.

Prusty et al. (2016) (9) [8]

In this paper, author reviews different agro-waste materials, which are used in concrete as a partial replacement of fine aggregate. Agro-wastes are used in self-compacting concrete and mortar, by performing fresh and hardened concrete test, and their properties are determine and compared. Agro-waste concrete containing bagasse ash, sawdust ash, and oyster shell are accomplished desire strength by replacing 20% of fine aggregate, which were maximum among all other agro-waste concrete. In addition to this inclusion of bagasse ash as fine aggregate in mortar increased the chloride penetration resistances.

Hemath Kumar et al. (2017) (10) [9]

The present study deals with the effects of natural fibers on some mechanical properties of the epoxy composites. This research was carried out by reinforcing the matrix (epoxy) resin with natural fiber (sugarcane fibers) and glass fiber. The natural fibers were exposed to chemical treatment before reinforcement. The hybrid composites reinforced with chopped glass and sugarcane fibers were produced using hand layup method. Each sample was fabricated with different 10, 20, and 30% by volume of sugarcane fiber. After preparation of composite material, the mechanical properties like flexural and impact strength were studied.

Ranjith et al. (2015) (11) [10]

In this paper, author are explained the process due to which sugarcane bagasse ash is found in sugar industries. Here, author was focused on examining the performance sugarcane bagasse ash concrete made by the partial replacement of ordinary Portland cement with different weight percentages (0, 5, 10, 15, 20, and 25%) in different curing environments.

Usman et al. (2014) (12)

In this study, researcher was examined silica and alumina potential of sugarcane bagasse ash obtained from Savannah Sugar Company Numan, Adamawa state of Nigeria. For above-mentioned aim, samples of sugarcane bagasse were burned in a furnace of metallurgical at three different control temperatures of 500, 600, and 700 °C, respectively. It was observed that the sugarcane bagasse ash has high silica and alumina content as compared with total content and both of which used reinforcing materials of aluminum matrix composites.

Kulkarni et al. (2013) (13)

In this paper, researcher was focused on making green and economical bricks and avoid ash disposable problem. For the same, sugarcane bagasse ash was utilized. They made bricks by replacing fly ash and lime in fly ash bricks by sugarcane bagasse ash in different proportion. Trial bricks of size (230 × 100 × 75) mm were tested.

Sivakumar et al. (2013) (14) [11]

In the present research, author was made an attempt to use sugarcane bagasse ash as a partial replacement in ordinary Portland cement (OPC) by 10% of weight. The chemical and morphology analyses were performed by SEM with EDS. The sample (OPC, bio-cement) was cured and hydrated with distilled water for 7 day and 28 day.

Ahmad et al. (2016) (15)

According to various research papers, it has been found that steel fibers give the maximum strength in comparison with glass and polypropylene fibers. Nowadays there exist many reinforcement techniques for improving the strength of those materials which lack load carrying and less durable capacity. Use of steel fiber to enhance the strength and reduce maintenance is an effective technology established in recent times. Fiber-reinforced concrete has been effectively used in different structural element like slab, beam, etc. precast element architectural elements, offshore structures, seismic region structures, crash barriers, isolated and combine footings, hydraulic structures, and many other applications.

Ram Meghe et al. (2014) (16)

The researcher presents the experimental study of the steel fibers reinforced self-compacting concrete. This was made by addition of different content of steel fibers. The result showed that due to inclusion of steels fiber, the split tensile strength was

increased and the optimum content of fiber for the same was found to be 1.75% and it was also observed that the steel fibers are used in the concrete to give the maximum strength as compared to other fibers such as glass fibers and polypropylene fibers.

Otuoze et al. (2012) (17)

They investigated the strength performance of concrete using partial blends of ordinary Portland cement (OPC) and sugarcane bagasse ash (SCBA). Sugarcane bagasse ash replaces with 0, 5, 10, 15, 20, 25, 30, 35, and 40 in terms of percentage of sugarcane bagasse ash by weight in the concrete. The result shows that the performance of concrete having up to 10% sugarcane ash replacement meeting with desire result and in mass concreting replacement up to 35% could be adapted.

Mehrotra and Irshad Masood (1992) (18)

There investigations indicate that bagasse ash has to be considered as a pozzolanic material like fly ash or any other conventional pozzolana. The authors consider that the material may be used for preparing lime ash mixture to be used locally as a mortar, especially in rural areas where availability is high.

Suvimol and Daungruedee (2008) (19)

They are studied the effect of pozzolanic activity and its application in cement, and they found that coarser ash is having 84–87% reactive and finer ash having 99–100% reactive; therefore, they recommended for the partially replacement of cement in making of concrete.

Corderio et al. (2008) (20)

In this research, they made concrete cube with 20% replacing of cement with SCBA by weight with embedded of steel rod and these cubes are put in salted water solution and corrosion rate was observed. The result shows that reinforced concrete containing SCBA has lowest rate of corrosion compared with normal reinforced concrete.

Babar et al. (2017) (21)

Author investigated the ductility and shear strength of fiber-reinforced concrete beams made by using hooked steel fiber without providing stirrups as shear reinforcement. In this investigation, the test beam specimens of $(1150 \times 125 \times 250)$ mm are cast and inclusion of steel fibers are varied from 2 to 0.5% of volume fraction, and the shear span-to-depth ratio (a/d) is varied like 1, 1.25, and 1.5, while longitudinal steel is kept constant, Under two-point loading, all the specimens was tested up to failure, and first crack load, failure load, and central deflection are observed precisely.

Nitin Kumar et al. (2015) (22)

Author presented the use of steel fibers as reinforcement material with concrete. In this study, the mixing of various materials weather chemicals or natural required for improving the strength and durability of parent substance with water cement ratio 0.35 was used. Precise investigation for M_{40} grade of concrete to examine the compressive, flexural and tensile strength of steel fiber-reinforced concrete is having fibers of 0, 1, 2, and 3% volume fraction. The result is shown that steel fiber-reinforced concrete increases strength toughness ductility and flexural strength of concrete.

Amin and Foster (2016) (23) [12]

In spite of the lots of awareness of steel fiber-reinforced concrete (SFRC) in practice and research, SFRC is yet to discover common application in load bearing or shear critical building structural elements. In this paper, results are presented on shear tests which have been conducted on ten ($5 \times 0.3 \times 0.7$) m simply supported beams with varying steel fiber reinforcement ratios. The tests have been performed, and the results are analyzed with complete material characterization which quantifies the post-cracking behavior of the SFRC.

Kawde et al. (2017) (24)

In this era of world, concrete is most used material for compressive strength for building construction. Tensile load carrying capacity is very low of concrete. This result leads concrete in brittle failure. To enhance concrete performance under tensile or dynamic loading, different types of the fibers are added to concrete. Inclusion of steel fiber of different volume fraction in concrete (SFRC) results in achieving desire tensile and flexural strength, shock and fatigue resistance; therefore, it is widely used in various fields of construction, irrigation, and architecture works.

3   Conclusion

As per the research studied above if we compare normal concrete with complete ordinary Portland cement and concrete with inclusion of sugar cane bagasse ash as some replacement with OPC blended concrete with SCBA is performed better. At lower replacements, the SCBA concrete performed better than ordinary concrete. Since sugarcane bagasse ash is an industrial waste product from sugar industries and utilization of this material as cement-replacing material reduces disposable waste problem of the industry as well as society. As the sugarcane bagasse ash is freely available, the low-cost concrete with desirable quality can be achieved. Hence, low-cost structure can be achieved as inclusion of steel fiber in normal concrete enhances different properties of concrete like strength and durability. But in above research inclusion of sugarcane bagasse ash and steel fiber in any concrete are not studied.

References

1. Nuntachai, C., Chai, J.: Utilization of bagasse ash as a pozzolanic material in concrete. Constr. Build. Mater. **23**, 3352–3358 (2009)
2. Srinivasan, R., Sathiya, K.: Experimental Study on Bagasse Ash in Concrete. Inter. J. Serv. Learn. Eng.**5**, 60–66 (2010)
3. Fairbairna, E.M., Americano, B.B., Cordeiro, G.C., Paula, T.P., Toledo Filho, R.D., Silvoso, M.M.: Cement replacement by sugarcane bagasse ash: CO_2 emissions reduction and potential for carbon credits. A J. Environ. Manage. **91,** 1864–1871 (2010)
4. Modania, P., Vyawahare, M.: Utilization of bagasse ash as a partial replacement of fine aggregate in concrete. Proc. Eng., **51**, 25–29 (2013)
5. Kawade, U., Rathi, V.: Effect of use of bagasse ash on strength of concrete. Constr. Build. Mater. **2**(7) (2013). ISSN:2319-8753
6. Aigbodion, V.S., Hassan, S.B., Ause, T., Nyior, G.B.: Potential Utilization of Solid Waste (Bagasse Ash). J. Miner. Mater. Charact. Eng. **9**(1), 67–77 (2010)
7. Sua-iam, G., Makul, N.: Use of increasing amounts of bagasse ash waste to produce self-com pacting concrete by adding limestone powder waste. J. Cleaner Prod. 6 June 2013
8. Prusty, J.K. et al.: Concrete using agro-waste as fine aggregate for sustainable built environment – A review. Int. J. Sustain. Built Environ. (2016)
9. Hemath Kumar, G., Babu, H., Purohit, V.R., Sahu, P., Rana, R.S.: Investigations on mechanical properties of glass and sugarcane fiber polymer matrix composites. In: 6th International Conference of Materials Processing and Characterization (ICMPC2016) Proceedings 4, pp. 5408–5420 (2017)
10. Ranjith, A., Sanjith, J., Kiran, B.M.: Experimental investigation on performance of sugarcane bagasse ash concrete in acidic environment. Indexed in Scopus Compendex and Geobase Elsevier, Chemical Abstract Services-USA, Geo-Ref Information Services-USA, List B of Scientific Journals, Poland, Directory of Research Journals. **08**(02), 471–476 (2015). ISSN 0974-5904
11. Sivakumar, M., Mahendran, N.: Expermintal studies of strength and cost analysis of concrete using bagasse Ash. Inter. J. Eng. Res. Tech. (IJERT). ISSN: 2278-0181, **2**(4) (2013)
12. Amin, A., Foster, S.J.: Shear strength of steel fibre reinforced concrete beams with stirrups. Eng. Struct. **111**, 323–332 (2016)
13. Vasantdada sugar institute sugar statistics of India

Analysis of Multi-storey Structures with Respect to Sequential Analysis

Nikunj D. Banugariya and S. S. Solanke

Abstract While examining a multi-storey building frame, routinely all the likely loads are applied in the wake of modeling the whole building frame. In any case, practically speaking the frame is developed in different stages. As needs be, the soundness of frame fluctuates at each stage. As we look to the method of rate of the loading, the development of the frame continues and some portion of the load is applied apparently, while the remaining piece of it is forced on fulfillment of the frame. There will be a change in loads consideration in linear static analysis in transient circumstance and consequently the results would not be appropriate and palatable. Subsequently the building structure ought to be dissected at each phase of development considering the load varieties. Finite element modeling considers the impacts of sequence of construction resulting in improvement of finite element analysis. Here it is termed as Construction Stage Analysis who considers all these constructional uncertainties. This paper deals with a two multi-story reinforced concrete building frames of various bay width and length, storey height, and number of stories utilizing ETABS 2016, trailed by the sequential stage examination of each model. Likewise, all full frame models are analyzed for static well as dynamic loads. At last, a relative investigation of axial forces and bending moments was done at each story for full casing model and construction stage model.

Keywords Structural loading · Design forces · High rise structure · Conventional analysis · Sequential analysis

1   Introduction

Static elastic finite element analysis, including summations of gravity loads was utilized by large designers, specialist and chiefs to determine the response of structures. The basic responses, i.e., axial loads, bending moments, and displacements,

N. D. Banugariya (✉) · S. S. Solanke
Department of Civil Engineering, G.H.R.C.E, Nagpur, India
e-mail: nbanugariya@gmail.com

of such normal analysis may progressively wander from real conduct while building height increase in development stage. Time-reliant, long-term deformations because of development sequence can cause redistribution of responses that would not be figured and considered by traditional strategies. Although staged analysis was muddled in nature, numerous imperatives must be checked at the time of analysis. At that point, nonlinear analysis is made simple and standard because of the headway of finite element modeling among designers and researchers that accelerate the reasonable structural design particularly for tall structures. Sequential analysis is produced into conspicuous part amid analysis a few understood analysis programming involves this arrangement in their analysis and configuration device. This, however, is not so boundless as far back as there is absence of data about its need and decision. Likewise as different analysis, construction stage analysis guarantees express objectives in configuration parts of the structures.

Since mid-1950s, the vulnerability of over abundance loads on slabs due to formworks and different development co-ordinations amid development is being examined. It was discovered that amid development slabs carry loads in abundance of administration life loads. The issue was all around investigated for the loads of formwork and imposed loads amid development. As earlier discussed due to time-dependent behavior of structure, results are not reliable in conventional analysis. To handle with the previously mentioned vulnerabilities, different methodologies were made. In late 80s, researchers studied the effect of structural loads only during development stage. Choi and Kim [1] studied a similar issue freely; however, they considered the impact of differential column shortening under dead loads and tragically gave careful consideration to the responses of different forces because of overabundance construction loads. Choi and Kim [1] used "One story at a single instance" investigation approach for tackling the issue. Be that as it may, it was past the human computational endeavors. In 1992, Chang-Koon et al. [2] proposed a simplified investigation approach known as "Correction Factor Method (CFM)" thinking about just dead loads. Vafai et al. [3] also dealt with the differential column shortening considering the creep and shrinkage of tall structure. Dinar et al. [4] and Shirhatti and Vanakudre [5] analyzed the reinforced concrete structure as well as steel structures and investigated a response of both materials using nonlinear staged analysis. In 2015, Dubey et al. [6] carried out the analysis considering all loads and defined a ratio of structural response considering Construction Sequence Analysis and Conventional Analysis.

It is clear from the above discussion that less attention has been paid on the impact of incomplete structure and the varied geometry as well as loading amid construction. Thus, this paper deals with the regularity as well as irregularity of structure apparently considering axial forces induced in the members.

2 Research Methodology

All the design checks like deflection, structural stability, and strength are performed by considering single-step loading in conventional design. Though the self-weight of high rise structure turns into an extensive fact while design and developing, sequential analysis considers the development stages which consider the residual stress of every storey of the structure independently to study the responses. In the analysis procedure, components are grouped with respect to floors to carry out more realistic analysis procedure. To represent the sequential load, case loads are assigned as per Indian Standards and nonlinear static load case is generated to analyze the structure step by step. Later, some response parameters are compared with respect to sequential analysis and conventional analysis. Various load combinations have been considered to carry out the structural analysis and design.

3 Sequential Analysis and Finite Element Modeling

It is assumed while designing a structure that all loads are applied simultaneously but it does not seem valid because of the floor by floor construction of building, apparently dead load acts sequentially. Figure 1a represents the linear static analysis procedure considering the single-step analysis termed as conventional analysis. Meanwhile more realistic results are obtained when structure is analyzed storey by storey considering nonlinear static sequential analysis as shown in Fig. 1b. Outcomes of a specific storey considering all possible loads are obtained in first step. Further the results of previous storey are stored by software and, when a story is added to the structure, past outcomes comes about were put away. This procedure is followed for every step. The joint of particular column where new column will be constructed in further step is used to store the residual stresses of that constructed column. At the point when the new story will be added to the structure, those stresses will be discharged and go about as an underlying parameters for advance investigation. In this manner, whole structure is grouped and analyzed by adding each groups step-wise. Though the nature of materials due to cracking and other effects is not linear as considered in conventional analysis, nonlinear analysis of structure gives more precise results.

To study the behavior of structure with respect to nonlinear sequential analysis over linear static analysis, using ETABS, two finite element models having identical plan but different height are considered. Keeping material properties and loadings same the structure is modeled. The sequential load case has been simulated for dead load only. Effects of time-dependent properties are not taken into account for sequential load case. Four models, two for conventional analysis and remaining for sequential analysis are used to carry out study. Figure 2. indicates the identical plan for all buildings.
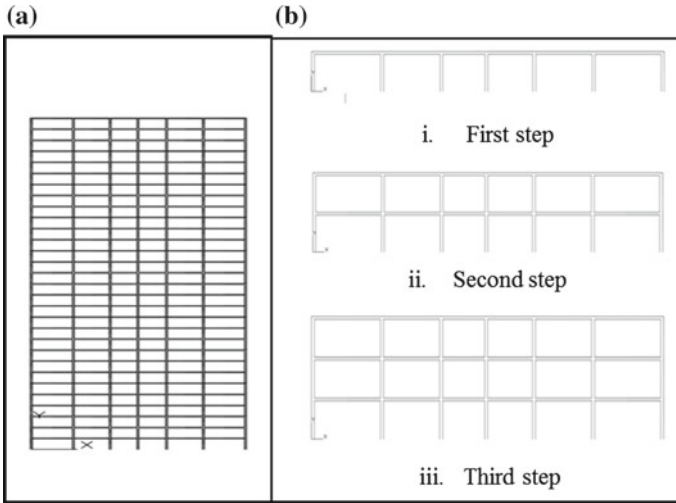
Fig. 1 Conventional analysis and sequential analysis
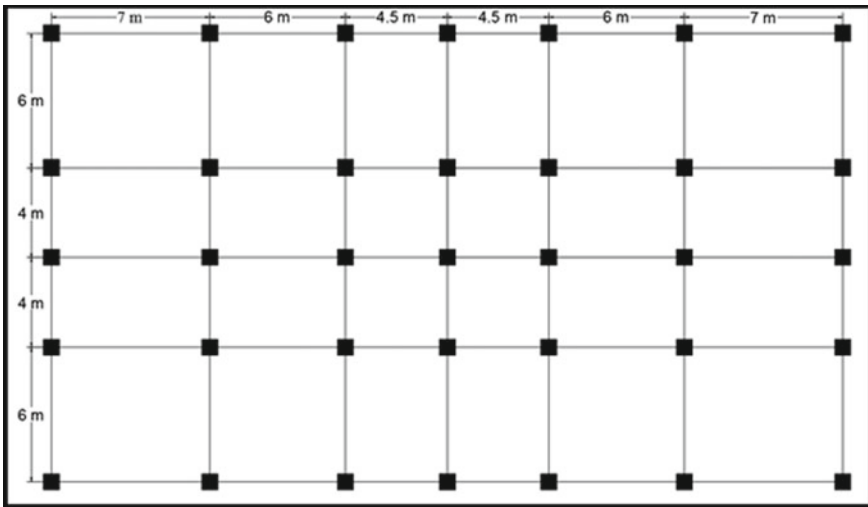
Fig. 2 Plan of the building

IS 875-Part 1(1987) and IS875-Part 2(1987) are referred for different dad load and live load considerations, shown in following Table 1. IS 875-Part 3(2015) is used to carry out wind load analysis for all finite element models.

It was assumed that construction of infill walls was carried out after construction of structural frame. Following Tables show the structural details of G+30 and G+45 storey building (Table 2).

Column sizes of G+45 storey structure are as follows: (Table 3)

Table 1 Loads considered

Material	Intensity/density
Density of concrete	25 KN/m^3
Floor finish	1 KN/m^2
Roof treatment	1 KN/m^2
Wall load: Internal wall External wall Parapet wall	16 KN/m 23 KN/m 11 KN/m
Live load: Floor Roof	3 KN/m^2 0.75 KN/m^2

Table 2 Structural Details

Grade of concrete	M30
Grade of steel	Fe500
Height of each storey	3 m
External wall	300 mm thick
Internal wall	150 mm thick
Column size (G+30 storey) Corner column Outer column Inner column	550 × 550 mm 600 × 600 mm 600 × 600 m, 650 × 650 mm, 700 × 700 mm
Beam size	350 × 450 mm
Slab	150 mm thick

Table 3 Column size of G+45 storey building

Corner columns	700 × 700 mm
Outer columns	750 × 750 mm, 800 × 800 mm
Inner columns	850 × 850 mm, 900 × 900 mm 950 × 950 mm

Table 4 shows the load combinations used for the conventional and sequential analysis in which DL, LL, WL stands for Dead Load, Live Load, and Wind Load, respectively.

Table 4 Load combinations used for analysis and design

1.5DL+1.5LL
1.2DL+1.2LL+1.2WLX
1.2DL+1.2LL−1.2WLX
1.2DL+1.2LL+1.2WLY
1.2DL+1.2LL−1.2WLY
1.5DL+1.5WLX
1.5DL−1.5WLX
1.5DL+1.5WLY
1.5DL−1.5WLY
0.9DL+1.5WLX
0.9DL−1.5WLX
0.9DL+1.5WLY
0.9DL−1.5WLY

4 Behavior of Structure with Respect to Sequential Analysis

The following Fig. 3 shows the key plan for identifying the columns and beams. Comparison of responses of structure with and without sequential analysis is done.
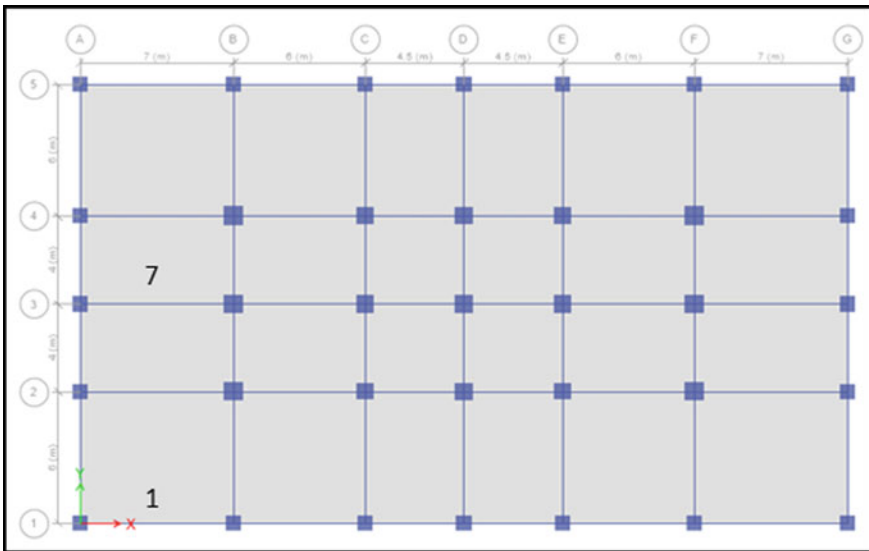
Fig. 3 Key plan of building

4.1 Comparison of Column Forces

The ratio α mentioned below has been obtained for outer and inner column 1A and 2B respectively for G+30 and G+45 storey building as shown in following figures.

Ratio of axial force of columns(α)

$$\text{Ratio } \alpha = \frac{\text{Axial Force considering sequential analysis}}{\text{Axial Force considering conventional analysis}}$$

4.1.1 For G+30 Storey Structure

From the results obtained by axial force variation in exterior and interior column 1A and 2B respectively it is clear that variations in the results are ranging from 3 to 18% (Fig. 4).

Axial deformation variation in exterior and interior column 1A and 2B respectively is shown in Fig. 5. Variations in the results show the overestimation of results in case of conventional analysis.

(i) Column 1A   (ii) Column 2B
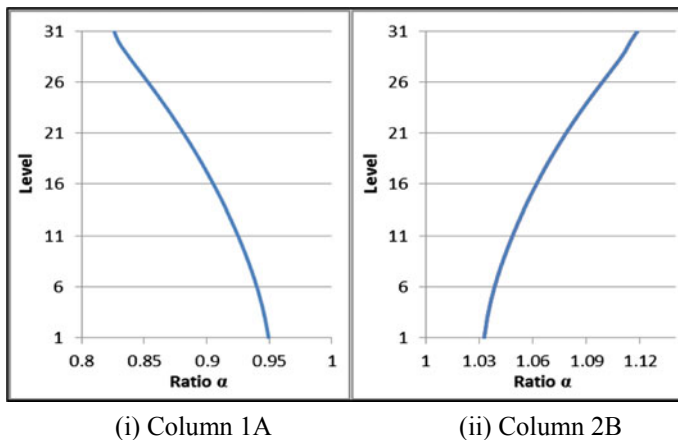
Fig. 4 Axial force variation in exterior and interior column
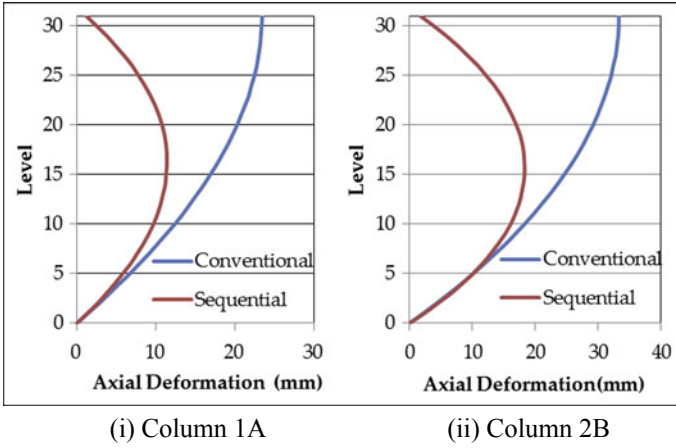
Fig. 5 Axial deformation variation in exterior and interior column
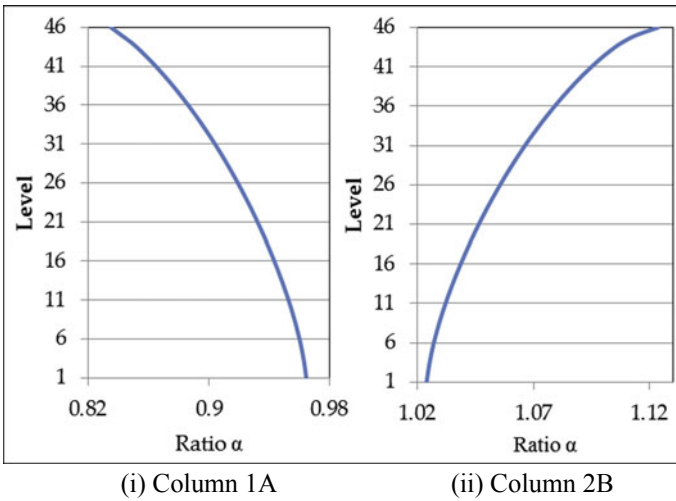
Fig. 6 Axial force variation in exterior and interior column

4.1.2   For G+45 Storey Structure

It is clear from the Fig. 6 that response of axial force variation in interior and exterior column shows the variation up to 16%.

Axial deformation variation in exterior and interior column is shown in Fig. 7, which states that results for conventional analysis are overestimated.

(i) Column 1A   (ii) Column 2B
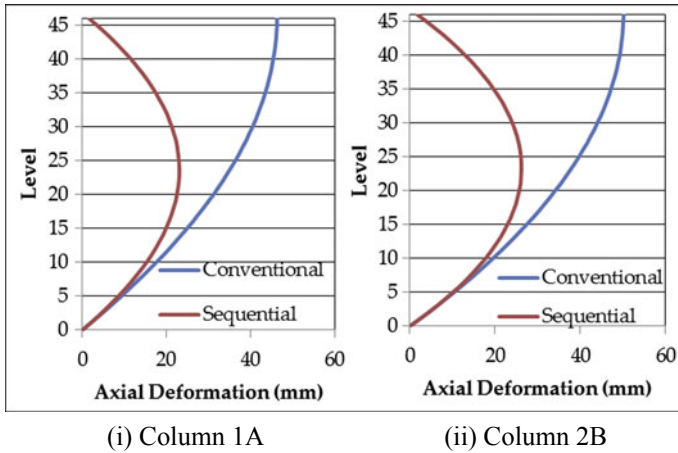
Fig. 7 Axial deformation variation in exterior and interior column

4.2 Comparison of Beam Forces

The ratio β mentioned below has been obtained for beam 1 and beam 7 respectively, as shown in Fig. 3. Responses of G+30 and G+45 storey building are shown in following figures.

Ratio of Bending Moments in Beams(β)

$$\text{Ratio } \beta = \frac{\text{Bending moment considering sequential analysis}}{\text{Bending moment considering conventional analysis}}$$

4.2.1 For G+30 Storey Structure

Ratio β defined for showing comparison of results of conventional and sequential analysis is obtained and displayed in Figs. 8 and 9. respectively. Bending moment variations at left end, middle span, and right end are shown, respectively.

Left End   Mid Span   Right End

Fig. 8 Bending moment variation in exterior beam
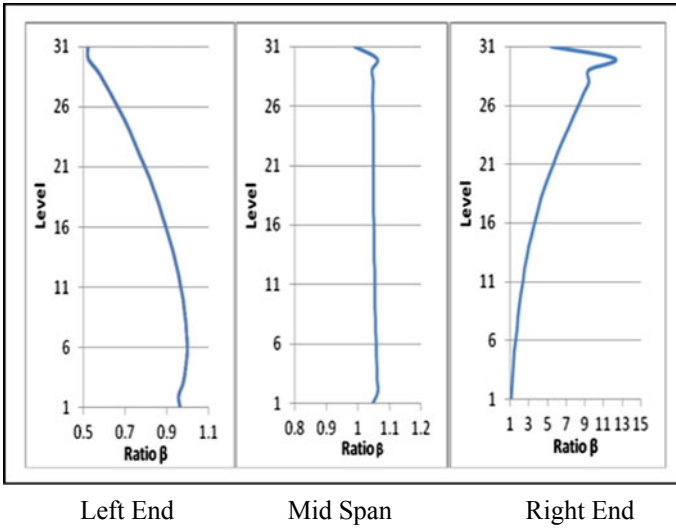
Left End   Mid Span   Right End
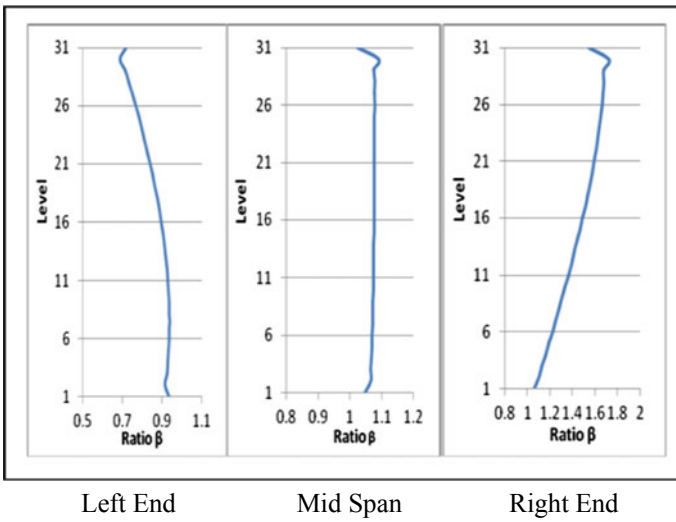
Fig. 9 Bending moment variation in interior beam

4.2.2 For G+45 Storey Structure

Results of bending moments variation at left end, middle span, and right end are obtained for exterior and interior beams and displayed in Figs. 10 and 11, respectively. Ratio β shows the comparison of conventional analysis with respect to sequential analysis.

Fig. 10 Bending moment variation in exterior beam

Left End   Mid Span   Right End

Fig. 11 Bending moment variation in interior beam

Left End   Mid Span   Right End
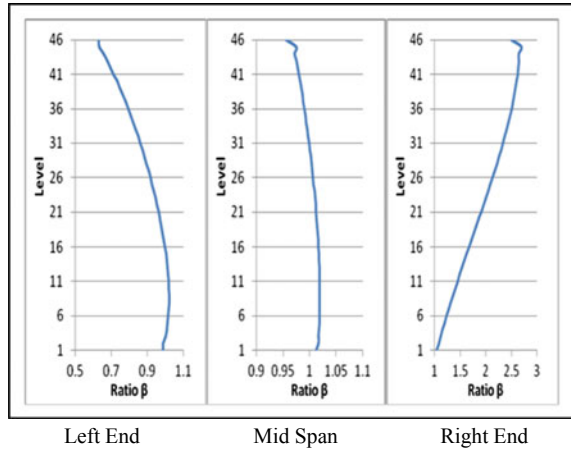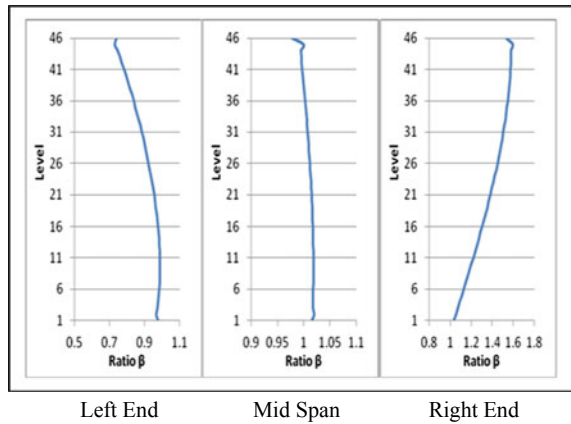
5 Conclusions

The study reveals that slenderness of structure increases as each additional floor creates a significant load upon the columns. To perform sequential analysis, considering nonlinear behavior of structure becomes significant with the increasing slenderness. In this paper, two different buildings G+30 and G+45 modeled with identical plan are considered. Analysis with respect to sequential analysis is carried out. Three response quantities, i.e., axial force, axial deformation in column, and bending moments in beam are studied. Ratio(α) and ratio(β) is generated taking both analysis cases into consideration.

The main observations were as follows: (1) Axial force increases in inner column, thus making it critical. (2) Deformations are underestimated in lower floors while same are overestimated in upper floors. (3) The location of the beams in plan plays vital role on the ratio of moments. The increase in the percentage of moment due to CSA is up to a maximum of 50, 100, and 10% at left end, right end, and mid span sections, respectively. (4) The variation in the response of ratio β shows more fluctuations in upper stories. (5) As construction of structure progresses time-dependent properties imparts more stresses on structural components and thus recently constructed upper floors shows more variation as compared to lower floors. As exterior columns carry generally half the load as carried by interior columns and same in case of beams, response quantities show variations in the pattern of loadings. (6) Responses of the structure as above clearly shows that results of axial force in columns are not same in both cases. This will result into variation in required reinforcement for the columns.

From above discussions, it can be concluded that inclusion of sequential analysis in regular practice is necessary to obtain more realistic design of structure.

References

1. Choi, C.K., Kim, E.D.: Multistory frames under sequential gravity loads. J. Struct. Eng. **111**(11), 2373–2384 (1985)
2. Choi, C.K., et al.: Simplified building analysis with sequential dead loads—CFM. J. Struct. Eng. **118**(4), 944–954 (1992)
3. Vafai, A., et al.: Calculation of creep and shrinkage in tall concrete buildings using nonlinear staged construction analysis. (2009): 409–426
4. Dinar, Y., Rasel, M.Md., Chowdhury, M.J.A.: Chronological Construction Sequence Effects on Reinforced Concrete and Steel Buildings. Inter. J. Eng. Sci. (IJES). **3**(1), 52–63 (2014). ISSN(e): 2319 – 1813 ISSN(p): 2319 – 1805
5. Shirhatti, T.G., Vanakudre, S.B.: The effects of P-delta and construction sequential analysis of RCC and steel building with respect to linear static analysis. Inter. Res. J. Eng. Technol. (IRJET) **2**, 501–505 (2015)
6. Dubey, N., Sonparote, R.S., Kumar, R.: Effect of construction sequence analysis on seismic performance of tall buildings. J. Civil Eng. Environ. Technol. **2**(11), 44–49 (2015)
7. Shrikar, S.N., Kumar, R., Sonparote, R.S.: Effect of staged construction analysis on seismic design and performance of RC buildings. Earthq. Eng. **2**, 436–449 (2014)

8. Das, G.G., Praseeda, K.I.: Comparison of conventional and construction stage analysis of a RCC building. IJSTE – Int. J. Sci. Technol. Eng. 3(03) (2016)
9. Rao, J.V.G., Ramesh Babu, D., Selvan, M., Kiran Kumar, V.: Study and comparison of construction sequence analysis with regular analysis by using E-TABS. Civil Eng. Inter. J. [CEIJ]TM. **2** (2016)
10. Pathan, K.M., Ali, S.W., Khan, H.T., Mirza, M.S., Waseem, M., Zubair, S.: Construction stage analysis of RCC frames. Inter. J. Eng. Technol. Res. **2**(3), 54–58 (2014)
11. Amin, S.R., Mahajan, S.K.: Analysis of multi storied Rcc building for construction sequence loading. Int. J. Mod. Trend Eng. Res. 2–4 July 2015. e-ISSN NO.:2349–9745
12. BIS, IS.: 875 (Part 1 and Part 2) Indian Standard Code of Practice for Design Loads (Other than Earthquake) for Buildings and Structures. Bureau of Indian Standards, New Delhi (1987)

Mixed Influence of Metakaolin (MK) and Steel Fiber on Mechanical Properties of Concrete

Pratik B. Shinde, P. Y. Pawade and Mayuri A. Chandak

Abstract The advances of concrete technology proved that the use of mineral admixture such as silica fume, coconut shells, egg shell powder, Fly ash, and GGBS are necessary and essential for producing high-performance concrete. In addition, incorporation of these materials immensely helps to address environmental problem related to damage being caused by extraction of raw materials, CO_2 emissions during cement manufacturing process and disposal of industrial waste by products. From last few decades, the use of metakaolin as a partial replacement to cement was increased tremendously only due to its high pozzolanic content. The present study shows the influence of metakaolin as a mineral admixture and steel fiber as an additional material, on properties of concrete. Metakaolin was blended with cement in various proportions to study the effect of strength on concrete. In this work, concrete was made up with Pozzolanic Portland Cement (PPC) to produce control mix and further replaced by metakaolin with 5, 10, 15, 20%, respectively. The mechanical properties of concrete were assessed by means of compressive strength, flexural strength of concrete. From the obtained results, 15% replacement of cement with metakaolin has higher compressive strength. The maximum compressive strength attained was 42.95 and 45.09 MPa. And it is greater than the normal concrete strength, i.e., 37.65 and 42.16 MPa for 28 and 90 days, respectively.

Keywords Metakaolin (MK) · Steel fiber (SF)

P. B. Shinde (✉)
Structural Engineering, G.H.Raisoni College of Engineering, Nagpur, India
e-mail: shinde_pratik.ghrcemtechstr@raisoni.net

P. Y. Pawade
Civil Engineering Department, G.H.Raisoni College of Engineering, Nagpur, India
e-mail: prashant.pawade@raisoni.net

M. A. Chandak
Applied Mechanics Department, P.I.E.T, Nagpur, India
e-mail: chandakmayuri1@gmail.com

1 Introduction

In recent decades, the construction industries have encountered many challenges. The positive approach of construction industry toward innovation will work as a channel for the development of durable, cheap, and new construction materials compared to the conventional ones, resulting low cost and energy competent structure. Nowadays, concrete is consumed up to that level, it reached on second rank in heavily consumed products in the world [1–5].

For manufacturing of cementitious materials, intensive energy was utilized. Along with it produce greenhouse gasses, like CO_2, which is the main cause of environment pollution. Another major issue is that civil industry consumes natural resources on large scale. So that to save energy consumption, reduce CO_2 emission, to control environmental pollution and minimize the utilization of natural resources, cement industries produce blended cements by using supplementary cementitious materials like fly ash, silica fume, limestone, pozzolan, and metakaolin.

In last few years, metakaolin (MK) was studied due to its high pozzolanic activity nature. It is not a by-product and secondary product as an industrial waste. It is a primary product which is generated from the dehydroxylation of kaolin clay under temperature of 700–850 °C [6, 7]. Kaiolin ($Al_2Si_2O_7$) is the main raw material in production of metakaolin. When metakaolin reacts with $Ca(OH)_2$, it produces C-S-H gel on certain temperature and reacts with CH, which results in production of alumina containing phases which includes C_4AH_{13}, C_2ASH_8, and C_3AH_6 [8, 9]. In high-performance concrete and high strength concrete, metakaolin shows better results with durability also. Many researchers reported the effects of metakaolin on the various factors of concrete like porosity, pore size distribution, compressive strength, durability, and pozzolanic reactions [1, 10–15].

Along with its better performance, concrete shows an average performance under subjected to tensile stress. Due to this reason, the use of fiber material was increased to improve the tensile nature of concrete [16–24]. Fiber orientation, concentration, distribution of fiber in mix, alignment, and aspect ratio, these are the main factors which contribute to enhance the mechanical properties of concrete [23].

This paper shows experimental study on the effect of metakaolin (MK) and steel fiber on the mechanical properties of concrete. In this study, the water ratio kept same that is 0.4 and steel fiber of length/aspect ratio 25/41.67. The steel fiber was added in the mix with 0.5, 1.0, and 1.5% of total weight of concrete. MK was added with 15% of total weight of binder. Then, results were analyzed by compressive strength, flexural strength at 28 and 90 days of curing period reported as follows.

Table 1 Chemical and physical properties of binder material [25]

Properties	Oxides	Cement (% by mass)	Metakaolin (% by mass)
Chemical Property	SiO_2	19.43	53
	Al_2O_3	5.64	43
	Fe_2O_3	4.00	1.2
	CaO	61.60	0.5
	Na_2O	0.11	0.12
	MgO	2.41	0.4
	K_2O	0.78	0.53
	L.O.I.	1.85	0.4
	TiO_2	–	2.27
Physical Property	Surface area (m^2/kg)	3.28	18,000
	Specific gravity	3.19	2.6

Table 2 Steel fibers properties

Shape	D (Ø) mm	L mm	Aspect ratio
Hooked end	0.6	25	41.67

2 Experimental Study

2.1 Materials

ACC brands (Concrete Plus) Pozzolana Portland Cement (PPC) having specific gravity 3.15 and fineness of 325 m^2/kg was used as a binder material. Properties of cement and MK are mentioned in Table 1. The coarse aggregate was used of size 10 and 20 mm size. Fine aggregate was used of locally available river sand. ViscoFlix-2230 + water reducing admixture was used for all the mixes to achieve slump between 140 and 170 mm for flexibility in handling, transporting, placing, and consolidating.

Locally available hooked end type steel fiber was used. The property of steel fiber is given in Table 2.

2.2 Mix Proportions

The water binder ratio was kept constant, i.e., 0.4 for making concrete. Mk was replaced by 5, 10, 15, and 20% of total binder weight for all mixes. Then, it was tested for compressive strength and flexural strength. Results are shown in Figs. 1 and 2. After that steel fiber was incorporated with 0.5, 1.0, and 1.5% of total weight of concrete with all metakaolin percentages in concrete. Therefore, total 14 different mix proportions were designed to study the influence of metakaolin (MK) and steel
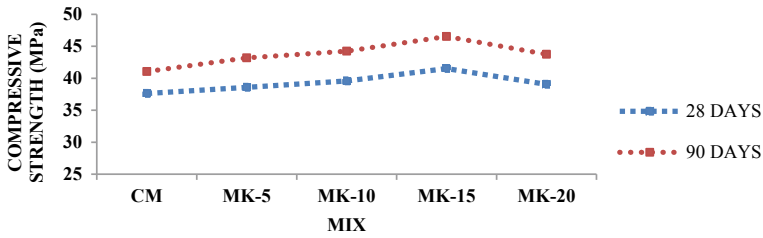
Fig. 1 Compressive strength with MK percentage
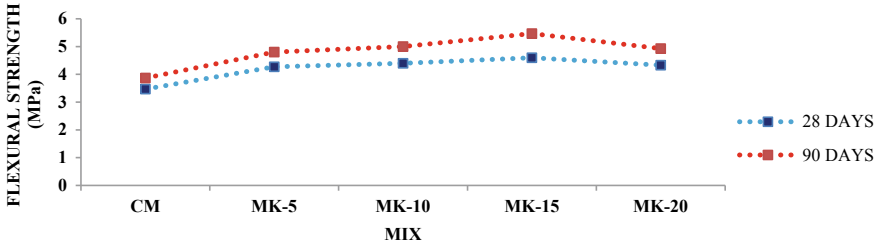
Fig. 2 Flexural strength with MK percentage

fiber on the mechanical properties of concrete. These mix details are given in Table 3.

2.3 Test Specimens

For the testing, various dimensioned samples were casted as follows,

Cube—150 × 150 × 150 mm
Beam—500 × 10 × 10 mm

The results were obtained by averaging of 3 readings of each test. Each test was conducted after 28 and 90 days of curing period.

2.4 Test Methods

Compression test and flexural test confirming to IS: 516-1959. The modulus of rupture (F_b) was calculated by,

$$F_b = \frac{PL}{BD^2} \tag{1}$$

Table 3 Mix proportion of plain, metakaolin concrete with and without steel fiber

Mix no.	Mix ID	Cement (Kg/m³)	MK (Kg/m³)	Water (kg/m³)	Fine Agg. (Kg/m³)	Coarse Agg. (Kg/m³)		Steel Fiber %	Steel Fiber kg	SP (kg/m)
						20 mm	10 mm			
1	CM	340	0	136	904	690	460	0	0	6.8
2	MK5 + 0.5	323	17	136	904	690	460	0.5	10.18	6.8
3	MK5 + 1.0	323	17	136	904	690	460	1	20.37	6.8
4	MK5 + 1.5	323	17	136	904	690	460	1.5	30.55	6.8
5	MK10 + 0.5	306	34	136	904	690	460	0.5	10.18	6.8
6	MK10 + 1.0	306	34	136	904	690	460	1	20.37	6.8
7	MK10 + 1.5	306	34	136	904	690	460	1.5	30.55	6.8
8	MK15 + 0.5	289	51	136	904	690	460	0.5	10.18	6.8
9	MK15 + 1.0	289	51	136	904	690	460	1	20.37	6.8
10	MK15 + 1.5	289	51	136	904	690	460	1.5	30.55	6.8
11	MK20 + 0.5	272	68	136	904	690	460	0.5	10.18	6.8
12	MK20 + 1.0	272	68	136	904	690	460	1	20.37	6.8
13	MK20 + 1.5	272	68	136	904	690	460	1.5	30.55	6.8
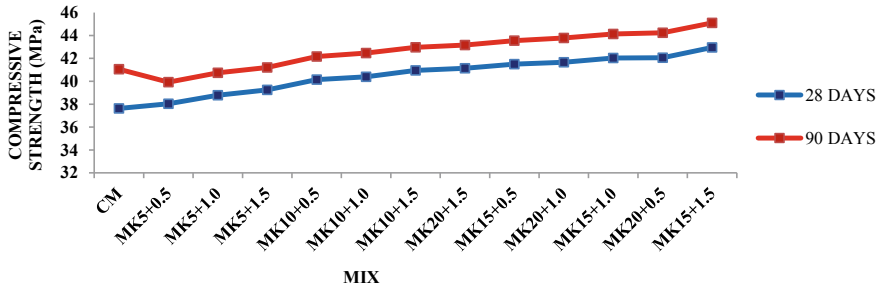
Fig. 3 Effect of steel fiber and MK on compressive strength

$$F_b = \frac{3PL}{BD^2} \tag{2}$$

where

P   Tensile load at failure (KN)
B   Width (mm)
D   depth (mm)
L   Support length (mm)
a   distance between the line of crack and next near support, measured on the center line

(1) When a > 200 mm for 150 mm sample or > 130 mm for 100 mm sample
(2) When a < 200 mm but > 170 mm for 150 mm sample or < 133 mm but > 110 mm for 100 mm sample.

3   Test Results with Discussion

3.1   Compressive Strength

Figure 3 gives the variation in compressive strength of concrete which was incorporated with MK and steel fiber. In which, 42.95 and 45.09 MPa are the maximum strength for 28 and 90 days, respectively. Percentage rate of gaining strength was decreased with respect to age of concrete. Replacement of cement with MK shows better increased in compressive strength as per results [2, 26–32]. About 0.5 and 1.0% incorporation of steel fiber gives relatively higher strength to plain concrete.
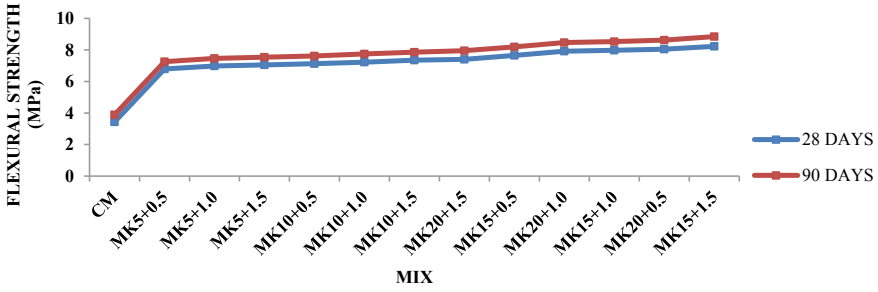
Fig. 4 Effect of steel fiber and MK on flexural strength
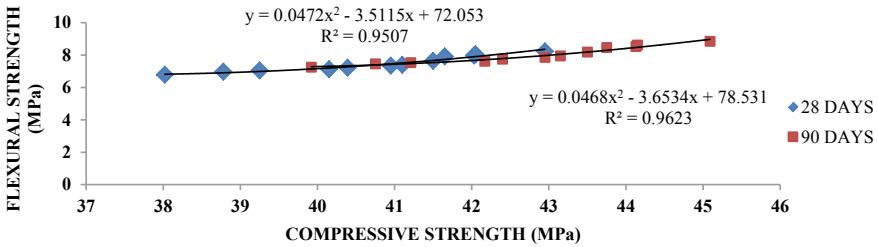
Fig. 5 Relation between compressive strength versus flexural strength

3.2 Flexural Strength

Figure 4 gives the variation in flexural strength for control mix, as well as concrete incorporated with steel fiber and MK. The maximum modulus of rupture was observed 8.23 and 8.85 MPa for 28 and 90 days, respectively. The nature of graph was continuously increasing. This nature of results was observed due to the small steel fiber, which have behavior to align in flow and high orientation density while mixing of concrete. It results in a better flexural strength.

3.3 Relation Between Compressive Strength Versus Flexural Strength

Figure 5 represents the relation between flexural strength (F_{cr}) versus compressive strength (F_{ck}). The results plotted for 28 and 90 days, respectively. After studying the relation, we can say that, if the compressive strength is high, then flexural strength will be higher. The relation equations with coefficient (R^2) were as given in Table 4.

Table 4 Relation equations with coefficient

Sr. No.	Age (Days)	Equation	R^2 Value
1	28	$F_{cr} = 0.047(F_{ck})^2 - 3.511x + 72.05$	0.950
2	90	$F_{cr} = 0.046(F_{ck})^2 - 3.653x + 78.53$	0.962

4 Conclusion

After observing and studying above results, we have the following conclusions,

- Mechanical properties of concrete were enhanced by replacement of cement with MK. It shows higher results in compressive strength and flexural strength for 15% replacement of MK to cement. The values were 42.95 and 45.09 MPa observed for 28 and 90 days. The increment was promised by incorporation of MK over plain concrete.
- The incorporation of steel fiber improves the results of concrete. The tensile strength capacity of concrete was improved remarkably. The smaller aspect ratio shows better flexural strength up to 8.23 and 8.85 MPa for 28 and 90 days, respectively. These better results were observed due to orientation and distribution of steel fiber in mixture.
- The demand of water was high because of high fineness of MK. To achieve desired workability, super plasticizer was used.
- Relation between compressive strengths versus flexural strength revealed that percentage addition of steel fiber and incorporation of metakaolin was affecting the mechanical properties of concrete considerably. When the results were compared with other authors, then it varies between ± 18%.

References

1. Sabir, B.B., Wild, S., Bai, J.: Metakaolin and cacined clays as Pozzolans for concrete: a review. Cem. Concr. Compos. **23**(6), 441–454 (2001)
2. Wild, S., Khabit, J.M., Jones, A.: Relative strength pozzolanic activity and cement hydration in uperplasticised metakaolin concrete. Cem. Concr. Res. **26**(10), 1537–1544 (1996)
3. Coleman, N.J., Page, C.L.: Aspects of the pore solution chemistry of hydrated cement pastes containing MK. Cem. Concr. Res. **27**(1), 147–154 (1997)
4. Frias, M., Cabrera, J.: Pore size distribution and degree of hydration of metakaolin–cement pastes. Cem. Concr. Res. **30**(4), 561–569 (2000)
5. Asbridge, A.H., Page, C.L., Page, M.M.: Effects of metakaolin, water/binder ratio and interfacial transition zones on the microhardness of cement mortars. Cem. Concr. Res. **32**(9), 1365–1369 (2002)
6. Klimesch, D.S., Ray, A.: Use of the second-derivative differential thermal curve in the evaluation of cement–quartz pastes with metakaolin addition autoclaved at 180_C. Thermochim. Acta **307**(2), 167–176 (1997)

7. Klimesch, D.S., Ray, A.: Autoclaved cement–quartz pastes with metakaolin additions. Adv. Cem. Based Mater. **7**(3), 109–118 (1998)
8. Changling, H., Osbaeck, B., Makovicky, E.: Pozzolanic reaction of six principal clay minerals: activation reactivity assessments and technological effects. Cem. Concr. Res. **25**(8), 1691–1702 (1995)
9. Zhang, M.H., Malhotra, V.M.: Characteristics of a thermally activated aluminosilicate pozzolanic material and its use in concrete. Cem. Concr. Res. **25**(8), 1713–1725 (1995)
10. Courard, L., Darimont, A., Schouterden, M., Ferauche, F., Willem, X., Degeimbre, R.: Durability of mortars modified with metakaolin. Cem. Concr. Res. **33**(9), 1473–1479 (2003)
11. Khatib, J.M., Wild, S.: Pore size distribution of metakaolin paste. Cem. Concr. Res. **26**, 1545–1553 (1996)
12. Curcio, F., DeAngelis, B.A.: Dilatant behavior of superplasticized cement pastes containing metakaolin. Cem. Concr. Res. **28**(5), 629–634 (1998)
13. Brooks, J.J., Johari, M.M.A.: Effect of metakaolin on creep and shrinkage of concrete. Cem. Concr. Compos. **23**(6), 495–502 (2001)
14. Li, Z., Ding, Z.: Property improvement of Portland cement by incorporating with metakaolin and slag. Cem. Concr. Res. **33**(40), 579–584 (2003)
15. Badogiannis, E., Tsivilis, S.: Exploitation of poor Greek kaolins: durability of metakaolin concrete. Cem. Concr. Compos. **31**(2), 128–133 (2009)
16. Gruber, K.A., Ramlochan, T., Boddy, A., Hooton, R.D., Thomas, M.D.A.: Increasing concrete durability with high-reactivity metakaolin. Cem. Concr. Compos. **23**(6), 479–484 (2001)
17. Bentur, A., Mindess, S., Diamond, S.: Pull out processes in steel fiber reinforced cement. Int. J. Cem. Compos. Lightweight Concr. **7**(1), 29–38 (1985)
18. Barros, J.A.O., Cruz, J.S.: Fracture energy of steel fiber-reinforced concrete. Mech. Compos. Mater. Struct. **8**(1), 29–45 (2001)
19. Banthia, N., Trottier, J.F.: Concrete reinforced with deformed steel fibres. Part II: Toughness characterization. ACI Mater. J. **92**(2), 146–154 (1995)
20. Khayat, K.H., Roussel, Y.: Testing and performance of fiber reinforced, self consolidating concrete. Mater. Struct. **33**, 391–397 (2000)
21. Quian, C.X., Stroeven, P.: Development of hybrid polypropylene–steel fibre reinforced concrete. Cem. Concr. Res. **30**, 63–69 (2000)
22. Yurtseven, A.E.: Determination of mechanical properties of hybrid fibereinforced concrete. MSc thesis, METU, Ankara, Turkey (2004)
23. Nili, M., Afroughsabet, V.: Property assessment of steel–fibre reinforced concrete made with silica fume. Constr. Build. Mater. **28**, 664–669 (2012)
24. Guneyisi, E., Gesoglu, M., et al.: Combined effect of steel fiber and metakaoline incorporation on mechanical properties of concrete. (Elsevier) composites: Part B **56**(2014), 83–9 (2013)
25. Al-Khaja, W.A.: Strength and time-depended deformations of silica fume concrete for use in Bahrain. Constr. Build. Mater. **8**, 169–172 (1994)
26. Ding, J.T., Li, Z.: Effects of metakaolin and silica fume on properties of concretes. ACI Mater. J. **99**, 393–398 (2002)
27. Güneyisi, E., Mermerdas, K.: Comparative study on strength, sorptivity, and chloride ingress characteristics of air-cured and water-cured concretes modified with metakaolin. Mater. Struct. **40**, 1161–71 (2007)
28. Güneyisi, E., Gesoğlu, M., Mermerdas, K.: Improving strength, drying shrinkage, and pore structure of concrete using metakaolin. Mater. Struct. **41**, 937–949 (2008)
29. Güneyisi, E., Gesoğlu, M., Karaoğlu, S., Mermerdas, K.: Strength, permeability and shrinkage cracking of silica fume and metakaoline concretes. Constr. Build. Mater. **34**, 120–130 (2012)
30. Kim, H.S., Lee, S.H., Moon, H.Y.: Strength properties and durability aspects of high strength concrete using Korean metakaolin. Constr. Build. Mater. **21**, 1229–1237 (2007)
31. Poon, C.S., Kou, S.C., Lam, L.: Compressive strength, chloride diffusivity and pore structure of high performance metakaolin and silica fume concrete. Constr. Build. Mater. **20**(10), 858–865 (2006)

32. Sanal, I., Özyurt, N.: Effects of formwork dimensions on the mechanical performance of fiber-reinforced cement based materials. In: 9th International congress on advances in civil engineering, 27 30 Karadeniz Technical University, Trabzon, Turkey; Sep 2010

Impact of Metakaolin and Steel Fibre on Mechanical Properties of Concrete

Mayuri A. Chandak and P. Y. Pawade

Abstract This study was based on experiments conducted to see the effect of Metakaolin (MK) concrete and Metakaolin (MK) concrete along with steel fibre on mechanical properties of concrete. The cement was replaced by metakaolin by 4, 8, 12, 16 and 20% of total weight of binder. Steel fibre (SF) used for the study has aspect ratio 83.33. Total 21 mix proportions were prepared for study. Compressive, split tensile and flexural strength tests were used to analysed the effect of metakaolin and steel fibre on concrete samples. These tests were conducted after the 28th day and 90th day of curing period. The present conducted study revealed that the incorporation of steel fibre and metakaolin (MK) shows significant changes on mechanical properties of concrete.

Keywords Compressive strength · Flexural strength · Metakaolin · Split tensile strength · Steel fibre

1 Introduction

Concrete is a versatile material of civil industry, it is used widely for construction because of the strengths it possesses. Now the incorporation of cementations materials, especially pozzolanic materials in mortar or concrete is the need of civil industry because it will reduce environmental effects and carbon content considerably in resulting products. That type of materials not only reduces cement content but also increase use of by-products and industrial waste .

The scenario of the use of concrete is considerably changed due to incorporation of pozzolanic materials like rice husk ash (RHA), fly ash, ground granular blast furnace slag, silica fume, metakaolin (MK). These materials are partially replaced with cement in high strength concrete [2, 8, 15, 16, 18]. These types of pozzolanic Materials give additional contribution in performance to concrete through reacting

M. A. Chandak (✉) · P. Y. Pawade
Department of Civil Engineering, G.H. Raisoni College of Engineering, Nagpur, India
e-mail: chandakmayuri1@gmail.com

with hydration product of Portland cement to create C-S-H gel is the main factor behind the gaining strength of concrete [2, 6, 17, 20] .

From last two decades, researchers are attracted towards the advantages, benefits and usage of metakaolin as a fractional substitute to cement. Metakaolin is made by calcinating of pure or refined kaolintic clay by varying temperature between 650 and 850 °C, fineness from 700 to 900 m^2/kg is obtained by grinding. A ground particle which has in micron size and inert impurities has carefully removed. According to many researchers, concrete having metakaolin gives excellence performance in terms of mechanical properties as well as durability properties [1, 7, 9, 12, 15, 21]. This approach is beneficially as well as environment friendly in many ways like minimizing rate of consumption of Portland cement which is responsible for CO_2 emission to atmosphere.

When concrete were subjected to tensile load its shows below average performance. For this reason we have to provide reinforcement in concrete. Now a day's use of steel fibre to improve mechanical properties of concrete is increased. Which is control and/or stop initial propagation of minor cracks. Fibre reinforced concrete [FRC] can resist certain amount of load under deflection [4]. The behaviour and performance of FRC varies with fibre material, its concentration, geometry, orientation and its distribution in mix [3, 18].

2 Experimental Study

Natural sand which confirming to (IS 383:2016), PPC confirming by (IS 1489:1991). Metakaolin was obtained by complete dehydroxylation of calcinations of kaolintic clay and this was taken as a fractional substitute of cement. The chemical properties of PPC and metakaolin [23] is given in Table 1.

Table 1 Physical and chemical properties of binder material

Properties	Oxides	Cement (%by mass)	Metakaolin (%by mass)
Physical properties	Surface area (m^2/kg)	310	16,800
	Specific gravity	3.15	2.5
Chemical properties	SiO_2	21.75	51.5
	Al_2O_3	5.15	40.2
	Fe_2O_3	3.23	1.23
	CaO	63.75	2.0
	Na_2O	0.33	0.12
	MgO	1.15	0.08
	K_2O	0.56	0.53
	L.O.I.	2.08	2.01
	TiO_2	–	2.27

Table 2 Characteristics of steel fibre

Shape	Diameter	Length	Aspect ratio
Hooked end	0.6 mm	50 mm	83.33

2.1 Characteristics of Steel Fibre

Steel fibre hooked end was used with aspect ratio of 83.33. The steel fibre is obtained from Shaktiman Stewols India (P) Ltd. in India. Vume fractions in percentage of steel fibres were 0.5, 1.0 and 1.5%. The properties of steel fibre are mentioned in following Table 2.

2.2 Mix Proportions

Total 21 mix series of concrete specimens were casted as per the proportions given in Table 3. Water: binder (W: B) ratio was constant for all mixes and that was 0.4. Total binder content was 372 kg/m^3 for all mixes. Only control mixes contain PPC without metakaolin (MK), but remaining all mixes was containing either metakaolin or metakaolin and steel fibre in various percentages. (% of total binder weight)

3 Test Method

The compressive strength test and flexural Strength test conforming to IS: 516-1959. The compressive strength test, cube specimens of dimensions $150 \times 150 \times 150$ mm were carried out by destructive test. Beam specimens of dimensions $100 \times 100 \times 500$ mm is used to carry out Flexural Strength (fb) test and determined by,

$$\mathrm{fb} = \frac{Pl}{bd^2} \tag{1}$$

(when a >200 mm for 150 mm specimen or >130 mm for 100 mm specimen) or

$$\mathrm{fb} = \frac{3Pl}{bd^2} \tag{2}$$

(When a <200 mm but >170 mm for 150 mm specimen or <133 mm but >110 mm for 100 mm specimen.)

Where, a is the distance, measured on the core line of the tensile side of the specimen between the line of fracture and the nearer support, b is the width in mm, d is the depth in mm, l represents supported length in mm and P is the load in KN. The

Table 3 Mix details of concrete samples

Trial Mix No.	Sample Identification	Cement (Kg/m³)	Metakaolin (Kg/m³)	Water (Kg/m³)	Steel Fibre (%)	Fine Aggregate (Kg/m³)	Coarse Aggregate (Kg/m³) 20 mm	Coarse Aggregate (Kg/m³) 10 mm	Super plasticizer (Kg/m³)
1	CM	372	0	148.8	0	672	824	538	2.42
2	MK4	357	15	148.8	0	672	824	538	2.42
3	MK8	342	30	148.8	0	672	824	538	2.42
4	MK12	327	45	148.8	0	672	824	538	2.42
5	MK16	313	59	148.8	0	672	824	538	2.42
6	MK20	298	74	148.8	0	672	824	538	2.42
7	MK4+0.5	357	15	148.8	0.5	672	824	538	2.42
8	MK4+1.0	357	15	148.8	1	672	824	538	2.42
9	MK4+1.5	357	15	148.8	1.5	672	824	538	2.42
10	MK8+0.5	342	30	148.8	0.5	672	824	538	2.42
11	MK8+1.0	342	30	148.8	1	672	824	538	2.42
12	MK8+1.5	342	30	148.8	1.5	672	824	538	2.42
13	MK12+0.5	327	45	148.8	0.5	672	824	538	2.42
14	MK12+1.0	327	45	148.8	1	672	824	538	2.42
15	MK12+1.5	327	45	148.8	1.5	672	824	538	2.42
16	MK16+0.5	313	59	148.8	0.5	672	824	538	2.42
17	MK16+1.0	313	59	148.8	1	672	824	538	2.42
18	MK16+1.5	313	59	148.8	1.5	672	824	538	2.42
19	MK20+0.5	298	74	148.8	0.5	672	824	538	2.42
20	MK20+1.0	298	74	148.8	1	672	824	538	2.42
21	MK20+1.5	298	74	148.8	1.5	672	824	538	2.42

split tensile tests were conforming to IS 5816-1999 for cylinder sample of diameter 150 and 300 mm long. The split tensile strength (T) of the specimen is given by,

$$T = \frac{2P}{\pi LD} \tag{3}$$

where, T—Split tensile strength, P–Maximum load applied (KN), L—cylinder Length (mm) and D—cylinder diameter (mm).

4 Test Results and Discussion

4.1 Compressive Strength

Variation in compressive strength of plain concrete and concrete containing metakaolin is shown Fig. 1. The compressive strength's of plain concrete was 46.60 and 49.00 MPa respectively for the age 28 and 90 days. The maximum compressive strength of 16% metakaolin concrete was 51.49 and 55.25 MPa respectively for 28 and 90 days of curing period. Variation in compressive strength of plain concrete and concrete containing metakaolin with steel fibre is shown in Fig. 2. The maximum values of compressive strength were 53.87 and 55.54 MPa for the age 28 and 90 days respectively. We observed from obtained results that; volume of SF influence the compressive strength. The incorporation of metakaolin in concrete provides significant increase and development in compressive strength [5, 7, 8, 10, 12, 13, 16, 22].
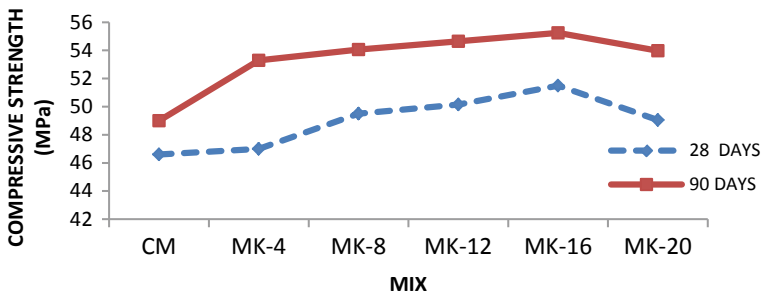
Fig. 1 Compressive strength of specimens with and without metakaolin (age −28 days and 90 days)

4.2 Split Tensile Strength on Cylinder

The effect of steel fiber on concrete was determined by the Split Tensile Strength test. The test results of split tensile strength on specimen with and without metakaolin were presented in the Fig. 3. For plain concrete split tensile strength was 2.03 and 2.25 MPa respectively for the age of 28 and 90 days. The maximum value of split tensile strength of 20% metakaolin concrete were 3.98 and 4.36 MPa respectively at the age 28 and 90 days. Variation in split tensile strength of plain concrete and concrete containing metakaolin with steel fibre is shown in Fig. 4. The maximum value of split tensile strength was 6.25 and 6.68 MPa for 28 days 90 days respectively. Another point is come under focus was that; SF shows better performance in tensile strength. And the reason behind that is distribution of steel fiber within the mix. By using small or short length steel fiber we can achieve homogenous distribution. Shorter steel fiber have a nature to stay parallel to flow direction and provide higher orientation density to mix during casting of concrete, that results concrete posses better tensile strength [11, 14, 19].
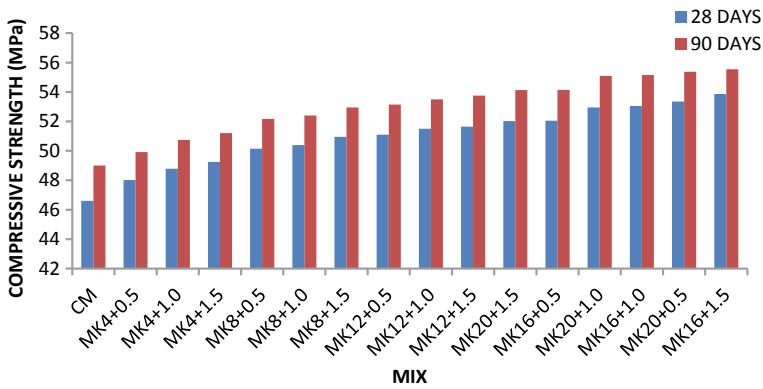
Fig. 2 Compressive strength of specimens versus replacement of metakaolin and steel fibre (age −28 days and 90 days)
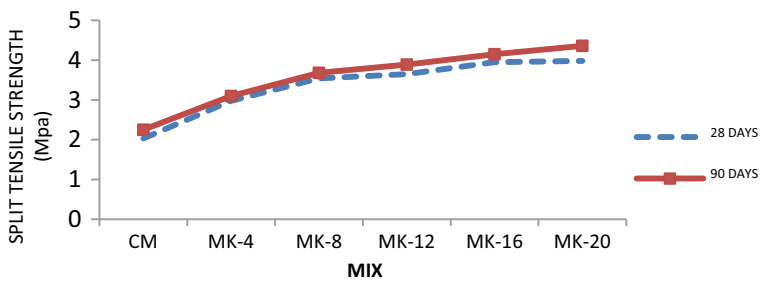
Fig. 3 Split tensile strength of specimens with and without metakaolin (age −28 and 90 days)
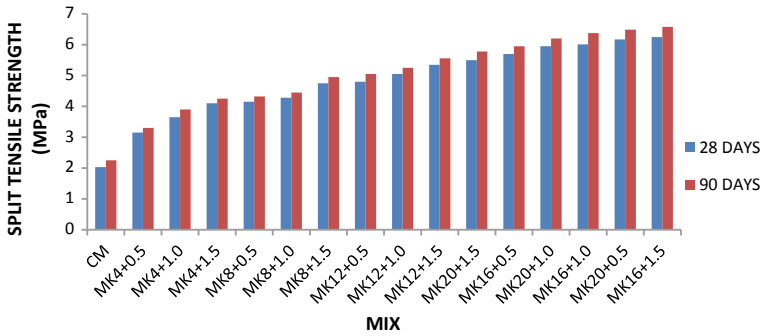
Fig. 4 Split tensile strength of specimens versus replacement of metakaolin and steel fibre (age − 28 days and 90 days)

4.3 Flexural Strength

Variation in flexural strength of plain concrete and concrete containing metakaolin is shown in Fig. 5. The flexural strength's of plain concrete was 3.43 and 3.89 MPa for thee age 28 and 90 days. The maximum flexural strength of 20% metakaolin concrete were 4.61 and 5.49 MPa respectively for the age 28 and 90 days. Variation in flexural strength of concrete containing metakaolin with steel fibre is shown in Fig. 6. The maximum values of flexural strength containing metakaolin along with steel fibre were 8.89 and 9.16 MPa respectively for 28 and 90 days.

4.4 Relations Between Mechanical Properties of Concrete

This approach is most common in researchers to analyse the results. The relationship between compressive strength and flexural strength is shown in Figs. 7 and 8 explains the relationship between compressive strength and split tensile strength. The regression equations with R^2 values were given in figure.
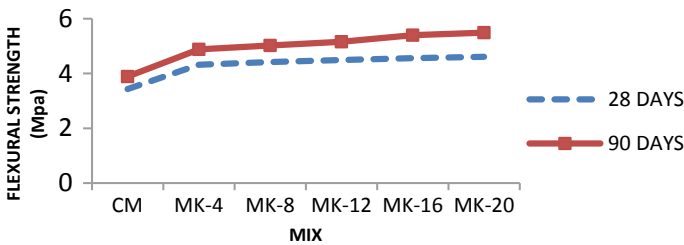
Fig. 5 Flexural strength test of specimens with and without metakaolin (age −28 and 90 days)

5   Conclusion

After the study of experimental results following conclusions may be drawn.

1. The weight density of concrete increases with increase in SF content.
2. Incorporation of metakaolin (MK) as a replacement material to cement shows improving results in mechanical properties over plain concrete. The maximum
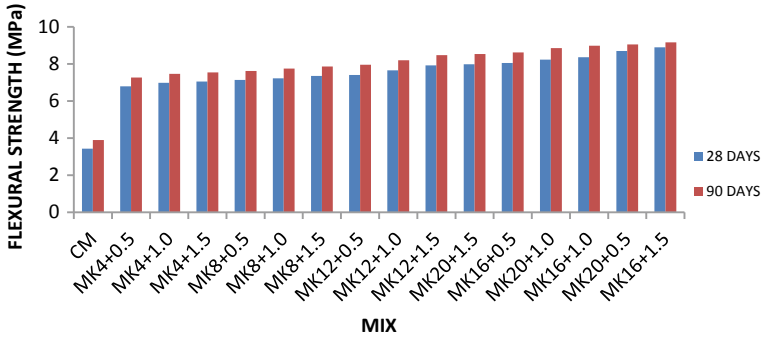
Fig. 6 Flexural strength of specimens versus replacement of metakaolin and steel fibre (age − 28 days and 90 days)
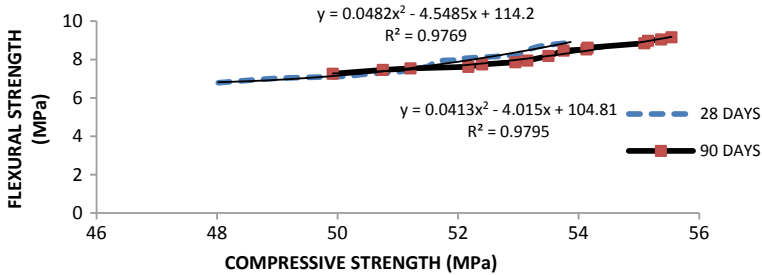
Fig. 7 Compressive strength versus flexural strength
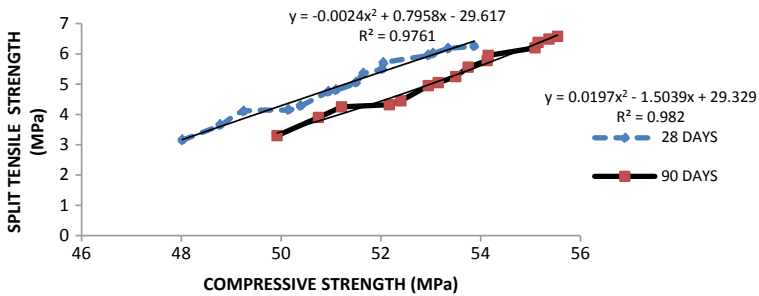
Fig. 8 Compressive strength versus split tensile strength

value of compressive strength was observed as 51.49 and 55.25 MPa for the age 28 and 90 days respectively for 16% metakaolin replacement. Along with steel fibre left foot prints in the form of increase in compressive strength. SF provides more compressive strength. It shows 53.87 and 55.54 MPa compressive strength of concrete with steel fibre for the age 28 and 90 days respectively. Over all, compressive strength was improved by incorporation of MK and steel fibre over plain concrete.

3. Due to SF considerable improvement was observed in split tensile strength as well as flexural strength of concrete. Split tensile strength of concrete was increasing continuously as per addition of steel fibre. This behaviour of steel fibre on split tensile and flexural strength was mainly due to its orientation and distribution in concrete mix.

4. The water content was increased as increase in percentage of MK. So that admixture was added to achieve workability.

5. From regression equations we say that, steel fibre and metakaolin contributes to enhance the mechanical properties of concrete.

References

1. Asbridge, A.H., Page, C.L., Page, M.M.: Effects of metakaolin, water/binder ratio and interfacial transition zones on the microhardness of cement mortars. Cem. Concr. Res. **32**(9), 13659 (2002)
2. Badogiannis, E., Tsivilis, S.: Exploitation of poor greek kaolins: durability of metakaolin concrete. Cem. Concr. Compos. **31**(2), 128–133 (2009)
3. Banthia, N., Trottier, J.F.: Concrete reinforced with deformed steel fibres Part II: Toughness characterization. ACI Mater. J. **92**(2), 146–154 (1995)
4. Barros, J.A.O., Cruz, J.S.: Fracture energy of steel fiber-reinforced concrete. Mech. Compos. Mater. Struct. **8**(1), 29–45 (2001)
5. Brooks, J.J., Johari, M.M.A.: Effect of metakaolin on creep and shrinkage of concrete. Cem. Concr. Compos. **23**(6), 495–502 (2001)
6. Changling, H., Osbaeck, B., Makovicky, E.: Pozzolanic reaction of six principal clay minerals: activation reactivity assessments and technological effects. Cem. Concr. Res. **25**(8), 1691–1702 (1995)
7. Coleman, N.J., Page, C.L.: Aspects of the pore solution chemistry of hydrated cement pastes containing MK. Cem. Concr. Res. **27**(1), 147–154 (1997)
8. Courard, L., Darimont, A., Schouterden, M., Ferauche, F., Willem, X., Degeimbre, R.: Durability of mortars modified with metakaolin. Cem. Concr. Res. **33**(9), 1473–1479 (2003)
9. Curcio, F., DeAngelis, B.A.: Dilatant behavior of superplasticized cement pastes containing metakaolin. Cem. Concr. Res. **28**(5), 629–634 (1998)
10. Ding, J.T., Li, Z.: Effects of metakaolin and silica fume on properties of concretes. ACI Mater. J. **99**, 393–398 (2002)
11. Guneyisi, E., Gesoglu, M., et al.: Combined effect of steel fiber and metakaoline incorporation on mechanical properties of concrete. (Elsevier) composites: Part B **56**(2014), 83–9 (2013)
12. Gruber, K.A., Ramlochan, T., Boddy, A., Hooton, R.D., Thomas, M.D.A.: Increasing concrete durability with high-reactivity metakaolin. Cem. Concr. Compos. **23**(6), 479–484 (2001)

13. Khatib, J.M., Wild, S.: Pore size distribution of metakaolin paste. Cem. Concr. Res. **26**, 1545–1553 (1996)
14. Khayat, K.H., Roussel, Y.: Testing and performance of fiber reinforced, self consolidating concrete. Mater. Struct. **33**, 391–397 (2000)
15. Klimesch, D.S., Ray, A.: Use of the second-derivative differential thermal curve in the evaluation of cement–quartz pastes with metakaolin addition autoclaved at 180_C. Thermochim. Acta **307**(2), 167–176 (1997)
16. Klimesch, D.S., Ray, A.: Autoclaved cement–quartz pastes with metakaolin additions. Adv. Cem. Based Mater. **7**(3), 109–118 (1998)
17. Li, Z., Ding, Z.: Property improvement of Portland cement by incorporating with metakaolin and slag. Cem. Concr. Res. **33**(40), 579–584 (2003)
18. Nili, M., Afroughsabet, V.: Property assessment of steel–fibre reinforced concrete made with silica fume. Constr. Build. Mater. **28**, 664–669 (2012)
19. Quian, C.X., Stroeven, P.: Development of hybrid polypropylene–steel fibre reinforced concrete. Cem. Concr. Res. **30**, 63–69 (2000)
20. Sabir, B.B., Wild, S., Bai, J.: Metakaolin and cacined clays as Pozzolans for concrete: a review. Cem. Concr. Compos. **23**(6), 441–454 (2001)
21. Wild, S., Khabit, J.M., Jones, A.: Relative strength pozzolanic activity and cement hydration in uperplasticised metakaolin concrete. Cem. Concr. Res. **26**(10), 153744 (1996)
22. Yurtseven, AE.: Determination of mechanical properties of hybrid fibereinforced concrete. M.Sc. thesis, METU, Ankara, Turkey (2004)
23. Zhang, M.H., Malhotra, V.M.: Characteristics of a thermally activated aluminosilicate pozzolanic material and its use in concrete. Cem. Concr. Res. **25**(8), 1713–1725 (1995)

Progressive Collapse Analysis of Composite Structure

Dhiraj Agrawal, Abhishek Gulhane and M. D. Goel

Abstract In the past few decades, effect of natural hazards such as earthquake, wind etc. on existing structures has attracted the attention of designers. Progressive collapse is nothing but a condition of indigenous failure of prime structural element which in turn leads to the collapse of connecting members and then it leads to the additional collapse. For the case of progressive collapse, damage is included in the model through the elimination of important structural component like column. The progressive collapse design guidelines primarily suggest the simplified analysis actions occurred due to the sudden removal of specific columns in a building. The study of analytical approaches for evaluating progressive collapse is carried out by linear static analysis using Alternate Path Method (APM) recommended in General Service Administration (GSA) guidelines and the same is presented in this study. This study involves the use of various general methods of progressive collapse design & evaluation based on numerical mock up and experimental information. For this study, a multistoried composite building (i.e. G+7) is considered. The prime objective of this study is to analyze the composite building by removing columns at different locations and finding out critical location of column vulnerable to progressive collapse and also prevention of progressive collapse of structure using linear static analysis. Location of removed column, Number of floors, vertical irregularity were studied and their influence was also carried out in this research.

Keywords Progressive collpase · Composite building · Displacement

D. Agrawal (✉) · A. Gulhane
Department of Civil Engineering, Yeshwantrao Chavan College of Engineering, Nagpur 441 110, India
e-mail: erdhiraj007@gmail.com

M. D. Goel
Department of Applied Mechanics, Visvesvaraya National Institute of Technology (VNIT), Nagpur 440 010, India

1 Introduction

Structural engineers are in front of various new innovations in designing safe structure due to an increase in the radical actions conceded on landmark buildings which has the prospective to cause great destruction, damage and menace to people. Progressive collapse analysis was carried out first time in 1968 after the fractional collapse of Ronan point apartment building in London, U.K. [1]. Design for mitigation of progressive collapse has always been a challenge in structural engineering due to a heightened awareness of blast and terrorist hazards. The output of the above research was reflected in terms of inclusion of distinct provisions in U. K. standards [1]. Many alternatives and suggestions have been proposed by numerous structural engineers and blast experts, and with continued research more alternatives are to be expected in the near future. Later in year 1995, unequal failure of Alfred P. Murrah Federal Building in Oklahoma City and entire collapse of towers of world trade centre in 2001, which were caused by terrorist attacks, generated interest among the engineering community in advanced research approaches related to progressive collapse analysis [2–8]. However, phenomenon of progressive collapse is becoming more recognized in the field of structural engineering with the advancement of research investigation in this area. It is to be noted that progressive collapse is the phenomenon of collapse of entire structure or large part of structure is get affected by failure or failure of small part of the structure.

Several authorities and various bodies have tried to develop the preventive measures against progressive collapse. Amid these efforts to create guidelines U.S. General Service Administration (GSA) and Department of Defence (DoD) by United Facilities Criteria (UFC)—New York, have given the thorough process related to various resisting methods of Progressive Collapse of Structures [1]. The competence aimed at progressive collapse is downcast in three autonomous stages based on the ductility demand, strength, and supply in the critical regions of affected structural members. A noteworthy benefit of established path of action is that, it can categorically account for dynamic effects related to the sudden removal of column through a simplified energy equivalence approach and hence it evades the requirement of nonlinear dynamic analysis. In progressive collapse mechanism, a solitary indigenous failure may lead to the significant deformation which in turn lead to the complete failure of the structure. Thus, progressive collapse is catastrophic structural phenomenon, that can occur because of accidents, human made blasts, natural hazards. The challenge exists in making decisions about the best solutions because of the inherent uniqueness that are to be encountered for each project. Also, there is little to no official design standards or guidelines available for engineers to follow to aide their decisions. Instead, the engineer must be well versed in blast resistance and progressive collapse research in order to have a good understanding of what it takes to build or retrofit a robust structure [1].

2 General Service Administration Guideline

General Services Administration (GSA) is a sovereign firm of US government, This body is formed in 1949 to assist & to provide the preliminary functioning of federal buildings [1].

2.1 Guidelines of GSA

GSA guidelines suggested that, risk aimed at progressive collapse of a building is determined seeing the instantaneous removal of first-storey columns situated at four different zones [1]:

Case C1—Removal of exterior column situated at middle of the short side.
Case C2—Removal of exterior column situated at middle of the long side.
Case C3—Removal of corner Column.
Case C4—Removal of interior column.

{These four cases are standard cases defined by the GSA guidelines; plan taken in this paper is square plan so long & short sides are same.}.

2.2 GSA Criteria

The Demand Capacity Ratio (DCR) of each primary and secondary member of the alternate path structure is calculated from the following equation [1]:

$$DCR = Q_{UD}/Q_{CE}$$

where,

Q_{UD} Acting force determined in the structural element.
Q_{CE} Expected ultimate, un-factored capacity of the structural element.

In order to prevent collapse of alternate path structure, DCR values for each structural element must be less than or equal to the following:

DCR ≤ 2.0 for symmetrical structure.
DCR ≤ 1.5 for unsymmetrical structure.

3   Methodology

In this section, progressive collapse analysis of a composite building (steel beam, steel column and RCC slab) of G+7 floors is carried out. The proposed building plan and structural elevation is as shown in Figs. 1 and 2, respectively. The beam sizes offered are ISMB 300 & column sizes are ISMB 600. B1, B2, B3, B4, B5, B6, and B7 are beams connected with column C1, C2, C3 & C4. The building is analyzed and designed in STAAD-PRO®, software. A basic model of G+7 storey is designed and analyzed for no loading (no external loads are applied) condition. After this analysis of basic model is completed, same model is subjected to earthquake loads (lateral loads) and analyzed. The model is then subjected to wind loading wherein, behavior of the structure under wind effects is studied. The load combination are applied by referring to IS 800:2007 for limit state of strength and limit state of serviceability. Progressive collapse analysis by linear statics is carried out as per General Service Administration (GSA) guidelines. Then, by referring to GSA guidelines, columns are removed one at one time and static linear analysis is carried out [1]. Here, three cases of column removal (corner column, side column, interior column) are studied. After columns are removed according to the three cases, reactions developed and the maximum bending moment occurred in the members are computed. Displacement of the members in structure is also premeditated. A comparative study of all the results is carried out wherein, most critical members of the structure are obtained. DCR ratios are evaluated for critical sections in the line of column removal. After complete analysis of the structure for all the three cases is completed and results are obtained and respective plots for the obtained results are out.

Model 1: General model (Fig. 2)
Model 2: Corner Column Removal model (Fig. 3)
Model 3: Interior column removal model (Fig. 4)

Fig. 1 Plan of the building considered in the present study
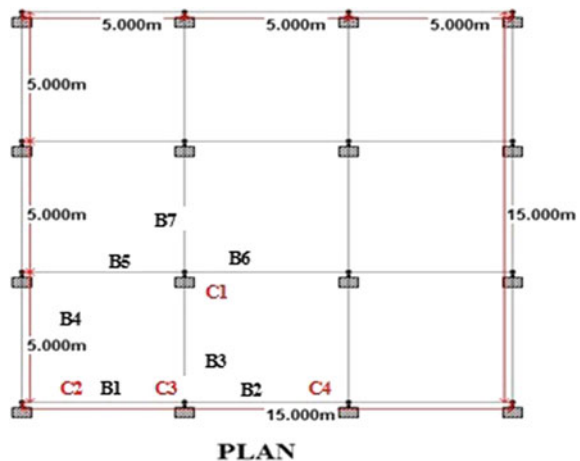
Fig. 2 Structural elevation of the building considered in the present study (Model 1)
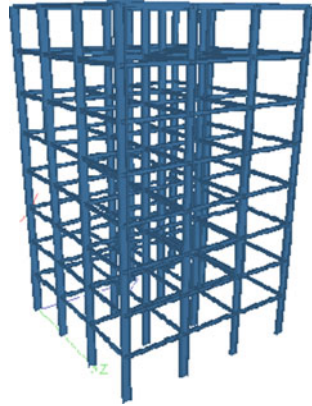
Fig. 3 Corner column removal model (Model 2)
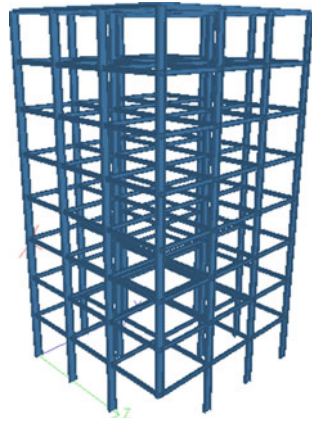
Fig. 4 Interior column removal model (Model 3)
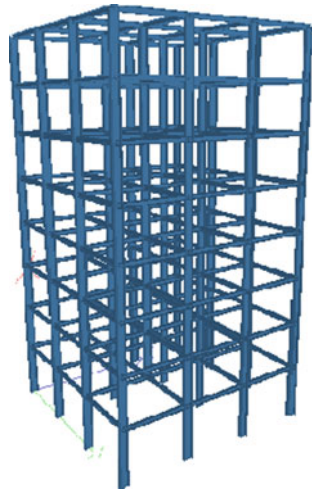
Fig. 5 Side column removal model (Model 4)
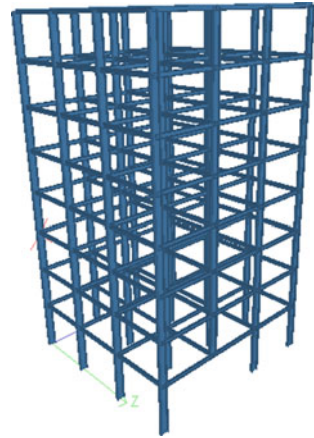
Model 4: Side column removal model (Fig. 5).

4 Results and Discussions

A model of G+7 story composite structure is analysed and designed by using STAAD-PRO® software. Then, by following GSA guidelines linear static analysis is carried out and condition of three cases of column removal are applied. In corner column removal model, load of removed column is transferred to the adjacent column and maximum bending moment is observed to occur in beam B1 and B4. In the side column removal model, load of removed column is transferred in the adjacent column in the vicinity of that column and the maximum bending moments is observed in beams B1, B2 and B3. When interior column is removed, load is balanced by adjacent column and the maximum bending moment is observed to occur in beams B3, B5, B6, and B7. Then dividing bending moments by the respective capacity of beam, DCR values for the beams are computed. The reactions and displacements are also computed. A comparative study is carried out between the three cases of column removal and accordingly the results are reported (Tables 1, 2, 3, 4, 5, 6, 7, 8, 9 and 10).

Figures 6, 7, 8, 9, 10, 11 and 12 shows the bending moment for beams B1, B2, B3, B4, B5, B6 and B7 under earthquake loading, respectively.

Figures 13, 14, 15, 16, 17, 18 and 19 shows the DCR for beams B1, B2, B3, B4, B5, B6 and B7 under earthquake loading, respectively.

Figure 20 shows the displacement for all the models considered in the present study. It shows that model 2 has maximum displacement amongst all the models considered in the present study (Fig. 21).

Table 1 Bending moments (kN-m) for general model (Model 1) under earthquake loading

	Basic model						
Story	B1	B2	B3	B4	B5	B6	B7
7	171.57	169.75	125.04	111.89	186.14	188.53	127.16
6	212.31	216.45	221.57	211.62	227.53	232.77	191.73
5	266.05	267.73	326.25	312.88	280.81	288.17	251.23
4	312.33	312.44	402.19	387.97	330.64	335.83	299.09
3	343.32	341.94	453.42	439.71	363.70	366.62	330.48
2	352.89	350.23	485.17	472.69	373.65	374.38	348.34
1	331.33	327.88	501.57	490.54	350.23	349.09	358.47
GF	257.54	254.09	531.23	520.26	270.73	268.34	350.94

Table 2 Bending moments (kN-m) for corner column removal model (Model 2) under earthquake loading

	Corner column removed						
Story	B1	B2	B3	B4	B5	B6	B7
7	459.12	329.88	128.36	297.09	190.81	213.25	142.20
6	489.27	358.36	222.78	349.47	237.19	260.76	212.55
5	504.55	391.13	332.58	369.25	295.54	319.35	270.92
4	522.37	424.88	411.93	422.32	351.56	371.71	319.75
3	542.69	451.58	466.15	459.81	389.59	405.51	351.34
2	567.65	458.73	501.01	484.92	402.56	413.81	368.96
1	597.93	440.80	520.93	501.00	378.95	385.34	378.77
GF	637.37	346.87	556.56	482.83	293.35	294.96	370.24

Table 3 Bending moments (kN-m) for interior column removal model (Model 3) under earthquake loading

	Interior column removed						
Story	B1	B2	B3	B4	B5	B6	B7
7	180.88	178.07	169.08	101.48	405.23	404.67	272.95
6	219.46	221.70	331.27	214.80	461.73	458.48	369.18
5	272.22	273.03	410.84	315.98	510.61	504.75	420.34
4	318.66	317.82	473.11	391.51	554.32	548.30	461.67
3	349.73	347.33	514.41	444.28	587.28	581.04	490.80
2	359.15	355.47	540.23	479.31	604.99	598.98	509.63
1	336.96	332.60	545.83	500.79	600.52	595.83	526.48
GF	261.62	257.48	601.66	537.52	560.25	555.66	499.83

Table 4 Bending moments (kN-m) for side column removal model (Model 4) under earthquake loading

	Side column removed						
Story	B1	B2	B3	B4	B5	B6	B7
7	427.21	422.23	233.52	114.45	195.86	197.82	234.70
6	482.41	474.40	289.02	212.89	237.78	239.49	298.37
5	527.23	517.44	360.31	317.71	287.55	294.50	346.46
4	567.70	558.89	412.82	395.45	337.29	342.11	383.63
3	598.53	590.70	448.65	449.76	370.15	372.77	409.35
2	615.24	608.79	471.17	485.65	379.69	380.19	427.70
1	611.07	606.94	484.14	507.10	355.45	354.17	430.84
GF	572.91	569.40	462.95	543.20	274.36	271.90	493.80

Table 5 DCR values for general model (Model 1) under earthquake loading

	Basic model						
Story	B1	B2	B3	B4	B5	B6	B7
7	0.79	0.79	0.58	0.52	0.86	0.87	0.59
6	0.98	1.00	1.03	0.98	1.05	1.08	0.89
5	1.23	1.24	1.51	1.45	1.30	1.33	1.16
4	1.45	1.45	1.86	1.80	1.53	1.56	1.39
3	1.59	1.58	2.10	2.04	1.68	1.70	1.53
2	1.63	1.62	2.25	2.19	1.73	1.73	1.61
1	1.53	1.52	2.32	2.27	1.62	1.62	1.66
GF	1.19	1.18	2.46	2.41	1.25	1.24	1.63

Table 6 DCR values for corner column removal model (Model 2) under earthquake loading

	Corner column removed						
Story	B1	B2	B3	B4	B5	B6	B7
7	2.13	1.53	0.59	1.38	0.88	0.99	0.66
6	2.27	1.66	1.03	1.62	1.10	1.21	0.98
5	2.34	1.81	1.54	1.71	1.37	1.48	1.25
4	2.42	1.97	1.91	1.96	1.63	1.72	1.48
3	2.51	2.09	2.16	2.13	1.80	1.88	1.63
2	2.63	2.12	2.32	2.25	1.86	1.92	1.71
1	2.77	2.04	2.41	2.32	1.76	1.78	1.75
GF	2.95	1.61	2.58	2.24	1.36	1.37	1.72

Table 7 DCR values for interior column removal model (Model 3) under earthquake loading

	Interior column removed						
Story	B1	B2	B3	B4	B5	B6	B7
7	0.84	0.82	0.78	0.47	1.88	1.87	1.26
6	1.02	1.03	1.53	0.99	2.14	2.12	1.71
5	1.26	1.26	1.90	1.46	2.37	2.34	1.95
4	1.48	1.47	2.19	1.81	2.57	2.54	2.14
3	1.62	1.61	2.38	2.06	2.72	2.69	2.27
2	1.66	1.65	2.50	2.22	2.80	2.77	2.36
1	1.56	1.54	2.53	2.32	2.78	2.76	2.44
GF	1.21	1.19	2.79	2.49	2.60	2.57	2.32

Table 8 DCR values for side column removal model (Model 4) under earthquake loading

	Side column removed						
Story	B1	B2	B3	B4	B5	B6	B7
7	1.98	1.96	1.08	0.53	0.91	0.92	1.09
6	2.23	2.20	1.34	0.99	1.10	1.11	1.38
5	2.44	2.40	1.67	1.47	1.33	1.36	1.60
4	2.63	2.59	1.91	1.83	1.56	1.58	1.78
3	2.77	2.74	2.08	2.08	1.71	1.73	1.90
2	2.85	2.82	2.18	2.25	1.76	1.76	1.98
1	2.83	2.81	2.24	2.35	1.65	1.64	2.00
GF	2.65	2.64	2.14	2.52	1.27	1.26	2.29

Table 9 Displacement values for different models

Zone V				
Floor level	Absolute displacement due to earthquake load (mm)			
	Model 1	Model 2	Model 3	Model 4
7	1244.38	1361.84	1276.10	1329.33
6	1186.23	1277.99	1216.29	1256.93
5	1081.72	1157.17	1111.75	1142.23
4	942.26	1006.87	973.23	995.05
3	778.58	836.27	811.80	825.65
2	599.48	653.51	636.80	642.87
1	411.84	466.25	456.32	454.04
GF	219.29	286.38	273.85	268.52

Table 10 Reactions developed after and before lateral forces

Column removed	Adjacent column	Reaction before column remove (kN)	Reaction after column removal (kN)
13	9	3114.74	4415.813
13	14	3135.26	5112.99
10	6	3499.8	4349.76
10	9	3114.74	4023.28
10	11	3499.85	4431.78
10	14	3135.26	3557.04
14	13	2544.83	3798.63
14	15	3135.26	4359.29
14	10	3499.846	4171.58

Fig. 6 Bending moment comparison of beam B1 for earthquake loading
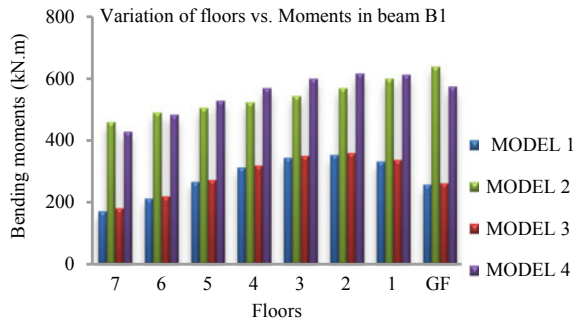
Fig. 7 Bending moment comparison of beam B2 for earthquake loading
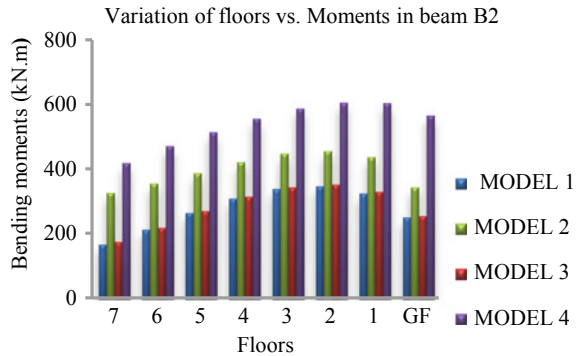
Fig. 8 Bending moment comparison of beam B3 for earthquake loading

Variation of floors vs. Moments in beam B3
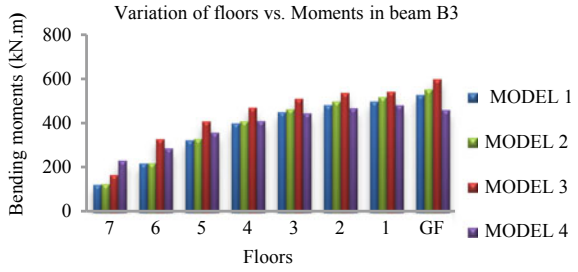
Fig. 9 Bending moment comparison of beam B4 for earthquake loading

Variation of floors Vs Moments in beam B4
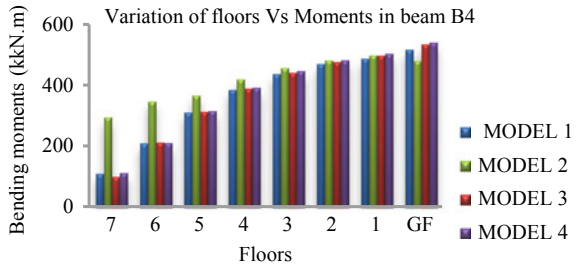
Fig. 10 Bending moment comparison of beam B5 for earthquake loading

Variation of floors vs. Moments in beam B5
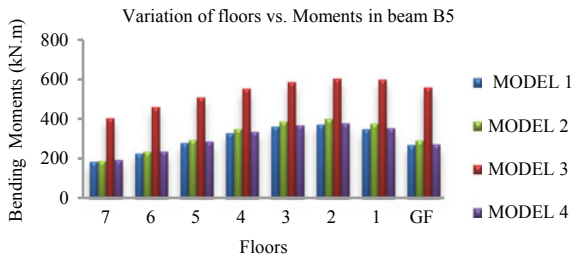
Fig. 11 Bending moment comparison of beam B6 for earthquake loading

Variation of floors vs. Moments in beam B6
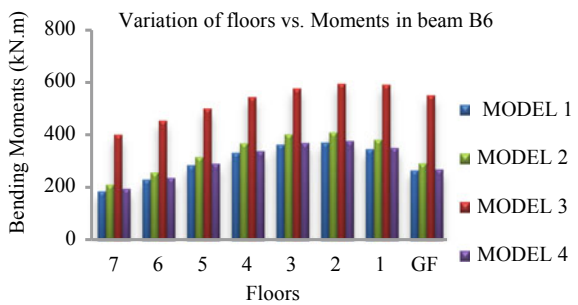
Fig. 12 Bending moment comparison of beam B7 for earthquake loading
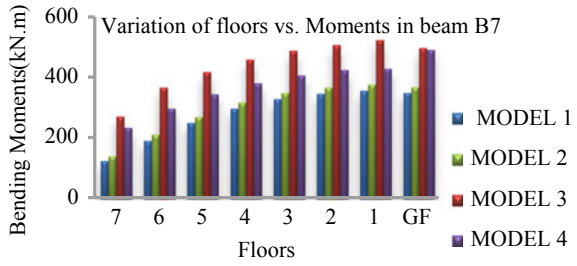
Fig. 13 DCR ratio comparison of different models of beam B1 forearthquake loading
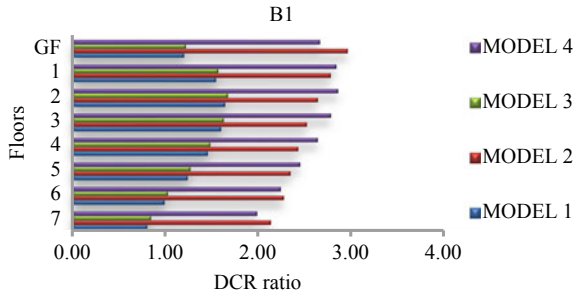
Fig. 14 DCR ratio comparison of different models of beam B2 forearthquake loading
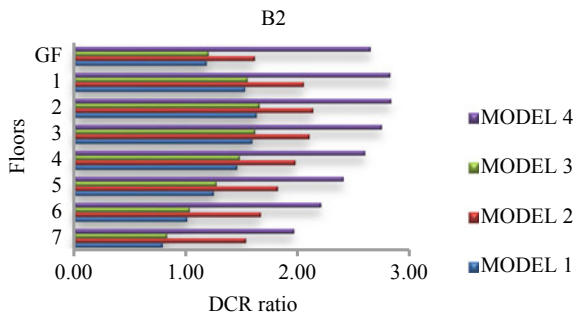
Fig. 15 DCR ratio comparison of different models of beam B3 forearthquake loading
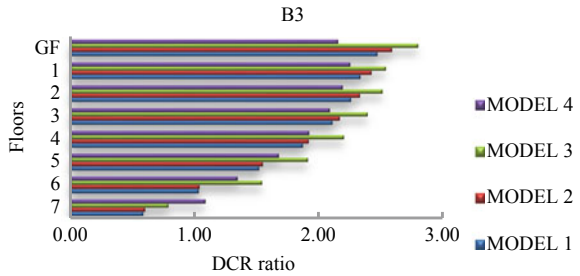
Fig. 16 DCR ratio comparison of different models of beam B4 forearthquake loading
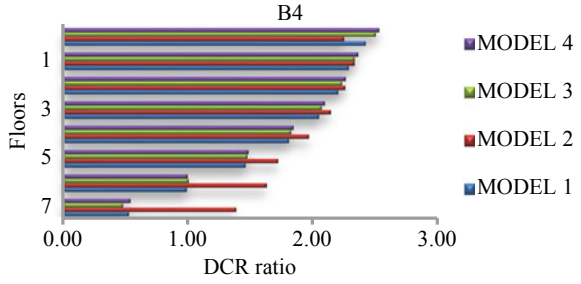
Fig. 17 DCR ratio comparison of different models of beam B5 forearthquake loading
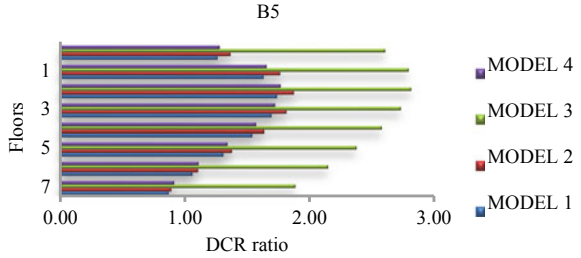
Fig. 18 DCR ratio comparison of different models of beam B6 forearthquake loading
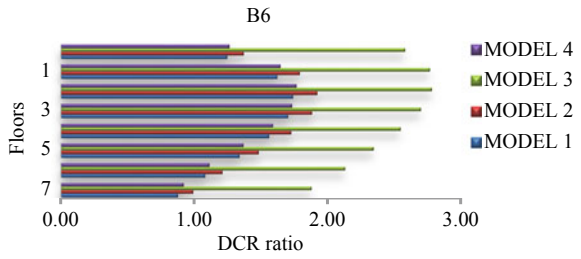
Fig. 19 DCR ratio comparison of different models of beam B7 forearthquake loading
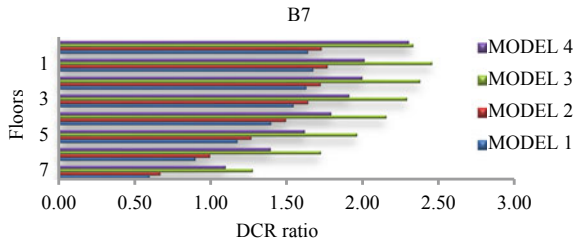
Fig. 20 Comparison of displacement for different model
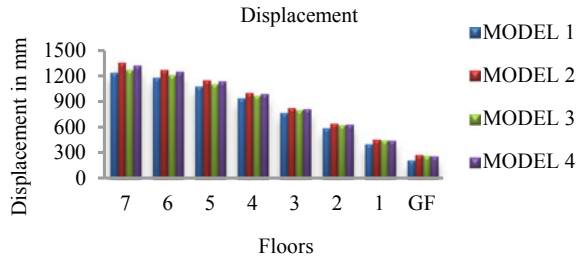
Fig. 21 Comparison of displacement of beam for different model
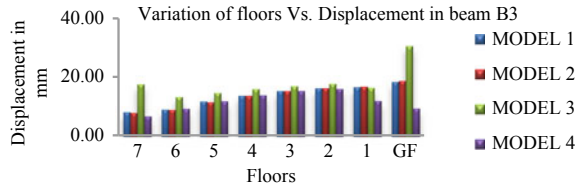
5 Conclusions

Grounded on this study and analysis, following conclusions are drawn,

1. By linear static method it is found that, lower storey beams are critical than upper storey beams in column loss scenario.
2. By linear static analysis, it is observed that the beam having DCR ratio for bending moment more than 2 will fail under sudden column loss condition. Hence, these beams need to be redesigned to arrest progressive collapse.
3. From the 3 cases of column removal, interior column loss is the most damaging.
4. A considerable difference is observed in the forces and bending moments from the initial condition (when no column is removed) due to the transfer of instantaneously applied load to the remaining undamaged structure as well as joints.
5. The nearest member of the removed column gets more affected due to transferring of load and it goes on decreasing when moving away from the removed column.
6. The alternate load path like providing bracing at floor level and increasing the size of members at outer face can be adopted advantageously to mitigate the progressive collapse.
7. Ground floor beams have maximum bending moment values as compared to the upper stories.
8. Interior column removal case develops maximum moments as compared to side and corner column removal cases.
9. Ground floor beams have maximum demand capacity ratio values as compared to upper stories.
10. CR values generated on beam in case of internal column removal are much higher than side and corner column removal.

11. Absolute displacement is maximum in case of corner column removal as compared to other in earthquake case.
12. In earthquake load case, beam B3 is connected to internal column and side column, DCR value obtained is maximum when internal column is removed.
13. In earthquake load case, beam B1 is connected to corner column and side column, DCR value obtained is maximum at GF due to corner column removal but on other floors the DCR values is maximum due to side column.
14. The reaction developed after removal of column is maximum when corner column is removed.
15. It is seen that, when interior column is removed maximum bending moment was occurred in the beams in comparison with removal of side & corner column. Due to this buckling of beams is occurred and it is maximum.

References

1. Bilow, D.N., Kamara, M.: U.S. General services administration progressive collapse design guidelines applied to concrete moment-resisting frame buildings. Structures Congress, Nashville, Tennessee, USA (2004)
2. Kim, J., Kim, T.: Assessment of progressive collapse-resisting capacity of steel moment frames. J. Constr. Steel Res. **65**(1), 169–179 (2009)
3. Fu, F.: 3-D Nonlinear dynamic progressive collapse analysis of multi-storey steel composite frame buildings. Eng. Struct. **32**(12), 3974–3980 (2010)
4. Alashker, Y., El-Tawil, S., Sadek, F.: Progressive collapse resistance of steel-concrete composite floor. J. Struct. Eng. **136**(10) (2010)
5. Sadek, F., Main, J.A., Lew, H.S., Bao, Y.: Testing and analysis of steel and concrete beam-column assemblies under a column removal scenario. J. Struct. Eng. **137**(9) (2011)
6. Song, B.I., Sezen, H.: Experimental and analytical progressive collapse assessment of a steel frame building. Eng. Struct. **56**, 664–672 (2013)
7. Gerasimidis, S.: Analytical assessment of steel frames progressive collapse vulnerability to corner column loss. J. Constr. Steel Res. **95**, 1–9 (2014)
8. Bandyopadhyay, M., Banik, A.K., Datta, T.K.: Progressive collapse of three-dimensional semi-rigid jointed steel frame. J. Perform. Constructed Facil. **30**(3) (2016)

Effect of Mineral and Chemical Admixture for Improvement of High-Performance Concrete

Bhalchandra V. Khode and Sujesh D. Ghodmare

Abstract Concrete is most versatile and widely used construction material. It has ability to mould when it is fresh. It also shows remarkable strength and durability when it is hard. It is the material with large synthesis with capita consumption of 1.5 tonnes per annum as far as India is concern. OPC concrete which is designed only considering the compressive strength parameter does not meet other functional requirements. It shows adverse results in aggressive environments in terms of energy adsorption capacity during repair and retrofitting works. It results in need to design HPC with superior performance. HPC mixtures consists of the similar material components to conventional concrete, but with the proportions specifically designed for providing the strength and durability required in terms of structural and environmental requirements for the project. Use of supplementary cementing material of specific mineral origin usually plays an important role resulting in HPC. They can be used for various purposes depending on their properties and requirements. Chemical composition of mineral admixtures used with very low water cement ratio plays the vital role in enhancing properties of concrete. The use of supplementary cementing materials to produce HPC improves the strength and durability of concrete and at the same time help to dispose the industrial by-product (waste) reducing the alarming environmental threats. This paper described the study carried out to check the use and suitability of marble and porcelain waste powders through strength activity test along with analysis of role of their chemical composition to produced HPC.

Keywords HPC · Mineral admixture · Durability · Marble powder · Porcelain powder super plasticizer

B. V. Khode (✉) · S. D. Ghodmare
Department of Civil Engineering, G. H. Raisoni College of Engineering, Nagpur, India
e-mail: bhalchandra.khode@raisoni.net

S. D. Ghodmare
e-mail: Sujesh.ghodmare@raisoni.net

Abbreviation

Al_2SO_4	Aluminium sulphate
C	Compressive strength
C_3S	Tricalcium silicate
C_2S	Dicalcium silicate
$Ca(OH)_2$	Calcium hydroxide
$CaCl_2$	Calcium chloride
D	No. of days
HPC	High-performance concrete
$MgSO_4$	Magnesium sulphates
MP	Marble powder
Na_2SO_4	Sodium sulphates
Nacl	Sodium chloride
PCC	Portland cement concrete
PP	Porcelain powder
SF	Silica flume
SiO_2	Silicon dioxide
W/C	Water cement ratio

1 Introduction

About 25 billion tones concrete globally has made tremendous strides in past. Concrete is no longer a material consisting of only cement, aggregates, water and admixtures. It is an engineered material nowadays with number of new constituents depending on specific requirements and the conditions with specific exposure in which it is used. Many improvements occurred in strength of concrete due to changes in constituent materials since 1950. For obtaining higher strengths in concrete, super plasticizers and other high water reducing agents (HWRA) with w/c ratio of about 0.25 were adopted as the new technology considering correlation between the w/c ratio, strength of cement and concrete. It is not possible to produce HPC exceeding the strength of 100 MPa by reducing the w/c ratio. This results into interdiction of mineral admixtures of high surface area and chemical admixtures in concrete when tested. In order to provide the quantitative information required for making sound decisions pertaining to the selection of mineral and chemical admixture in combination with Portland cement. This requires the more effective utilization of supplementary materials and or cement, enhancing the life cycle performance. This is also helpful in reducing the cost of the structure. In this paper, it is tried to develop HPC of above M70 grade using supplementary cementing materials basically procured from industrial and other wastes. It is also tried to investigate the strength and durability aspect of HPC-M70 grade and to establish the influence of the used mineral and chemical admixtures on their properties. Kjellsen et al. [1] studied the

effective strength of performance concrete to produce M140 grade concrete using W/B ratio from 0.25 to 0.4. The 10% cement was also replaced with silica flume. Kjellsen et al. [1] evaluate the parameters like compressive strength, tensile strength, flexural strength, modulus of elasticity and fracture energy of HPC mixes with 10% of silica fumes. Zain and Radin [2] studied properties like compressive strength and Modulus of Elasticity of HPC with SF, CGBSF, FA and Portland cement using W/B = 0.25. Erdem and Kirca [3] proposed concrete using binary systems, incorporated with SF 5, 10 and 15% by mass and ternary mixes. They used FA 10, 20 30 and 40% by mass of total binder content. Malagavelli and Rao [4] tested the compressive strength and tensile strength of M30 grade HPC by replacing cement with ground granulated blast furnace slag (0, 40, 50, 60%), and sand replaced with Crusher dust. Muthupriya et al. [5]) evaluated the compressive strength of HPC of M60 grade with various replacement levels of SF and FA. Ravel et al. [6] replaced ceramic waste up to 50% by weight of cement and compared strength with conventional strength achieved up to 30% replacement of cement without effecting properties of fresh and hardened concrete. Pacheco et al. [7] examined the feasibility of using ceramic waste in M25 grade HPC and observed that 20% replacement of cement give a minor strength but durability and performance increases of concrete. Chandana et al. [8] prepared M30 grade HPC with 20% cement replacement with ceramic powder. When tested, strength and durability results reflected that concrete with partial replacement cement with ceramic powder had lost a minor strength but increased durability performance. In this paper, the experiments were conducted replacing cement with porcelain and marble powder by 5, 10, 15 and 20%. To enhance on strength and durability aspect of HPC-M70 grade made from waste based supplementary cementing material and establish the influence of mineral admixtures and chemical admixtures on different properties.

2   Porcelain and Marble Powder

Marble is being commonly used as the building material since long times. The industry disposal of the marble powder which is a very fine powder is the notified environmental problems all around the word. At many places, this marble dust is settled using sedimentation and then dumped in different areas resulting in environmental pollution. It is also threatening for both agriculture field and public health. Therefore, if this marble dust originating from various industrial sectors like construction, glass, paper, etc., is used properly, it may help to protect the environment. Marble dust effectively used either to produce new products as well as an admixture as the natural sources avoiding dumpsites of marble waste. Ceramic materials are usually nonmetallic and inorganic which are the primary compounds of oxygen. It is also the compounds like carbon, nitrogen and silicon. Ceramic products are used for preparing the artistic objects and tableware but it also commonly used for various industrial and technical items which includes sewer pipe and electrical insulators. Tables 1 and 2 show chemical and physical characteristics of both waste powders. The chemical

Table 1 Chemical characteristics of marble powder and porcelain powder

Characteristics	Marble powder(MP)	Porcelain powder(PP)
$Fe_2O_3 + AL_2O_3 + SiO_2$	76.9	90.52
MgO	1.7	1.02
SO_3	1.2	0.06
Na_2O	1.4	2.31
CaO	0.32	1.87
K_2O	0.05	2.23
LOI	2.9	0.48

Table 2 Physical characteristics of marble and porcelain powder

Characteristics	Marble powder (MP)	Porcelain powder (PP)
Specific gravity of MP and PP	2.5	2.1
Water absorption of MP and PP	0.8	0.3
Specific surface area (m^2/kg)	535	528
Particles retained on 75 micron IS Sieve	1.23	1.41

composition of porcelain and marble powder varies considerably, depending on the source and technique. These powders contain silica, alumina, iron oxides and different oxides and alkalis. Other characteristics of marble and porcelain powder also affect its reactivity, such as fineness and crystallizes the structure.

3 Experimental Procedure

The experimentation was started by cement mixture containing ordinary Portland cement and at least one supplementary cementing material called as binary blended cement. It is used to improve workability and reduce the cost. The mix proportion shown in Table 3 was made for the concrete with slump 140 mm and the M70 grade of concrete. The replacement of cement with porcelain and marble powder by 5, 10, 15 and 20% the mix design is a combination of empirical results and mathematical calculation based on the absolute volume method. The water contribution by super plasticizer is part of the mixing water. Mixing of ingredients was done according to specification given in IS516 (1959) for cubes, cylinder and also beams. The specimens were removed from the mould after 24 h and were kept submerged in curing tank. After curing for the period of 1, 3, 7, 28, 56 and 91 days, the specimen was dried before testing. Compression test, split tensile, flexural test, shear test and ultrasonic pulse velocity tests were conducted for HPC with different pozzolanic blending. Details of the test carried out are summarized in Table 3.

Table 3 Details of mechanical properties

Parameter	Size of specimen	Age of test in days	Test standards
Compressive test	Cube (150 × 150 × 150 mm)	1,3,7,28,56,91	IS 516 (1959)
	Cylinder (150 × 300 mm)		
Split tensile test	Cylinder (150 × 300 mm)	1,3,7,28,56,91	IS 516 (1999)
Flexural strength	Beam (150 × 150 × 700 mm)	7,28,56,91	IS 516 (1999)
Shear strength	150 × 150 × 150 mm cube size mould with wooden block of 150 × 90 × 90 mm (inverted L-Shape)	28,56,91	AS per JSCE
Quality of concrete (ultrasonic pulse velocity test)	Cube (150 × 150 × 150 mm) Cylinder (150 × 300 mm)	28,56,91	IS13311-1 (1992)

4 Results and Discussion

Experimentation is carried out on different test for each model of compression test, split tensile, flexural test, shear test and ultrasonic pulse velocity tests were conducted for HPC with different pozzolanic blending. From these observations, the value of compressive strength with no of days is plotted in graphs as shown in Figs. 1, 2, 3, 4, 5 and 6. Regression analysis was adopted to represent the data in terms of equations. Analysis was carried out for the data obtained for each test separately.

The general equation obtained for compression test, split tensile, flexural test, shear test on carrying the regression analysis on the observed data for each test is
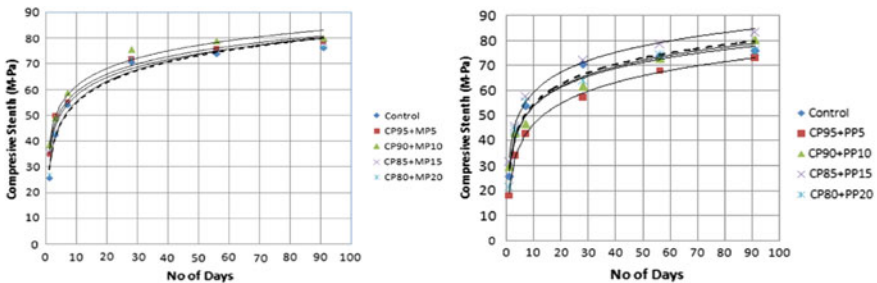
Fig. 1 Compressive strength of marble and porcelain powder-based HPC (cube)
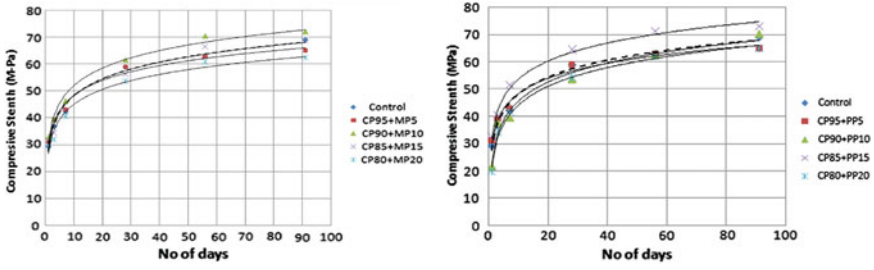
Fig. 2 Compressive strength of marble and porcelain powder-based HPC (cylinder)
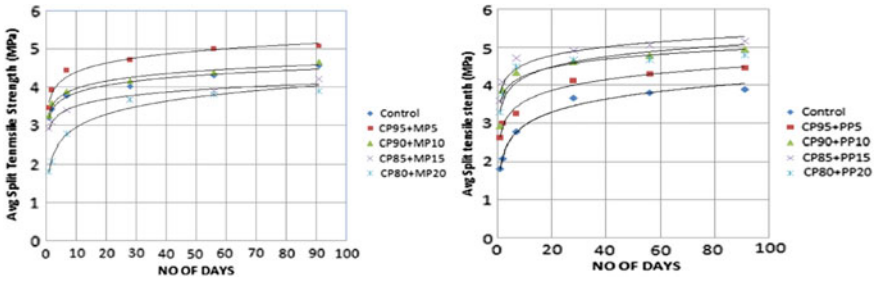
Fig. 3 Marble and porcelain powder-based HPC (split tensile strength)
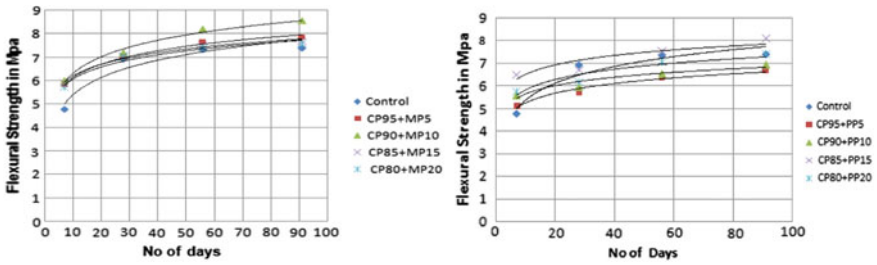
Fig. 4 Marble and porcelain powder-based HPC (flexural strength)
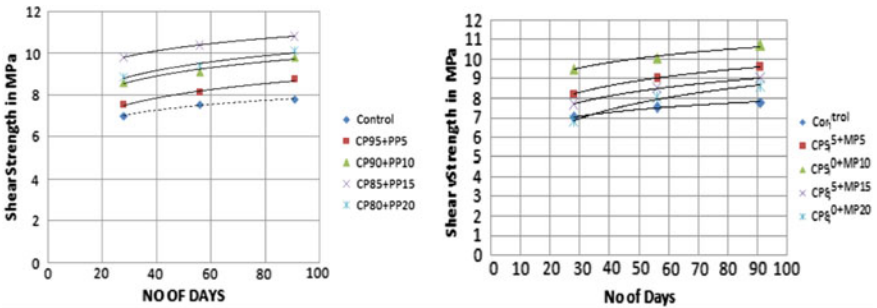
Fig. 5 Marble and porcelain powder-based HPC (shear strength)
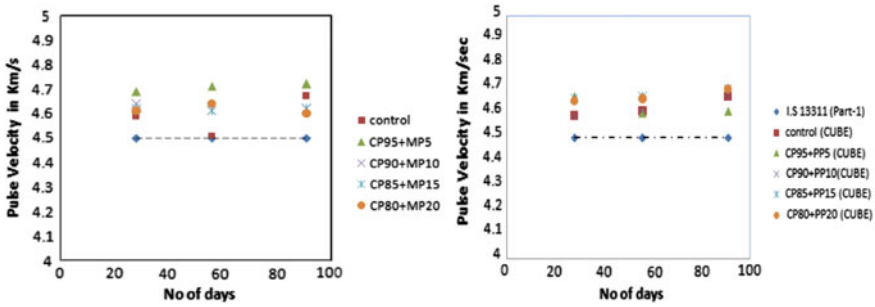
Fig. 6 Marble and porcelain powder (ultrasonic pulse velocity)

Eq. 1. It is found that logarithmic curve fits well to obtain relation between strength and number of days and is expressed as

$$C = A_o \ln(D) + A_1 \tag{1}$$

where

C Compressive strength
D No. of days

Observations were taken and that values of coefficients A_0 and A_1 along with the R^2 values for Porcelain and marble powder mix designed using 5, 10, 15 and 20% are shown in Table 4. The variation of days with compressive strength, split tensile test, flexural test and shear test is shown in Figs. 1, 2, 3, 4, 5 and 6.

5   Summary and Conclusion

The experiment-based results for test conducted to study the effect of cementations mineral admixture reflected detail insight of various strength and durability aspects of binary blended HPC. On the basis of experimental study, the following conclusions can be drawn.

(1) The result of test to check the mechanical properties and durability properties of various binary HPC shows a considerable improvement in performance of concrete. The parameters like compressive strength split tensile and flexural strength along with shear strength at early and after long period may show the increase in comparison with control mix for 15% replacement of porcelain and 10% replacement of marble powder.

(2) The ultrasonic pulse velocity tests have also confirmed the improvement in quality of concrete produced with binary blends.

Table 4 Coefficients for marble and porcelain for different mix design

Test	Marble powder				Porcelain powder			
	Mix design	A_0	A_1	R^2	Mix design	A_0	A_1	R^2
Compression test (Cube)	Control	11.38	29.05	0.974	Control	11.28	29.05	0.974
	C95+MP5	9.729	36.86	0.986	C95+PP5	11.93	19.22	0.996
	C90+MP10	9.764	39.14	0.981	C90+PP10	10.84	28.80	0.982
	C85+MP15	9.907	35.15	0.986	C85+PP15	11.43	33.12	0.994
	C80+MP20	11.24	29.68	0.973	C80+PP20	11.34	27.73	0.951
Compression test (Cube)	Control	8.973	27.59	0.988	Control	8.973	27.59	0.999
	C95+MP5	7.923	30.23	0.985	C95+PP5	7.927	30.22	0.985
	C90+MP10	9.330	30.56	0.986	C90+PP10	10.02	22.64	0.972
	C85+MP15	8.973	27.63	0.965	C85+PP15	9.450	32.06	0.922
	C80+MP20	8.022	26.57	0.971	C80+PP20	9.858	21.63	0.994
Split tensile strength	Control	0.282	3.205	0.982	Control	0.496	1.807	0.983
	C95+MP5	0.281	3.317	0.966	C95+PP5	0.413	2.626	0.982
	C90+MP10	0.341	3.612	0.969	C90+PP10	0.387	3.314	0.884
	C85+MP15	0.263	2.894	0.974	C85+PP15	0.326	3.802	0.926
	C80+MP20	0.496	1.807	0.983	C80+PP20	0.311	3.539	0.878
Flexural strength	Control	1.068	2.920	0.917	Control	1.068	2.920	0.917
	C95+MP5	0.832	4.211	0.992	C95+PP5	0.628	3.794	0.965
	C90+MP10	1.020	3.962	0.985	C90+PP10	0.531	4.425	0.923
	C85+MP15	0.716	4.559	0.981	C85+PP15	0.606	5.107	0.823
	C80+MP20	0.747	4.340	0.975	C80+PP20	0.656	4.326	0.905
Shear strength	Control	0.608	4.800	0.980	Control	0.668	4.800	0.989
	C95+MP5	1.150	4.406	0.990	C95+PP5	1.022	4.088	0.985
	C90+MP10	1.011	6.107	0.979	C90+PP10	1.030	5.106	0.959
	C85+MP15	1.147	3.892	0.999	C85+PP15	0.855	6.955	0.999
	C80+MP20	1.516	1.837	0.991	C80+PP20	1.030	5.106	0.959

(3) Using porcelain or marble powders in making concrete can solve several environmental problem and may help in reduction of CO_2 emission in environment as cement can be saved. It may also avoid exploration of large quantities of raw material from the earth keeping the landfill area unoccupied as the waste material will be effectively reutilized by construction industry.

References

1. Kjellsen, K.O., Hallgren, M., Wallevik, O.H.: Fracture mechanical properties of high performance concrete-influence of SF. Mater. Struct. **33**, 552–598 (2000)
2. Zain, M., Radin, S.S.: Physical Properties of high performance concrete with admixture exposed to a medium temperature range 20–50 °C. Cem. Concr. Res. **30**, 1283–1287 (2000)
3. Erdem, T.K., Kirca, O.: Use of binary and ternary blends in high strength concrete. Constr. Build. Mater. **22**, 1477–1483 (2008)
4. Malagavelli, V., Rao, P.N.: High performance concrete with GGBS and ROBO sand. Inter. J. Eng. Sci. Technol. **2**(10), 5107–5113 (2010)
5. Muthupriya, P., Subramanian, K., Vishnauram, B.G.: Experimental investigation on high performance reinforced concrete column with SF and FA as admixture. Asian J. Civ. Eng. (Build. Hous.) **12**, 597–618 (2011)
6. Ravel, A.D., Patel, I.N., Pitrida, J.: Re-use ceramic industry waste for elaboration of eco-efficient concrete. Inter. J. Res. Studies, **2**(3), 103–105 (2013)
7. Pacheco Torgal, F., Shahasavandi, A., Jalali, S.: Mechanical properties and durability of concrete with partial replacement of Portland cement by ceramic wastes. WASTES Solution, Treatments and opportunities 1st international conference (2011)
8. Chandana, S., Bata Krishna, K., Saha, P., Shyam, C.K.: A study of sustainable industrial waste material as partial replacement of cement. In: IACSIT Combatore Conference, vol. 28, pp. 161–169 (2012)

Comparative Analysis of ECC by Partial Replacement of Cement with Slag Sand

Akshay A. Gulghane and Chintaman Bari

Abstract Bendable concrete is one of the emerging term nowadays which is also called as ECC (Engineered Cementitious Composites) developed by Dr. Victor C. Li in 2001. Compressive strength of concrete is comparatively very high than tensile strength. But for the resistance to unknown tensile forces due to reversal of stresses as in case of earthquakes is the normal concrete fails catastrophically. Newly developed ECC is having higher tensile strength with same compressive strength. Cost of ECC is comparatively high than normal concrete due to the presence of PVA, (Polyvinyl Alcohol Fibers). The main aim was to study the change in the original properties of ECC with the partial replacement of conventional cement with the slag sand. The study was done on both compressive strength and split tensile strength after 7 days and 28 days of curing. The cement in the ECC was replaced by slag sand, that is waste from iron industry in the percentage of 10, 20, and 30 by weight of cement.

Keywords ECC · PVA · Silica sand · Slag sand

1 Introduction

The complete development of the fiber reinforced concrete materials has undergoes various stages. The ultra modern-day versions of these continuous fiber reinforcements are projected by the textile cement reinforced concrete materials that can be the prestressed. In the modern years, couple classes of high-performance RCC have emerged. The Ductile materials have the very high tensile strength around 12 MPa and a ductility of the value around 0.02–0.06% and ECC developed and manufactured at the University of Michigan, with a very moderate tensile strength of 4–6 MPa and comparatively a higher ductility of 3–5%. ECC can particularly be considered as the family of versatile material with the range of tensile strength along with ductility's that can be clearly adjusted simultaneously very much depending on the demands

A. A. Gulghane (✉) · C. Bari
G. H. Raisoni College of Engineering, Nagpur 440016, India
e-mail: akshaygulghane@gmail.com

of any particular civil structure. ECC also represents a dominant family of materials with different and efficient functions in addition to the common and regular characteristics of much higher tensile, greater ductility, and very fine multiple cracking. ECC is class of the High-Performance Fiber Reinforced Cementitious Composite (HPFRCC) next to the DUCTAL. ECC is special type of concrete basically mortar (as it only consists of fine aggregate not coarse aggregate) designed with the special fibers called as PVA (Polyvinyl Alcohol Fiber). The maximum amount of fiber is restricted only to 2%. Higher amount of flexibility than used in traditional concrete, ECC acts appreciably more as a metal than compared to the glass. Convention concrete is more considered as a brittle, ceramic, and rigid in physical characterization. It can certainly suffer catastrophic failure when it is strained in particularly moderate intensity earthquake or by continuous overuse. It is covered with purposefully fully covered RCC fibers that hold it in sturdy state. ECC remains completely bonded, summed up, and comparatively safe to use even at tensile strains rises up to the 5%. Conventionally used concrete sum up with failure and not able to carry any further load at 0.01% tensile strain. Modern-days builders are purposefully using these reinforce concrete structures with steel bars to make sure these relative cracks must be as small as possible that can be. But some of the cracks that are relative large and much wide that cannot recover easily, so the water and the partially present salts can insert up to the steel section causing sever corrosion that further defoliate of the structure. But the cost is higher than normal concrete, so to decrease the cost of concreting, suitable measures must be taken without hampering the overall strength of the structure.

2 Literature Review

Various research was carried on ECC and some of them are discussed below.

Deshpande and Murnal [1] studied Ductile properties of Concrete using Engineering Cementitious Composite. They completely investigated the said property of normal concrete that can be tremendously improved by using PVA fibers in variable amount in place of coarse aggregate and cement partially replaced by fly ash. The concrete cubes, cylinders, beams, and slabs are experimentally investigated in laboratories. Flexure strength of ECC is 60% more than conventional concrete, though compressive strength of ECC and convention concrete is nearly same. Split tensile strength of ECC is about 32% more than conventional concrete. Composite beams reinforced with FRP bars are slower than RC beams reinforced with FRP bars after cracking.

Hind et al. [2] had studied numerical and parametric studies on flexural behavior of ECC beams by considering the effect of slag and micro-pva fiber. Their aim was to study the mechanical performance of ECC beams with respect to the effect of aggregate size and amount by employing nonlinear finite element method. The compressive strength testing, split cylinder tensile strength at 3, 7, 14, and 28 days, respectively, conducted and flexural strength of prism and optimum percentage of

bentonite was find out by replacing different percentage of bentonite and 60% of steel slag by weight of cement and coarse aggregate for a mix of M20 grade concrete.

Sharmila and Nadu [3] studied on behavior of Hybrid Fibre Engineered Cementitious Composites. A particular experimental investigation was precisely carried out on the variable replacement of conventional cement by desire admixture of fly ash and GGBS to check down the various properties of ECC. About 70% of the total cementitious content is variably replaced by the mineral admixture (flyash) and further the fly ash is variably replaced by GGBS. Further to analyze all these composite behavior, about 0.5% of steel fiber and 1% of PVA fiber were added to the matrix. Compressive strength rises by 45.4%, split cylinder tensile strength increases about 50%, and flexural strength of concrete increases by 14.5%. GGBS when added separately has no particular impact on the strength properties, but when it is combined together with PVA, it shows better improvement in the strength. This is due to the formation of a chemical bond between them which enhances the strength of ECC.

Li [4] studied about the research and development of Engineered Cementitious Composites (ECC) over the couple of decade since its invention. The very importance of micromechanics in the construction materials design engineering is emphasized. Observations of unique characteristics of ECC based over a very wide range of theoretical as well as preside experimental research are examined. The specific advantageous use of ECC in certain categories of structural, its repair, and its retrofitting applications is reviewed particularly.

3 Objectives

From the above literature review, following objectives are selected for present study.

(1) To study the properties of ECC.
(2) To study complete properties related to ECC with partial replacement of cement with the slag sand.

4 Experimental Programme

4.1 Materials of ECC

Cement: Cement used is the general Ordinary Portland Cement with flyash or Portland Pozzolona Cement (PPC). In this experiment, PPC of 53 grade was used (Ultratech Cement).

Silica Sand: Sand is naturally occurring granular material composed of finely divided rock and mineral particle as shown in Fig. 1. Silica sand passing from 1.18 mm sieve was used. Its density is about 2.6 kg/m3. Properties of Silica sand is given below in the Table 1 (Figs. 1 and 2).

Table 1 Properties of silica sand

Constituent	Properties
Color	Brown/yellowish
SiO_2	96.90%
Fe_2O_3	0.29%
K_2O	0.07%
$A_{l2}O_3$	1.00%

Fig. 1 Silica sand

Fig. 2 Polyvinyl Alcohol Fibers

Super Plasticizer: This is particularly utilized to control rheological properties of the made fresh concrete. Zentoament FBV was used as superplastisizer.

Poly Vinyl Alcohol (PVA) Fiber: PVA fiber specially has very high strength and a high modulus of elasticity compared to other specific general organic fibers. It is of length 5–6 mm length with elongation 6–10%. One of the remarkable properties of PVA is the strong bond with cement matrix, because of formation of particular layer of Ca (OH)$_2$ mainly called as interfacial transition zone. This zone is not observed in the other fiber such as poly propylene (PP) fiber. PVA fiber manufactured in China was used, as shown in Fig. 2.

Water: Potable water is suited and used for concrete mix. It was free from alkali, oil, grease, and other impurity.

4.2 Materials of ECC10, ECC20, ECC30

Cement, fiber, and water were used same as in case of ECC but cement was partially replaced as 10, 20, and 30% with the silica sand passing from 90 micron sieve.

Slag Sand: Slag sand is one of the waste products from the iron industries. Slag sand is also sieved from 1.18 mm sieve. Slag sand from Bhagvati Ferro Metal Pvt. Ltd, was used. It's cost is about 2500Rs/brass which is nearly about 55% less than silica sand and 40% less than natural river sand. Properties of slag sand are given below in Table 2.

Table 2 Properties of slag sand

Constituent	Properties
Color	Blackish
SiO_2	44.25%
Fe_2O_3	24.10%
CaO	4.60%
Al_2O_3	9.10%
M_gO	0.40%
Cr_2O_3	Nil
Total Alkali	2.80%
M_nO	8.10%
P_2O_5	0.32%
Silt	Nil
Loss on Ignition at 900 °C	5.20%

Table 3 Mix proportion of ECC, ECC10, ECC20, ECC30

Mix	Cement	Sand	Slag	PVA (% of cement)	Super plasticizer (%)
ECC	1.0	1	0.0	1.5	2
ECC10	0.9	1	0.1	1.5	2
ECC20	0.8	1	0.2	1.5	2
ECC30	0.7	1	0.3	1.5	2

4.3 Mix Proportion of ECC

The mix design of ECC concrete is mainly and basically based on the microme-chanics concept which depends on fiber–matrix interaction. Steady-state cracking phenomenon is seen particularly in the ECC instead of Griffith cracking due to the attachment of microfiber with the mortar at ends. It predominately forms thus bridging action which increases the strength. PVA fiber design was thus evaluated with the help of pull out test for micromechanics which cannot be possible in normal lab rotary. Hence for the study ideal mix proportions present in the literature of ECC concrete, was used as the guidelines to determine the proportion of various constituents in the concrete. The ideal Mix proportion small for ECC which was taken as reference is given in Table 3.

Also the mixture of ECC10, ECC20, ECC30, i.e., replacement of cement in ECC with 10, 20, 30% slag sand is also shown in Table 3. The water cement ratio adopted was 0.35.

4.4 Casting

The mixing of ECC, ECC10, ECC20, and ECC30 is done using hand mixing method. The dry mix is prepared with silica, sand, and cement for ECC. Then, about 50% of water is added. Once water is added, PVA fiber is added in designed proportion. Finally, plasticizer with remaining water is added to form homogeneous mixture.

For ECC10, ECC20, and ECC30, the replacement of the cement is done by silica sand which is sieved from 90 microns IS sieve. The cubes were casted of standard size 150 × 150 × 150 mm, and the cylinder of size 300 × 150 mm was also casted by filling mixture in layers and tamping was done for each layer appropriately.

5 Testing

5.1 Compressive Test

As per the cement association of India (2003), compressive strength of concrete is that value at which material fails completely under uniaxial compressive stress. At the end of 7 and 28 days (counted from time of mixing of water with cement and aggregates), three cubes are taken out from curing tank. The excess amount water is allowed to drain off, and then, the cubes are placed in a compression testing machine (CTM). Load is applied gradually till the failure occurs in the respective cubes. The results are shown in Fig. 3.

5.2 Split Tensile Strength Test

Tensile strength is very low in concrete. It is very difficult to measure tensile strength directly, so split tensile strength confirming IS 5816:1999 was used. The load is applied at gradual rate and continues it fails. The results of split tensile test are as shown in Fig. 4.
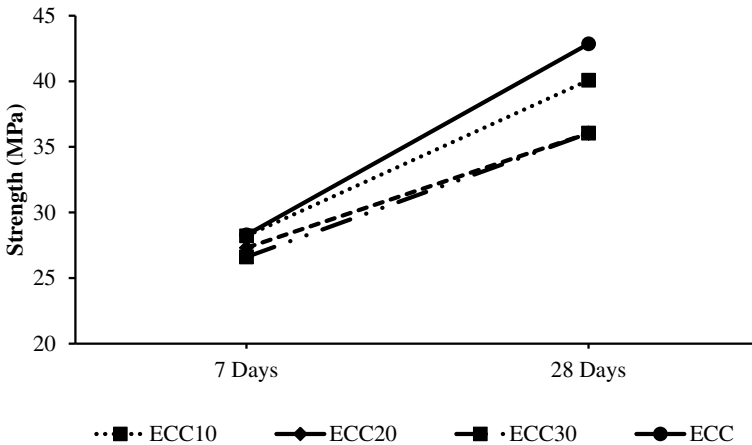
Fig. 3 Comparison of Compressive strength for 7 days and 28 days
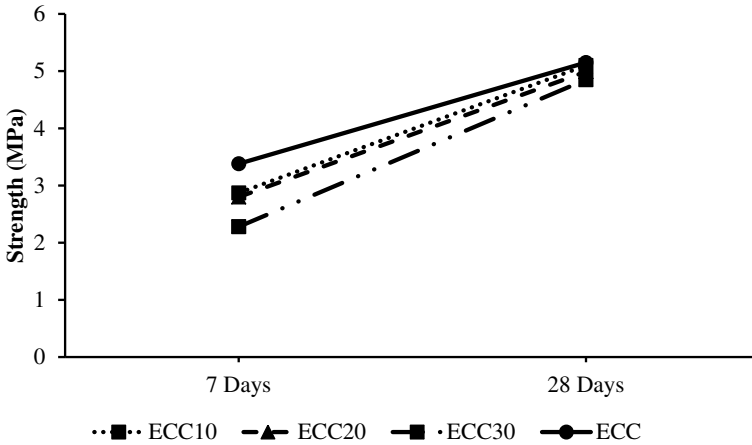
Fig. 4 Comparison of Split tensile strength for 7 days and 28 days

Table 4 Cost analysis of ECC, ECC10, ECC20, ECC30

Type	Rs. Cost/m³
ECC	20,594
ECC10	18,631.5
ECC20	16,669
ECC30	15,719

6 Cost Analysis

The comparative cost analysis of ECC, ECC10, ECC20, ECC30 has been done for per meter cube quantity, and following cost is computed as shown in Table 4.

7 Conclusions

The ECC was found to be having more ductility as compared to normal concrete.

- The experimental compressive strength of ECC10 is about same as ECC after 7 days and about 93.53% after 28 days.
- The experimental compressive strength of ECC20 is about 96.53% of ECC after 7 days and about 84.10% after 28 days.
- The experimental compressive strength of ECC30 is about 94.02% of ECC after 7 days and about 84.10% after 28 days.
- The experimental split cylinder tensile strength of ECC10 is 84.91% of ECC after 7 days and 99.02% after 28 days.

- The experimental split tensile strength of ECC20 is 82.84% of ECC after 7 days and 96.89% after 28 days.
- The experimental split tensile strength of ECC30 is 67.45% of ECC after 7 days and 94.17% after 28 days.
- Cost reduction is about 9.52, 19.05 & 23.67%, respectively, for ECC10, ECC20, and ECC30.

References

1. Deshpande, U.L., Murnal, P.B.: Ductile concrete using Engineered Cementitious Composites. Inter. J. Eng. Res. **5013**(5), (2016)
2. Hind, M.K., Ozakça, M., Ekmekyapar, T.: Numerical and parametric studies on flexural behaviour of ECC beams by considering the effect of slag and Micro-PVA fibre J. Adv. Res. Appl. Mech. **21**(1), 1–21 (2016)
3. Sharmila, S., Nadu, T.: Behaviour of hybrid fibre engineered cementitious. Int. J. Sci. Environ. Techn. **5**(5), 3539–3545 (2016)
4. Li, V.C.: Engineered Cementitious Composites (ECC)—Tailored Composites through Micromechanical Modeling. Fiber Reinf. Concr. 01–38 (1997)

Analysis and Characterizations of Modified Caesalpinia Bonduc (MCB) Seed Coat in the Process of Defluoridation

Ranjit N. Patil, P. B. Nagarnaik and B. J. Godbole

Abstract The researchers and philosophers mainly focused on the quality and quantity of drinking water from last some decades. In this research investigation, the seed coats of Caesalpinia bonduc were found a predominant promising herb for the defluoridation from ground water. Method of adsorption was selected for analysis and experimental program for the range of pH (2–14), dose (0.5–5.0 g/L), time of contact (0–420 min), initial concentration of fluoride (2.5–15 mg/L), particle size (75–600 μm) with the agitation speed (150 rpm). Analyzed data checked for isotherms and found well fitted in case of Langmuir isotherm.

Keywords Fluoride · Adsorption · TCM · Isotherm

1 Introduction

Water is an elixir for life. But today pure drinking water has become a scarcity. Majority of the population is drinking more or less contaminated water. There are different reasons for the contamination of water like natural forces and industrial effluent. The major reason for contamination of water is fluoride [1]. Water scarcity is a global problem; where 2 billion peoples are affected. India is also facing the same crisis where millions of people are not able to get pure drinking water and are compelled to drink contaminated water. Poor sections of the society are deprived of pure drinking water and are consuming contaminated water, eventually they fall ill

R. N. Patil (✉)
Department of Civil Engineering, Priyadarshini Bhagwati College of Engineering,
Nagpur, M.S, India
e-mail: ranjeetpatilpbce@gmail.com

P. B. Nagarnaik
G. H. Raisoni College of Engineering, Nagpur, M.S, India

B. J. Godbole
Department of Civil Engineering, G. H. Raisoni College of Engineering,
Nagpur, M.S, India

and sometimes it may result in epidemics [2]. Day by day the demands of water get increase and at the same time the quantity of acceptable drinking water gets reduced. In 1997–98, total 629 BCM needed to grow and by the year 2050 it will be projected to grow 1180 BCM. It is due to the growth in the sector of agriculture, industrialization, modern urbanization, economic growth increases the existing demand of water. Hence, it creates a huge gap between demand and supply of ground water. The quality of water gets also affected because of large consumptions in the sector of agriculture, industrial, and domestic as well (Uberoi 2003).

Caesalpinia bonduc (Sagargota tree plant) is one of the medicinal herbs found across to our nation. In this investigation study, the adsorption capacity of MCB was studied by using batch experimental analysis which follows the dose, initial fluoride concentration, time of contact, pH, and particle size of adsorbent parameters. The isotherm study covers Freundlich and Langmuir.

Caesalpinia Bonduc Plant: Medicinal Plant, found in the hotter part area of India. It is also found in Sri Lanka and Burma countries. It has a height up to 15.00 m. At 1000 m altitude, it is found in Himalayas.

2   Materials and Methods

Analytical (AR) grade chemicals were selected and used in present research study. The solution of stock prepared by using 2.21 g of sodium fluoride and the double distilled water of quantity 1000 ml. After the stock solution, working samples were prepared by selecting required appropriate stock dilution [3].

Adsorbent and its Preparation

Seeds of Caesalpinia bunduc were collected, separated, and stored. The seed coat then sun dried and cut into required size. The dried coats washed with normal demonized water for the removal of dust particles and trash as well. Then, the seed coats were kept for 24 h. in oven at a 110 °C temperature. Completely dried coats were then cooled in desiccators. The seed coats were then pulverized and kept in muffle furnace at a 900 °C temperature for 2.5 h. for activation. This was then chemically activated and used for further study [4, 5].

3   Experimental Methods

The method of adsorption is a suitable chip method widely used in the defluoridation process. The observing parameters in the process are dose, pH, agitation, initial concentration of fluoride ions, particle size. The experimental studies used plastic bottles of capacity 250 ml and the test sample containing 100 ml. The pH controlled by 0.1 N HCl or 0.1 N NaOH. The fluoride quantity was checked by spectrophotometer throughout the experimentations [6, 7].

4 Results and Discussion

4.1 Physical Characterizations

Proximate analysis		Ultimate analysis	
Parameters	MCB	Parameters	MCB
% Moisture Content	2.16	% Hydrogen	3.40
% Volatile Matter	18.34	% Nitrogen	0.54
% Ash Content	37.36	% Carbon	39.55
% Fixed Carbon	42.14	% Oxygen	43.49

From the proximate analysis, it has been observed that the percentile amount of fixed carbon found 42.14% which was further used after process in batch experimentation analysis [5, 8]. From the ultimate (CHN) analysis, it has been confirmed that the amount of carbon content has been found good in case of modified Caesalpinia bonduc MCB.

SEM Analysis

Figure 1 shows the SEM micrograph of modified Caesalpinia bonduc seed coat which was chemically treated unloaded adsorbent of MCB. SEM observations of chemically activated adsorbents carbon obtained from thermal degradation of natural materials recorded its complex and porous surface texture which helps in the process of defluoridation [5, 8].

4.2 Effect of Dose

In the process of determination of dose quantity in the fluoride ions, removal process from ground water contained 5 mg/L of fluoride. From this laboratory study, the results show the percentage removal capacity of Caesalpinia bonduc used in varying dose ranges from 0.5 to 5 g/L and used as an effective low-cost herb and bioadsorbent in adsorption analysis as shown in Fig. 2 [9]. The result of analysis shows the % increase in removal of fluoride ions as the dose increases. The upper uptake capacity of MCB noted 90.21% for a dose quantity of 0.8 g/L.

4.3 Effect of PH

In the process of adsorption, pH is one of the important parameters which plays vital role in the defluoridation. For the optimum dose study analysis, 2–14 pH range were selected. Maximum uptake capacity 90% was observed at pH 8.7. The removal of
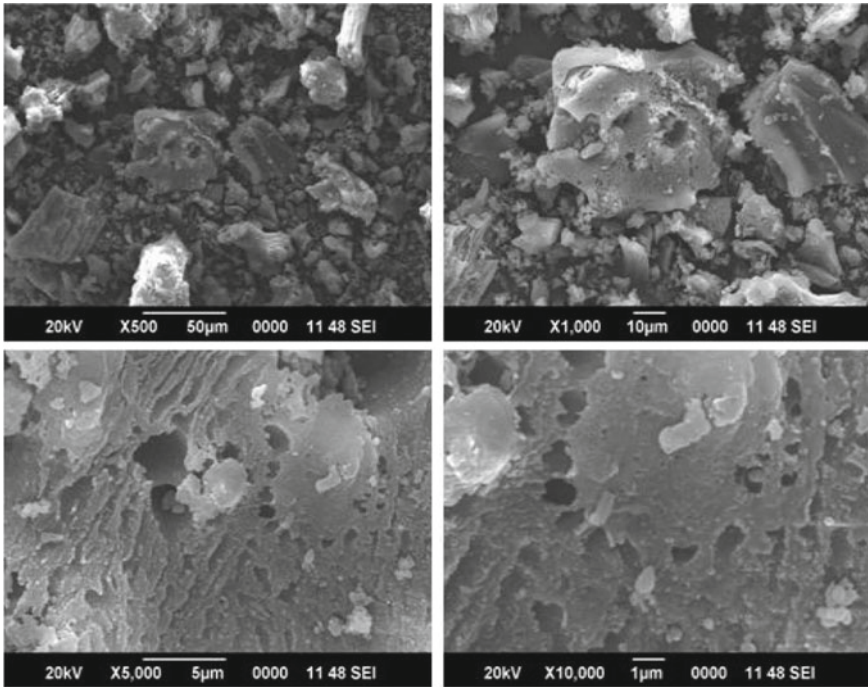
Fig. 1 SEM analysis
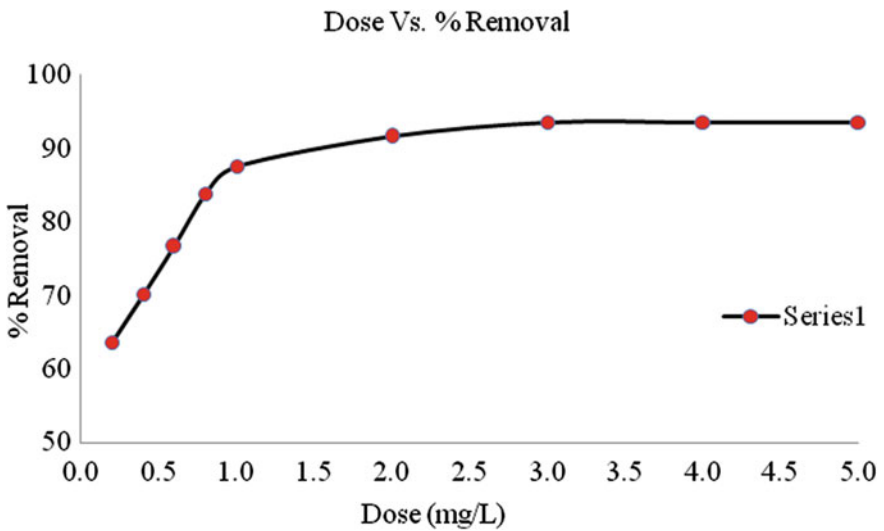
Fig. 2 Dose and removal %
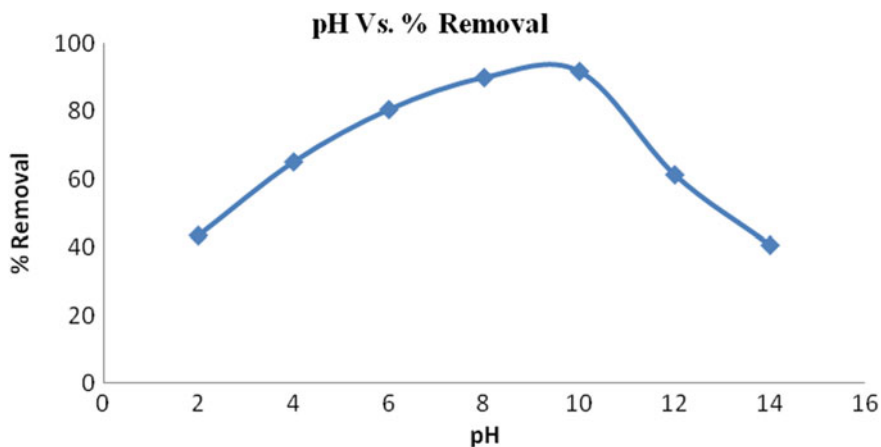
Fig. 3 pH and removal %

fluoride ions increases with increase in pH. The pH falls suddenly after the pH 8.7 and the capacity of removal decreased with increase in pH as shown in Fig. 3. From the observed result, the profile of graph shows down after rechase maximum removal capacity, it may be due to the formation of weak hydrofluoric acid [10].

4.4 Initial Concentration Study and Effects

The study of literature shows the variation in fluoride ions worldwide. In some countries, it is observed very less and in others found very high. In India, some of the states and area found higher fluoride ranges. This is one of the studies which provides the removal capacity of MCB for the initial concentration ranges 2.5–15 mg/L [11, 12]. The increase in percentage removal observed with decreased in initial concentration and vice versa shown in Fig. 4.

4.5 Particle Size Effect

The uptake capacity of adsorbent (MCB) is also based and depends on the particle size. The particle size 75–600 μm was used in this research. The result shows the maximum removal capacity of MCB at lower particle size as shown in Fig. 5.
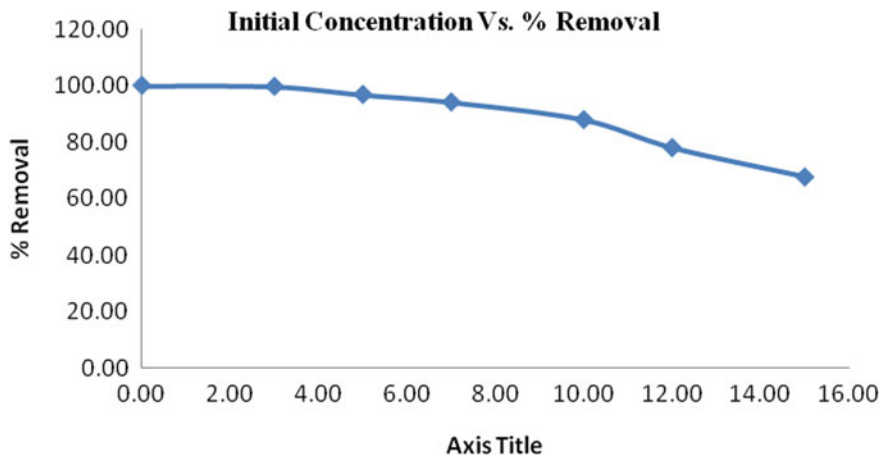
Fig. 4 Initial concentration and removal %
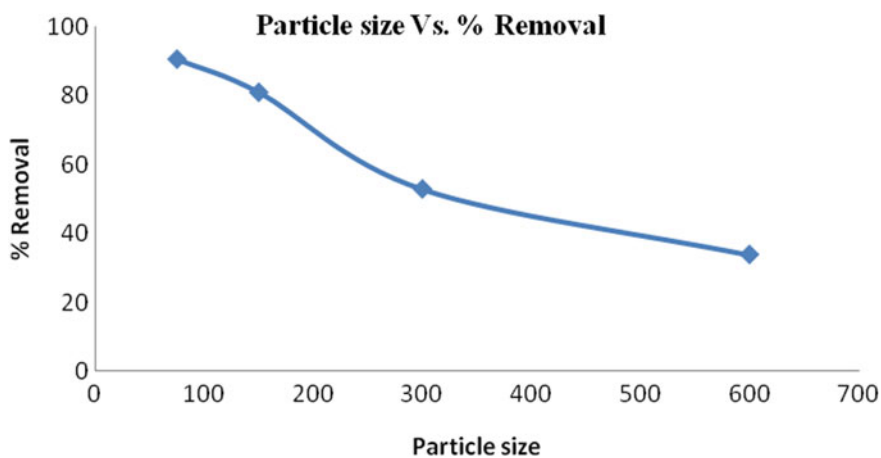
Fig. 5 Particle size and removal %

4.6 Effect of Contact Time

The study of equilibrium in the process of adsorption is an essential parameter in this study. The removal capacity of adsorbent was observed with increase in time of equilibrium. The removal percentage observed maximum at 60 min. as shown in Fig. 6.
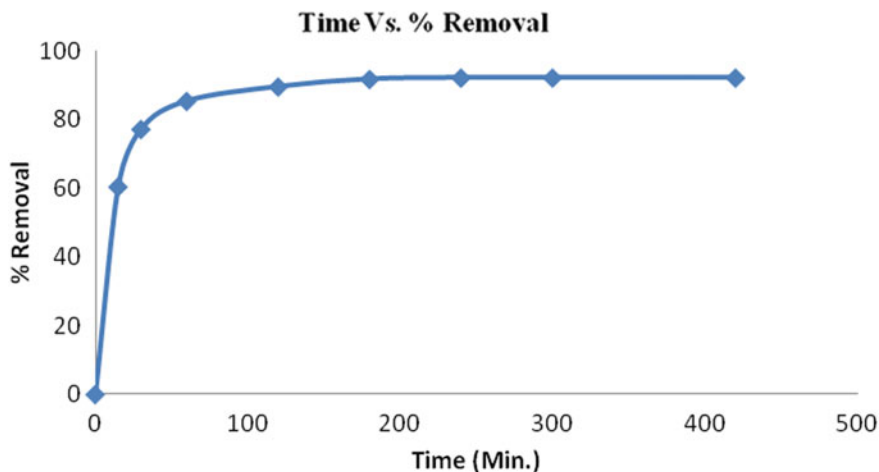
Fig. 6 Contact time versus % removal
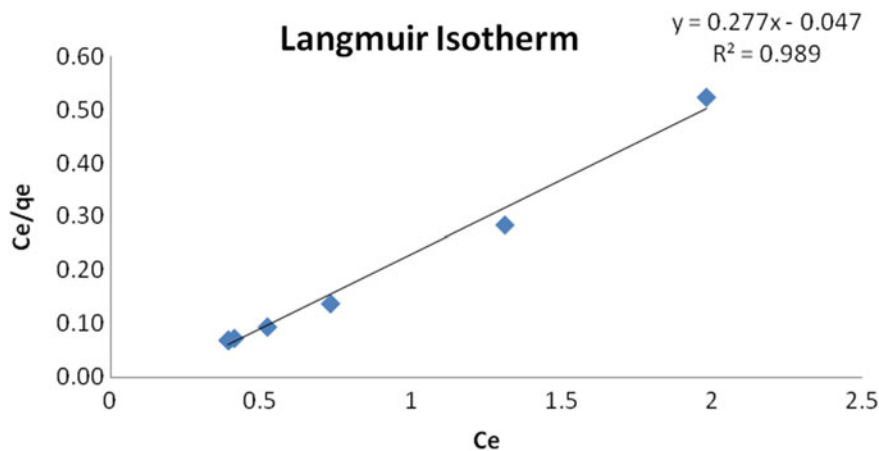
Fig. 7 Langmuir adsorption isotherm

4.7 Model of Adsorption

From the analysis, the data were prepared and the adsorption model observed get fitted well in the isotherm of Langmuir. This study results show the isotherm achieved good adsorption uptake capacity as shown in Figs. 7 and 8.

Freundlich Isotherm

$$y = -0.233x + 1.546$$
$$R^2 = 0.941$$
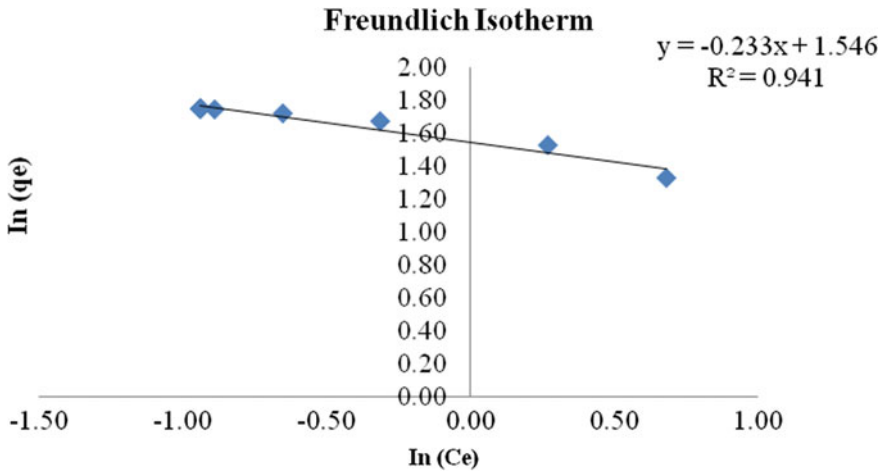
Fig. 8 Freundlich adsorption isotherm

5 Conclusion

This MCB adsorbent laboratory analysis study concludes on the basis of observed readings in the standard laboratory conditions.

1. The MCB has good fluoride uptake capacity used, when it has modified.
2. The maximum (optimum) dose of MCB was found 0.8 g/L for 5 mg/L initial fluoride concentration.
3. Adsorption capacity at pH 6.5–8 was noted more.
4. The optimum time of equilibrium was found 60 Min.
4. The % removal percentage of removal observed more in case of minimum particle size.
5. The adsorption equilibrium data follows Langmuir isotherm than Freundlich isotherm.

References

1. Abe, I., Iwasaki, S., Tokimoto, T., Kawasaki, N., Nakamura, T., Tanada, S.: Adsorption of fluoride ions onto carbonaceous materials. J. Colloid Interface Sci. **275**(1), 35–39 (2004)
2. Patil, Ranjit N., Nagarnaik, P.B., Agrawal, D.K.: Removal of fluoride from ground water by using modified bark of terminalia chebula (Haritaki). Inter. J. Civ. Eng. Technol. **7**(6), 21–30 (2016)
3. Waghmare, Sanghratna, Arfin, Tanvir, Rayalu, Sadhana, Lataye, Dilip, Dubey, Samujjwala, Tiwari, Sangeeta: adsorption behaviour of modified zeolite as novel adsorbents for fluoride removal from drinking water: Surface phenomena, kinetics and thermodynamics studies. Inter. J. Sci. Eng. Technol. Res. (IJSETR) **4**(12), 4114–4124 (2015)

4. Patil, Ranjit N., Nagarnaik, P.B., Agrawal, D.K.: Removal of fluoride from ground water by using treated bark of phyllanthus emblica (Amla) Tree. Inter. J. Civ. Eng. Technol. **7**(6), 11–20 (2016)

5. Patil, R.N., Nagarnaik, P.B., Agrawal, D.K.: Removal of fluoride from water by using bio-adsorbents: a state of art. Inter. J. Pure Appl. Res. Eng. Technol. **3**(9), 272–279 (2015)

6. Raichur, A.M., Basu, M.J.: Adsorption of fluoride onto mixed rare earth oxides. Sep. Purif. Technol. **24**, 121–127 (2001)

7. Simons, R.: Trace element removal from ash dam waters by nano filtration and diffusion dialysis. Desalination **89**, 325–341 (1993)

8. Wu, X.M., Zhang, Y., Dou, X.M., Yang, M.: Fluoride removal performance of a novel Fe–Al–Ce trimetal oxide adsorbent. Chemosphere **69**(11), 1758–1764 (2007)

9. Rao, M., Parwate, A.V., Bhole, A.G.: Uptake of Nickel from aqueous solution using low cost adsorbent. Enviromedia **20**(4), 669–675 (2001)

10. Rao, M., Parwate, A.V., Bhole, A.G.: Uptake of Nickel from aqueous solution using low cost adsorbent. Enviromedia **20**(4), 669–675 (2001)

11. Patil, R.N., Nagarnaik, P.B., Agrawal, D.K.: An experimental analysis of adsorption behavior of HTB for the removal of fluoride. Inter. J. Eng. Res. Technol. Special issue, 89–90

12. Waghmare, S.S., Arfin, T., Manwar, N., Lataye, D.H., Labhsetwar, N., Rayalu, S.: Preparation and characterization of polyalthia longifolia based alumina as a novel adsorbent for removing fluoride from drinking water. Asian J. Adv. Basic Sci. **4**(1) (2015). 12–24ISSN (Online): 2347–4114

Punching Shear Distribution of Flat Slab with Opening Adjacent to Column

K. N. Kadam and Saurabh Ingole

Abstract Flat slab though have pleasant aesthetes is critical in punching shear. The flat slab may have openings for various architectural concerns such as stairways or elevators, the transition of gas, electricity, water and air-conditioning systems, etc. This opening may be anywhere in the slab, but the most favourable location is the one next to the column since continuity of the carpet area is undisturbed. But, providing an opening adjacent to column implies providing the opening at the most critical location. Due to an opening adjacent to the column, the punching shear capacity is most affected, which results in the failure of the structure. One shall also notice the vulnerability of such type of failures since this type is a failure, brittle in nature; there are no signs of failure as a warning. The failure is sudden and may cause the collapse of the whole structure. To avoid such type of failure, one shall analyse the structure at the time of construction itself and take safety measure at the time of construction itself. The objective of this study is twofold—firstly, the size of the opening and secondly, the location of the opening in the flat slab. In this paper, seven different models/specimens have studied in which six models have an opening of size 1.2 × 1.2 m, 2 × 2 m or 3 × 3 m adjacent to column face. Openings are placed parallel to the face of the column or diagonal to the face of the column. And first model is the control specimen without opening. All these models are analysed by finite element analysis-based software CSI SAFE 2016.

Keywords Flat slab · Opening adjacent to the column · Opening · Punching shear · Flat plate

1 Introduction

The flat slab is a type of two-way reinforced concrete slab widely adopted for construction such as large-scale supermarket, store and underground garage, bridge

---

K. N. Kadam · S. Ingole (✉)
Department of Applied Mechanics, Government College of Engineering, Amravati, India
e-mail: saurabhing94@gmail.com

decks, etc. Also, it is used frequently in high-rise buildings for various different purposes or in buildings with flexible spatial arrangements during their lifespan. Flat plate slab is a very common and competitive structural system, in which columns directly support floor slabs without beams. Flat slabs are preferred for the construction of in situ concrete frame building. In these slabs, a square or near square grid is used [1]. They may have openings for architectural concerns such as stairways or elevators, the transition of gas, electricity, water and air-conditioning systems, etc. Due to the opening, the discontinuity occurs in the natural load path of the structure. This results in unbalanced shear force and bending moments. The main concern while designing a flat slab is the consideration of punching shear capacity. Providing an opening affects the punching capacity of the structure. Punching shear failure is a brittle type of failure and thus is the most dangerous once. Punching shear failure is a sudden failure and may result in the collapse of whole structure [2–5].

The size and location of opening have a high impact on the punching shear capacity [6]. Depending upon the size of opening and location of opening, the amount of steel required also increases [6]. Providing an opening makes the situation critical, but among these situations, providing an opening adjacent to the column is the most critical one. Opening adjacent to column affects the punching shear capacity of the flat slab at very large scale. Since flat plate slab is already vulnerable to punching shear, an opening adjacent to the column in such slab may cause great effect on the design parameters of the flat slab [7, 8]. So the effects of these openings on the punching shear behaviour of flat slab-column systems must be examined carefully [9–11]. The punching shear failure should be examined and the design must stay on the conservative side for safety purpose. Effects of these openings adjacent to the column on the punching shear behaviour of flat slab-column systems are to be examined carefully [12–14].

2 Specimen Details and Material Properties

A flat slab model of having four bay in both the direction is considered which resembles with most of the commercial buildings. The 250-mm-thick slab is directly rested upon columns. The size of the column is taken as 0.8×0.8 m. The size of each slab panel is 8×8m. The plan view of the model is given in Fig. 1. To ensure that punching shear takes place, no column capital nor drop panned is provided and neither any shear strengthening is done. The design of the flat slab is done using CSI software SAFE2016 by finite element method. Dead load of 6.25kN/m^2 and live load of 3.5kN/m^2 is applied on slab, and factor of safety of 1.5 is applied to the total load. Thus, the total factored load applied on the slab is 14.625kN/m^2. The clear cover of 15 mm is provided at the bottom face as well as at top face of the slab [6]. The grade of concrete used is M20, and grade of steel used is Fe415. Totally seven models are designed out of which six models have an opening of different sizes at the different location adjacent to column, and first model is the control specimen without opening.
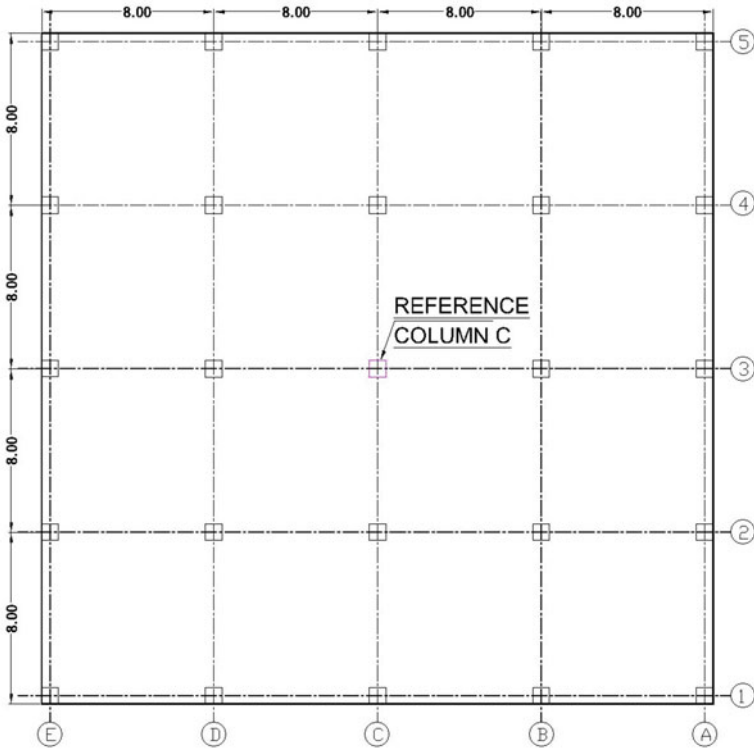
Fig. 1 Plan view of the model (All dimension in m)

Table 1 Model specification details

Case	Location	Size of opening
I	–	No opening
II	Parallel to column face	1.2 × 1.2 m
III	Parallel to column face	2 × 2 m
IV	Parallel to column face	3 × 3 m
V	Diagonal to column face	1.2 × 1.2 m
VI	Diagonal to column face	2 × 2 m
VII	Diagonal to column face	3 × 3 m

The square opening of size 1.2 × 1.2 m, 2 × 2 m or 3 × 3 m is provided at the various location near reference column C. Details of size and location of the opening in specimens are given in Table 1.

Table 1 shows details of the specimen, specimen 1 shows the control model without opening, and other six models have the opening of different size at the
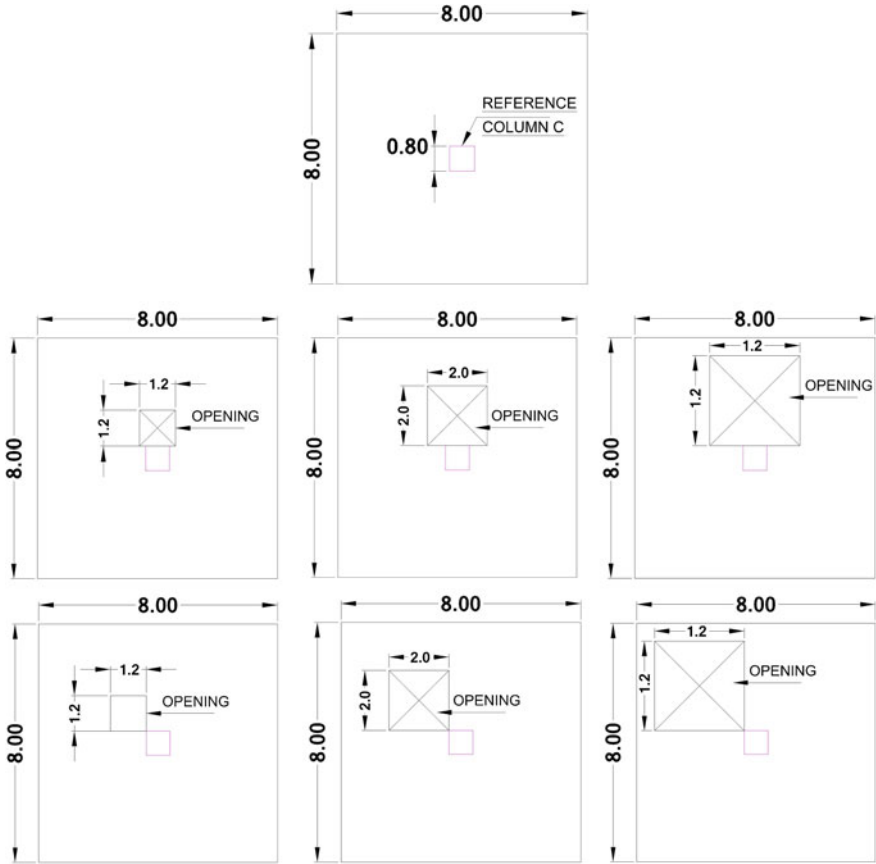
Fig. 2 Opening layout scheme of models. (Dimensions in m)

different locations as per shown in Fig. 2. The different size and location of opening help to understand the behaviour of the discontinuous flat slab.

3 Numerical Analysis

A three-dimensional finite element program 'SAFE' is used for the numerical analysis of seven flat slab models. In this analysis, the material is defined as M20 for the grade of concrete and Fe415 as the grade of steel. All the seven case are modelled and analysed by using the 'Automatic slab mesh option' for the meshing of the slab. Minimum reinforcement ratio used for cracking is 0.12% as per IS 456. In this software depending upon size and location of opening, the percentage of steel is affected and the deflection is constant for all the seven case. Due to opening, the designed

shear stress in the structure increases which results in the increment of punching shear ratio [6], where punching ratio is,

$$\text{Punching Shear Ratio} = \frac{\text{Maximum Designed Shear Stress}}{\text{Shear Stress Capacity}}$$

where shear stress capacity is calculated by $(0.25\sqrt{fck})$ and maximum design punching shear stress is calculated by,

$$\tau_v = \frac{Vu}{b_0 d}$$

where

Vu Shear force acting on the member
b_0 Punching shear perimeter
d Depth of slab

The shear stress capacity of the concrete is 1.118 N/mm^2 for M20 grade of concrete. The shear stress capacity depends upon the grade of concrete and the shear reinforcement provided. Since no shear strengthening is done in any of the models, the shear stress capacity is only due to concrete.

For,

Punching Shear ratio ≤ 1 (Implies the Structure/Model is safe)
Punching Shear ratio > 1 (Implies the Structure/Model fails in punching)

4   Effect of Opening in Flat Slab

The opening is provided adjacent to the column, due to which load path of the structure is disturbed. Providing an opening adjacent to column makes the structure more vulnerable to failure. In order to make the structure safe, proper analysis of the structure must be done and the structure must be designed accordingly. Opening adjacent to column causes high effect on the punching shear behaviour of the structure. The punching shear perimeter is located at the distance d/2 from the column face, where d is the depth of column. The opening adjacent to column implies the discontinuity in punching shear perimeter, due to which the punching strength is highly affected. The effect of opening on punching shear perimeter can be understood more precisely from the Fig. 3.

Form Fig. 3, it is noted that the size and location of opening situated adjacent to column affects the punching shear perimeter of the column. The reduced in punching perimeter directly affects the shear strength of the member.

Since design punching shear is inversely proportional to punching shear perimeter, the decrease in punching shear perimeter increases the design punching shear of the
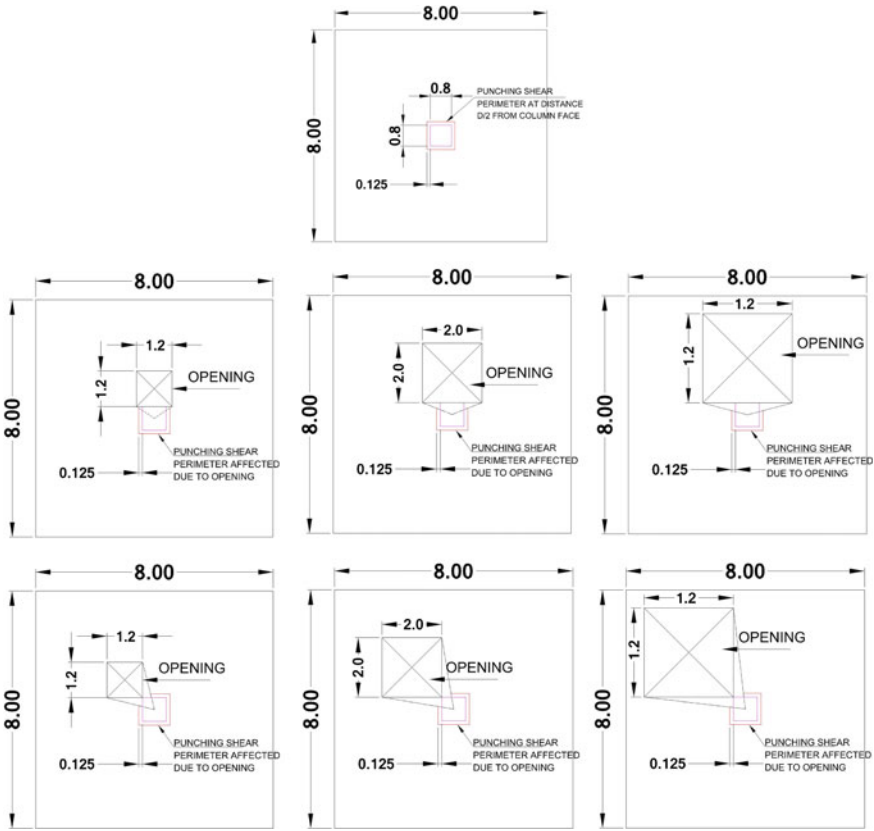
Fig. 3 Effect of opening on punching shear perimeter (Dimensions in m)

member. For all seven cases, the maximum/designed shear stress is calculated using
the finite element-based software. Table 2 shows the results obtained from the finite
element-based software CSI SAFE.

From the results obtain from SAFE, it can be noted that punching shear strength
is highly affected due to the opening adjacent to column face. The punching shear
strength depends upon two parameters since the depth of slab is kept constant; first is
punching shear parameter, and second is the area of the opening. Providing opening
affects the punching parameter as shown in Fig. 3, whereas size of the opening is
directly proportional to the shear force acting on the member. Since the opening is
always considered as an unloaded area of the structure, the load acting in the opening
area is zero, which results in the decrease in shear force at the support.

In order to make the structure safe in punching, proper shear strengthen must be
done. Also, opening in flat slab disturbs the natural load path of the structure/member
which results in the change of the requirement of the steel in the flat slab. From the
results, it can be noted that the size of the opening is directly proportional to the area

Table 2 Punching shear capacity of the specimens

Case	Punching shear perimeter	Punching shear ratio at column C	The percentage decrease in punching shear capacity with respect to case I	Percentage increase in reinforcement required with respect to case I	
				At top face	At bottom face
I	4.2 m	0.9181	–	–	–
II	2.8 m	1.6746	82.40%	18.7%	42.85%
III	2.52 m	1.622	76.67%	18.7%	88.88%
IV	2.38 m	1.3556	47.65%	18.7%	106.89%
V	3.413 m	1.1728	27.74%	0.4%	51.12%
VI	3.326 m	1.0673	16.25%	4.03%	74.88%
VII	3.269 m	1.1238	22.40%	8.13%	84.61%

of steel required at the bottom, i.e., as the opening size increases the area of steel required also increases. This is due to the flexural behaviour of the slab, whereas for the area of steel required at the top face, the location of opening plays an important role.

5 Conclusions

This paper represents a numerical analysis of flat slab with the opening adjacent to column face. The results are obtained for all the seven cases without providing any shear reinforcement so that the effect of size and location of the opening in the flat slab can be studied and compared. Based on the numerical results and discussions, the following conclusions are obtained,

i. The punching shear capacity of the flat slab without opening is higher than the flat slab with the opening.
ii. The punching shear capacity is lowest in case II, i.e., opening of size 1.2×1.2 m parallel to the face of the column. Since the punching shear perimeter (b_0) is reduced by 33.33%, whereas there is not considerable decrease in the unloaded area, i.e., the size of the opening, due to which shear force acting on member is not much affected.
iii. From the results, it is concluded that adjacent openings diagonal to the face of the column are more efficient than the openings parallel to the face of the column.

Form the above study, it is also concluded that, there is a necessity to provide shear strengthening in the form of shear reinforcement or stud rail or by column head or column drop or combination of these; otherwise, the structure will fail in punching shear irrespective of increase in reinforcement at top and bottom face of the slab.

References

1. Li, R., Young, S.C., Zhang, S.: Punching shear behaviour of concrete flat plate slab reinforced with carbon fibre reinforced polymer rods. Compos. B **38**(5), 712–719 (2007)
2. Harajli, M.H., Soudki, K.A.: Shear strengthening of interior slab-column connections using carbon fibre-reinforced polymer sheets. J. Compos. Constr. **7**(2), 145–153 (2003)
3. Faria, D.M., Einpaul, J., Ramos, A.M., Ruiz, M.F., Muttoni, A.: On the efficiency of flat slabs strengthening against punching using externally bonded fibre reinforced polymers. Constr. Build. Mater. **73**, 366–377 (2014)
4. Guandalini, S., Burdet, O.L., Muttoni, A.: Punching tests of slabs with low reinforcement ratios. ACI Struct. J. **106**(1), 87–95 (2009)
5. Al-Saawani, M.A., El-Sayed, A.K., Al-Negheimish, A.I.: Effect of basic design parameters on IC debonding of CFRP-strengthened shallow RC beams. J Reinf. Plast. Compos. (2015)
6. Kadam, K.N., Ingole, Saurabh: Redistribution of punching shear in flat slab with opening. IJIRSET J. **7**(3), 2234–2239 (2018)
7. Florut, S.-C., Sas, G., Popescu, C., Stoian, V.: Tests on reinforced concrete slabs with cut-out openings strengthened with fibre-reinforced polymers, Elsevier (2014)
8. Ebead, U., Marzouk, H.: Strengthening of two-way slabs using steel plates. ACI Struct. J. **99**(1), 23–30 (2002)
9. Abdulrahman, Bassam Q., Wua, Zhangjian, Lee, S.: Cunningham, experimental and numerical investigation into strengthening flat slabs at corner columns with externally bonded CFRP. Constr. Build. Mater. **139**, 132–147 (2017)
10. Li, R., Young, S.C., Zhang, S.: Punching shear behaviour of concrete flat plate slab reinforced with carbon fibre reinforced polymer rods. Compos. B **38**(5), 712–719 (2007)
11. Kadam, K.N., Shaikh, Viquaar: Behaviour of flat slab a study by finite element analysis. IJIRSET J. **7**(3), 2213–2218 (2018)
12. Jendele, L., Cervenka, J.: Finite element modelling of reinforcement with bond. Comput. Struct. **84**(28), 1780–1791 (2006)
13. Anil, O., Kina, T., Salmani, V.: Effect of opening size and location on punching shear behavior of two-way RC slabs. Mag. Concr. Res. (2014)
14. Durucan, C., Anil, Ö.: Effect of opening size and location on the punching shear behaviour of interior slab-column connections strengthened with CFRP strips. Eng. Struct. **105**, 22–36 (2015)

Soft Sensor for TSS in Effluent of Primary Clarifier of Industrial Effluent Treatment Plant

Nital Patel, Jayesh Ruparelia and Jayesh Barve

Abstract Measurement of TSS is of interest and important to accomplish good quality control in wastewater treatment plants. This paper covers work towards the development of a soft sensor to estimate total suspended solids (TSS) in the effluent of a primary clarifier subsystem in a typical industrial effluent treatment plant (IETP). The data pre-processing has been done using 3σ edit rule, and statistical technique has been applied for the development of soft sensor to predict the clarifier effluent TSS as a function of clarifier influent flow rate and influent TSS. The data set has been collected from real-life plant located at Ahmedabad. A set of data is used for the soft sensor development, and other set of data has been used for model validation. The performance analysis has been evaluated based on the absolute percentage error, and it is observed that the absolute percentage error is less than 20%.

Keywords Primary clarifier · Soft sensor · Total suspended solids · Effluent · Wastewater

1 Introduction

The observance of environmental pollution issues and safety rules contribute to increase the complexity of the various industries. Companies are required to respect laws that enforce more and more strict limits on product specifications and pollutant

N. Patel (✉)
Instrumentation & Control Engineering Department, Nirma University,
Ahmedabad 382481, India
e-mail: nital.patel@nirmauni.ac.in

J. Ruparelia
Chemical Engineering Department, Nirma University, Ahmedabad 382481, India
e-mail: jr@nirmauni.ac.in

J. Barve
GE Global Research, Bangalore 560066, India
e-mail: barve.jayesh@gmail.com

emissions of industrial plants. As one of the aspects to fulfil these requirements is development of sophisticated instrumentation systems, software sensors provide an alternative to hardware sensors. In this context, research on developing soft sensors for various parameters has been extensively carried out in last decade [1]. A literature review on data driven soft sensing methods adopted for biological wastewater treatment plants has been discussed by Haimi et al [2]. Fuzzy network and influent quality-based approach for the prediction of effluent suspended solids (SS), effluent chemical oxygen demand (COD) and effluent pH has been presented by Pai et al [3]. Adaptive network-based fuzzy inference system has been developed by Wan et al [4] for the prediction of SS and COD. A data mining approach for predicting the total suspended solids in wastewater has been developed by Verma et al [5].

This paper is organized as follows. In Sect. 2, soft sensor development methods are discussed. Section 3 comprises considered plant and data collection. Statistical soft sensor model and error analysis are explained in Sect. 4. Section 5 comprises concluding remarks.

2 Soft Sensors and Its Development Techniques

Soft sensors are valuable tool in many different industrial fields of application, including refineries, chemical plants, cement kilns, power plants, pulp and paper industry, food processing, nuclear plants, urban and industrial pollution monitoring, etc. [1].

As shown in Fig. 1, soft sensor is a model which processes easily measurable variables and estimate hard to measure variable. It is also known as state observer, software-based sensor or virtual sensor. Soft sensors offer a number of attractive properties:

- They represent a low-cost alternative of expensive hardware sensors.
- They can work in parallel with hardware sensors, giving useful information for fault detection tasks.
- They allow real-time estimation of data, overcoming the time delays introduced by slow hardware sensors.

There are main three approaches used for building the soft sensors: First principle modelling (physical modelling), multivariate statistics and artificial intelligence modelling such as neural networks, fuzzy logic and hybrid methods. First principle modelling technique requires good knowledge of the system and involves mathematical
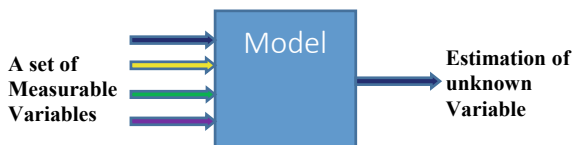
Fig. 1 Soft sensor concept

modelling of the respective process. Multivariate statistics and artificial intelligence methods are termed as purely data-driven techniques. In data-driven techniques, soft sensor model is developed using historical data obtained from the plant. Before using the data for model development, pre-processing like outliers detection and data filtering are applied [1]. A number of strategies exist for the detection of outliers, e.g. edit rule 3σ, parameters of Jolliffe, linear regression residual analysis etc.

For edit rule 3σ using estimated mean, normalized distance for every data sample can be estimated using following expression [6].

$$d_i = \frac{x_i - \text{mean}_x}{\sigma_x} \tag{1}$$

The assumption made is that data follow the normal distribution to get probability for absolute value of normalized distance d_i greater than 3 which is about 0.27%. The x_i observation is taken as an outlier when $|d_i|$ is more than this threshold.

Jolliffe method depends on d_{1i}^2, d_{2i}^2, d_{3i}^2 parameters which are estimated on z variables. These parameters are determined using principal component analysis or projection to latent structure to the model variables. Following expressions were used to estimate the parameters.

$$d_{1i}^2 = \sum_{k=p-q+1}^{p} z_{ik}^2 \tag{2}$$

$$d_{2i}^2 = \sum_{k=p-q+1}^{p} \frac{z_{ik}^2}{l_k} \tag{3}$$

$$d_{3i}^2 = \sum_{k=p-q+1}^{p} z_{ik}^2 l_k \tag{4}$$

Here i is the ith sample of projected variable, p is number of inputs, q is no. of principal components with variance less than 1, z_{ik}, is ith sample of kth principal component and l_k is variance of kth component.

Suitable limits of the three statistics introduced in Eqs. 2, 3 and 4 are to be used as criterion for detecting the outliers.

The third technique for outlier detection is the residual analysis of linear correlation (Warne et al.) which rely on multiple liner regression among independent and dependent variables in the form as shown below:

$$y = X\beta + \varepsilon \tag{5}$$

Here y is a vector of system output data, X is collecting input variable data of matrix, β is a vector of parameters and ε as a vector of residuals. In order to estimate β, least square method is applied using expression (6).

$$\hat{\beta} = (X^T X)^{-1} X^T y \tag{6}$$

The estimated output $\hat{y}$ and model residual $\hat{r}$ are to be obtained using:

$$\hat{y} = X \hat{\beta} \tag{7}$$

$$\hat{r} = y - \hat{y} \tag{8}$$

The plots of residuals with 95% confidence interval were prepared and data whose confidence interval did not cross zero axis were taken as outliers.

3   Treatment Plant and Collection

3.1   Treatment Plant

The objective of central effluent treatment plant (CETP), Vatva, Ahmedabad is to remove pollutants from industrial wastewater as per the government of Gujarat norms. There are 680 units of the Vatva industrial estate located in the total area of about 14 km^2. The internal collection system is installed to collect effluent of each unit. Moreover, 92 sump rooms are constructed to connect all these 680 units. From sump rooms, wastewater flows by gravity to the six pumping stations. Finally, wastewater is pumped to CETP for the treatment. Fig. 2 shows the outline of treatment process.

As shown in Fig. 2, the pretreated effluent is pumped to the equalization tank where 24 h of residence time provided under maximum flow condition. From the equalization tank, the wastewater flows to flash mixer wherein selected flocculants and coagulants are mixed and effluent is sent to clariflocculator. In the clariflocculator, the coagulation and flocculation of suspended solids, colloids and some of the dissolved pollutants take place. At the inlet as well as outlet of the clariflocculator pH, chemical oxygen demand (COD), biochemical oxygen demand (BOD), total organic carbon (TOC), total dissolved solids (TDS) and total suspended solids (TSS) are measured per day for the performance monitoring of clariflocculator. The flocculator overflow is sent to dissolve air flotation. The concentration of suspended solids is maintained less than 100 mg/l in the dissolved air flotation. During these steps, some organic matters removed in colloidal state which results into marginal reduction in the COD. The effluent is sent to aeration tank by gravity where organic matter reduction is carried out by microorganisms present in the activated sludge. The effluent from the aeration tank flows through secondary clarifier. In the secondary clarifier, suspended solids settled down by gravity subsequently discharged from bottom of the clarifier.
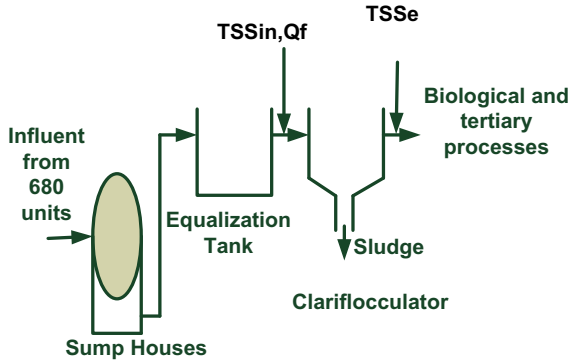
Fig. 2 Schematic of central effluent treatment plant, Vatva, Ahmedabad
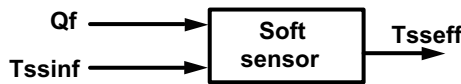
Fig. 3 Soft sensor model for the estimation of TSS_{eff}

3.2 Clariflocculator and Soft-Sensor Model

In this research work, considered process is clariflocculator which is a equipment that comprises flocculation and clarification in a single tank. As shown in Fig. 3, the inner tank serves as flocculation area and the outer tank acts as clarification zone. Thicker solids flow out from the bottom of the tank and clear water flows at the top of the tank. Influent and effluent samples are taken at every 3 h. The plant is operated in three shifts. All the samples of three shifts are combined together and analysed in laboratory for pH, TOC, TDS, TSS, COD and BOD. The plant data for the period of July-December 2015 were collected for this work. This dataset comprises influent flow rate (Q_f), influent total suspended solids (TSS_{inf}) and effluent total suspended solids (TSS_{eff}). The soft sensor is developed for the clariflocculator that estimates TSS_{eff} based on knowledge of Q_f and TSS_{inf}, as shown in Fig. 3.

3.3 Data Set and Outlier Detection

The developed statistical model is based on data set of Q_f, TSS_{inf} and TSS_{eff}. Influent flow rate, influent total suspended solids and effluent total suspended solids are shown in Figs. 4, 5 and 6, respectively.

Before using the data set for model development, it is required to filter out outliers from the data set. The 3σ edit rule is applied for the outlier detection. The outliers representation in Q_f and TSS_{inf} data are shown in Fig. 7 and 8, respectively.
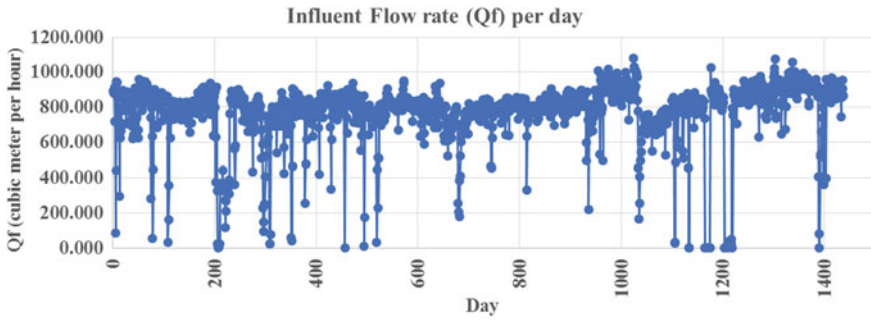
Fig. 4 Influent flow rate per day
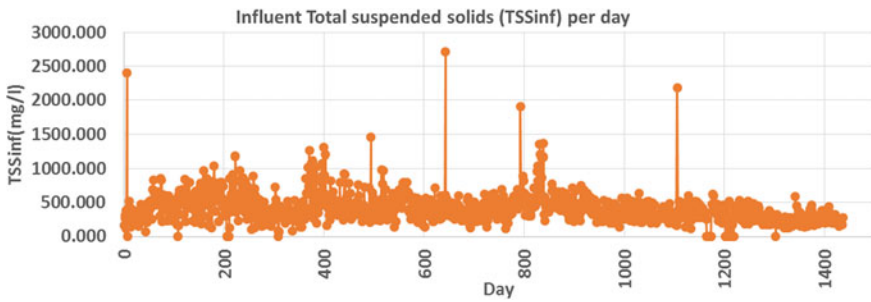
Fig. 5 Influent total suspended solids per day
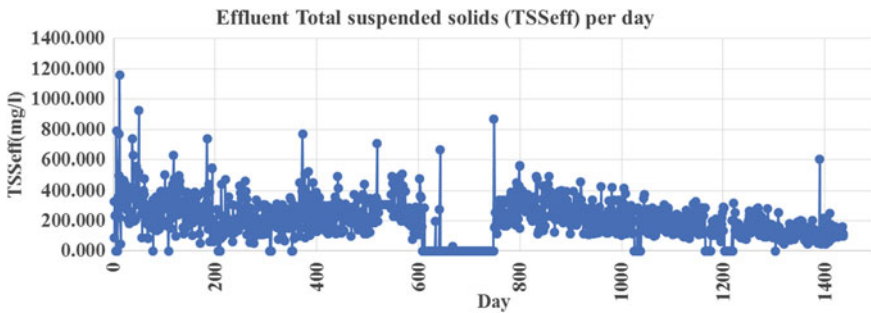
Fig. 6 Effluent total suspended solids per day

4 Statistical Soft Sensor Model and Error Analysis

The soft sensor model has two inputs Q_f and TSS_{inf} and one output TSS_{eff}. The total number of available observations was 1410 including outliers and missing data as 384. After removing the outliers and missing data, 80% data points were used for statistical model development and 20% data points were used for the model
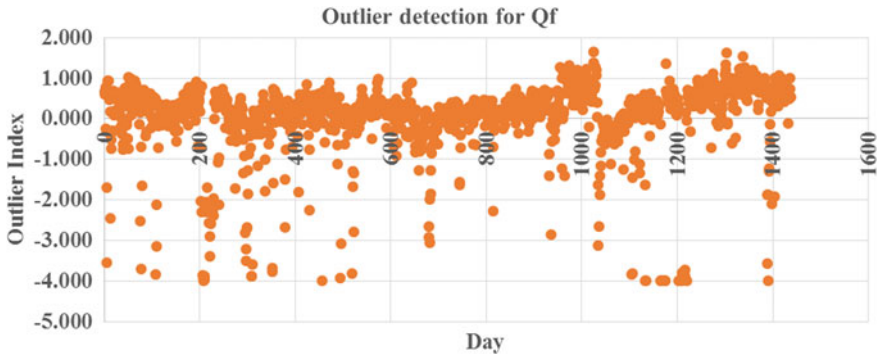
Fig. 7 Outliers representation for Q_f data
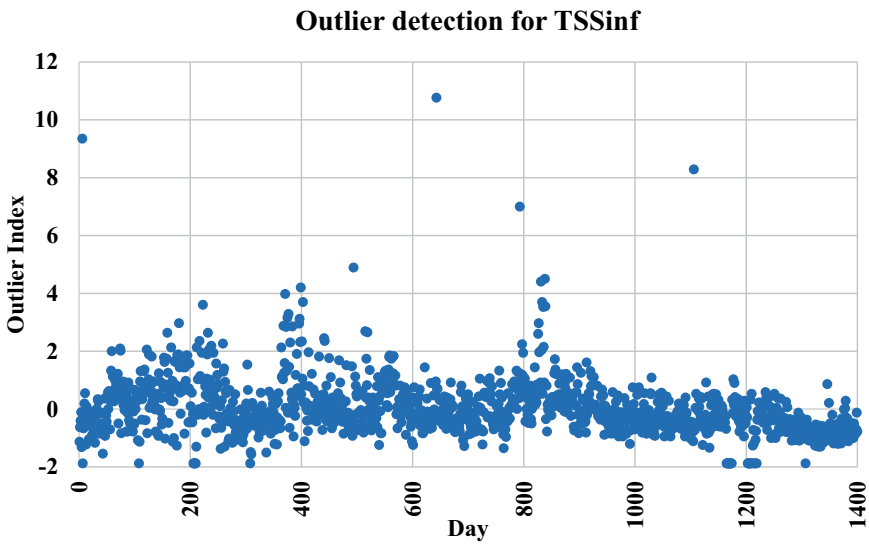
Fig. 8 Outlier representation for TSS_{inf} data

validation. The model has been developed using data analysis toolbox in Excel and equation is as follows:

$$TSS_{eff} = 87.8 + 0.0255 * Q_f + 0.289 * TSS_{inf} \tag{9}$$

The predicted TSS_{eff} and measured TSS_{eff} is plotted as shown in Fig. 9.

The data samples having index greater than 3 or −3 are considered as outliers, and the corresponding data samples are discarded in model development.

The histogram for absolute percentage error is presented in Fig. 10. As per the histogram out of 208 observations, 167 observations fall under the prediction absolute
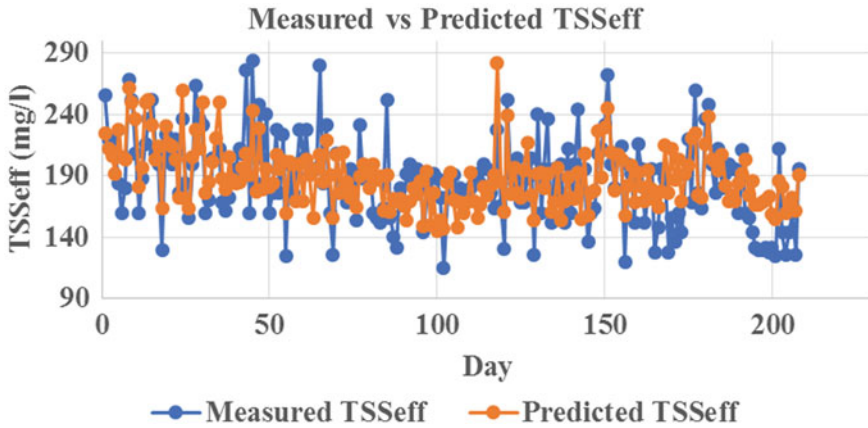
Fig. 9 Measured TSS$_{eff}$ versus predicted TSS$_{eff}$
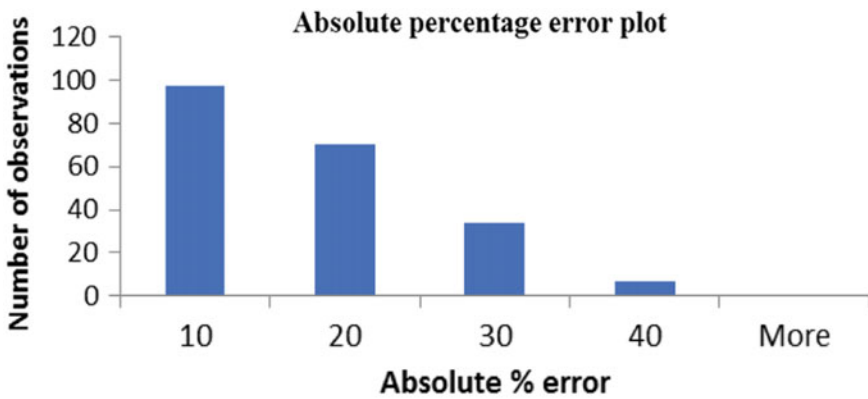
Fig. 10 Histogram representation of absolute percentage error versus number of observations

percentage error less than 20%. The cause of the error is due to measurement error of TSS$_{inf}$ and Q_f.

5 Conclusion

A soft sensor is developed to estimate total suspended solids (TSS) present in the effluent of clariflocculator using influent flow rate and influent TSS. It is found to be fitting well with the available plant data and can be useful to reduce time-consuming and tedious TSS measurements and hence the resources, time and cost for the industrial ETP plant.

References

1. Fortune, L., Grazia, S., Xibilia, M.G.: Soft-Sensors for Monitoring and Control of Industrial Processes, Springer Publication, pp. 27–51 (2007)
2. Haimi, H., Mulas, M., Coronab, F., Vahala, R.: Data-derived soft-sensors for biological wastewater treatment plants: An overview. Environ. Model Softw. **47**, 88–107 (2013)
3. Pai, T.Y., Yang, P.Y.: Predicting effluent from the wastewater treatment plant of industrial park based on fuzzy network and influent quality. Appl. Math. Model. **35**, 3674–3684 (2011)
4. Wan, J., Mingzhi Huang, M.: Prediction of effluent quality of a paper mill wastewater treatment using an adaptive network-based fuzzy inference system. Appl. Soft Comput. **11**, 3238–3246 (2011)
5. Verma, A., Wei, X., Kusiak, A.: Predicting the total suspended solids in wastewater: A data-mining approach. Eng. Appl. Artif. Intell. **26**, 1366–1372 (2013)
6. Warne, K., Prasad, G., Rezvani, S., Maguire, L.: Statistical and computational intelligence techniques for inferential model development: a comparative evaluation and a novel proposition for fusion. Eng. Appl. Artif. Intell. **17**, 871–930 (2004)

Comparative Analysis of BRTS and MRTS—An Approach Required for Selection of System

Sujesh D. Ghodmare, Preeti Bajaj and Bhalchandra V. Khode

Abstract   As cities grow in size, the vehicular trips on roads increase substantially. This necessitates adopting strategy to debilitate private transit modes and support public transport once the traffic volume level along any transit corridor in one way surpasses 8000 people for every hour. The introduction of a rail based Mass Rapid Transit System (MRTS) or Bus Rapid Transit System (BRTS) becomes essential. It has been observed that in developed countries, making arrangements for mass transit system start when population of city surpasses 1 million, and the system is in position when the city population is 2–3 million and once the population exceeds 4 million planned extensions to the MRTS are quickly taken up. Both the mass transit systems are taken into consideration and compared for analyzing the benefits and limitations of the systems. The comparative analysis was done by considering different BRTS and MRTS. In terms of investment, the both systems are very costly. In terms of environmental impact, the MRTS is more effective than BRTS. It was also observed that if Intelligent Transportation System is incorporated the service of both systems may result in enhanced efficiency. It can be stated that the combination of various public transportation systems should be planed during the stages of design considering the integrated approach as a need for good public transportation system

Keywords   Rapid transit system · Private transit mode · Environmental impact · Enhanced efficiency

1   Introduction

Many choices are available as far as the transit systems are taken into consideration for public transportation . It includes public bus, bus rapid transit (BRT), light rail

S. D. Ghodmare (✉) · B. V. Khode
Department of Civil Engineering, G. H. Raisoni College of Engineering, Nagpur, India
e-mail: sujesh.ghodmare@raisoni.net

P. Bajaj
Department of Electronics Engineering, Nagpur, India

transit (LRT), commuter rail system, metro rail transit system (MRTS). The transit system which can satisfy the needs of both users and operators and its success in terms of sustainability depends on the optimal design and its aspects related to service. Generally the planning process for public transportation system is targeted to provide the higher LOS at affordable cost with ease of access, less travel time, reliable providing safe and comfortable journey with minimum environmental impact. When it comes to select the particular transit system, the conventional techniques for the purpose of analysis fail to consider the various nonmonetary issues. These issues are well connected with the society at large and sustainability and have considerable impact on the final choice. Prime minister of India Mr. Narendra Modi well said during his one of speech "Let us create streets for PEOPLE not for VEHICLES" .

Both BRTS and MRTS are the systems which require the huge amount of investment in order to provide the good level of service (LOS) and comfort level to the users [1]. This makes it essential to compare these two transit systems as both the systems are capable of serving about one million passengers per day. There are many points for consideration on the basis of which there are two different groups supporting BRTS and MRTS. There are number of parameters on the basis of which an attempt has been made to compare BRTS and MRTS to help decision makers to suggest regarding the selection of either system are discussed in this paper. The major highlighting characteristics are flexibility, life span of vehicles, investment, environmental impacts, etc. are tried to elaborate for BRTS and MRTS in following sections.

1.1 Metro Rail Transit System (MRTS)

MRTS is a well-known urban electronic transportation system. Using rail tracks, it is capable of providing the high-frequency service with considerable capacity. The main characteristics of this system is its independence from other vehicles, roads, and pedestrians as the system is designed for performing the operations using physically separated infrastructure. The system is also well-known as metropolitan rail, subway, tube, elevated, underground railway in different parts of world.

1.2 BUS Rapid Transit System (BRTS)

BRTS is the public transportation system which is bus-based service operated on limited stops [2]. It usually operates on dedicated lanes on the basis of special rights. It generally operates on surface but in some cases grade separation is provided to avoid the intersections or populated city centers. BRTs were first introduced in Brazil in 1982. With the aspect of specific system design, the capital cost of BRTS is 10–90 times less than the MRTS system. Capacity and speed are the main characteristics of BRTS. Nowadays the system incorporated with the use of modern devices such

Fig. 1 MRTS-Delhi Metro
"Heritage Line"(India)

Fig. 2 BRTS-Pune (India)

as global positioning system(GPS), signal priority system, smart cards, electronic display boards, etc. are also enhancing the reliability of the system (Figs. 1 and 2).

2   Historical Development of MRTS and BRTS

2.1   Bus Rapid Transit System (BRTS)

Though the planning for various BRTS started in about 1930, the concept of BRTS was first evolved in 1974 in Brazil at Curitiba. Due to its advantages, number of many BRT systems was implemented by the various authorities. According to Global BRT data source, 2012 BRTS is successfully running in about more than 146 cities through the 150 BRT systems across the world with capacity to serve about 25 million passengers per day over about 3700 km of dedicated way. The concept of BRTS was first emerged to replace the rail transit lines with express bus system on freeway in central areas of Chicago. After this during 1955–1959, the Washington D.C. transit plan proposed the 86 mile BRTS (W. C. Gilman and Co. 1959). This indicates that

transit operators are working for improvement of service to customers as per the need and requirement since 1930.

Later on BRTS was developed in many other cities of Alegre, Brazil (1977), Pittsburgh, US (1977) America (Meirelles 2000). In 1996, Quito started BRTS based on electric trolley bus system. At present, the Sao Paulo BRTS is the largest BRTS system with about 250 km of dedicated lane providing service to about 3.2 million trips to the users per day.

2.2 Metro Rail Transit System (MRTS)

Metro the very common word nowadays is the word came in picture from "Paris Metropolitan" and applied to almost all subway systems. It is also regarded as the rapid transit rail system. As recorded in year 2014, about 168 MRTS are providing services across the globe.

Though the idea of underground railway was first proposed in 1830, and the line was build in 1854, the world's first metropolitan rail system was opened on 10 January 1863 between Farrington and Paddington of London. It was the underground system working on steamed train, served about 38,000 passengers on first day and was not proper.

After this in 1872, a British company was registered to build the MRTS which started serving the users on 17 January 1875. In 1897 in Boston, US build the subway tunnel which is in use till date also. In 1913, the oldest subway was opened in Argentina. The world's longest metro system in existence currently was opened on 17 October 1919 in Madrid. After this, the Barcelona metro was opened in 1924 followed by Japan (Tokyo) in 1927 and Osaka in 1933 followed by Moscow in 1935 which is the most busiest MRTS with 186 stations and 308 km track.

After this, the implementation of new MRTS system in various countries such as Toronto (1954), Canada (1966), Brazil (1974), South Korea (1974), Kolkata (India, 1984), Cairo (1987), Singapore (1987), Taiwan (1996), Iran (1999), UAE (2009), Saudi Arabia (2011) were started, and the list is still increasing.

2.3 Barriers to Rapid Transit System—MRTS and BRTS

Rapid transit systems help in enhancing the travel conditions and can be considered as an attempt to attain the sustainability. Still there are number of unavoidable challenges in the process of implementation of MRTS and BRTS [3]. According to Wright, 2007 enlisted political interference, institutional bias and capacity, technical capacity, finance, geographical limitations, and physical limitations as the barriers that generally emerge in case of developing countries during rapid transit projects.

2.4   Comparative Analysis Between MRTS and BRTS

MRTS and BRTS are also well-known as the high capacity public transit systems. Due to successful results, the popularity of the both systems is increasing day by day. In some cities, the BRTS is also introduced to make public transportation more attractive in competition to private vehicles [4]. After the successful implementation of Bagota BRTS in Colombia, it was proposed and adopted by different countries including India.

Same is the situation with MRTS and number of new projects of either BRTS or MRTS, under rapid transit system is increasing day by day. Based on these facts, it becomes necessary to analyze the MRTS and BRTS according to its economical, social, and environmental impact. Though BRTs requires comparatively less initial investment and has good capacity to serve the transportation system due its number of deficiencies, it has to face public criticism as was happened on few corridors [5]. The deficiencies such as untrained drivers, less speed, low frequency, problems due to private vehicles and pedestrians, lack of supporting infrastructure and parking spaces, etc. This type of situations has generated in depth debate on the issue of selection between MRTS and BRTS. Basically choice between BRTS and MRTS is based on present and forecasted passenger demand, characteristics of the corridor, financial capacity of the community [6]. Therefore, if the characteristics of BRTS and MRTS are reasonably understood and if the accurate estimation of the travel demand is assured, it becomes possible to take the proper decision to select either of the system in rational consideration [7]. Therefore, it is very important to compare the various parameters of both BRTS and MRTS.

In this paper, it has been tried to compare the MRTS and BRTS on the basis of some selected important parameters such as requirement of space and catchment area, speed of journey, passenger carrying capacity, accessibility, safety, users perception and modal split, environmental impact, economic impact, mobility benefits, cost and benefit, and PROS and CONS as explained below

2.5   Factors Affecting the Choice Between BRTS and MRTS

1. **Popularity, Users Perception, and Modal Shift**

The rapid transit systems have the capability to provide the high-quality public transit system which ultimately results in user's satisfaction [8]. This quality parameter is responsible for the modal shift from private to public transit system (Deng and Nelson 2010).

As shown in Fig. 3, popularity of BRTS is more due to its generous characteristics such as flexibility, extent, low fare rates, etc. In many studies, it was reflected that the popularity of the BRTS was quite high [9]. As far as rush hours are taken into consideration, both MRTS and BRTS are accepted by users as an alternative to the private vehicles (Deng and Nelson 2010).

Fig. 3 Popularity of MRTS
and BRTS

	London	Maxico	Hong Kong	Singapore	Chennai	Delhi
■ Popularity(%) BRTS	62	86	57	61	79	90
■ Popularity(%) MRTS	38	14	43	39	21	10
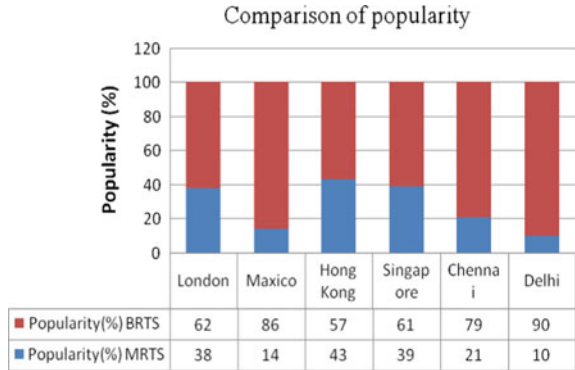
Fig. 4 Evolution of MRTS
and BRTS
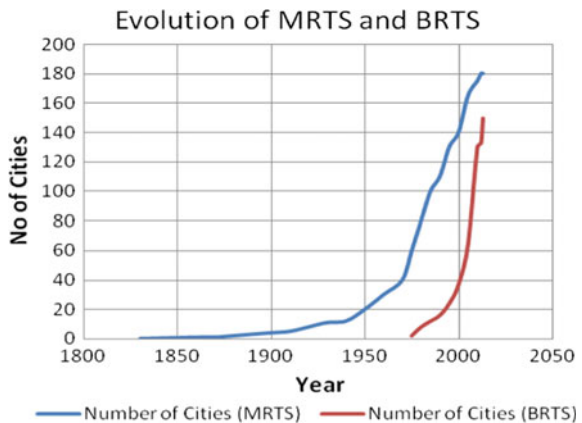
The overall impact of all above parameter is the acceptance of the authorities to MRTS as the sustainable mode of transportation. As shown in Fig. 4, this resulted in proposal of many no of new MRTS projects in different cities all over the world. The graph clearly indicated that the number of MRTS projects is increasing at huge rate as compared to the new BRTS projects. If this trend continues, the number of successfully implemented MRTS projects will be more than 300 by year 2050.

2. **Requirement of Space or Catchment Area**

MRTS requires very less road space in comparison with BRTS. It requires no space if underground system is proposed and approximately 2 m width is required if elevated system is proposed. However, it has the capacity equivalent to the nine lanes of bus traffic and 33 lanes of private traffic on either way.

As an example, the BRTS at few stretched of Delhi can be taken into consideration. The six-lane road was also affected seriously due to implementation of BRTS resulting in heavy traffic congestion for many hours.

3. **Speed of Journey**

Fig. 5 Average minimum and maximum speed of different modes
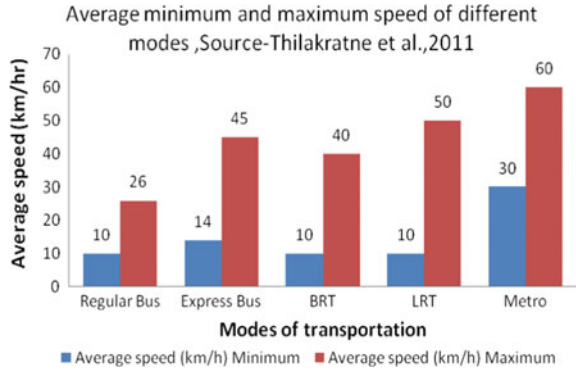
Fig. 6 Average minimum and maximum capacity of different modes
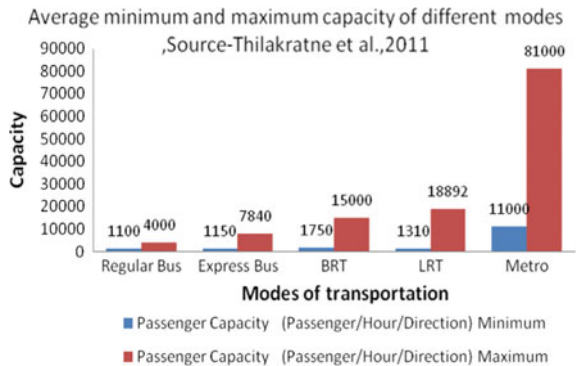
The operating speed and speed of journey of any rapid transit system is mainly influenced by spacing between stops, design of corridor, and many other factors. BRTS generally prefer the limited stops in comparison with the regular bus service which results in extra traveling by passengers in many cases (Fig. 5).

Though the extended green time increases the speed of BRTS system considerably the average speed of journey and operating speed are recorded to be very less as compared to MRTS. As shown in the graph, above metro has the highest speed when compared to the other rapid transit modes. The main reason for this is the zero interference of the other modes of road transit system.

4. **Transit Capacity**

Transit capacity is generally represented as the capacity in passenger per hour per direction which the particular mode of transportation can comfortably and safely accommodate. The operator generally attempts to provide the capacity as per the demand because if demand is not satisfied, many service qualities are negatively affected. Therefore, assurance of adequate capacity is important. The total capacity consists of vehicle capacity, station capacity, and corridor capacity (Fig. 6).

As shown in the graph above, the overall capacity (maximum and minimum) in terms of passenger/hour/direction of MRTS is superior to all other rapid transit

modes. It can be noted that there is huge difference between the capacity of MRTS and BRTS. The maximum capacity of MRTS is about 81,000, and minimum is 11,000 passenger/hour/direction while for BRTS it is 15,000 and 1750, respectively. Therefore, the level of service of MRTS is also superior in case of MRTS.

5. Accessibility and Mobility Benefits

Accessibility in case of rapid transit system depends on many factors. These factors again have the impacts on dwell time, comfort of passengers, transit capacity, ridership, level of acceptance etc. Many features are added to the transit mode to enhance the accessibility. In case of BRTS as maximum stretch is of at grade type, the access to the system is more convenient than MRTS. But it maximizes the risks also. Whereas in case of MRTS, maximum corridors are elevated along with the stations which rises the issue of accessibility. But several measures such as additional door channels, battery operated vehicles, enhancing the wheel chair security, free or paid bicycles, etc. are introduced by MRTS operators. These features increase the connectivity, and as a result, the accessibility to the MRTS is comparatively improved.

Both metro rail transit system and bus rapid transit systems have the ability to enhance the transit ridership within the effective area of the corridors. BRT system is attractive as it is affordable due to the advantages it has along with lower capital investments. Its infrastructural investment is also less as compared to the requirements of MRTS. The one of major advantage of BRTS and MRTS is the capability of shaping land use in the form of spatial distribution within the region. This can be made possible by establishing connectivity between centralized urban area with the suburban area. Land use policies, travel demand management, and growth management in integrated way are the parameters which has the capabilities to offer the solution for different challenges during the operation period which can result in sustainability of the system.

6. Safety Improvement

The measure of safety is represented by the frequency and level of accidents and injuries experienced by the users. The performance parameters for measuring the safety level are rate of accidents and public perception.

Based on the public perception through various surveys, both BRTS and MRTS have the high safety levels which reduces issues and conflicts at stations and along the corridors. The advanced technologies such as camera monitoring facilitate active management of system quick responses to crime and incidents along with its reduction. On the basis of various investigations, it can be stated that apart from the common facilities due to less connectivity with the road traffic, MRTS has low rate of accidents as compared to BRTS.

7. Environmental Impact

As required for a good transit service, both BRTS and MRTS have positive role in reducing the air pollution from the transportation system. This is mainly due to reduction in use of number of private vehicles, propulsion system, alternative fuel, use of solar energy, and emission control regulation by different authorities. The level

Fig. 7 Pollution Level by
different modes

Pollution level by different modes

	Private Car	Taxi	Regular Bus	BRT	Rail	Motor
Pollutant CO2 (Ton)	140	116.9	19.8	4.7	7.5	62
Pollutant Nox)kg)	746	662	168.4	42	17.5	90
Pollutant Oil (ton)	49.2	41	6.9	1.6	2.6	21.8
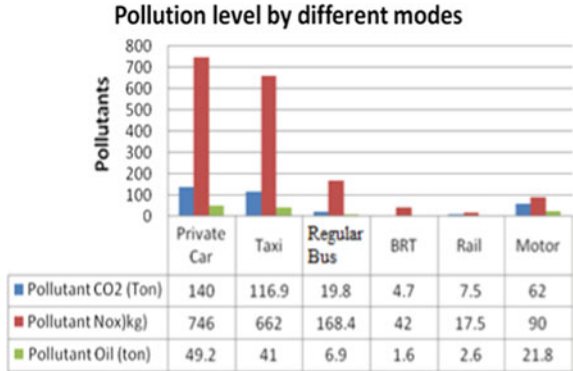
Fig. 8 Energy efficiency of
different modes

Energy Efficiency (MJ per pass of km) Source- J. Kenworthy 2008, Droege)
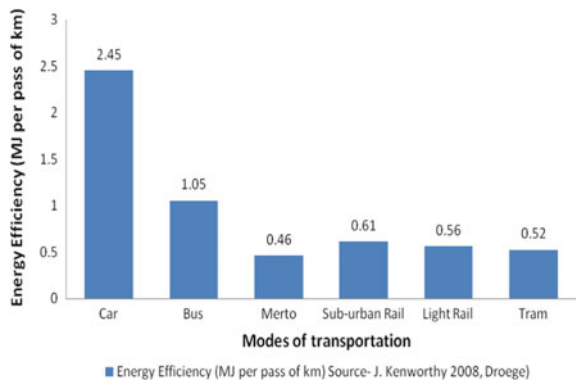
of output depends mainly on percentage modal shift, travel time reduction, speed of journey, etc. As per the data available, MRTS requires near about 50% less energy per passenger to be carries in comparison with BRTS. Furthermore advantages of MRTS are its reliability, comfort level, safety, etc. Journey time reduces by about 50–75% by MRTS (Kumar 2011) (Fig. 7).

As shown in above graph, private car is the main culprit in enhancing the intensity of pollution followed by taxi and regular buses. Both BRTS and MRTS have the less impact. As BRTs is generally operated on the conventional fuel, it has comparatively more impact in increasing the pollution than MRTS which runs on propulsion system. The another reason for less impact by MRTS is the enhanced utilization of solar energy for different operations (Fig. 8).

As shown in above graph, MRTS is the most energy efficient mode of transportation as compared to other modes followed by other rail systems. It can also be observes that car which represents the major private transit mode gives the worst results in terms of energy efficiency followed by the bus as a mode of transportation.

8. **Economic Impact**

Fig. 9 Capital investment
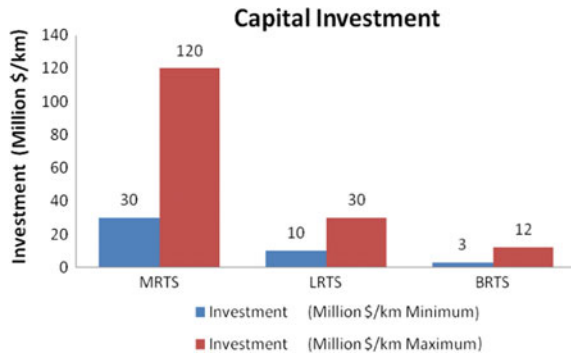
Generally the implementation of project as far as the transportation system is concerned in urban area is decided on the basis of cost benefit analysis and geometric constrains. According to Mark L. Tourner Marc Le, selection between MRTS and BRTS is mainly related to the number of passengers/hour. If it is 3000 passengers/hour BRTS should be adopted and if it is more MRTS should be adopted. It can also be stated that metro has its own class and should be implemented when demand exceeds the capacity of BRTS and high speed of the journey is expected.

Both BRTS and MRTS have the positive impact on economic status. It can be stated that both system are capable of influencing the transit-oriented development resulting in the increment in land values, improves scope for employment and opportunities, etc. It has been observed by many researchers that, because of the difference between cost of implementation and characteristics of surrounding localities the MRTS has more potential of development which causes more positive economic impact.

9. Cost and Benefits

BRTS is the very much cost effective in comparison with other public transit systems as its capital investment per kilometer is less (Levinson et al. 2003 and FTA 2004). This makes BRTS an affordable and attractive public transit system if the budget is the main concern. Hossain (2006) stated that cost of implementation of BRTS is about US$ 1.3 million/Kilometer, whereas for metro project in Bangkok was about US$ 43.4 million/kilometer (Fig. 9).

Metro systems have number of systems depending on its capacities. If the system has the capacity ranging from 60,000 to 90,000 Phpdt (Passenger per hour per direction) it is heavy capacity system. For medium and light capacity systems the range is 40,000 to 50,000 and 25,000 to 30,000 Phpdt respectively (DMRC experience, Kumar 2011). Similarly the cost/km for different systems varies. It was about 275 (Rs.Cr.) for heavy capacity underground system and 110 for heavy capacity elevated system. For medium capacity, it was estimated to 220 and 85 and light capacity it was estimated to 200 and 75, respectively (DMRC experience, Kumar 2011) (Table 1).

When compared, the cost of different mass transit system also shows the huge variations in both capital cost and operating cost. It was observed that the average capital cost (2000 US$/mile in millions) for BRTS, LRT, and MRTS was about

Table 1 Cost of different transit modes (Deng and Nelson 2011)

Parameter	BRTS	LRTS	MRTS
Average Capital Cost (2000 US$/mile in millions)	13.46	34.7	168.51
Average Operating Cost (2000 US$/vehicle revenue mile in millions)	4.73	12.22	8.54

Fig. 10 Construction time required
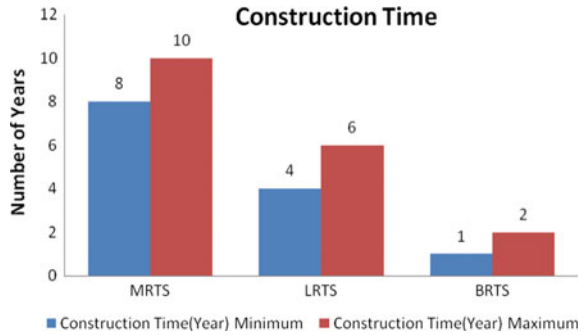
13.46, 3470, and 168.51, respectively (Deng and Nelson 2011). Deng and Nelson also observed that the average operating cost (2000 US$/vehicle revenue mile in millions) for BRTS, LRT, and MRTS was about 4.73, 12.22, and 8.54, respectively. It clearly indicated that the cost investment for all mass rapid transit systems is huge. Still BRTS requires comparatively less investments (Fig. 10).

As per bus rapid transit planning guide, 2007, Page-70, it can be stated that the capital cost investment for underground MRTS is highest. It is about 40 to 350 million US $ per kilometer. For elevated MRTS, the cost is comparatively less but still ranges between 40 and 85 million US $ per kilometer. But both systems have the maximum passenger carrying capacity per hour per direction up to 50,000–70,000, respectively. The capital cost for BRTS ranges from few million US $ per kilometer to 15 million US $ per kilometer but the maximum passenger carrying capacity per hour per direction is also less. It ranges from 5000 to 43,000 approximately.

The MRTS projects require the huge capital cost per kilometer of the corridor. Also it is the general trend that the operator has to arrange for the entire cost of the project. In case of BRTS operator is responsible for cost of transport vehicles and operation and maintenance cost as in case of BRTS all other infrastructural facilities are borne by the government authorities of the benefited area. But when compared, it is generally argued that MRTS requires huge investment. Actually for the purpose of comparison to support the decision criteria, every proportional parameter must be taken into consideration and not only the favoring parameters for both the systems (Litman 2009 and 2010).

3 Conclusion

As discussed above, both systems have their own valuable characteristics. But if few parameters such as initial investment and time of construction of project are considered secondary MRTS is superior to BRTS in almost all considerations. That is the reason that metro is serving about 112 million passengers per day. BRTS is also serving in about 156 cities across the world with about 26 million passenger ridership per day. The important issues regarding successful and proper implementation of MRTS and BRTS are assessment of requirements and public perception. For both MRTS and BRTS should be designed as per the requirements of their potential users. Integration with almost all modes of transportation is also the need to make the system more efficient and sustainable. If the challenges and risks are not handled properly, it may result in reduction in ridership and exclusion by the potential users such as elders, children, women, especially abled and minorities.

Any public transit system can only become successful if it is capable of encouraging users to shift from private vehicles to the new system. Every transit system has its own characteristics but the good public transit system should be the combination of different transportation systems. These different systems should be complimentary to each other and not in competing with each other. From the stage of design itself the system should be developed based on integrated approach. Similarly the experience gained from various projects the aspects related to operation and maintenance can be applied and implemented for upcoming projects to promote the social acceptance and for ensuring the sustainable development.

Hence, it can be stated that both MRTS and BRTS have the upsides and downsides. BRTS can provide service to more destinations, activity centers but has limitations in attracting the riders per capita. MRTS can provide service to less destinations but has huge impact on development of area nearby the corridor and the stations and has great per capita ridership. Overall it can be concluded that due to some parameters in case of MRTS which cannot be obtained through BRTS, MRTS has lower cost per passenger kilometer and can be thought of as the more sustainable public transit system to be promoted in the urban and suburban areas of emerging metropolitan cities.

References

1. Wright, L., Fjellstorm, K.: Mass transit options. Eschborn, Germany.GTZ (2003)
2. Vedagiri, P., Arasan, V.T.: Estimating modal shift of car travelers to bus in introduction of bus priority system. J. Transp. Syst. Eng. Infrastruct. Technol. **9**(6), 120–129 (2009)
3. Niraj Sharma et al.: Critical issues related to metro rail projects in India. J. Infrastructural Dev. **5**(1), 67–86 (2013)
4. Rangrajan, A: BRTS-bus rapid transit system in pune: modeling, simulation and feasibility analysis. In: Proceedings of International Conference on Industrial Engineering and Operations Management Dhaka, Bangladesk, January 9–10, 2010781 (2010)

5. Xisong Dong et al.: Research on bus rapid transit (BRT) and its real time scheduling, IEEE (2011). 978-1-4577-0574-8/111
6. Wang, Yuanqing, et al.: Modal sift behaviour impacts from the introduction of metro service: Case study of Xi'an China. J. urban plann. Dev. ASCE/September **139**(3), 216–225 (2013)
7. Litman, T.: Evaluating public transit benefits and costs, Victoria: Victoria Transport Policy Institute (2004)
8. Wirasinghe, S.C.et al.: Bus Rapid Transit (BRT)_ A Review. J. Urban Sci. (2013). https://doi.org/10.1080/12265934.2013.777514
9. Satiennam, Thaned, et al.: A study on the introduction of bus rapid transit system in asian developing cities _ A case study on bangkok metropolitan administration project. IATSS Res. **30**(2), 2006 (2006)

Prediction of Groundwater Withdrawal for a Composite Coal Mine Over a Mine Life: A Case Study

Prashil P. Shukla, Ashish P. Shukla, Amol R. Zilpe and Avinash P. Saraf

Abstract There are three opencast Coal Mine pits in the area, namely Pandharkawda OC, Marki OC, and Mini Marki OC. The Opencast Pit at Marki has an area of 44 ha and will attain a maximum depth of 50 mbgl with open pit mine life of 10 years. Pandharkawda Opencast is having an area of 40 ha with maximum depth of 45 mbgl having opencast mine life of 9 years. Mini Marki OC is the third small Opencast Pit which will start production in 28th Year i.e., after the closure of Pandharkawda Underground. It has a small area of 7.25 ha with life span of 3 Year (28th to 30th Year). Thus, the total opencast mining area is 91.25 ha. In the area, two underground (UG) patches are proposed namely Marki and Pandharkawda UG which will commence production after completion of opencast workings. These sections will attain a maximum depth of 150 mbgl. Life span of Marki UG will be 20 Years (10th to 27th Year) and that of Pandharkawda UG will be 18 Years (9th to 27th Year). Coal Mine is producing coal @ 0.30MTPA peak since 2017. The Coal Mine was operated for 3 years from 2011 to 2013 and again resumed production since 2017. Hence, the opencast mine Pandharkawda OC, Marki OC will last its operation till first 9 years, and underground Coal Mine will continue from 9th year onwards till 27th year. Total planned mine life of Marki Mangli-I Coal Mine is around 20 years whereas Mini Marki OC will start its operation from 27th years onwards till 30th year. Study for prediction of groundwater withdrawal for subjected Coal Mine was carried out pre-monsoon and post-monsoon period in year 2016 to quantify the groundwater withdrawal from coal mining operations. The predicted quantity of groundwater withdrawal from Coal Mine is used by mine management to create groundwater recharge structure to compensate the groundwater discharge during mine operations.

P. P. Shukla (✉) · A. P. Shukla · A. R. Zilpe
Environmental Consultant-Impact Assessment, Enviro Techno Consult Pvt. Ltd., Nagpur, India
e-mail: prashilshukla@yahoo.com

A. P. Shukla
e-mail: apshukla@yahoo.in

A. R. Zilpe
e-mail: azilpe2003@yahoo.com

A. P. Saraf
Gondwana Geological Society, D.G.M., Nagpur, India

1 Introduction

Coal Mining (may be by opencast or underground method) depletes groundwater table during excavating coal. It is very important to assess the quantity of groundwater withdrawal during the mining operation. Major sources of groundwater withdrawal from a coal mining activity are

(i) Groundwater seepage during mining activity and (ii) groundwater withdrawal by means of bore wells/tube wells for domestic and drinking purposes.

Considering seepage rate, carrying pump test, studying local geology, lithology subject to proposed depth of Coal Mine, pumping of groundwater from bore wells used for domestic purpose groundwater withdrawal is assessed.

2 Literature Review

This project has been arrived at after study in the literature available, various reports in scientific and nonscientific publications regarding groundwater withdrawal, hydrogeological data available, guidelines of Central Ground Water Agency, Groundwater Survey and Development Agency, Ministry of Environment, Forest and Climate Change. The purpose of the literature review is to consider all the available literature on the subject and help to arrive at a judicious view based on factual status of groundwater withdrawal from a subjected Coal Mine.

3 Methodology

The hydrological and hydrogeological studies of the core zone (mining lease area) and buffer zone (10 km radius area from lease boundary) and impact of mining on the water regime are assessed by collecting hydrogeological data of key wells by visiting them in the field, studying present groundwater conditions, present groundwater withdrawal, and status of groundwater development. The pre- and post-monsoon data was collected from 10 dug wells of buffer zone. The fluctuation of water levels in surrounding area of the proposed mines as recorded through monitoring wells was interpreted in relation to mining depth and its impact on quantity of water. The present report embodies the findings of detailed hydrological and hydrogeological studies carried out for core and buffer zones of Marki Mangli-I Coal Mine and impact of mining activity on water regime.
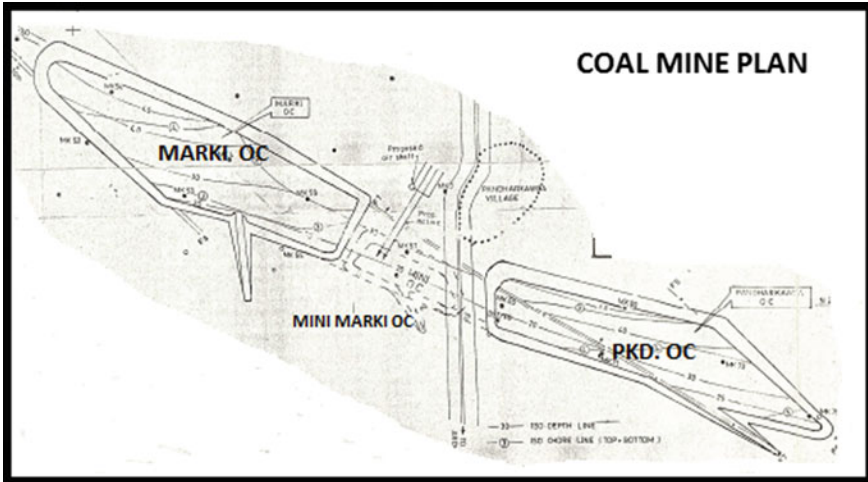
Fig. 1 Coal Mine plan of case study

4 Collection of Data and Interpretation

Marki Mangli-I Coal Mine (N 19° 50′ 47″ and E 78° 46′ 41″) is located over five villages namely Marki Khurd, Marki Buzurg, Ganeshpur, Pandharkawda, and Pardi in Tahsil-Jhari Jamni, District-Yavatmal (MS). The area is covered by Survey of India Toposheet No.56 I/9 and I/13 and its mining lease covers an area of 682.78 ha (Refer Fig. 1) (Table 1).

Well data interpretation w.r.t. reduced level and groundwater flow direction is drawn as (Figs. 2 and 3).

Pump Test:

Pump test continued for 700 min when pumping level stabilized indicating steady state with drawdown of 46.44 m, while interpretation of pump test data has been done by Cooper and Jacob's Method which has indicated transmissivity of 37.41 m^2/day and hydraulic conductivity of 0.53 m/day taking aquifer thickness of 70 m. This is very low value of hydraulic conductivity.

5 Assessment of Groundwater Seepage and Extraction

Groundwater Seepage, Extraction OC Operations

Three opencast pits in the area named Marki, Pandharkawda, and Mini Marki OC. The opencast mine at Marki has an area of 44 ha and will attain a maximum depth of 50 mbgl with a life span of 10 years. Pandharkawda Opencast pit is having an

Table 1 Groundwater wells observation[a]

S. no.	Village	Type of well	Depth of well	Diameter of well	Aquifer	Reduced Level during Oct. 2016	Reduced level during May 2016	Latitude (Deg-decimal)	Longitude (Deg-decimal)
1.	Jhari	DW	10.58	4.5	Basalt	98.1	93.7	19.8624	78.7275
2.	Kadakdari	DW	8.33	4.2	Basalt	99.35	96.2	19.9042	78.7823
3.	Sindiwadhona	DW	4.65	4.8	Basalt	99.55	94.7	19.8782	78.8666
4.	Rajur	DW	15.78	4.58	Limestone	96.33	94.3	19.7608	78.8233
5.	Patan	DW	10.42	4.48	Shale	96.1	89.9	19.8043	78.7018
6.	Kharboda	DW	12.2	4.82	Shale	97.2	90.8	19.8188	78.7218
7.	Jhamni	DW	9.37	4.5	Basalt	97.85	94.1	19.8625	78.7279
8.	Salebati	DW	14.5	4.5	Basalt	97.05	93.1	19.8717	78.7617
9.	Marki	DW	15.8	0.165	Sandstone	87.85	86.2	19.8638	78.7759
10.	Pikiwadhana	DW	12	4.5	Basalt	99.05	94.6	19.8846	78.8475

[a] All dimensions are in meter
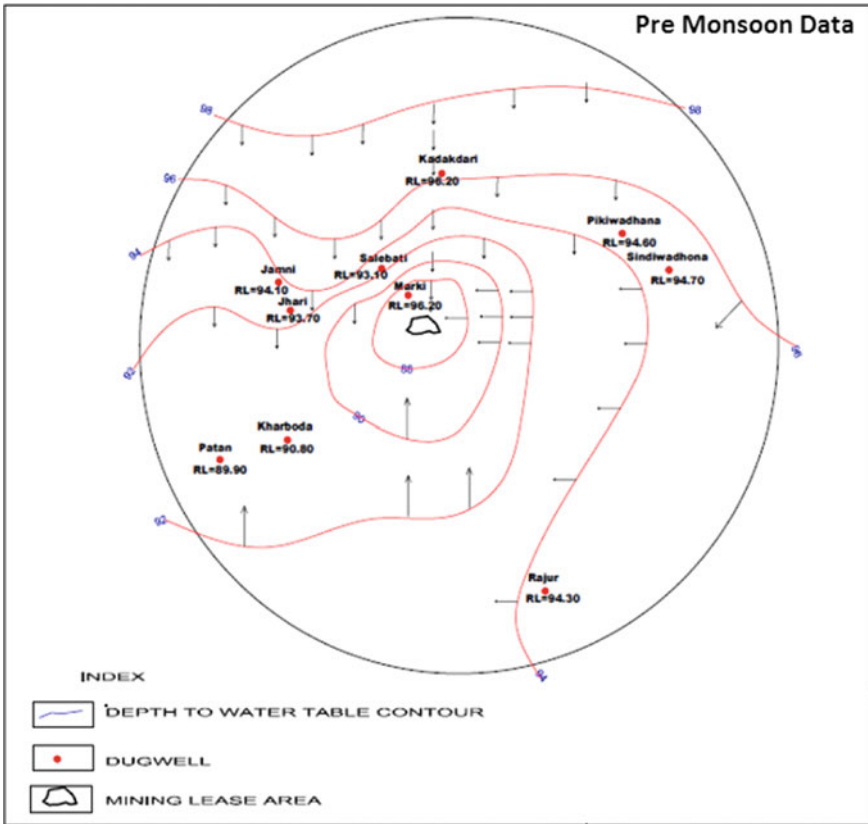
Fig. 2 Well data interpretation w.r.t. reduced level and groundwater flow direction for pre-monsoon period

area of 40 ha with maximum depth of 45 mbgl and life span of 9 years. Mini Marki is the third OC mine and will start its operation in 28th year, i.e., after closure of Pandharkawda Underground section. It has a small area of 7.25 ha with life span of 3 year (28th to 30th Year). Thus, the total opencast mining area is 91.25 Ha. When the opencast mining is initiated and depth of mining goes below water table, an inflow of groundwater will start accumulating in mining pits. This inflow will gradually increase as the mining activity spreads and will be maximum when opencast mining pits achieve maximum open area and depth. This mine seepage will need to be withdrawn to have smooth opencast mining.

Seepage from aquifer zone will not commence till pits achieve depth of more than 20 m as Barakar sandstone is encountered at a depth of 20 m. This Barakar sandstone is overlain by ferruginous clays belonging to Kamthi which do not release much water. Whatever water that gets collected from direct rainfall and subsurface
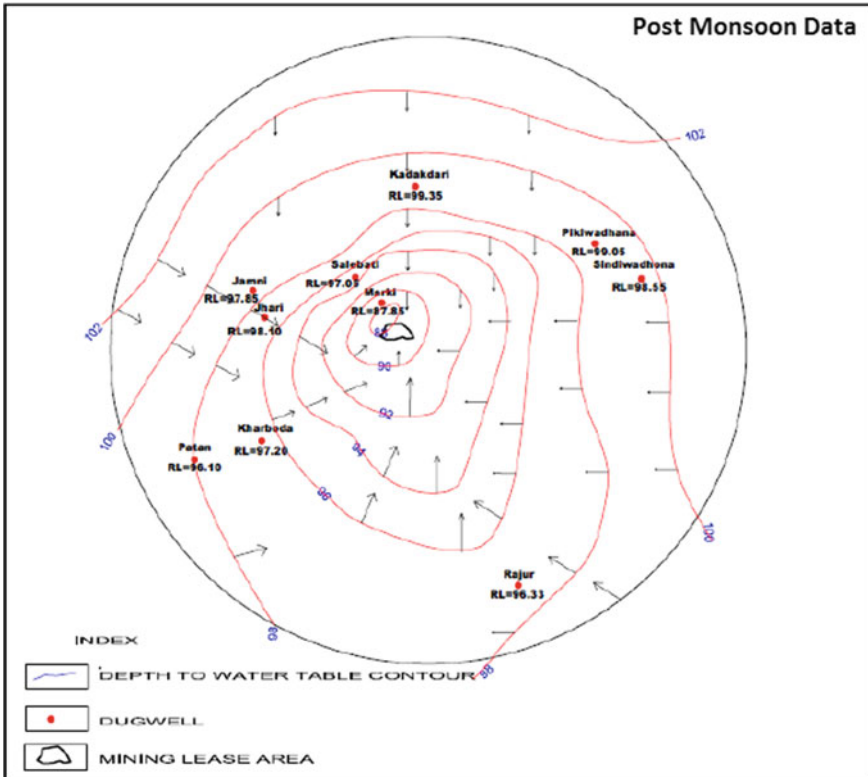
Fig. 3 Well data interpretation w.r.t. reduced level and groundwater flow direction for post-monsoon period

inflow of groundwater after the depth of 20 m, will be pumped by multistage, heavy duty centrifugal pumps.

The maximum quantity of groundwater seepage into the mine that will be required to be pumped out in each opencast mine located at Marki and Pandharkawda OC is estimated as below.

1. Groundwater seepage at Marki OC pit–**300 m³/day** × 365 days = 109,500 m³/year (0.109 MCM/year).
2. Groundwater seepage at Pandharkawda OC pit–**275 m³/day** × 365 days = 100,375 m³/year (0.1003 MCM/year).
3. Groundwater seepage at Mini Marki OC pit–**50 m³/day** (starts after 27 years).
4. Withdrawal for domestic purpose from two tube wells in Marki and Pandharkawda OC pit—06 m³/day × 2 mines = **12 m³/day** × 365 days = 4380 m³/year (0.00438 MCM/year).
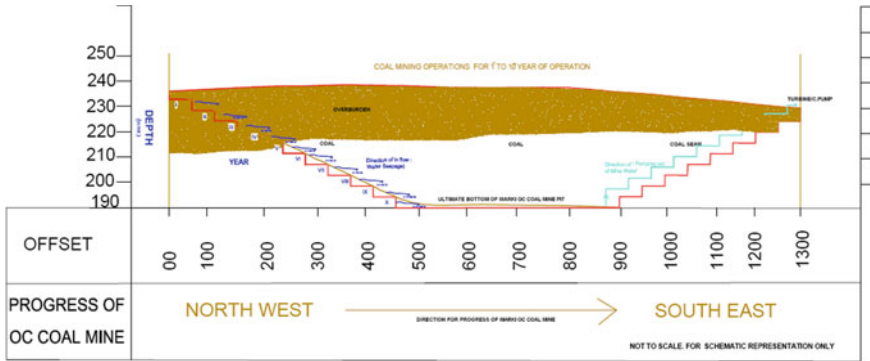
Fig. 4 Progressive depth of Coal Mine versus lateral advancement of Coal Mine working for Marki OC
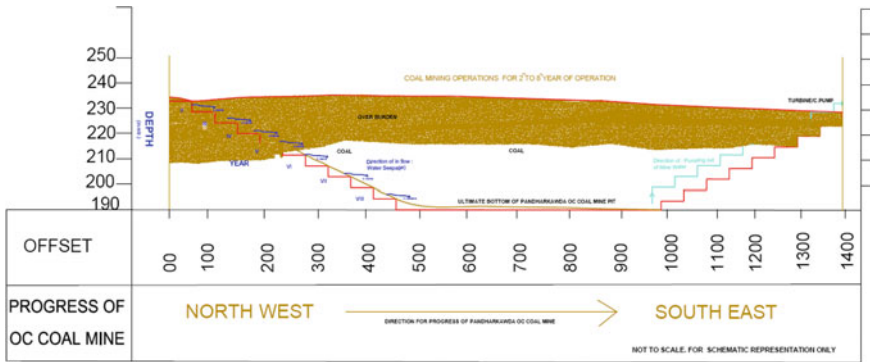
Fig. 5 Progressive depth of Coal Mine versus lateral advancement of Coal Mine working for Pandharkawda OC

Maximum Groundwater seepage and withdrawal at any given point of time during OC operations—**587 m³/day** × 365 days = 214,259 m³/year (0.2142 MCM/year) (Figs. 4 and 5).

Groundwater Seepage and Extraction for Underground Operations

Two underground (UG) sections are proposed in the area namely Marki and Pandharkawda OC, and they will commence after completion of opencast mining activity. These mines will attain a maximum depth of 150 mbgl. The life span of Marki Underground will be 20 Years (11th to 30th Year) and that of Pandharkawda Underground will be 18 Years (10th to 27th Year). When the underground mining is initiated and extends to maximum depth of 150 mbgl, the main aquifer zone consisting of fine-to medium-grained sandstone will be encountered where groundwater occurs under sub-confined state due to confining beds of the shale. The groundwater inflow in the working underground sections will not be much as mining by board and pillar method will be followed by sand stowing. The sandstones have very low hydraulic conduc-

tivity of 0.5 m/day as revealed by pump test data. It means very limited quantity of groundwater will be received in the mine openings. The inflow in mine openings will be mainly from overlying carbonaceous shale which has very low hydraulic conductivity and also through fractures connected to shale and coal seam from overlying sandstones as witnessed in surrounding coal mining areas. As the mining will be mainly confined to coal seams, water stored in coal and its associated shale will be received in the mine working area.

Groundwater Seepage and Extraction

The linear length of the mine at any given time will not be more than 100 m and its width will be around 144 m of course duly supported by pillars. It is safe to assume that water within 100 m (50 m on either side) of the mine opening will drain under gravity along the length of mine opening and will release about 181 m^3/day in the mine working area.

- Maximum surface area along the mine length: 14,480 m^2.
- Taking average specific yield of coal and shale: 1.25% or 0.0125 as fraction.
- **Groundwater seepage in working mining area: 14,480 × 0.0125 = 181 m^3/day**.

Thus, the maximum quantity of groundwater seepage that will be required to be pumped out during this stage of mining operations is estimated as below.

1. Groundwater seepage in Marki and Pandharkawda UG—181 m^3/day × 2 mines = **362 m^3/day** × 365 days = 132,130 m^3/year (0.13213 MCM/year).
2. Groundwater seepage retained by OC mine pits—232.5 m^3/day × 2 mines = **465 m^3/day*** × 365 days = 169,725 m^3/year (0.1697 MCM/year) [*300 m^3/day for Marki OC + 275 m^3/day for Pandharkawda OC].
3. Domestic purpose in Marki and Pandharkawda UG—0.6 m^3/day × 2 mines = **12 m^3/day** × 365 days = 4380 m^3/year (0.00438 MCM/year).
4. Total groundwater extraction—362 m^3/day (from 1) + 465 m^3/day (from 2) + 12 m^3/day (from 3) = **839 m^3/day** × 365 days = 306,235 m^3/year (0.3062 MCM/year).

Hence, during UG mining operations maximum daily total groundwater extraction will be limited to 839 m^3/day from 10th year onward mining operation by underground method.

6   Conclusion

Maximum groundwater seepage and withdrawal at any given point of time during OC operations of Marki Mangli-I Coal Mine—587 m^3/day × 365 days = 214,259 m^3/year (0.2142 MCM/year).

*Maximum groundwater seepage and withdrawal at any given point of time during UG operations of Marki Mangli-I Coal Mine—**839 m³/day** × 365 days = 306,235 m³/year* (*0.3062 MCM/year*).

This predicted quantity of groundwater withdrawal from Coal Mine is used by mine management to create groundwater recharge structures to compensate the groundwater discharge during mine operations.

Impact of Ash Disposal in Coal-Based Thermal Power Plant on Groundwater Quality and Availability

Prashil P. Shukla and Ashish P. Shukla

Abstract Ash disposal in particular and environment management in general has become a second important activity after generation of power by thermal method. A typical coal-based thermal power plant in taluka of Umred, Vidarbha is selected, generating power around 2×35 MW/day. Total ash bund area is around 4.5 ha. Daily Coal consumption is around 650 TPD to generate 35 MW/day. Daily water consumption is around 380 cum/day. Optimum daily power generation is around 32–34 MW/day. Per day slurry bottom ash pumped into Ash Pond is 52 TPD. Ash bund slurry samples, overflow from ash bund and groundwater samples were collected in December 2017 and May 2018. This study reveals that ash water is expected to recharge shallow aquifer around the bund and ash water channel.

Keywords Ash disposal · Coal-based thermal power plant · 2×35 MW

1 Introduction

Majority of power generation plants are based on coal as a fuel. A typical process diagram for a thermal power plant is as below (Fig. 1).

Process energy conversion involved in thermal power plant is schematically shown below (Fig. 2).

Indian coal used at this thermal power plant has following composition on average basis is as below (Table 1).

Ash generation at boiler during combustion of coal is schematically drawn below (Fig. 3).

It is evident from process flow diagram of subjected thermal power plant is that flue gases and ash are the combustion products of coal during thermal power generation. Ash is classified into bottom and fly ash. Percentagewise bottom ash is 20% of coal consumed, and later is 80%. Present system of disposal of bottom ash is to carry its

P. P. Shukla (✉) · A. P. Shukla
Gondwana Geological Society, D.G.M., Nagpur, India
e-mail: prashilshukla@yahoo.com

PROCESS FLOW DIAGRAM FOR THERMAL POWER PLANT
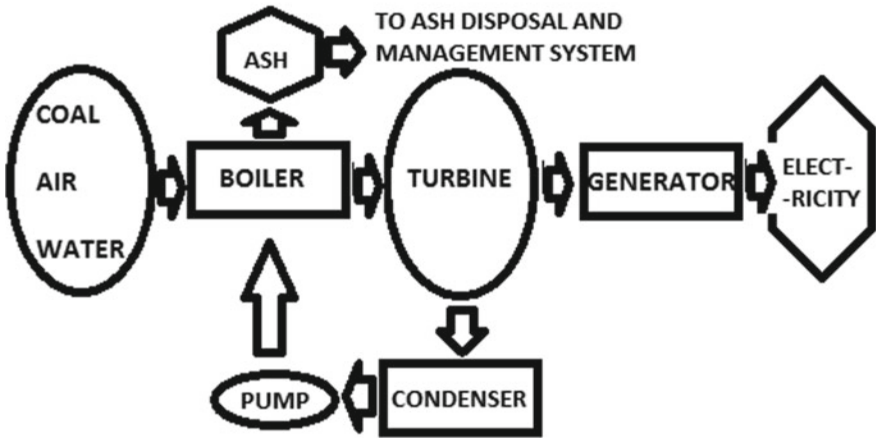
Fig. 1 A typical process diagram for a thermal power plant

ENERGY CONVERSION AT THERMAL POWER PLANT
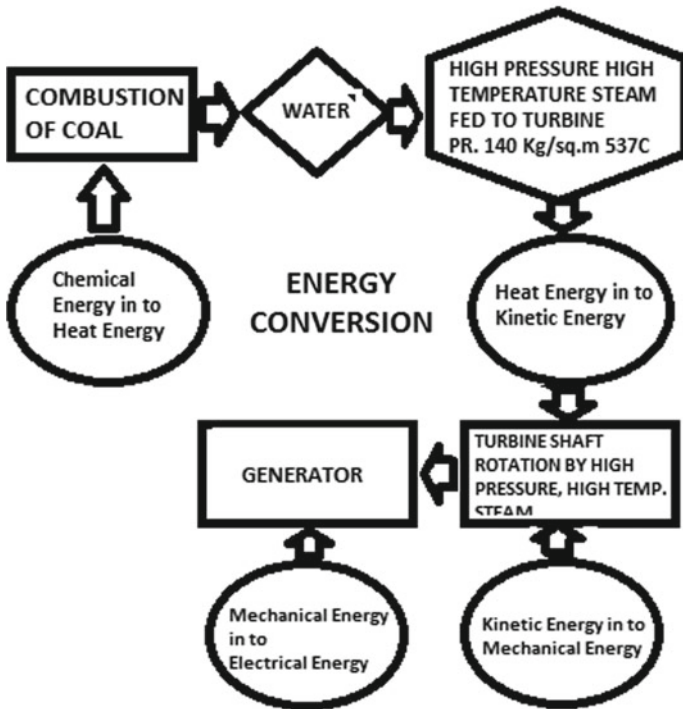
Fig. 2 Process energy conversion involved in thermal power plant

Table 1 Composition of Indian coal used at this thermal power plant

Composition	Unit	Value
Coal heating value	Kcal/Kg	3000–4000
Sulphur content	%	0.35–0.40
Ash content	%	35–42
Moisture content	%	7.5–9.0
Nitrogen content	%	0.8–1.0
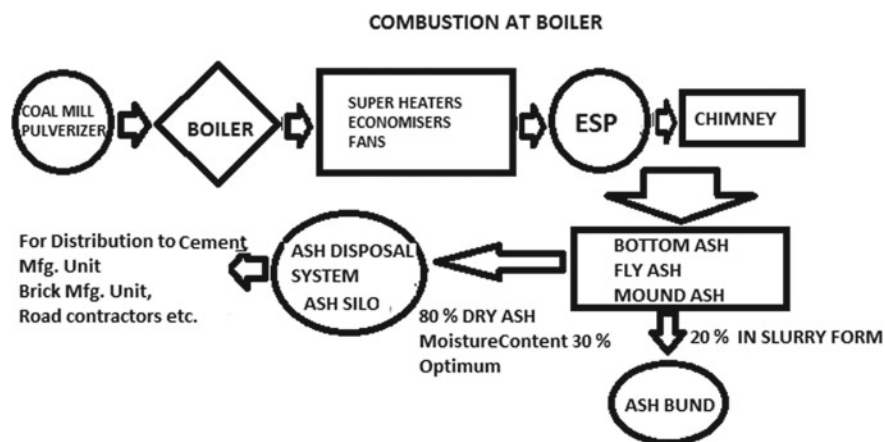
Fig. 3 Ash generation at boiler during combustion of coal in thermal power plant

15–20% slurry in water to a designated site called "ash bund". Of late, high-density slurry system has been introduced to reduce water consumption during transportation of bottom ash. In this system, 70–80% slurry in dough form is pumped to ash pond.

Ash disposal practice being adapted by thermal power plant have invited wrath of common people without verification of facts about interaction of environment with fly ash disposal practice for a given situation.

Thermal power plants in Maharashtra region have been erected during last four decades when the environmental concerns were of low priority. However, after introduction of recent environmental protection laws and guidelines, thermal power plants have to pay more attention to a number of operations during power generation.

Important activity during thermal power generation is "Ash Disposal Practices".

Scenario of present ash disposal guidelines by MoEF & CC, Govt. of India is being revised from time to time, and power plants are being coerced for their implementation.

Several ash bunds have been examined during the Environmental Impact Assessment studies which have been carried for environmental clearance by MOEF & CC.

Studies hitherto have shown that a more detailed investigation is justified with regard to ash bund particularly because (i) it can have direct interaction with the

terrestrial, aquatic and gaseous/air quality system of environment and (ii) a new ecosystem is being developed at most ash bunds.

Out of three segments of ecosystem around ash bund, namely land, air and water, the latter two are dynamic systems while land has been permanently impacted. These two systems, namely air and water, are dynamic because

(i) Fresh slurry is being introduced everyday which has interaction with gaseous environment also.

(ii) Water in the slurry when delivered at ash bund evaporates, percolates or is decanted in the area around and under the ash bund.

Hence, an industry undertaken for study is chosen in such a way that it is under continuous operation for last 8 years and generating power at its optimum capacity and complying ash disposal guidelines of MoEFCC, GOI.

2 Literature Review

This project has been arrived at after study in the literature given in cited references herein, various reports in scientific and nonscientific publications regarding impact of ash bunds on environment. Purpose of literature review is to consider all the available literature on the subject and help to arrive at a judicious view based on factual status of environment in the most vulnerable around ash bund. Literature available for ash disposal practices in thermal power plant has been referred and validated for subjected coal-based thermal power plant in taluka of Umred in Nagpur district.

3 Methodology

Requirement for these investigations will include (i) Survey of ash bund area (2 km radius), (ii) monitor environmental data with respect to groundwater table, quality, water quality of surface sources, if any, (iii) comparison between quality of ash water with groundwater in the monitored area with respect to Indian standards for groundwater quality IS:10500, (iv) Arrival on the conclusion over impacts on groundwater quality and groundwater availability due to disposal of ash in thermal power plant.

4 Survey of Ash Bund Area (2 Km Radius)

Ash bund is built over 4.5 ha area compacted with high-density soils, provided with impervious clay lining with sides of ash bund with linings. Capacity of ash bund is around 50 m^3. Around the ash bund, there are agricultural farms producing a single

crop of cotton, soya bean, toor. There are three notified lakes at a distance of 1.07 km on North, 1.57 km on West and 3.00 km on East of the ash bund.

5 Comparison of Ash Bund Water with Groundwater

Ten samples were collected out of which 4 samples were either the ash slurry or overflow from ash bund, remaining six were from bore wells around the ash bund within peripheral distance of 2 km area. These are the main sources impacting receptors. Receptors of these sources were three lakes at a distance of 1–3 km, soil or the shallow aquifer.

6 Impacts on Groundwater Quality and Groundwater Availability

Ash bund is a source which would affect the receptors, three lakes at a distance of 1–3 km, soil or the shallow aquifer. Analysis of ash slurry/overflow in winter and summer shows that all parameters except suspended solids are within acceptable norms of water quality standards in India for agriculture and potable water supply after treatment (refer Table 2). The only treatment needed will be clarification by plain or aided settling.

Also ash water passes through soil layers of ash dykes. Hence, soil particles can absorb heavy metal hydroxides.

7 Conclusion

Ash water is expected to recharge shallow aquifer around the bund and ash water channel. This study is utilized by industry to identify the ash bund as one of the groundwater recharge structure for the subjected industry.

Table 2 Comparison between ash water and groundwater quality as per Indian standards

Parameters	Unit	Ash water	Groundwater	Permissible limits as per IS 10500: 2012	Permissible limits as per IS2490:1982	Designated use for irrigation purpose (CPCB Standards)
Temperature	°C	28.0–32.0	25.0–30.0	–	45 °C at point of discharge	–
Turbidity	NTU	12–300	Nil	5	–	–
Suspended solids	mg/l	50–990	Nil	–	600	200
Dissolved solids	mg/l	320–840	290–1390	2000	2100	2100
pH		7.2–8.9	7.7–8.1	6.5–8.5	5.5–9.0	6.0–8.5
Alkalinity as $CaCO_3$	mg/l	113–176	157–250	–	–	–
Hardness as $CaCO_3$	mg/l	90–520	370–1100	–	–	–
Calcium as Ca	mg/l	29–120	150–250	200	–	–
Magnesium as Mg	mg/l	4–37	20–156	100	–	–
Sodium as Na	mg/l	75–245	20–96	–	–	–
Iron as Fe	mg/l	0.2–2.0	BDL–0.4	0.3	–	–
SAR	meq/100 gm	2.0–5.8	0.13–3.8	–	–	26
Bicarbonates as HCO_{3-}	mg/l	120–190	185–750	–	–	–
Chlorides as Cl	mg/l	65–320	140–780	1000	–	–
Sulphates as SO_4	mg/l	10–120	80–250	400	1000	–

Data collected in December 2017 (winter) and May 2018 (Summer)

References

1. Sahoo, D.K., Behara, A., Mishra, P., Mehar, N.S.: Environmental Impact and Utilization of Fly Ash: A Case Study of IB-Thermal Power Plant
2. Mathur, A.K.: N.T.P.C. Noida, Research Article, Seminar Collection (2000)
3. Sinha, R.: Fly Ash Disposal and Utilization: Indian Scenario. Department of Civil Engineering, I.I.T. Kanpur, July 1999
4. Naresh, D.N.: Management of ash disposal. In: Indian Geotechnical Conference (2010)
5. Asokam, P., Saxena, M., Asolekar, S.R.: Coal Combustion Residues—Environmental Implications and Recycling Potential
6. Ghosh, K.G., Mukharjee, K., Saha, S.: Fly Ash of Thermal Power Plant: Review of Problems and Management Options with Special Reference to Barkeshwar Thermal Power Plant, Eastern India
7. Ghazali, M., Kaushal, O.P.: Characteristics of Fly Ash from Thermal Power Plant and its Management Along with Settling Pond Design
8. Kanchan, S., Kumar, V., Arya, S., Sharma, S.: Effect of Fly Ash Disposal on Ground Water Quality near Parichha Thermal Power Plant Jhansi: A Case Study

MoEFCC, Government of India/Central Pollution Control Guidelines/Indian Standards

9. Ash disposal guidelines by MoEFCC, Government of India 8.0.763(E) dated 14 Sept 1999
10. Ash disposal guidelines 2015 by MoEFCC, Government of India S.O. 1396 (E) dated 25 Mar 2015
11. Guidelines for handling of all types of FlyAsh generated by Thermal Power Plants 2013 by C.P.C.B
12. National Ambient Air Quality Standards 2009
13. Indian standards for ground water IS: 10500:2012
14. Indian standards for industrial and sewage effluents discharge IS: 2490-1982
15. Environmental Protection Laws, Government of India
16. Standards for thermal power plant regarding discharge of effluent CPCB guideline as per EPA act 1986
17. MoEFCC, Government of India notification GSR 422(E),1993 for general standard for discharge of environmental pollutants

Damage Detection of Shear Strengthened (Originally Deficient) Reinforced Concrete Beams Using EMI Technique

S. N. Khante and Akash Kodam

Abstract Reinforced concrete (RC) structure is the most familiar structure in the field of civil engineering. It is necessary to monitor the health of these RC structures as it undergoes several changes during its life span and as such various techniques are available to do so. Electro-Mechanical Impedance technique (EMI) is a newly invented non-destructive technique which is becoming very popular in the community of Structural Health Monitoring (SHM) in which PZT sensors (surface bonded or embedded) are used as smart materials. These sensors are as such very sensitive and brittle in nature which are available in small dimension (10 mm × 10 mm × 0.2 mm). Due to this reason, these sensors are used in the form of Smart AGgregate (SMAG). This fabricated SMAG is embedded in the monitored structure. This research work focuses on detection of damage of shear deficient-reinforced concrete (RC) Beam before and after strengthening in shear. The Beams were rendered artificially deficient in shear in the form of no shear reinforcement. PZT sensor is used in form of SMAG. The conductance responses were obtained by connecting the SMAG to LCR meter. Further these signatures were used for damage detection and quantification. RMSD index is used for damage quantification. Further loading the specimens under Universal Testing Machine (UTM), damages were given till visible cracks. These induced damages and its severity were identified using EMI Technique.

Keywords Reinforced concrete beam · Conductance · Susceptance · Electro Mechanical-Impedance (EMI) · PZT sensors · Structural health monitoring (SHM)

S. N. Khante (✉) · A. Kodam
Department of Applied Mechanics, Government College of Engineering, Amravati, India
e-mail: snkhante@yahoo.com

A. Kodam
e-mail: akashkodam@gmail.com

1   Introduction

Failure of beam (shear) mainly occurs when their shear capacity fall below their flexural capacity. Thus, this type of failure of beam should be as such avoided due to brittle nature of beam. They fail without any warning and cracks are mainly diagonal in nature and are larger than flexural cracks. Hence to avoid these kind of failures, shear strengthening and identification of shear strength becomes important. For strengthening of reinforced concrete beam in shear Embedded Through Section (ETS) Technique is used which is as such a new technique. In this technique, bars of steel or FRP materials are placed in the holes which are drilled in the section. CFRP or GFRP material is used for strengthening the beam due to their various properties.

SHM is process in which continuous health monitoring of the structures is possible for incipient to severe damages. The EMI technique is a technique used for Structural Health Monitoring and experimental study also shows that this technique is sensitive to damages around the transducers [1–3]. In this technique, PZT patches are used as sensors. These sensors are used as transducers for SHM [4]. These PZT patches can be used as surface bonded or embedded. Khante and Gedam [5] experimentally investigated that embedded PZT in form of SMAG is more effective than surface mounted, and damages are effectively detected. Shanker [6] conducted experiment on concrete and steel beams and investigated the possibility of an PZT (embedded) as a sensor by using impedance-based method. Gedam and Khante [7] studied the effectiveness of SMAG with varying orientation. Negi et al. [8] after using PZT patch (embedded) in reinforced concrete beam studied three different configurations of PZT. Annamdas et al. [9] monitored fresh concrete using EMI technique and suggested double protection wrap method with both metal and non-metal of embedding PZT sensors. Breveglieri et al. [10] studied the evaluation of ETS efficiency on reinforced concrete beams. The investigation on different ETS configuration was done. The present study focuses on detection of damages of shear strengthened RC beams and its severity using EMI technique.

2   Electro-Mechanical Impedance (EMI) Technique

The EMI Technique in which PZT sensors are used is as such a new technique. The range of sensing of PZT patch is 0.4–2 m. The patch behaves as a thin bar which undergoes axial vibration. When an electric field is applied to patch, it dynamically expands and contracts. Both the end points of the patch can be assumed to encounter equal impedance Z from the host structure.

The complex electro-mechanical admittance Y of the coupled system is given by:

$$Y = 2\omega\, j\, \frac{wl}{h}\left[(\mathord{\in}_{33})^T + \left(\frac{Z_a}{Z + Z_a} \right)(d_{31})^2 \bar{Y}^E \left(\frac{\tan(kl)}{kl} \right)(d_{31})^2 \bar{Y}^E \right] \qquad (1)$$

d_{31} Piezoelectric strain coefficient of the PZT material,

E Complex Young's modules under constant electric field,

$\in^T 33$ Complex electric permittivity at constant stress,

Z Mechanical impedance (structural system),

Z_a Mechanical impedance (PZT patch) (function of Stiffness, Mass and Damping)

ω Angular frequency

$k1$ The wave number.

The electro-mechanical admittance consists of real and imaginary part called conductance and susceptance, respectively. Hence, the magnitude of complex admittance can be calculated as given in Eq. (2)

$$Y = \sqrt{G^2 + B^2} \tag{2}$$

where

Y Electro-mechanical admittance

G Conductance

B Susceptance.

Root mean square deviation (RMSD) has been used to associate the damage or material changes with changes in the signature. It is given by Eq. (3)

$$M = \sqrt{\frac{\sum(G_2 - G_1)^2}{\sum G_1^2}} \times 100\% \tag{3}$$

where

M Root mean square deviation

$G1$ Baseline signature of PZT conductance

$G2$ Corresponding conductance at each monitoring time.

3 Experimental Approach

3.1 General

For performing structural health monitoring using EMI technique, four concrete beams were cast. The experiment is done to identify damage severity of concrete beams and sensitivity of PZT sensors which was used in the form of SMartAGreggate (SMAG).

Table 1 Summary of all four beam

Designation		Details
Beam 1	(C)	Healthy
Beam 2	(0S 1)	Shear deficient
Beam 3	(0S 2)	Shear deficient strengthened with steel bars (10 mm)
Beam 4	(0S 3)	Shear deficient strengthened with CFRP bars (10 mm)

Fig. 1 Schematic SMartAGgregate (SMAG)
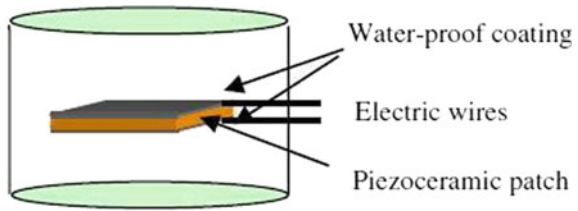
3.2 Materials and Specimen

The tests were carried out on concrete beams. The PZT sensor was used in the form of SMAG. Total four reinforced concrete specimens were casted. The summary of all the four beams is given in Table 1. The materials used for shear strengthening of RC beam are Carbon Fiber Reinforced Polymer (CFRP) bars and steel bars. For fabrication of SMAG PZT patch (10 mm × 10 mm × 0.2 mm) was soldered to coaxial cable wires. The form work of simple card board with 30 mm diameter was filled with mortar to half of its depth, PZT was bonded on the top surface of this cement block using epoxy (Araldite) and allowed it to set for 24 h. The card board was filled to its full depth with the cement mortar. After curing it for 7 days, the card board was removed from cement block and SMAG was finally ready to use. The Schematic SMAG is shown in Fig. 1. The performance of this sensor was studied on the R.C. beams. The details of all the specimens are shown in Table 1, and the dimensions and properties of Beam 1 (C) are shown in Table 2. The instrument used is LCR meter whose frequency range is from 20 Hz to 2 MHz.

3.3 Experimental Approach

The experimental setup consisted of one control/healthy beam and three RC beam which were shear deficient in the form of no shear reinforcement. The reinforcement of the beams is shown in Figs. 2 and 3. The monitoring span was ($L1 = 0.312$ m) which was taken as ($L1/d = 2.5$) and steel stirrups 6@90 mm were placed at center

Table 2 Material properties and dimensions of control beam

Dimension/properties	Value
Length (L)	1000 mm
Cross section	100 mm × 125 mm
Grade of cement (OPC)	53
Grade of steel	Fe 500
Reinforcement bars	2#10 mm dia @ top and bottom
Stirrups	6 mm dia @ 90 mm C/C

Fig. 2 Reinforcement of control beam

Fig. 3 Reinforcement of shear deficient beams

of beam span so as to avoid shear failure in that particular span. The SMAG was placed at center of beam and wired to LCR meter. The frequency of sensors was swept from 100 to 400 kHz to obtain conductance signatures. For strengthening the shear deficient beam, vertical holes of 12 mm diameter were drilled in the beam core in portion of the span which is shear deficient and 25 mm cover was kept intact from bottom of beam so that the adhesive should not flow through that bottom part of the beam. Then, the holes were cleaned with the help of the blower until the dust was completely removed and epoxy resin was poured into the holes. The bars were cut in the required length and were placed in the holes removing the resin which is in excess. This test was conducted in two different stages, i.e., in the first stage signatures for only healthy condition of the beams and in second stage for the damaged condition of beams are obtained.

In the second stage, damage was given in the form of significant visible cracks by loading the specimen under Universal Testing Machine (UTM) as shown in Fig. 4. The ultimate transvers loads at failure carried by the specimen are shown in Table 3. The damaged specimen in which SMAG is present is wired to LCR meter. The frequency was swept from 100 to 400 kHz. These vibrations are transferred to structures and reflect back from the same PZT patch through waves, which will thus indicate the health of the structure. The conductance (G) is measured directly through LCR meter, and graph of conductance versus frequency is plotted. Same procedure was adopted for first stage. Then, the data for healthy and damaged state were compared.

Table 3 Load carried by each specimen at failure

Specimen		Load (kN)
Beam 1	(C)	55
Beam 2	(0S 1)	35
Beam 3	(0S 2)	39
Beam 4	(0S 3)	42

Fig. 4 Beam 1 (control) loaded on UTM and connected to LCR meter

4   Results and Discussions

The healthy signature of the beams was taken. The beam was loaded on Universal Testing Machine. The schematic loading arrangement is shown in Fig. 5. SMAG was connected via cable to LCR meter, and corresponding response was recorded after damage. The conductance values were recorded by LCR meter in the range of 100–400 kHz. The conductance signature and RMSD graphs were plotted. Similar procedure is repeated for all the specimens.

4.1   Damage Detection of RC Beam 1 (C)

The Beam 1(C) when loaded exhibited cracking (Fig. 6). It was observed from Fig. 7 that, as the damage was introduced in the beam, the conductance signatures changed. As introduced damage was small in nature, and the conductance signatures
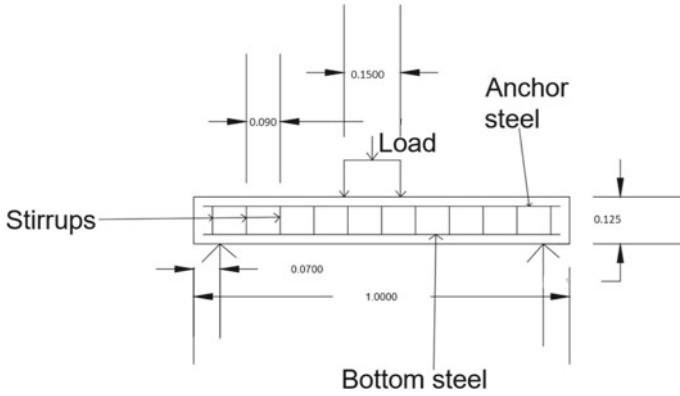
Fig. 5 Schematic diagram of loading
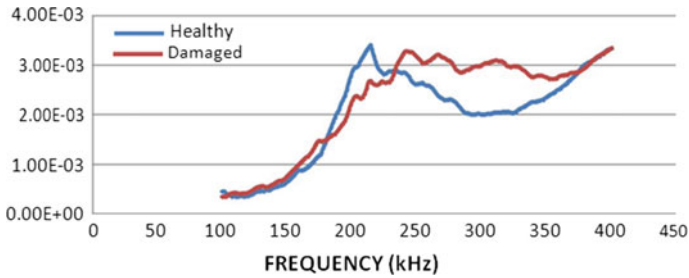
Fig. 6 Conductance graph for healthy and damaged of beam 1 (C) specimen

Fig. 7 Damaged beam 1 (C) with visible crack

was shifted accordingly. Noticeable changes were observed in conductance signature. The damage index was quantified by using conductance signature. The damage index was found out to be 4.13% (Fig. 14).
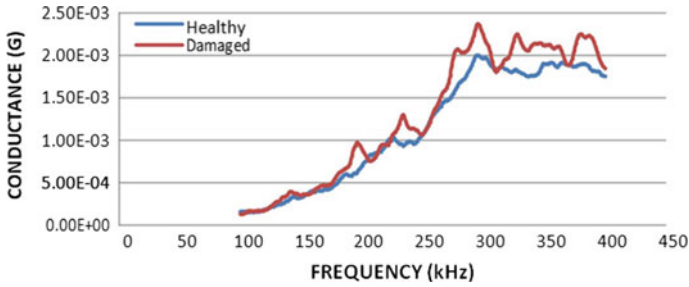
Fig. 8 Conductance graph for healthy and damaged of beam 2 (0S 1) specimen

Fig. 9 Damaged beam 2 (0S 1) with visible cracks

4.2 Damage Detection of RC Beam 2 (0S 1)

The shear deficient beam 2 (0S 1) was shear strengthened and its healthy signature was obtained. The beam was loaded to introduce damage (Fig. 8). This specimen failed at 35 KN load. It was observed from Fig. 9 that, as the damage was introduced in the beam, the conductance signatures changed. Since the introduced damage was very large, the conductance signatures were shifted by large values. Therefore, conductance signature was more effective in observing the variation. The damage index was quantified by using conductance signature. The shifting of graph both horizontally and vertically is more as compared to Beam 1 (C) specimen. Clear shifting in the recorded conductance responses for healthy and damaged state shows effectiveness of SMAG. The damage index recorded was 24.19% (Fig. 14).
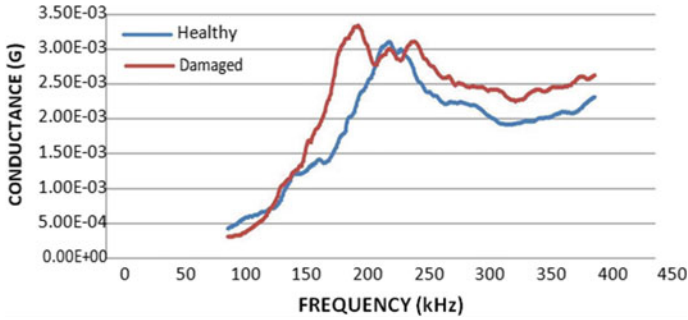
Fig. 10 Conductance graph for healthy and damaged of beam 3 (0S 2) specimen

Fig. 11 Damaged beam 3 (0S 2) with visible cracks

4.3 Damage Detection of Beam 3 (0S 2)

This specimen failed at 39 kN load. The loaded specimen with cracks at failure is shown in Fig. 10. It was observed from Fig. 11 that, due introduction of damage in the form of crack the subsequent conductance signature altered. The damage index was again quantified by using conductance signature only. The horizontal and vertical shifting of the graph is less as compared to Beam 2 (0S 1) specimen. The damage index recorded was 19.82% (Fig. 14).
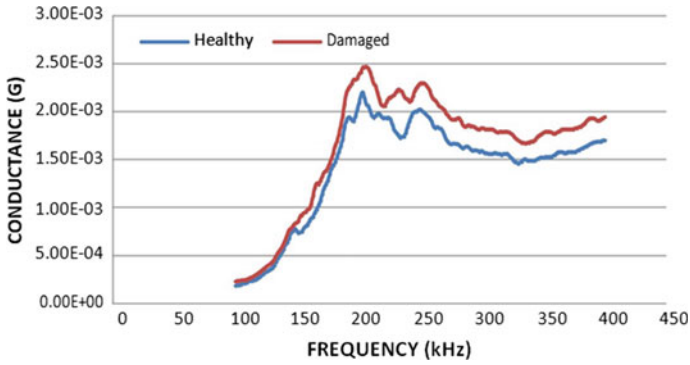
Fig. 12 Conductance graph for healthy and damaged of beam 4 (0S 3) specimen

Fig. 13 Damaged beam 4 (0S 3) with visible cracks

4.4   Damage Detection of RC Beam 4 (0S 3)

The loaded and cracked specimen is shown in Fig. 12. This specimen failed at 42 kN load. It was observed from the Fig. 13 that, due to introduction of damage in the beam, the conductance signatures changed. The shifting of graph is less as compared to Beam 3 (0S 2) specimen. The damage index recorded was 16.21% which was quantified by RMSD Index (Fig. 14).

Higher RMSD Index shows that Beam 2 (0S 1) is more damaged and has less shear strength comparatively. The sensitivity of SMAG is more for this beam (Figs. 8, 9 and 14).
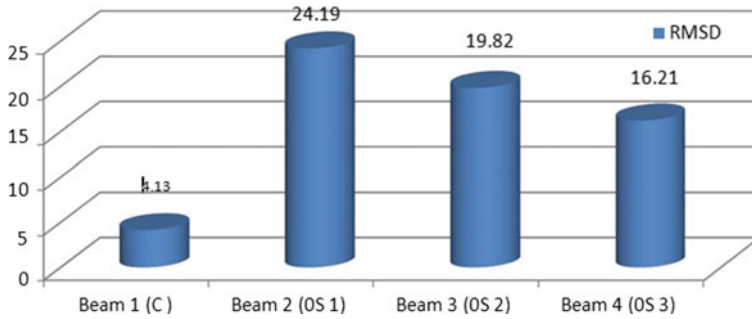
Fig. 14 RMSD indices

5 Conclusions

The test was thus performed on four reinforced concrete beams. PZT patch was used in the form of SMAG. Damage was detected by change in output signatures obtained from LCR meter. Damage was quantified with help of RMSD index.

1. Damages and its extent in RC Beams are effectively detected with SMAG. It is observed that there is significant shift in the curves after damage. The vertical and horizontal shifting of curves is the indication of damage present in specimen.
2. Shift in vertical and lateral direction in the recorded conductance responses shows the effectiveness of SMAG.
3. The beam with more shear strength was damaged less (least cracking) and has less RMSD Index.
4. Similarly Beam having less shear strength has higher RMSD index because of more damage in the form of extensive cracking.

References

1. Park, S., Ahmad, S., Yun, C.B., Roh, Y.: Multiple crack detection of concrete structures using impedance based structural health monitoring techniques. Exp. Mech. **46**(5), 609–618 (2006)
2. Tawie, R., Lee, H.: Monitoring the strength development in concrete by EMI sensing technique. Constr. Build. Mater. **24**(9), 1746–1753 (2010)
3. Khante, S.N., Jain, R.: Identification of strength gain of precast concrete during initial period using reusable PZT. Int. J. Innov. Res. Sci. Eng. Technol. **6**(1), 716–722 (2017)
4. Park, G.: Assessing structural integrity using mechatronic impedance transducers with application in extreme environments. Ph.D. dissertation. Virginia Polytechnic Institute and State University, Blacksburg, VA (2000)
5. Khante, S.N., Gedam, S.R.: PZT based smart aggregate for unified health monitoring of RC structures. Open J. Civ. Eng. **6**, 42–49 (2016)
6. Shanker, R.: An integrated approach for structural health monitoring. Thesis-Indian Institute of Technology, Delhi (2009)

7. Gedam, S.R., Khante, S.N.: Experimental investigation on sensitivity of smart aggregate embedded in reinforced concrete beam. Open J. Civ. Eng. **6**, 653–669 (2016)
8. Negi, P., Kaur, N., Bhalla, S., Chakraborty, T.: Experimental strain sensitivity investigations on embedded PZT patches in varying orientations. In: Proceedings of 9th Biennial Conference on Structural Engineering Convention (SEC 2014), 22–24, Dec 2014, pp. 2615–2620. New Delhi (2014)
9. Annamdas, V., Yang, Y., Soh, C.: Impedance based concrete monitoring using embedded PZT sensors. Int. J. Civ. Struct. Eng. **1**(414), 424 (2010)
10. Breveglieri, M., et al.: Embedded through-section shear strengthening technique using steel and CFRP bars in RC beams of different percentage of existing stirrups. Compos. Struct. **126**(2015), 101–111 (2014)

Assessment of Multi-storied RC Framed Structure Using Passively Damped Viscous Dampers

Purva J. Kalamkar, Shital S. Wani and Pradip D. Jadhao

Abstract The main aim of this study was to analyze 10-storied structure by using dampers and without dampers for the performance of building including different cases like changing the position of dampers, changing the number of dampers, and analyze the seismic performance of the structure. Also the performance should be calculated on the basis of changing damping ratio. In the present paper, study of nonlinear dynamic analysis of 10-storied RCC building is considered. The building under consideration is modeled with the help of SAP-2000 software. Time history analysis is performed on the basis of different ground motion records. Nonlinear analysis is considered for the performance of seismic analysis of the structure. Story displacement, maximum bending, and shear force calculated on the basis of nonlinear analysis of the structure. It is observed that the change in position of dampers will also give better results for improving the performance of structure.

Keywords Viscous damper · Energy dissipation · Dynamic analysis

1 Introduction

From a very long time, natural forces have been always disturbing the living survival. Even though human being always trying to control the nature and coexist with it, from all other disasters, most destructive and hazardous disaster is earthquake. Earthquakes occur due to release in energy on the earth surface which creates seismic forces. They occur with different intensities, sometimes they are so trivial that they do not recognize but sometimes they are so strong due to which high storied structure may

P. J. Kalamkar (✉) · S. S. Wani · P. D. Jadhao
K.K.W.I.E.E.R., Nashik, India
e-mail: purva125@gmail.com

S. S. Wani
e-mail: sswani@kkwagh.edu.in

P. D. Jadhao
e-mail: pdjdhao@kkwagh.edu.in

also collapse or cause major damage to infrastructure and kill thousands of people or the whole city may get destroyed in some fraction of time. During a seismic event, ground acceleration, i.e., input energy which transforms into kinetic and potential energy should be absorbed or dissipated through heat. For strong earthquake, a large amount of energy is absorbed by hysteretic action in the form of damage to structure. For the many designers, the main approach to protect the structure against effect of earthquake is to increase the stiffness of the structure.

Actually stiffness of structure will be increased by placing dampers in earthquake resisting design of building. There are fields of earthquake which are used for the dynamic analysis which has made some techniques and some evolution of software techniques on computer and use of powerful testing facilities.

Studying on different literature surveys, it is observed that axial deformations were considered on the basis of continuum-based models [5]. The sequential quadratic programming method was used for finding the optimization problem for objective function and constraint equations [1]. The damping mechanism under coupled shear wall also introduces for transforming shear forces [6]. Governing equations was established by using Timoshenko beam theory and Hamilton's principle. Experimental investigation was done for damping performance of viscoelastic material by the application of constrained layer damping treatment [7]. Non-local finite element analysis was performed for viscous damped beams [8]. Fundamental frequencies of tall buildings were evaluated on the basis of beam behavior [9]. Seismic response analysis was performed for two adjacent buildings connected with MR dampers [10]. Steel MRF's were designed by application of viscous dampers and collapse resistance as well as plastic mechanism evaluated [11]. Dissipated energy was evaluated on the basis of seismicity for design of steel structure using fluid viscous dampers [13]. Positions of steel braces were changed, and the maximizing performance position of braces was found out [14]. Vibration analysis was considered for beam with partially distributed internal viscous damping [15]. Literature survey also studied for the seismic risk assessment of linear and nonlinear fluid viscous dampers [16].

Previous studies have demonstrated that, capacity design rules for columns having high-performance steel moment resisting frames with viscous dampers should be found for collapse resistance as well as drift performance and also the properties of viscous dampers should be calculated by changing the damping ratio. The investigation required for the analytical techniques, stochastic linearization approaches, and also time variant hazard function approximation.

2 Design of Structure

Ten storied structure is modeled on FEM-based software, i.e., SAP2000 for time history analysis in which total 10 cases are considered. First case is considered as structure without placing damper, and remaining nine cases are considered as placement of dampers in order to change the number of dampers with respect to their locations. The total work done is considered by changing the damping ratio of the

Table 1 Details of structure

Type of structure	SMRF
Grade of concrete	M20
Plan size	12×6 m
Total area	72 m^2
Number of stories	10
Building height	32.2 m

Table 2 Section properties

Size of column	350×500 mm
Size of beam	230×400 mm
Size of slab	120 mm thick

Fig. 1 Plan view
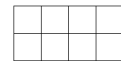
Fig. 2 Elevation view
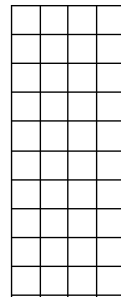
damper. Initially two steps are considered. In first step, $G + 9$ storied structure is modeled as per Indian standards referring the IS codes. For first case, the structure is considered as without application of dampers at any location and the analysis results were found out. Then, for remaining nine cases dampers are applied in order to change the number of dampers with respect to their positions. These all cases are designed for damping ratio 10% as well as 15%. There are total 20 different models are analyzed separately. Above all cases are done under the ground motion of Elcentro, Bhuj, Dharmsala, and Uttarshi separately. The structures are designed as per the codal provisions given in Indian Standard. Damper used for modeling are nonlinear fluid viscous dampers which are connected at the different floor levels. The dampers are used for reducing the stiffness factor of the structure, the damper property used for modeling are taken as the Taylor's devices. Tables 1 and 2 show all the data used for modeling the structure and section properties of RC members. Figures 1 and 2 show plan view and elevation view of the structure.

3 Application of Dampers

Case 1 is modeled as without damper application but further nine cases are considered as according to the application of dampers with respect to the different places. All the cases are designed for damping ratio 10 and 15%. In this model, ISMB150 section is selected for connecting the damper member, from this information we will easily find out the stiffness property of the damper. Equation of stiffness (K) calculated as follows [2]:

$$K = AE/L \tag{1}$$

where K = stiffness property of damper, A = Area of steel member, L = length of member where damper is applying, Damping coefficient is calculated as shown in Eq. (2) [4]:

$$C_0 = 2\,m\omega\xi \tag{2}$$

where C_0 = damping coefficient, m = total seismic mass of structure, ω = natural frequency = $2\pi/T$ [12] and ξ = damping ratio. Dampers are placed in a structure so as to reduce the seismic forces induced in the structure due to earthquake. Seismic force gets reduced due to application of dampers; hence, the stiffness of the structure also gets increased. Generally dampers are placed in the tall structures which are having height more than 30 m. Dampers are the devices which absorbs or dissipate the vibration caused by the earthquake to the structure and to increase damping and stiffness as well. In this case, FVD250 type of damper is used. While modeling the structure with viscous damper, the dampers are applying to building at different positions as shown in Fig. 3.

Table 3 shows time period comes after modeling structure for mode 1, which comes as 1.82 s and m is the seismic mass, i.e., the total seismic weight considered for the design of building including weight of column, weight of beam slab, floor finish of slab, total live load, and total dead load applied on the structure. K is the stiffness, and damping coefficients are considered as according to the values come for damping ratio 10 and 15%. Above all values are applied to the property of damper, which is considered as a Taylor's device FVD 250. The modeling is done for nonlinear analysis for Elcentro ground motion record. Figure 3 shows arrangement of dampers in different manner for all nine cases.

4 Modeling of Structure

After analyzing, results are noted for the values of maximum displacement at each story for all ten cases, as soon as the earthquake is applied to any of the structure, the lateral displacement is generated due to the motion of earthquake, it means there is
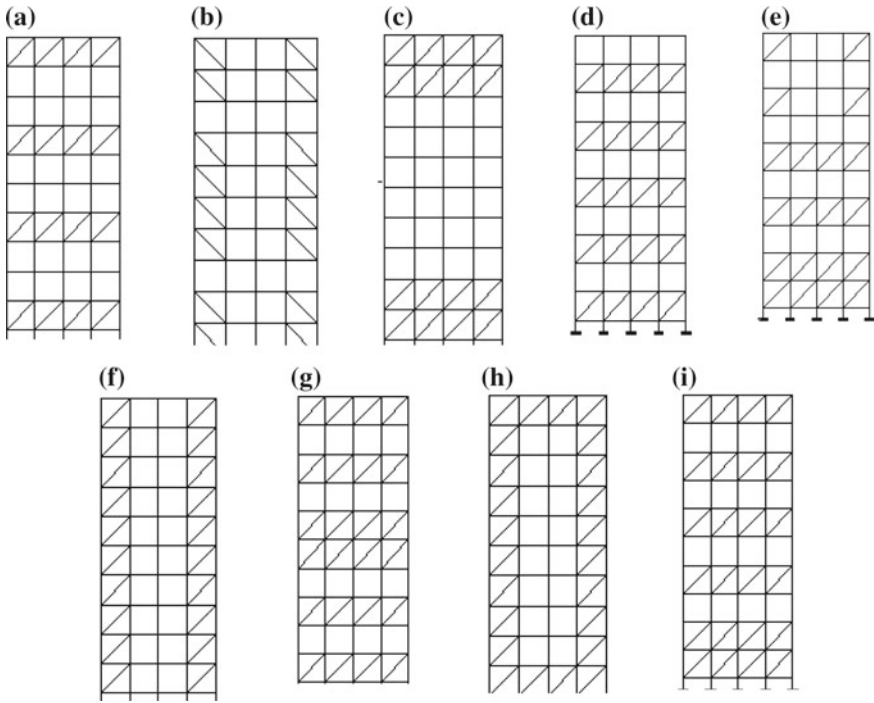
Fig. 3 Different arrangement of dampers

Table 3 Dampers calculating values

Time period	1.82 s
Seismic mass	2,037,138 N/s^2
Stiffness value	88,167.05 kN/m
Damping coefficient	
For 10%	1405.84 kN/s^2
For 15%	2108.77 kN/s^2

displacement force generated due to earthquake [3]; hence, the value of displacement is note down for the case of EQx only.

5 Results for the Analysis of Elcentro Ground Motion

See Figs. 4, 5, 6, 7, 8 and 9.

Fig. 4 Story displacement for damping ratio 10%
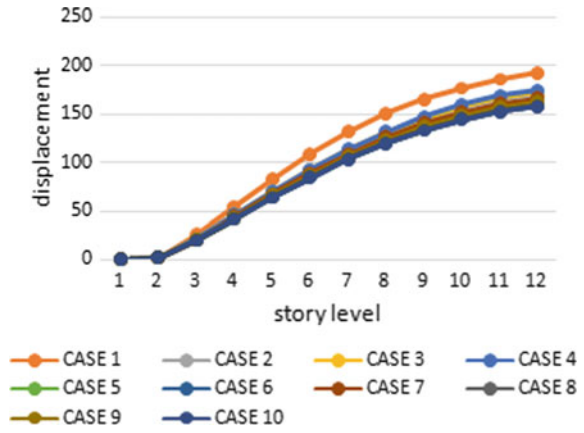
Fig. 5 Story displacement for damping ratio 15%
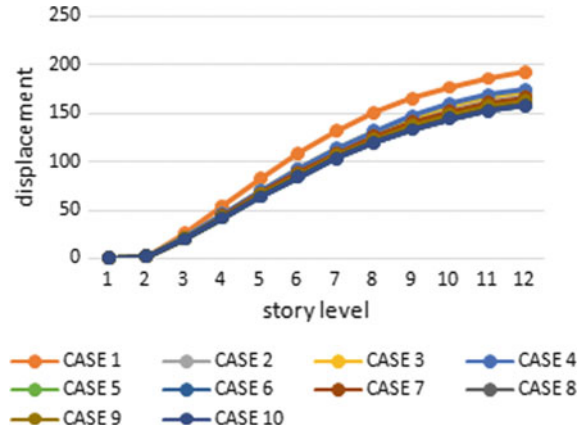
Fig. 6 Base shear for damping ratio 10%
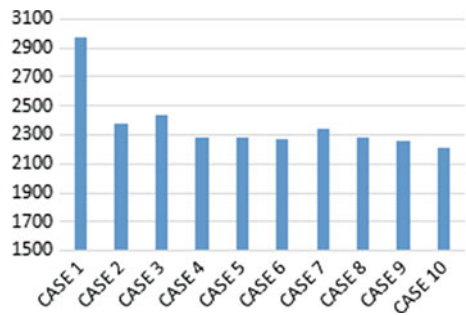
Fig. 7 Base shear for damping ratio 15%
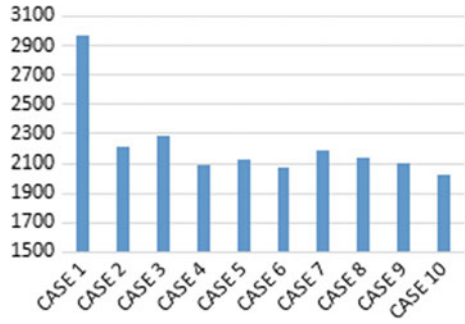
Fig. 8 Max BM and SF for damping ratio 10%
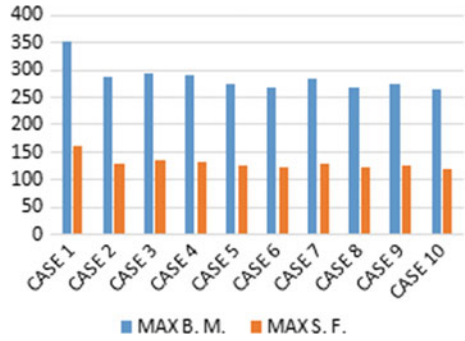
Fig. 9 Max BM and SF for damping ratio 15%
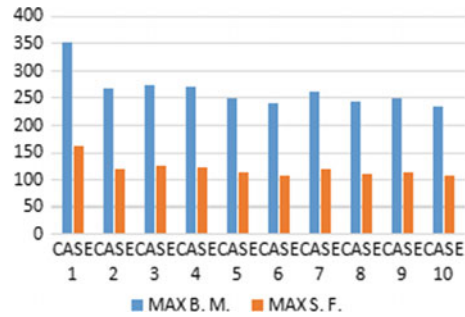
6 Results for the Graph for Damping Force Versus Displacement for Elcentro Ground Motion

See Figs. 10 and 11.

Fig. 10 For case 6 for 10% damping
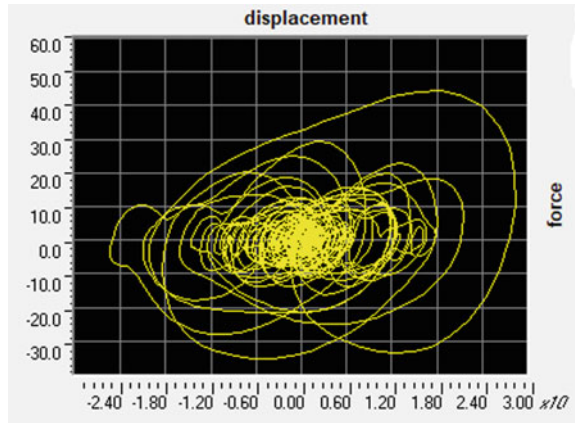
Fig. 11 For case 6 for 15% damping
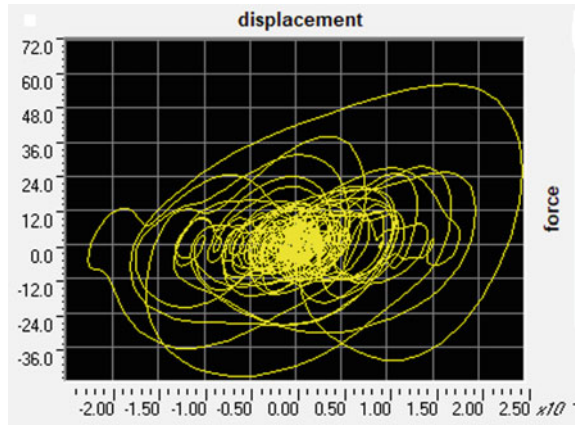
7 Discussion

Observing graph for story displacement for Elcentro ground motion, it is seen that displacement for case 1, i.e., structure without damper having displacement as 192.3 mm while displacement for case 2 is 171.8 mm for 10% damping, it means that, if some number of dampers are attached to the structure, the displacement going to be reduced by 20.46 mm but when the same number of dampers attached by only changing the position of damper displacement is going to be increased by 1 and 2 mm, respectively, for case 3 and case 4 by comparing with case 2. Hence, comparing case 2, case 3, and case 4, most appropriate case is case no 2. Now again increasing the number of dampers displacement going to be reduced by 30, 33, and 26 mm for case 5, case 6, and case 7 comparing with case 1; hence, the most effective case in between these three is case no 6. Similarly again increasing the number of dampers for remaining case and comparing the results, we get 33, 29, and 34 mm reducible displacement as

comparing with case 1. In these three, case 10 is the most effective case. Comparing all these models, the most efficient cases are case 6, case 8, and case 10 but, the max reduction in displacement is carried by case 10 only.

Similarly observing for case of damping ratio changing with 15% for same Elcentro ground motion record, it is seen that displacement for case 1, i.e., structure without damper having displacement is 192.269 mm while displacement for case 2 is 162.068 mm for 15% damping. While number of dampers are attached to the structure, the displacement going to be reduced by 30.201 mm but when the same number of dampers attached by only changing the position of damper displacement is going to be increased by 1 and 3 mm, respectively, for case 3 and case 4 by comparing with case 2. Hence, comparing case 2, case 3, and case 4, most appropriate case is case no 2. Now again increasing the number of dampers displacement going to be reduced by 43.51, 41.15, and 37.81 mm for case 5, case 6, and case 7 comparing with case 1; hence, the most effective case in between these three is case no 5. Similarly again increasing the number of dampers for remaining case and comparing the results, we get 47.78, 42.67, and 49.63 mm reducible displacement as comparing with case 1. In these three, case 10 is the most effective case. Comparing all these models, the most efficient cases are case 6, case 8, and case 10 but, the max reduction in displacement is carried by case 10 only. Comparing all the cases as same as that of above the most efficient cases is case 8 and case 10.

8 Conclusion

This study is based on viscous damping models for multi-storied reinforced concrete framed structure. Scarcely any years the fluid viscous dampers have been placed in many structures. Seismic performance can be increased by placing the dampers into structure. The seismic performance of multi-storied structure for structure with and without viscous fluid damper was discussed in this paper. Seismic performance based on nonlinear fluid viscous damper. Different properties were calculated by changing damping ratio values for comparison purpose. Based on above study, following conclusions are drawn:

- Vertical displacement of the structure is necessary for determining the characteristics of the structure.
- While changing the damping ratio, characteristics of the structure also changed.
- Slight increase in damping ratio gives drastic change in the characterization in the structure.
- Attachment of fluid viscous damper will improve the performance of structure and collapse probability will also decrease.
- It is observed that the change in position dampers will also give better results for improving the performance of structure.
- For best performance of structure, it is needed to find the appropriate number of dampers and position of dampers.

References

1. Carlos, A.: Optimal design of passive viscous damping system for building under seismic excitation. J. Constr. Steel Res. **90**, 253–264 (2013). Elsevier
2. Chopra, A.K.: Dynamics of structures, theory and applications to Earthquake Engineering. University of California at Berkeley. ISBN-81-203-1043-8
3. Duggal, S.K.: Earthquake Resistant Design of Structures, 2nd edn. Department of Civil Engineering, Motilal Nehru National Institute of Technology, Allahabad. ISBN-13-9780198083528
4. George, D.: Maximum Damping forces for structures with viscous dampers under near source earthquakes. Eng. Struct. **68**, 1–13 (2014). Elsevier
5. Hadi, F., Antonio, C.: Analysis of passively-damped coupled shear walls using continuum-based models. Eng. Struct. **148**, 739–754 (2017). Elsevier
6. Hadi, M., Antonio, C.: Investigation of the effect of viscous damping mechanism on structural characteristics in coupled shear walls. Eng. Struct. **116**, 121–139 (2016). Elsevier
7. Hujare, P.: Experimental investigation of damping performance of viscoelastic material using constrained layer damping treatment. Proc. Mater. Sci. **5**, 726–733 (2014). Elsevier
8. Indian standard 1893 (part 1): 2002: Criteria for earthquake resistant design of structure. fifth revision, Bureau of Indian Standard
9. Indian standard code of practice for design loads (other than earthquake) for buildings and structure second revision
10. Indian standard plain and reinforced concrete code of practice, fourth revision
11. Mehdi, B., Ali, G.: Seismic performance assessment of steel moment-resisting frames equipped with linear and nonlinear fluid viscous dampers with the same damping ratio. J. Constr. Steel Res. **136**(2017), 215–228 (2017). Elsevier
12. Narkhede, D.I., Sinha, R.: Shock vibration control of structures using fluid viscous dampers (2012)
13. Ras, A.: Seismic energy dissipation study of linear fluid viscous dampers in steel structure design. Alexandria Eng. J. **55**(3), 2821–2832 (2016). Elsevier
14. Theodore, L.K.: Assessment of capacity design of columns in steel moment resisting frames with viscous dampers. Soil Dyn. Earthq. Eng. **88**, 215–222 (2016). Elsevier
15. Ting, C., Jia, H.: Vibration analysis of beam with partially distributed internal viscous damping. Int. J. Mech. Sci. **51**(11–12), 907–914 (2009). Elsevier
16. Tubaldi, E., Barbato, M.: Performance based seismic risk assessment for building equipped with linear and nonlinear viscous dampers. Eng. Struct. **78**, 90–99 (2014). Elsevier

Design and Experimental Study of Voided Slab with Proposed New Shape of Void Former

Check for updates

Vikas P. Bhamare, Pradip D. Jadhao and Abhijit J. Pawar

Abstract Use of voided slab is spreading all over the world in recent times. Voided slab system has many advantages over conventional solid slab and some drawbacks also. There is a lot scope for studying the voided slabs in India. The compatibility of these foreign techniques must be workout with Indian standards. This paper presents experimental study of voided slab considering Indian Practices and proposes a new shape of void formers to improve the stiffness of voided slab.

Keywords Voided slab · Two way slab · Void former · Flexural test on slab

1 Introduction

Voids in slab was developed already in 90s in foreign countries and applied to the numerous projects. But it was just introduced a few years ago in India and started to apply to the some projects. In voided slab systems, the concrete under less stresses of central portion of cross section had removed and void formers ware placed to create void. The saving of concrete reduces CO_2 emission, reinforcement, seismic load, which also saves fossil fuel or energy and void former utilizes the recycled plastic. This ecofriendly effects make it sustainable green building, which is accepted in European countries and some more places in world.

The voided slab system is not new to European countries; as Bubble Deck from UK, Cobiax from Switzerland and U-Boot Beton from Italy patented their techniques around 20 years before. It is spreading worldwide rapidly.

V. P. Bhamare (✉) · P. D. Jadhao · A. J. Pawar
Department of Civil Engineering, K. K. Wagh Institute of Engineering Education and Research, Nashik, India
e-mail: vikasbhamare96@gmail.com

P. D. Jadhao
e-mail: pdjadhao@kkwagh.edu.in

A. J. Pawar
e-mail: ajpawar@kkwagh.edu.in

In India, it is all new concept of use of void formers in slabs. Nowadays there is a need of large span slabs which is the main limitation for conventional flat slabs. Also it increases the overall dead load of structure which increases the amount of steel reinforcement and quantity of concrete. The voided slab offers large span and with reducing the dead load. The construction cost increases every day as voided slab saves material and reduced cost of construction, and it is going to be very beneficial in construction industry.

To ensure the safety and life span of structure in Indian tropical zone, it is necessary to work out the compatibility of these foreign techniques with Indian standards. The awareness and confidence on voided slabs in construction industry is very less in India, the lack of research on voided slabs and void formers is responsible for it. So the research on voided slabs in India is necessary, to gain popularity in construction industry.

Fanella et al. [3] proved that such systems can be designed using the provisions of the American Concrete Institute (ACI) for strength and serviceability and can satisfy the minimum requirements for vibration control and fire resistance.

Parikh and Bhagat [7] compared and studied the voided flat plate slab and solid flat plate slab. They found that voided flat plate slabs have low stiffness than that of solid flat plate slabs.

Tiwari and Zafar [10] concluded Bubble Deck performs better than normal conventional solid slabs. The internal forces and maximum stresses in the voided deck were up to 40% lesser than solid slab due to reduced dead weight by use of HDPE spheres. The deflection was little greater by 10% since the stiffness reduces from the presence of bubbles/spheres.

The main objective of the study was to propose flat slab with voided system in Indian practice. In this study, the new shape of void formers has been proposed to optimize the stiffness modification factor. The study also validates the theoretical analysis with experimental work.

2 Void Formers

2.1 Study of Various Shapes

There are various shapes of void formers which are using to form voids in slab nowadays. In Bubble Deck circular void formers are used, whereas Cobiax and air deck uses the elliptical and circular shape also, and U-Boot Beton uses a square and rectangular shape void former. These are most popular techniques of voided slab uses a patented shape and design of void former.

The shape of void formers in Bubble Deck and Cobiax is spherical and elliptical so removing same amount of concrete from top and bottom zone which is under less stresses of central portion of cross section. Result of this is reducing stiffness of slab. So stiffness modification factor had been introduced. As their technique had
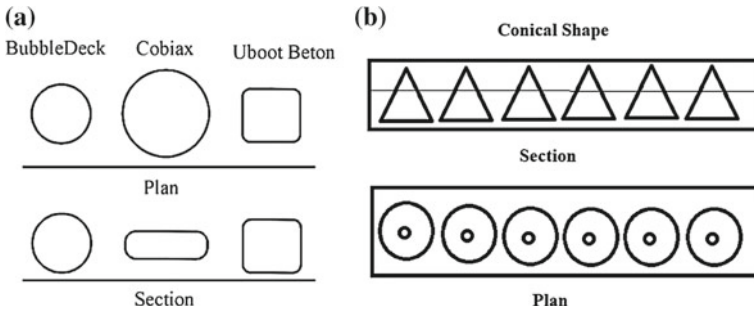
Fig. 1 **a** Various approximate shapes of void formers. **b** Proposed shape of conical void former

patented, their calculations of stiffness modification factor are confidential. There are no certain guidelines available on stiffness modification factor. Hence, there is an attempt on optimizing stiffness modification factor and weight reduction factor. As these parameters depend on shape and volume of void former, it has been tried to change the shape of void former from spherical to conical with same volume so the concrete in top layer is increased and the stiffness is increased, ultimately stiffness modification factor is reduced (Fig. 1).

2.2 Proposed Conical Shape

The proposed conical shape has its own advantages and disadvantages. This shape allows more concrete in upper layer of slab and removes more concrete from bottom side, which gives more compressive resistance in same quantity of concrete. The logic behind conical shape is removing less concrete of compressive zone and more from tensile zone where it is less useful. The role of concrete in tensile zone is to transfer the stresses to reinforcement in bottom. According to method mentioned by Tiwari and Zafar [10], stiffness modification factor was calculated from moment of inertia of section. In that almost same moment of inertia of both sphere and cone had been calculated, and it gives almost same stiffness modification factor. This method is not accurate; there is need of FEM analysis.

The manufacturing of HDPE void former is not possible for small quantity because the die of specific shape to manufacture is costlier. So for research work, the thermocol is selected to make void formers of required shape. The density of selected thermocol is more than regular one, and it is also possible to manufacture locally. The conical shape thermocol void former is not costlier for small quantities and research works. As the void former does not contribute to flexural and shear strength of slab, their only role is to provide voids in slab (Fanella et al. [3]) (Fig. 2).
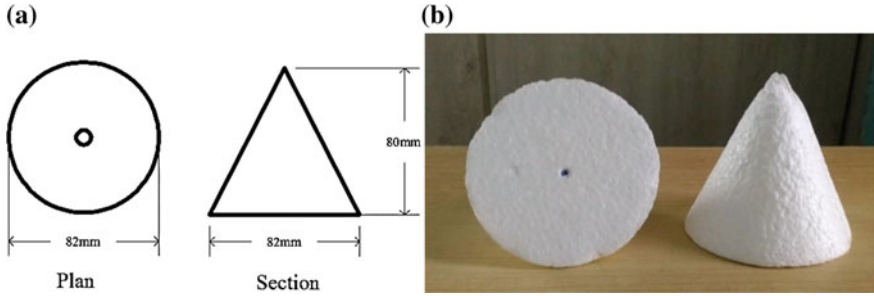
Fig. 2 **a** Dimensions of conical void former. **b** Conical void former of thermocol

3   Experimental Work

According to the research papers of Bubble Deck [16] and Cobiax [15], their design of voided slab is like regular solid slab design and the U-Boot Beton's design is made by grid of ribs in slab.

On the basis of Bubble Deck's and Cobiax's information sources and research paper of Parikh and Bhagat [7], it was decided to design the voided slab like regular solid slab by IS 456:2000 provisions with basic detailing of reinforcement except use of mild steel. Total three specimens of slab were cast which are configured as follows.

- Slab Size: 1.5 m × 1.5 m × 0.1 m
- Concrete Grade: M25 (1:2.11:2.99)
- Steel Grade: Mild Steel (Fe250) (6 mm diameter)
- Cement: PPC-53 Grade
- Curing Period: 28 Days (water ponding).

The quantity of fine aggregate was increased in concrete mix design to reduce the placing and compaction problems in the presence of void formers.

3.1   Solid Slab (Control Specimen)

In solid slab, the mild steel reinforcement was used, consists total 7 bar of 6 mm diameter in both directions at spacing of 250 mm C/C with alternate bent up bars (Fig. 3).

3.2   Type I Voided Slab

In type I voided slab, the conical void is placed. The 100 conical void formers had placed in 10 rows and 10 columns with 10 mm spacing in both directions. The
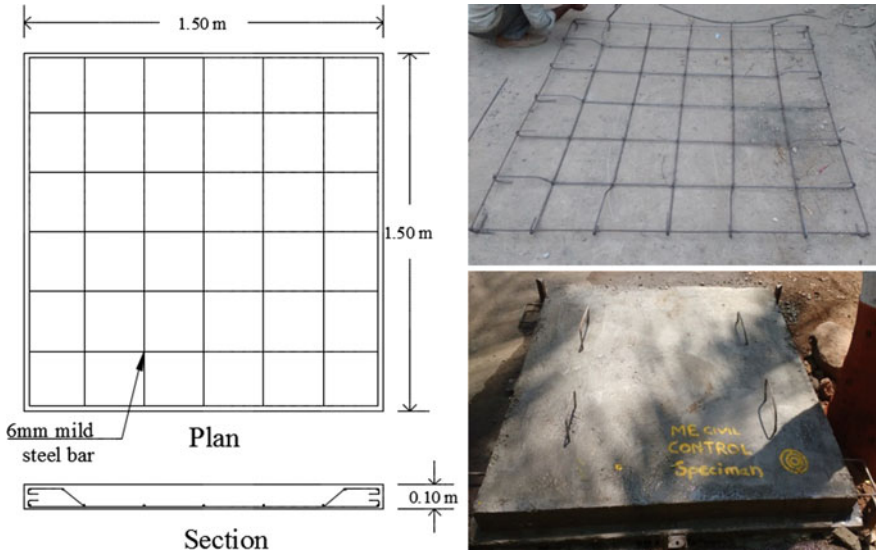
Fig. 3 Reinforcement details of solid slab

welded mesh of 16 gauge thickness with 50 mm × 50 mm spacing and size of around 1 m × 1 m was placed above reinforcement and bounded with binding wire. The void formers of thermocol ware fixed on welded mesh by strong adhesive uses in crafting. The void formers save almost 6–7% concrete. The reinforcement is same as in that of solid slab. The amount of concrete saved is less because of small depth of slab.

The welded mesh can resist tension, so it increases the area of steel in cross section by 26 mm^2. Compare to main steel of 198 mm^2, it is very less but almost 13% of main reinforcement (Fig. 4).

3.3 Type II Voided Slab

In this type II voided slab, the same amount of void formers is used, which saves same amount of concrete. Only the reinforcement and its pattern had changed. For type II voided slab, the frame of 6-mm bar was welded with welded mesh to fix void former on it and to support the reinforcement. Mild steel galvanized iron wire of 3.4 mm diameter was used as reinforcement in similar amount as that of other slabs. So this slab had similar type of behavior like large scale slab. And it can make the grid of ribs with reinforcement at bottom (Fig. 5).
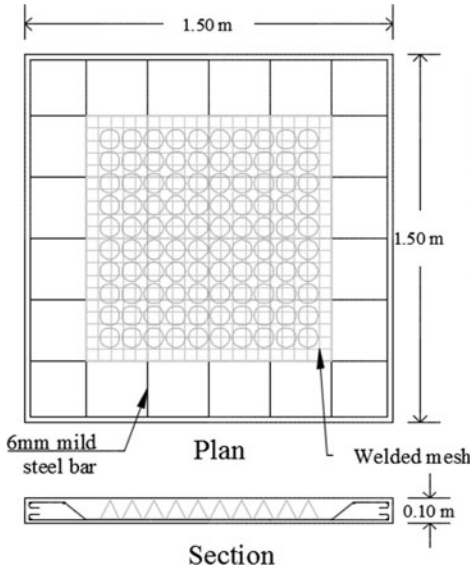
Fig. 4 Reinforcement details of type I voided slab
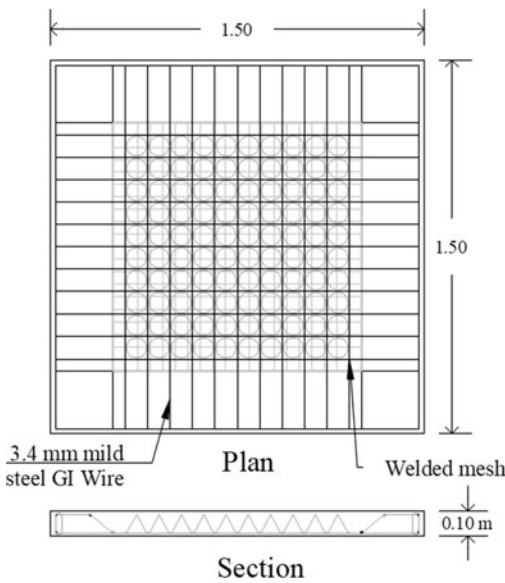
Fig. 5 Reinforcement details of type II voided slab

3.4 Test Setup

The flexural test on slabs was conducted by manual operating hydraulic machine on loading frame of a capacity of 100 tones. Uniformly distributed load was applied to slab through sixteen points. The distance between two roller supports is 1.3 m, and the area enclosed is divided into four equidistant lines.

The wooden block of size 5 cm × 5 cm × 5 cm had been used. Below that wooden plate of 10 cm × 10 cm × 1 cm had placed to distribute load more uniformly over the area. Above wooden block, the low capacity I section of 100 × 100 × 50 had been used in two layers four section in one layer and three above that. The double welded heavy channel section has transferred load of hydraulic jack to I section (Figs. 6 and 7).
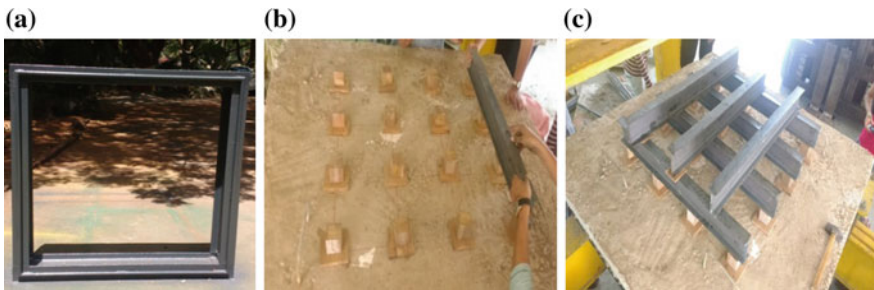
Fig. 6 a Roller support frame. **b** Arrangement of wooden block on sixteen points. **c** Loading arrangement of I sections

Fig. 7 Flexural test setup

4 Results and Discussion

The Results of each specimen discussed separately to provide details of behavior of specimen under testing. The values of load discussed below are reading of pressure gauge of hydraulic jack. All graphs of load versus deflection were plotted considering central (maximum) deflection only.

4.1 Solid Slab (Control Specimen)

From reading and the plotted graph, it was observed that the deflection was zero for initial gradual load up to 10 kN. The first crack was at a load of 105 kN where sudden increase in deflection was observed and crack was getting wider continuously as load was increasing. After that the rate of deflection was increased and slab reached to its ultimate load carrying capacity. Further reading showed that there was increase in deflection under sustained load.

From the crack pattern of solid slab, it is clear that the slab transferring load in two way action as all major cracks propagated diagonally from central portion toward corners. The crack pattern shows that the pure uniformly distributed load was acted on slab. The crack width is little larger at ultimate load, as it has less minor cracks which indicate that the overall performance was good.

4.2 Type I Voided Slab

Type I voided slab was showing very less deflection up to 20 kN loading. The first crack was at 85 kN loading where also sudden increase in deflection observed. The type I slab takes same ultimate load carrying capacity of 190 kN with less deflection of 10.2 mm as compared to 13 mm of solid slab. It means that the stiffness of type I slab is not reduced in the presence of conical shape void former. The additional reinforcement of welded mesh which is 13% of main reinforcement has not affected much to deflection and load carrying capacity. It had less quality of steel than main steel and placed above main reinforcement.

The crack pattern is not perfect as that of solid slab; as it showed less diagonal cracks than solid slab. The overall crack pattern shows that the uniformly distributed load was acted in two way on slab. The crack widths are little lesser at ultimate load than solid slab because it takes less deflection.

4.3 Type II Voided Slab

Type II voided slab was not showing deflection up to 10kN loading. The first crack was observed at 90 kN loading. It does not clear from deflection readings, as it not showing instant deflection; but from the rate of deflection which is increased after 90 kN. After that the cracks were getting wider continuously and then slab reached at its ultimate load carrying capacity.

The type II slab had more ultimate load carrying capacity of 215 kN with more deflection of 16 mm but compared to type I, and solid slab, it gives 11.5 mm deflection at 190 kN load which is more than type I and less than solid slab. The results state that the stiffness of type II slab is not reduced in the presence of conical shape void former, but the ultimate load carrying capacity increased due to more distributed reinforcement of galvanized iron wire. Because of reinforcement type slab acts like ribbed slab as it forming grid of it. And its deflection is more due to more ultimate loading capacity.

The cracks in type II slab are more than solid slab. Crack pattern is also perfect as it shows more density of cracks and diagonal propagation from center to corners. It also shows the two way action, and the uniformly distributed load was transferred correctly on slab. The crack width is same at ultimate load like solid slab because the number of cracks is more but ultimate loading is also more than solid slab.

The void formers are used to reduce the concrete from slab. The amount saved from conical void formers is shown in Table 1.

The values of load observed from pressure gauge and deflection from dial gauge are shown in Table 2.

From Fig. 8 of graph, it can be observed that the line of load versus deflection of solid and type I slab propagated in same manner. But the type I slab performs more than solid giving less deflection (Fig. 9).

Table 1 Amount of concrete used

Slab type	Amount of concrete used (m^3)	Amount of concrete saved (m^3)	% concrete saved
Solid	0.225	–	–
Type I voided	0.2113	0.01408	6.26
Type II voided	0.2113	0.01408	6.26

Table 2 Observed load and deflection

Slab type	Maximum load (kN)	Maximum load (kN/m^2)	Maximum deflection (mm)
Solid	190	112.43	13
Type I voided	190	112.43	10.2
Type II voided	215	124.26	16
	At 190	112.43	11.5
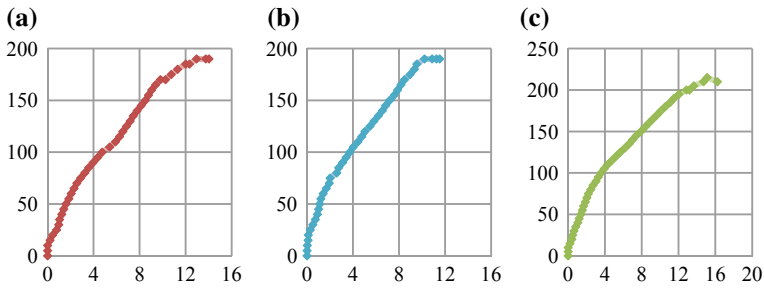
Fig. 8 Graphs **a–c** shows the load versus deflection of solid, type I and type II slab
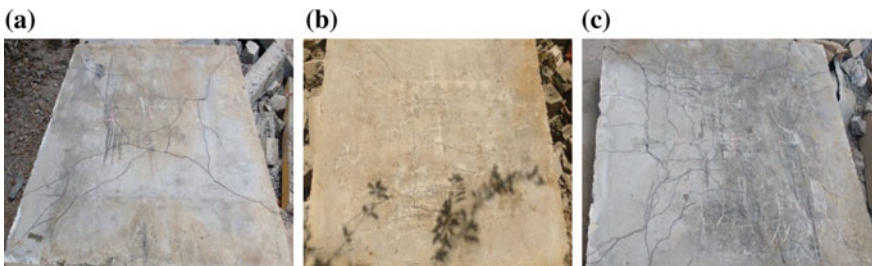
Fig. 9 **a–c** Shows the crack pattern of solid, type I and type II slab

The type II voided slab perform less compare to type I slab, and perform more than solid slab in terms of deflection. On the other hand, it is better at ultimate load carrying capacity than both type I and solid slab. Both the type I and type II voided slabs perform better than solid slab in different parameters (Fig. 10).

5 Conclusion

From the analysis and design of flat slab as per IS 456:2000, it has been found out that in current guidelines, the stiffness modification factor is not specified or explained in any analytical procedure. The weight reduction factor can be applied by making direct changes in load calculations of voided slab. So voided slab or voided flat slab can be designed by codes considering appropriate stiffness modification factor.

Voided slab systems are more suitable or efficient for large depth slabs, more the depth of slab more concrete will be saved and give more benefits.

From the flexural test results of slabs, it has been concluded that

- Voided slab is giving equal flexural strength like solid slab, and the stiffness is not reduced by conical void formers.
- Both the type I and type II voided slab performs better than solid slab in deflections.
- That means the conical void former optimized the strength of section of slab.

Fig. 10 Combined load versus deflection graph of all slab
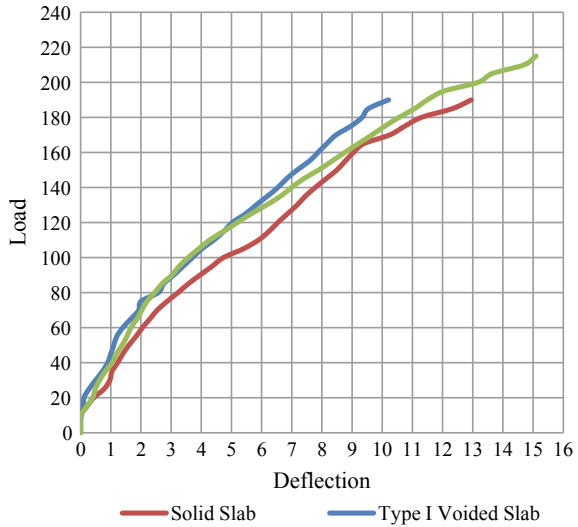
- The proposed conical shape void former is effective, and it definitely increases the stiffness of voided slab compared to spherical shape.

More study is required in Indian practice on voided flat slab considering stiffness and deflection of voided flat slab.

References

1. Björnson, G.: BubbleDeck two-way hollow deck. Bubble Deck®, Sept 2003
2. Dwived, A.K., Joshi, H.J., Raj, R., Mishra, P.P., Kadhane, M., Mohabey, B.: Voided slab design: review paper. IJRSI **IV**(I), 220
3. Fanella, D.A., Mahamid, M., Mota, M.: Flat plate–voided concrete slab systems: design, serviceability, fire resistance, and construction. © 2017 American Society of Civil Engineers. https://doi.org/10.1061/(asce)sc.1943-5576.0000322
4. Ibrahim, A.M., Ali, N.K., Salman, W.D.: Flexural capacities of reinforced concrete two-way bubbledeck slabs of plastic spherical voids. Diyala J. Eng. Sci. **06**(02), 9–20 (2013). ISSN 1999-8716
5. Jang, T.-Y., Kim, S.-M., Kim, S.-D.: New eco-friendly two-way void slab. Int. J. Sustain. Build. Asia. SB10SEOUL
6. Lai, T.: Structural behavior of BubbleDeck® slabs and their application to lightweight bridge decks. Massachusetts Institute of Technology, © Tina Lai, All rights reserved, June 2010
7. Parikh, K.B., Bhagat, S.: Comparative study of voided flat plate slab and solid flat plate slab. Int. J. Innov. Res. Dev. **3**(3) (2014). ISSN 2278-0211. www.ijird.com
8. Parikh, K.B., Bhagat, S.: Parametric study of R.C.C. voided and solid flat plate slab using SAP 2000. IOSR J. Mech. Civ. Eng. (IOSR-JMCE) **11**(2), 12–16. e-ISSN: 2278-1684, p-ISSN: 2320-334X. Ver. VI www.iosrjournals.org (2014)
9. Purushottam, Y.J., Hemantkumar, T.Y.: Analytical study of solid flat slab and voided slab using ANSYS workbench. Int. Res. J. Eng. Technol. (IRJET) **03**(10) (2016)

10. Tiwari, N., Zafar, S.: Structural behaviour of bubble deck slabs and its application: main. IJSRD Int. J. Sci. Res. Dev. **4**(02) (2016). ISSN: 2321-0613
11. Valivonis, J., Skuturna, T., Daugevičius, M., Šneideris, A.: Punching shear strength of reinforced concrete slabs with plastic void formers. Constr. Build. Mater. **145**, 518–527 (2017). ScienceDirect. www.elsevier.com

Books

12. Punmia, B.C., et al.: Reinforced Concrete Structures
13. Shah, V.L., Karve, S.R.: Illustrated Reinforced Concrete Design. 5th edn. Structures Publications. Jal-Tarang, 36, Parvati, Pune-411009

Codes of Practice

14. ACI 318-2014
15. Cobiax: Lightweight concrete slabs. www.cobiax.com
16. http://www.bubbledeck.com/
17. IS 456:2000

Part III
Industrial Engineering for Sustainable Development

Dr. Pramod V. Walke Conference Organizing Chair

Introduction

In all over the world, Industrial Engineering for sustainable Development plays a vital role towards the technology enhancement in turns of good quality products as per the versatile demand by the day to days life. It bringing major revolution in turns of the quality and quantity of all engineering applications. This goal of achieving high quality products are done by advancement technique in Industrial engineering like Additive Manufacturing, Virtual Instrumentation and Operations Management in industry for sustainable development.

In the "International conference on Smart Technologies for Energy, Environment and Sustainable Development, 2018 (ICSTEESD-18)", two technical sessions have been organized for addressing the technical challenges, opportunities, and research innovation related to Industrial Engineering for Sustainable Development.

Both sessions have been chaired by Prof. Dr. Akira Nishimura of MIE University (Japan), who has specialization in Energy System Design, photocatalyst, Fuel Cell, fluid dynamics with two decades international experience in the world's prestigious universities. The research papers of this section have highlighted various technical issues related to Additive Manufacturing, Binary Logistics Regression Analysis, "Study Of Springback Effect In Industrial Grade Materials Polypropylene Alloys And Composites", Virtual Instrumentation and Operations Management, Industry 4.0 etc.

www.ghrce.raisoni

Dr. P. V. Walke Conference Organizing Chair
International conference on Smart Technologies for Energy,
Environment and Sustainable Development, 2018 (ICSTEESD-18);
Head of Mechanical Engineering Department, G.H. Raisoni College
of Engineering, Nagpur, Maharashtra, India

Development of Finned Tube Type Adsorber Bed for Adsorption Cooling System

Bhushan C. Behede and Uday S. Wankhede

Abstract Adsorption cooling system consists of the specifically designed heat exchanger which is filled with adsorbents (silica gel). The flow of refrigerant is regulated inside the heat exchanger by regulating valves. Heat exchanger filled with adsorbents called a 'Thermal compressor' is used to build the pressure in the system. It is a replacer for the mechanical compressor in a Vapor Compression Refrigeration System (VCRS). This heat exchanger is experimentally evaluated in the adsorption cooling system which is developed for air-conditioning of subcompact vehicle of 1 TR capacity. Coefficient of Performance (COP) and Specific Cooling Power (SCP) are the performance parameters evaluated from the experimentation. Temperature of hot source is varied from 45 to 60 °C and for 15 min of cycle time, maximum COP obtained is up to 0.55, whereas minimum obtained is 0.14. On another hand, SCP is observed up to 348 W/kg. Here, the design of thermal compressor plays an important role. SCP and COP of the system are to be maximized by increasing heat transfer and mass transfer rates. Poor design of heat exchanger leads to decrease in heat transfer and mass transfer rates which will reduce SCP and COP of the system. Heat transfer rate of the heat exchanger is enhanced by increasing heat transfer area, and mass transfer rate is enhanced by decreasing the thermal resistance between adsorbent–adsorbate particles.

B. C. Behede (✉)
G. H. Raisoni Institute of Engineering and Management, Jalgaon, Maharashtra, India
e-mail: bhushanbehede@gmail.com

U. S. Wankhede
Government College of Engineering, Chandrapur, Maharashtra, India

1   Introduction

The story of sorption refrigeration systems starts when the human world realized to fight with problems arising due to global warming and ozone layer depletion. Energy demand has been enormously increasing day by day and naturally occurring earth-fuel storage is about to finish. Now, there is a strong need to find some alternative energy sources or to conserve the abundantly available excess thermal energy present in many thermal processes [1]. According to International Institute of Refrigeration, almost 15% of utilized energy is consumed for air-conditioning purposes. Moreover, this amount is going to increase rapidly in coming years because comfort requirements are increasing continuously [2].

Vapor Compression Refrigeration System (VCRS) has very good COP and widely accepted by almost all refrigeration industries; however, this system is more electricity consumable in many cases [3]. VCRS uses refrigerant, which contains CFCs, HCFCs, and HFCs. These environmentally harmful refrigerants are ruled out by various treaties like Montreal protocol (1987), Kyoto protocol (1997), and European regulation commission 2037/2000 which concerns with global climatic change [4]. Hence, sorption refrigeration systems have been gaining the attention of many researchers and now strong need is to develop a global model of an adsorption colling system which would be accepted by refrigeration industries.

ADCS consists of the main component as 'Heat Exchanger' (called as Heart of the system) filled with adsorbent materials (silica gel), a condenser, an expansion device, and an evaporator, main components along with valves forming a cycle, as shown in Fig. 1 [5].

Interconnecting valves are incorporated to initiate the flow of refrigerant. Heat exchanger packed with the specific amount (in kg's) of an adsorbents is used to build pressure in the system, called as a 'Thermal compressor', which replace the mechanical compressor in a VCRS. A complete cycle can be divided into two half cycles as 'Heating—Desorption—Condensation' and 'Cooling—Adsorption—Evaporation' [5].

Conventional ADCS is facing the problem of low COP and SCP, because of having poor mass transfer and heat transfer rates inside an adsorber bed heat exchanger. With prior to solve this problem, there is a strong need to design and fabricate or to

Fig. 1 Basic layout of ADCS
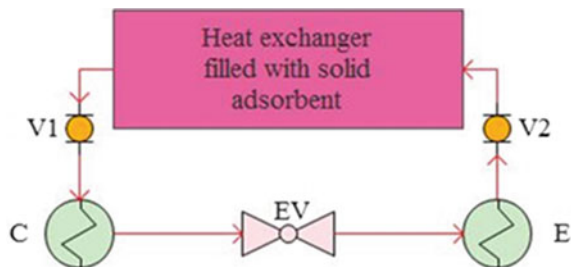
modify the available designs of an adsorber bed heat exchanger in such a way that the heat transfer rate, as well as mass transfer rate, will boost and thermal resistance will decrease [6]. With this aim, the main objective of the present work was to design and fabricate an improved, global, and dynamic model of an adsorber bed heat exchanger for ADCS. A further objective of present work was to develop a sophisticated methodology to evaluate the performance of an ADCS.

2 Literature Review

Here some existing methods were adopted by researchers and discussed same to increase the performance of ADCS [7].

2.1 Design of an Adsorber Bed Heat Exchanger

Cycle time increases due to low heat and mass transfer rate. Poor design of an adsorber bed leads to decrease in mass transfer rate which results in low SCP of the system. Heat transfer rate of the heat exchanger can be enhanced by increasing the heat transfer area, and mass transfer rate is enhanced by decreasing the thermal resistance between adsorbent–adsorbate particles and by creating voids. The main goal is to increase the heat transfer and mass transfer rate by improving adsorber bed heat exchanger design [6, 8].

2.2 Using Extended Surfaces

Use of different types of the fin on the outer surface improves heat transfer rate. Surface area between adsorbent–adsorbate increases by providing fins. Different types of heat exchangers as shown in Fig. 2 can be made by using different types of fins [6, 9].

Sharafian et al. [7] listed various types of heat exchanger design used in waste heat-driven ADCS. Effect of an adsorber bed design on SCP, COP, and adsorber bed to the adsorbent mass ratio (AAMR) is compared with nine types of heat exchanger designs as shown in Fig. 2. Types of heat exchangers compared are spiral plate, shell and tube, hairpin, annulus tube, plate fin, finned tube, plate tube, a simple tube, and plate type. Among them, plate fin and finned tube heat exchangers have higher heat and mass transfer rate than plate type and simple tube type heat exchangers. Finned tube type heat exchanger is the most suitable because of having improved heat transfer and mass transfer rate.
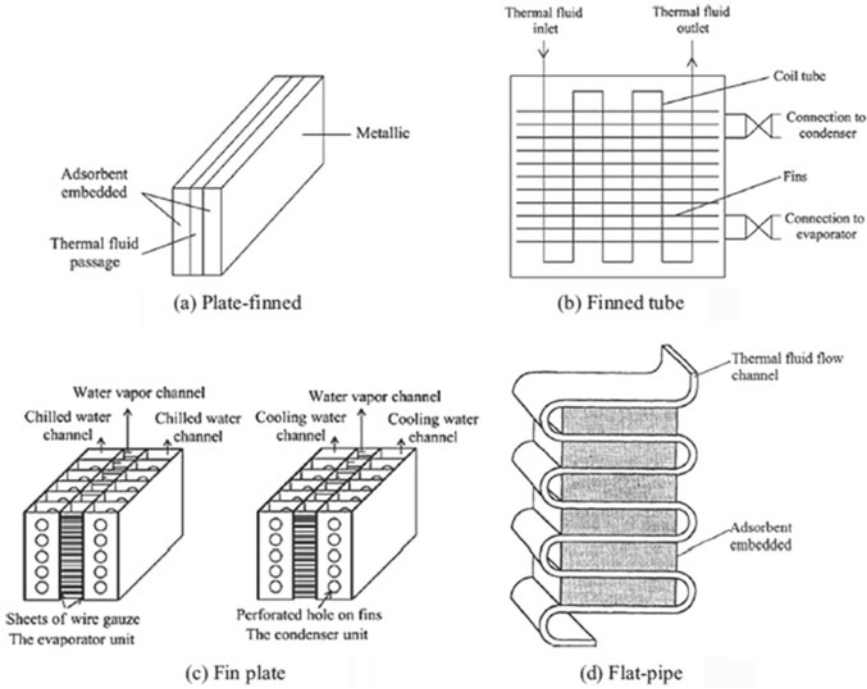
Fig. 2 Different types of heat exchanger configurations [8]

2.3 Coating

An adsorbent material is coated around a pipe or fin to generate high-speed heat transfer and mass transfer rate. The coating material is prepared by a consolidated adsorbent material with a suitable binder. Coating material should have good mechanical stability and adhesive property [6]. Andrea Frazzica et al. [9] did an experimental evaluation of a binder-based coating adsorbent developed for chilling purposes. SAPO-34 is used as a commercial adsorbent, and Bentonite clay is used as a binder. This adsorbent is compared with monolayer and multilayer of loose grained adsorbents. Experimental results show that 0.6 mm thickness is most suitable to achieve higher volumetric-specific cooling power (VSCP). Larger thickness reduces VSCP which is not acceptable.

Low COP and SCP are major barriers in the way of commercialization of adsorption cooling technology. Less heat and mass transfer rates are the reasons behind the ADCS having low COP and SCP. In the upcoming years, more research is required to improve COP and SCP values of an ADCS [10].

2.4 Modified Cycles

The basic cycle has low efficiency. Single bed ADCS produces intermittent cooling power. Two-bed ADCS has been developed so far. Modification in basic cycle improves the performance of double and multi-bed ADCS. Heat recovery, mass recovery, combined heat, and mass recovery, thermal wave, forced convective thermal wave, cascading are the modifications in basic cycle. These methods increase complications in the working on the basic cycle but COP and SCP improve compared to earlier designs [11, 12]. Review of ADCS with modified cycles is summarized in Table 1.

3 Adsorber Bed Heat Exchanger

Heat exchanger incorporated in the present work is a finned tube type. It is state-of-the-art device which aims both heat transfer and mass transfer characteristics to be fulfilled. Major parts consist of heat transfer channel surrounded by rectangular fins, and the complete assembly is known as Mass Transfer Channel (MTC), which is firmly placed in outer casing with the help of flanges. The whole structure can be evacuated from one end. Selection is as follows.

3.1 Mass Transfer Channel (MTC)

- Material used for tubes—copper
- Orientation—coiled tubes
- Shape—Rectangular
- Fins:

  - Type—Square fins
  - Material—aluminum
  - Space between two fins—18 mm.

- Outer casing:

  - Material—G. I. Sheet.

Main components were designed, and other components such as condenser, expansion device, evaporator, etc. are selected according to refrigerating load. An air-cooled heat exchanger is utilized as condenser while flooded type heat exchanger is incorporated as an evaporator where chilled water is yielded which can be further used for desired applications. Line diagram of the heat exchanger with details is pictured in Fig. 3. Adsorber bed heat exchanger is modeled on the 3-D interface by using CATIA V5 R20, as shown in Fig. 4. MTC placed in outer casing is shown in Figs. 5

Table 1 Review of ADCS with modifications in working cycle

References	Scheme of modification	Adsorbent + adsorbate	Comments
[12]	Mass recovery	Silica gel + Water	• An experimental prototype is developed having plate fin type HEX, with 16 kg of adsorbent/bed • It has been concluded that heating and cooling effect during the mass recovery process improves the cooling output • The mass recovery scheme is best suitable when low-temperature heat source is available
[13]	Double bed ADCS with mass recovery	Silica gel + Water	• Chilled water outlet temperature obtained is lower than conventional single bed system • Simulation results show that the cooling capacity of the proposed system is 40% higher than conventional systems
[14]	Mass recovery between beds + cascading	Upper cycle – Silica gel + water Lower cycle – Silica gel + water	• A COP of the proposed system is greater than a conventional system • It has been concluded that heating and cooling effect during the mass recovery process improves the cooling output
[15]	Mass recovery between beds + cascading	Upper cycle – Silica gel + water Lower cycle – Silica gel + water	• The proposed system is best suitable for low-temperature heat source

(continued)

Table 1 (continued)

References	Scheme of modification	Adsorbent + adsorbate	Comments
[16]	Cascading	Upper cycle + lower cycle: adsorbent/refrigerant switched using Simulink/MATLAB software are as follows Maxsorb/R134a + Maxorb/Propane, ATO/Ethanol + Maxsorb/R507A, ATO/Ethanol + Maxsorb/Propane, and Maxsorb/R134a + Maxsorb/R507A	• MAxsorb + R134a and Maxsorb + propane reported as better performance than others because of high pressure of R134a and high latent heat of propane • 30.0% increase in COP and 30.1% increase in SCP over basic single bed ADCS • ATO/Ethanol + Maxorb/Propane combination is cheapest among all
[17]	Cascading	Upper cycle – Activated carbon + R134a Lower cycle – Activated carbon + R507a	• With $T_{evp} = -10$ °C, the system is reported suitable for freezing applications and process industries where large amount of waste heat is available at around 70 °C
[18]	Thermal wave (square type) without mass recovery, with adiabatic mass recovery and with isothermal mass recovery	Zeolite-NaX + Water Heat transfer model – Water	• Simulation results show that the COP of the reversible cycle is maximized, then COP of the TW cycle is 40–75% lower than reversible but greater than, simpler cycle and heat recovery cycle with two isothermally spatial (2SIB) beds
[19]	Cascading + heat and mass recovery between upper cycle beds	Upper cycle – Zeolite + Water (two beds) Lower cycle – Silica gel + Water (single bed)	• With cascading around 50% higher COP obtained than basic two-bed ADCS without heat and mass recovery, and 35% higher COP than heat and mass recovery between 230 °C. However, beyond 230 °C, increase in COP is negligible

Fig. 3 Line diagram of an adsorber bed heat exchanger. Description (1) copper tube inlet, (2) copper tube outlet, (3) rectangular-shaped aluminum fin, (4) insulation, (5) medium meshed metallic net, (6) outer casing, (7) mass transfer channel (MTC), (8) leak proof enclosure, (9) inlet for adsorbate, (10) outlet for adsorbate
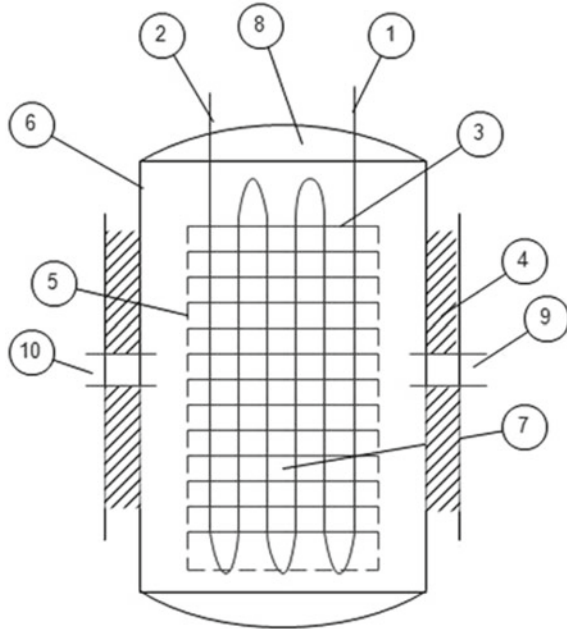
and 6. Silica gel is filled compactly in and around the copper tubes between the gap of the fins to reduce the thermal resistance, and metallic net is wrapped to hold the adsorbents with tubes.

All the parts of an adsorber bed heat exchanger are listed below the caption. The same design is adopted for both the adsorber bed heat exchangers. Mass transfer channel (Callout 7) is refillable and has a compact structure. MTC consists of a copper tube having an inlet (Callout 1) and outlet (Callout 2), through which heat transfer fluid circulated. Copper tube has five turns, and rectangular-shaped aluminum fins (Callout 3) were fixed around the periphery of the tube. Gap available between the fins is utilized for filling of an adsorbent material. Metallic net of medium mesh (Callout 5) is wrapped around the channel to prevent the falling of an adsorbent material. The mass transfer channel is enclosed completely in the outer casing (Callout 6) and fitted with the help of leak proof enclosure (Callout 8). Insulation (Callout 4) is provided around the outer casing. Provision for the flow of an adsorbate (Refrigerant) is made in the midway of bed, which has an inlet (Callout 9) and outlet (Callout 10).

4 Experimental Setup

Line diagram of a complete experimental setup shows connections of all primary and secondary components as shown in Fig. 7. The experimental setup consists of a two

Fig. 4 Modelling of adsorber bed heat exchanger on CATIA V5 R20
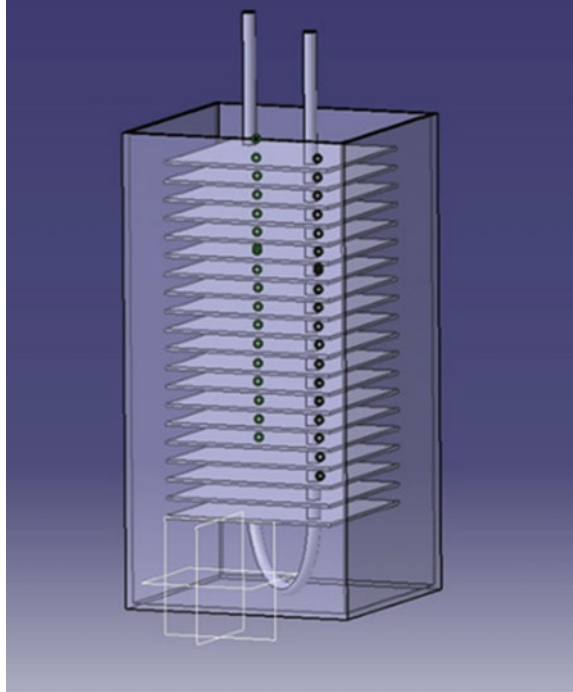
adsorber bed heat exchangers, air-cooled condenser, an expansion device (Capillary tube), and an evaporator. The other supplementary setup consists of parts of a hot and cold water tank, pumps, in-way and out-way circuits, heater, valves, etc. Two adsorber beds of same configurations are incorporated as a thermal compressor in the system. Two beds operate during their respective half cycles. Common air-cooled condenser and evaporator are connected to the adsorber beds with the help of valves. Valves are operated manually in order to evaluate the system for changing parameters. The function of valves in the refrigerant line is to regulate the flow of an adsorbate through adsorber bed, followed by a condenser, evaporator, and back to the adsorber bed. Valves present in the in-way and out-way circuits are used to regulate the flow of cold and hot water in the adsorber bed heat exchangers. Two reservoirs used in the system to provide hot and cold water. Hot and cold water is being circulated in the system with the help of pumps. Submersible pump dipped in the cold water tank is used to circulate chilled water through the evaporator. Rotameters are fitted in the pipeline of hot and cold water after the pumps. The temperature at the different locations is measured by k-type thermocouples and indicated by digital indicator present on the control panel. Pressure gauges used to measure pressure. The separate external arrangement is provided in the system to create a vacuum to charge adsorbate.

Fig. 5 Mass transfer
channel (MTC)
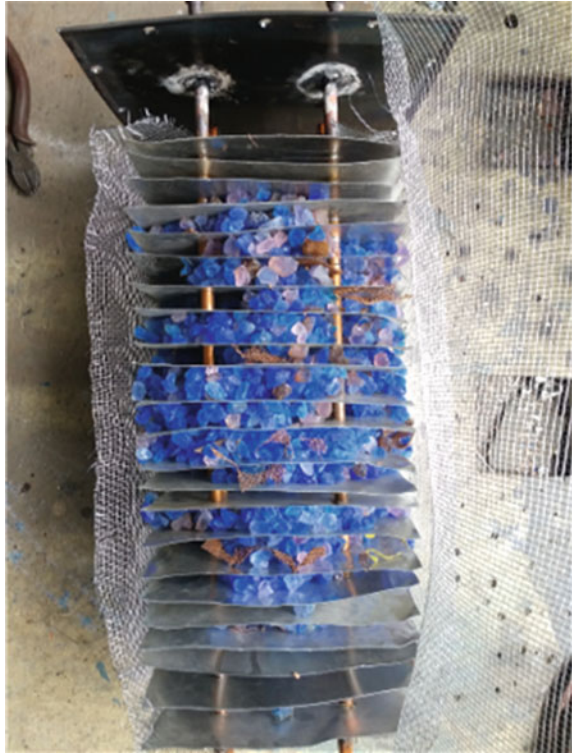
Fig. 6 MTC placed in the
outer casing
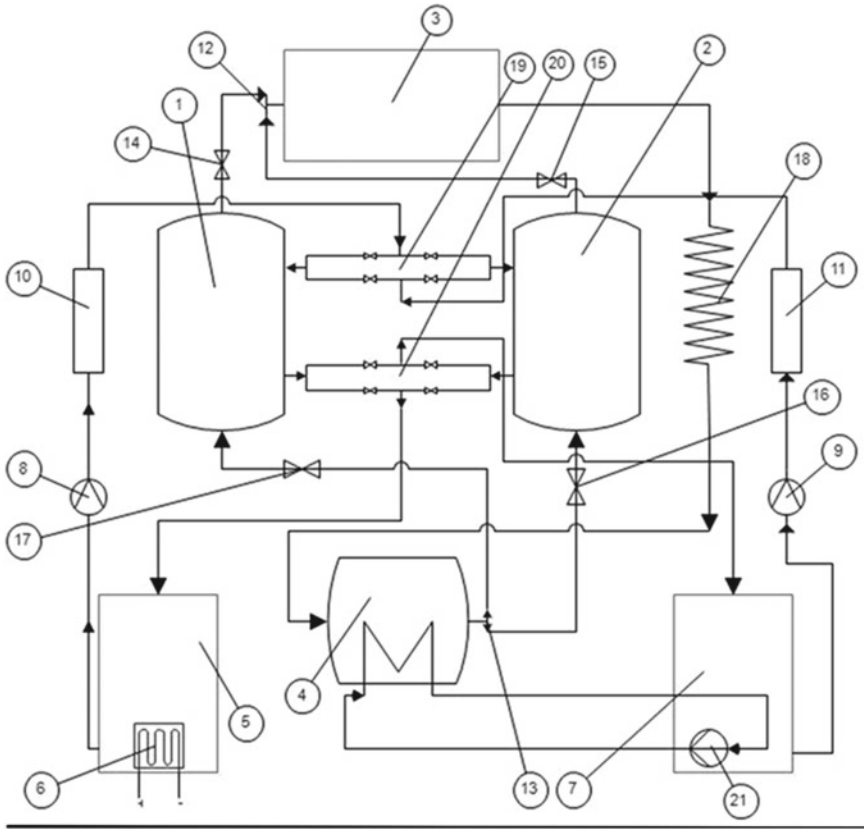
Fig. 7 Line drawing of complete experimental setup. Description (1) adsorber bed 1, (2) adsorber bed 2, (3) air-cooled condenser (with Fan), (4) evaporator, (5) hot water tank, (6) heater, (7) cold water tank, (8) pump delivering hot water, (9) pump delivering cold water, (10) rotameter in the hot water line, (11) rotameter in the cold water line, (12) T-joint at the inlet of condenser, (13) T-joint at the outlet of an evaporator, (14) valve connecting adsorber bed 1 with condenser through T-joint 12, (15) Valve connecting adsorber bed 2 with condenser through T-joint 12, (16) valve connecting adsorber bed 2 with evaporator through T-joint 13, (17) valve connecting adsorber bed 1 with evaporator through T-joint 13, (18) expansion device—capillary tube, (19) common in-way circuit for both the beds, (20) common out-way circuit for both the beds, (21) submersible pump

5 Adsorber Bed to Adsorbent Mass Ratio (AAMR)

AAMR is the ratio of adsorber bed mass other than adsorbent to adsorbent mass. AAMR is the term used to check the design of the adsorber bed heat exchanger with its fabrication. The metal of adsorber bed heat exchanger which is other than adsorbent material is known as the dead mass of the system and the actual mass of an adsorbent material is known as the live mass of the system. AAMR represents the dead-to-live ratio of ADCS [20]. It is well and good if AAMR is greater than one.

$$\text{AAMR} = m_{\text{Adsorber}}(\text{kg})/m_{\text{Adsorbent}}(\text{kg})$$

where

- $m_{\text{Adsorber bed}}$ = Mass of adsorber bed heat exchanger with no adsorbent = 5.227 kg.
- $m_{\text{Adsorbent}}$ = Mass of adsorbent material filled = 5 kg.

Hence,

$$\text{AAMR} = 5.227/5$$
$$\textbf{AAMR} = \textbf{1.054}.$$

6 Experimentation

The two-bed ADCS consists of two adsorber bed heat exchangers, the whole system is divided into two parts: one part is adsorber bed 1, and another part is adsorber bed 2. Both the beds connected with in-way and the out-way circuit through which hot and cold water supply can be done. Consider, adsorber bed 1, i.e., one part is undergoing the desorption process. During this, hot water is supplied to bed 1. The desorption process followed by condensation process in the condenser and refrigerant is expanded in the evaporator by a capillary tube. In the evaporator, the refrigerant is used to cool atmospheric water, which is supplied by a submersible pump. At the same time, another part is supplied with cold water and receives refrigerant which is expanded in the first part. This process is switched after halftime of cycle elapsed. Now, the second part is ready for being first part and the first part will be second. All operations were switched, and this switching time is neglected. During this time, positions of valves interchanged. The position of valves is as follows (Fig. 8; Table 2).

Table 2 Operation of valves according to process

Adsorber bed	Process	Valves in the Refrigeration line				Valves in the in-way circuit				Valves in the Out-way circuit			
		V1	V2	V3	V4	1	2	3	4	1	2	3	4
1	Des	On	Off	On	Off	On	Off	Off	On	Off	On	On	Off
2	Ads	On	Off	On	Off	On	Off	Off	On	Off	On	On	Off
1	Ads	Off	On	Off	On	Off	On	On	Off	On	Off	Off	On
2	Des	Off	On	Off	On	Off	On	On	Off	On	Off	Off	On
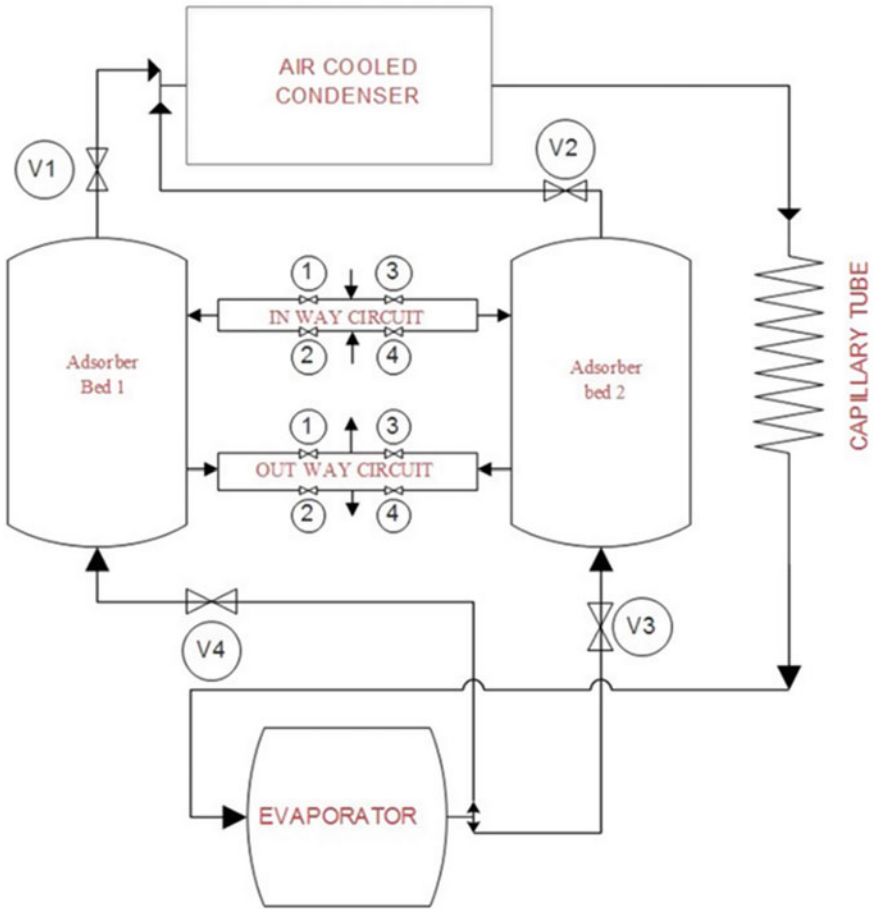
Fig. 8 Position of valve

7 Experimental Cases and Formulation

To compute different performance parameters and to establish a relation between them, it is necessary to keep constant some operating parameters and some to be changed accordingly. Experimentation is carried out by adopting three unic cases as follows:

7.1 Case A: By Varying Mass Flow Rate of a Hot and Cold Source for a Range of Operating Conditions at the Constant Cycle Time

In this case, the mass flow rate of the hot and cold source is varied in the range of 3–15 LPM of water. Cycle time is decided 10 min earlier but, to compensate the effect of switching time, the cycle time is kept constant at 15 min. Three inlet temperatures of hot source are analyzed as follows:

1. For (T_h)in = 50 °C, (T_c)in = 30 °C and $(T_{chilled})$in = 30 °C.
2. For (T_h)in = 55 °C, (T_c)in = 30 °C and $(T_{chilled})$in = 30 °C.
3. For (T_h)in = 60 °C, (T_c)in = 30 °C and $(T_{chilled})$in = 30 °C.

7.2 Case B: Keeping Constant Mass Flow Rate of a Hot and Cold Source for Varying Operating Conditions at Constant Cycle Time

In this case, the mass flow rate of the hot and cold source and cycle time kept a constant while the inlet temperature of the hot source is varied from 45 to 60 °C.

7.3 Case C: Keeping Constant Mass Flow Rate of a Hot and Cold Source for Varying Operating Conditions at Varying Cycle Time

In this case, the mass flow rate of hot and cold source kept constant and inlet temperature of the hot source along with cycle time is changed (Table 3).

8 Results and Discussion

Results were obtained by doing a complete experimentation with three different cases. Base case operating conditions are assumed to determine the nominal performance parameters and a working model of the double-bed ADCS is analyzed to calculate those parameters. Then, the analytical study is conducted in order to find out the effect of different parameters on the performance of the system. Different types of analysis tools are used to compare the results. Effective discussion has been done which is mentioned in subsequent sections.

Table 3 Formulation

Parameter	Symbol	Equation used for calculation	Unit	Reference
Heat supplied to the desorber bed	Q_h	$\dot{m}_h$ (kg/s) $\times$ C_{ph} (kJ/kg °C) $\times \Delta T_h$ (°C)	kW	[21]
Heat extracted from the adsorber bed	Q_c	$\dot{m}_c$ (kg/s) $\times C_{pc}$ (kJ/kg °C) $\times \Delta T_c$ (°C)	kW	
Heat released at the condenser	Q_{cond}	U (kW/m^2) $\times$ A (m^2) $\times \Delta T_{cond}$ (°C)	kW	
Cooling effect obtained at the evaporator	Q_e	$\dot{m}_w$ (kg/s) $\times C_{pw}$ (kJ/kg °C) $\times (\Delta T_{Chilled})$ (°C)	kW	
Coefficient of performance	COP	Q_e (kW)$/Q_h$ (kW)	–	
Specific cooling power	SCP	$\dfrac{Q_e (W) \times t_{ads} \text{ (min.)}}{m_{Adsorbent} \text{ (kg)} \times t_{cycle} \text{ (min.)}}$	W/kg	
Total cycle time	t_{cycle}	$t_{ads} + t_{des}$	min.	
Adsorber bed to adsorbent mass ratio	AAMR	$m_{Adsorber}$ (kg)$/m_{Adsorbent}$ (kg)	–	

8.1 Comparison of Trend of COP's for Varying Mass Flow Rates of the Hot Source at Constant Cycle Time

The trend of COP observed is the same at any operating condition when cycle time is kept constant. The range of COP values is maximum when the temperature of the hot source is around 60 °C but, the trend observed is unpredictable for earlier values of mass flow rates of hot source. Beyond 10 LPM of water, COP remains almost constant for all operating conditions. Nature of increase in COP is well predictable in the range of mass flow rate of the hot source of 10–15 LPM of water. It is well and good to keep mass flow rate of the hot source in the range of 10–15 LPM of water. Figure 9 shows an effective comparison of three different ranges at same cycle time. Almost same and low values of COPs are obtained at the starting, for all the three operating conditions. The reason is the very low mass flow rate of hot water. For higher values of the mass flow rate of hot source, COP increases, when inlet temperature of hot source supplied is increased. At the starting, hot source inlet temperature of 60 °C is well and good enough to build adsorbate vapor in the system in provided cycle time. If we compare COP values at a higher mass flow rate, then COP around 0.55 obtained when hot source inlet temperature is around 60 °C and COP obtained is 0.41 and 0.44 when the temperature of the hot source is 50 and 55 °C, respectively.
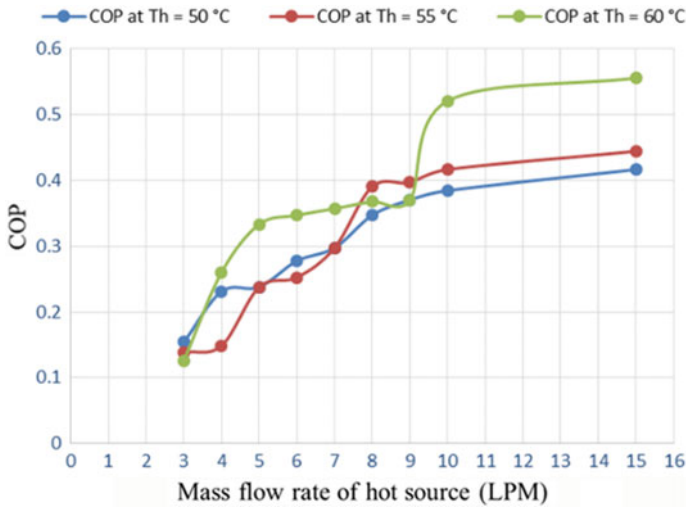
Fig. 9 Different COP trends obtained at different inlet temperatures of hot source against mass flow rate of hot source at constant cycle time

8.2   Effect of the Mass Flow Rate of the Hot Source on Specific Cooling Power (SCP)

SCP increases linearly with the increase in mass flow rate of the hot source as shown in Fig. 10. Low SCPs were observed at the lower mass flow rates of hot source. Up to 10 LPM of water, it is difficult to predict the trend of the increase in SCP because of very small variation of evaporative power. As soon as the mass flow rate of the hot source increases beyond 10 LPM of water, more heat is transferred to the bed. In the evaporator, we get large temperature drop and hence more evaporative energy can be extracted. Very low values of SCPs were observed at the lower mass flow rate of the hot source as shown in Fig. 10. SCP of around 50 W/kg of adsorbent is reported at the mass flow rate of 3 LPM of water for all set of operating conditions in the operating range. It is not sufficient to operate the system at these low mass flow rates. We require SCP round 350 W/kg of the adsorbent for 1 TR system. We should supply hot source in the range of 55–60 °C at 15 LPM of water as the mass flow rate of the hot source in order to obtain SCP around 350 W/kg of adsorbent. It is also observed from above figure that the hot source inlet temperature near about 50 °C is not sufficient to get desired value of SCP because of low heat transfer rates at lower temperatures. Higher SCP is always preferable as large temperature drop obtained in evaporator within a constant cycle time to get sufficient cool air in the cabin of the vehicle.
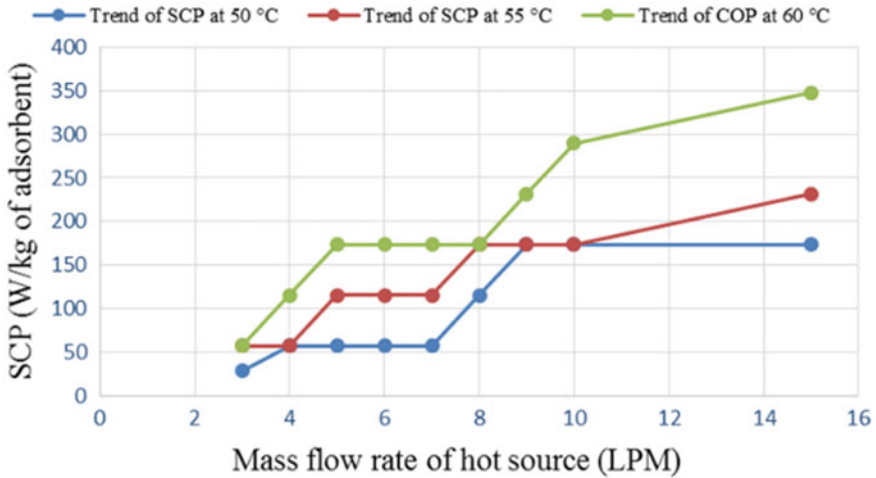
Fig. 10 Trend of SCPs against varying Mass flow rate of the hot source in the range of operating conditions

Fig. 11 Variation in COP against the inlet temperature of hot source
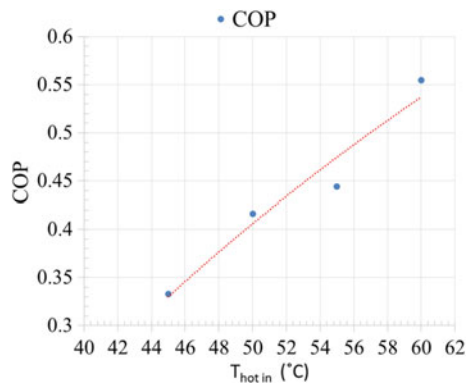
8.3 Effect of Temperature of the Hot Source on Coefficient of Performance When the Mass Flow Rate of Hot and Cold Source Kept Constant at Constant Cycle Time

To evaluate the performance of ADCS against the temperature of the hot source, a temperature range of hot source from 45 to 60 °C is adopted. COP is calculated for the mass flow rate of the hot source at 15 LPM of water. This value of mass flow rate of the hot source is adopted because higher COPs observed through earlier experimentation. In this case, the system is made operating continuously with an interval of cycle time. The result is plotted and shown as Fig. 11.

From above figure, it is clear that COP is increasing with the increase in the inlet temperature of the hot source in the range of 45–60 °C. The inlet temperature of the

Fig. 12 Increment in COP at different temperature of hot source
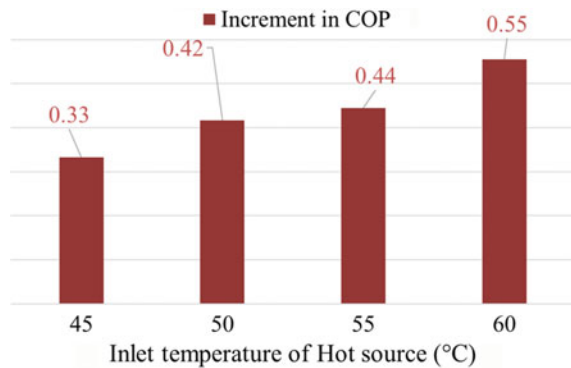
hot source keeps changing in the range while the mass flow rate of hot source and cycle time is kept at 15 LPM of water and 15 min. Due to the virtue of experimentation facility, experimentation at a higher temperature of the hot source is not possible, but whatever the range is examined, it is the well-accepted range in subcompact vehicles where the hot source is radially available at an average temperature within this range. If we look at the vehicle condition at the starting of the engine or if the condition is of cold starting, then we have a hot source inlet temperature around 45 °C. At this inlet temperature, we have a low COP obtained, but as the engine runs continuously then, the inlet temperature of hot source also increases and we ensure an increase in COP values.

At the starting of the engine after completing the one-half cycle of 15 min, we get COP = 0.33 (as shown in Fig. 12), provided at 45 °C of the inlet temperature of the hot source, 30 °C of the inlet temperature of the cold source and chilled water inlet temperature, as shown in Fig. 12. The flow rate of the hot and cold source is set at 15 LPM of water. As the temperature of hot source inlet temperature is increased at 50 °C, we get an increase in COP for the same cycle time. Maximum COP is obtained around 0.55 at the 60 °C of hot source.

9 Conclusions

Experimental investigations have been done on the finned tube adsorber bed heat exchanger to confirm the performance of the system. SCP and COP are performance parameters of the system. A global and dynamic prototype of the finned tube adsorber bed heat exchanger has been developed which works on the principle of an adsorption. Here, a simple and sophisticated methodology has been developed to calculate the performance parameters (SCP and COP) of the system. Fabrication work has been done very well where AAMR is maintained greater than one.

Effect of varying performance parameters on the finned tube adsorber heat exchanger has been determined by studying nature of curves and variation in values.

The mass flow rate of the hot source is adopted around 15 LPM of water. At this value of mass flow rate, maximum COPs and SCPs have been observed. Further, values of COP and SCP remain constant (very marginal change) even if the mass flow rate of the hot source is increased.

References

1. Hassan, H.Z., Mohamad, A.A.: Thermodynamic analysis and theoretical study of a continuous operation solar-powered adsorption refrigeration system. Energy **61**, 167–178 (2013)
2. Sharafian, A., Bahrami, M.: Adsorbate uptake and mass diffusivity of working pairs in adsorption cooling systems. Int. J. Heat Mass Transf. **59**(1), 262–271 (2013)
3. Rouf, R.A., Alam, K.C.A., Khan, M.A.H.: Solar adsorption cooling and hot water supply for climatic condition of Dhaka. Proc. Eng. **105**(ICTE 2014), 705–712 (2015)
4. Yeo, T.H.C., Tan, I.A.W., Abdullah, M.O.: Development of adsorption air-conditioning technology using modified activated carbon—a review. Renew. Sustain. Energy Rev. **16**(5), 3355–3363 (2012)
5. Fernandes, M.S., Brites, G.J.V.N., Costa, J.J., Gaspar, A.R., Costa, V.A.F.: Review and future trends of solar adsorption refrigeration systems. Renew. Sustain. Energy Rev. **39**, 102–123 (2014)
6. Demir, H., Mobedi, M., Ülkü, S.: A review on adsorption heat pump: Problems and solutions. Renew. Sustain. Energy Rev. **12**(9), 2381–2403 (2008)
7. Sharafian, A., Bahrami, M.: Assessment of adsorber bed designs in waste-heat driven adsorption cooling systems for vehicle air conditioning and refrigeration. Renew. Sustain. Energy Rev. **30**, 440–451 (2014)
8. Li, X.H., Hou, X.H., Zhang, X., Yuan, Z.X.: A review on development of adsorption cooling—novel beds and advanced cycles. Energy Convers. Manag. **94**, 221–232 (2015)
9. Frazzica, A., Füldner, G., Sapienza, A., Freni, A., Schnabel, L.: Experimental and theoretical analysis of the kinetic performance of an adsorbent coating composition for use in adsorption chillers and heat pumps. Appl. Therm. Eng. **73**(1), 1020–1029 (2014)
10. Hassan, H.Z., Mohamad, A.A.: A review on solar-powered closed physisorption cooling systems. Renew. Sustain. Energy Rev. **16**(5), 2516–2538 (2012)
11. Choudhury, B., Saha, B.B., Chatterjee, P.K., Sarkar, J.P.: An overview of developments in adsorption refrigeration systems towards a sustainable way of cooling. Appl. Energy **104**, 554–567 (2013)
12. Akahira, A., Alam, K.C.A., Hamamoto, Y., Akisawa, A., Kashiwagi, T.: Experimental investigation of mass recovery adsorption refrigeration cycle. Int. J. Refrig **28**(4), 565–572 (2005)
13. Akahira, A., Alam, K.C.A., Hamamoto, Y., Akisawa, A., Kashiwagi, T.: Mass recovery adsorption refrigeration cycle—improving cooling capacity. Int. J. Refrig. **27**(3), 225–234 (2004)
14. Alam, K.C.A., Akahira, A., Hamamoto, Y., Akisawa, A., Kashiwagi, T.: A four-bed mass recovery adsorption refrigeration cycle driven by low temperature waste/renewable heat source. Renew. Energy **29**(9), 1461–1475 (2004)
15. Akahira, A., Alam, K.C.A., Hamamoto, Y., Akisawa, A., Kashiwagi, T.: Mass recovery four-bed adsorption refrigeration cycle with energy cascading. Appl. Therm. Eng. **25**(11–12), 1764–1778 (2005)
16. Dakkama, H.J., Elsayed, A., Al-Dadah, R.K., Mahmoud, S.M., Youssef, P.: Investigation of cascading adsorption refrigeration system with integrated evaporator-condenser heat exchanger using different working Pairs. Energy Proc. **75**, 1496–1501 (2015)
17. Habib, K., Saha, B.B., Chakraborty, A., Koyama, S., Srinivasan, K.: Performance evaluation of combined adsorption refrigeration cycles. Int. J. Refrig **34**(1), 129–137 (2011)
18. Taylan, O., Baker, D.K., Kaftanoğlu, B.: COP trends for ideal thermal wave adsorption cooling cycles with enhancements. Int. J. Refrig. **35**(3), 562–570 (2012)

19. Liu, Y., Leong, K.C.: Numerical study of a novel cascading adsorption cycle. Int. J. Refrig **29**(2), 250–259 (2006)
20. Sharafian, A., McCague, C., Bahrami, M.: Impact of fin spacing on temperature distribution in adsorption cooling system for vehicle A/C applications. Int. J. Refrig **51**, 135–143 (2015)
21. Shara, A., Bahrami, M.: Critical analysis of thermodynamic cycle modeling of adsorption cooling systems for light-duty vehicle air conditioning applications. Renew. Sustain. Energy Rev. **48**, 857–869 (2015)

Oil- and Aluminum-Based Thermal Storage System Using Flat Plate Solar Collector

Vednath P. Kalbande and Pramod V. Walke

Abstract The energy demand in the world is increasing day by day, and fossil fuel shortages are also increasing. Solar energy and renewable energy resources become more important. Most of the Indian population is lives in rural area and use wood for the cooking purpose. The thermal energy storage is popular in this era for the cooking purpose. Thermal energy storage system based on solar collector is developed for the cooking of bread in mind. The oil- and aluminum-based energy storage system is used for experimentation and having same storage potential and to store the energy in storage contain phase change material which have melting temperature of 210–220 °C. Energy collected by solar collector heated the fluid (i.e., soybean oil) contained in receiver tube and carry the energy to storage space. The self-circulation unit is introducing between storage and solar collector which contain soybean oil as a heat transfer fluid. Main aim of the concept is to store energy during day and utilized it in nighttime for cooking purpose.

Keywords Aluminum-based storage · Oil-based storage · Phase change material · Self-circulation · Solar collector · Thermal storage

1 Introduction

The objective of the research work is to encourage and to develop prototype of thermal storage system using solar collector for the purpose of cooking and water heating. The main aim is to examine the thermal storage system temperature for whole day and energy in the system. Also the using sensible heat storage solar energy can be store during daytime and utilized in night [1, 2]. Most percent of the Indian population is lives in rural area. The primary fuel source for the cooking is wood due

V. P. Kalbande (✉) · P. V. Walke
Department of Mechanical Engineering, G. H. Raisoni College of Engineering, Nagpur, India
e-mail: v.kalbande@raisoni.net

P. V. Walke
e-mail: pramod.walke@raisoni.net

to which emits the CO_2 in environment, and it is harmful for health. So to reduce such problem solar energy is the better option. Using solar collector solar energy can collect and store into the thermal energy storage system for various applications. The thermal energy storage (TES) heat capacity and physical model is explained by Nyeinga et al. [3]. Nowadays different solar cooker is available in the market such as direct and indirect solar cooker. The indirect solar cooker is based on thermal energy storage system in which solar energy can store and utilized in nonsunny days. The phase change material is introduced in the thermal energy storage system to store the energy. Van den Heetkamp [4] with an idea from Lovseth et al. [5] studied multipurpose concentrating solar energy system is of particular interest. The solar box cooker is the simplest version of solar cooker by using solar panel for collecting the solar energy [6]. Compare the cooking time for different types of food using solar energy-based thermal storage system [7]. The traditional and most important India bread is called chapatti. It is 20–30 cm in diameter and is cooked at a temperature of 160 °C.

2 Self-circulation and Heat Capacity

2.1 Self-Circulation Unit

The self-circulation principle is a better option for the solar thermal storage system. Due to the gravity difference, fluid is circulated in the system so does not necessitate the use of a pump and a well-designed system will then regulate its temperature by itself. This principle is already widely used in the thermosyphon solar hot water systems [8]. The self-circulation is based on the Darcy-Weisbach equation [9]. The analysis details of self-circulation unit are as follows,

Volumetric mass flow in m^3/s,

$$Q = AU \tag{1}$$

where A = Cross-sectional area of tube, m^2

$$A = \frac{\pi}{4} \times D^2$$

U = Velocity of working fluid, m/s.

The self-circulation is based on the Darcy-Weisbach equation

$$\frac{\Delta P}{L} = \lambda \rho \frac{U^2}{2} \frac{1}{D} \tag{2}$$

where ΔP = Pressure drop, Pa.

$L =$ Length of tube (m), $D =$ Diameter of pipe (m), $\rho =$ Density of working fluid (Kg/m^3), $\lambda =$ Darcy friction factor for laminar flow

$$\lambda = \frac{64}{\text{Re}} = \frac{64\mu}{\rho DU} \tag{3}$$

and

$$\Delta P = \Delta\rho h g \tag{4}$$

where,

$\Delta\rho =$ Density difference (Kg/m^3), $g =$ Gravitational acceleration (m/s^2), $h =$ Height of column (m), $\mu =$ Dynamic viscosity (Kg/ms).

From Eqs. (2), (3) and (4)

$$\frac{\Delta\rho g h}{L} = \frac{64\mu}{\rho DU} \rho \frac{U^2}{2} \frac{1}{D}$$

$$U = \frac{g h D^4 \Delta\rho}{32\,\mu L} \tag{5}$$

From Eqs. (1) and (5)

$$Q = \frac{g h D^4 \pi \, \Delta\rho}{128\,\mu L}$$

2.2 Heat Capacity

Heat capacity can be determined by following equation, in Watt.

$$Qh = mCp\Delta T$$

where

Qh Heat Capacity
m Mass flow rate, Kg/s
Cp Specific heat of working fluid, kJ/Kg K
ΔT Temperature difference, K.

3 Data Collection

3.1 Material

3.1.1 Aluminum Alloy

The main component of the heat storage is an aluminum cylindrical block. Aluminum was chosen as conducting material because of its high conductivity and low density. It also has a good resistance to oxidation. However, pure aluminum is too soft for carving and machining. An alloy of aluminum is selected [11–14].

3.1.2 Stainless Steel

Stainless steel is used for the oil-based tank storage and the main supply line for the experiment. Oil-based tank is the outer shell on which the aluminum plate is mounted with the aluminum tubes.

3.1.3 Solar Salt

The homogeny binary mixture of 60% $NaNO_3$ and 40% KNO_3 was used as a PCM. It is known as solar salt or Hitec XL [3]. The melting temperature of $NaNO_3$ is 310 °C, whereas KNO_3 has melting point of 330 °C. The mixture of the solar salt has a melting temperature between 210 and 220 °C which makes it well suited for injera cooking [7, 10–14].

3.1.4 Soybean Oil

Soybean oil is used as the working fluid. It flows through the thermal storage system. The soybean oil is better option due to its desirable properties.

4 Experimental Setup

The experimental setup as shown in Fig. 1 consists of a flat plate solar collector with length and width of the 1.8 and 1 m, respectively. The solar collector higher temperature capacity is 175 °C. There were two thermal storage system used for the experimentation is as follows,

1. Oil-based thermal storage system
2. Aluminum-based thermal storage system.
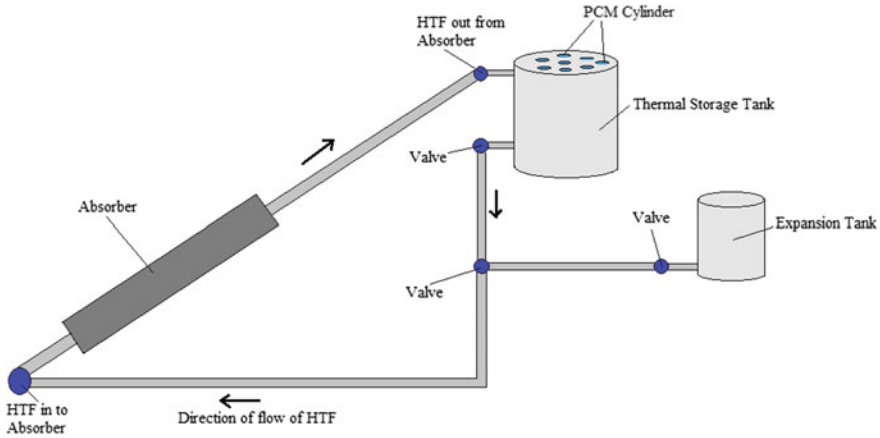
Fig. 1 Schematic of experimental setup

The setup is common for both the above thermal storage system. The collector is kept at 30° angle of elevation. The pipe fitting is done by the G.I. pipes, with the help of sockets of stainless steel. The internal diameter of circulating fluid flow line pipe is 25 mm. The valve is fitted in the flow pipe to control the flow.

The storage tank has a valve fitting at the outlet and connected to the inlet of the solar collector. The solar collector outlet valve is connected to the thermal storage tank. The outlet of the thermal storage tank is connected to the reservoir tank. The complete setup is insulated with glass wool material of thickness 50 mm. The glass wool has an aluminum foil sheet at the outside.

4.1 Oil-Based Thermal Storage Unit

The oil-based thermal storage unit is made of aluminum and steel material. The outer tank of storage is made from stainless steel to store the working fluid. The tank is to be exposed to the atmosphere, so to avoid the corrosion of the tank which is caused by the oxidation of the metal with the moisture present in the atmosphere. The oxidation of stainless steel does not take place as it is galvanized with the anti-corroding metals. The tank is of 250 mm diameter and height of 200 mm for opening the inlet and the exit of the working fluid. The top plate is made from aluminum material of thickness 10 mm. The holes on the top plate were made with an angle of 72° between them so as to store maximum heat. The first five holes of 25 mm diameter were made at a distance of 50 mm and another five holes of same diameter at a distance of 80 mm from center holes. The each hole on the top plate makes an angle of 72° to with each other as shown in Fig. 2.
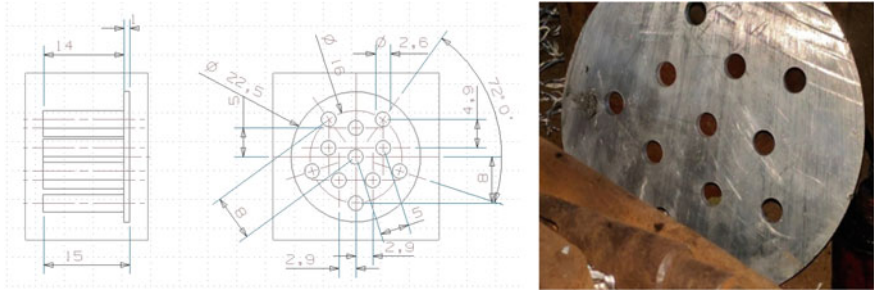
Fig. 2 Top plate dimensions and image

Fig. 3 Top plate, salt cylinder assembly and 3D model of full assembly of oil-based tank

The top plate has 11 sets of holes of 25 mm diameter. The salts cylinders of aluminum having 25 mm diameter is fixed with top plate for storing energy as shown in Fig. 3.

The base plate, top plate, and cylinder are gas welded to fix in oil tank. The complete thermal storage is sealed by liquid cement and leak proof is done. The thermal storage oil tank has two holes for inlet and outlet.

At the outlet of the tank, a valve is fitted to regulate the flow of working fluid. The whole assembly of the oil-based thermal storage is insulated with glass wool material and PCM material is poured inside the salt cylinder.

4.2 Aluminum-Based Thermal Storage Unit

The aluminum-based storage is made from block of solid aluminum cylinder of 255 mm diameter and 250 mm length as shown in Fig. 4. Three plates were cut out of the aluminum block of thickness 10 mm. The two sets of grooves are drilled by the help of lathe machine. After the machining of the block, it is again drilled for the PCM chambers by the drill machine. The same set of holes, which is in oil-based thermal storage, is produced on the top plate of the aluminum storage as shown in Fig. 5.
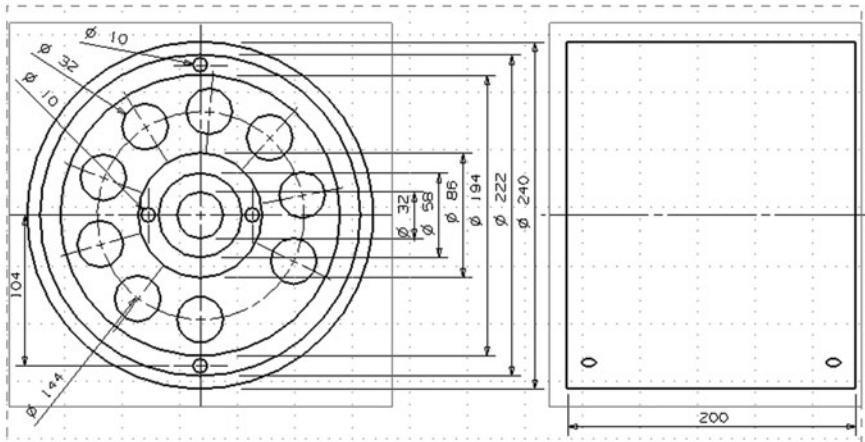
Fig. 4 Aluminum-based tank dimension
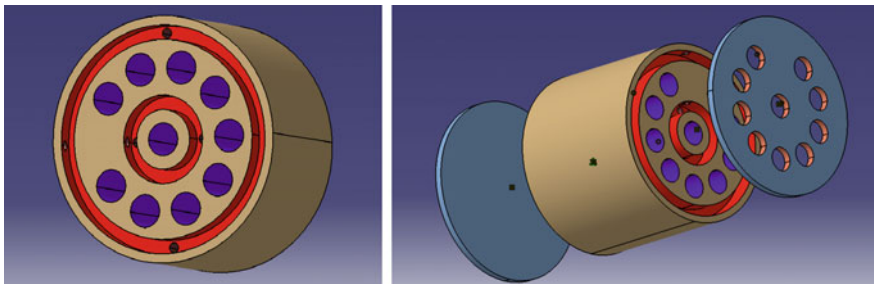
Fig. 5 3D Model and assembly of aluminum-based thermal storage system

The top plate and the base plate is gas welded with the block. The block of aluminum-based storage has two holes for inlet and outlet, respectively. At the outlet of the storage, a valve is fitted to regulate the flow of working fluid. The whole assembly of the aluminum-based thermal storage is insulated with glass wool material, and PCM material is poured inside the salt cylinder.

The soybean oil will be the working fluid. The oil will be stored in the reservoir tank from where it would be passed to the collector for heating. The oil flow will be self circulating because of the difference in the density of the working fluid. The oil will get heated up in the collector and then passed to the thermal storage tank where it will transfer heat to the PCM material. The PCM material will absorb the heat and change its phase from solid to liquid. The heat absorbed by the PCM material can be used for cooking purpose. After the oil is passed from the thermal storage tank, it is then passed to the reservoir tank and the cycle continues.

5 Testing and Experimentation

The solar collector is facing toward the south direction to collect maximum solar radiation. The apparatus is tested on the day when maximum temperature is about 43 °C and average temperature 38 °C at the outlet. After an hour interval, the temperature again recorded and it is found to be 82 °C after an hour. The temperature is recorded by the help of thermocouple, and it is shown in digital temperature indicator. The temperature reaches its maximum for some time and remains constant, and then, it will gradually decrease after some hours. When the temperature of the storage tank reached nearly up to 102 °C the PCM material stared to change its phase.

The oil-based system temperature at the outlet of the absorber has reached its maximum at the first hour while establishing the circulation. The low mass flow in the loop at the beginning due to high viscosity of fluid in the pipe can be eliminated by keeping oil longer time in the absorber. The pressure drop in the loop increases in the channels of aluminum storage due to extra frication which results into the loss of significant amount of energy in the pipe. The Tout absorber is reached higher in the oil-based system and decreases the temperature drop due to higher mass flow of fluid. For the aluminum-based thermal storage system obtained nearly same temperature in storage at inlet and salt cylinders.

6 Result and Discussion

The aluminum-based storage is tested on a $P = 1.06$ kW heating element twisted around the absorber. From the experiment, it is observed that the melting temperature of the salts is not obtained in storage. The oil-based thermal storage unit temperature is reached around 110 °C. Higher temperature of absorber is obtained by keeping each particle for longer time in absorber.

The temperature of absorber and storage unit is shown in Fig. 6 for both the thermal storage system. The absorber temperature reaches to 135 °C in 8 h of time. Whereas aluminum- and oil-based thermal storage unit temperature reached up to the 90 and 110 °C, respectively, as shown in Fig. 7.

The above graphs show that the solid–solid phase change around 110 °C and oil-based thermal system shows more efficient than aluminum-based thermal storage system.

Experimental characteristics of energy are shown in Tables 1 and 2.

7 Conclusion

Considering a self-circulation loop filled with soybean oil, for an equivalent heat capacity, a oil-based thermal storage system is more efficient than aluminum-based
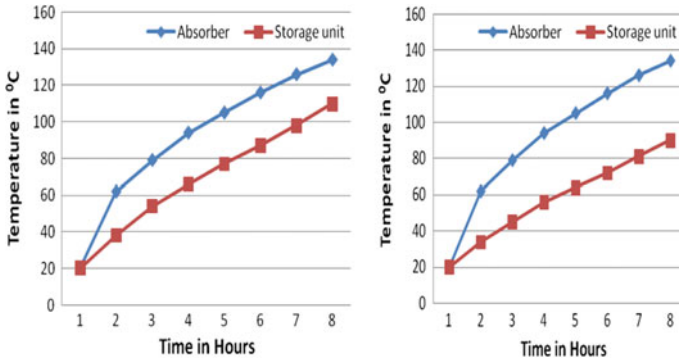
Fig. 6 Graph between temperature and time in hours for absorber and storage unit

Fig. 7 Graph between
temperature and time in
hours for oil-based and
aluminum-based storage unit
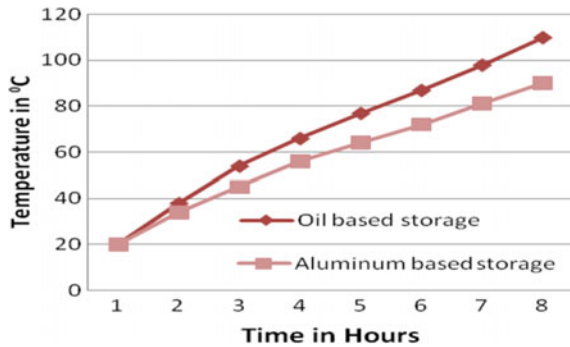
Table 1 Characteristics of aluminum-based storage system

Material	Volume (m^3)	Mass (Kg)	Specific heat (kJ/KgK)	Energy 20–90 °C (kJ)
Aluminum	0.007129	19.24	0.953	1283.50
Oil	0.000238	0.1953	2.079	28.42
Salts	0.001125	2.026	1.2	170.18
Total				1482.11

Table 2 Characteristics of the oil-based thermal storage system

Material	Volume (m^3)	Mass (Kg)	Specific heat (kJ/KgK)	Energy 20–110 °C (kJ)
Aluminum	0.001331394	3.5947	0.953	308.32
Oil	0.011309734	9.2581	2.079	1732.29
Salts	0.001555088	2.7991	1.2	302.31
Iron	0.000319679	2.4295	0.46	100.58
Total				2443.50

thermal storage system. The oil stays for a long period in the storage to release its energy. Lower frication in the storage is effect on outlet temperature of storage and mass flux in the loop. The oil-based thermal storage unit is much efficient than the aluminum-based thermal storage unit. The system coupled with a flat plate solar collector to show the ability to store solar energy using flat plate solar collector. Concerning solar cooking, the storage temperature shows a potential for the boiling. The absorber temperature is same for both the storage unit. The oil-based storage unit temperature is higher than aluminum-based storage unit. It can be concluded that the oil-based thermal storage can be used for the applications.

References

1. Buddhi, D., Sahoo, L.K.: Solar cooker with latent heat storage: design and experimental testing. Energy Convers. Manag. **38**(5), 493–498 (1997)
2. Nahar, N.M.: Performance and testing of a hot box storage solar cooker. Energy Covers. Manage. **44**(8), 1323–1331 (2003)
3. Nyeinga, K: Dynamic model for small scale concentrating solar energy system with heat storage. In: Physics Department. Makerere University, Kampala, Uganda (2012)
4. Van den Heetkamp, R.: The development of small solar concentrating systems with heat storage for rural food preparation. Phys. Scr. **2002**, 99 (2002)
5. Loveseth, J.: Small multi-purpose concentrating solar energy systems. In: Proceeding of the 10 Solar PACES International Symposium (2000)
6. Okello, D: Rock bed stove suitable for solar cookers with thermal energy storage systems (Potential for solar cooking in Uganda). In: Physics. Makerere University, Makerere, Uganda (2012)
7. Foong, C.W.: Experimental and numerical investigations of small scale double-reflector concentrating solar system with latent heat storage. Department of Energy and Process Engineering. NTNU. Norwegian University of Science and Technology (2011)
8. Joshi, S.V., Bokil, R.S., Nayak, J.K.: Test standards for thermosyphon-type solar domestic hot water system: review and experimental situation. Sol. Energy **78**, 761–798 (2005)
9. Romeo, E., Royo, C., Monzon, A.: Improved explicit equations for estimation of the friction factor in rough and smooth pipes. Phys. D **239**, 1318–1328 (2010)
10. Hoff, C.: Heat Storage for solar based concentrator. Master thesis. Department of Energy and Process Engineering, Norwegian University of Science and Technology (2012)
11. Mussard, M., Nydal, O.J.: Comparison of oil and aluminum-based heat storage charged with a small scale solar parabolic trough. Appl. Therm. Eng. **58**(1–2), 146–154 (2013)
12. Mussard, M., Nydal, O.J.: Charging of a heat storage coupled with a low cost small scale solar parabolic trough for cooking purposes. Sol. Energy **95**, 144–154 (2013)
13. Mussard, M., Gueno, A., Nydal, O.J.: Experimental study of solar cooking using heat storage in comparison with direct heating. Sol. Energy **98**(Part C), 375–383 (2013)
14. Kalbande, V.P., Rambhad, K.S., Walke, P.V.: Performance of solar collector for thermal storage system using nanofluid: a review. IJAEFEA **2**(1), 6–11 (2015)

Effect of Ground Condition on the Storage Zone Temperature of Salinity Gradient Solar Pond

Shyamal G. Chakrabarty, Uday S. Wankhede, Pramod V. Walke and Trushar B. Gohil

Abstract Salinity gradient solar pond is an integral thermal energy collection and storage device. Energy extracted from the storage zone can be utilized for power generation, process heating, drying agriculture products, and desalination. In case of buried solar pond, the thermal performance of the pond is highly dependent on the ground conditions. A numerical model was used to investigate the effect of depth of ground water table and thermal conductivity of the soil on the storage zone temperature. The model used has a good agreement with the experimental data. It was found that storage zone temperature and warm-up period is highly influence by the ground conditions.

Keywords Solar pond · Ground water table · Warm-up period · Storage zone

Nomenclature

A	Area (m^2)
C_p	Specific heat of NaCl (MJ/kg °C)
h	Fraction of solar radiation
I	Incident solar radiation (MJ/m^2-h)

S. G. Chakrabarty (✉) · U. S. Wankhede · P. V. Walke
Department of Mechanical Engineering, G. H. Raisoni College of Engineering, Nagpur 440016, India
e-mail: shyamal2706@gmail.com

U. S. Wankhede
e-mail: udaywankhede74@gmail.com

P. V. Walke
e-mail: pramod.walke@raisoni.net

T. B. Gohil
Department of Mechanical Engineering, Visvesvaraya National Institute of Technology, Nagpur 440010, India
e-mail: trushar.gohil@gmail.com

k	Thermal conductivity of NaCl (MJ/m °C)
k_g	Thermal conductivity of ground soil (MJ/m °C)
S	Salinity (%)
T	Temperature (°C)
t	Time (h)
x	Layer thickness (m)
X_g	Depth of ground water table (m)
UCZ	Upper convective zone
NCZ	Non convective zone
LCZ	Lower convective zone
Q_{losses}	Heat losses (MJ)
Q_{load}	Amount of heat extracted (MJ)
Q_{rad}	Radiation heat loss (MJ)
Q_{evap}	Evaporation heat loss (MJ)
Q_{conv}	Convection heat loss (MJ)
$Q_{sidewall}$	Side wall heat loss (MJ)
Q_{ground}	Ground heat loss (MJ)

Greek Symbols

ρ	Density of NaCl (kg/m^3)
β	Fraction of incident beam entering into water

1 Introduction

The world is facing major challenges in the field of energy security, global warming, and climate change. The solution of this problem lies in the exploration of green and efficient energy technologies. Though modern renewable technologies for generation of thermal energy have tremendous potential but are still limited to use because of its high investment cost. Solar pond provides an interesting option for simultaneous thermal energy collection and storage. A number of researchers [1–10] have explored the area of solar pond and its applications.

The cost of a solar pond was found to be much less than the conventional flat plate collectors. However, it was also reported that cost of solar pond is strongly dependent upon site selection factors such as cost of excavation and candidate salt. Whereas its thermal performance is a function of site-specific factors such as solar irradiation, ground thermal conductivity, and depth of ground water table Srinivasan [6].

Zhang and Wang [11] developed a simulation model to study the ground thermal storage capacity. Saxena et al. [12] investigated the storage zone temperature for different depth of ground water table. Kanan et al. [13] conducted simulation to study effect of ground conditions under a solar pond on the performance of solar

air-conditioning system. Ganguly et al. [14] concluded that heat can be extracted from ground below the solar pond. The present study aimed to investigate the effect of depth of ground water table considering different types of soil on the storage zone temperature.

2 Numerical Model

A transient simulation model of salinity gradient solar pond was developed based on the model presented by number of researchers [7, 9, 15–17] to investigate the storage zone temperature for different depth of water table and thermal conductivity of the soil. Solar pond considered in this present study comprises of UCZ, NCZ, and LCZ having thickness 0.2, 0.4, and 0.3 m, respectively, and 8 m^2 area [18]. UCZ and LCZ were assumed as a single layer because it has uniform temperature throughout its thickness. NCZ was divided into equal layers of 0.1 m thickness.

Heat conservation equation of UCZ

$$\rho(S, T)C_p(S, \rho)\left(\frac{\partial T}{\partial t}\right) = \frac{\partial}{\partial x}\left(k(S, T)\left(\frac{\partial T}{\partial x}\right)\right) + I\beta A\left(\frac{\partial h}{\partial x}\right) - Q_{losses_{ucz}} \quad (1)$$

Heat conservation equation of NCZ

$$\rho(S, T)C_p(S, \rho)\left(\frac{\partial T}{\partial t}\right) = \frac{\partial}{\partial x}\left(k(S, T)\left(\frac{\partial T}{\partial x}\right)\right) + I\beta A\left(\frac{\partial h}{\partial x}\right) - Q_{losses_{NCZ}} \quad (2)$$

Heat conservation equation of LCZ

$$\rho(S, T)C_p(S, \rho)\left(\frac{\partial T}{\partial t}\right) = \frac{\partial}{\partial x}\left(k(S, T)\left(\frac{\partial T}{\partial x}\right)\right) + I\beta A\left(\frac{\partial h}{\partial x}\right) - Q_{load} - Q_{losses_{LCZ}} \quad (3)$$

Properties of sodium chloride solution were considered to be the function of temperature and salt concentration [7]. Heat losses from UCZ, NCZ, and LCZ were given as follows:

$$Q_{losses_{ucz}} = Q_{rad} + Q_{evap} + Q_{conv} + Q_{sidewall} \quad (4)$$

$$Q_{losses_{NCZ}} = Q_{sidewall} \quad (5)$$

$$Q_{losses_{lcz}} = Q_{ground} + Q_{sidewall} \quad (6)$$

Heat loss from the UCZ and LCZ was obtained according to the procedure used by Sayer et al. [17]. Heat loss from side wall and heat load was not considered in

Table 1 Properties of different soil

Types of soil	Moisture (%)	K_g (W/m °C)
Fine sand (dry)	0	0.15
Coarse sand (dry)	0	0.25
Sandy soil	7.9	1.082
Clay and sandstone	4.4	1.7
Fine sand (sat.)	24.6	2.75
Coarse sand (sat.)	20.2	3.72

this study. Fraction of solar radiation was calculated as per the method discussed by Bryant and Colbeck [19].

Different types of soil considered for the investigation are shown in Table 1 given by Kanan et al. [13]. The depth of ground water table was varied from 1, 2, 3, 4, 5, 10, 15, 20, 25, 30, and 50 m.

3 Result and Discussion

A numerical code was developed to solve Eqs. (1), (2) and (3) by using MATLAB code. Data of 22 years average values of solar radiation, ambient temperature, wind velocity, and relative humidity were obtained from NASA (accessed in POWER Surface meteorology and Solar Energy [20], Available from: https://asdc-arcgis.larc.nasa.gov/sse/, last accessed 2018), considering solar pond location in Kuwait City [18].

Figure 1 presents the variation of storage zone temperature for operational period of one year of solar pnd located in Kuwait City. Experimental data given by Ali [18] and data obtained from present numerical model having thermal conductivity $k_g = 2.5$ W/m °C for wet soil and $k_g = 1.28$ W/m °C for clay soil as mentioned by Wang and Akbarzadeh [7] were compared. There is a good approximation between model and experimental data.

The variations of storage zone temperature for different types of ground soil at a fixed depth of water table of 5 m are demonstrated in Fig. 2. Fine sand (dry) has the maximum storage zone temperature throughout its operational period as the heat loss to the ground water table is less due to lower thermal conductivity of the soil. Whereas coarse sand (sat.) has the minimum storage zone temperature.

Figures 3 and 4 show the temperature distribution of storage zone for different depth of the ground water table. It can be seen that fine sand (dry) has a minor difference in the variation of temperature for different depth of 1–50 m, whereas in case of coarse sand (sat.), considerable difference of temperature for different depth was observed due to higher thermal conductivity. For depth of 1–10 m, significant impact on temperature was found. And this effect reduces when the depth increases beyond 10–50 m. Therefore, proper insulation is necessary for shallow depth of water
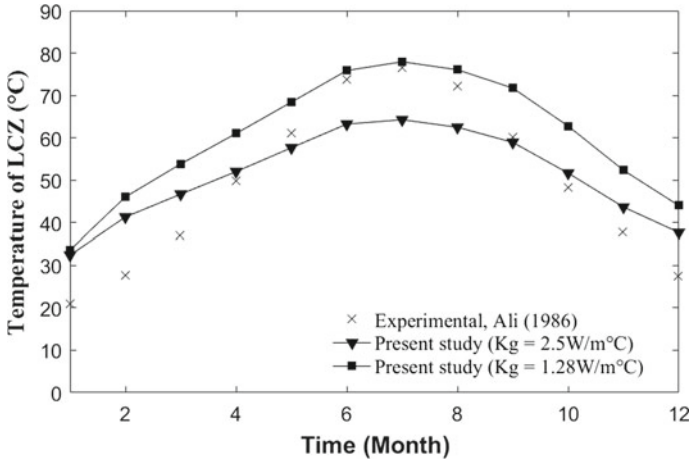
Fig. 1 Variation of storage zone temperature of solar pond located in Kuwait city for duration of one year

Fig. 2 Variation of storage zone temperature for different types of ground soil considering 5 m depth of water table
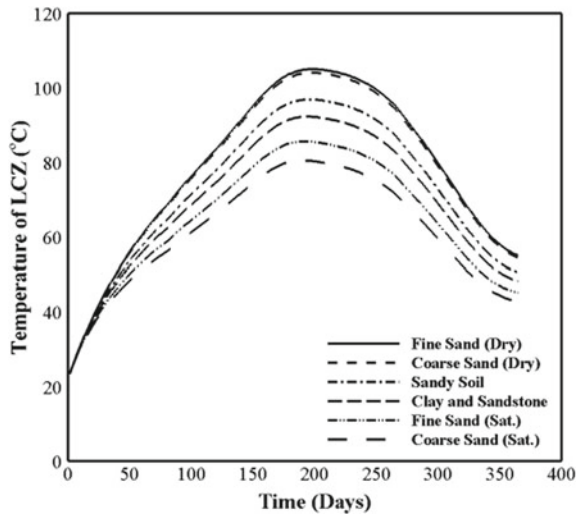
table. Maximum temperature of storage is obtained in case of higher depth of ground water table [12]. The dependence of storage zone temperature for different depth increases as the thermal conductivity of soil increases and depth of ground water table reduces. Similar phenomena were observed for clay and sandstone.

From Fig. 5, it was observed that maximum value of temperature was achieved for fine sand (dry) compared with other types of soil. Beyond the depth of 10–15 m, there was a minor difference in the maximum temperature achieved for all types of soil considered in this study.
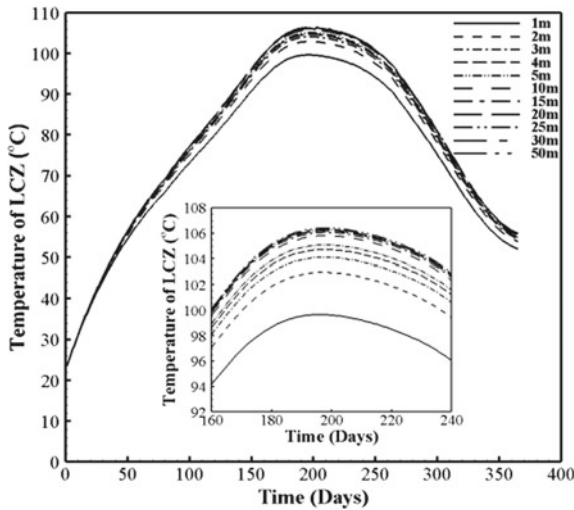
Fig. 3 Storage zone temperature for different depth of ground water table considering fine Sand (dry) ($k_g = 0.15$ W/m °C)
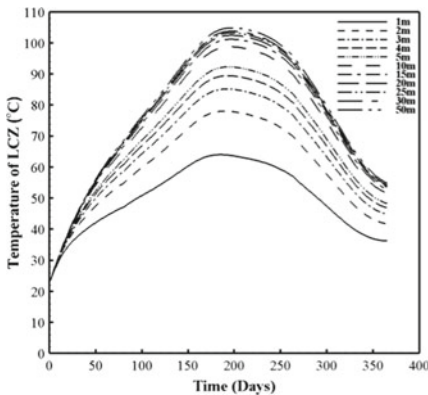
(a) Clay and Sandstone $k_g = 1.7$W/m˚C **(b)** Coarse Sand (sat.) $k_g = 3.72$W/m˚C
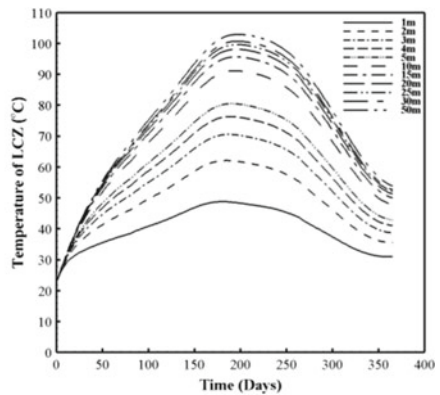
Fig. 4 Variation of storage zone temperature for different depth of ground water table

It can be seen from Fig. 6 warm-up period required for different types of soil has significant impact for the depth up to 15 m and its influence decreases beyond 15 m. Marginal effect in warm-up period was observed for the soil having lower value of thermal conductivity. Whereas considerable increase in warm-up period was observed for coarse sand (sat.). There was a minor variation in the warm-up period required for different types of soil beyond the depth of 15 m.

Fig. 5 Maximum storage zone temperature for different depth of ground water table
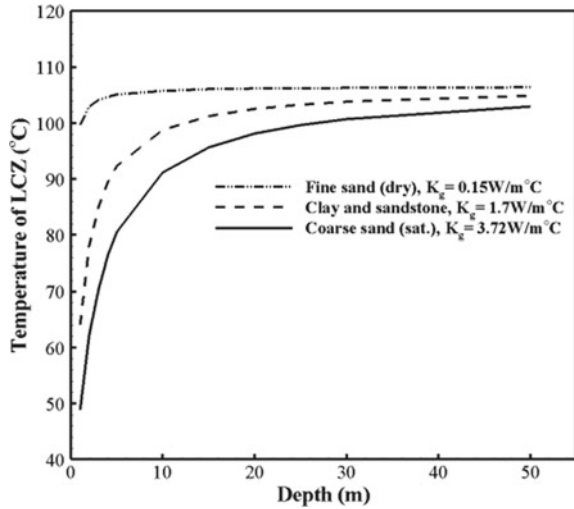
Fig. 6 Warm-up period for different depth of ground water table
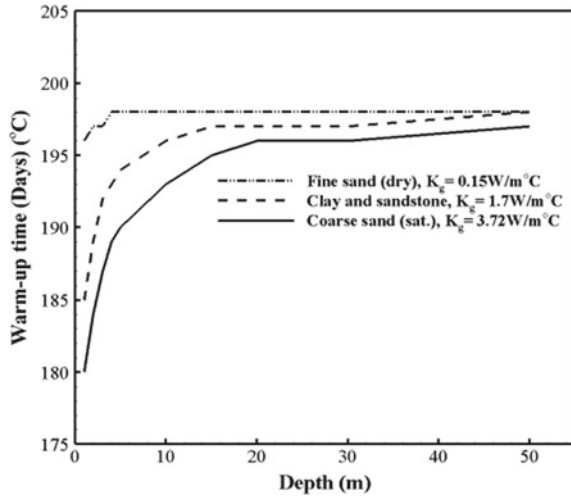
4 Conclusion

The effect of depth of ground water table and thermal conductivity was investigated using a numerical model. The model presented has a good agreement with the experimental result. The dependence of storage zone temperature rises as the thermal conductivity of soil increases and ground water table depth decreases. Warm-up period increases with increase in depth of pond. The thermal conductivity of the soil has a very minor impact on warm-up period.

References

1. Weinberger, H.: The physics of the solar pond. Sol. Energy **8**(2), 45–56 (1963)
2. Tabor, H., Matz, R.: Solar pond: status report. Sol. Energy **9**(4), 177–182 (1965)
3. Tabor, H.: Solar ponds as heat source for low-temperature multi-effect distillation plants. Desalination **17**(3), 289–302 (1975)
4. Tabor, H.: Non-convecting solar ponds. Philos. Trans. R. Soc. A Math. Phys. Eng. Sci. **295**(1414), 423–433 (1980)
5. Hull, J.R.: Solar pond ground heat loss to a moving water table. Sol. Energy **35**(3), 211–217 (1985)
6. Srinivasan, J.: Solar pond technology. Sadhana **18**(1), 39–55 (1993)
7. Wang, Y.F., Akbarzadeh, A.: A study on the transient behaviour of solar ponds. Energy **7**(12), 1005–1017 (1982)
8. Karakilcik, M., Kiymaç, K., Dincer, I.: Experimental and theoretical temperature distributions in a solar pond. Int. J. Heat Mass Transf. **49**(5–6), 825–835 (2006)
9. Date, A., Yaakob, Y., Date, A., Krishnapillai, S., Akbarzadeh, A.: Heat extraction from non-convective and lower convective zones of the solar pond: a transient study. Sol. Energy **97**, 517–528 (2013). Elsevier Ltd
10. Suárez, F., Ruskowitz, J.A., Childress, A.E., Tyler, S.W.: Understanding the expected performance of large-scale solar ponds from laboratory-scale observations and numerical modeling. Appl. Energy **117**, 1–10 (2014)
11. Zhang, Z.M., Wang, Y.F.: A study on the thermal storage of the ground beneath solar ponds by computer simulation. Sol. Energy **44**(5), 243–248 (1990)
12. Saxena, A.K., Sugandhi, S., Husain, M.: Significant depth of ground water table for thermal performance of salt gradient solar pond. Renew Energy **34**(3), 790–793 (2009)
13. Kanan, S., Dewsbury, J., Lane-Serff, G.F., Asim, M.: The effect of ground conditions under a solar pond on the performance of a solar air-conditioning system. Energy Proc. **91**, 777–784 (2016)
14. Ganguly, S., Date, A., Akbarzadeh, A.: Heat recovery from ground below the solar pond. Sol. Energy **155**, 1254–1260 (2017). Elsevier Ltd
15. Tundee, S., Terdtoon, P., Sakulchangsatjatai, P., Singh, R., Akbarzadeh, A.: Heat extraction from salinity-gradient solar ponds using heat pipe heat exchangers. Sol. Energy. **84**(9), 1706–1716 (2010). Elsevier Ltd
16. Abbassi Monjezi, A., Campbell, A.N.: A comprehensive transient model for the prediction of the temperature distribution in a solar pond under mediterranean conditions. Sol. Energy **135**, 297–307 (2016). Elsevier Ltd
17. Sayer, A.H., Al-Hussaini, H., Campbell, A.N.: New theoretical modelling of heat transfer in solar ponds. Sol. Energy **125**, 207–218 (2016). Elsevier Ltd
18. Ali, H.M.: Mathematical modelling of salt gradient solar pond performance. Int. J. Energy Res. **10**(4), 377–384 (1986)
19. Bryant, H.C., Colbeck, I.: Technical note a solar pond for london? Sol. Energy **19**, 321–322 (1977)
20. POWER Surface Meteorology and Solar Energy (SSE). Available from: https://asdc-arcgis.larc.nasa.gov/sse/. Last accessed 02 Apr 2018

Wear Behavior of Polytetrafluoroethylene Composites: A Review

Suraj Kolhe, Abhijeet Deshpande and Kiran Wangikar

Abstract Polytetrafluoroethylene is a synthetic fluoropolymer produced by the polymerization of tetrafluoroethylene. It possess properties like high density (2.2 g/cm^3), high flexural strength, nonsticky, high electric and corrosion resistance, hydrophobic, chemically inert, low friction coefficient (0.01), and high thermal stability (327 °C). Due to low friction, it can be used in friction and wear applications such as piston rings, bearings, clutches, and guide ways. But due to extreme ductile nature, it shears off easily and possess high wear rate. So certain reinforcement component will be added in pure PTFE in order to enhance its mechanical as well as wear properties. Carbon, bronze, glass, alumina, MoS_2, graphite, PEEK, potassium titaniate whisker (PTW), etc. are widely used reinforcement materials. Right selection of various reinforcement materials has greater impact on mechanical properties of PTFE composite material. Therefore, this paper aimed at detailed study of selection of reinforcement component suitable for various applications.

Keywords Polytetrafluoroethylene (PTFE) · Friction coefficient (μ) · Wear rate · Filler (reinforcement) · Weight fraction · Load · Sliding velocity · Sliding time · Transfer film

1 Introduction

Polytetrafluoroethylene (PTFE) is a fluorocarbon commercially known as Teflon which is a DuPont company registered trademark. It is white or gray waxy solid, tough, strong, and non-flammable. It found applications for wiring purpose in

---

S. Kolhe (✉)
Department of Mechanical Engineering, Vishwakarma Institute of Information Technology (VIIT) Pune, Kondhawa (Bk), Pune 411048, India
e-mail: soorajkolhe06@gmail.com

A. Deshpande · K. Wangikar
Department of Mechanical Engineering, Vishwakarma Institute of Information Technology (VIIT) Pune, Kondhawa (Bk), Pune 411048, India

aerospace, as an insulator, computer function, handling, and storing corrosive chemicals, nonstick coatings, etc. PTFE can be widely used as a non-metallic material in various applications due to the reasons like extremely low friction coefficient, thermally stable, and possess high chemical resistance. PTFE has the third lowest coefficient of friction. It can be used in the friction and wear application. PTFE when rubbed against surface forms transfer film on that surface which is a vital reason for to the reduced wear. However, the use of PTFE is limited by the poor mechanical properties like the low load carrying capacity, huge wear rate. This is overcome by adding various filler materials as reinforcements in pure PTFE. The most commonly used fillers are carbon, glass, graphite, bronze, MoS_2, alumina, PEEK (polyetheretherketone), and potassium titaniate whisker (PTW). Along with this, other fillers are used such as ekonol, polyethersulphone, and poly-*p*-phenyleneterephthalamide (PPDT) fibers.

Carbon is widely used as compared to other fillers due to the following reasons: wear resistance increased by adding carbon to the base material, increases the tensile strength, impact strength and also the hardness. Moreover, with small addition of carbon, mechanical properties improve considerably when compared to other fillers [1], which need to be added in large proportions. Appropriate percentage of carbon found to be 15% [2]. Treatment of carbon with rare earth also improves the mechanical properties and reduces the wear rate [3].

Glass when used as filler in PTFE improves the hardness and tensile strength. It also reduces wear rate and improves the load bearing capability of the composite and the transfer film forming capability on the counter surface. Glass fibers are abrasive in nature and possess less wear resistance than carbon [1, 4]. Optimum percentage of glass varied from 15 to 25.

Bronze is ductile metal. It forms highly smooth, uniform, thin film on counter surface than most of the fillers which is vital cause in reducing the wear rate [5, 6]. But when used in low percentage, it cannot contribute to the wear performance due to its ductile nature. So it is used in between 40 and 60% in PTFE composite. Bronze in combination with PTFE possess highest tensile strength between 15 and 20% and has appropriate hardness [7]. It is generally used in combination with MoS_2 which is solid lubricant in filler percentage of (55 bronze + 5 MoS_2) % [1].

MoS_2 is scratch resistant solid lubricant used in combination with the other fillers in PTFE composite (glass, bronze) [1, 4, 8]. Alone with PTFE possess high wear rate than other composite.

PEEK has high hardness, and like PTFE, it is also noncorrosive, nonreactive, and hydrophobic and has very strong bonding with PTFE and increases the hardness when used with PTFE as filler. Within 20–40% addition of PEEK wear rate of PTFE/PEEK composite found to be at an order of 10^{-9} mm³/Nm. Optimum percentage of PEEK in PTFE is 20% [9].

Ekonol as filler in PTFE decreases tensile strength, elongation at break but increase the modulus and improve the wear rate. Optimum filler content is 20% (10^{-6} mm³/Nm). Ekonol when used in combination with slight percentage, carbon nanotube PTFE improved the tensile strength, modulus and elongation up to breaking location, creep resistance. Optimum filler percentage of ekonol and c in PTFE

composite is 20% Ekonol, 1% carbon nanotube at which wear rate is in the range 10^{-7} mm^3/Nm [10]

Potassium titanate whisker (PTW) as filler on PTFE improves the tensile strength, hardness, and impact strength. It can be used for high load high-temperature applications [11]. Optimum filler percentage is 15%. Friction coefficients (μ) and wear rates for PTW/PTFE composite follow the order $\mu_{dry} > \mu_{water} > \mu_{alkali}$ and $W_{water} > W_{dry} > W_{alkali.}$ It is favorable for alkaline condition but unfavorable for water lubrication. Wear rate was at an order of 10^{-6} mm^3/Nm [2].

Addition of nano-ZnO in PTFE improves the wear resistance. PTFE/nano-ZnO forms thin and tiny transfer film on the counter face. PTFE/nano-ZnO has high friction coefficient as compared to other PTFE composite. About 15% nano-ZnO filler gives best wear performance and wear rate at an order of 10^{-5} mm^3/Nm [12].

Alumina as filler in PTFE improves the mechanical properties and reduces the wear. It is favorable for $N_2 + O_2$ but unfavorable for the lubricated conditions [13]. Least wear rate is up to 10^{-6} mm^3/Nm. PTFE alumina composite forms transfer film on the counter surface. Appropriate percentage varies from 12 to 20%. Nanoalumina particles require less percentage (5%) and performance equivalent to 20% micro alumina particles [13, 14].

Wear has greater impact of material (40–60%), load (10–20%), sliding distance, sliding velocity, interaction of load and material [15].

Polyethersulphone filler in PTFE reduces friction coefficient. It is suitable for high-load low-velocity application. 1200 N is the critical load, and 150–200 °C are the critical temperature. About 20% is the optimum filler percentage. Wear rate is 10^{-7} mm^3/Nm [16].

Graphite is used as the solid lubricant along with the other fillers in PTFE composite. Addition of graphite to PTFE cannot improve property significantly. It makes the material softer and reduces the coefficient of friction significantly with slight addition. Addition of graphite to PTFE carbon composite reduces wear rate remarkably than without use of graphite. Percentage of filler addition varied from 1 to 10% approximately [4].

About 10% poly-*p*-phenyleneterephthalamide (ppdt) fibers in PTFE have great resistance near to carbon and more than glass on smooth surface at low velocity and load [4].

2 Literature Review

Bhushan and Wilcock [1] studied the wear behavior of different polymeric composites using reciprocating screening tester operating at 1200 cycles and stroke of 40 mm, 0.69 MPa pressure, 100-h test duration in nitrogen atmosphere at room temperature with counter surface of nitride water cooled SAE 7140 steel. Specific wear rates obtained for different PTFE composite with different fillers 0.07×10^{-6} mm^3/Nm (Carbon Dixon 7035), 0.80×10^{-6} mm^3/Nm (15% graphite powder), 0.13×10^{-6} mm^3/Nm (10% Glass + 15% CdO-graphite-Ag (Dixon)), 0.17×10^{-6}

mm^3/Nm (bronze + MoS2), 0.35×10^{-6} mm^3/Nm (25% glass fiber), 0.3×10^{-6} mm^3/Nm (glass fiber (GL-15)), 0.16×10^{-6} mm^3/Nm (polyamide powder). Low friction attributed to the thicker transfer film on the metal plate. They observed that very smooth surface (0.05 μm) caused the high wear rate while rough surface (0.81 μm) caused low wear rate due to thick, uniform, and attaching transfer film forming. Transverse groove found to cause more rapid wear than longitudinal grooves due to cutting action. They concluded that as transfer films were important, precoating with PTFE was recommended.

Bijwe et al. [17] studied the effect how the filler and reinforcing of fiber affects on abrasive wear behavior of polymeric composites and fillers used are glass, graphite, glass, carbon, bronze, MoS$_2$. They carried out test on pin on disk wear apparatus at 0.43 m/s by varying loads from 1 to 6 N for time of 4 min. Disk rotated at 120 rpm and wear track radius was 3.5 cm. Silicon carbide paper mounted on steel disk to observe abrasive wear phenomena. Abrading distance varied from 25 to 200. They measured loss in mass and converted to volume loss with the help of density. From results wear resistance found in the order Nylon > PEI (polyetherimide) > PTFE > PI (polyimide). Fillers (except bronze filled polytetrafluoroetylene) found to detrimental to wear rate. They observed polymer without fillers had the better wear performance. Effect of filler found to be worse in case of PEI and PI. They observed least affectance on abrasive wear after the filler incorporation. Fillers in particulate shape found to be more detrimental to abrasive wear performance. Graphite found to be the most unsuitable filler but found to be less detrimental in combination with PTFE in PI. Role of PTFE in abrasive wear performance was subjected to the type of binder. Wear performance of PI in combination with the graphite was improved but failed when used with PEI alone. Abrasive wear performance for PTFE composite followed the order PTFE + 55% bronze + 5% MoS$_2$ > PTFE > PTFE + 25% glass fiber > PTFE + 25% Carbon. Specific wear rate of PTFE and its composite found to be diminishing with increased load. Ultimate endurance strength found to be decreased after the filler addition in all the composite.

David et al. [9] studied the wear and friction characteristics of PEEK (polyetheretherketone)/PTFE (polytetrafluoroethylene) composite by varying the percentage of PEEK from wt% of 0, 5, 10, 20, 30, 40, 50, 70, and 100 using a linear reciprocater test apparatus in which stainless steel used as another opposing surface. They performed tests in standard laboratory conditions with applied pressure of 6.35 MPa, speed used of 50 mm/s, and 0.5–140 km length of sliding velocity for a 20 wt% PEEK filled sample. They averaged the friction coefficient for whole experiment. The friction coefficient obtained $\mu = 0.111$ for 50 wt% composite to $\mu = 0.363$ for unfilled PTFE. They observed ultra low wear rate for PEEK/PTFE composite. The wear rates ranging from $K = 2.3 \times 10^{-9}$ mm^3/(Nm) for a 20 wt% PEEK specimen to $K = 6 \times 10^{-4}$ mm^3/(Nm) for PTFE in the absence of PEEK. Scanning electron microscopy concluded that PEEK/PTFE composite had the strong and unique connection between the PTFE and PEEK which is answerable to the ultra low wear rate of the PTFE/PEEK composite which is very useful in wear applications.

Cheng et al. [10] did the wear study of PTFE with poly-p-oxybenzoate (also known as Ekonol) and carbon nanotubes (CNTs) as fillers. Apparatus used for wear

test was a ball-on-block reciprocating UMT-2 tribometer at room temperature, and relative humidity was 50%. The reciprocating friction stroke was 5 mm and tests carried out for 15 N normal load at 10 Hz reciprocating frequency. The friction time was 60 min. The counterpart (ball of 3 mm in diameter) manufactured from GCr15. From the results, they observed that PTFE composite with 20 wt% Ekonol and 1 wt% CNT possessed most tensile strength and also possess highest modulus and reduce elongation at break in comparison with pure PTFE, micro- and nanoscale PTFE composites. From result, they also observed that Ekonol and CNT fillers together improved creep resistance of PTFE composites. They also did the scanning electron microscopy for tensile fracture surface and wear surfaces. They indicated that for tensile fractured surfaces, the surfaces of Ekonol particles are covered by individual CNTs. From the tests and results, they also concluded that the Ekonol and CNT fillers as composite slightly increased the friction coefficient but great decrease in the specific wear rate of 10,000 times in comparison with pure PTFE. Scanning electron microscopic carried out to observe of the worn surfaces revealed that the multiscale composite had very smooth wear surface. Therefore, wear resistance was improved immensely.

Wang et al. [2] investigated the friction, wear behavior, as well as mechanical properties of polytetrafluoroethylene (PTFE) reinforced by the potassium titaniate whisker (PTW) and short carbon strands (CF) subjected to dry, wet, and alkaline (10 wt% NaOH) conditions using ring on ring wear machine [(MPX 2000) friction and wear tester] having stainless steel ring as counterpart with roughness 0.3 to μm at ambient conditions (25 °C temperature) at sliding velocity 1.4 m/s and normal load of 200 N with friction time of 30 min under dry friction of pure PTFE and 120 min for samples dissolved in lubricants. Highest tensile strength and hardness obtained for 20% CF/PTFE composites, whereas 15 wt% for PTW/PTFE composites. They obtained high impact strength for 10% CF/PTFE composites, whereas 5 wt% for PTW/PTFE composites. Friction coefficient decreases with increase in the filler content for both the composites up to 15% and then again starts increasing gradually. They found least coefficient for 15 wt% composites (0.12 for PTW/PTFE composite and 0.15 for carbon/PTFE composite). Friction coefficients (μ) and wear rates for CF/PTFE and PTW/PTFE composite found in the order $\mu_{dry} > \mu_{water} > \mu_{alkali}$ and $W_{water} > W_{dry} > W_{alkali}$. PTW found to be unsuitable for water lubricated condition where there was extreme rise in wear rate. From results, they conclude that both CF/PTFE and PTW/PTFE showed better wear resistance under alkali and dry conditions. They observed that wear resistance of PTW/PTFE was more that of CF/PTFE up to 15 wt% filler after that the comparison was reversed. The found the wear for both composite in the order 10^{-6} mm^3/Nm.

Shangguan et al. [3] studied the surface treatment outcome on tensile strength and wear properties of carbon fiber (CF) PTFE composites. Surface treatment was given by air oxidation and rare earth [(RE) (LaCl$_3$)]. They carried out tensile test on strong material testing machine at room temperature. They performed friction and wear test on reciprocating ball on disk at varying loads 6, 9, 12, 15 N with reciprocating sliding frequency 10–215 Hz with sliding velocities from 0.1 to 0.25 m/s at room temperature and relative humidity 45–55% under dry sliding conditions and 60-

min test timing. Test revealed that tensile properties of the CF-PTFE composites having treatment by air oxidation and rare earth were useful to those of the untreated CF-PTFE composite. The RE treatment was most promising to enhance the tensile properties due to improvement of interfacial adhesion of the CF-PTFE composites. From graph, they concluded for all composites, friction coefficient increases with load. Friction coefficients (μ) and specific wear rates for CF/PTFE composite were in the order $\mu_{\text{untreated}} > \mu_{\text{air oxidated}} > \mu_{\text{RE treated}}$ and $\mu_{\text{untreated}} > \mu_{\text{air oxidated}} > \mu_{\text{RE treated}}$. They found friction coefficient of all composite reduced with increase in reciprocating sliding frequency.

Shi et al. [18] investigated wear and friction properties along with mechanical characteristics of carbon nanofiber (CNF) filled polytetrafluoroethylene (PTFE) composite in varying percentage of 0.1, 0.5, 1, 1.5, 2, 2.5, and 3%. Loads ranged from 50, 100, 150, and 200 N with sliding speeds of 0.692 and 1.39 m/s. Test was carried out on ring wear apparatus. From result obtained, they concluded that decrease in friction coefficient up to 0.5% filler content and then increment found. During sliding, CNF walked out from composite acted as spacer and prevented direct contact of mating surfaces and reduced friction coefficient. Increase in friction coefficient caused due to the filler accession on worn surface. Wear volume loss decreased with increase in filler percentage up to 2% and then again started to increase. High friction and volume loss was obtained for pure PTFE at high sliding speeds due to rapid transfer film drawing. For PTFE CNF composite, they found low coefficient of friction and slightly high wear volume loss at high velocity. They found best wear resistance for 2% filler percentage which was 100 times the unfilled PTFE. Friction coefficient found to be decreased with increasing load, whereas wear volume loss and specific wear rate increased with load increment. From worn surface analysis, they obtained plucked marks due to destruction of subsurface from pure PTFE told that adhesion was prime wear mechanism. Less plucked marks and narrow nicks obtained for PTFE CNF composite told that filler reduced adhesive wear. Pure PTFE was rough transfer film which can degrade easily during friction. Smooth and coherent transfer film obtained for 2 weight (wt)% CNF PTFE composite indicated that CNF increased strength and bond between transfer film and counterpart surface. They found increase in impact strength for filler addition and highest found for 1 wt% (25.7 kJ/m^2) which was 40% higher than pure PTFE. Tensile strength as well as elongation at break increased by 20 and 70% for 1 wt% CNF due to increased cross-linking and then decreased. Specific wear rate was in order of 10^{-5} mm^3/Nm.

Hu et al. [12] investigated friction and wear nature of PTFE filled with nanosized ZnO filled composite in varying percentage from 2.5 to 30 wt%. They carried out test on block on ring wear apparatus at room temperature. Addition of ZnO reduced the wear than pure PTFE. Lowest wear rate found for 15% filler content at which specific wear rate was 1.3×10^{-5} mm^3/Nm at 200 N load and 0.431 m/s sliding velocity after which wear rate again starts increasing. From test, they obtained decreased friction coefficient PTFE filled with ZnO with the increase in load as well as sliding speed. Volume loss was increased with increase in load but slight fluctuations with the sliding velocity. A change in the microstructure was observed after insertion of ZnO powder in PTFE which was one of the antiwear mechanism. Insertion of ZnO

reduced the adhesive of PTFE and uniform and tiny transfer film of PTFE composite was formed on the counter surface.

Krick et al. [13] studied the wear phenomena of alpha phase alumina powder (80 nm particle size and 5 wt%) used as polytetrafluoroethylene (PTFE) composite on linear reciprocating wear tester at contact pressure of 6.3 MPa, 25.4 mm stroke length and 50.8 mm/s sliding speed at ambient conditions. Load applied was 250 N at 50,000 cycles. They found that specific wear rate of PTFE/alumina had depended on the environment surrounds it. Specific wear rate decreased with increase in humidity. They observed that nitrogen and nitrogen oxygen environment were suitable PTFE/alumina composite where ultra low wear rate obtained which was in the order of 10^{-7} mm^3/Nm, whereas unfavorable in water environment where the wear rate increased 3 orders of magnitude than nitrogen oxygen environment. For N_2 and $N_2 + O_2$, thin uniform transfer film was obtained for PTFE/alumina composites. This was due to formation of transfer film was inhibited in submerged water condition. The wear rate in the order of 10^{-4} mm^3/Nm was observed for nitrogen and nitrogen oxygen environment. In nitrogen environment, lowest friction coefficient for PTFE/alumina composites obtained for 10% relative humidity. Among given environmental state, lowest friction coefficient was obtained for submerged water conditions.

Sawyer et al. [14] done the study wear as well as friction nature of PTFE with alumina particles (40 nm particle size) as filler and filler concentration varied from 0 to 20 wt%. They carried out test on reciprocating tribometer with steel as counter surface. They carried out test at 604 MPa contact pressure, 50 mm stroke length, and 50 mm/s sliding velocity at room temperature. Friction coefficient varied from $\mu = 0.15$ to $\mu = 0.2$. They observed increased wear resistance increase in the filler content. At 20 wt%, wear resistance increased to 600 times unfilled PTFE (specific wear rate = 1.2×10^{-6} mm^3/Nm). They could not found optimum filler content. Specific wear rate obtained in the order of 10^{-6} mm^3/Nm. Small alumina particles surrounded by the PTFE particles preventing wear of the PTFE by disrupting the subsurface crack propagation. Smooth and continuous transfer film formed on the counter face for all filler content being the another reason of the reduced wear rate. Nondestructive nature of the nanofillers to transfer film helped in keeping stable or slight fluctuations of the friction coefficient.

Song et al. [8] studied effect of adding glass fiber and molybdenum disulfide to wear and friction of polytetrafluoroethylene (PTFE) composite with chopped carbon fiber (CF) as filler (composite B). The weight percentage of carbon fiber was kept constant 20 wt%. PTFE/CF/glass composite (composite D) was prepared by adding 5% glass fiber. PTFE/CF/Molybdenum disulfide composite (composite C) was prepared by adding 5% molybdenum disulfide. Finally PTFE/CF/glass fiber/molybdenum disulfide composite (composite E) was prepared by adding 5% glass fiber and 5% molybdenum disulfide. They carried out wear test on electrohydraulic servo PV friction testing apparatus at room temperature. They kept constant velocity (1, 2, 3 m/s) and pressure was increased by 1 MPa after every 30 min. They used steel ring as counter surface. Wear test carried out at 1 m/s at which pv limits (p = pressure, v = velocity) obtained for composite B = 5 MPa m/s, C = 5.5 MPa m/s, D =

6.5 MPa m/s, $E = 9.5$ MPa m/s. Highest storage modulus and elastic deformation resistance obtained for composite C. They found increased friction coefficient with increased velocities and decreased load. MoS_2 reduced the wear rate due to its scratch resistant nature and reducing stress concentration on fibers, best antiwear property found at 1 m/s. Wear rate of C increased greatly at 3 m/s due to failure of transfer film. Composite C was suitable to operate under low velocity conditions. They observed that composite D showed worst antiwear property due to severe abrasive wear but above 2 m/s it forms tough and homogeneous transfer film which helps in reducing the wear of the transfer film. Combination of MoS_2 and glass fiber helped to improve he pv limit and the wear resistance and favorable under high velocities. The pv limit of composite E obtained was 9.5 m/s at 1 m/s and 15 m/s at 2 m/s. 2 m/s found to be the best. Wear rate was obtained in the order of 10^{-6} mm^3/Nm.

Unal et al. [19] investigated the wear behavior of polytetrafluoroethylene (PTFE) and its composites on pin on disk wear apparatus with varying sliding speeds 0.32, 0.64, 0.96, 1.96 m/s under varying loads of 5, 10, 20, and 30 N at room temperature. Composites studied are PTFE, PTFE + 17% glass fiber, PTFE + 25% bronze, PTFE + 35% carbon fiber. They found decrease in friction coefficient for the PTFE and composites with increase in load. They found when load increased beyond the critical value friction and wear increased. Decreased specific wear rate with increase in load obtained for the PTFE composites and no admirable effect on specific wear rate with increase in sliding speeds. Wear process attributed to fracture, tribochemical effects, and plastic flow as well as transfer film formation. Thin and uniform transfer film was formed in case of PTFE and PTFE/glass composite where disruption of transfer film was observed in case of bronze- and carbon-filled composite. Least wear rate obtained for glass/PTFE composite in order of 10^{-9} mm^3/Nm. Wear performance followed the order PTFE + 17% glass fiber > PTFE + 25% bronze > PTFE + 35% carbon fiber > PTFE.

Sachin [20] studied wear behavior of polytetrafluoroethylene (PTFE) and its composites including glass and carbon as filler. He used pin on disk apparatus for wear testing under ASTM G99 standard. He cut composite samples into pin shape for testing. SiC paper mounted on steel disk. He tested samples at 8 m/s sliding speed, abrading distances of 45, 90, 120 m, and loads of 5, 10, and 20 N. He used grit size about 400, 800, 1200 during test. Glass fiber and carbon was 15 and 25% by weight. From results obtained, he found that volume loss increased with abrasive size, load, and distance. Furthermore, specific wear rate decreased with increasing grit size, load, sliding distance, whereas slightly with compressive strength. He concluded that carbon-filled composites were slightly more wear resistant than glass fiber reinforced PTFE matrix. Wear rate was obtained in the order of 10^{-6} mm^3/Nm.

Yan et al. [21] obtained the mechanical properties of PTFE/10 wt% nano-EG composites reinforced with the different nanoparticles as nano-Al_2O_3 (A composite), nano-Cu (B composite), nano-SiO_2 (C composite), nano-TiO_2 (D composite) with 10% filler percentage manufactured by cold briquetting and hot pressing sintering technology. Tensile strength and hardness obtained for each composite. Shore D hardness obtained for pure PTFE, A, B, C, D composite are 52.5, 82.5, 66, 60, 68, and tensile strength (in MPa) obtained were 14, 32, 21, 15, 17. They observed after

addition of fillers both hardness (82.50) and tensile strength (32) sufficient improved than pure PTFE and O composite possessed highest hardness and tensile strength among the tested composites. Composite O, C, D did not possess sufficient yield strength. They found that stress relaxation resistance of composite B was higher than composite although the relaxation limit of A was higher than B. Composite C and D showed brittle behavior. Stress relaxation time prolonged and stress limit was increased than pure PTFE of all the composites.

Venkateswarlu et al. [7] studied the filler effects on mechanical properties of polytetrafluoroethylene (PTFE) composites by using different fillers such as glass, granite, graphite, garnet, alumina, antimony trisulphide, carbon, marble, mica, sand, bronze, wollastonite, porcelain, china clay, and tixolex—25 on mechanical properties such as hardness, tensile strength, and % elongation of pure PTFE and different PTFE composites with varying filler concentration (filler content 5–50%). They carried out hardness and tensile test on durameter hardness tester and universal testing machine. They found increased hardness with increasing filler content in antimony trisulphide, sand, granite, porcelian filled PTFE. They observed increased hardness up to 25% and then start decreasing in glass, graphite garnet, alumina, and bronze filled PTFE. They found increased hardness up to 30% and then decreased. For mica and wollastonite, hardness increased up to 15% and then decreased. They obtained highest hardness for 15, 20, and 25% garnet filled PTFE, 50% in marble filled PTFE, and 40% in porcelain filled PTFE. Hardness is an important property in wear as it is the resistance to scratch. Tensile strength is also important in wear as it is the resistance to shearing off of one layer with other material. Appropriate elongation required in applications such as piston rings. They found highest tensile strength for 5% bronze/PTFE. They concluded that there was the effect on hardness and tensile strength on PTFE after addition of filler. They found decrease in tensile strength and elongation with increasing filler content. They concluded that bronze can be used in applications of optimum tensile strength and elongation required.

Wang et al. [22] investigated the water absorption effect on wear behavior of polytetrafluoroethylene (PTFE) composite using carbon (CF/PTFE composite) and basalt fibers (BF/PTFE composite) as fillers. Sample of composites submerged in water and kept at 23 °C for 24 h. They carried out friction and wear test on block on ring test apparatus at load 200 N, sliding speed 0.5 m/s. Test duration was 120 min for water lubrication and 60 min for dry conditions at room temperature. Friction coefficient (μ) found to be decreased for PTFE and its composite in water lubrication but only slight decrease was observed for basalt fiber filled PTFE ($\mu = 0.2$). Friction coefficient was found to be 200 times and 6 times more than pure PTFE and CF/PTFE composite. There was the minute change in the shore hardness, tensile strength, compressive, and flexural strength very less water absorption for PTFE and CF/PTFE but remarkable change for the basalt fiber as compared to other two composites was observed. This was due to the poor fiber/matrix adhesion of basalt fiber with PTFE caused more water absorption. Strong bonding presented between the carbon and PTFE. Improved fiber matrix adhesion resisted the water intake. They observed smooth, fine furrows, and slight plastic deformation in PTFE indicated abrasive wear mechanism due to which transfer film retained there. Very smooth film was

obtained for CF/PTFE composite with not able to see scratches properly. Serious plastic deformation, peeling, wide furrows observed in case of BF/PTFE composite due to which transfer film hardly retained there. Wear rate found in the order of 10^{-5} mm^3/Nm.

Gujrathi et al. [15] studied the wear behavior of polytetrafluoroethylene (PTFE) reinforced with 25 and 35 wt% carbon fiber. They carried out test on pin on disk apparatus by varying loads from 1, 2, 3 kg, sliding speeds 1.09, 2.019, 3.29 m/s, sliding distance 2, 4, 6 km using Taguchi approach. They used statistical regression analysis to obtain the correlation between the two or more variable using least square method. They used design expert-7 software to obtain multiple regression models to establish correlation between wear parameters such as sliding velocity, load, time, and sliding wear. They observed that addition of filler reduced the wear rate. From the results established, they conclude that material affected dominantly in the wear (57.29%), followed by load (10.61), sliding distance (2.198), sliding velocity (0.219), interaction of load and material (19.435). Formation of protective layer between the pin and counter face found useful to reduce the wear volume loss.

Zuo et al. [16] studied wear behavior of polyethersulphone (PES) reinforced polytetrafluoroethylene (PTFE) composite by using ring on disk friction and wear apparatus normal loads(400, 800, 1000, 1200, and 1400 N, i.e., 2.77, 5.54, 6.93, 8.31, and 9.70 MPa), with sliding speeds (0.482, 0.750, 1.003, 1.204 m/s), and five ambient temperatures (25, 65, 100, 150, 200 °C). Test time was 60 min. Friction coefficient of pure PTFE, PTFE/PES, virgin PES obtained steady-state value within 60 min. They observed least friction coefficient of PTFE/PES composite (0.12) than PES (0.306) and PTFE (0.148). They found decreased specific wear rate of PTFE/PES composite with increased filler content. Specific wear rate of PES/PTFE found to be decreased with increased sliding speed. They found best antiwear property at 0.48 and 0.75 m/s. 0.75 m/s was the critical velocity. Increased velocity increased wear rate drastically. They tested composite under varying loads at 0.482 m/s. Friction coefficient found to be decreased for the composite with increased load up to 1000 N. Specific wear rate increased suddenly when the load reached to 1200 N. 20 wt% PES/PTFE composite found to have optimum specific wear rate (8×10^{-7} mm^3/Nm) at 0.48 m/s and least found for 40 wt% PES/PTFE composite (5.5×10^{-7} mm^3/Nm). After testing under pv (p = pressure, v = velocity) limits, they found that the friction and wear performances of PES/PTFE composites at high loads are far better than that at high speeds. About 40 wt% composite was chosen to test under different ambient temperature. They found slightly higher values at the temperatures of 100 and 150 °C than at 25 and 65 °C. Specific wear rate of PES/PTFE found to be increased drastically when temperature reached to 200 °C. Temperature range 150–200 °C found to be critical. 0.75 m/s was the critical velocity. Worn surface analysis showed farrows and indentation were seen in 10 wt% PES/PTFE and not seen in 20% and 40 wt% PES/PTFE composite. They observed that PES/PTFE composite only applicable to low velocity application under high loads. PES had not take part in forming the transfer film.

Mu et al. [11] done the wear and friction study of PTFE/PEEK (15 wt%) reinforced by potassium titaniate whisker (PTW) or short carbon fiber (CF) (15 wt%) at

elevated temperatures (160, 180, 200, 220, and 240 °C), by using different loads (100 and 200 N), and various sliding speeds (0.7 and 1.4 m/s) on ring on block friction apparatus. They observed 30% less friction coefficient of PTFE/PEEK/PTW composite than PTFE/PEEK/CF composite at any temperature. They found decreased friction coefficient for CF/PTFE/PEEK composite with increasing temperature and increased friction coefficient for PTFE/PEEK/PTW composite with increased temperature. Wear rate found to be increased with increasing contact temperature for both the composites. When the temperature increased PTFE/PEEK matrix surface become softer and easy peeling of composites occurred. They found that there was 10–40% wear rate variation of PTFE/PEEK/PTW composite than PTFE/PEEK/CF composite. The wear rate of PTW/PTFE/PEEK composites is only 20% of CF/PTFE/PEEK composites at 200 N, 1.4 m/s, and 240 °C. Stable wear rate was observed in between 180 and 240 °C. Wear rate and friction coefficient found to be decreased with increasing sliding velocity at all contact temperatures. Small size of PTW made transfer film smoother which reduced the wear rate. Wear rate and friction coefficient found to be decreased with increasing sliding load at all contact temperatures. They found that there was 45–70% wear rate variation of PTFE/PEEK/PTW composite than PTFE/PEEK/CF.

Wang et al. [5] studied the wear activity of PTFE/bronze composites transfer films with filler percentage varied from of 5 to 30% under the load of 0.5, 1, 2, 3 N under varying sliding time (5 to 60 min). They carried out test on DFPM reciprocating tribometer at 0.2 m/s sliding speed. They found increased thickness of transfer film with increased bronze content. Increased sliding time found to be helpful to form transfer film with more ductility and continuity but did not possess any effect on tribological properties. Higher bronze content found to improve the tribological properties reduced friction and enhanced wear life and also transfer film became more and more smooth. Increasing bronze content made the wear debris to be thinner some stayed on worn surface some stick to counter surface. They found bronze in the transfer film effectively capable of resisting shear force. They observed decreased wear life of transfer film with increased load. Good ductility of bronze with PTFE found to be helpful to reduce the friction coefficient.

Tevrüz [6] studied the wear behavior of 60% bronze filled PTFE dry journal bearing using journal friction apparatus' of Tecquipment, from England with different pressures, sliding velocities, sliding time, and sliding distance. Experiment was done in two parts first part to find out effect of load and velocity, and second part was to found effect of sliding distance and sliding time. They found increased and decreased wear loss and friction coefficient, respectively, with increased load and sliding velocity and stabled after some time. Friction coefficient increased with increase in temperature. Wear found in 60% bronze filled PTFE 20–30% less than 35% carbon-filled PTFE bearings, 3–7 times more than 25% glass field PTFE bearing was observed. Stable value of friction coefficient attributed to continuous transfer film was formed on the counter surface. Decreased friction coefficient with increased pressure due to formation of smooth transfer film was observed. According to Hoechst at about 20 °C, friction coefficient increased due to change in phase structure and remains stable up to 327 °C. Increased load leads to increase temperature which prevents formation of transfer film by causing the filler material to be uncovered.

Pasha et al. [23] studied the wear behavior of polytetrafluoroethylene (PTFE) 25% glass and 40% bronze used as filler on pin on disk apparatus by applying loads from 20, 40, 60, 80, 100 N, and sliding velocities from 1.5 to 5.5 m/s and sliding distance from 500 to 2500 m. They found increased weight loss with increase in sliding load for all composite at constant sliding velocity and sliding distance. Glass reinforcement reduced weight loss up to some extent. They observed drastic improved wear resistance for 40% bronze/PTFE composite. Weight loss increased with increase in sliding velocity was observed for all composite. About 40% bronze filled composite found to have better wear resistance. They found increased weight loss with increase in sliding distance for all composite at constant load and sliding speed. In SEM (Scanning electron microscopy), they observed large patches of PTFE compared its composite on worn surface. They observed smooth surface for PTFE with bigger debris patches attached. It was also observed that for 25% glass filled PTFE composite a thin transfer film was formed on the disc surface. Transfer film of pure PTFE formed on the counter surface seemed to be thick and lumpy where for 40% bronze filled PTFE, it was found to be thin, smooth, and uniform. Similar case found for glass filled composite but less uniform and thinner than bronze filled composite. Highest adhesive strength between transfer film and counter face found in case of bronze filled composite leaded to decrease wear loss compared to other two specimens. At higher speed due to yielding of matrix occurs due to heat generation and plastic flow of the material due to which increased wear loss observed. At 5.5 m/s and 100 N load due to high heat matrix breaks and transfer film formation disrupted. Copper fluoride formed due to local degradation of PTFE and bronze which help to reduce the wear by reducing the interface temperature by acquiring contact area rather than the chemical action.

Swati and Deore [24] investigated the specific wear rate of glass and bronze filled PTFE with 25% glass and 15 and 30% bronze as filler content. They carried out test on pin on disk wear apparatus under loads of 1, 2, and 3 kg and sliding velocity 3.77 m/s, 5.03 m/s, and 6.28 m/s under ambient conditions. Taguchi Approach was used. They used L9 orthogonal array to find out the effect of load, sliding velocity, and sliding distance. The wear rate obtained was 1.583×10^{-5}, 2.046×10^{-5}, 2.481×10^{-5} g/m, respectively, for PTFE with 30% bronze, PTFE with 25% glass, and PTFE with 15% bronze, respectively. They found increased wear rate with increasing load and sliding distance decrease with increasing sliding velocity. Based on the various factors studied, the composite ranked for wear performance as 30% bronze filled PTFE > 25% glass filled PTFE > 15% bronze.

Bagale et al. [25] studied wear activity of polytetrafluoroethylene (PTFE) with filler 40% carbon and 40% bronze with loads acting 2, 3.54 N and sliding speeds of 1.5 and 2.8 m/s. They carried out test on pin on disk wear apparatus with steel as counter face at room temperature. They observed significant improvement in wear resistance with carbon as filler than bronze. They found decrease in wear rate of pure PTFE by 42% after addition of 40% bronze and 81% after adding 40% carbon Wear performance followed the order PTFE/carbon > PTFE/bronze > PTFE.

Khedkar et al. studied wear activity of polytetrafluoroethylene (PTFE) with fillers as carbon, graphite, E glass fibers, MoS2, and poly-*p*-phenyleneterephthalamide

(PPDT) fibers. They carried out test at on pin on disk apparatus at 5 N load and 0.5 m/s velocity. Hardness and wear resistance found to be increased in all the composites. Hardness (Shore D) followed the order: 18% carbon + 7% graphite > 20% glass fibers + 5% MoS2 > 10% PPDT fibers > 97.5% PTFE + 2.5% PPDT > 75.0% PTFE + 25% E glass fibers > 85.0% PTFE + 15% E glass fibers > Pure PTFE. Wear resistance followed the order: 18% carbon + 7% graphite > 20% glass fibers + 5% MoS2 > 10% PPDT fibers > 75.0% PTFE + 25% E glass fibers > 97.5% PTFE + 2.5% PPDT > 85.0% PTFE + 15% E glass fibers > Pure PTFE. Specific wear rate obtained with fillers 18% carbon + 7% graphite, 20% glass fibers + 5% MoS2, 10% PPDT fibers and pure PTFE were 8×10^{-5} mm^3/Nm, 11×10^{-5} mm^3/Nm, 12×10^{-5} mm^3/Nm and 94×10^{-5} mm^3/Nm, respectively. Friction coefficient affected slightly and remains low. Addition of MoS$_2$ to Glass/PTFE composite improved the wear resistance. Also wear process found to be depending on the thermal conductivity and thermal stability. Increase in thermal conductivity increased the wear resistance.

3 Conclusion

It was observed that 15% carbon can be used for medium pressure application in PTFE as filler. For high-pressure application, 15% carbon + 5% graphite is suitable. Optimum filler content of glass in PTFE is 20% and is useful for low-pressure application. About 60% bronze is favorable for low pressure application, whereas 55% bronze + 5% MoS$_2$ is favorable for high-pressure application in PTFE composite due to scratch resistant nature of MoS$_2$ and act as solid lubricant. Optimum filler content of alumina is approximately 12–20% and is favorable in N$_2$ and N$_2$ + O$_2$ atmosphere and unfavorable for lubricated conditions and also favorable for high-pressure applications. PEEK with optimum filler content of 20% in PTFE matrix is favorable in high-pressure and high-temperature application, in bone dry conditions and possess ultra low wear rate. 15% Potassium titaniate whisker (PTW) is suitable for alkaline and dry conditions and also for high-pressure high-temperature applications. About 15% ZnO in PTFE is useful in high-pressure applications but possess high wear rate compared to other PTFE composites. About 20% Ekonol + 1% carbon nanotube is useful in low-pressure application. About 20% polyethersulphone in PTFE is favorable for high-pressure medium-temperature application.

References

1. Bhushan, B., Wilcock, D.F.: Wear behavior of polymer compositions in dry reciprocating sliding. Wear **75**, 41–70 (1982)
2. Wang, H., Feng, Z., Shi, Y., Lu, X.: Effect of fibrous filler on friction on wear of PTFE composite under dry and wet condition. China Particuol. **5**(6), 414–419 (2007)
3. Shagguan, Q., Cheng, X.: Effect of rare earth on tribological properties of carbon fiber reinforced PTFE composites. J. Rare Earth **25**(2007), 469–473 (2007)

4. Khedkar, J., Negulescu, I., Meletis, E.I.: Sliding wear behavior of PTFE composites. Wear **252**, 361–369 (2002)
5. Wang, Y., Yan, F.: A study on tribological behaviour of transfer films of PTFE/bronze composites. Wear **262**, 876–882 (2007)
6. Tevrüz, T.: Tribological behaviours of bronze-filled polytetrafluoroethylene dry journal bearings. Wear **230**, 61–69 (1999)
7. Venkateswarlu, G., Sharada, R., Rao, M.B.: Effect of fillers on mechanical properties of PTFE compoisite. Arch. Appl. Sci. Res. **7**(7), 48–58 (2015)
8. Song, F., Wang, Q., Wang, T.: Effect of glass fiber and MoS_2 on tribological behaviour and PV limit of chopped carbon fiber reinforced PTFE composite. Tribol. Int. **104**, 392–401 (2016). S0301-679X(16) 00027-X
9. David, L., Burris, W., Sawyer, G.: A low friction and ultra low wear rate PEEK/PTFE composite. Wear **261**, 410–418 (2006)
10. Cheng, H., Cheng, X.: Mechanical and tribological behavior of polytetrafluoroethylene composites reinforced by carbon nanotubes and poly-*p*-oxybenzoate, High Perform. Polym. **25**, 611–621 (2013)
11. Mu, L., Feng, X., Zhu, J., Wang, H., Sun, Q., Shi, Y., Lu, X.: Comparative study of tribological properties of different fibers reinforced PTFE/PEEK composites at elevated temperatures. Tribol. Trans. **53**(2), 189–194 (2010). ISSN: 1040-2004 (Print) 1547-397X (Online)
12. Li, F., Ke-ao, H., Li, J., Zhao, B.: The friction and wear characteristics of nanometer ZnO filled polytetrafluoroethylene. Wear **249**, 877–882 (2002)
13. Krick, B.A., Ewin, J.J., Blackman, G.S., Junk, C.P., Sawyer, W.G.: Environmental dependence of ultra-low wear behavior of polytetrafluoroethylene (PTFE) and alumina composites suggests tribochemical mechanisms. Tribol. Int. **51**(2012), 42–46 (2012)
14. Sawyer, W.G., Freudenberg, K.D., Bhimaraj, P., Schadler, L.S.: A study on the friction and wear behavior of PTFE filled with alumina nanoparticles. Wear **254**, 573–580 (2003)
15. Gujrathi, S.M., Dhamande, L.S., Patare, P.M.: Wear studies on polytetrafluoroethylene (PTFE) composites: Taguchi approach. Bonfir. Int. J. Ind. Eng. Manag. Sci. **3**(2), 47–51 (2013)
16. Zuo, Z., Song, L., Yang, Y.: Tribological behaviour of polyethersulfone-reinforced polytetrafluoroethylene composite under dry sliding condition. Tribol. Int. **86**, 17–27 (2015)
17. Bijwe, J., Logani, C.M., Tiwari, U.S.: Wear: influence of filler and fibre reinforcement on abrasive wear resistance of some polymeric composites. Wear **138**, 77–92 (1990)
18. Shi, Y., Feng, X., Wang, H., Lu, X., Shen, J.: Tribological and mechanical properties of carbonnanofiber filled polytetrafluoroethylene. Wiley Interscience (2005). https://doi.org/10.1002/app.23951, 7 Dec 2005
19. Unal, H., Mimarolu, A., Kadioglu, U., Ekiz, H.: Sliding friction and wear behavior of PTFE and its composite under dry sliding conditions. Mater. Des. **25**, 239–245 (2004)
20. Sachin, Y.: Analysis of abrasive wear behavior of PTFE composite using Taughi's technique. Coagent Eng. **2**, 1000510 (2015)
21. Yan, Y., Jia, Z., Yang, Y.: Preperation and mechanical properties of PTFE/nano-EG composites reinforced with nanoparticles. Proc. Environ. Sci. **10**, 929–935 (2011)
22. Wang, J., Chen, B., Liu, N., Han, G., Yan, F.: Combined effects of fibre/matrix interface and water absorption on the tribological behaviors of water lubricated-polytetrafluoroethylenebased composites reinforced with carbon and basalt fibres. Compos. Part A **59**, 85–92 (2014)
23. Pasha, B.A.M., Budan, D.A., Basavarajappa, S., Yadav, S.M., Nizamuddin, B.A.: Dry sliding wear behaviour of PTFE filled with glass and bronze particles. W. S. Maney & Son Ltd. Received 3 Feb 2011. Accepted 19 Mar 2011 https://doi.org/10.1179/1751584x11y.0000000006
24. Patil, S.P., Deore, E.R.: Prediction of specific wear rate of glass and bronze filled PTFE composites. Int. J. Curr. Eng. Technol **5**(6), 3901–3906 (2015). E-ISSN 2277-4106, P-ISSN 2347-5161
25. Bagale, D., Shekhavat, S., Chaudhari, J.: Wear analysis of polytetrafluoroethylene ant it's composites under dry conditions using design-expert. Int. J. Sci. Res. Publ. **3**(1), 1–5 (2013). ISSN 2250–3153

Predictive Model for Vibrations Induced at the Bearings of Spinning Charkha

Shilpa P. Bhorkar, V. N. Bhaiswar, J. P. Modak and G. D. Mehata

Abstract This paper presents the mathematical modeling for vibrations induced at the bearings of spinning charkha. Vibrations may generate due to various causes. These generated vibrations may lead to damage of the yarn, the quality of yarn, it may also affect on the consumption of energy as far as charkha is concerned. So it is very important to analyze or to predict the vibration induced in any machine before breakdown occurs. It helps to optimize the parameters given above. In order to achieve all these, firstly causes of vibration have been found out which is based on the machine structure and various factors. Vibration analysis is the only perfect way to detect or predict or to find out the faults in any machine. Likewise here vibration spectrums have been taken on various bearing locations of charkha, by using FFT analyzer, and model formation has been carried out. Here in this paper, field database mathematical modeling has been used by using one of the tools that is multiple linear regression analysis.

Keywords Spinning · Mathematical model · Vibration · FFT analyzer

1 Introduction

Cotton is basically the short staple species *Gossypium herbaceum*, and its production is done in most of the parts of Maharashtra. Cotton also has great importance and application both at home and export. Cotton crop provides fiber for the textile industry. It is also used in food and oil industry. Cotton is a versatile product in its performance and natural comforts too. It is also used to make all kinds of cloths and

S. P. Bhorkar (✉) · V. N. Bhaiswar
Mechanical Engineering Department, G. H. Raisoni College of Engineering, Nagpur, India
e-mail: vinchurkar.shilpa@gmail.com

J. P. Modak
Mechanical Engineering Department, P.C.E., Nagpur, India

G. D. Mehata
Aeronautical Engineering Department, P.C.E., Nagpur, India

homewares as well as for industrial purposes like tents, hotel sheets, army uniforms, etc.

All these products are produced in mill, also known as cotton mill. It is a factory in which spinning or weaving machineries are used for the production of yarn cloth from cotton [1].

A spinning wheel called as charkha is a device for spinning thread or yarn from natural or synthetic fibers. "Charkha" was the physical embodiment and symbol of Gandhiji's constructive program. It gives feeling of Swadeshi independency because spinning wheel is at the center of a network of cotton grovers, carders, weavers, distributers and users as well.

So by observing charkha's importance, the present paper is focusing on the issue of vibrations induced in its bearings. The charkha is a sensitive apparatus, so there are not many points trying to spin on it before it sets up correctly. Charkha has various components like gears, cam and follower, pulleys, rollers, bearings, spindles, etc. Gears made from composite materials are widely used. Due to lower weight-to-stiffness ratio, composite gears may be replaced by conventional material gears. Improper design of gears causes increase in load capacity and reduces weight size, and vibration level may get increased [2]. Misalignment, unbalance, improper bearings, etc., lead to failure of charkha.

And to overcome this problem, vibration signatures are the best indicators to detect bearing failure and to predict failure of charkha.

2 Need of Predictive Model to Ascertain the Faults Increased in Charkha

Vibration analysis is the best tool to predict the faults incurred in machines, before getting break down. And by this, vibration signature technique can improve the reliability, productivity, and efficiency of machine and also health of bearings.

Rolling element bearings plays a vital role in most widely used machineries including charkha also. Under various operating conditions, various loading conditions and different life span of bearings, various causes of bearing failure are rise in temperature, surface distress, dirt, misassemble, misalignment, lubrication, overloading, corrosion, etc. There are many more techniques to analyze vibration, but FFT is one of them which is widely used in all industries. From the study, various causes of bearing failure are identified and they are as follows:
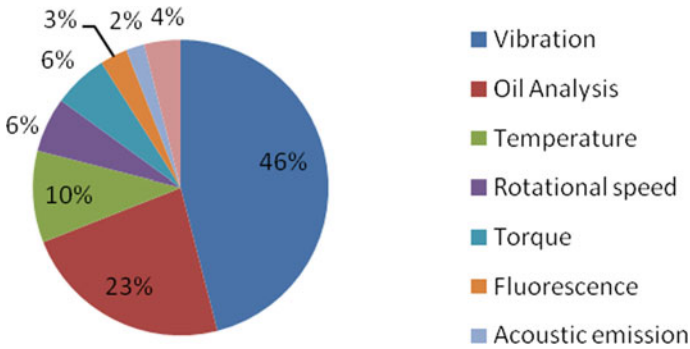
Generally, problem arises or occurs in bearings and then it propagates in other parts of machine.

From the above figure, one can observe the major cause of bearing failure is vibration. That is why one needs to carry out vibration analysis.

3 An Approach to Formulate the Predictive Model for the Induced Vibrations at Bearings

In present work, it has been decided to formulate mathematical model based on field database. In this regard, field survey has been carried out and solar operated spinning machine has been selected. Solar-operated spinning machine is shown in figure below:

Machine having weight of 40 kg, motor of 60 W, runs at variable speed but standard maximum speed is 1500 rpm. This spinning machine has eight spindles on which output, i.e., final yarn, wound out. On each of the gears and spindle, bearings are provided for smooth working of spinning machine.

4   Dimensions of Machines Components

Sr. No.	Description	Unit (mm)
1	Shaft diameter	12
2	Shaft length	650
3	Machine pulley diameter	135
4	Center distance between machine pulleys	60
5	Mean radius of bearing cap	29
6	Thickness of bearing cap	5
7	Width of bearing cap	6.2
8	Inner diameter of bearing	10
9	Outer diameter of bearing	30
10	Bearing width	9
11	Length of feed rollers	560
12	Diameter of feed rollers	25.8
13	Spindle length	220

5   Model Formulation

The search for development of mathematical model in such a way that one can predict failure due to vibration. It ends at a good analytical technique. This technique is nothing but the formulation of mathematical model which gives the relationship between causes and effects.

5.1   Process of Model Formulation

It includes Identifying variables:

Sr. No.	Variables	Type	Symbol	Unit	Dimensional formula
1	Motor speed	I	N_m	rpm	T^{-1}
2	Speed of main shaft	I	N_s	rpm	T^{-1}
3	Diameter of main shaft	I	D_s	mm	L^1
4	Length of shaft	I	L_s	mm	L^1
5	Material density of shaft	I	ρ_s	gm/mm^3	M^1L^3
6	Center distance between machine pulleys	I	$C_{p1}-C_{p8}$	mm	L^1
7	Material density of machine pulleys	I	ρ_p	gm/mm^3	M^1L^3
8	Volume of machine pulley	I	Vol_p	mm^3	L^3
9	Machine pulley diameter	I	$D_{p1}-D_{p9}$	mm	L^1
10	Mean radius of bearing cap	I	R_{mb}	mm	L^1
11	Thickness of bearing cap	I	T_b	mm	L^1
12	Width of bearing cap	I	B_{bcap}	mm	L^1
13	Material density of bearing cap	I	ρ_{bcap}	gm/mm^3	M^1L^3
14	Modulus of elasticity of bearing cap material	I	E_{bcap}	gm/mm s^2	$M^1L^{-1}T^{-2}$
15	Inner diameter of bearing	I	d_{bi}	mm	L^1
16	Outer diameter of bearing	I	d_{bo}	mm	L^1
17	Bearing width	I	B_b	mm	L^1
18	Material density of gear	I	ρ_g	gm/mm^3	M^1L^3
19	Gear ratio	I	G	Dimensionless	Dimensionless
20	Gap between feed rollers	I	$g_{f1}-g_{f2}$	mm	L^1
21	Length of feed rollers	I	$L_{f1}-L_{f3}$	mm	L^1

(continued)

Sr. No.	Variables	Type	Symbol	Unit	Dimensional formula
22	Diameter of feed rollers	I	D_{f1}–D_{f3}	mm	L^1
23	Material density of top arm (rubber)	I	ρ_t	gm/mm^3	M^1L^3
24	Speed of spindles	I	N_{sp}	rpm	T^{-1}
25	Length of spindles	I	L_{sp}	mm	L^1
26	Number of spindles	I	n	Dimensionless	Dimensionless
27	Length of thread from machine pulley to spindle through tension pulley	I	L_{thr}	mm	L^1
28	Length of oscillating roller follower from pin joint to roller	I	$L_{orf\,p}$	mm	L^1
29	Length of oscillating roller follower from pin joint to cam center	I	$L_{orf\,c}$	mm	L^1
30	Material density of roller	I	ρ_{rolf}	gm/mm^3	M^1L^3
31	Weight of cam	I	W_{cam}	gm	M^1
32	Length of lever from roller to plate of spindle	I	L_{lev}	mm	L^1
33	Moisture content in roving	I	W_{mro}	gm	M^1
34	Quantity of roving processed in certain time	I	Q_{nrov}	gm	M^1
35	Thickness of follower lever	I	T_{lev}	mm	L^1
36	Total quantity of roving	I	Q_{tyr}	gm	M^1
37	Acceleration due to gravity	I	g	mm/s^2	L^1T^{-2}
38	Vibration amplitude	D	Y_1	mm/s	L^1T^{-1}
39	Processing time	D	PT	sec	T^1
40	Energy consumed	D	EC	gm-mm^2/s^2	$M^1L^2T^{-2}$
41	Productivity	D	P	gm/s	$M^{-1}T^{-1}$

These variables mentioned in above table are (1) independent variables or causes, (2) dependent variables or effect, and (3) extraneous variables. The independent variables may vary according to the choice of designer or these are the causes to arise dependent variables while dependent variables may only vary if there is a variation in the independent variable. The extraneous variables are random and one does not have any control over it. For the present work, above vantage variables have been identified.
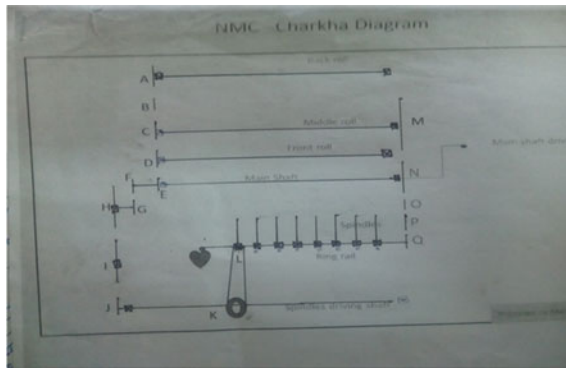
Various bearing locations

6 Reduction of Variables Through Dimensional Analysis

In this stage, all independent variables have been reduced down into a group of pi (π) terms. One can do it with the help of dimensional analysis technique. This technique gives the ability to reduce any form of variables with less time. Basic steps followed here are:

1. Identification of variables which are independent
2. By using Buckingham's method, get dependent and independent pi terms.

Input pi terms

π_1	π_2	π_3	π_4
$\dfrac{N_s}{N_{sp}}$	$\dfrac{d_s*C_{p1}-C_{p8}*T_b*d_{bi}*B_b*L_{f1}-L_{f3}*L_{sp}*L_{orfp}*L_{lev})}{(L_s*D_{p1}-D_{p9}*B_{bcap}*d_{bo}*g_{f1}-g_{f3}*D_{f1}-D_{f3}*L_{thr}*L_{orfc}*t_{lev})}$	$\dfrac{\rho_g*\rho_{rolf}*Vol_p*W_{cam}*Q_{nrov}}{\rho_t*\rho_{bcap}*r_{mb}*W_{mrov}*Q_{tyr}}$	$\dfrac{E_{bcap}*g*G*n}{\rho_{bcap}*(N_m^4*R_{mb}^3)}$

Responses are:

Vibration amplitude (Motor)		
Horizontal	Vertical	Axial
$\pi_5 A(M)$	$\pi_5 B(M)$	$\pi_5 C(M)$
$\dfrac{Y_1 A(M)}{R_{\text{mb}} * N_{\text{m}}}$	$\dfrac{Y_1 B(M)}{R_{\text{mb}} * N_{\text{m}}}$	$\dfrac{Y_1 C(M)}{R_{\text{mb}} * N_{\text{m}}}$

Vibration amplitude (Main shaft bearing)		
Horizontal	Vertical	Axial
$\pi_5 A(B)$	$\pi_5 B(B)$	$\pi_5 C(B)$
$\dfrac{Y_1 A(B)}{R_{\text{mb}} * N_{\text{m}}}$	$\dfrac{Y_1 B(B)}{R_{\text{mb}} * N_{\text{m}}}$	$\dfrac{Y_1 C(B)}{R_{\text{mb}} * N_{\text{m}}}$

Vibration amplitude (Spindles)		
Horizontal	Vertical	Axial
$\pi_5 A(S)$	$\pi_5 B(S)$	$\pi_5 C(S)$
$\dfrac{Y_1 A(S)}{R_{\text{mb}} * N_{\text{m}}}$	$\dfrac{Y_1 B(S)}{R_{\text{mb}} * N_{\text{m}}}$	$\dfrac{Y_1 C(S)}{R_{\text{mb}} * N_{\text{m}}}$

6.1   Data Generation

It was decided to take vibration reading in three directions which are mutually perpendicular to each other that is horizontal, vertical, and axial directions. For this reading has been taken on spinning machines at various locations like motor bearings, main shaft bearings, spindles etc. at different speeds and different loading conditions.

6.2 Sample Spectrum taken on Motor
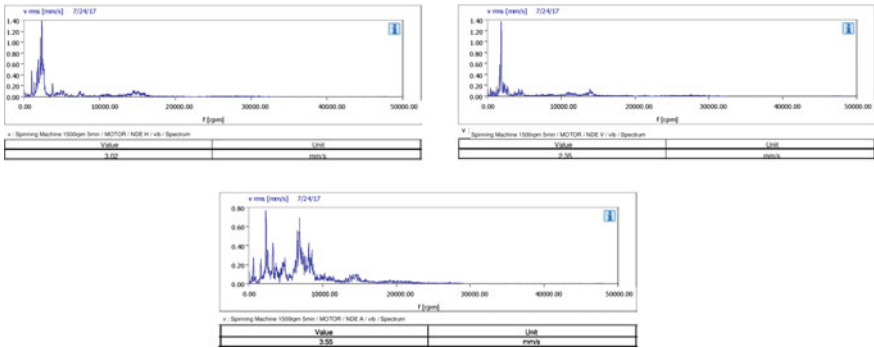
Sample spectrums

Sample readings:

π_1	π_2	π_3	π_4
0.00255	0.06144	0.001473	5.13306E−11
0.002731	0.06144	0.002379	3.62705E−11
0.002541	0.06144	0.001175	4.173E−11
0.002985	0.06144	0.009626	2.70263E−11
0.0028	0.06144	0.001388	4.34645E−11
0.002155	0.06144	0.002509	5.98234E−11
0.002501	0.06144	0.001437	5.42513E−11
0.002692	0.06144	0.002514	5.15834E−11

Π_{5A} (M)	Π_{5B} (M)	Π_{5C} (M)	Π_{5A} (B)	Π_{5B} (B)	Π_{5C} (B)	Π_{5A} (S)	Π_{5B} (S)	Π_{5C} (S)
0.000255783	6.933E−05	0.000278638	0.062603	0.038775	0.811359	1.272424	0.006237	37.93105
0.000223925	4.3869E−05	0.000163817	0.042217	0.030874	0.815475	1.219932	0.008586	32.90858
8.63408E−05	0.00010178	7.46414E−05	0.062766	0.033056	0.750071	0.981921	0.013586	32.71021
0.000207579	4.1423E−05	0.000232684	0.038509	0.049233	0.5722	2.25374	0.005672	27.36685
0.00017925	9.9633E−05	7.41551E−05	0.043347	0.042871	1.004738	1.286793	0.010611	41.15845
0.000215893	5.339E−05	0.000225704	0.033114	0.044895	0.85664	2.281514	0.013389	18.87194
0.000160294	6.3981E-05	0.000189133	0.030579	0.050241	0.645971	1.789408	0.012081	39.1553
0.000261044	9.5055E−05	0.000249157	0.047203	0.043302	0.822502	1.076611	0.010527	38.1722

7 Multiple Regression Analysis

After this process, multiple regression analysis has been carried out and the model formed due this is as follows:

1. **Vibration at motor**:

   a. In horizontal direction: $Y_1A(M) = 0.8864 - 9.459\,\pi_1 + 26.054\,\pi_3$
   b. In vertical direction: $Y_1B(M) = 0.551 + 0.3825\,\pi_1 + 8.7\,\pi_3$
   c. In axial direction: $Y_1C(M) = 0.62 + 115.98\,\pi_1 + 23.74\,\pi_3$

2. **Vibrations at main shaft bearings**:

   a. In horizontal direction: $Y_1A(B) = -1.67 + 621.51\,\pi_1 + 20.33\,\pi_3$
   b. In vertical direction: $Y_1B(B) = -3.36 + 9.6\,\pi_1 + 9.41\,\pi_3$
   c. In axial direction: $Y_1C(B) = 2.56 - 9.631\,\pi_1 + 7.78\,\pi_3$

3. **Vibrations at spindles**:

   a. In horizontal direction: $Y_1A(S) = 4.71 + 5.33\,\pi_1 + 7.47\,\pi_3$
   b. In vertical direction: $Y_1B(S) = -5.104 + 5.05\,\pi_1 + 2.3\,\pi_3$
   c. In axial direction: $Y_1C(S) = -4.501 - 1.054\,\pi_1 + 1.5\,\pi_3$

8 Result and Discussion

A multiple regression was carried out to investigate all independent variables π_1, π_2, π_3, π_4 which could significantly predict vibration of motor of spinning machine that is charkha. The results of the regression indicated below.

(i) **For motor vibration horizontal**:

A significant regression equation has been found: ($F(16,86) = 171.3955$, $p < 1.7163E^{-56}$) with an R^2 of 0.9623 that is the model explained 96.28%.

Predicted vibration of motor in horizontal direction is equal to $0.8864 - 9.45924\,\pi_1 + 0\,\pi_2 + 26.054\,\pi_3 + 0\,\pi_4$,

where π_1 related to speed, π_2 related to geometric properties, π_3 related to flow properties or weight-related properties, and π_4 related to miscellaneous variables.

Motor vibrations increased 26.054 unit weight-related and 9.459 unit which is related to speed.

(ii) **For motor vibration vertical**:

A significant regression equation has been found: ($F(16,86) = 134.7$, $p < 2.57E^{-52}$) with an R^2 of 0.9531 that is the model explained 95.31%.

Predicted vibration of motor in vertical direction is equal to $0.551 + 0.3825\,\pi_1 + 8.7\,\pi_3$,

where π_1 related to speed, π_2 related to geometric properties, π_3 related to flow properties or weight-related properties, and π_4 related to miscellaneous variables. As π_2, π_4 coordinates are zero, hence not mentioned.

Motor vibrations increased 8.73 unit weight-related and 0.3825 unit which is related to speed.

(iii) **For motor vibration axial**:

A significant regression equation has been found: ($F_{(16,86)} = 267.43$, $p < 2.74721E^{-64}$) with an R^2 of 0.9758, that is the model explained 97.58%.

Predicted vibration of motor in axial direction is equal to $0.62 + 115.98\,\pi_1 + 23.74\,\pi_3$,

where π_1 related to speed, π_2 related to geometric properties, π_3 related to flow properties or weight-related properties, and π_4 related to miscellaneous variables. As π_2, π_4 coordinates are zero, hence not mentioned.

Motor vibrations increased 23.74 unit weight-related and 115.98 unit which is related to speed.

(iv) **For main shaft bearing vibration horizontal**:

A significant regression equation has been found: ($F_{(16,86)} = 104.36$, $p < 6.08E^{-48}$) with an R^2 of 0.9403 that is the model explained 94.03%.

Predicted vibration of motor in axial direction is equal to $-1.67 + 621.51\,\pi_1 + 20.33\,\pi_3$,

where π_1 related to speed, π_2 related to geometric properties, π_3 related to flow properties or weight-related properties, and π_4 related to miscellaneous variables. As π_2, π_4 coordinates are zero, hence not mentioned.

Motor vibrations increased 20.33 unit weight-related and 621.51 unit which is related to speed.

(v) **For main shaft bearing vibration vertical**:

A significant regression equation has been found: ($F_{(16,86)} = 4.77E + 31$, $p < 0$) with an R^2 of 1, that is the model explained 100%.

Predicted vibration of motor in axial direction is equal to $-3.36 + 9.6\,\pi_1 + 9.41\,\pi_3$,

where π_1 related to speed, π_2 related to geometric properties, π_3 related to flow properties or weight-related properties, and π_4 related to miscellaneous variables. As π_2, π_4 coordinates are zero, hence not mentioned.

Motor vibrations increased 9.41 unit weight-related and 9.6 units which is related to speed.

(vi) **For main shaft bearing vibration axial**:

A significant regression equation has been found: ($F_{(16,86)} = 1.15E + 31$, $p < 0$) with an R^2 of 1, that is the model explained 100%.

Predicted vibration of motor in axial direction is equal to $2.56 - 9.631\,\pi_1 + 7.78\,\pi_3$,

where π_1 related to speed, π_2 related to geometric properties, π_3 related to flow properties or weight-related properties, and π_4 related to miscellaneous variables. As π_2, π_4 coordinates are zero, hence not mentioned.

Motor vibrations increased 7.78 units weight-related and 9.631 units which is related to speed.

(vii) For spindle vibration horizontal:

A significant regression equation has been found: ($F(16,86) = 1.69E + 31$, $p < 0$) with an R^2 of 1, that is the model explained 100%.

Predicted vibration of motor in axial direction is equal to $4.71 + 5.33\,\pi_1 + 7.47\,\pi_3$,

where π_1 related to speed, π_2 related to geometric properties, π_3 related to flow properties or weight-related properties, and π_4 related to miscellaneous variables. As π_2, π_4 coordinates are zero, hence not mentioned.

Motor vibrations increased 7.43 units weight-related and 5.33 units which is related to speed.

(viii) For spindle vibration vertical:

A significant regression equation has been found: ($F(16,86) = 1.75E + 31$, $p < 0$) with an R^2 of 1, that is the model explained 100%.

Predicted vibration of motor in axial direction is equal to $-5.104 + 5.05\,\pi_1 + 2.3\,\pi_3$,

where π_1 related to speed, π_2 related to geometric properties, π_3 related to flow properties or weight-related properties, and π_4 related to miscellaneous variables. As π_2, π_4 coordinates are zero, hence not mentioned.

Motor vibrations increased 2.53 units weight-related and 5.05 units which is related to speed.

(ix) For spindle vibration axial:

A significant regression equation has been found: ($F(16,86) = 2.15E + 32.$, $p < 0$) with an R^2 of 1, that is the model explained 100%.

Predicted vibration of motor in axial direction is equal to $-4.501 - 1.054\,\pi_1 + 1.5\,\pi_3$,

where π_1 related to speed, π_2 related to geometric properties, π_3 related to flow properties or weight-related properties, and π_4 related to miscellaneous variables. As π_2, π_4 coordinates are zero, hence not mentioned.

Motor vibrations increased 1.5 units weight-related and 1.054 units which is related to speed.

9 Conclusion

For such type of research work, a researcher must go for multiple tools to investigate the model. So the model formed in MATLAB is further investigated using ANN and thereafter authenticity of model has been considered.

References

1. Baldonado, M., Chang, C.-C.K., Gravano, L., Paepcke, A.: The Stanford digital library metadata architecture. Int. J. Digit. Libr. **1**, 108–121 (1997)
2. Bruce, K.B., Cardelli, L., Pierce, B.C.: Comparing object encodings. In: Abadi, M., Ito, T. (eds.) Theoretical Aspects of Computer Software. Lecture Notes in Computer Science, vol. 1281, pp. 415–438. Springer-Verlag, Berlin (1997)

Bone Drilling Parameters and Necrosis: An In Vitro Study

Rajesh V. Dahibhate and Santosh B. Jaju

Abstract Implant screw fixation and bone drilling are the two one after another processes. If certain operating parameters are not observed, necrosis may result. Necrosis can be explained as an unfavorable form of cell injury whereby integrity of cell membrane is lost and the extracellular space if filled with an uncontrolled release of products of cell death. This process starts an inflammatory response in the surrounding tissue which attracts leukocytes and phagocytes which remove the dead cells. However, collateral damage to surrounding tissues by microbial damaging substances released by leukocytes inhibits the healing process and lengthens patient rehabilitation period or even unsuccessful implant fixation and post-operative complications. This research work is initiated with review work, as the literature on this topic is having contrary conclusions and so review of previous investigators experimentation's on the effects of spindle speed, depth of drilling and feed rate on temperature distribution and correlation among them is made. Conclusions based on histopathological analysis and bone mineral density with in vitro study are very important. This review work attempts to organize the previous work on bone drilling parameters and its correlation with necrosis.

Keywords Bone drilling · Histopathology · Microtome · Drilling parameters

1 Introduction

Implant fixation and bone drilling are the two inseparable processes in orthopedic surgery, but with it necrosis also comes into act. Necrosis can be explained as an unfavorable form of cell injury whereby integrity of cell membrane is lost and the extracellular space if filled with an uncontrolled release of products of cell

R. V. Dahibhate (✉) · S. B. Jaju
Mechanical Engineering Department, G. H. Raisoni College of Engineering, Nagpur, India
e-mail: dahibhaterv@gmail.com

S. B. Jaju
e-mail: santosh.jaju@raisoni.net

death. Here the dead cells are eliminated by an inflammatory response that attracts leukocytes and phagocytes. However, collateral damage to surrounding tissues by microbial damaging substances released by leukocytes inhibits the healing process and lengthens patient rehabilitation period or even unsuccessful implant fixation and post-operative complications. Thus, unnoticed necrosis may be converted and consequence in a build-up of decomposing dead tissue and cell debris around the site of the cell death. The nucleus changes in necrosis are characterized by the manner in which its DNA breaks down, the nucleus fades or the nucleus shrinks, and the chromatin condenses the shrunken nucleus fragments to complete dispersal. Similarly plasma alterations are also observed in necrosis like loss of microvillus and cell blebbing. George Axhausen, (1877–1960) a leading jaw surgeon of his time from Berlin University of Dentistry known for his pioneer studies in the field of jaw, facial surgery, and especially to the palate gaps, focused necrosis.

Denaturing of bone alkaline phosphate above 56 °C is considered to be a reason for necrosis. Other factors responsible for necrosis are toxins, infection, or trauma. Mechanical trauma generally involves cellular physical damage, damage to blood vessels, and associated tissues. In thermal effects, disruption of cells as these are exposed to extremely high or low temperature for external factors result in necrosis.

2 Literature Survey

The authors [1] developed drill bits from stainless steel piping with 4.5 mm outside diameter. k-type thermocouples were "bedded" inside at the bottom of hollow pipe. The tip of tube was closed by welding. The drill bit then fluted to helix angle of 23° and ground to 90°, 80°, 70° point angles. For the bone storage, a container with saline water, heating element with thermostat control to maintain human body temperature of 37 °C is used. To calculate bone hardness, simple handheld barber Coleman impresser is employed instead of Rockwell or Brinell hardness tester. During drilling, it is observed that, in case of bovine bones, for a depth of 3 mm, the temperature varies from 38 to 26 and then 29 °C, as speed increases from 400 to 1200 and then 2000 rpm. Whereas for a depth of 9 mm, it ranges 102–117 °C for 400–1200 rpm. In case of human bones for a depth of 5–6 mm, temperature ranges from 80, 68, and 75 °C for 400, 1200, and 2000 rpm. The thrust force measured is 48, 25, and 23 N for 400, 1200, and 2000 rpm, respectively. Thus, temperature drop in both the cases in the range of 400–1200 rpm is related to reduction in thrust force, whereas temperature increase over 1200–2000 rpm is related to drop off in torque rate and thrust change. During the research work, it is also observed that the mechanical properties of bone are anisotropic [1] and density or mass of bone mineral (calcium hydroxyapatite Ca_{10} $(PO_4)_6OH_2$) in a medium consist of biological materials like minerals, bone marrow, muscles, and fats. Observation under optical microscope indicates traces of burning along with faint smell from where drill bit proceeded into the hole. Again bovine bone is more hard and thick (7–9 mm) as compared to human ulna (3–5 mm) and so generates more heat. The authors also pointed that placing of thermocouples on

the surface near the drilling sight by earlier researchers gives unsatisfactory results due to insulating property of bone. Point angles of 70°, 80°, 90°, and rake angle 23° have no significant effect on temperature rise and drilling speed of 800–1400 rpm with drill bit diameter 3.2 mm provide temperature to manageable conditions. The heat is dissipated primarily by blood and tissue fluids and partially by the bone chips. Drilling speed and heat generated are proportional parameters. Depth of bone and poor conductivity is the two factors responsible for temperature rise to 55 °C.

The aim of this study [2] is to measure and compare the temperature rise during drilling a femoral cortex of animals and humans. The animals selected are rabbit and dog. In experimental setup, a special drill guide was used to maintain a fixed distance of 0.5 mm between drilling site and heat sensitive thermocouples ample saline cooling at room temperature was maintained. In case of rabbit, for a drilling duration of 5 s, the mean temperature recorded was 40 °C. The temperature increase of 8 °C from initial temperature was rapidly. When drilling stopped, the temperature fell unexpectedly to 32 °C, Bone thickness was 1.5 mm and drill diameter 3 mm, point angle 118° and helix angle 30°. When the same procedure applied for two adult dog's, bone thickness 3.5 mm and duration of drilling is 15 s, temperature recorded was 56 °C in lateral cortex and the peak temperature for medial cortex was 65 °C, i.e., almost increase of 10 °C. In case of human's clinical study, the average time for drilling is 18 s and temperature recorded was 96 °C, even though saline cooling was applied. The cortical thickness was around 6.5 mm. The author also discussed that the experimental conditions vary from situation to another as all measurements were taken on livings under anesthesia and that could be the reason of temperature variation. Another reason is possible drilling techniques in experimental and surgeons. Clogged flutes of drilling tool increases torque and so specific cutting energy and increases temperature, this phenomenon is more prominent as drill depth increases. Another reason is coolant cannot reach the depth of drill. Karaca et al. [3] studied optimum operating conditions to avoid defects during surgeries. The parameters controlled are drill speeds 230, 570, and 1080 rpm for drill tip angle 85°, 118°, and 130° and drill force 50, 100, and 150 N. The specimens selected were fresh male and female calf tibias and multidisciplinary factors like bone sex, bone mineral density were considered. The comments were temperature increases with drill tip angle. Similarly augmented bone mineral density and female samples were the factors favorable for temperature rise. Maximum temperature reduces with hike in feed rate and drill force, and the grounds may be increase in feed rate decreases drill time. Maximum temperature of 73.9 °C was reached at bone mineral density of 2.43 g/cm^2, for corresponding values of drill speed 1080 rpm and drill force of 40 N. Drill tip influences the drill performance and drilling becomes more difficult as inevitably it produces high friction. The authors also discussed two kinds of bone damages, one the necrotic tissue and second the volume of osteocytes responsible in regenerating the bone tissue after drilling. Multiple regression showed a high degree of correlation ($R = 0.85$) between bone mineral density, drill force, and drill speed.

As drilling is performed inside a hole, it prevents most of the direct observation techniques to evaluate the process and so it is difficult to understand the complexity of process [4]. This paper presents three-dimensional thermo-mechanically coupled

finite element model of drilling process. The observations are mentioned below. The thrust force can be explained as the force applied by the rotating drill bit to the work piece, and the thrust force increases drastically with increase in cutting speed. Torque is applied by the spindle speed to maintain the drill rotation.

1. Thrust force increase with increase in feed rate due to the fact that the shear area is elevated.
2. Torque also increases with feed rate; however, the consequence of cutting speed on torque was more dominant than cutting speed.
3. Thrust force increases with increase in cutting speed and feed. Changing feed rate has linear effect on thrust force.
4. Cutting speed (v) = drill bit rpm X3.14 × Diameter of drill.
5. Feed rate (mm/min) = drill bit rpm × feed (mm/rev).
6. Time to machine = time/feed rate.
7. Material removal rate = 3.14 × D2.feed rate/4.

The objective of the work of Sean R. H. Davidson et al. [5] was to calculate thermal conductivity of bone. It is a well-known fact that bone is an anisotropic in nature but in this study it is prominently explained that it is isotropic for thermal conductivity. 0.1-cm-thick slices of bovine cortical bone were prepared, with average surface area across which heat applied was 0.1 cm^2. Temperature was measured with k-type thermocouples. The heat flow equation, Fourier's equation $Q = K.A.\Delta T/t$ referred. The conductivity measurement was divided into three groups: longitudinal, circumferential, and radial directions, and the thermal conductivity values were 0.58, 0.53 and 0.54 W/m K, respectively. According to author, this variation is due to difference in animal type, age, and bone site. This also reflects the difference in composition. Largest indicator difference is 0.05 W/m K (8.9%) of mean conductivity is between the circumferential and longitudinal direction, which is negligible. Bone density is considered to be an important aspect as it is closely related to bone conductivity. To measure bone density, single or dual energy absorptiometry (SXA & DXA) projection imaging techniques are used. Other findings related are specific heat capacity of bone is 1256 J/Kg K. Thermal conductivity is 0.53 W/m K.

3   Experimental Apparatus and Procedure

To avoid the vibrations and to achieve accuracy, CNC drilling machine is used. The drill bit specifications can be discussed as, surgical drill bit diameter was 3, 6, and 9 mm, preferred drill tip angle is 118°, and corresponding Rake angle value is 35 °C, whereas helix angle selected is 28°. **The specimen, as earlier researchers preferred bovine or canine, in this research work it is a rib bone of six-month-old sheep collected from a local butcher. The sheep was slaughtered and immediately the rib bone collected, kept in a container filled with saline water and used for drilling**. During the drilling process, it was kept in phosphate buffer solution (sodium salt) with pH of 7.4 for this stock solution A comprised of ($Na_2HPO_4 \cdot 2H_2O$),

0.2 molar solution containing 35.61 g/L or ($Na_2HPO_4 \cdot 12H_2O$), 0.2 molar solution containing 71.64 g/L, whereas Stock solution B comprised of ($NaH_2PO_4 \cdot 2H_2O$), 0.2 molar solution contains 27.67 g/L or ($NaH_2PO_4 \cdot 2H_2O$), 0.2 molar solution containing 31.21 g/L on making the addition of both A and B, (X ml of (A) + Y ml of(B)), diluted to a total solution quantity of 200 ml that is $X = 19.0$, $Y = 81.0$, pH = 7.4. For 100 ml solution quantity, density of solution A is 3.561 g/100 ml and density of solution B is 3.121 g/100 ml. The solution was maintained at 37.8 °C to simulate live body temperature. The temperature at the drilling site is measured with the help of an infrared thermometer. The speed ranges preferred were four and are as 600, 1200, 1800, and 2400 rpm. The speed selection is based on the range of the speeds recommended in the literature for the drilling of bone. The drill bit diameter was 3, 6, and 9 mm, and feed rates used were 0.3, 0.6, 0.9, and 1.2 mm/s. These feeds were chosen arbitrarily, since during orthopedic surgeries, the feed rate varies from operating person, i.e., surgeon to surgeon, and in the case of a particular surgeon, there will also be a variation, since the drill is to be handled manually. After each drilling, the specimens were dipped in bottles containing 10% formalin. After a long gap of 45 days and an interval of every 4 days, the chemical solution was replaced with a new one (Fig. 1 and Table 1).

Fig. 1 Histopathological image

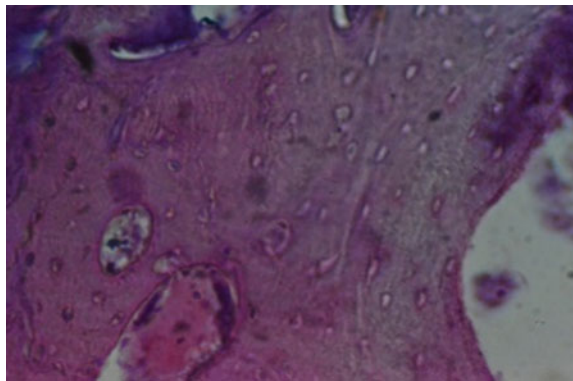
Table 1 Temperature generated during related drill speed (rpm) and feed rate (mm/s)

Sr. No.	Drill speed (rpm)	Drill feed rate (mm/s)	Temperature at drill site (°C)		
			3 mm	6 mm	9 mm
1	600	0.3	41.2	46.5	54.2
2	1200	0.6	43.5	47.8	56.5
3	1800	0.9	44.6	49.9	58.4
4	2400	1.2	45.2	51.3	60.2

4   Conclusions

The measurements as recorded by previous researchers when summarized indicate a great fluctuation although the operating principles are same. Use of electrical source and parameters like temperature gradient, heat flow and specimen dimensions were the some aspects. Zelenovs [6] faces the problem that the heat may escape to surrounding instead of through the specimen. Lunskdog [7] used resistive wire to heat the specimen at one end while other end connected to copper heat sink. Temperature was measured by thermocouple placed across the length drilled drills here the heat loss through the specimen and heat sources, and drilled holes have to be considered from above survey we can summarize that the experimental setup is a challenging task for accurate results. The apparatus used by the Biyikli [8] can be considered as an accurate one as in this one-dimensional heat flow was measured by insulating the specimen by which experimental error is reduced but in this also accurate sizing of specimen is achieved by machining which can change the physical properties of bone so if specimen of different dimensions can be adopted, it will be a great feature. Aouzgia [9] noted that circumferential direction temperature rise is less as compared to longitudinal direction and on the basis, anisotropic nature of cortical bone was claimed, contrarily Lunskdog [7] claimed for longitudinal direction. Juenlee [10] the opposing factors like higher heat generation and low thermal conductivity reduces the effect of drilling parameters like speed rate and feed rate. High conductivity of drill bit as compared to bone the drill tool will cool the drilling site by conduction. The chip stream also convects the heat from drilling site. The drill bit material also affects the heat removed by it, about 50–60% of heat generated when steel is used. The thermal conductivity $K = 0.28$ W/m K and $h = 0.182$ corresponding to thermal conductivity 0.42 W may be due to less water content in bone also affects the thermal conductivity also provides the data to calculate the amount of mechanical energy absorbed as thermal power into the bone (0.6–0.7% is converted to thermal power) and here the term torque dominates the power consumption, this mechanical power is converted to heat which is partitioned into drilling tool, chips containing bone debris and bone specimen. Osteocytes begin to die with temperature increase above 50 °C, and if temperature even exceeds 70 °C, enzymes and proteins required for recovery will get damaged concurrent with biochemical damage to cells [9]. The simplest method of evaluating thermal conductivity consists of creating a "1-D" heat flow. Fourier's law is also used to measure conductivity. The use of sensors has limitations as the dimensions of the sensors are relatively large. Larger drills contribute to better elimination of heated bone chips and debris by which more efficient drilling with lesser increase in bone temperature metal chips carry 85% of heat generated but due to poor conductivity bone chips carry lesser percentage of heat. Thermal gradient exists from the heat source as the high temperature to the cooler specimen. Higher temperature gradient more heat transfer will occur and will continue till the gradient is maintained. The balance heat gain and loss will decide the ultimate temperature. When these two phenomenon's are equal, state of equilibrium is achieved, in equilibrium the specimen temperature is a function of exposure temperature and

thermal conductivity but in case of biological tissues as the exposure time is usually too short, equilibrium is not reached and so in the non-equilibrium case the temperature is function of temperature exposure and exposure time, whereas the specific heat capacity is constant [7]. usually thermocouples are placed 0.5–1 mm from drilling site used axial positioning of thermocouples [5] also noted that there are significant differences in conduction values across the longitudinal, circumferential direction, and no significant differences along radial and circumferential direction and so the information of two thermal properties of specific heat and thermal conductivity is very essential. Karaca [3] mentioned the difference in thermal properties with respect to species too. Bachus [11], in his paper referred four forces 57, 83, 93, and 130 N. Thermocouples were placed 0.5, 1, and 2 mm away from drilling site. When reading of thermocouple, 0.5 mm distance is observed; it shows 67.24, 47.2, 35.17, and 34.66 °C for thermocouples 1.0 mm distance away from site is observed it shows 57.86, 45.05, 34.50, 33.22 °C, and for 2 mm distant thermocouples 52.79, 41.46, 31.62, 31.88 °C. From this, we can interfere that only at 57 N, local application temperature is above 50 °C, up to 2 mm away from cutting site for 48 s. When a load of 83 N time reduced to 45 s afterward for 93 and 130 N temperatures remain below 50 °C. So we can conclude that as the drilling force is increased, temperature is reduced. The reason behind this may be the time required to penetrate the cortex bone is reduced. But if we observe the research of other investigators, they have not concluded the same interference as Bachus [11] have. The reason is that the cutting tool parameters they have referred are different for example like dental studies utilized speed range from 125 to 100,000 rpm and force between 1.5 and 24 N, with dental burrs, extra skeletal pins, and drill bits, whereas orthopedic researchers had employed 60–700 rpm with 60 and 120 N.

References

1. Hillery, M.T., Shuaib, I.: Temperature effects in the drilling of human and bovine bone. J. Mater. Process. Technol, 302–308 (1999)
2. Eriksson, A., Alberektsson, T., Albrektsson, B.: Heat caused by drilling cortical bone. Acta Orthop. Scand. **55**, 629–631 (1984)
3. Karaca, F., Aksakal, B., Kom, M.: Influence of orthopedic drilling parameters on temperature and histopathology of bovine tibia: an in vitro. Med. Eng. Phys. **33**, 1221–1227 (2011)
4. Ahemad, N.: Effect of changing drilling parameters on thrust force and torque. IDOSI Publications, Middle East J. Sci. Res. (2014)
5. Davidson, S.R.H., James, D.F.: Measurement of thermal conductivity of bovine cortical bone. Med. Eng. Phys. **22**, 741–747 (2000)
6. Zelenov, E.S.: Experimental investigation of the thermophysical properties of compact bone. Mech. Compos. Mater. **21**, 759–762 (1985)
7. Lundskog, J.: Heat and bone tissue. Scand. J. Plast. Reconstr. Surg. Hand Surg. Suppl. **9** (1972)
8. Biyikli, S., Modest, M.F., Tarr, R.: Measurement of thermal properties for human femora. J. Biomed. Mater. Res. **20**, 1335–1345 (1986)
9. Abouzgia, M.B., James, D.F.: Temperture rise during drilling through bone. Int. J. Oral Maxillofac. Implants **12**(3), 342–353 (1997)

10. Lee, J.E., Ozdoganlar, B., Rabin, Y.: An experimental investigation on thermal exposure during bone drilling. Med. Eng. Phys. **34**, 1510–1520 (2012)
11. Bachus, K.N., Rondina, M.T., Hutchinson, D.T.: The effect of drilling force on cortical temperature and their duration: an in vitro study. Med. Eng. Phys. **22**, 685–691 (2000)

Identification of Performance Measures for Supply Chain Performance Measurement in Textile Enterprise

Pranav G. Charkha and Santosh B. Jaju

Abstract Supply chain performance has gained significant importance in the last two decades. Almost every sector has utilized its implementation benefits. Unlike, manufacturing sector, supply chain management is very critical and complex in process industry such as textile industry. Textile industries' supply chain in India is very lengthy and complex, so as its performance measurement. This paper proposed to develop a conceptual framework based on the literature review and discussion with experts. Framework proposed utilizes the essence of balanced scorecard perspective, in order to overcome some of the earlier literature gaps.

Keywords Supply chain management · Performance measurement system · Supply chain performance measurement · Textile industries

1 Supply Chain Performance Measurement System (SCPMS)

Supply chain management has gained a significant importance among the practitioners, academicians and researchers as well in the last two decades [1]. Supply chain management envelopes entire life cycle of the product, initiating from raw material procurement to manufacturing and finally to customers through proper distribution channels [2]. In the recent past, the concentration is shifted from manufacturing units to across the units and or across the organization/enterprises. Today's businesses have confined boundaries due to outsourcing, globalization, enhanced application of information technology and improvement in integration [3]. The said parameters

P. G. Charkha (✉)
Department of Mechanical Engineering, Datta Meghe Institute of Engineering Technology & Research, Wardha, Maharashtra, India
e-mail: pgcharkha@gmail.com

S. B. Jaju
Department of Mechanical Engineering, G. H. Raisoni College of Engineering, Nagpur, Maharashtra, India

have triggered the firms to initiate better managerial perspectives. These perspectives must be assisted by a sufficient set of performance measures in order to ensure efficiency and effectiveness. To ensure, supply chain to be efficient and effective, performance measurement of supply chain system proved to be best alternative to achieve supply chain excellence. Performance measurement system (PMS) played vital role in its development as well for its supply chain. It is very rightly said that "What can't be measured, can't be improved" [4]. Following traditional performance measurement system, practitioner faced frequent drawbacks such as consideration of financial measures, lack of connection between organization's strategies and measurements, lack of stakeholder consideration [5, 6]. There are variety of objectives of performance measurement system such as identify whether customer is satisfied and ensure the flexibility and effective as well efficient utilization of internal resources carried out, with introduction of some innovative practices which provides better learning opportunities for personnel involved in process and ultimately achieving the maximum gains for firm/business enterprise [7, 8]. Hence, consideration of supply chain as shown in Fig. 1 is very important in the development of supply chain performance measurement system (SCPMS) [9]. There have lot of efforts done in developing SCPMS as well exploring the concept of SCPMS along with availability and selection of appropriate performance measures. Study focused on scant of research paper on performance measures/metrics. Various researchers have contributed to state of the art of SC performance with different perspectives as per their unique vision. Most of the studies reviewed the literature in SC performance concentrate considering specific division of supply chain, whereas few studies considered performance of SCs as a whole. Another attempt has been made to determine the key performance metrics in SCs [10]. Yet another contribution has done by another study suggested framework using resource, output and flexibility as performance measures [11]. On the other hand, it is agreed that, currently available PMS possess few limitations, first, it usually applies financial measures without any process perspective and secondly evaluation is confined to directly measurable or accountable indicators [12–15]. The answer to these limitations is that modern performance measurement system should support the organization strategies considering nonfinancial measures and focusing majorly on the features/characteristics of the industry. Some types of industries need very specific measurement system characteristics and thereby left difficulty in developing a generic performance measurement system [11]. Hence, to recognize the value drivers, practitioners/managers must have performance measurement system designed to capture information on all perspectives of business divisions by not only using the financial results [10]. Reason for failure in using only financial measures was because of their historical orientation, lacking in forward-looking perspective, not relating to organization's strategic performance and not considering the operational efficiency and effectiveness [16]. On the contrary, new PMS should take into account a wider perspective for the satisfaction of all the stake holders of the business, which are firm's management, customer-targeted, employees involved [17–19]. It should give an insight into firms about the skills and systems that your employees needed (innovation and learning) to innovate and build the right strategic capabilities and efficiencies (internal business
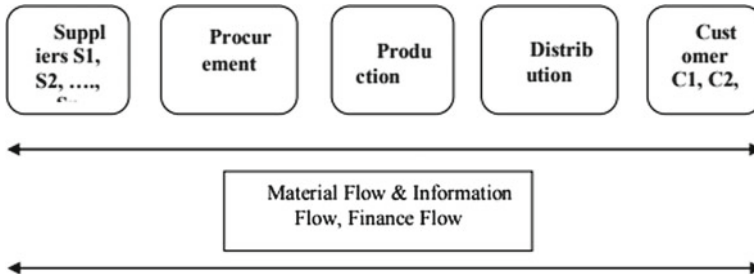
Fig. 1 Generalized supply chain

perspective) that deliver specific value to the market (customer perspective) which eventually lead to higher shareholder value (financial perspective) [20].

2 Textile Supply Chain

Textiles and clothing sector have been one of the leading process industries of South Asia in terms of its contribution to output, employment and trade. Today, the textile industry sector employs 35.0 million people (second largest employer), generates 1/5th of total export earnings and contributes 4% to the GDP, thereby making it the largest industrial sector in India [21, 22]. Being second largest contributor to the Indian economy, the core textile industry of developing country like India is still very unorganized in managing its resources either in the form of raw material (cotton, jute, silk, wool, etc.), work in process (yarn, rough fabric), finished product (finished fabric) [21] as shown in Fig. 2. Textile supply chain as shown in Fig. 2 has unique features that justify a separate supervision of its supply chain. Some prominent features are mentioned below:

1. Process industry
2. Long fragmented and complex supply chain
3. Multiple intermediate procurement stages
4. Complex production processes
5. Long distribution channels.

3 Research Problem

Most of the studies conducted in the area of supply chain performance evaluation have concentrated on supply chain of discrete part manufacturing industries. Process industry supply chains have not received the equal weightage as they require [9, 23]. The textile industry supply chain is one type of process industry differentiating itself
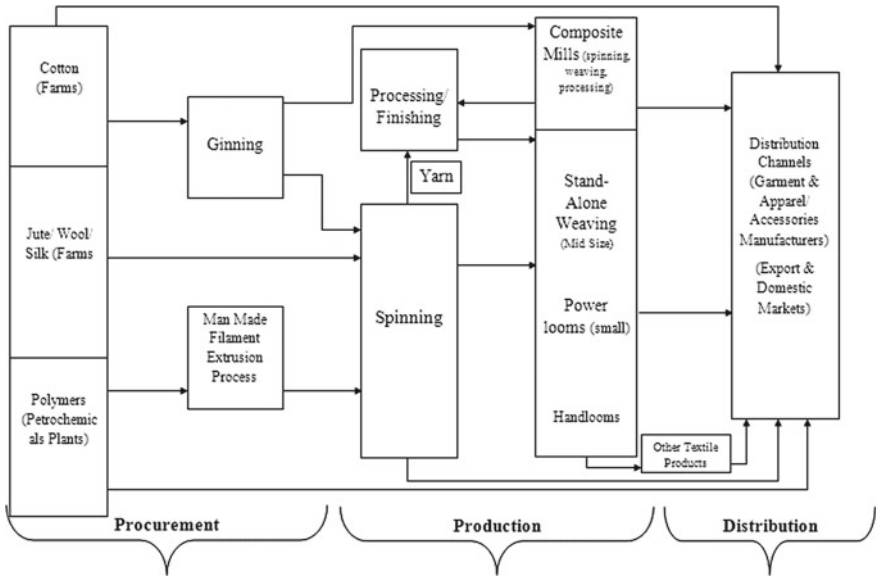
Fig. 2 Textile supply chain

from other supply chains due to its distinguishing features. Apart from characteristics mentioned earlier, textile supply chain has design variations, high risks are involved, and ruination of product is among some common issues [24, 25]. Other issues like less awareness regarding making the technical textiles R&D intensive, rationalizing cost at every process division of supply chain, establishing coordination between textile industry and relevant trade firms to make supply chain more efficient are still to be explored. Another important issue in textile supply chain is integration of intermediate division which not only increases lead time but also adds to cost [26]. Hence, it becomes very important to identify specific performance measurement for textile supply chain. Conventional measure for supply chain evaluation such as cost and return on investment may not be adequate to assess the performance. There are other qualitative performance measures which affect the supply chain performance. Balanced approach needs to be adopted while evaluating the supply chain performance focusing on the related intermediate process division of supply chain. Our research proposes to evaluate textile supply chain which can help to identify the list of crucial performance measures. For this, we should identify the right combination of procurement strategy, efficient production strategy and distribution strategy to deliver to potential markets which are more attractive, fruitful, stable and suitable for the business success. This will help to evaluate the resources and various strategies which will support the long-term goals of a textile business [27]. All these issues are very important in attaining the satisfaction of all stakeholders keeping strategic perspective in mind. In order to evaluate the performance of supply chain, the objectives of the paper are:

  i. To validate the framework designed for assessing the supply chain performance in case companies

 ii. To determine the relative weight of all the perspectives (i.e., financial, customer, internal business process, innovation and learning), and also to determine the relative weight of all criteria under each of the perspectives on the basis of the responses of experts from industry for which case study is conducted.

4 Methodology

In the current research study, we proposed a generic model to evaluate the performance of textile supply chain with due consideration to its features and characteristics. In existing literature, there is no model which identify the crucial performance measures and quantify them for textile supply chain. Hence, the selection of appropriate performance measure to assess textile supply chain is an important factor; also, the importance level of performance measure is an aspect of concentration. This study has categorized the criteria under each of BSC perspectives. In such a situation, AHP has proven its benefits to establish pairwise comparison in order to determine relative importance of performance measure with respect to one another [28, 29]. AHP is also used to establish priorities among the criteria and alternative. The study uses the combination of BSC and AHP techniques. The study identified characteristics of textile industry, and since these are generic issues of textile supply chain, they are aligned to four perspectives of BSC and treated as strategic objectives of textile supply chain. As stated earlier, right combination of strategies at procurement, production and distribution process division is important, and we have selected these three process divisions as an alternative to estimate their importance toward overall supply chain performance with respect to criteria and sub-criteria. In order to validate the need of the study, list of performance measures identified, criteria, alternative and the relevance of study as a whole, with expert identified are from industry, academia and consultants working in domain area of supply chain management (SCM), textile industry and operation management (OM) etc., with an average experience of more than 15 years. In all, 15 subject matter experts (SMEs) were contacted, out of which, 13 agreed to interact. Thirteen experts consist of six from textile industry (integrated units) located in central India, four are academicians teaching to textile engineering with adequate knowledge of SCM and having management qualification, whereas the last three are consultants and working members of state's textile corporation and textile association of India. In all, total of three rounds of interaction were undertaken and results were refined. Structure list of questions was used in each round to understand the philosophy of SCM, performance measurement in textile industry. The questions involve subjective and objective responses as well. Very renowned comparison scale developed by Likert was used to estimate the agreement toward the existence of identified BSC perspectives as criteria and sub-criteria in the framework. The mean values and CoV values are calculated for the existences of accepted sub-criteria. Also, reliability of responses is measured using Cronbach's

Table 1 First-level BSC perspective consensus as criteria

Sr. no.	BSC perspective as performance criteria	Mean	Coefficient of variation
1	Financial perspective	4.6	0.11
2	Customer perspective	4.4	0.124
3	Internal business process perspective	4.8	0.09
4	Innovation and learning perspective	4.2	0.075
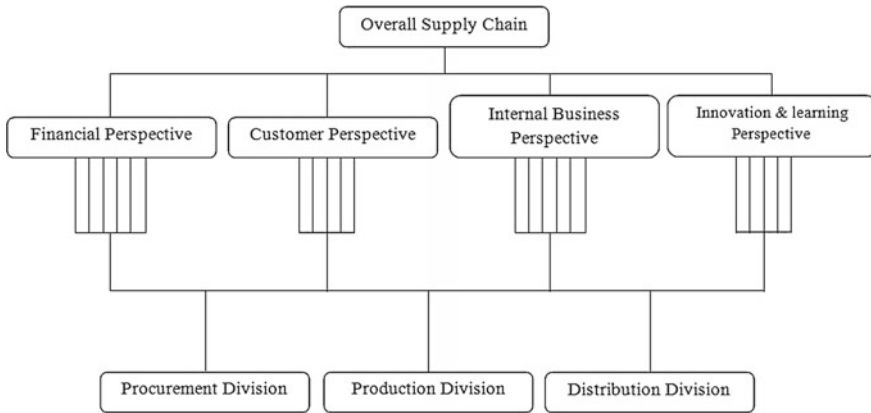
Fig. 3 Hierarchical representation of problem

alpha. Experts were given choice of suggesting any additional criteria/sub-criteria as shown in Tables 1 and 2. Experts were given a choice of suggesting or adding additional criteria/sub-criteria. Finally, out of 53 identified measures, 20 were consented to be the part of framework. Along with 20, 2 new performance measures were added as per expert's suggestion, namely "use of quality engineering/quality management techniques" and "employing information technology and knowledge management technologies" abbreviated as "use of QE/QM techniques" and "employing IT/KM technology," respectively.

Final list of performance measures under each perspective criteria is mentioned below, whereas final framework is developed as shown in Fig. 3. This final framework and semi-structured questionnaire are used to undertake case studies in four case companies to be discussed in next section.

Table 2 CoV for performance sub-criteria and Cronbach's alpha estimation of reliability under every performance criteria

Sr. no.	Performance measurement criteria (BSC perspectives)	Performance sub-criteria	Mean	COV	Cronbach's alpha
1	Financial perspective	Net profit vs productivity ratio	3.4	0.36	0.8253
		Rate of return on investment	4.8	0.093	
		Supplier's cost-saving initiatives	4.6	0.108	
		Supplier's rejection rate	3	0.408	
		Information carrying cost	4.2	0.106	
		Inventory carrying cost	4.7	0.092	
		Cost per hour of operation	4.6	0.109	
		Manufacturing cost	4.6	0.111	
		Variation against budget	3	0.333	
2	Customer perspective	Quality of goods delivered	4.6	0.109	0.8497
		Customer satisfaction	4.6	0.111	
		Customer query time	4.2	0.106	
		Delivery performance and lead time	4.8	0.093	
		Quality of delivery documentation	2.8	0.298	
		Range of product and services	2.6	0.295	
		Effectiveness of delivery invoice methods	2.8	0.298	
		Effectiveness of distribution planning schedules	4.6	0.111	
		Level of customer-perceived value of product	3.2	0.407	

(continued)

Table 2 (continued)

Sr. no.	Performance measurement criteria (BSC perspectives)	Performance sub-criteria	Mean	COV	Cronbach's alpha
3	Internal business process perspective	Frequency of delivery	3.4	0.335	0.8025
		Capacity utilization	4.8	0.093	
		Planned process cycle time	4.6	0.111	
		Total cash flow time	3.6	0.316	
		Total supply chain cycle time	4.6	0.111	
		Product development cycle time	4.4	0.120	
		Flexibility to meet particular customer needs	4.4	0.120	
		Level of supplier's defect-free deliveries	3	0.408	
		Extent of cooperation to improve quality	4.8	0.093	
4	Innovation and learning perspective	Order entry method	2.2	0.280	0.7885
		Delivery reliability	2.6	0.319	
		Accuracy of forecasting	4.8	0.093	
		Range of products/services	2	0.5	
		Supplier's booking procedures	2.4	0.475	
		Buyer–supplier partnership level	4.8	0.093	
		Employee satisfaction and skill orientation	4.8	0.093	
		Supplier assistance in solving technical problems	2.8	0.296	
		Supplier ability to respond to quality problems	3	0.408	
		Use of IT/KM technologies	4.4	0.120	
		Use of QE and QM techniques	4.8	0.093	

5 Conclusion

Supply chain management has major impact on all industries in today's era of globalization [30]. The consequence of adopting specific supply chain performance practices should offer motivation to practitioner/managers to review the situation of an enterprise. An efficient SC depends on its performance. SC configuration varies from industry to industry. Process industry like textile needs specific SC. It should also have definite strategy for its different process divisions (procurement, production and distribution). Effect of various SC performance measures is very important and analyzed in this study. Selection of performance measures is done by analyzing the features/characteristics of textile supply chain and validated with subject matter experts. Supply chain performance is problem of multi-criteria decision making. Various performance measures were utilized in earlier studies, and most of them consist of financial parameters only. Though, cost has direct relation with profit and also an easy measurement to decide effectiveness of SC. But misconception about measuring supply chain performance using cost and other financial measures only should be avoided. In recent research studies, quality as a measure was strongly preferred for most industry, especially process ones [31]. Hence, supply chain performance measures in this study are categorized under different BSC perspectives (financial, customer, internal business process, and innovation and learning) used to find out relative impact on each other and on supply chain's strategic process division. Quantification of these measures has no definite ground, and 22 performance measures under 4 BSC perspectives are categorized based on expert's opinion, with 2 new measures (employing IT/KM technologies and use of QE/QM techniques) as contribution to this study. Based on perspective as criteria and sub-criteria and alternative for assessing supply chain performance, a hierarchical framework is designed as mentioned in Fig. 3.

References

1. Agrawal, S., Singh, R.K., Murtaza, Q.: Prioritizing critical success factors for reverse logistics implementation using fuzzy-TOPSIS methodology. J. Ind. Eng. Int. **12**, 15–27 (2016). https://doi.org/10.1007/s40092-015-0124-8
2. Aria Nezhad, M.G., Makuie, M., Khayatmoghadam, S.: Developing and solving two echelon inventory system for perishable items in a supply chain: case study (Mashhad Behrouz Company). J. Ind. Eng. Int. **9**, 39 (2013)
3. Babazadeh, R., Razmi, J., Ghodsi, R.: Supply chain network design problem for a new market opportunity in an agile manufacturing system. J. Ind. Eng. Int. **8**, 19 (2012)
4. Kaplan, R.S., Nortan, D.P.: The Balanced Scorecard-Measures that Drive Performance. Harvard Business School (1992)
5. Bhagwat, R., Sharma, M.K.: Performance measurement of supply chain management: a balanced scorecard approach. Comput. Ind. Eng. **53**(1), 43–62 (2007)
6. Bhagwat, R., Sharma, M.K.: Performance measurement of supply chain using the analytical hierarchy process. Prod. Planning Control: Manag. Oper. **18**(8), 666–680 (2007)

7. Bhagwat, R., Chan, F.T.S., Sharma, M.K.: Performance measurement model for supply chain management in SMEs. Int. J. Glob. Small Bus. **2**(4), 428–444 (2008)
8. Bhagwat, R., Sharma, M.K.: An application of the integrated AHP-PGP model for performance measurement of supply chain management. Prod. Planning Control: Manag. Oper. **20**(8), 678–690 (2009). https://doi.org/10.10080/09537280903069897
9. Shah, N.: Process Industry Supply Chains: Advances & Challenges. Comput. Chem. Eng. **29**, 1225–1235 (2005)
10. Gunasekaran, A., Patel, C., McGaughey, R.: A framework for supply chain performance measurement. Int. J. Prod. Econ. **87**(3), 333–348 (2004)
11. Beamon, B.M.: Measuring supply chain performance. Int. J. Oper. Prod. Manag. **19**(3), 275–292 (1999)
12. Bigliardi, B., Bottani, E.: Performance Measurement in the Food Supply Chain: A Balanced Scorecard Approach, vol. 28, no. 5/6, pp. 249–260. Facilities-Emerald Publication
13. Bititci, Cavalieri U.S., Cieminski, G.: Implementation of performance measurement system: public and private sector. Prod. Planning Control: Manag. Oper. **16**(2), 99–100 (2005)
14. Browne, J., Devlin, J., Rolstadas, A., Andersen, B.: Performance measurement: the ENAPS approach. Int. J. Bus. Transform **1**(2), 73–84 (1998)
15. Teng, S.G., Jaramillo, H.: A model for evaluation and selection of suppliers in global textile and apparel supply chains. Int. J. Phys. Distrib. Logistics Manage. **35**(7), 503–523 (2005)
16. Singh, R.K., Sharma, M.K.: Prioritizing the alternatives for flexibility in supply chain. Prod. Plann. Control: Manage. Oper. **25**(2), 176–192. https://doi.org/10.1080/09537287.2013.782951 (2014)
17. Gopal, P.R.C., Thakkar, J.: A review of supply chain performance measures and metrics: 2000–2011. Int. J. Prod. Perform. Manag. **61**(5), 518–547 (2012). Gunasekaran, A., Patel, C., Tirtiroglu, E.: Performance measures and metrics in supply chain environment. Int. J. Prod. Oper. Manag. **21**(1/2), 71–87 (2001)
18. Hall, D.C., Saygin, C.: Impact of information sharing on supply chain performance. Int. J. Adv. Manuf. Technol. **58**(1–4), 397-409. https://doi.org/10.1007/s00170-011-3389-0 (2011)
19. Thakkar, J., Kanda, A., Deshmukh, S.G.: Supply chain performance measurement framework for small and medium scale enterprises. Benchmarking: Int. J. **16**(5), 702–723 (2009)
20. Kaplan, R.S., Nortan, D.P.: Using the BSC as a strategic management system. In: Best of HBR Managing for Long term (2007)
21. Chandra, P.: The textile & apparel industry in India. In: Oxford Companion to Economies in India (2006)
22. Lam, J.K.C.: Textile & apparel supply chain management in Hong Kong. Int. J. Cloth. Sci. Technol. **18**(4) (2006). https://doi.org/10.1108/09556220610668-491
23. Cao, N., Zhang, Z., To, M.K., Ng, K.P.: How are supply chain coordinated?—an empirical observation in textile-apparel businesses. J. Fashion Mark. Manag. **12**(3), 384–397 (2008)
24. Moghaddam, R.T., Forouzanfar, F., Ebrahimnejad, S.: Incorporating location, routing, and inventory decisions in a bi-objective supply chain design problem with risk-pooling. J. Ind. Eng. Int. **9**, 19 (2013)
25. Swaminathan, J.M.: Managing supply chain operation in India. *Book on Building Supply Chain Excellence in Emerging Economies*, pp. 137–154 (2006)
26. Bedi, J.S.: Report on Assessing the prospects for India's Textile & Clothing Sector. National Council of Applied Economic Research (2009)
27. Chandra, C., Kumar, S.: An application of system analysis methodology to manage logistic in textile supply chain. Supply Chain Manag.: Int. J. **5**(5), 234–245 (2000)
28. Chan, Y.C.L.: An analytic hierarchy framework for evaluating balanced scorecards of healthcare organizations. Can. J. Adm. Sci. **23**(2), 85–104 (8) (2006)
29. Dalalah, D., Oqla-Al, F., Hayajneh, M.:Application of Analytical hierarchy process in multi criteria analysis of selection of cranes. Jordan J. Mech. Ind. Eng. **4**(5), 567–578 (2010). ISSN: 1995-6665
30. Singh, R.K., Sharma, M.K.: Selecting competitive supply chain using fuzzy AHP and extent analysis. J. Ind. Product. Eng. **31**(8), 524–538. https://doi.org/10.1080/21681015.999723 (2015)

31. Varma, S., Wadhwa, S., Deshmukh, S.G.: Evaluating petroleum supply chain performance: application of analytical hierarchy process to balanced scorecard. Asia Pac. J. Mark. Logistics **3**, 343–356 (2008)
32. Bourne, M., Neely, A.: Implementing performance measurement system: a literature review. Int. J. Bus. Perform. Manag. **5**(1), 1–23 (2003)
33. Chan, F.T.S.: Performance measurement in a supply chain. Int. J. Adv. Manuf. Technol. **21**, 534–548 (2003). https://doi.org/10.1007/s001700300063
34. Charkha, P.G., Jaju, S.B.: Supply chain performance measurement system: an overview. Int. J. Bus. Perform. Supply Chain Model. **6**(1), 40–60 (2014)
35. Charkha, P.G., Jaju, S.B.: Designing innovative framework for supply chain performance measurement in textile industry. Int. J. Logistics Syst. Manag. **6**(1), 216–230 (2014)
36. Cooper, M.C., Lambert, D.M., Pagh, J.D.: Supply chain management: more than a new name for logistics. Int. J. Logistics Manag. **8**(1), 1–13 (1997)
37. Digalwar, A.K., Sangwan, K.S.: An overview of existing performance measurement frameworks in the context of world class manufacturing performance measurement. Int. J. Serv. Oper. Manag. **9**(1), 60–82 (2011)
38. Jadhav, J.R., Mantha, S.S., Rane, S.B.: Analysis of interactions among the barriers to JIT production: interpretive structural modeling approach. J. Ind. Eng. Int. **11**, 331–352 (2015a). https://doi.org/10.1007/s40092-014-0092-4
39. Jadhav, J.R., Mantha, S.S., Rane, S.B.: Roadmap for Lean implementation in Indian automotive component manufacturing industry: comparative study of UNIDO model and ISM model. J. Ind. E. Int. **11**, 179–198 (2015). https://doi.org/10.1007/s40092-014-0074-6
40. Kumar, S., Luthra, S., Haleem, A.: Customer involvement in greening the supply chain: an interpretive structural modeling methodology. J. Ind. Eng. Int. **9**, 6 (2013). Conference 2016, LNCS, vol. 9999, pp.1–13. Springer, Heidelberg (2016)

Influence of Process Parameters on Abrasive Water Jet Machined Pockets on Inconel 718 Alloy

Vivek V. Bhandarkar, Rahul A. Jibhakate and T. V. K. Gupta

Abstract The proposed work area is 'Abrasive Water Jet Machining (AWJM)' due its various advantages over the conventional machining. AWJM is a non-traditional machining process in which material is removed by the erosion process where a very high pressure and very high velocity jet of abrasive particles and water slurry strikes on the work piece material (Momber and Kovacevic in Principles of abrasive water jet machining. Springer, [1]). Milling blind pockets is majorly used in the areas of automobiles, aerospace, and defense sectors. Here, for these applications, Inconel 718 is commonly used material which is very difficult to be machined by using conventional machining processes [2]. In many sectors like Aerospace, preference is given to high strength with less weight of the materials. The research work includes the use of 'Taguchi method' of Design of Experiments. It also includes finding the influence of particular process parameters on each selected output parameter, analysis of variance (ANOVA), and regression analysis for each output parameter. For this purpose, traverse speed and water pressure have been selected as process parameters, and pocket size, pocket depth, and surface roughness have been selected as output parameters.

Keywords Abrasive water jet machining · Taguchi · ANOVA · Regression analysis · Design of experiments · Main effects plot

1 Introduction

In abrasive water jet machining, fine abrasive particles and water are mixed in suitable proportion and its slurry in a small stream is forced on the surface of the work piece

---

V. V. Bhandarkar (✉) · R. A. Jibhakate
G. H. Raisoni College of Engineering, Nagpur 440016, India
e-mail: vivek.bhandarkar@raisoni.net
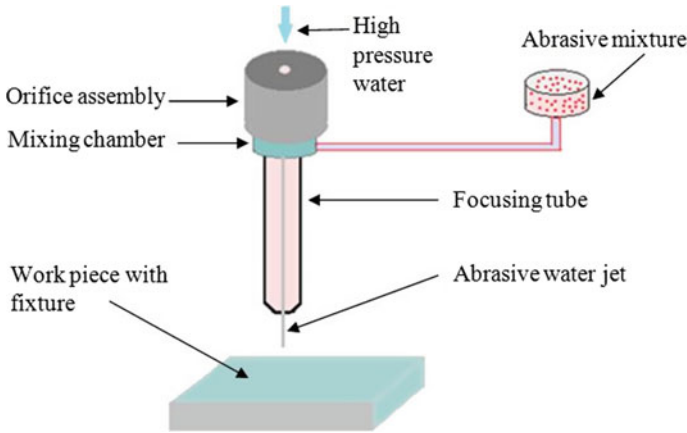
T. V. K. Gupta
VNIT, Nagpur 440010, India
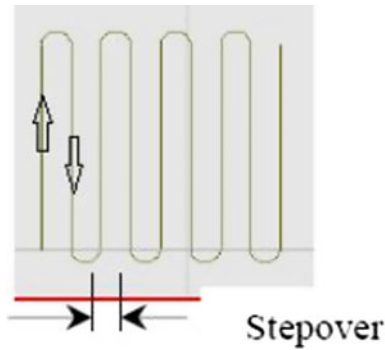
Fig. 1 Schematic of AWJM

Fig. 2 Traversing direction

material through a fine nozzle. This impact of the abrasive particles on the work piece surface causes the erosion process due to which the material gets removed [1].

Inconel 718 alloy is a nickel-chromium alloy resistant to corrosion as well as oxidation to a great extent [3]. Hence, it can be used at a very high temperature and also in corrosive atmosphere. Moreover, a large variety of mechanical properties can be obtained by heat treatment [4]. Figure 1 shows the schematic of AWJM.

In the areas like Automobile, blind pocket milling has a lot of applications. In these areas, material weight is reduced keeping the strength in acceptable limits [5]. Figure 2 shows the direction along which the abrasive water jet traverses, whereas Fig. 3 shows the sample of pocket milled surface.
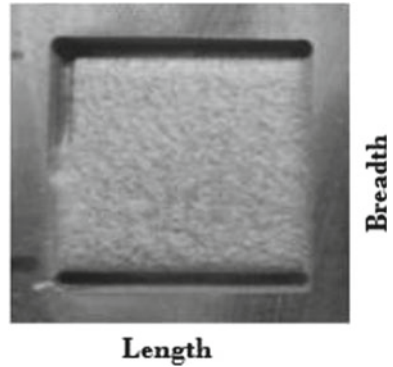
Fig. 3 Sample pocket

Table 1 Fixed parameters during the experimentation

Parameters	Values
Abrasive type	Silica sand
Abrasive size	80 # (177 microns)
Stand of distance (SOD)	2 mm
Jet impact angle	90°
Jet diameter	0.76 mm
Step over	0.76 mm

2 Experimentation

Design of experiments (DOE) is a widely used technique for statistical problems. In the 1920s, it was introduced by R. A. Fisher in England. The reason behind this was to study the effect of multiple variables simultaneously. This method is also called as Taguchi method. In this method, orthogonal arrays are used which estimate the effects of various factors on response mean and variation [6]. L16 orthogonal array was selected in this work. Following table shows fixed parameters during the Experimentation (Table 1).

3 Analysis and Results of Measured Output Parameters

Size of pocket (Length and Width), depth of pocket, and surface roughness were selected as the output parameters and were measured using USB microscope, coordinate measuring machine (CMM), and Mitutoyo surface roughness tester, respectively. All these measuring equipments are available in VNIT, Nagpur.

ANOVA was performed for each output parameter. The conclusion from this analysis is as given below (Table 2).

Above ANOVA table exhibits that water pressure influences more for the length of pocket followed by the traverse speed. Similarly, the other output parameters get influenced as shown in the ANOVA table.

Regression analysis was performed for each output parameter. All the results were statistically significant for 'P' value less than 0.05. For all output parameters, the value of is greater than 50%. This indicates that the regression equations or models developed for all output parameters are acceptable.

Main effects plot in terms of means was obtained for each output parameter. Figures 4, 5, 6 and 7 show the main effects plots for length, width, pocket depth, and surface roughness, respectively.

The observation from these plots is as shown in following table (Table 3).

Table 2 ANOVA results

Parameters	Contribution on output parameters			
	Length (%)	Width (%)	Pocket depth (%)	Surface roughness (%)
Traverse speed	42.89	59.30	30.6	13.68
Water pressure	57.11	40.69	69.39	86.31

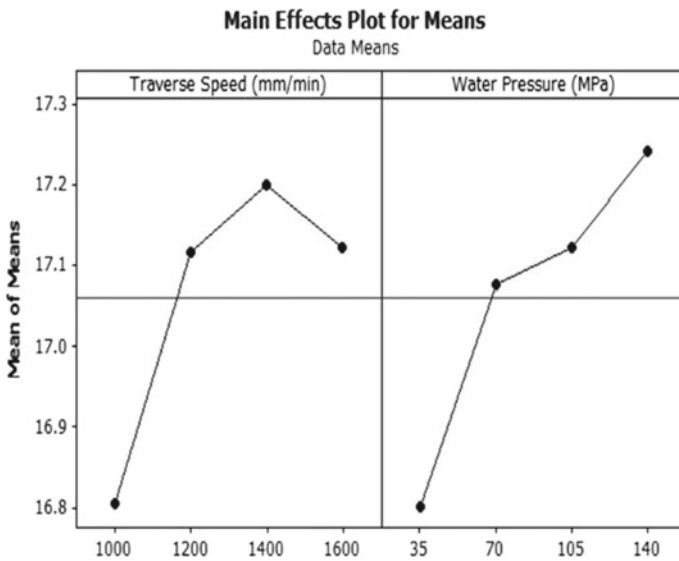**Fig. 4** Main effects plots for length in terms of mean of means

Main Effects Plot for Means
Data Means

Fig. 5   Main effects plots for width in terms of mean of mean

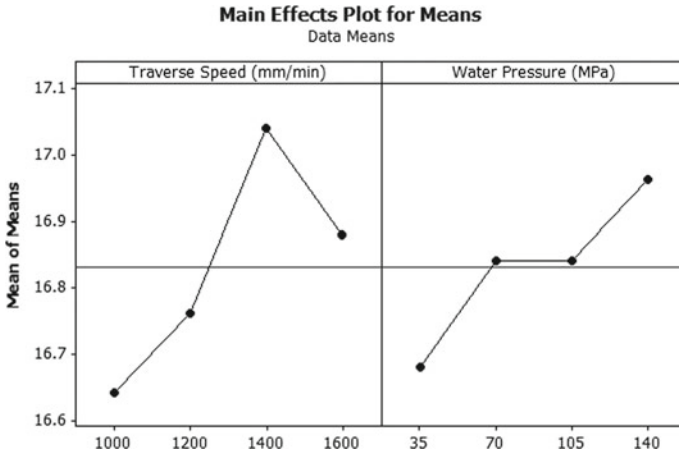**Main Effects Plot for Means**
Data Means

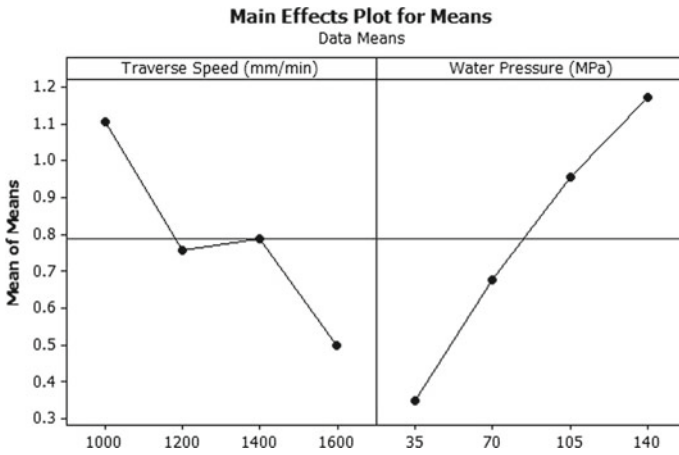Fig. 6   Main effects plots for pocket depth in terms of mean of means

Table 3   Observations from main effects plot

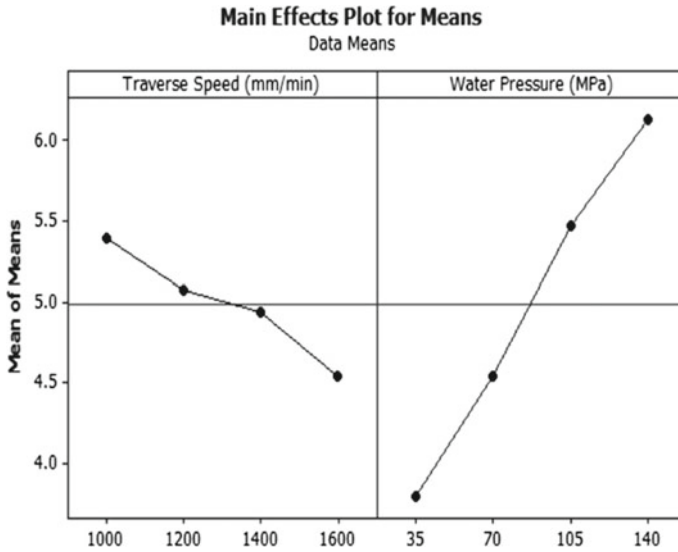| Output parameter	Observation
Length	Increased when the traverse speed was increased
Width	Increased when the water pressure was increased
Pocket depth	Decreased with the increase in traverse speed
Surface roughness	Increased with the increase in water pressure

Main Effects Plot for Means
Data Means

Fig. 7 Main effects plots for Surface roughness in terms of mean of mean

4 Conclusion

The design of experiments performed for the proposed work was successful. The ANOVA and regression analysis conducted was acceptable. Moreover, the work may be expanded by considering few more process parameters and output parameters.

References

1. Momber, A.W., Kovacevic, R.: Principles of Abrasive Water Jet Machining. Springer
2. Sreekesh, K., Dr. Govindan, P.: A review on abrasive water jet cutting. Int. J. Recent Adv. Mech. Eng. (IJMECH) **3**(3) (Aug 2014)
3. Hascalik, A., Caydas, U., Gurun, H.: Effect of traverse speed on abrasive waterjet machining of Ti–6Al–4 V alloy. Mater. Des. **28**, 1953–1957 (2007). Elissa, K.: Title of paper if known (unpublished)
4. www.specialmetals.com
5. Arola, D., Ramulu, M.: Material removal in abrasive waterjet machining of metals Surface integrity and texture. Wear **210**, 50–58 (1997). Maxwell, J.C.: A Treatise on Electricity and Magnetism, vol. 2, 3rd edn. Clarendon, Oxford, pp. 68–73 (1892)
6. Phadke, M.S.: Quality Engineering Using Robust Design. Pearson

Polypropylene Alloys and Composites—A Review

Ashish R. Thakre, R. N. Baxi and Pramod V. Walke

Abstract In the twenty-first century, composites of domestic polymer material with natural fibers are gaining considerable importance due to numerous valid reasons such as environmental protection, balancing ecosystem besides consumer demands, and allied legislation issues. Thus, the quest of manufacturing industries for generating new material is boosted tremendously. Blends and composites of polypropylene have been popularly used since about last thirty to forty years to manufacture completely innovative novel materials. These materials have combined entity characteristics of the basic module polymers. The success of these synthesized blends and composites is entirely dependent on compatibilization of the parent polymers with the additives. Improvisation in the blend morphology, enhancement in contact area adhesion, and furthermore consequently improvement in the concert service of blend are the basic outcomes of the compatibilization. Blends of polypropylene (PP) with synthetic and natural fibers are gaining special importance because they allow increment in the thermal and mechanical properties of the new material that combined with the process ability of the PP. The new material developed is definitely a cost-effective and largely being used in automotive sector besides its uses in various other industrial sectors. The mechanical properties (flexural strength, impact strength, stiffness, higher strength-to-weight ratio, and modulus) and thermal properties like heat deflection temperature are having great importance in case of polypropylene.

Keywords Polypropylene · Thermoplastic · Composites · Natural fibers · Composite fibers · Blend · Compatibilization

A. R. Thakre (✉) · R. N. Baxi · P. V. Walke
Department of Mechanical Engineering, G. H. Raisoni College of Engineering, Nagpur, India
e-mail: ashish20jan2000@yahoo.com

R. N. Baxi
e-mail: r_baxi@yahoo.com

P. V. Walke
e-mail: pramod.walke@raisoni.net

1 Introduction

Steep growth in production of polypropylene and its use is well-known during three to four decades. Polypropylene is popularly mortal use within diverse sector of diligence such as textile, chemical, electrical, automotive, household, agriculture, packing, transportation, and many more. Market consultancy and management research indicated that PP witnessed huge growth during last decade and also forecasted that demand for PP is likely to crossover its 4–5% average annual growth rate of past decade in the coming days [1].

Polypropylene (PP), one of the domestic polymeric resin materials, be the earliest artificial polymer (with ordered arrangement of pendant group) to become industrially popular. Life form higher strength-to-weight ratio and high orderliness in its crystalline structure, polypropylene shows high hardness, stiffness, and tensile strength. Thus, owing toward low density, it is far and wide replacing traditional materials in automobile sector, electrical plus domestic apparatus, furnishings industry, and casing usages and many such applications. PP is derivative of non-renewable fuel resources, and basically, it is not degradable within environment, which can core ecological hazards if not properly made to dispose. Therefore, many government and public forums communities be currently added aware regarding the impact of non-recyclable plastic on the entire earth, including its ill effects on entire ecosystem plus on top of the visual look of modern cities also barren land. Success in the production of biodegradable polymers now definitely evolved with entirely new idea of this solid dissipate board techniques since these biodegradable materials are designed in such a manner so as to degrade under normal environmental situation at the max in using low-end technology and allied solid waste treatment facilities [2].

The mixture in the form of blend of organic material such as starch and inorganic polymers is responsible in favor of this environmental imbalance. The starch is one of the constituents of these biodegradable polymers as its properties be somewhat parallel toward the petrochemical-based polymers. In plenty of cases, it has attempted to use renewable with sustainable materials on the way to arrange biodegradable PP composites to trim down its adverse environment bang. Therefore, compatibilization was done mainly through modification of PP with glycidyl methacrylate (GMA), acrylic acid (AA), maleic anhydride (MA), and groups [3]. Ease of processing is the main driving force for polypropylene (PP) being widely used commodity polymer. Cost-effective, basic crux property, and towering hurdle property toward wetness are the added features of this material. However, the limitation of the high oxygen permeability needs to be taken care in some cases. PP and nylon 6 are immiscible throughout the entire choice of composition top toward mediocre property that necessitates the requirements in favor of compatibilization. Compatibilized of polymer blends toward attain miscible blends has been broadly deliberate in excess of the preceding decade [4].

Another outcome is a raise in linkage by segment limits of generous upper-stress transport. In order to obtain this, the bonding linking between the three phases such as compatibilizing copolymer fetters. One more outcome is the prohibition of agglom-

Fig. 1 Chemical compatibilization of constituents
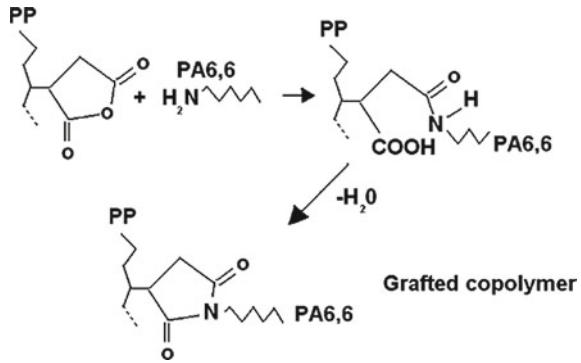
eration of the second stage via modifying the segment margin edge. It is normally common to commence compatibility among polyolefins and polyamides which are by element alterations. Carboxyl groups in the form of pendant are introduced keen on polyolefins by graft with maleic anhydride (MAH), and this forms compound link with the polyamide using the fatal amino groups as shown in Fig. 1.

The presence of a rejoinder among the nylon 6 and MAH, amino end group be proven in the chips removal of the PP, judgment of the numeral of finish group, and thermal investigation using DSC of the remains. In added advance to boost the properties of polyolefin/polyamide, blends contain the adding of acrylic acid/butyl acrylate/styrene terpolymers with the adding of nylon 6—polybutene multi-block copolymer.

2 Literature Review

The contributions of various researchers have been discussed below.

Sigdel et al. [5] explained, since it is very cost-effective, wood plastic composite (WPC) is generating a tremendous increase in the market of wood and allied composites product. Researchers made an attempt to fabricate WPCs by sawdust of pinewood flour which is otherwise treated as waste of wood/furniture diligence. In this experimentation comparatively, study of composite of PP-g-MAH and pinewood flour and composite of recycled PP-g-MAH and pinewood flour with different wt% were studied. The Composites were prepared in twin-screw extruder. Specimens were prepared in injection molding machine. Properties like tensile strength, flexural strength, hardness, and water absorption test for 2 and 24 h were carried out.

Conclusion—Tensile strength in both cases increases with increase in MAPP at 0–4%; flexural strength in both cases increases with increase in MAPP at 4 and 8%. Hardness of composite is maximum at 4% of MAPP in both cases. Water absorption is least at 8% MAPP in both composites. DSC proves that melt temperature, after incorporation of pinewood flour, remains close to that of pure material. This

paper revealed that recycled PP can be good than virgin PP with proper content of compatibilizer for reducing the cost of the product.

Future scopes—Different experimentation can be done by using wood material such as sawdust, plywood, solid wood, hardwoods, Oak wood which can be added and studied.

Aranburu and Eguiazábal [3]: Study of polypropylene (PP) as parent phase and polyamide-12 (PA12) like another binary constituent was carried out in this work by the use of compatibilization. These blends were prepared using injection molding method by adding modified 20% maleic anhydride copolymer (PP-g-MA) to the PP, manufactured by a degree graft PP (gPP). PA12 plays role of a nucleating agent and on top of the cooling crystallization of the gPP, and a one more crystallization peak of the grafted PP seen in the PA12-concentrated blend indicates the modification in the crystalline structure. This might because of change in the crystalline structure of the blends in the PA12-concentrated blends, the lucid cut enhancement in the crystallinity of the grafted PP period, which might be responsible for the enhancement in its chain longevity and also contributed in the enhancement in modulus.

Single screw extrusion was used to mix PP (80%) and MAH (20%) in this study. This grafted PP was directly mixed with PA12 in injection molded machine. Different wt% of PA12 was added to synthesize the blend in this experimentation. The compatibilized gPP/PA12 and uncompatibilized PP/PA12 blend in different wt%. The properties using DMA, DSC, SEM, and mechanical were carried out on the blends.

Conclusion—It was observed that addition of compatibilizer showed slight increase in Tg in PA12 blends. The use of compatibilizer led to a clear decrease in the particle size of PP-g-PA12. The crystallinity of the PP-g-PA12 increased significantly as in gPP it remains constant. Young modulus of the blends showed appreciable synergic manners throughout compositional range.

Suggestions/future scope—Similar type of experimentation can be done by using different polysters, for example, *polyethylene naphthalate* (*PEN*), polyethylene terephthalate (PET), *nylon 66, nylon 6, polybutylene terephthalate* (*PBT*)*, nylon 1,6, and polytrimethylene terephthalate* (*PTT*).

Gupta and Aftab [2]: Biopolymer in the form of potato starch was considered as one of the constituents and the achieve of potato starch presence on motorized. Structural property of polypropylene–starch blends enclose has been analyzed. Researchers suggested that using maleic anhydride grafted PP as coupling agent improves the bond strength involving starch and base polymer matrix since interfacial force among the two, i.e., reinforcement material and polymeric base material has through effect on the properties of blend mixture. In this experimentation, the composition of starch is assorted from 15 to 30%, and moreover, interface bonding mediator (i.e., PP-g-MA) was used as 10% in proportion. Corotating twin-screw extruder was used for compounding the blends. Various mechanical properties were evaluated. Observation stated that the tensile and impact strength remained more or less unvarying, but flexural strength of the blend enhanced by 45%, and decrease in entitlement strain amid rising starch contented in the blend was noticed [2].

Findings:

- Enhancement in mechanical properties was seen in PP and starch blending using PP-g-MAH as the coupling agent.
- The flexural strength increases in PP due to interfacial adhesion of 25% starch originate.
- Impact strength and tensile strength almost remain constant.

The same were validated using FTIR, SEM, and MFI which showed upgrading in interfacial bond between starch and polymer.

Suggestion/future scope—(1) Other bio-starches can be used such as corn starch, wheat starch, and rice starch, and properties can be observed and studied, (2) biodegradability can be measured in each case.

Kant et al. [6]: It is established fact that talc is common significant filler used pro polypropylene (PP). Use of non-halogen fire retardants with PP be real studied by researchers. It was observed that this does not generate any poisonous gas and sarcastic smoke through incineration. The flammability of PP spirit gets lowered by addition of flame retardants. Talc and PP composite in different wt% were prepared in this study. Talc is used as filler in PP. The composite be equipped with injection molding machine. Mechanical properties like tensile strength, flexural strength, and ultimate modulus were investigated in this study.

Conclusion—Flexural modulus indicated superior result for 30–50% talc-filled PP. Tensile strength increases with increase in filler %.

Suggestion/future scope—Experimentation can be done and tested by using different fillers such as silica, $CaCo_3$, clay, carbon fiber, and graphite.

Essabir et al. [7]: Composites of polypropylene (PP) combined with Nut-shells of Argan (NA) particles were prepared in this study. Researchers focused on the collective effects of equally particle size and speck load on the mechanical and thermal properties of composite. In the processing of these blends, PP and Nut-shells of Argan were prepared using compatibilizing agent based on styrene and butadiene. Three different sizes and different NA particle wt% were used for blending. Twin-screw extruder was used for processing of blends. The compatibilized PP matrix was blended by NA particles at different fiber substance by a two roll mill. Morphological and structural properties were analyzed using SEM, FTIR. Thermal analysis and mechanical testing were studied using DSC and Instron tensile testing machine, respectively.

Conclusion—With the reduction in particle size indicated clear cut enlarge in the Young's modulus. Results also showed that increase in Young's modulus is starting the apply of particles when compared to the orderly PP. Advantageous grow of 42.6, 26.7, and 2.9% at 20 wt% bit loading, for subdivision series 1, 2, and 3, correspondingly, was observed. Besides this, an extraordinary increment in the Young's modulus be seen as diminish the particle volume. The thermal constancy of composites exhibits its minor drop-off (256–230 °C).

Suggestion/future scope—

- Various other regional seeds/hard nut shells can be tested, for example, coconut shells, almond shells, rice husk, karanji seed nut shell, ground nut shell can be explored as a future scope.
- Use of Micron and nano-sizes can be studied as the future.
- Use of different interfacial agents needed to be studied.

Cerqueira et al. [8]: In this study, composite of cellulose preheated sugarcane bagasse fibers and PP were prepared with a composition of 5–20 wt% and mixed in the thermokinetic mixer. Mechanical properties, FTIR, and morphological test were carried out.

Conclusion—The composites of PP with one of the constituents as biomaterial efficiently increase in the tensile, impact strength, flexural and in comparison with the virgin polymer material.

Suggestions/future scope—Experimentation can be done by using similar fibers that obtain in our regions such as bamboo fiber, banana fiber, seed fiber, coconut fiber, and hibiscus sabdariffa fiber need to be studied for addition.

Hufenbach et al. [9]: The important outcome of this research indicates that the reinforcement using textile thermoplastic and manufacturing PP composites offers enormous relevance. Anisotropic obviously needs the detailed study of the directional dependent material properties. A multilayered flat-bed weft-knitted glass fiber/PP composite was compared amid two resources, i.e., a NCF-GF/PP composite and a woven GF/PP composite. The advantage of this novel material turns out to be so perceptible if away of plane loading is occupied on three-dimensional hassle state happen.

Suggestion/future scope—MAH-PP grafted compatibilizer can also be studied so as to compare the effect of different compatibilizer [11].

Ikai et al. [10]: Considering health hazardous effects of asbestos, PVA material was developed. But due to higher cost of PVA researchers focused the efforts to build up a confined elevated robust polypropylene. Researchers presents the towering robustness polypropylene fibers property, its built-up method, impact resistance, and mechanical presentation improved actions, compared to fiber–cement goods obtainable inside the local Brazilian market.

Suggestion/future scope—Various other reinforcement designs can be explored.

Dr. Shivnand et al. [11]: Polymer and environmental issue is great challenge for polymer industry. Awareness regarding environmental issues is promoting cost-effective. The main focus of this study is to manufacture the natural fiber composites with appropriate dispensation/manufacturing method also to verify mechanical properties while subjected to bending,

It is proved in the study that the tensile strength in addition to flexural properties increases by the increase in fiber content in the composite. Though, the tensile strength decreases after a certain percentage of addition of fibers. Compared to untreated hemp fiber, no noteworthy change in the tensile strength has been pragmatic for treated hemp fiber fortification. The flexural strength/modulus of the composite was upper compared to unadulterated polypropylene (PP) for fiber loadings.

Suggestion/future scope—Recycle PP can be used. (From the concern of environment, use of recycled PP will be beneficial besides further cost reduction.)

Srisawat et al. [12] focused on melt spun fume silica particle, crammed polypropylene (PP) string fibers which were geared up in pilot plant.

Findings—Researchers studied the SEM analysis of spun PP filament fibers with silica as additive. In the SEM images of the fiber, the morphology shows that the direct proportional of increase % silica leads to enlarge silica particle density, and at the same time, the agglomeration issue gets triggered. With low % silica loading, shear force applied during spinning seems to be effectual enough to disaggregate the silica agglomeration. It is found that catch-up speeds play a crucial job in a gain in fiber crystalline. It was observed that the range beyond (2.5 wt%) silica loading is not preferable for filler dealing out as well as measurement of fiber properties. The thermal constancy of PP fibers might be improved when filled by water repelling silica in comparison with water-loving silica. DSC analysis showed that the crystallization temperature of silica filled composite fiber was originated to be more than those of virgin PP fiber because of this sooner cooling rate, faster processing time was obtained.

Suggestion/future scope—Use of nanoparticles can be studied as the future scope.

Rezaei et al. [13]: In this literature, short carbon fiber reinforced polypropylene (SCF/PP) composite be geared up by way of melt blending and hot-pressing technique. It is observed that carbon fiber is the best reinforcement material for synthesizing PP composites since it reveals all the supreme properties. The finding leads to the fast expansion and achievement in use for many applications of these PP SCF composites over the last decade. It is publicized that a heighten in fiber extent be capable of increase in the thermal permanence of SCF/PP composites and recover the damp property to the greatest possible extent.

Suggestion/future scope—Effect of aspect ratio on different characteristics can be done.

Shashidhara et al. [4]: In this study, researchers studied blends of PPCP and nylon 6 compatibilized via accumulation (PP-g-MAH).

Study reported the use of PP (70%) and nylon 6(30%). To study the effect of PP-g-MAH on mechanical and thermal properties of N6 and PP, blend was the motto of this experimentation. PP-g-MAH has enhanced the interfacial adhesive among two constituent phases. The use of compatibilizer shows improvement in the tensile strength value. Marginal increment in the impact strength was seen. There is no noteworthy impact on the thermal properties of the blend by compatibilization [14].

Suggestion/future scope (1) Study of wear properties can be done, and (2) effect of different compatibilizer needed to be studied.

Bilewicz et al. [14]: The multi-laminar structure of polymer nano-composites performed by non-conventional practice of injection molding was observed in this study. Researchers, during this study, evolved the methodology of using DOE traditional system and fixed out with another mold externally operated using artificial intelligence and pressure machine (capacity of 150 bar hydraulic pressure). They have found out that this brings advantage of closing highly developed and added structure during manufacturing. Nano-composites of PP with formed layered struc-

ture on nano- and micro-level are certainly the domestic polymer PP thus transformed into high concert engineering materials with notable escalation and with interests and rising branch in core science and applied science.

Injection molding of PP Ferromatik Milacron k-85 equipped with shear controlled orientation in injection molding (SCORIM) was studied by varying the process parameters such as melt temperature, stroke time, and stroke number. Thus, conventional injection molding and non-conventional injection molding of PP were compared in this study. Self-reinforced composite was resulted by non-conventional injection molding. This resulted in improvements in mechanical properties. This method can be competently used to get high recital nano-composites lacking pretreatment. Morphological study was carried out in this work.

Suggestion/future scope—TEM studies can be done of morphological aspects of the multi-laminar PP composites in the advanced direction.

Hua et al. [15]: Filler material is important as one of the additives in the plastic component manufacturing resin materials. Evaluation of the flow and mechanical properties of filled wood flour in PP/PET blend in the form of wood plastic composites is objective of this study. (PP/PE) blends be grafted with (MAH) to improve the interfacial union. The fluid flow properties were premeditated by use of energetic quantity. Corotating twin-screw extruder was used to process PP/PE blend (80/20) and wood fiber composites. MAH and dicumyl peroxide were used as compatibilizer (10:1). The addition of MAH resulted in the enhancement of mechanical properties.

Improvements in mechanical properties were noticed. Wood fiber has numerous inbuilt return above conformist reinforcing materials such as profusion, expenditure effectiveness, and lighter in weight.

Future Scope—CFD analysis can be done.

Khalid et al. [16]: Biodegradable plastics are in tremendous demand. In this work, cellulose was consequent as of oil palm empty fruit bunch fiber (EFBF) by customary ASTM D1104 method. This cellulose and EFB fibers were compounded in various ratios up to 50 wt% with polypropylene (PP) using Brabender twin-screw compounder. The tensile strength and flexural modulus of cellulose are much more on privileged side than EFBF composite.

Future Scope—(1) Similar type of experimentation can be done by using different biomaterials (which are commonly being grown in the respective geographical regions) like bamboo fibers, etc. (2) It has been observed from the research that if suitable coupling agent be used then mechanical properties may be further improved.

Sarami et al. [17]: Blend of polypropylene (PP) and polyethylene terephthalate (PET) was prepared screw extruder. Fiber configuration subsequently was passed out all the way through the spinneret. PP-*g*-GMA was used as catalyst. The belongings of PET content and PP-*g*-GMA as a compatibilizer be too analyzed systematically. The properties mechanical and morphology of compatibilized and uncompatibilized PP/PET fibers be broadly studied and utilized analytical tools such as (SEM) and tensile testing machine. Fibers from PET and PP blends were prepared using reacting and non-reacting additives such as PP-G-MAH.

Future scope—Effect of different processing parameters such as screw geometry and barrel temperature can be altered in this study.

Viana et al. [18]: Effect of process parameters on morphology and mechanical properties of an injection molded poly(ethylene terephthalate), PET, was reported in this study. Standard tensile specimen of PET prepared in injection molding at different temperature. This specimen was characterized by thermomechanical environment, WAXS, DSC, hot recoverable strain test, and mechanical characterization.

Future Scope—(1) Variation in the mold temperature upon crystallization kinetics (which is contributing in the production of perform during molding) can be studied for blends of PET-PP. (The same can be compared in compatibilized and in uncompatibilized case.) (2) Crystallization kinetics of PP can be studied by similar variation of mold temperature near its glass transition temperature (in order to relate processing and morphology development in respective cases.)

Somit Neogi et al. [19]: Wear characteristics of polypropylene (PP) isotactic, polyethylene terephthalate (PET), and their blends evaluated in this study. Blends of PP and PET with different composition were prepared. The sliding wear of the test specimen as a meaning of applied pressure and composition in dry condition next to a stainless steel counter face was studied. Researchers suggested that wear rate decrease with the adding of PET in the blend. The morphology and worn surface of PP/PET blends were studied.

Future Scope—(1) Further mechanical properties can be studied. (2) Effect of compatibilizers for enhancement of properties can be further explored.

Afshari et al. [20]: Investigation of ternary blend of nylon 6 (N6), polypropylene (PP), and polypropylene grafted maleic anhydride (PP/N6/PP-g-MAH) as compatibilizer with 50% of nylon 6 was done by the researchers. Increase in size of discrete nylon 6 droplets lead to a reduction in viscosity. The amount of PP-g-MAH in 80/20 blends increased.

Future Scope—Correlation of the properties which are identified that further needed to be investigated.

Conclusion—Worldwide growing environmental consciousness is cheering scientific follow a line of investigation into the progress of cost-effective, environmentally welcoming, and added sustainable polymeric material for multiple usages. The research by various authors in the field of polypropylene-based alloys and composites has been more demand in bio-composite and natural fibers. The various properties like mechanical and thermomechanical have been analyzed, and still there is ample amount of gap which is identified in the form of the future scope in the literature reviewed.

References

1. Growth opportunities for PP resin in the Global Composite Industry.: Luncintel, Market research and management consulting (2016)
2. Gupta, A.P., Aftab A.: Study of flexural, tensile, impact properties and morphology of potato starch/polypropylene blends. Int. J. Adv. Res. **2**(11) 599–604 (2014)
3. Aranburu, N., Eguiazába.J.I.: Improved mechanical properties of compatibilized polypropylene/polyamide-12 blends. Int. J. Polym. Sci. Article ID 742540, p. 8 (2015)

4. Shashidhara, G.M., Biswas, D., Pai, B.S., Kadiyala, A.K., Feroze, G.W., Ganesh, M.: Effect of PP-g-MAH compatibilizer content in polypropylene/nylon-6 blends. Polym. Bull. **63,** 147–157 (2009). https://doi.org/10.1007/s00289-009-0074-7

5. Sigdel, D.D., Dr. Giri, R.: Study on pinewood/recycled polypropylene composite, IJARIIE-ISSN (O)-2395–4396, **2**(4), 186–191, 2016

6. Kant, S., Urmila, J.K., Pundir, G.: Study of talc filled polypropylene—a concept for improving mechanical properties of polypropylene **02**(04), 411–415 (2013)

7. Essabir, H., Hilali, E., Elgharad, A., El Minor, H., Imad, A., Elamraoui, A., O.Al Gaoudi.: Mechanical and thermal properties of bio-composites based on polypropylene reinforced with Nut-shells of Argan particles. Mater. Des. **49**, 442–448 (2013). http://dx.doi.org/10.1016/j.matdes.2013.01.025

8. Cerqueiraa, E.F., Baptistab, C.A.R.P., Mulinaria, D.R.: Mechanical behaviour of polypropylene reinforced sugarcane bagasse fibers composites. Procedia Eng. **10**, 2046–2051 (2011). https://doi.org/10.1016/j.proeng.2011.04.339

9. Hufenbach, W., Böhm, R., Thieme, M., Winkler, A., Mäder, E., Rausch, J., Schade, M.: Polypropylene/glass fibre 3D-textile reinforced composites for automotive applications. Mater. Des. **32,** 1468–1476 (2011). https://doi.org/10.1016/j.matdes.2010.08.049

10. Ikai, S., Reichert, J.R., Rodrigues, A.V., Zampieri, V.A.: Asbestos-free technology with new high toughness polypropylene (PP) fibers in air-cured Hatschek process. Constr. Build.Mater. **24**, 171–180 (2010)

11. Dr.Shivnand, H.K., lnamdar, P.S., Sapthagiri, G.: Evaluation of tensile and flexural properties of hemp and polypropylene based natural fiber composites. In: 2nd International Conference on Chemical, Biological and Environmental Engineering (ICBEE 2010), 978-1-4244-8749-3/10/$26.00 © 2010 IEEE, pp. 90–95 (2010)

12. Srisawat, N., Nithitanakul, M., Srikulkit, K.: Characterizations of fibers produced from polypropylene/ silica composite. J. Metals Mater. Mine. **19**(1), 53–58 (2009)

13. Rezaei, F., Yunus, R., Ibrahim, N.A.: Effect of fiber length on thermomechanical properties of short carbon fiber reinforced polypropylene composites. Mate. Des. **30**, 260–263 (2009)

14. Bilewicz, M., Dobrzański, L.A., Viana, J.C.: Morphological aspect of multilaminar PP composite. J. Achiev. Mater. Manuf. Eng. **37**(02), 598–606 (2009)

15. Gao, H., Song, Y-M., Wang, Q.-W., Han, Z., Zhang, M.-L.: Rheological and mechanical properties of wood fiber-PP/PE blend Composites. J. For. Res. **19**(4), 315−318, (2008). https://doi.org/10.1007/s11676-008-0057-9

16. Khalid, M., Ratnam, C.T., Chuah, T.G., Ali, S., Thomas S.Y., Choong, Y.: Comparative study of polypropylene composites reinforced with oil palm empty fruit bunch fiber and oil palm derived cellulose. Mater. Des. **29**, 173–178 (2008)

17. Sarami, R., Kashani, M.R.: Study of polypropylene/polyethylene terephthalate blend fibres compatibilized with glycidyl methacrylate. Iran. Polym. J. **17**(4), 243–250 (2008)

18. Viana, J.C., Alves, N.M., Mano, J.F.: Morphology and mechanical properties of injection molded poly(Ethylene Terephthalate). Polym. Eng. Sci. **44**(12), 2174–2184 (2004)

19. Neog, S., Hashmi, S.A.R., Chand, N.: Role of PET in improving wear properties of PP in dry sliding Conditio. Bull. Mater. Sci. **26**(6), 579–583 (2003)

20. Afshari, M., kotek, R., Haghighat, M., Dast, H.N., Gupta, B.S.: Effect of blend ratio on bulk properties and matrix- fibril morphology of polypropylene/nylon 6 polyblend fibres. Polymere **43**, 1331–1341 (2002)

Experimental Study on the Performance of Standing Wave Thermoacoustic Refrigeration System

Ashish S. Raut, Uday S. Wankhede and S. N. Ramteke

Abstract This paper presents the experimental study on the thermoacoustic refrigeration system performance with respect to specific critical operating factors. Experimentations were carried out upon the thermoacoustic refrigeration system under different operational conditions. The experimental setup consists of 3D printed stack to obtain better cooling effect. Substantial aspects which impact on the performance of the system were identified. The results show that the performance of system was improved.

Keywords Thermoacoustic refrigerator · 3D printed stack · COP

1 Introduction

Nowadays it is very much important to design and develop the environmental friendly refrigeration systems, to avoid global warming and ozone layer depilation effect. Along with that it should abolish the usage of environment harmful refrigerants; many researchers are further concentrating and applying efforts to develop the substitute working fluids (refrigerant) and also various alternate refrigeration technologies. Approaching in various kind of alternate technology is the thermoacoustic refrigeration system and that creates refrigeration effect commencing sound (acoustic). Thermoacoustic is study which concentrated on interaction of acoustic and thermodynamics. Acoustic or sound waves have the coupled pressure and oscillation displacement. These acoustic waves drive the gas parcel and interact with the boundaries which effect the alteration of thermal effect. Thermoacoustic effect which is the

A. S. Raut (✉)
G. H. Raisoni College of Engineering, Nagpur 440016, India
e-mail: ashish.raut.ytl@gmail.com

U. S. Wankhede
Government College of Engineering, Chandrapur 442402, India

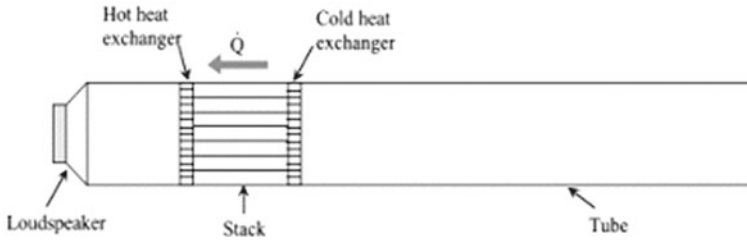S. N. Ramteke
VMF, Nagpur 440014, India

Fig. 1 Thermoacoustic refrigerator

energy alteration of acoustic or sound work engaged to transportation of heat (thermoacoustic refrigerator) shown in Fig. 1; on the other hand, the conversion provided heat energy into acoustic or sound (thermoacoustic engine).

The thermoacoustic refrigerator or cooler alters the acoustic standing wave into gradient of temperature. Thermoacoustic refrigeration system contains the resonator tube, associated with loudspeaker or acoustic signal generator and filled with inert gas medium. Two heat exchanger and stack are placed inside the resonator. The acoustic signal generator creates an acoustic standing wave at the essential frequency which interacts with a porous medium known as stack. In general, stack geometry is parallel plates, and it is manufactured with Mylar. The working fluid (gas) within tube (resonator) of thermoacoustic refrigeration system relates thermodynamically through the plates of stack, associated properly to path of pulsation of acoustic standing waves backing by working gas. Two notable properties which product as of interaction among acoustic waves and compact periphery of plates of stack are immersion of acoustic power near to apparent of plates as well as a heat flux at exterior of plates in the route of sound pulsation.

2 Literature Review

Swift [1, 2] recognized the primary calculations in addition perceptions intended for thermoacoustic concept in addition to the primary history of thermoacoustics. Jebali et al. [3] deliberate the effectiveness of thermoacoustic refrigeration system lay open to flexible load. Hot side heat exchanger of the arrangement was kept by the side of atmospheric temperature by circulating water, whereas the temperature of cold side heat exchanger was wide-ranging toward attain some amount of temperature variances beside of stack. The refrigerating capacity was calculated for these temperature variances despite the fact of variable working frequency. Design of involvement of advance and motionless influences in addition to loss on thermoacoustic flow of heat remained implemented. Outcomes from experimentation indicated that the stack both end temperature deviation along with that the operating frequency is directly affect

over refrigerating power. On resonance frequency, the highest refrigeration effect was obtained.

Bai et al. [4] explored consequence of inert gas (working fluids), length of resonator tube, thermoacoustic refrigeration system initial pressure (charging pressure) and temperature of heat exchangers, and its effects on the system performance. During the experimentation, Bai et al. not considered variable cooling load effect on thermoacoustic system performance. Zhou et al. [5] utilized wire mesh of copper as a stack in his study and examine whole system performance on the basis of operating frequencies, copper mesh stack length and mesh size, charging and dynamic pressure, and the operating fluid. By means of boundary layer, approximation for short stack optimization in design was done by Wetzel and Herman [6–8]. During the study on thermoacoustic system, high-speed cinematography and holographic interferometry blend were used to find the thermoacoustic effects on stack. Along with that operating fluid communication with stack also investigates and design steps summary was given for additional study. A mathematical study on thermal stratified movement in the vicinity of stack was done by Worlikar et al. [9–11]. Along with that nearby the heat exchanger effect of energy flux density was studied for design of heat exchangers. Belcher et al. [12] elaborate most suitable inert gases (working fluids) in thermoacoustic refrigeration system.

3   Experimental Setup

The heart of thermoacoustic system is the stack, whatever thermoacoustic phenomenon happens that happen in stack only. This porous medium experiences maximum losses due to viscous resistance and thermal losses. The stack material has an important as the specific heat capacity and thermal conductivity of stack material having vital part in heat transmission process. The effectiveness of the thermoacoustic refrigeration system is exact reliant on the performance of stack [13]. Which also depends upon the stack length L_s, its center position x, spacing among the two layers y_o, and this is depending upon the δ_k (thermal penetration depth) and δ_v (viscous penetration depth). As the stack has very much importance and in general stack is manufacture with Mylar and with parallel plate or spiral geometry, which having many losses, so to avoid it in this study stack is fabricated with 3D printing technology to achieve the accurate dimensions, also the PLA is use as a stack material, which having better thermo physical properties than Mylar.

The thermoacoustic refrigerator system effectiveness is obtained through coefficient of performance which is nothing but relationship among cooling power to acoustic (sound) work delivered to stack. Tijani et al. [14] defined in his study the acoustic power, $W_n = W/\text{pmaA}$ and normalized cooling power $Q_{cn} = Q_c/\text{pmaA}$. To obtain the efficient resonator tube design, the length parameter $\lambda/4$ was implemented; however, to create an open end situations in system instead of spear buffer, the cone type shape buffer was used. The resonator tube comprises large and small diameter portion. For slightest energy losses relationship among the small and large

tube diameters was 0.45. The other physical quantity measuring instruments was also attached to experimental setup at various locations such as temperature measurement by thermocouples, charging pressure and fluctuating pressure by pressure measuring sensors, operating frequency was generated by frequency meter, etc.

$$Q_{cn} = \frac{\delta_{kn} D^2 \sin 2x_n}{8\gamma(1+\sigma)\wedge} \times \left(\frac{\Delta T_{mn} \tan x_n}{(\gamma-1)BL_{sn}} \frac{1+\sqrt{\sigma}+\sigma}{1+\sqrt{\sigma}} - 1 + \sqrt{\sigma} - \sqrt{\sigma}\delta_{kn} \right)$$

$$W_n = \frac{\delta_{kn} L_{sn} D^2}{4\gamma}(\gamma-1)B\cos^2 x_n \times \left(\frac{\Delta T_{mn} \tan_{xn}}{BL_{sn}(\gamma-1)(1+\sqrt{\sigma})\wedge} - 1 \right)$$

$$- \frac{\delta_{kn} L_{sn} D^2}{4\gamma} \frac{\sqrt{\sigma} \sin^2 x_n}{B\Lambda}$$

4   Result and Discussion

Experimentation was carried out under several working environments such as variable frequency, variable charging pressure, different stack geometry and materials, and operating gas, etc. The resonance frequency of resonator is finding out by giving a frequency sweep. The value of resonance frequency found by experimentally is 474 Hz. This resonance frequency value is near to the design frequency 500 Hz. In same way, experimentations done at various charging pressure so as to confirm that the resonance frequency are independent of working gas pressure. For the measurement of cooldown temperature, experimentation was carried out. The thermoacoustic refrigerator is run at the resonance frequency and 20 W of electrical power input. To understand the influence of charging pressure on cooldown, the experimentation is done at various charging pressure such as 2, 4, 6, 8, and 10 bar. To avoid heating of acoustic driver, at different charging pressure, experimentation is carried out for 30 min, after each run, the electric power is switch off, so that the cold end temperature reach to atmospheric temperature.

The cooldown curves for different charging pressure are shown in Fig. 2. When the acoustic driver is switched on, there is a rapid formation of temperature gradient across the stack due to thermoacoustic enthalpy flow. The stack end closer to acoustic driver (pressure antinode) begins to heat up while the other end (near pressure node) begins to cool down. It is observed from the cooldown curve that after starting the experimentation, a quick reduction in temperature is observed up to first eight minutes for all charging pressure, the curve is smooth, and then suddenly slight temperature rise in all curve; then, in next ten minute, temperature drop is found but curves are not smooth. And in last ten minutes, it is found that the temperature reduction rate is very slow or become constant. The influence of charging pressure can also be seen, the cold end temperature is lower for higher value of charging pressure and low for low charging pressure. The reason behind this is $\Gamma \ll 1$, which causes very high thermoacoustic enthalpy flux to flow within stack commencing cold side to hot side. In other words, the reason behind this is at high charging pressure, the working
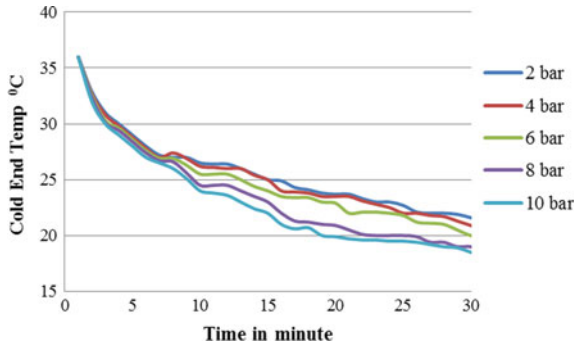
Fig. 2 Cool-down curve

fluid displacement is also high which enhance the heat transfer rate, similarly at low charging pressure the heat transfer rate is low.

The experimentation conducted to find out the temperature difference among the cold heat exchangers and hot heat exchangers for different frequency. For this test, the charging pressure is 10 bar, time duration 3600 s, and the waged fluid is helium. Test is conducted for different frequency such as 200, 300, 400, 474, and 500 Hz. For each frequency test, the acoustic driver run for 3600 s and temperature is note down for both heat exchangers; then allow heat exchangers to reach up to the atmospheric temperature, and then, next frequency test run is conducted.

It is observed from Fig. 3, at the beginning 200 and 300 Hz frequencies create near about same temperature difference, and near about 480 s, it is observed that the both frequencies temperature gradient difference varies but temperature gradient path is near about same. Whereas 400 Hz frequency also follows the same path; but at the end of 3600 s, all three frequencies having different temperature difference, which is shown in Fig. 4 The design frequency 500 Hz and the experimentally found optimum frequency 474 Hz creates maximum temperature difference at the beginning and then after its rate of temperature difference reduces. Both frequencies having the same path of temperature gradient, but at the end of 600 s, the optimum frequency creates maximum temperature difference among all other frequencies till the end to experimentation.

The stack material and stack geometries having directly impact on the performance of thermoacoustic system. Till date various researchers utilized Mylar as stack material, because of fabrication difficulties and Mylar available in sheets, many researchers developed only spiral and parallel stack. Also it is very difficult to fabricate the stack with desired dimension with conventional machining process. In this study, the stacks are manufactured with 3D printing technology, it will help to develop stack in different shapes and in desired dimensions with high accuracy.

To find the effect of various stack geometries on the performance of thermoacoustic refrigerator, various types of stack geometries are fabricated with the help of 3D printing technology such as spiral, parallel, mesh, circular, honeycomb, etc. and tests
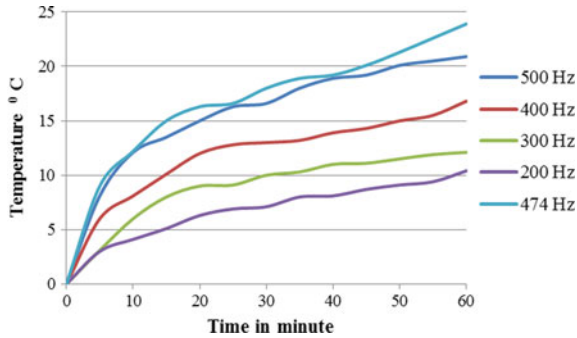
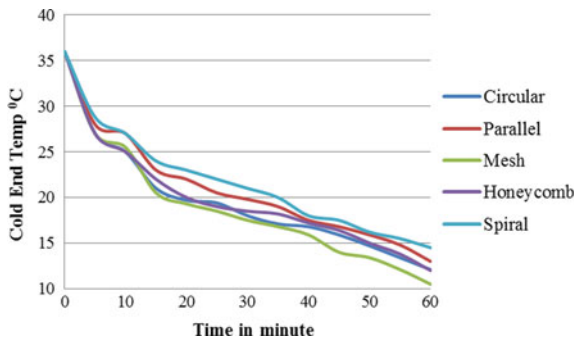**Fig. 3** Temperature difference versus operating frequency

Fig. 4 Effect of different stack geometries

are conducted in same environment for different geometries. Figure 4 displays the results achieved from the tests. From Fig. 4, it is clearly shown that the mesh type stack geometry obtained the lowest temperature during test. Whereas the honeycomb and circular stack are just above than the mesh type stack result, and the most commonly used stacks spiral and parallel having high temperature as compared to mesh stack. The reason behind this is the stack geometry (mesh), where the optimum value of δk and δv was obtained. Also the heat exchangers geometry is similar to stack and because of this the acoustic wave is not disturbed, so the thermoacoustic refrigerator produces maximum cooling.

5 Conclusion

The operating parameters that govern the performance of a given configuration of thermoacoustic refrigerator are the charging pressure of the working medium, the driving frequency, the dynamic pressure, and the mean temperature. In standing wave thermoacoustic refrigerator, the attainable cold temperature and the cooling power

crucially depend on the dynamic pressure and operation near the resonant frequency of the system. In addition, off-resonance operation hampers the dynamic pressure drastically and hence is detrimental to the system performance. Along with those results shows that the 3D printed stack enhance the performance of system, also the stack material and stack geometries play very important role.

References

1. Swift, G.W.: Thermoacoustic engines. J. Acoust. Soc. Am. **84**(4), 1145–1180 (1988)
2. Swift, G.W.: Thermoacoustics: A Unifying Perspective for some Engines and Refrigerators. Acoustical Society of America, New York (2002)
3. Jebali, F., Lubiez, J.V., Francois, M.X.: Response of a thermoacoustic refrigerator to the variation of the driving frequency and loading. Int. J. Refrig. **27**, 165–175 (2004)
4. Bai, X., Jin, T., Chen, G.B.: Experimental study on a thermoacoustic prime mover. In: Proceedings of the 1998 conference on cryogenics and refrigeration, ICCR, Hangzhou, China, pp. 522–525 (1998)
5. Zhou, S., Matsubara, Y.: Experimental research of the thermoacoustic prime mover. Cryogenics **38**(6), 813–822 (1998)
6. Wetzel, M., Herman, C.: Design optimization of thermoacoustic refrigerators. Int. J. Refrig. **20**(1), 3–21(1997)
7. Wetzel, M., Herman, C.: Experimental study of thermoacoustic effects on a single plate—part 1. Heat Mass Transfer **36**(1), 7–20 (2000)
8. Wetzel, M., Herman, C.: Experimental study of thermoacoustic effects on a single plate—part 2. Heat Mass Transfer **35**(6), 433–441 (1999)
9. Worlikar, A.S., Knio, O.M.: Numerical simulation of a thermoacoustic refrigerator I—unsteady adiabatic flow around the stack. J. Comput. Phys. **127**, 424–451 (1996)
10. Worlikar, A.S., Knio, O.M., Klein, R.: Numerical simulation of a thermoacoustic refrigerator II—stratified flow around the stack. J. Comput. Phys. **144**(2), 299–324 (1998)
11. Worlikar, A.S., Knio, O.M.: Numerical study of oscillatory flow and heat transfer in a loaded thermoacoustic stack. Numer. Heat Transfer A: Appl. **35**(1), 49–65 (1999)
12. Belcher, J.R., Slaton, W.V., Raspet, R., Bass, H.F., Lightfoot, J.: Working gases in thermoacoustic engines. J. Acoust. Soc. Am. **105**(5), 2677–2684 (1999)
13. Raut, A.S., Dr. Wankhede, U.S., Dr. Walke, P.V.: Design and optimization of stack for eco-friendly thermoacoustic refrigeration system. Int. J. Sci. Technol. Eng. **4**(6), ISSN (online): 2349-784X, pp. 21–27 (2017)
14. Tijani, M.E.H., Zeegers, J.C.H., De Waele, A.T.A.M.: Design of thermoacoustic refrigerators. Cryogenic **42**, 49–57 (2002)

Roadmap for Lean Implementation in Testing Laboratory

Vijayshri Mahobiya, Santosh B. Jaju, D. J. Tidke and Ramesh R. Lakhe

Abstract Accuracy in result is the main feature of any testing laboratories. Accurate result and timely report not only useful to make decision but also helps to laboratory to remain competitive in the market. Elimination of nonvalue added activity is important to obtain accurate and timely result. This paper addresses the lean wastes occur in testing laboratory. Also suggest roadmap for lean implementation in testing laboratory. Case study shows that application of lean manufacturing tools is able to eliminate nonvalue added activities also provide not only faster process but also gain customer satisfaction.

Keywords Lean manufacturing · Lean wastes · Lean tools · Road map · Testing laboratory

1 Introduction

In today's era, clinicians reliance on laboratory test results to make decisions is increasing and as a result testing laboratories have assumed great importance in healthcare services [1]. Nowadays laboratory is committed to providing clients with high-quality laboratory testing which results in improving patient care and employee safety. Implementation of lean manufacturing will facilitate achievement of this objective. This paper aimed at enhancing the performance of testing laboratory

V. Mahobiya (✉)
G. H. Raisoni College of Engineering, Nagpur, India
e-mail: vmahobiya20@gmail.com

S. B. Jaju
Department of Mechanical Engineering, G. H. Raisoni College of Engineering, Nagpur, India

D. J. Tidke
Anand Mine Tools Pvt. Ltd., Nagpur, India

R. R. Lakhe
Director Shreyas Quality Management System, Nagpur, India

through lean manufacturing. It also provides framework as to how lean manufacturing can be implemented to testing laboratory for performance improvement.

2 Review of Related Work

According to oxford dictionary, lean means 'efficient'. The term was coined by John Krafcik who was working on the International Motor Vehicle Programme (IMVP). The term entered the management lexicon via Krafcik's [2] Sloan Management Review article when it was used to describe the Toyota Production System [3]. Book Machine that changes the world made lean popular. Lean manufacturing more focuses on waste elimination. Waste can be defined as nonvalue activity that does not contribute in terms of profit or customer does not pay for it. Basic mura are eight types but one more waste include by some authors is Complexity/Unevenness Mura [4–6]. Complex solutions tend to produce more waste and are harder for people to manage. Re-prioritization is defined as starting one task, being interrupted (phone, e-mail, page), and changing to another task before the first task is completed by Mayo Medical Laboratories 2007. To eliminate these wastes, lean showcase offered many tools and techniques which can improve productivity result quality, reduces lead time, and obtain better operational control.

Large pool of tools contains more than 100 different tools, each having a specific focus [7]. Synergistic benefits can often be achieved using a combination of tend to combine tools to improve the overall performance of the organization performance improvement initiatives [8, 9]. Many Practitioner [10, 11].

3 Lean Performance Measurement Framework

The success of lean requires a consistent and repeatable methodology for implementation. Anita Susilawati et al. [12] include hierarchical levels of organization and multiple criteria for the lean manufacturing practice performance indicators. Based on the theoretical frame of reference of lean, it was decided that five criteria of lean laboratory performance measures would be adopted in this study: lead time, waste reduction, customer satisfaction, on time delivery, and safety. Table 1 describes the criteria, measures its description along with source. Proposed roadmap consists of 5 phases more or less follows the lean principle and is applicable for testing laboratory.

First phase is conceptual, which helps to identify customer voice and the need of lean manufacturing. Second phase is situation analysis, as the name suggests it helps to understand the present condition of the system. VSM tool is introduced in this phase. Next phase is implementation design. It has SWOT analysis and FSM to identify tools and target. The implementation phase provides waste-free system by applying tools. Last phase is evaluation, in this phase evaluate the performance and as a output gain the confidence and efficient and productive system. The approach

Table 1 Criteria for performance measure

Criteria	Measures	Description	Source
Lead time	Talk time, cycle time	The time between the initiation and completion of the process	Anand et al. [13], Shah and Ward [14], Fullerton and McWatters [15]
Waste reduction	Over production, waiting, inventory	Eliminate the nonvalue added activity	Anand et al. [13], Ahlstrom [16], Portioli-Staudacher [17], Selau et al. [18]
Customer satisfaction	Customer demand, no of referees	How services supplied by the laboratory meet or surpass customer expectation	Womack and Jones [19], Escobar and Revilla [20], Carlborg et al. [21]
On time delivery	No of report deliver with in promise time	Sample/report/result deliver on date to be promised	Anand et al. [13], Cua et al. [22], Shah and Ward [14], Womack and Jones [19]
Safety	No of accidents	Control of the recognized hazards in order to achieve an acceptable level of risk	Anand et al. [13], Brown and O'Rourke [23]

behind this framework is to identify similarity between manufacturing and laboratory. Table 2 shows the description of roadmap for lean implementation.

4 Case Study

ABCD testing laboratory was established in the year 1958 under societies registration act XXI of 1860. ABCD testing laboratory is committed for excellence in R&D in Environmental Science and Engineering Research and related services to Government, Industry and Society. For analyses of various parameters in water samples, carry out its testing activities in such a way, so as to meet the requirements of International Standard and to satisfy the needs of the customers. During certification, management felt that the arrangement of the laboratory includes extra process time, increase searching time, efforts, and also cause of accident. Management of laboratories is committed to the development and implementation of the management system and continually improving its effectiveness. To achieve the target, it needs to identify the waste or problem area in the system. This they do through lean manufacturing.

Table 2 Description of roadmap for lean implementation

Phase	Steps	Input	Effect	Out put
Conceptual	✓ Identify the need of lean ✓ Decide the target/objective ✓ Building Lean Expert Team ✓ Training for lean implementation ✓ Prepare check list	Customer need, lean team, training, check list	Understand the need of lean in customer terms	Value, target, work force, knowledge of lean
Situation analysis	✓ Data collection (list of equipment, present process ✓ Review lesson learned on lean ✓ Collection of data (time, information, sample flow) ✓ Current process mapping (VSM) ✓ Identify waste	VSM	Unhide waste, identify area of improvement	Understand the present situation
Implementation design	✓ Categories the waste ✓ Waste analysis ✓ Identify tool for elimination of waste ✓ Analysis for applying Lean ✓ Documenting the current state map ✓ Future state map(with decided target)	SWOT analysis FSM	Helps to decide tools, target	Tools, target
Implementation	✓ Apply 5S concept ✓ Design lean tool implementation ✓ Training ✓ Evaluation the implementation ✓ Lean implementation document ✓ Standardize the Lean Practice	5S, lean tools	Organize work place, remove waste	Organized work place, waste-free system
Evaluation	✓ Lean implementation document ✓ Standardize the Lean Practice ✓ Expanding lean practices ✓ Decide new target ✓ Continues evaluation of performance	Lean document Compare after and before situation	Standardize process	Improvement Efficiency, confidence Competitive-ness

5   Research Methodology

To achieve the desired improvement, it is important to unhide and eliminate the nonvalue added activates. Testing laboratory follows the steps monitioned in the framework for implementation of lean manufacturing in. It includes Building Lean Expert Team and Training, identify the need of the laboratory, visual inspection, process flow chart, value stream mapping, identify nonvalue added activity, method for elimination of wastes, and corrective measures.

6   Analysis and Results

Team member collects all the information. This process needs lots of correction and detailed concern. Many software are available to draw VSM but pencil paper is best way to draw it. When compile all the collect data in trams sequence of the operation, required time to finish respective operation. lead time of testing process 244 min. According to the current state map, the total value added time, such as testing and pretesting, is only about 189 min. In this case study, the current state map was reviewed and discussed with the process team. During the discussion, the team identified numerous nonvalue added activities and waste. Carefully analysis of the work place shows that undefined testing area creates problem and some time it creates the chances of accident. Searching material, unorganized laboratory, poor maintains are the causes of nonvalue added activity and accident. After analysing all the factors, the lean event team suggested tools. After carefully analysis, it is suggested that new laboratory arrangement is required. Existing layout has no specific areas like hot area dry are and wet area. The lean event team also suggested that the laboratory apply 5S, Poka-Yoke, Visual Management, Training, and Kaizen. Once all tools are applied successfully, next step is to evaluate the performances of the laboratory by comparing the data to be collected after one year. This lean transformation required time and brain storming. After one year, statistical data are collected. Table 3 shows the comparison of the key performance before and after implementation. After lean implementation, lead time decreased by 39 min. The target of lean manufacturing is to remove wastes, and it is achieved by eliminated 18 wastes. Customer satisfaction in terms of demand is increased.

7   Conclusions

Proposed systematic procedure here extends this concept to transform laboratory into lean laboratory that has customer-triggered working processes, faster and systematic task tracking, and reduced costs due to a reduction in nonvalue added activities. After implementation of suggested lean manufacturing frame work, positive results were

Table 3 Comparison of key performance before and after lean implementation

PI	Description	Before	After	Out put
Lead time	Time between sample enter to deliver report	244	205	Value, target, work force, knowledge of lean
Waste reduction	No of waste eliminate	18	0	Understand the present situation
On time delivery %	Report to be deliver in promise date	53	80	Tools, target
Customer satisfaction	Demand increase	366	408	Organized work place, waste-free system
Safety	No of accident	3	0	Safety

gained. Future study can be carried out in developing a generalized field database model for improving performance of the testing laboratory.

References

1. Forsman, R.W.: Why is the laboratory an afterthought for managed care organizations? Clin. Chem. **42**(5), 813–816 (1996)
2. Krafcik, J.F.: Triumph of the lean production system. MIT Sloan Manag. Rev. **30**(1), 41 (1988)
3. Samuel, D.E.: Exploring UK lean diffusion in the period 1988 to. Doctoral dissertation, Cardiff University (2011)
4. Thakur, A.: A review on lean manufacturing implementation techniques: a conceptual model of lean manufacturing dimensions. REST J. Emerg. Trends Model. Manuf. **2**(3), 62–72 (2016)
5. Rajesh Kumar, M., Metha, D., Metha, N.K.: Lean Manufacturing practices: problems and prospects. Faculty of Engineering - Hunedoara, Romania Tome X. Fascicule 3, pp. 119–124 (2012)
6. Dutta, E.A.B., Banerjee, E.S.: Review of lean manufacturing issues and challenges in manufacturing process. Int. J. Res. Bus. Manag. **2**(4), 27–36 (2014)
7. Laursen, M.L., Gertsen, F., Johansen, J.: Applying lean thinking in hospitals-exploring implementation difficulties (2003)
8. Gowen III, C.R., McFadden, K.L., Settaluri, S.: Contrasting continuous quality improvement, Six Sigma, and lean management for enhanced outcomes in US hospitals. Am. J. Bus. **27**(2), 133–153 (2012)
9. Sánchez, A.M., Pérez, M.P.: The Use of lean Indicators for Operations Management In services. Int. J. Serv. Technol. Manag. **5**(5–6), 465–478 (2004)
10. Koning, H., Verver, J.P., Heuvel, J., Bisgaard, S., Does, R.J.: Lean six sigma in healthcare. J. Healthc. Qual. **28**(2), 4–11 (2006)
11. Silva, I.B.D., Miyake, D.I., Batocchio, A., Agostinho, O.L.: Integrando a promoção das metodologias Lean Manufacturing e Six Sigma na busca de produtividade e qualidade numa empresa fabricante de autopeças. Gestão & Produção (2011)
12. Susilawati, A., Tan, J., Bell, D., Sarwar, M.: Develop a framework of performance measurement and improvement system for lean manufacturing activity. Int. J. Lean Thinking **4**(1), 51–64 (2013)
13. Anand, G., Ward, P.T., Tatikonda, M.V., Schilling, D.A.: Dynamic capabilities through continuous improvement infrastructure. J. Oper Manag **27**(6), 444–461 (2009)

14. Shah, R., Ward, P.T.: Lean manufacturing: context, practice bundles, and performance. J. Oper. Manag. **21**(2), 129–149 (2003)
15. Fullerton, R.R., McWatters, C.S.: The production performance benefits from JIT implementation. J. Oper. Manage. **19**(1), 81–96 (2001)
16. Ahlstrom, P.: Lean service operations: translating lean production principles to service operations. Int. J. Serv. Technol. Manag. **5**(5–6), 545–564 (2004)
17. Silva, C., Tantardini, M., Portioli Staudacher, A., Salviano, K.: Lean production implementation: a survey in Portugal and a comparison of results with Italian, UK and USA companies. In: 17th international annual EurOMA conference, pp. 1–10 (2010)
18. Selau, L.P.R., Pedó, G.B., Senff, D.S., Saurin, T.A.: Produção Enxuta no Setor de Serviços: caso do Hospital de Clínicas de Porto Alegre - HCPA. Revista Gestão Industrial **1**(5), 122–140 (2009)
19. Womack, J.P., Jones, D.T.: Lean consumption. Harv. Bus. Rev. **83**(3), 58–68 (2005)
20. Escobar, D., Revilla, E.: The customer service process: the lean thinking perspective (2005)
21. Carlborg, P., Kindström, D., Kowalkowski, C.: A lean approach for service productivity improvements: synergy or oxymoron? Manag. Serv. Qual. Int. J. **23**(4), 291–304 (2013)
22. Cua, K.O., McKone, K.E., Schroeder, R.G.: Relationships between implementation of TQM, JIT, and TPM and manufacturing performance. J. Oper. Manag. **19**(6), 675–694 (2001)
23. Brown, G.D., O'Rourke, D.: Lean manufacturing comes to China: a case study of its impact on workplace health and safety. Int. J. Occup. Environ. Health **13**(3), 249–257 (2007)

Durability Analysis of Titanium Engine Valves Using CAE

Anuradha Jagdish Thakare and Ashok J. Keche

Abstract The automotive engine valves in an enclosed internal combustion engine are perpetually underneath variable loading when the engine is in operation condition. The fatigue failures occur because of the alternating compressive and tensile stresses throughout its revolutions. The design of the valve is critical for the engine performance, fatigue life, linear vibration, and durability. To increase the performance of engine, the tribological characteristics are to be identifying by using light-weight valves made of titanium alloy. The objective of this paper was the comparative analysis of proposed titanium alloy with existing steel alloy to predict the maximum stresses, temperature distribution in the valve at the high temperature and pressure ranges. Thermo-mechanical analysis of new valve design has done using CAE (ABAQUS). In addition, this study has done valve fatigue durability using stress life approach and evaluating the design of safety and fatigue factor of safety.

Keywords Engine valves · CAE analysis · Ti6Al4V · Durability analysis · Fatigue life

1 Introduction

The automotive industry business is continually exigent higher durability and reliability of the internal combustion engine valves. Recent trends in light-weight design for high-speed and high-performance vehicle to support fluctuation. What is the main target of bigger environmental and pollution norms which make always the scope for choice of titanium material because of its strength-to-weight ratio for increase durability. If the valves area is lighter, it permits a lot of radial cam profiles that shut

A. J. Thakare (✉)
Department of Mechanical Engineering, Aurangabad, Maharashtra, India
e-mail: anuradhathakare293@gmail.com

A. J. Keche
Department of Mechanical Engineering, Maharashtra Institute of Technology, Aurangabad, Maharashtra, India

and open the valves more quickly for better performance and low-end torque. This section depends on the design requirement and the application where it is going to function inside the engine. Normally this is optimizing based on the loads coming for it and the space availability. The main purpose of the valves is to draw the air—fuel mixture into the cylinder and release exhaust gas out. The valves are subject to alternating stresses of compression to tension, stress, and impact force. The material selection criteria of the valves are critical, as it has to undergo an alternating load leading to fatigue failure. The cyclic loading is a very important factor in the design of valves [1–4]. The increase in cross section of valves affects the overall balancing of the engine. The basic purpose of selecting titanium is to achieve better sealing, flexibility, and uniform stress distribution. Now if the balancing requirement of the engine gets increases, then the engine overall vibration is increased which leads to the failure of its component. To keep a fine balance between valve weight and its component design, optimization of weight is required.

In this paper, we are going to be addressing engine valves for experimental fatigue testing and validation of its design. The failure location of the valve is identified with the help of CAE analysis and perform fatigue life test with the help of SN approach. The design of the connecting rod is modified to make it pass the fatigue life. After the modification of the design, again experimental validations are carried out to validate the results from the analysis.

2   Literature Review

For previous couples of decades, a very less industrial analysis, research work has found in engineering analysis using FEA for regular steel valves. Finite element analysis methodology for analysis and its visualization using CAE analysis considered robust procedure both in the academic way and industrial way designed to simulate stress analysis using engineering calculations under maximum static loads. An analytical understanding is important for valve stresses behavior on proposed reference boundary conditions before having a balanced design based on heat transfer and stress–strain FEA increasing durability.

Zade [1], in this paper, mentioned high pressure enclosed in the combustion chamber the stresses iatrogenic during a valve because of high within the combustion chamber spring force and the cam force for the optimization of fillet radius of inlet valves. The results obtained through static structural analysis counsel that the optimized value of fillet radius is 14 mm shows safe results and is chosen for additional work that is for material optimization, which shows sensible improvement compared to allowable stresses. The alloy AISI 1541 shows less stress, as compared to alloy 21-2 N with higher allowable stress, and therefore, for valve improvement, this material is best.

Pandey and Mandloi [2] conducted experimental investigation of valve failures by observing and analyzing the changes in microstructure of valves as reflected by, images taken through a SEM. For this purpose, a number of specimens were prepared of the engine valves that failed under service and the changes were marked against the new valves. From the observation, it is proving that high-temperature conditions affect the microstructure of failed valves that is the grain size, boundaries, and the distribution of carbide particles through the material matrix and the more severe effects are observed for exhaust valves against new valves. A discernible change has been observed in the microstructure of the valve material after operating at high temperature. In high temperature, the size of grain, also a change that reduces the level of valve hardness in turn, causes more wear.

Lavhale et al. [3] in this paper the failure of inlet and exhaust valve caused by different reasons due to fatigue, thermal loading, wear, corrosion, and erosion were discussed. These failures are affecting mechanical properties of the material and the engine performance. In addition, the various tools and techniques for the fracture analysis were studied. Carbon deposition on the valve neck leads to poor sealing that creates a hot spot on the valve sealing face, which results in channeling effects. From the results, it concludes that the exhaust valves fail more than the intake valve.

Rao et al. [4] this paper conducted the theoretical calculation of an exhaust valve design for a four-wheeler petrol engine by using three-d model thermal analysis to determine the mode shapes of the valve for the number of modes when it is closed and open at 5000 cycles. In this EN 52 and EN59, material alloy is used for optimization while analysis. From the results, we observed that total savings per annum is 20 lakhs and lead time is reduced by 2 days.

3 Experimental Program of Engine Valves

The functioning of the valves is critical in the operation of the automotive engine. In a four-stroke cycle, the valves are constantly under a tensile load and compressive load during its operation. The loads always vary in nature in a continuous alternating fashion, which leads to a major fatigue failure. In any design of the component, its operating condition is very important and as per that, its impact on product life is highly dependent. For this purpose, it needs to check the durability of engine valves regularly for better improvement.

3.1 Finite Element Modeling of Engine Valve

A finite element model has created to simulate an engine valve, which undergoes fatigue fracture during durability cycles. To provide ideal virtual simulation inter-action, the FEA model builds after creating a finite element model to simulate a titanium and steel alloy valve, respectively. The valve material input data used for

Table 1 Mechanical and thermal properties of proposed titanium alloy and existing steel alloy (21-4N & EN-52) valve material

Specification data	Titanium valve	21-4N	EN-52
Young's modulus (Gpa)	113.8	211	207
Thermal conductivity (W/m K)	6.7	18.7	21
Poisson's ratio	0.34	0.3	0.31
Density (g/cm^3)	4.43	7.65	7.75
Specific heat (J/g K)	0.52	0.49	0.46
Expansion coefficient (10^6/K^{-1})	16.2	16.5	12–14
Yield strength (Mpa)	880	580	565

Fig. 1 Finite element model of valve

proposed titanium (Grade 5) alloy and existing steel alloy 21-4N & EN-52 are given in Table 1.

A three-dimensional solid element meshing was developed in valve structure. For better results of deformation, meshing should be fine along the valve area. The load is uniformly distributed along the valve head area and thus the meshing along the face area so that the combustion pressure strikes all the parts of the angular region of the valve head. The meshed model of the valve is shown in the diagram below (Fig. 1).

3.2 Engine Valve Thermal Modeling

The thermal stresses of the valves we get through the analysis of a 3D linear steady-state thermal analysis. During the combustion process, the operating temperature of the inlet valves reaches up to 500–600 °C and of the exhaust valves is between 700 and 850 °C, at this temperature, the thermal analysis is carried out. The load is impacted in the face and guide with uniform distribution, and the boundary condition has applied the temperature for both alloys in case of the inlet and exhaust valve diagram are as shown below.

A CASE I: TITANIUM
See Figs. 2 and 3.
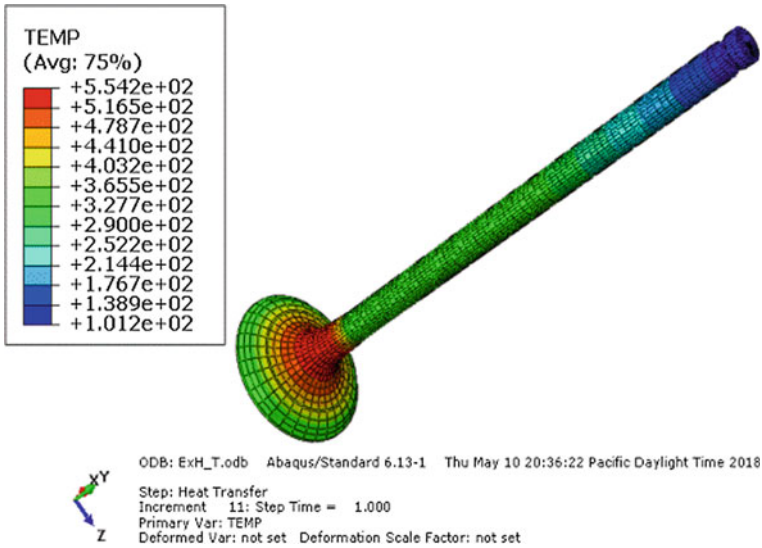
Fig. 2 Titanium exhaust valve thermal value
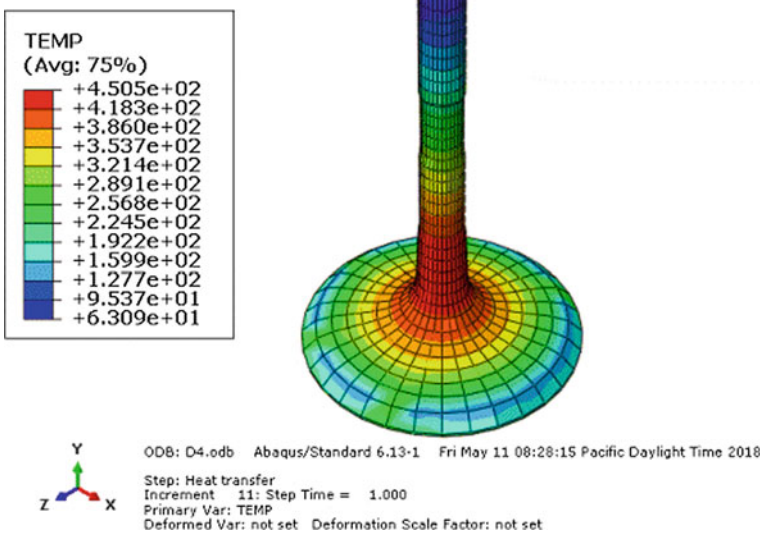
Fig. 3 Titanium inlet value thermal value

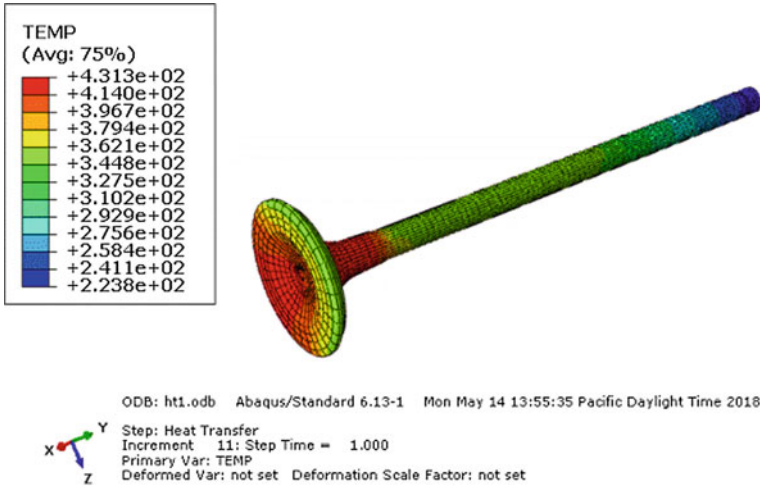A CASE II: STEEL
See Figs. 4 and 5.

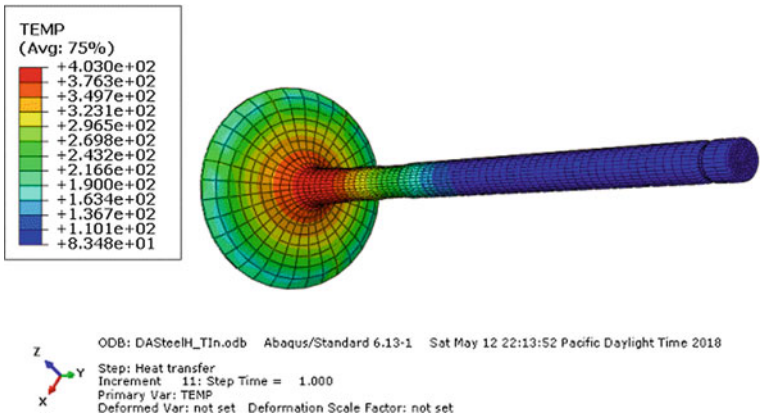**Fig. 4** 21-4N exhaust valve thermal value

Fig. 5 EN-52 inlet valve thermal value

3.3 Thermo-Mechanical Stress Analysis Results

The thermo-mechanical analysis is carried out on valves during its operating condition under valve train dynamics, and the combustion pressure, thermal temperature, load, and impact closing velocity was analyzed by CAE. The combustion pressure of 200 Mpa is applied on the face of the valve. The Lancaster and Tie constrains are applied under the boundary condition to valve created for static analysis. For results that are more accurate, we had coupled stresses with heat transfer. The thermo-mechanical coupled analysis results for both alloys intake and exhaust diagram are as shown below (Figs. 6, 7, 8 and 9).

3.4 Fatigue Behavior of Engine Valve

To ensure a high probability, it is necessary for engine valve manufacturers to have a valve fatigue life model for future product design. This is one of the objectives of this present work to check the fatigue life of the valves for both exhaust and inlet valves. The demand for higher durability from the automotive industry has become a need to predict failure life of valves under various operating conditions. The design and the safety factor are terms designed for a structure we do this to know the additional load that will cause the structure to fail. If a structure having a factor of safety of two will fail at twice the design load [5–8].
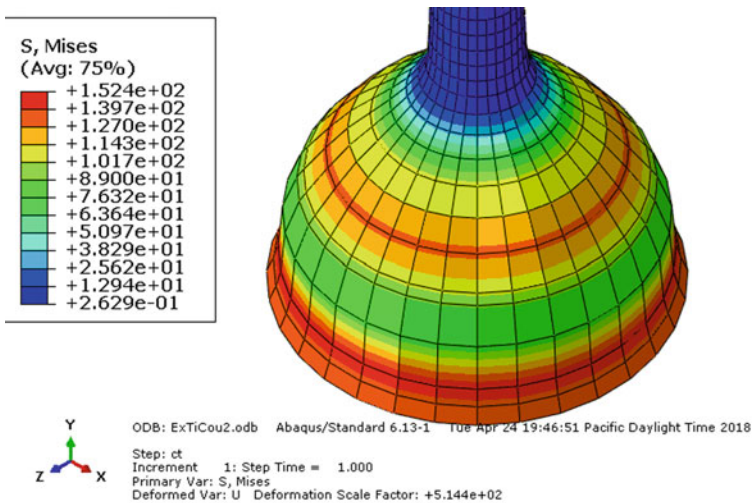
Fig. 6 Von-Misses stresses showing on the titanium exhaust valve
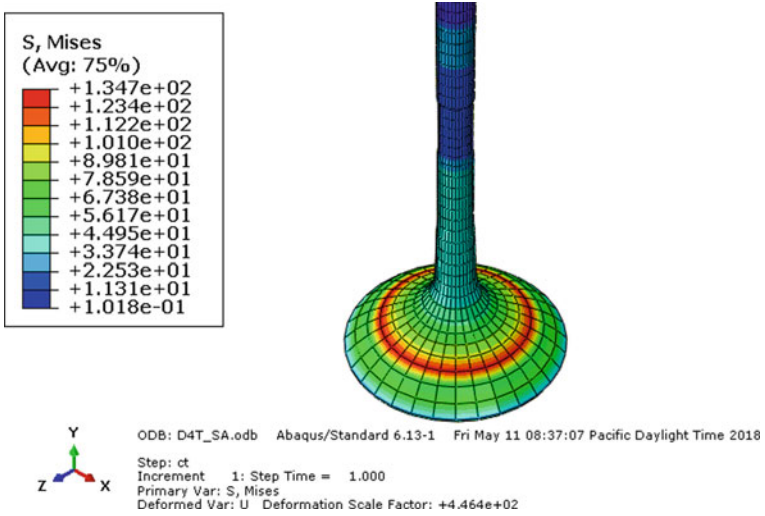
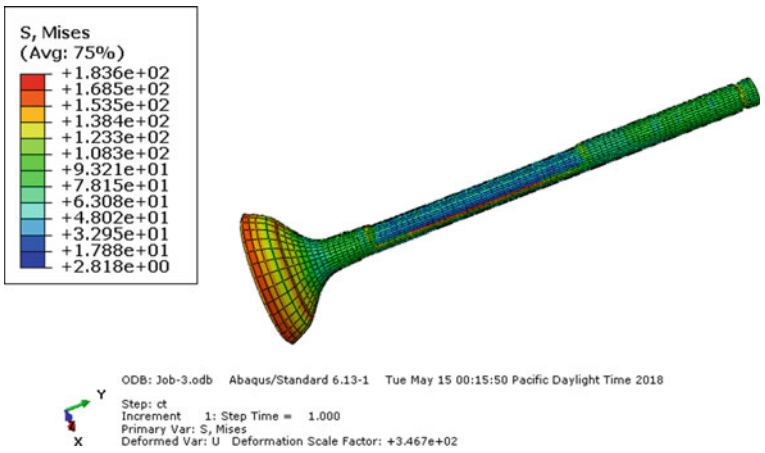**Fig. 7** Von-Misses stresses showing on the titanium inlet valve

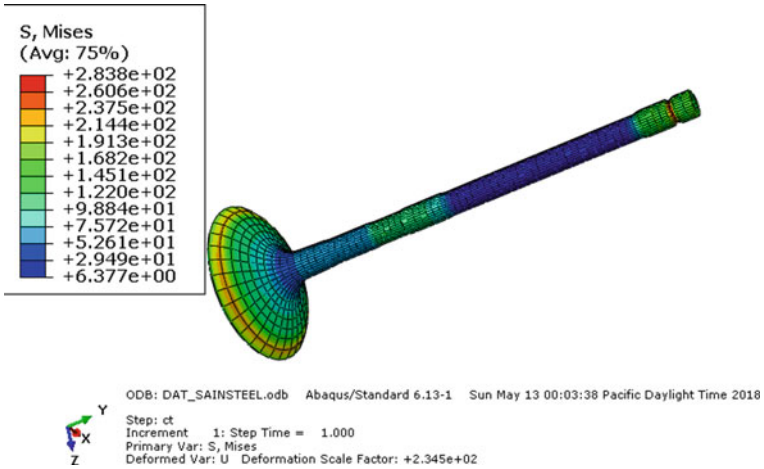**Fig. 8** Von-Misses stresses showing the 21-4N exhaust valve

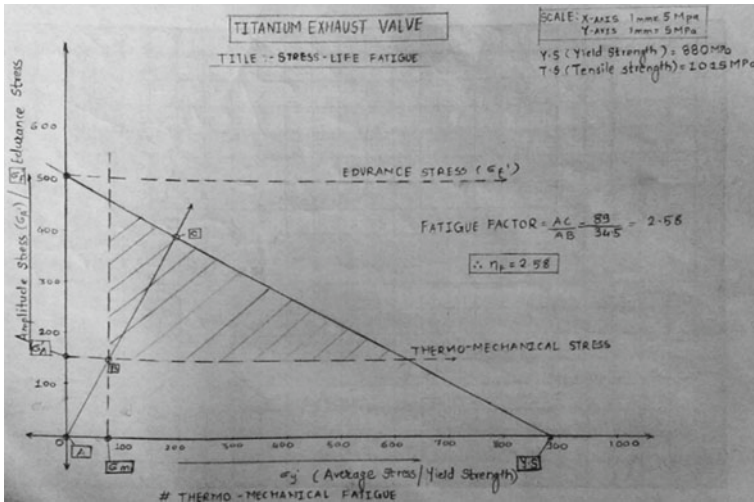Fig. 9   Von-Misses stresses showing on the EN-52 inlet valve

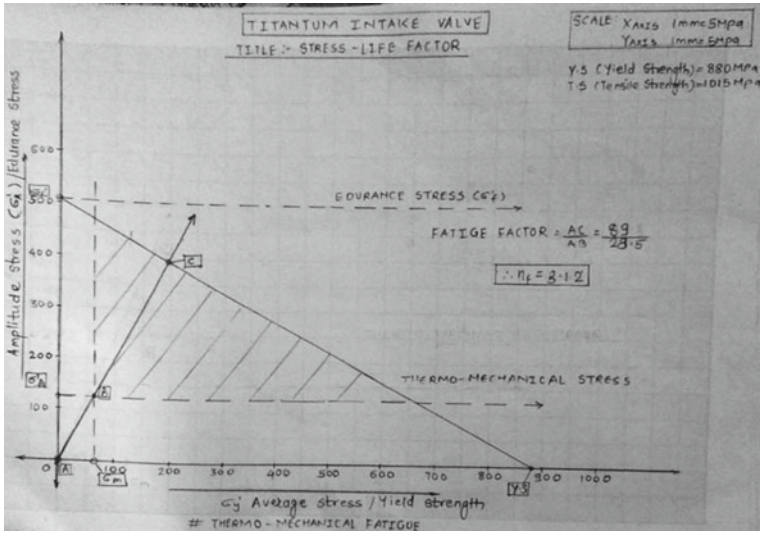Fig. 10   Titanium exhaust valve fatigue behavior
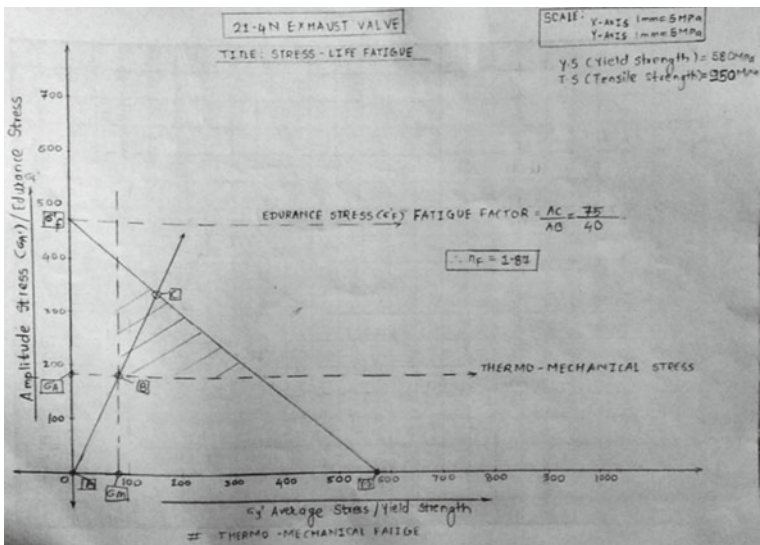
Fig. 11 Titanium inlet valve fatigue behavior
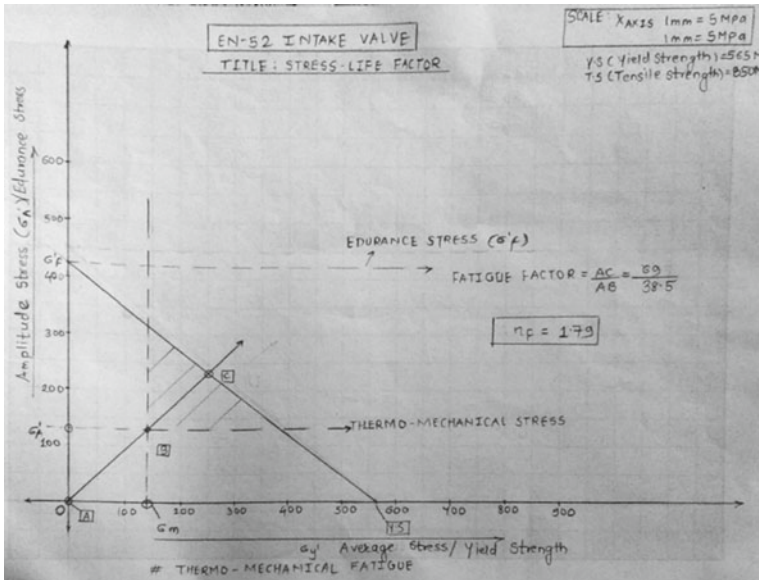

Fig. 12 21-4N exhaust valve fatigue behavior

Fig. 13 EN-52 inlet valve fatigue behavior

The fatigue graphs for steel alloy and titanium alloy as shown below: (Figs. 10, 11, 12 and 13).

4 Conclusions

Following are the conclusions of valve thermal-stress behavior and fatigue assessment by CAE analysis as shown:

(1) Thermo-mechanical stresses of the proposed and existing valve have been fairly analyzed by using CAE.

(2) Titanium exhaust valve design of safety 2.58 and of the titanium Inlet valve is 3.12 that means the structure is safe in comparison with steel alloy. Thus, it is also proved that the titanium alloy has enough potential as an optimal better material for the engine valve in comparing to 21-4N and EN-52 steel alloy for better engine performance.

(3) Valve fatigue life can be reasonably assessed by using the SN method which is the main purpose of life prediction.

(4) The aim main is achieved, and strength-to-weight ratio of titanium is high in comparison with steel alloy. The overall reduction in mass of titanium is 10.8% and of steel is 18.8%.

References

1. Zade, M.R.: Optimization of the inlet valve of IC engine using finite element analysis. Int. Res. J Eng. Tech. (IRJET) **3**(10), 451–454 (Oct 2016)
2. Pandey, A., Mandloi, R.K.: Effects of high temperature on the microstructure of automotive engine valves. Int. J. Res. Appl. **4**, 122–126. ISSN: 2248-9622 (Mar 2014)
3. Lavhale, Y.K., Salunke, J.: Overview of failure trend of inlet & exhaust valve. (IJMET) Int. J. Mech. Eng. Sci. Tech. **5**(3), 104–113 (Mar 2014)
4. Rao, B.S., Chandu, D.G.: Petrol engine exhaust valve design, analysis and manufacturing processes. Int. J. Mech. Eng. Robot. Res. **3**(4), 395–401 (Oct 2014)
5. Rao, Y.M.S.C., Ramakrishna, V.V., Krishna, S.M.: Structural, and Thermal Analysis of Poppet Valve made of different composite materials. Int. J. Mech. Eng. Technol. **2**(9), 939–944 (Dec 2015)
6. Raghuwanshi, N.K., Pandey, A., Mandloi, R.K.: Failure analysis of internal combustion engine valves: a review. Int. J. Innov. Res. Sci. Eng. Tech, 173–181 (2012)
7. Yu, Z.W., Xu, X.L.: Failure analysis and metallurgical investigation of diesel engine exhaust valves. Eng. Fail. Anal. **13**, 673–682p (2006)
8. Kumar, G.U., Mamilla, V.R.: Failure analysis of internal combustion engine valves by using Ansys. Am. Int. J. Res. Sci. Tech. Eng. Math., 169–173 (2014)

Selection of Blank Size for Deep Drawing of Rectangular Parts

Arvind B. Bodhe, Nitin K. Mandavgade and Amit Tajne

Abstract Sheet metal fabrication plays key role in the area of fabrication. It is used to manufacture various parts like from hinges to automobile bodies. A sheet metal blank is a flat part of sheet which is used to form different shapes in pressing machine. The process of deep drawing begins with holding a blank in between die and punch. The selection of blank size is one of the tedious jobs. This paper suggested an appropriate method for selecting the proper blank size for rectangular parts which required deep drawing process. In this paper, a number of methods suggested by various researchers for blank size are studied. The method suggested by Daniel Dallas is found to be more suitable for rectangular part such as choke used in tube light. The research gaps are identified, and suitable method is suggested through experimentation for specific rectangular drawing parts.

Keywords Deep drawing · Metal forming · Rectangular blank

1 Introduction

Deep drawing, first developed in the 1700s, has been studied extensively and become an important metalworking process. Typical parts produced are beverage cans, pots, pans, containers of all shapes and sizes, sinks, and automobile panels. To produce a desired shape, the material is formed which is accomplished by straining it beyond the yield point, so that it will take a permanent shape and retain it [1]. A hydraulic or mechanical press is generally used for deep drawing work [2]. A blank is a flat piece

A. B. Bodhe (✉) · N. K. Mandavgade
Nagpur Institute of Technology, Nagpur, India
e-mail: bodhe2013@gmail.com

N. K. Mandavgade
e-mail: nkmandavgade@gmail.com

A. Tajne
S. B. Jain Institute of Technology, Management and Research, Nagpur, India
e-mail: amit.tajne@gmail.com

of sheet metal used to form different shapes. The process of deep drawing begins with a metal blank held in between punch and die in press machine which used to produce the part [3]. The shape of blank plays one of the vital roles to have good quality parts.

2 Literature Review

Sheet metal formation for choke of tube light is very tedious job. The development of blank size required more appropriate method to optimize the method of blank formation. The work carried out by various researcher in same area has been reviewed with objective to decide the proper method and to identify the gaps in literature.

Gopinathan [4] elaborated the deep drawing processes for circular, rectangular parts. It is mentioned that deep drawing and deep drawing of special shapes have gained considerable importance in the fabrication of sheet metal components.

It is discussed that for circular deep drawing, the blank is circular, whereas for rectangular deep drawing, the initial blank may or may not be rectangular. It may be circular, elliptical, or any other shape, depending upon the drawing ratio and the tool geometry.

Kim and Kobayashi [5] described an approximate geometrical method which determine velocity field with parameters in the deformation domain. The blank shapes are determined at several punch steps. Majlessi and Lee [6] suggested a finite element technique. It is suitable for the pressing of square shapes. In this type of work, deformation theory of plasticity is used. The first position of these elements is computed by minimizing the potential energy.

Iseki and Murota [7] proposed a finite element procedure for determining the optimum shape and size of a blank for deep drawing of a non-axisymmetric cup with a flat-headed punch. The blanks are designed by the repetition method of the strain-hardening characterization.

Cao and Li [8] analyzed metal pressing of a symmetric part with a complex geometry. Their design yields are of a lower maximum void volume. This indicates more meaningful forming process but requires slightly higher press load. Analytical methods from finite element are enriched by mesh adaptivity, failure criteria, wrinkling and surface defects, springback, and contact algorithms. It is now possible to simulate new process and design of blank. Gea and Ramamurthy [9] represented a computer aided tool for blank design optimization of deep drawn parts. The methodology is based on the maximizing the drawability in the deep drawing process. Yao and Cao [10] assessed the corner failure depths in the deep drawing of 3D panels using simplified 2D numerical and analytical models. They proposed to use an axisymmetric finite element model with an enlarged tooling. The blank size is used to calculate the corner failure height in a 3D part forming.

Krishnan and Cao [11] estimated the optimal blank holder force trajectory, in segmented binder, using Auto-Regressive Moving-Average model ARMA model. According to them, variations in blank holder forces also had an effect on drawing

process. These forces are varied to control the wrinkle formation as well as tearing in the part. Sitaraman et al. [12] described the knowledge-based system and compared process sequences output by the system with corresponding process. Peng and Cao [13] applied the homogenization method to determine the effective elastic constants of unidirectional fiber-reinforced composites. Comparison between the obtained results and available experimental data as well as analytical results from mechanics of materials approach and Halpin-Tsai equations validated the efficiency and accuracy of die homogenization method in estimating material constants of composites. They applied this method to determine the material constant of plain woven composite and used them as initial inputs in the simulation of composite stamping.

Hino et al. [14] developed the design optimization system using high- and low-fidelity finite element simulations. Kirn and Yang [15] predicted the location and relative possibility of wrinkling initiation. The wrinkling in the door inner stamping can be found using his theory. Hsu and Lee [16] showed that the drawability as measured in the drawing of round cups can be generalized to cover cups of all possible shapes by a careful analysis of the definition of draw ability and that such an analysis involved the deformation caused by the drawing operation.

From the above literature review, it may be concluded that the calculation part of blank is missing. No such work is identified which can calculate the dimensions for rectangular parts.

3 Blank Calculation and Development

It is extremely important to determine the size of the blank for drawing the component accurately and to reduce the cost. The size of the blank is determined by knowing the volume of the component to be drawn, which must be equal to the volume of the blank [17]. In most calculations, it is assumed that the sheet thickness remains constant during the (drawing) process. The constant volume condition is satisfied when the surface area of the blank and the component are equal. This assumption is correct for simple parts with circular symmetry since both wall thickening and wall thinning occur in these components such that the mean value of the wall thickness remains approximately constant [18]. In complex shapes, stretching of sheet due to localized drawing results into thinning and thickening in regular manner.

Followings are some methods which may be used to find the blank size for deep drawing of the rectangular parts—

- (i)   Blank suggested by Frank Wilson:
- (ii) Blank suggested by Daniel Dallas:
- (iii) Blank suggested by Prof. Kurt Lange:
- (iv) Blank suggested by Dr. S. K. Basu:
- (v)   Blank suggested by V. Gopinathan:

A rectangular press part such as choke shell used in tube light is selected for experimentation. This part has dimension of 100 mm × 50 mm × 38 mm. Its part
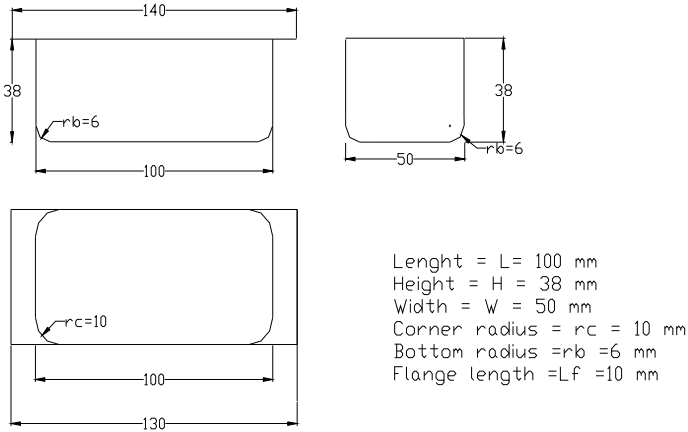
Fig. 1 Part drawing of rectangular deep draw part
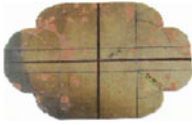
Fig. 2 Rectangular pressed part

drawing is shown in Fig. 1. After deep drawing, this part will look like as shown in Fig. 2. The part details are given as below:

L = Length = 100 mm
W = Width = 50 mm
H = Height of Shell = 38 mm
r_c = Corner radius = 10 mm
r_b = Bottom radius = 06 mm

Blanks are calculated by various methods and developed for experimentation. Following are some methods to find the blank size of rectangular shell.

Blanks are worked out using different methods for blank size calculations. Blank layout is prepared with the help of permanent marker; the layout is drawn on the mild steel metal sheet of size of 0.23 mm thickness. Different sets of 10 blanks are prepared for each method suggested by Frank Wilson, Daniel Dallus, Prof. Kurt Lange, Dr. S. K. Basu, V. Gopinathan and method used in M/s S.S. Metal Craft company are as shown in Table 1. These blanks are prepared for experimentation. Frank Wilson suggested the blank with dimension of 182.86 mm × 132.86 mm with corner radius of blank, i.e., R_c = 30.73 mm. Daniel Dallas suggested the blank with dimension of 176 mm × 126 mm with corner radius of blank, i.e., R = 34.06 mm. Prof. Kurt Lange

Table 1 Blank developed by various researchers

Blank developed by	M/S. S.S.Metal Craft	Suggested by Frank Wilson	Suggested by Daniel Dallus
Photograph of blank	Having length of 165 mm and Width of 124 mm		
Blank developed by	Suggested by Prof. Kurt Lange	Suggested by Dr. S. K. Basu	Suggested by V. Gopinathan
Photograph of blank			

suggested the blank with dimension of 176.84 mm × 126.84 mm with corner radius of blank, i.e., $R = 37.86$ mm. and modified radius $R' = 47.21$ mm. Dr. S. K. Basu suggested the blank with elliptical shape with major axis of 182.84 mm and minor axis of 126.84 mm. V. Gopinathan suggested the blank with dimension of 174.9 mm × 124.9 mm) with corner radius of blank, i.e., $R = 28.35$ mm.
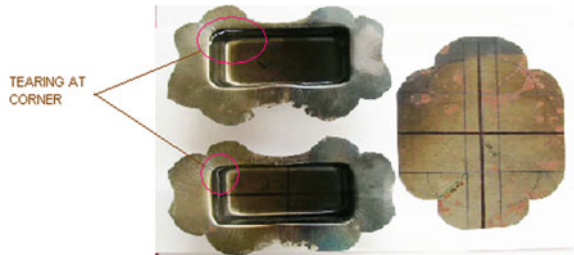
4 Experimentation

Shapes of blanks are worked out using different methods of blank size calculations. The different type of blanks must be tried for press working to see the different shape of flanges. For purpose of comparison, the dimension of basic component is maintained same. The basic dimensions are width, length, height, thickness, corner radius, flange length, and bottom radius. General machines are used for experimentation such as shearing machine, mechanical press (of 50 Ton), and mechanical press (of 10 Ton) for trimming. This experiment attempts to reveal the details of drawing process. For example shape of flange, wrinkle formation, earring, tearing of the sheet, ironing, slip band, cracks at various position, puckers, bulges out, etc. can be clearly observed for all the blanks that are drawn in the experimentation process. After observation, it will be fairly easy to decide the blank dimensions for the best output.

Fig. 3 Pressed part by method used in company

Fig. 4 Blank and pressed part by Wilson method

TEARING AT CORNER

5 Analysis of Experimental Result

The blank sizes are calculated and developed by using various methods. These blanks are pressed in experimental setup. The observations are made as shown in Table 2. With the help of these observations, analysis is done by considering various methods to find out the best blank size for rectangular part considered for experimentation.

It is analyzed that the parts produced from the blanks developed by method used in company have tearing defects. Large wrinkle are observed on flange 54.42 cm^2 is trimming area out of 204.60 cm^2 as blanks area. 26.59% of blank area is wastage as trimming area as shown in Fig. 3. One part is rejected. Hence, this method used in company for blank development for drawing electric choke is not recommended.

The final parts from the blanks suggested by Wilson method have tearing and earring effects, and hence, all the parts were rejected. Out of 198.61 cm^2 blank area, 57.48 cm^2 trimming area was observed. About 28.94% of blank area was wasted as shown in Fig. 4. Hence, this blank is not recommended.

The parts from Dallus method had no defects. All parts had superior quality, and all parts were accepted. Out of 191.23 cm^2 blanks area, 41.87 cm^2 trimming area was observed. Only 21.22% of blank area was wasted as trimming area as shown in Fig. 5. Hence, Dallus Method for blank development for drawing electric choke is recommended.

The final parts from the blanks suggested by Prof. Kurt Lange's method had tearing defects. Medium-sized wrinkle was observed on the flange. Quality of parts was found to be poor. Out of 200.54 cm^2 blank area, 39.48 cm^2 trimming area was

Table 2 Details various defects with blank wise

Blank made as per	Area of blank (cm²)	Blank corner shape	Trimming area in cm² & in %	Wrinkle per cm	Others defect		Tearing	Accepted or rejected
					Earring	band slip		
Suggested by Frank Wilson	198.61	Concave	57.486 cm² 28.94%	12	Yes at side flange	No	Yes at corner 10 out of 10	None of the parts were accepted
Suggested by Daniel Dallus	191.23	Cosine wave	41.87 cm² 21.22%	6 very small	No	No	No	Accepted 100% (Excellent quality)
Suggested by Prof. Kurt Lange	200.54	Round	39.48 cm² 19.69%	9 medium size	Yes	No	No	May be accepted 7 part out of 10 are ok but poor quality 70%
Suggested by Dr. S. K. Basu	200.16	Elliptical	15.64 cm² 7.58% of blank area	9 medium size	Yes 6/9	Yes At back side	Yes 6/10	Rejected
Suggested by V. Gopinathan	210.45	Double radius	37.28 cm² 17.71% of blank area	5 large size at corner height	No	No	Yes 3 out of 10	Rejected (3 parts out of 10 is o k) 30% of final parts are accepted
Company used	204.60	Right angled	54.42 cm²	15			At corners 4 out of 10	

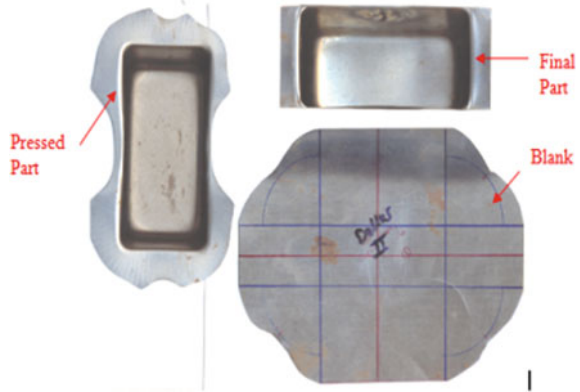**Fig. 5** Blank, pressed part and final part by Dallus method

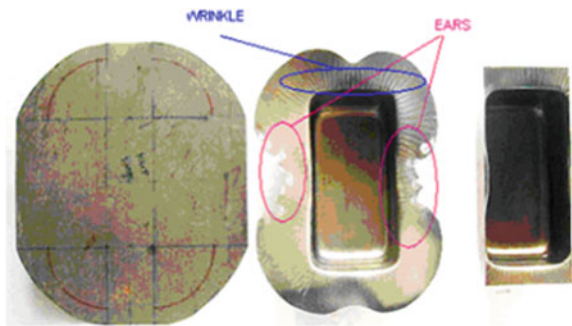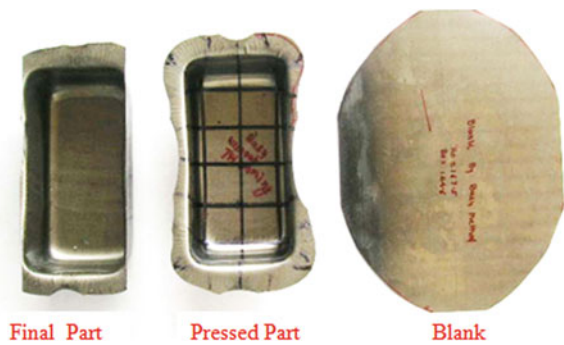**Fig. 6** Pressed part by Kurt Lange method

Fig. 7 Blank, pressed part and final part by Dr. S. K. Basu method

observed. Approximately 19.69% of blank area was wasted as trimming area as shown in Fig. 6. Therefore, this method is not recommended.

The final parts from the blanks suggested by Dr. S. K. Basu's method had tearing defects. Medium-sized wrinkles were observed on flange. All parts were rejected due to shorter length on side flange. Out of 200.16 cm^2 blank area, 15.64 cm^2 trimming area was observed. About 19.69% of blank area was wasted as trimming area as shown in Fig. 7. Hence, this method is not recommended.

Blank   Pressed Part
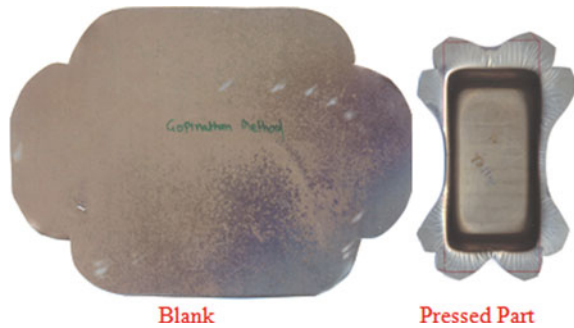
The final parts from the blanks suggested by Mr. Gopinathan's method had tearing defects. Medium sized wrinkles were observed on flange. Only 3 parts out of 10 parts were accepted. Out of 210.45 cm^2 blank area, 37.28 cm^2 trimming area was observed. About 17.71% of blank area was wasted as trimming area as shown in Fig. 8. Hence, this method is also not recommended.

6 Conclusion

After experimentation and analysis, it is observed that the method used in company had tearing defects. Large wrinkles were observed on flange. Quality of parts was found to be good. Out of 204.60 cm^2 as blank area, 54.42 cm^2 trimming area is observed. About 26.59% of blank area was wasted as trimming area. One part was rejected out of nine parts. Therefore, the method used in company for blank development (for drawing Electric Choke) is not recommended. The parts from Dallus method had no defects. All parts had superior quality, and all parts were accepted. Out of 191.23 cm^2 blanks area, 41.87 cm^2 trimming area was observed. Only 21.22% of blank area was wasted as trimming area. Hence, Dallus Method for blank development for drawing electric choke is recommended.

References

1. ASTME: Fundamentals of Tool Design. Prentice Hall of India Ltd, New Delhi (1964)
2. Wilson, F., Harvey, P.: Die Design Handbook. McGraw Hill, New York (1964)
3. ASM: Metals Handbook, 9th edn, vol. 14. ASM (Ohio)
4. Gopinathan, V.: Optimum blank profile for rectangular deep drawing. Indian J. Technol. **15**, 330–333 (1977)
5. Kim, N., Kobayashi, S.: Blank design in rectangular cup drawing by an approximate method. Int. J. Mach. Tool Des. Res **26**, 125–135 (1986)
6. Majlessi, S.A., Lee, D.: Deep drawing of square shaped sheet metal parts. J. Eng. Ind. **115** (1993)

7. Iseki, H., Murota, T.: On the determination of the optimum blank shape of non-axisymmetric drawn cup by the finite element method. Bull. JSME **29**, 1033–1040 (1986)
8. Cao, J., Li, S.: Analysis of an axisymmetric deep drawn part forming using reduced forming steps. J. Mater. Process. Technol.
9. Gea, H.C., Ramamurthy, R.: Blank design optimization on deep drawing of square shell. IIE Trans. (1998)
10. Yao, H., Cao, J.: Assessment of corner failure depths in the deep drawing of 3D panels using simplified 2D numerical and analytical model. ASME Trans. **123**, 248–256 (2001)
11. Krishnan, N., Cao, J.: Estimation of optimal blank holder force trajectories in segmented binders using an ARMA model. J. Manuf. Sci. Eng. **125**, 763–770 (2003)
12. Sitaraman, S.K., Kinzel, G.L., Allan, Taylan: A knowledge based system for process sequence design in axisymmetric sheet metal forming. J. Mater. Process. Technol. **25**, 247–271 (1991)
13. Peng, X.Q., Cao, J.: Material characterization in forming structural composites. Polytech. Univ. 100th Anniversary Special Issue
14. Hino, R., Yoshida, F., Toropov, V.V.: Optimum blank design for deep drawing using interaction of high and fidelity simulation. In: ICTAM, 21, pp. 15–21 (2004)
15. Kirn, J.B., Yang, D.Y.: Prediction of wrinkling initiation in sheet metal forming processes. Eng. Comput. **20**, 6–39 (2002)
16. Hsu, T.C., Lee, S.Y.: A definition of drawability and its relation to deformation in the drawing of square cups. **4**, 340–345 (1976)
17. Dallas, D.: Tool and Manufacturing Engineers Hand book. McGraw Hill, New York (1976)
18. Bodhe, A.B., et al.: Comparison and evaluation of blank optimization technique—a case study. In: The 17th international conference on flexible automation and intelligent manufacturing (FAIM' 2007) held in Malvern, Pennsylvania, USA, 18–20 June (2007)

Binary Logistics Regression Analysis to Assess Employability of Engineering Graduates in IT Sector

Vijay N. Kalbande, Chandrahas C. Handa and Amit W. Bankar

Abstract An attempt has been made to identify employability skills of engineering graduates. The skills that influence the performance of engineering graduates in campus placement are assessed. In this paper, various skills were identified and correlated with each other by using statistical tools such as chi square test and T-Test using SPSS-20. Binary logistic regression mathematical model was developed which predicts Probability of Employment of engineering graduates in campus placement recruitment process of multinational companies in IT sector. Sensitivity analysis was carried out to check impact of input variables like Aptitude, Communication, Technical, and Personality skills on Employability. Aptitude is the major deciding skill to get early employment in campus placement recruitment process of the company.

1 Introduction

There is significant increase in demand of technocrat due to globalization. To fulfill the increasing demand of technocrats, the engineering institutes have also increased tenfold in India [1]. The number of technical institutes has increased by many folds. This has directly affected quality and employability of students [2]. To promote industrial and economic growth, it is essential to develop competent technical man-

V. N. Kalbande (✉) · A. W. Bankar
Nagpur Institute of Technology, Nagpur, India
e-mail: drvijaykalbande@gmail.com

A. W. Bankar
e-mail: amitb9275@gmail.com

C. C. Handa
KDK College of Engineering, Nagpur, India
e-mail: chandrahashanda@rediffmail.com

power. The institute and industry needs to work shoulder to shoulder to develop the technocrats through active interaction between them.

The companies invest lot of time and money on training engineering graduate recruited through campus placement to make them ready for work. The study has revealed that the employability of engineering graduate is very low. To make engineering graduates employable in IT and IT services, they need to be trained during their program. Feedback from employers says that only 25% of technical graduates are employable after probation period [3]. Also, only 7% are employable when all skill factors like technical skills, analytical skills, and communication skills are considered together. Study reveals that around 80% of the students do not have required problem solving and analytical skills [4]. As per the study FICCI and the WB, 64% of employers are unsatisfied with skill sets of engineering graduates [5].

The most of the researchers suggests to upgrade the quality of technical institute by using SQC, TQM, Six Sigma, QC, Industry–Institute Partnership, etc. [6–8]. The few of them have assessed influence of employability skills of engineering graduate on employability based on stakeholder's opinion. In this research, employability skill is measured using questionnaire method which is validated by the stakeholders such as HR executives, Senior Training and Placement Officers (TPO) of various Engineering institutes, Corporate trainers and Students/Alumni (selected through campus recruitment and working satisfactorily after successful completion of probation period). The mathematical model is developed by using binary logistic regression to assess probability of employment based on their employability skills.

2 Literature Review

Most of the research in this area is based on opinion of stakeholders to predict employability.

Jonck et al. [9] acknowledged that in previous study on employability suggests to focus on curriculum design and teaching methods.

Nenzhelele et al. [10] have stated that in today's work environment is turbulent. Employability is important for unemployed as well as currently employed individual. Institutes are responsible to produce employable graduates. There is a gap between skills required by industry and skills offered by institutes. Study suggests more of experimental learning to reduce the skills gap.

Sermsuk et al. [11] explored the employability skills through employer's perspective. The study is conducted through an interview and a survey with the employers/supervisors from many companies or from business owners. The survey shows that the skills required for employment are personal management skills, fundamental skills, and teamwork skills.

Venkatesh et al. [12] have focused on the importance of soft skills and positive attitude as perceived by industry with specific reference to fresh engineers, right from the time of industrial revolution. As the times passed by, the need of the community

and society changed drastically, the demands rose with more specifics, technology grew by leaps, and finally the products and services changed for the better.

Chithra et al. [13] studied the perception of employers as well as the employees toward employability skills required for entry level engineering graduates in multinational software companies. The study concluded that, the students with work experience have better awareness of the employability skills than the students with no work experience.

Rosenberg et al. [14] have examined the required employability skills for job, receipt of these skills in institute, and additional training required to upgrade these skills after graduation. The research has triangular design approach. The attitudes of three distinct groups—recent graduates, the faculty, and employers who recruit them were studied. The paper suggests strengthening the skill to make the graduates employable.

Gokuldas et al. [15] identified predictors of employability of undergraduate engineering students in campus recruitment drives of Indian software companies. It was observed that knowledge of engineering and proficiency in English language are important predictors of continuous employability of engineering graduates in campus interviews of software services companies.

Rao et al. [16] concluded that there is a gap exists between the employer wants and the deliverance of the graduates' skills. Employer is not ready for experimenting things; they expect that employee should perform at his best.

3 Methodology

The study is carried out in engineering institutes affiliated to RTM Nagpur University, Nagpur. The performance of final year engineering graduate students who have completed graduation in year 2013 is considered as population. The questionnaire method is used to collect primary data and measure performance of students on identified employability skills. Random and convenience sampling technique is used to collect samples. The secondary data (placement record) of first 5 multinational IT Sector companies are collected from Training and Placement Department of technical institutes.

4 Variable Identification

The dependant variable of this study is recruitment of students in campus placement. It has two binary outcomes, i.e., placed or not placed. If students get selection in first 5 opportunities in multinational IT sector companies, they are considered as placed student and mathematically coded as '1', and if not selected, then coded as '0'.

The independent variables, i.e., employability skills are identified from literature review on employability of engineering graduate. As per the review, forty one

skills are identified to be responsible for employability [17–20]. Recruiters, students/alumni, TPO's, and corporate trainers are considered as stakeholders. The opinion of the 45 stakeholders is taken into consideration to select 22 important employability skills. Confirmative factor analysis method is used to group these 22 skills into four major skill factors. The four major skill factors are aptitude, communication, technical, and personality.

5 Sample Size Determination

The population of engineering students in technical institutes of Nagpur University, Nagpur with 60% and above marks from SSC onwards in academics is considered. The population size is approximately 12,000. Yamane [21] formula is used to determine sample size with level of precision 5% as shown below

Sample Size = Population size/(1 + Population size * e^2)
Population Size = 12,000, $e = 0.05$ Precision error with 5%
Sample Size = 12,000/(1 + 12,000 * 0.0025) = 333.33 (required).

In binary logistic regression, the sample size is calculated based on number of independent variable. A minimum of 50 cases per independent variables is recommended in binary logistic regression. In this study, four employability skills were considered as independent variable to assess employability. So the required number of samples for designing the model to represent the population size is more than 200 (4 * 50 = 200 Samples).

As per the above two references, samples above 333 are adequate to design the mathematical model. In this study, 362 samples are used to design the binary logistic regression model.

6 Data Collection

To obtain the primary data, Engineering Graduate Employability Test (EGET) is designed and conducted in various engineering institutes of Nagpur University, Nagpur for 2000 students. The Secondary data are collected from engineering institutes. The samples are filtered based on the research study constraints and smoothened by using Box Plot statistical tool to 362 samples.

Table 1 Kaiser–Meyer–Olkin (KMO) and Bartlett's test on 362 samples

Kaiser–Meyer–Olkin adequacy and Sphericity	Yes/no output dataset	Recommended value
Adequacy	0.712	Kaiser (1974) Acceptable > 0.5 Mediocre −0.5 to 0.7 and Good −0.7 to 0.8
Approx. chi square	411.091	
Degree of freedom	10	
Significance (*P*)	0.000	
Adequacy of dataset	Good	

7 Data Analysis

The analysis of collected data is carried out by using statistical tools, i.e., chi square test, T-Pair Test, and SPSS-20 [22, 23]. The adequacy and Sphericity of 362 samples is tested by Kaiser–Meyer–Olkin (KMO) and Bartlett's test as shown in Table 1.

The adequacy value 0.712 is found good (Kaiser 1974, 0.7–0.8). The Sphericity of Sample data is confirmed by Bartlett's test, which tested chi square 411.091 with degree of freedom 10 and it is found significant, $P = 0.000$ ($P < 0.05$). The influence of Aptitude, Communication, Technical, and Personality skill factor on Employability are tested and confirmed by chi square test. The correlation between factors is checked by using T-pair test, and it is found to be positively correlated with each other. Sensitivity analysis is carried out to check impact of predictor variables on employability. The empirical model is developed to assess Probability of Employment (employability) based on four independent variables (Employability skills) by using Binary Logistic Regression model in SPSS 20.

8 Results and Discussion

T-Pair test is conducted with significance level 5% to check correlation of independent variables with each other and ranked based on correlation as shown in Table 2. It is observed that all employability skills are having significant positive correlation with each other. Aptitude skill shows stronger (0.322) correlation with Technical skill whereas weaker (0.166) correlation with Personality skill. This strong correlation between aptitude and technical skill indicate that the students who have high aptitude skill are also good at technical skill.

The influence of independent variables on Probability of Employment is checked by using chi square test and binary logistic regression analysis at 5% significance level by using SPSS-20 as shown in Table 3. All independent variables have significant ($P < 0.05$) influence on Employability of Engineering graduates. It is also observed that Aptitude skill is the major deciding factor to get early employment in campus placement recruitment process of the IT firm.

Table 2 T-pair test to check correlation between predictors by using SPSS-20

Pair of employability skills	No of samples	Correlation	Sign. value P	Rank
Aptitude and communication	362	0.265	0.000	4
Communication and technical	362	0.270	0.000	3
Technical and personality	362	0.315	0.000	2
Aptitude and technical	362	0.322	0.000	1
Aptitude and personality	362	0.166	0.002	6
Communication and personality	362	0.196	0.000	5

Table 3 Chi square and Wald coefficient of employability skills

Employability skills	Pearson chi square	DOF	Sign. value (P)	Chi square from χ^2 Std. table	Diff. of χ^2	Walt coefficient	Rank
Aptitude skill	123.86	22	0.00	33.92	89.99	54.733	1
Communication skill	64.62	11	0.00	19.65	44.97	16.84	3
Technical skill	115.5	18	0.00	28.86	86.64	51.29	2
Personality skill	43.93	20	0.00	31.41	12.52	5.37	4

Table 4 Summary of binary logistic regression model

Step	−2 Log likelihood	Cox and Snell R square	Nagelkerke R square
1	220.633	0.534	0.716

Binary logistic regression model is developed for considering 95% confidence level and is summarized in Table 4. The combine impact of all independent variables on the dependent variable is determined by Nagelkerke R Square (0.716) and Cox and Snell R Square (0.534) which indicates the strong relationship between them. All variable are significantly contributing to predict employability.

The Wald Test Coefficient is the way to find out the significance of independent variables used in a model. The test can be used for a multitude of different models including those with binary variables or continuous variables. Table 5 indicates that aptitude factor (Wald Coefficient: 54.733) contributes largely, whereas personality factor (Wald Coefficient: 5.371) contributes less to predict Employability.

The model fitness in logistic regression is the likelihood ratio test, which is simply the difference of chi square of null model and model containing the predictors. The result of Cox and Snell's R^2 indicates that 53.4% variation in the dependent variable is explained by the predictor variable which is found to be good for this model.

Hosmer and Lemeshow test is conducted to check Goodness of fit of the model as shown in Table 6. It is observed that the calculated P Value 0.189 is greater than

Table 5 Result of binary logistic regression model

Employability skills	B coeff.	Wald coeff.	DOF	Rank	Sig.	Exp(B)	95% C.L. for Exp(B)	
							Lower	Upper
Aptitude	0.379	54.733	1	1	0.000	1.461	1.321	1.615
Communication	0.283	16.842	1	3	0.000	1.327	1.159	1.520
Technical	0.498	51.290	1	2	0.000	1.645	1.436	1.885
Personality	0.130	5.371	1	4	0.020	1.139	1.020	1.272
Constant	−14.414	85.122	1		0.000	0.000		

Table 6 Goodness of fit (model diagnosis)

Hosmer Lemeshow test			
Step	Chi square	Degree of freedom	Significance
1	11.23	8	0.189

Table 7 Accuracy of placed and unplaced group at cutoff point

Cut off value	% accuracy of placed group	% accuracy of unplaced group
0.2	94.5	63.4
0.3	92	72
0.4	90	79.5
0.5	87.6	85.7
0.6	85.1	90.1
0.7	82.6	92.5
0.8	74.6	97.5

the 0.05. It is also observed that chi square calculated 11.23 is less than chi square 15.50 from standard chi square distribution table. The successes of test indicate that the model has good fit.

Cutoff value was found out to get optimum accuracy of model to assess probability of employment. The cutoff point was varied from 0.2 to 0.8 and calculates predicted accuracy of placed and unplaced group as shown in Table 7.

The gradient of the curve was evaluated to determine best cutoff point value to achieve a desire balance between predicted accuracy of placed and unplaced group in % as shown in Fig. 1.

From curve, it is observed that the predicted accuracy of placed group changes inversely proportional with cutoff point. The optimum value of predicted accuracy of placed group is 87.76%, and unplaced group is 85.70% at 0.5 cut-off value. Hence, binary logistic regression model is found out by taking cutoff point 0.5. The sensitivity analysis is carried out to check impact of individual skill on output employability. To find out the predicted employability, vary one input variable, keeping other variables

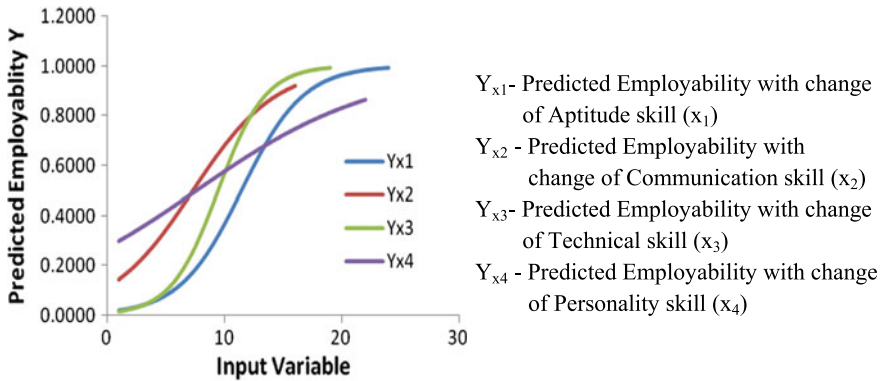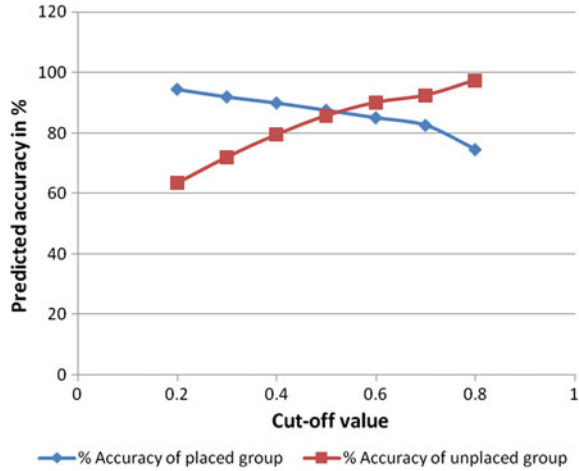**Fig. 1** Cutoff point versus predicted accuracy of placed and unplaced group

Fig. 2 Input variables versus predicted employability

Y_{x1}- Predicted Employability with change of Aptitude skill (x_1)

Y_{x2} - Predicted Employability with change of Communication skill (x_2)

Y_{x3}- Predicted Employability with change of Technical skill (x_3)

Y_{x4} - Predicted Employability with change of Personality skill (x_4)

constant. The graph is plotted between independent variables and their predicted probability of employment as shown in Fig. 2.

From curve, it is observed that, the students having 100% aptitude and technical skills may have maximum probability of placement. Hence, students need to have excellent aptitude skill and technical knowledge to get assured employment in campus placement for IT sector.

9 Conclusions

From analysis, it is concluded that all input variables are significantly contributing to predict probability of employment in campus placement recruitment process of IT

Sector companies. It means being good at one skill cannot facilitate 100% probability of employment in IT Sector. Aptitude is the major deciding skill factor to get early employment in campus placement. All independent variables are having positive correlation with each other. The model helps students and trainer to understand level of skills set required by IT Sector well in advance, which allows them to work upon weak areas. Further employers may use this approach to find out quality engineering talent from untapped region and provide equal opportunities to fresh engineers. All of these means that the institute needs to focus on skill set required to make graduates employable and make rigorous efforts to develop them, to make them competent and employable.

References

1. Manda, S., Kumar, N.: Status of technical education in India—emerging issues and challenges. Scribd Digit. Libr. 67–72 (2012)
2. PurpleLeap Study: Low Employability Skills Among Engineering Students, in Andhra Pradhesh. Reachout's News Bureau (2009)
3. Survey Conducted by Federation of Indian Chambers of Commerce and Industry (FICCI) and World Bank, Employability of Fresh Engineering During Training Period (2009)
4. Karapetrovic, S., Rajamani, D.: An approach to the application of statistical quality control technique in engineering courses. J. Eng. Educ. 269–276 (1998)
5. Handa, C., et al.: Research activity in un-aided engineering colleges a review, need and hurdles. J. Eng. Educ. (2011)
6. Jonck, P., et al.: Human capital evaluation of graduates from the faculty of management sciences employability skills in South Africa. Acad. J. Interdiscip. Stud. **3**(6), 265–274 (2014)
7. Nenzhelele, T.E., et al.: Employability through experiential learning course in open distance learning institution. Mediterr. J. Soc. Sci. **5**(20), 1602–1612 (2014)
8. Sermsuk, S., et al.: Employment conditions and essential employability skills required by employers for secondary school graduate. Proc.—Soc. Behav. Sci. **116**, 1848–1854 (2014)
9. Venkatesh, B.R., et al.: A study of the importance of soft skills and positive attitude as perceived by industry with specific reference to fresh engineers. Int. J. Res. Commer. Manag. **4**(1), 78–84 (2013)
10. Chithra, R., et al.: Employability skills—a study on the perception of the engineering students and their prospective employers. Glob. J. Manag. Bus. Stud. **3**(5), 145–155 (2013)
11. Rosenberg, S., et al.: Basic employability skills: a triangular design approach. Educ. Train. **54**(1), 7–20 (2012)
12. Gokuldas, V.K., et al.: Predictors of employability of engineering graduates in campus drives of Indian software services companies. Int. J. Sel. Assess. **19**(3), 313–319 (2011)
13. Rao, A.A., et al.: Employability in MNCs: challenge for graduates. Interdiscip. J. Contemp. Res. Bus. **3**(4), 189 (2011)
14. Kalbande, V., Handa C.: Identification of important parameters and skills required by Engineering students in campus placement process. Int. J. Eng. Res. **3**(S2), 319–325 (2015)
15. Yuzainee, M.Y.: Employability skills for an entry level engineer as seen by Malaysian employers. In: At 2011 IEEE, Global Engineering Education Conference (EDUCON), pp. 80–85 (2010)
16. French, B., et al.: An examination of indicators of engineering students' success and persistence. J. Eng. Educ. 419–425 (2005)
17. Sacre, M., et al.: Characteristics of freshman engineering students: models for determining student attrition in engineering. J. Eng. Educ. 139–149 (1997)

18. Kalbande V., Handa C.: Developing a mathematical model to check employability of mechanical engineering students. In: 2nd International Conference on Industrial Engineering, Surat, pp. 861–865 (2013)
19. William, B.: Exploratory factor analysis: a five step guide for novices. J. Emerg. Prim. Health Care **8**(3) (2010)
20. Felder, R., et al., A longitudinal study of engineering student performance and retention I. Success and failure in the introductory course. J. Eng. Educ. 15–21 (1993)
21. Yamane, T.: Statistics, an Introductory Analysis, 2nd edn. New York: Harper and Row (1967)
22. Park, Kang, Kerr, Peter: Determinants of academic performance: a multinomial logit approach. The J. Econ. Educ. **21**(2), 101–111 (2012)
23. Kalbande, V., Handa, C.: Developing a model to correlate employability of engineering graduate with employability skill sets in campus placement for IT sector. Online Int. Interdiscip. Res. J. **VI**(I), 128–137 (2016)

Process Parameters Optimization of Drip Pipe Extrusion Process Using Taguchi Approach

Vrushali M. Shete and Ashok J. Keche

Abstract In the present analysis work, a plastic extrusion process that's used for production of drip irrigation pipes is optimized using Taugchi approach. It's vital to spot and optimize the process parameters, to assure quality extrusion pipe producing. Conjointly it's essential to find out the defects in it. For analysis work Akash Drip Industries, company was elite. Taguchi technique is employed to optimize the method parameters, temperature and take-off speed. The experiment was conducted for 3 totally different material providers as supplier changes properties of material aiming to modified due to parameter setting throughout producing of material. Taugchi L9 orthogonal array is chosen for experimental designing and experiment was analyzed exploitation business Minitab18 computer code. After interpretation of values, optimized factor settings were chosen to predict minimum defects. The result unconcealed that using optimized values of things proportion defects for uneven wall thickness decreased from average of 4.19, 4.103, 5.04 to 1.38, 1.66, and 1.18 severally for 3 material suppliers.

Keywords Plastic pipe extrusion · Design of experiment · Taguchi loss function · S/N ratio

1 Introduction

Plastic Extrusion could be a high-volume producing method wont to turn out product of continuous lengths of constant cross section like pipes and tubes. To optimize the manufacturing processes, several strategies are developed and used over the years. Amongst all processes Design of experiments is that the most generally used technique. This is often one in all the foremost thoroughgoing approaches in product and method development. The foremost perspective to DOE is Full Factorial Design and Taguchi technique. Orthogonal array could be a technique recommended by Taguchi

V. M. Shete (✉) · A. J. Keche
Department of Mechanical Engineering, MIT, Aurangabad, India
e-mail: shetevm@gmail.com

to review impact of many control factors over entire parameter space. Exploitation OA technique we tend to need lesser variety of experiments to be conducted, however Full Factorial style needs sizable amount of experiments to be conducted. To measure the performance characteristics which are deviating from the expected target value the concept of the loss function counseled by Taugchi. The value of this loss function is further regenerate into signal-to-noise(S/N) ratio. There are 3 S/N ratios of common interest that are: a. nominal-the-best, b. larger-the-better, and c. smaller-the-better. In present work smaller-the-better kind of control function, was employed in scheming the S/N magnitude relation. Akash Dip industry is a manufacturer of variety of best in class drip irrigation pipes, located close to Renapur, Dist. Latur-413527 (India).

2   Literature Review

Gadekar et al. [1] found that the inappropriate setting of operational parameters, recent machineries, compounding material with wrong proportion, poor testing and examination of material are the causes for the scrap within the company. Improper setting of operational parameters kept on an outsized share of the explanation for scrap and nonconformity of the merchandise. Taguchi's technique of design of experiment for setting of optimum operational parameters is employed for minimizing scrap rates. Rao et al. [2] executed the design and optimization of extrusion process using Taguchi method and finite element analysis of temperature and extrusion load during extrusion of aluminum 6061 alloy. Taguchi L9 design matrix used for experimental run. Analysis of variance (ANOVA) technique is used to check the importance of the input variables on the output responses. The optimal process parameters are obtained using Taguchi's approach. Kumar et al. [5] used Taguchi technique for optimization of process parameters in extrusion blown film machinery. To review the performance parameters on tensile strength orthogonal array and signal/noise ratio enforced. For higher quality characteristics bigger S/N ratio is chosen. Therefore, level with the greatest S/N ratio was elite. In these analysis four factors like melting temperature, winding speed, extrusion speed and pressure were elite for conducting experiments. By use of acceptable orthogonal array experiments were conducted. Afterward by measuring the tensile strength, Signal to Noise ratio was calculated. Exploitation MINITAB 17 computer code Main impact plots for S/N ratios were drawn and optimum parameter values were obtained. Narasimha et al. [7] targeted on to search out the basis causes for the prevalence of defects and wastes in plastic extrusion method. To spot the basis causes of those defects the cause and effect diagram was enforced. The important causes were the take off speed, temperature, vacuum pressure, screw speed and material properties as are often seen from cause and effect diagram. Exploitation Taguchi's principle of loss function the quality loss for the present performance variation was calculated and demand for improvement was verified.

Table 1 The categories of defects with frequency data for-1 month observation

Sr. no	Type of quality defects	Frequency of defect
1	Uneven wall thickness	70
2	Off-center	4
3	Diameter variation	52
4	Crack	14
5	Discontinuity in drilling	26
6	Rough surface finishing	12
	Total	178

Fig. 1 In-line drip pipe

3 Problem Statement

The present analysis work is administered at Akash Drip Industries, Renapur. The categories of defects determined with frequency are as shown in Table 1. The subsequent information is employed for investigation purpose.

Product: In-line Drip Pipe

Size: Diameter = 16 mm, Wall Thickness = 0.45 mm, Length = 300 m (Fig. 1).

4 Methodology

In present work design of Experiments (DOE) using Taguchi's design for optimization of the process parameters is employed. The fundamental steps related to design of experiments (DOE) using Taguchi approach:

   i. Recognition of objective function to be optimized
  ii. Recognition of noise factor
 iii. Recognition of the control factors and their levels
  iv. Selection of appropriate orthogonal array
   v. S/N calculation and experimentation
  vi. Prediction of optimized setting from Taguchi analysis

vii. Prediction of optimum control factors levels and its performance.

4.1 Recognition of Objective Function

Our objective is to minimize the uneven wall thickness defect of drip pipe. Hence, objective Function: Smaller-the-Better is employed to reduce the response. S/N Ratio for this function:

$$S/N = -10 \log_{10} \left(1/n \sum_i^n y_i^2 \right) \tag{1}$$

where, n = Sample Size, and y = % defect in that run.

4.2 Recognition of Process Parameters

The factors that have an effect on the drip pipe dimensions and cause the defect of uneven wall thickness are as per Table 2.

The factors that considerably have an effect on the performance are taken into consideration in constructing matrix experiment. All alternative factors are considered as Noise Factors. The subsequent 3 parameters that are most affecting are designated for performing the matrix experiment:

  (i) Take-off speed (m/min)
 (ii) Temperature 1(°C) (Barrel zone 1)
(iii) Temperature 2(°C) (Coating zone 1).

4.3 Recognition the Control Factors and Their Levels

The extrusion setup has various thermocouples connected to the extruder and coating machine. The most important temperatures are BZ1 and CZ1 that are to be set and alternative are to be accrued incrementally within the increments as in extruder BZ1 and BZ2 increments are by nearly 5 °C, in extruder SC, MZ1, DZ1 by 25 °C and in

Table 2 Factors that have an effect on production of drip pipe

Control factors	Noise factors
Take-off speed	Vacuum pressure
Temperature 1	Relative speed of auxiliary
Temperature 2	–

coating zone increments by 25 °C. For optimization purpose base temperature BZ1 (Temperature T1) and CZ1 (Temperature 2) is chosen as control factors. Because the material provider changes the defects incidence range and the parameter settings also changes. Hence there's need to optimize these control factors for every of the provider. So, experiments are designed differently for every material provider and process parameters are optimized consequently. The factors and their levels are shown Table 3.

4.4 Selection of Orthogonal Array

The Taguchi optimization technique starts with choice of associate accetable orthogonal array. The minimum number (min N) of runs within the array may be determined as follows:

$$N_{\min} = (L - 1)F + 1 \tag{2}$$

where, L = number of levels, F = number of factors.
   where, $L = 3$ and $F = 3$.
   Now Taguchi's array is chosen for experimentation having minimum seven numbers of experiments. Total 9 experiments were administered as a result of the foremost appropriate orthogonal array for experimentation having three factors and three levels is L9 array.

4.5 Experimental Programme

With relation to the above OA, nine experiments were conducted with their factors and their levels as mentioned in Table 3. The defect uneven wall thickness for every experiment was measured and % defects for every supplier calculated. For every supplier want one separate experimental array of nine runs. Thickness variation of

Table 3 Control factor levels for three suppliers

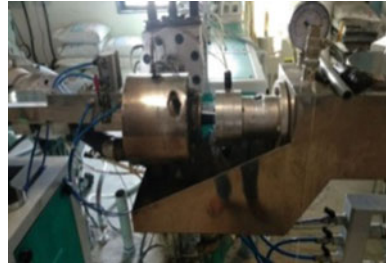|	Vardhaman Polymers, Ahemadnagar			Lata Industries, Latur			Bansal Polymers, Hyderabad		
Control factors	Level			Level			Level		
Unit	1	2	3	1	2	3	1	2	3
Take-off speed (m/min)	19	22	25	18	21	23	22	25	27
Temp. 1 (°C)	158	163	169	169	176	182	152	160	164
Temp. 2 (°C)	171	178	182	182	188	192	163	171	178

Fig. 2 Temperature control panel

Fig. 3 Machine control panel

Fig. 4 Die section

the pipe was measured using the screw gauge. Each of the above nine experiments were conducted three times (27 experiments for every supplier) to account for the variations which will occur because of the noise factors. The temperature instrument panel to manage temperatures, the machine control panels to manage takes off speed and different parameters and also the die section of machine are shown in Figs. 2, 3 and 4 severally.

5 Results and Discussion

Experimental work is administered at Akash Drip Industries, Renapur, Latur for 3 different material suppliers particularly Vardhaman Polymers Ahemadnagar, Lata Industries Latur, Bansal polymer Hyderabad. The experimental results are mentioned in Tables 4 and 5. Sample Calculation:

Table 4 OA with control factors for three suppliers

Exp. no.	Vardhaman Polymers, Ahemadnagar			Lata Industries, Latur			Bansal Polymers, Hyderabad		
	Take-off speed	Temp. 1	Temp. 2	Take-off speed	Temp. 1	Temp. 2	Take-off speed	Temp. 1	Temp. 2
1	19	158	171	18	169	182	22	152	163
2	19	163	178	18	176	188	22	160	171
3	19	169	182	18	182	192	22	164	178
4	22	158	178	21	169	188	25	152	171
5	22	163	182	21	176	192	25	160	171
6	22	169	171	21	182	182	25	164	163
7	25	158	182	23	169	192	27	152	178
8	25	163	171	23	176	182	27	160	163
9	25	169	178	23	182	188	27	164	171

Table 5 Percentage of defects for different suppliers

Exp. no.	1	2	3	4	5	6	7	8	9
Vardhaman Polymers, Ahemadnagar	4.688	3.333	4.412	4.762	8.065	7.273	3.226	3.279	5.172
Lata Industries, Latur	3.279	4.478	1.852	2.083	4.286	7.353	6.154	3.030	4.412
Bansal Polymers, Hydrabad	3.846	7.143	4.688	2.857	5.882	5.714	3.448	4.839	6.944

The percentage of defect per shift

$$= (\text{Number of defective products having uneven wall thickness})/$$

$$(\text{Total number of units produced per shift}) * 100 \qquad (3)$$

It was found that, total 65 units are produced per shift out of that 7 defective units having uneven wall thickness.

% defect = 7/65 * 100 = 10.769% … (Putting values in Eq. 3).

After conducting the experiment, the results were converted into S/N ratio values. For these experimentation and analysis using Taguchi results are adopted with the assistance of Minitab-18 software package. Smaller-the-better kind of control function was employed in calculating the S/N ratio. Main effects plot for the main effect terms viz. factors take-off speed, temperature 1 and, temperature 2 are shown in Figs. 5 and 6.

6 Confirmation Experiment

Confirmation experiments conducted using the factor levels obtained by S/N ratio plot, using Taguchi method, for each supplier the level of factors found different. Total three experiments were conducted and their % defects values were checked. It can be seen that the results are having minimum defects (Table 6).

7 Conclusion

The Following conclusions are drawn from the current study:

(1) The experimental results show that the temperature and take-off speed are the main parameters which will have an effect on uneven wall thickness defect.
(2) The optimum values for influential factors for lesser percentage defects in drip pipe extrusion are obtained from Taguchi's methodology for various material suppliers.

Table 6 Confirmation experiment

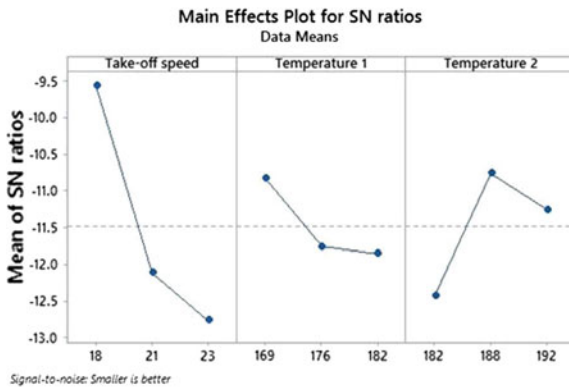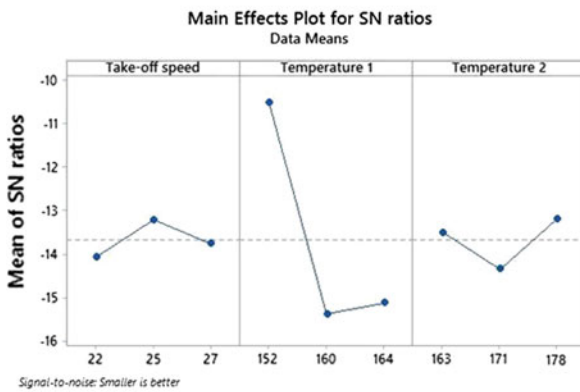| Supplier name	Optimized values of factors			% defects
	Take-off speed	Temp. 1	Temp. 2	
Vardhaman Polymers, Ahemadnagar	22	169	182	1.38
Lata Industries, Latur	23	182	182	1.66
Bansal Polymers, Hyderabad	22	160	171	1.18
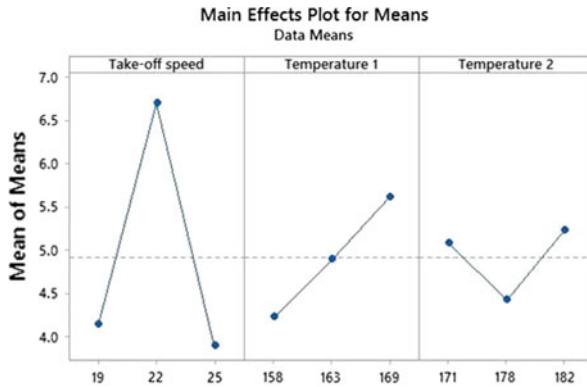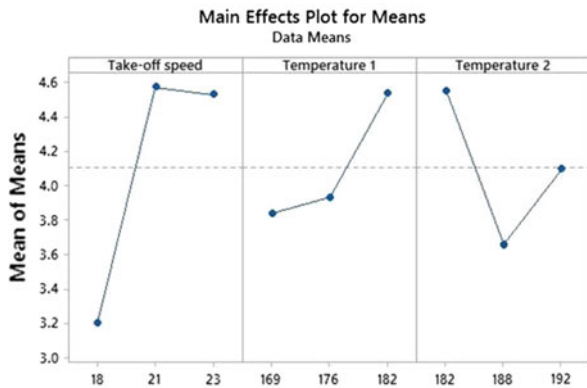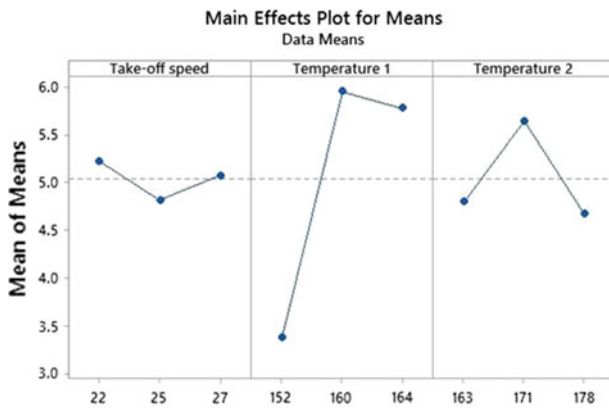
Fig. 5 Main effects plot for means
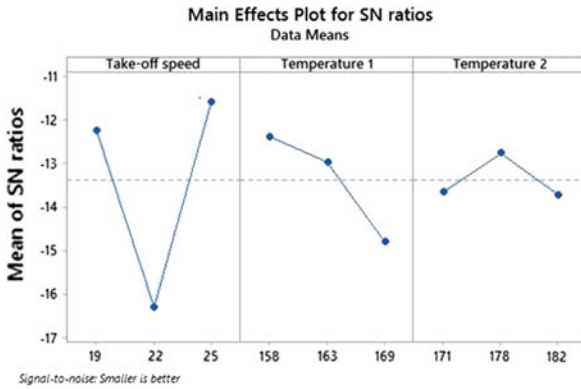
Vardhaman Polymers, Ahemadnagar

Lata Industries, Latur

Bansal Polymers, Hyderabad

Fig. 6 Main effects plot for S/N ratios

Using optimized values of factors percentage defects for uneven wall thickness reduced from average of 4.19, 4.103, 5.04 to 1.38, 1.66, and 1.18 severally for 3 material suppliers particularly Vardhaman Polymers Ahemadnagar, Lata Industries Latur and Bansal Polymers Hyderabad.

(4) The current work helps to boost the quality of product and to optimize drip pipe extrusion process.

References

1. Gadekar, S.S., Khan, J.G., Dalu, R.S.: Analysis of process parameters for optimization of plastic extrusion in pipe manufacturing. Int. J. Eng. Res. Appl. **5**(5) (Part 1), 71–74 (2015). www.ijera.com. ISSN: 2248-9622
2. Rao, T.B., Gopala Krishna, A.: Design and optimization of extrusion process using FEA and Taguchi method. Int. J. Eng. Res. Technol. (IJERT) **1**(8) (2012). ISSN: 2278-0181
3. Taguchi, G., Elsayed, E.A.: Quality Engineering in Production Systems. McGraw-Hill Book Company, New York (1989)
4. Levy. S., Carley, J.F.: Plastice Extrusion Technology Handbook. 2nd ed. ISBN: 9780831111854 (2005)
5. Kumar, D., Kumar, S.: Process parameters optimization for HDPE material in extrusion Blown film machinery using Taguchi method. IOSR J. Mech. Civil Eng. (IOSR-JMCE) **12**(4), 1–3 (2015)
6. Maddock, B.H.: Factors affecting quality in polyethylene extrusion. Mod. Plastics **34**(8), 123–136 (1957)
7. Narasimha, M., Rejikumar, R.: Plastic pipe defects minimization. Int. J. Innov. Res. Dev. **2**(5) (2013)
8. Roy, R.K.: Design of Experiments Using the Taguchi Approach: 16 Steps to Product and Process Improvement. Wiley Inter-science publication, ISBN 0-471-36101-1
9. Raju, G., Sharma, M.L., Meena, M.L.: Recent methods for optimization of plastic extrusion process: a literature review. Int. J. Adv. Mech. Eng. **4**(6), 583–588 (2014)
10. Kerealme, Srirangarajalu, N., Asmare, A.: Parameter optimization of extrusion machine producing UPVC pipes using Taguchi method: a case of Amhara pipe factory. Int. J. Eng. Res. Technol. (IJERT) **5**(01) (2016). ISSN: 2278-0181
11. Sharma, G.V.S.S., Umamaheswara Rao, R., Srinivasa Rao P.: A Taguchi approach on optimal process control parameters for HDPE pipe extrusion process. J. Ind. Eng. Int. **13**, 215–228 (2016)

Nanofluids—A Novel Approach of Enhancing the Heat Transfer

Prashant P. Shingare, Vilayatrai M. Kriplani and R. S. Shelke

Abstract Nanofluids have numerous advantages over traditional heat transfer fluids. Among previous 10–20 years, extensive work had carried out in this emerging area of nanofluid heat transfer. Single and multi walled carbon nanotubes since having very high thermal conductivities, yields in higher enhancement rates even with smaller concentrations of these nanofluids. In this review paper major contributions made in enhancement of heat transfer by various researchers in last few decades are summarized having emphasis on enhancement techniques by using nanofluids only. So, this article will provide a brief insight of the work carried out till date in nanofluid heat transfer area for the incoming research in this field.

Keywords Nanofluids · Heat transfer · Thermal conductivity · Volumetric concentration

Nomenclatures

μm	Micrometer (1 μm = 1×10^{-6} m)
CVD	Chemical vapour deposition
CFD	Computational fluid dynamics
GA	Gum Arabic
MWCNTs	Multi walled carbon nanotubes
nm	Nanometer (1 nm = 1×10^{-9} m)
PVA	Polyvinyl alcohol

P. P. Shingare (✉) · V. M. Kriplani · R. S. Shelke
Department of Mechanical Engineering, G H Raisoni College of Engineering,
Nagpur 440016, India
e-mail: prashant_wrr@rediffmail.com; prashant.shingare@raisoni.net

V. M. Kriplani
e-mail: v.vmk@rediffmail.com; vilayatrai.kriplani@raisoni.net

R. S. Shelke
e-mail: rupesh.shelke@raisoni.net

Re   Reynolds number
SDBS   Sodium dodecyl benzene sulfonate
SDS   Sodium dodecyl sulfate
SEM   Scanning electron microscope
SWCNT   Single walled carbon nanotubes
TEM   Transmission electron microscope

1 Introduction

Higher rate of heat transfer in forced convection cooling is always in demand and is a major technological challenge faced by various types of industries such as transportation, microelectronics, air conditioning, chemical processes and manufacturing. Enhancement in heat transfer is a major key aspect in developing compact heat exchangers which will be having low cost with light weight & size and also high efficiency.

The cooling fluids which are traditionally used like water, ethylene glycol, propelene glycol and engine oil have lower thermal conductivities as well as lower thermal coefficient of heat transfer. On the contrary, solid particles comprising of metals and metal oxides mostly have much higher thermal conductivities than these fluids, suspension of which in these fluids will result into heat transfer enhancement. A step ahead in this regard was the use of macrometric and even micrometric size of such particles suspending in these fluids which suffers major drawback in terms of sedimentation, clogging of flow channels and eroding pipes and channels. Nanotechnology provides the solution for these drawbacks in terms of nanofluids.

This terminology of nanotechnology was first introduced by Taniguchi (Tokyo science University) in the year of 1974. According to him Nanotechnology basically comprises of processing, separation, consolidation and deformation of materials by means of one atom or one molecule. Nanofluid is a term which was coined by Choi and Eastman in 1995. Nanofluids are usually made from one of the types of base fluids and at least one type of nanoparticles having at least one dimension sized from 01 to 100 nm.

Nanoparticles have few unique qualities like large ratio of surface area to the volume which is nearly 1000 times higher for particles having diameter of 10 μm. This large surface area results into improvement in heat transfer capabilities as well as increases the steadiness of the suspension. Extremely large quantity of total surface area has been provided by nanoparticles, therefore they are having strong potential for heat transfer applications. Now a days utilization of these nanofluids is increasing for different applications including microelectronics, utility of solar energy in generating power, transportation, lighting, and micro—electro mechanical systems (MEMS). Recent nanofluid techniques includes suspension of these nanofluids in the coolants and lubricants, metal cutting fluids and hydraulic fluids to enhance their thermophysical properties like capacity of load carrying, antiwear and friction reducing characteristics among the moving mechanical components.

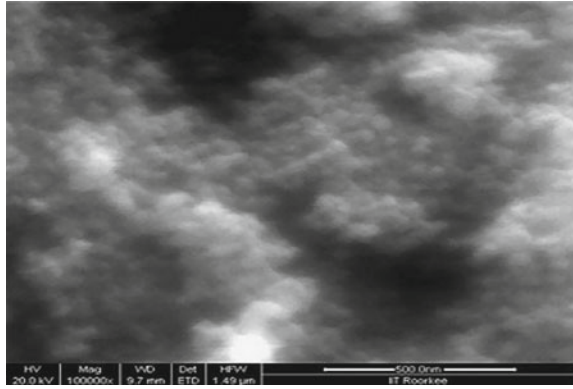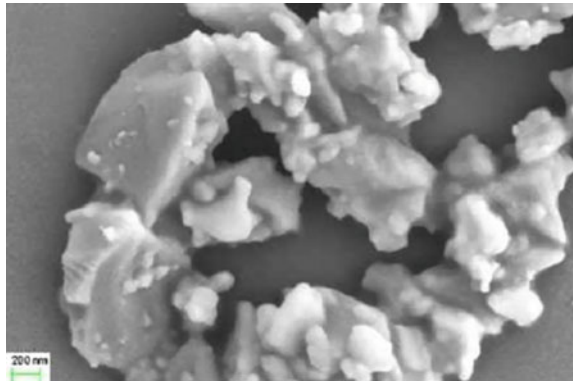**Fig. 1** SEM image of the agglomerated ZnO nanoparticles [1]

Fig. 2 SEM image of SiC powder sample dispersed in fluid medium [2]

In this review paper an attempt has been made to summarize the contributions given by different researchers in enhancing the heat transfer by means of nanofluids. This paper also presents a brief overview of the research work carried out till date in this emerging area of enhancing the heat transfer by means of nanofluids for the new researchers. In this review paper focus has been given on the types of nanoparticles used, their sizes, volumetric concentrations, type of flow channel and type of flow under study (Figs. 1, 2, 3 and 4).

2 Review on Nanofluid Heat Transfer Enhancement Techniques

Khullar et al. [4] have conducted experiments with Al_2O_3 nanofluid, prepared by two step method and used base fluid as transformer oil with surfactant oleic acid 4% by volume. Nanofluid concentrations used were 0.1, 0.2 and 0.5% by volume. Sonication was carried out for one and half hour. They reported that nanofluids
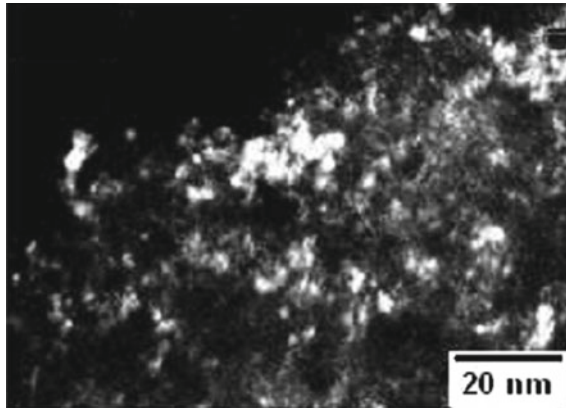
Fig. 3 TEM image of CuO nanoparticles [3]

Fig. 4 SEM image of CuO nanoparticles [3]

have higher thermal conductivities by 2.1, 2.6 and 4.5% than that of base fluids related to the respective concentrations used. With increased temperature, density and viscosity of the nanofluids goes on decreasing while at increased concentration, density as well as viscosity is higher. Coefficient of heat transfer was higher at higher flow rates which finally improves thermal conductivity of nanofluids. Zeinali Heris et al. [5] have carried out experimentation on forced convective heat transfer in the laminar flow range for water based Al_2O_3 nanofluids which were allowed to flow in a plain pipe at uniform wall temperature. According to them the coefficient of heat transfer improves along with the rise in the volumetric concentration of the nanoparticles.
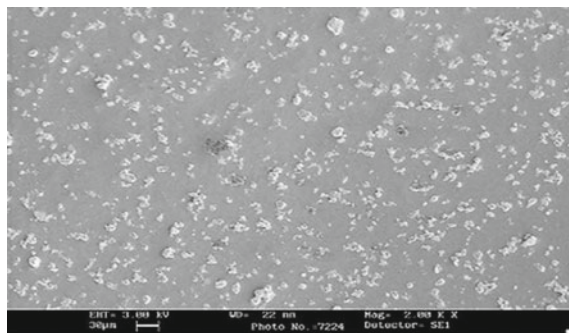
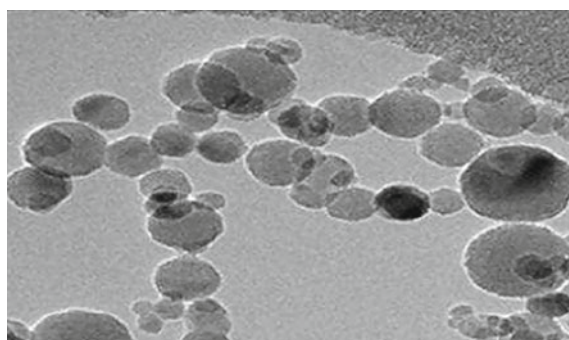**Fig. 5** SEM image of A1$_2$O$_3$/water nanofluid [7]

Fig. 6 TEM image of the A1$_2$O$_3$ nanoparticles [6]

Synthesis as well as characterization of ZnO nanoparticles and also its nanofluids using a base fluid as polyvinyl alcohol had carried out experimentally by Singh et al. [1]. Sythesization of crystalline ZnO nanoparticles were done by applying single step chemical method where as the nanofluids were made by means of dispersion of nanoparticles with PVA solution by ultrasonication process conducted in an ultrasonicator. They reported that the amount of crystallinity for the nanoparticles is dependent on evaporation rate obtained through its synthesis. Also there exists a non linear relationship between the ultrasonic velocity and temperature for the nanofluid under study. Almohammadi et al. [6] have carried out experimental work on the analysis of convective coefficient of heat transfer as well as pressure drop with water based Al$_2$O$_3$ nanofluids. Flow pattern utilized during their studies was laminar and experimentation was done under uniform heat flux criteria. Water based Al$_2$O$_3$ nanofluids having 0.5 and 1% volumetric concentrations were used while the nanoparticle diameter was 15 nm. The result shows that convective coefficient of heat transfer gets enhanced as the nanoparticle volumetric based concentrations are increased (Figs. 5 and 6).

It was observed that the heat transfer coefficient improves by 11–20% with 0.5% concentration by volume and enhanced by 16–27% with 1% concentration by volume when differentiated to the distilled water. In their experimentation any significant increase in friction factor for the nanofluids under study was not recorded.

Fakoor-Pakdaman et al. [8] have investigated characteristics of pressure drop for the MWCNT nanofluid which flows in a helically coiled vertical tube. The base fluid used was heat transfer oil and the flow pattern under test was laminar flow. The tube wall temperature was maintained uniform at nearly 95 °C in order to obtain boundary conditions of isothermal nature. Ratio of pitch to that of tube diameter varies from 1.6 to 6.1 and diameter ratio of coil to that of tube ranges from 14.1 to 20.5. Experimental data reveals that MWCNT nanofluids tested have higher pressure drop rate as compared to that of base fluid and this rate of pressure drop does not depends on the type of geometry of tube through which the nanofluids are flowing. Further rise in the pressure drop across the test section occurred when the nanofluids flow inside the helically coiled tube instead of that of a straight tube and that increase was found to be exponential in nature. This enhanced pressure drop is as high as 3.5 times as compared to the flow with base fluids when MWCNT nanofluids having 0.4% particle concentration by weight were flowing in a helically coiled vertical tube.

The variations in temperature, ultrasonication time and surfactant additives and their effects towards the thermal and physical properties of MWCNT was evaluated experimentally by Sadri et al. [9]. Three surfactants which were tested are GA, SDBS and SDS. At various temperatures the viscosity and thermal conductivity for the nanofluid suspensions has been measured. They reported that higher enhancement in thermal conductivity is obtained with GA surfactant as compared to others i.e. SDS & SDBS. Also they observed that nanofluid dispersion, thermal conductivity and viscosity gets altered with the variation in sonication time. When the sonication time and temperature was increased, nanofluids thermal conductivity was also observed to be significantly increased. At 45 °C temperature, the maximum heat transfer increase of the order of nearly 22% was observed for 40 min sonication time. An increase in MWCNT nanofluids viscosity was recorded when the sonication time was increased upto 7 min and after that subsequent increase in sonication time resulted into decrease in thermal conductivity (Figs. 7, 8 and 9).

Sajadi and Dizaji [10] have experimentally investigated pressure drop and heat transfer for water based Al_2O_3 nanofluids flowing in a circular tube having uniform wall temperature. Volume fraction of nanoparticles inside the base fluid was 1 and 2%. Experimental analysis was done for the turbulent flow pattern for which the Reynolds number was varied from 5000 to 30,000. The results reveals an increase in the coefficient of heat transfer of nearly 12% for 2% nanoparticle concentration. With increasing nanoparticle volumetric concentration it was observed that pressure drops associated with the use of nanofluids also goes on increasing. Experimental result shows that nanofluids are having higher overall performance compared to that of clean water. Abdul Hamid et al. [11] have investigated heat transfer properties of TiO_2 nanofluid with respect to temperature under forced convection. The experiment has been carried out under constant heat flux boundary conditions having Reynolds
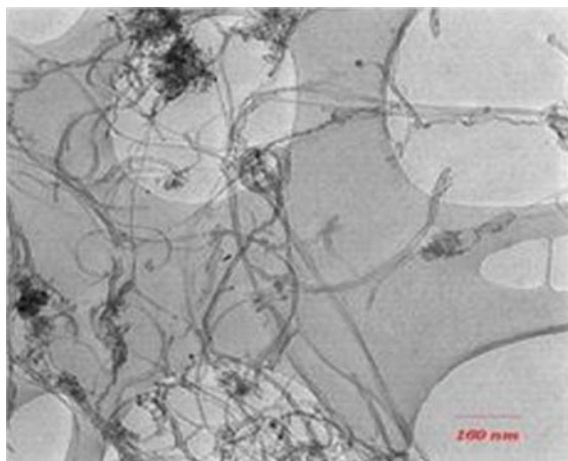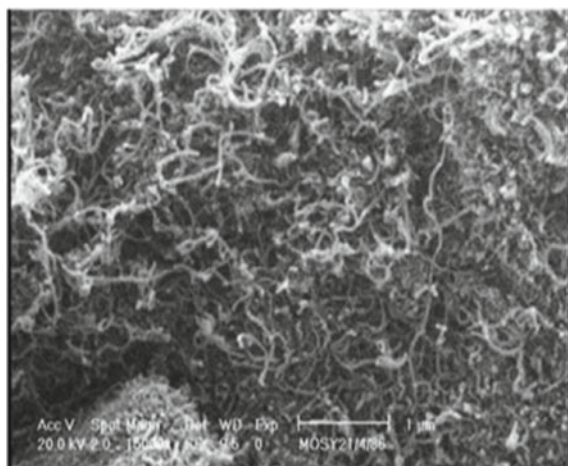
Fig. 7 TEM images of MWCNT [8]

Fig. 8 SEM images of MWCNT [8]

number lower than 25,000 and TiO_2 nanofluid concentrations ranging from 0.5 to 1.5%. Thermal conductivity enhancement of 22.75 and 28.92% was observed at 50 and 70 °C at the respective nanofluid concentrations. It has been observed that working temperature influences the performance of nanofluids considerably. Considerable improvement in enhancement of heat transfer for TiO_2 nanofluids were accounted to their enhancement in thermal properties because of the presence of nanoparticles, particularly at higher volumetric concentration and at an elevated working temperature.
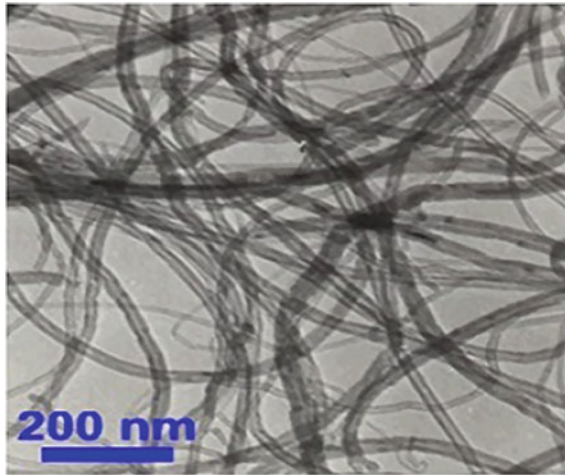
Fig. 9 TEM image of MWCNT nanofluids [9]

Wan et al. [12] have carried out investigations with demonized water based MWCNT nanofluids prepared through the method of chemical vapour deposition. The volumetric concentration was varied from 0.01 to 0.05%. To minimize the agglomeration of the MWCNT, extremely little quantity of surfactant namely Sodium Dodecyl Sulfate (SDS) was added. They observed sudden enhancement at lower temperatures and particularly for MWCNTs having volumetric concentration of nearly 0.03% with base fluid as water, which can be recognized to generation of CNT chains having much higher conductivities in the medium. The enhancement in the thermal conductivities based on the temperature variations can be understood with the help of theory of Brownian motion since chains of carbon nanotubes are formed at elevated temperatures due to instability which results from increase in temperature.

Ganesh Kumar et al. [13] have investigated different thermophysical properties and density of MWCNT having base fluid as a combination of Ethylene Glycol in Water. For measuring density of nanofluids, the method of standard volumetric flask was used and fair agreement was reported with mixing theory. A maximum of 11% enhancement for thermal conductivity was reported for nanofluids having 0.9% weight concentration. Nanofluids Viscosity ratio increases with rise in temperature and nearly twice enhancement was recorded specially for the temperature variation of 30–40 °C. Piratheepan and Anderson [14] have performed experimental investigations on the heat transfer characteristics of MWCNT nanofluids inside a straight circular tube within the turbulent flow region. They conclude that using the MWCNT nanofluid, pumping power was increased and convective heat transfer characteristics decreases. So they suggested that MWCNT nanofluids could not be considered as an appropriate media for heat transfer for the forced turbulent flow regime under study. For the nanofluids comprising of Fe_3O_4 nanoparticles and deionized water, heat transfer properties under forced convection were investigated by Ma et al. [15]. Test

section comprises of horizontal copper tube and tests were conducted in transition region for which, the Reynolds numbers ranges from 2500 to 5000. The results had revealed that coefficients of heat transfer for Fe_3O_4 nanofluids falls as the nanoparticles concentrations increases for the transition regime of flow which differs from initial expectation.

Thermal and hydrodynamic behavior of Al_2O_3, CuO and TiO_2 nanofluids was numerically investigated by Balla et al. [16], for the flow inside a uniformly heated tube. The volumetric concentration was varied from 0 to 4%, whereas Re range used was 100–1000. They observed that Nusselt number as well as coefficient of heat transfer increases as the nanofluid volumetric concentration is increased with an increase in pressure losses. Kalbasi and Saeedi [17] analyze CuO with water nanofluids numerically for the flow in a circular tube with the varied nanoparticle volumetric concentrations under the conditions of uniform heat flux. They reported that the predicted Nusselt numbers reveals better agreements with correlation proposed by Gnielinski. Their results indicate that as the concentration by volume of nanoparticles increases, the corresponding heat transfer rate along with wall shear stress goes on increasing. In their work, the Reynolds number was varied from 20,000 to 100,000 with volumetric concentration of 0–4%. Hussein et al. [18] have conducted experimental study on the thermal characteristics of different nanoparticles namely TiO_2, Al_2O_3 and SiO_2 by using base fluid as water. Heat transfer under forced convection in the turbulent flow region for which the Reynolds number is varied from 5×10^3 to 50×10^3, in a heated horizontal tube have been numerically simulated. On the contrary, for the flat tube, heat transfer rises by nearly 6% and pressure drop falls by around 4% when compared to circular tube.

Nanoparticle heat transfer for turbulent pipe flow has been carried out on theoretical basis by Corcione et al. [19]. Behavior of nanofluids is mostly like single phase fluid rather than that of traditional mixture of solid and liquid, is the basic idea on which this research is based. Corcione et al. [19] have reported that, the amount of optimized loading of particle required for highest amount of heat transfer at uniform driving power was found to be practically same with that of criteria of minimum operational cost at uniform rate of heat transfer; for all the possible mixture of solid with that of liquid phases. The optimal amount of volume fraction increases by increasing the bulk temperature of nanofluid, increasing the Reynolds number and by decreasing the ratio of length to diameter of the tube, where as it was virtually found to be not dependent on the size of suspended nanoparticles.

Enhancement in heat transfer for helically coiled tube inspite of straight tube along with oil based CuO nanofluid was investigated experimentally by Hashemi and Akhavan-Behabadi [20]. Experimentation was carried out in lower laminar region, Reynolds number ranging from 10 to 150. Higher heat transfer rates have been observed for helical tubes than that of simple straight tube. Convective coefficient of heat transfer for water, Cu with water, Al with water, Al_2O_3 with water and TiO_2 with water comprising of 2% concentration of nanoparticle were analyzed for the counter flow heat exchanger by Hasanuzzaman et al. [21]. They reported that convective coefficient of heat transfer as found for Cu with water, AI with water, Al_2O_3 with water and TiO_2 with water nanofluids were 81, 63, 66 and 64% higher when differentiated to that of pure water respectively. They reports an increase in the effectiveness of the heat exchanger by virtue of use of nanofluids.

Experimental performance for enhancement of heat transfer and requirements of pumping power were done using CuO nanafluids by Sahin et al. [22]. Flow region used for tests was turbulent in nature with concentration by volume of the nanofluids varied from 0.5 to 4%. They reveals that as per as the amount of heat transfer is concerned, the CuO nanofluid having volumetric concentration more than 0.5% are not suitable. The maximum heat transfer enhancement were reported for CuO nanofluids at volumetric concentration of 0.005 at Reynolds number of nearly 16,000 and lowest heat transfer enhancement was found for the Reynolds number of 20,000 having volumetric concentration of 0.02. Haghighi et al. [23] have conducted experiments on nanofluids namely Al_2O_3 and TiO_2 having water as base fluid having concentration of 9% by weight. They mentioned an increase of 15% in the coefficient of heat transfer at the same Reynolds numbers. On the other hand for constant pumping power criteria, coefficient of heat transfer for water based Al_2O_3 nanofluids remained unchanged while 10% decrease in coefficient of heat transfer was reported for TiO_2 nanofluids.

3 Summary of Literature Review

Ref. no.	Bibliographic information		Nanofluids details			Type of tube/channel	Flow pattern—Re range	Results/findings/conclusions in short
	Name of the authors	Type of paper	Nanofluids used	Base fluids	Conc. (%)			
[5]	S. Zeinali Heris et al.	EXPT	Al_2O_3	Water	0.2–2.5% by volume	Circular tube	700–2050	Ratio for coefficient of heat transfer for the nanofluid as that for water of 0.2 and 2.5% concentration increases from 1.08 to 1.16 and 1.22 to 1.41 by varying the Peclet number from 2500 to 6000 and 2600 to 6000 respectively
[19]	Massimo Corcione	TH	CuO, TiO_2 and Al_2O_3	Water & EG	Not given	Circular $L/D =$ 50–1000	2300 to 5×10^6	Both cases like constant pumping power (CPP) and constant heat transfer rate (CHTR) were considered
[20]	S. M. Hashemi, M. A. Akhavan-Behabadi	EXPT	CuO	Oil (SN-500)	0.5, 1 and 2% by weight	Horizontal helical tube	Laminar (10–150)	For the uniform concentration of the Nanoparticles significant enhancement in the rate of heat transfer were recorded by incorporating the helical tube than that of plain straight tube. As compared to that of flow of base oil in straight tube, the largest index of performance of 1.26 was reported for the tested nanofluid flow having 2% nanoparticle concentration by weight having the Reynolds no. of nearly 41

(continued)

(continued)

Ref. no.	Bibliographic information		Nanofluids details			Type of tube/channel	Flow pattern—Re range	Results/findings/conclusions in short
	Name of the authors	Type of paper	Nanofluids used	Base fluids	Conc. (%)			
[7]	P. C. Mukesh et al.	EXPT	Al_2O_3	Water	0.1, 0.4 and 0.8 by volume	Shell & Helically coiled tube HE	5100–8700	Maximum enhancement in the overall coefficient of heat transfer & inner Nu was recorded as 24 and 28%, at 0.8% nanoparticle concentration by volume with maximum increase of inner heat transfer coefficient of 25%
[16]	Hyder H. Balla et al.	Numerical	Al_2O_3, CuO & TiO_2	Water	0 to 4% by volume	Circular tube	Laminar 100–1000	The results reveals that both Nusselt number as well as coefficient of heat transfer for nanofluids are dependent on and also increases with the increase in concentration by volume of nanoparticles. Similarly for each value of concentration, the increase in heat transfer is more for the highest valve of Reynolds's number
[17]	Mansour Kalbasi & Alireza Saeedi	Numerical	CuO	Water	0–4 by volume	Circular tube	Turbulent (20,000–1,00,000)	They revealed that the Nusselt No. as well as the coefficient of heat transfer for nanofluids basically depends on nanoparticles and they increases with the concentration by volume of nanoparticles. Also an increase in shear stress was found with the increase in volumetric concentration of nanoparticles

(continued)

(continued)

Ref. no.	Bibliographic information		Nanofluids details			Type of tube/channel	Flow pattern—Re range	Results/findings/conclusions in short
	Name of the authors	Type of paper	Nanofluids used	Base fluids	Conc. (%)			
[4]	Anuj Khullar et al.	EXPT	Al_2O_3	Transformer oil	0.1–0.5	Circular tube	72–400	The pressure drop with nanofluids was found to be lower than that of base fluid when the flow rates were varied and lower pressure drops were observed with the higher amount of nanofluid concentrations
[1]	D. K. Singh et al.	EXPT	ZnO	Polyvinyl alcohol	—	NA	NA	It had been reported that for ZnO with PVA nanofluid, the changes in temperature for ultrasonic velocity were mainly dependent on volumetric concentration of dispersed particles in the region of low frequency
[6]	H. Almohammadi et al.	EXPT	Al_2O_3	Disttiled water	0.5 and 1.0	Circular tube	Laminar flow	The average coefficient of heat transfer was found to be increased by 11–20% with volumetric concentration of 0.5% and increased by 16–27% with volumetric concentration of 1% as differentiated to that of distilled water
[8]	M. Fakoor-Pakdaman et al.	EXPT	MWCNT	Heat transfer oil	0.063, 0.125 and 0.251	Vertical helically coiled tube	Laminar 10–2000	Exponential increase in pressure drop was recorded for helical coiled tube as compared to that of straight tube and pressure drop was found to be decreasing with the increase in the ratio of coil diameter to the tube diameter

(continued)

(continued)

Ref. no.	Bibliographic information		Nanofluids details			Type of tube/channel	Flow pattern—Re range	Results/findings/conclusions in short
	Name of the authors	Type of paper	Nanofluids used	Base fluids	Conc. (%)			
[9]	Rad Sadri et al.	EXPT	MWCNT	Distilled Water	0.5% by wt. and 0.25% GA	NA	NA	GA dispersant was found to be superior over SDS and SDBS in terms of enhancement of thermal conductivity when added to MWCNT nanofluids for increasing its stability
[10]	A. R. Sajadi and A. F. Dizaji	EXPT	Al_2O_3	Water	1 and 2% by volume	Horizontal tube	Turbulent (5000–30,000)	Friction factor was found to be independent of concentration of nanofluids. However, the pressure drop increases with the increase in concentrations of nanofluid. Enhancement in overall performance was reported for the Al_2O_3 nanofluids having water as the base fluid
[11]	K. Abdul Hamid et al.	EXPT	TiO_2	Ethylene glycol	0.5 to 1.5% by volume	Circular tube	Less than 25,000	In the light of the results obtained, maximum enhancement is 28.5% compared to that of base fluid having 1.5% concentration by volume and the working temperature of 70 °C. The effect of temperature is significant in relation to heat transfer performance at high volume concentrations and high temperature in the range studied

(continued)

(continued)

Ref. no.	Bibliographic information		Nanofluids details			Type of tube/channel	Flow pattern—Re range	Results/findings/conclusions in short
	Name of the authors	Type of paper	Nanofluids used	Base fluids	Conc. (%)			
[12]	Meher Wan et al.	EXPT	MWCNTs + deionised water)	Deionised water	0.01, 0.03 and 0.05	Circular tube	—	Due to generation of CNT chains which are highly conductive, a sudden enhancement was recorded at the volumetric concentration of 0.03% for CNTs with base fluid as water in particular lower temperature range. Percolation phenomena is useful for understanding this sudden enhancement in thermal conductivity
[13]	J. Ganesh kumar et al.	EXPT	MWCNT	Water + ethylene Glycol	0.3–1.5 mass conc.	NA	NA	With MWCNT having concentration of 0.9% by weight, maximum enhancement of 11% in the thermal conductivity was reported. Brownian motion is found to be responsible for the temperature dependence of heat transfer enhancement

(continued)

(continued)

Ref. no.	Bibliographic information		Nanofluids details			Type of tube/channel	Flow pattern—Re range	Results/findings/conclusions in short
	Name of the authors	Type of paper	Nanofluids used	Base fluids	Conc. (%)			
[14]	M. Piratheepan and T.N. Anderson	EXPT	MWCNT	Water	1–2 gm/lt.	Double pipe HE	Turbulent	A significant decrease in the heat transfer characteristics was observed with the use of MWCNT s particularly in turbulent region of flow. So, it can be concluded that use of MWCNT nanofluids in the forced convective turbulent flow region is not a good choice in terms of enhancement in heat transfer
[15]	Jie Ma et al.	EXPT	Fe_3O_4	Deionized water	Not given	Horizontal tube	Transitional flow region	In this study, Fe_3O_4 with phenol formaldehyde resin (PFR) nanofluid having water as base fluid was prepared by the approach of facile hydrothermal. However, increase in the concentration of Fe_3O_4 nanoparticles was found to be disadvantageous for raising the forced convective efficiency of heat transfer in transitional flow region

4 Conclusions

It can be concluded from the Literature survey that the uniform distribution or mixing of nanoparticles in the base fluids, known as nanofluids, remarkably improves the thermal as well as physical properties of these traditional fluids. The major drawback of these nanofluids are little drop in pressure associated with the enhancement of heat transfer and another one is the long run stability of nanoparticles which are being dispersed in the base fluid. The difficulty of stability had been overcome by adding the surfactants in nanofluid but only to the certain extend and not for larger durations. For MWCNT, adding surfactant is a common practice than in case of metal oxide nanoparticles.

The enhancement in heat transfer recorded by using the nanofluids is much more than that of one which is predicted by heat transfer standard correlations as applied to nanofluids, considering them to be single phase. The presence of solid nanoparticles which are highly conductive in the nanofluids, leads to much higher increase in coefficient of heat transfer for these nanofluids but is not only the reason for heat transfer enhancement. Brownian motion plays a vital role in augmentation of heat transfer obtained due to the addition of nanoparticles. Also other parameters like particle interactions and fluctuations, basically at elevated Peclet numbers may also results into the change of flow structures and ultimately which leads in heat transfer enhancement because of the dispersion of nanoparticles.

Owing to remarkably lower cost and ease of manufacturer of the metal oxides forms of nanoparticles as compared to pure metals, these metal oxides forms like Al_2O_3, CuO, SiO_2, TiO_2, Fe_3O_4 and ZnO has more attracted for use in nanofluids. Also amongst these varied range of metal oxides, Al_2O_3 and CuO are more popular owing to their easy suspension qualities in base fluids. For the wider range of applications involving heat transfer, the exact understanding as concerned to the fundamentals which are involved in case of the heat transfer for nanofluids and also the wall friction are of prime importance for the development of these nanofluids. Although many efforts had already been taken by different scientists and researchers in last few decades on the development of heat transfer with nanofluids, further experimental based investigations and also the in-depth theoretical understanding about the different mechanisms involved in heat transfer are needed for detailed analysis of heat transfer as well as fluid flow performance for the nanofluids.

References

1. Singh, D.K., Pandey, D.K., Yadav, R.R., Singh, D.: A study of nanosized zinc oxide and it's nanofluid. Pramana J. Phys. **78**(5), 759–766 (2012). https://doi.org/10.1007/s12043-012-0275-8
2. Manna, O., Singh S.K., Paul, G.: Enhanced thermal conductivity of nano-SiC dispersed water based nanofluid. Bull. Mater. Sci. **35**(5), 707–712 (2012). https://www.ias.ac.in/article/fulltext/boms/035/05/0707-0712

3. Lanje, A.S., Sharma, S.J., Pode, R.B., Ningthoujam R.S.: Synthesis and optical characterization of copper oxide nanoparticles. Adv Appl Sci Res **1**(2), 36–40 (2010)

4. Khullar, A., Sharma, S., Gangacharyulu, D.: Heat transfer and pressure drop of nanofluids containing aluminum oxide with transformer oil in horizontal pipe. Int. J. Theoretical Appl. Res. Mech. Eng. (IJTARME) **2**(4), 137–143 (2013)

5. Zeinali Heris, S., Nasr Esfahany, M., Etemad. S.Gh.: Experimental investigation of convective heat transfer of Al_2O_3/water nanofluid in circular tube. Int. J. Heat Fluid Flow **28**, 203–210 (2007). https://doi.org/10.1016/j.ijheatfluidflow.2006.05.001

6. Almohammadi, H., Nasiri Vatan, Sh., Esmaeilzadeh, E., Motezaker, A., Nokhosteen, A.: Experimental investigation of convective heat transfer and pressure drop of Al_2O_3/water nanofluid in Laminar flow regime inside a circular tube. World Acad. Sci. Eng. Technol. **6**, 08–24 (2012)

7. Mukesh Kumar, P.C., Kumar, J., Suresh, S.: Experimental investigation on convective heat transfer and friction factor in a helically coiled tube with Al_2O_3/water nanofluid. J. Mech. Sci. Technol. **27**(1), 239–245 (2013). https://doi.org/10.1007/s12206-012-1206-9

8. Fakoor-Pakdaman, M., Akhavan-Behabadi, M.A., Razi, P.: An empirical study on the pressure drop characteristics of nanofluid flow inside helically coiled tubes. Int. J. Therm. Sci. 206–213 (2013). https://doi.org/10.1016/j.ijthermalsci.2012.10.014

9. Sadri, R., Ahmadi, G., Togun, H., Dahari, M., Newaz Kazi, S., Sadeghinezhad, E., Zubir, N.: An experimental study on thermal conductivity and viscosity of nanofluids containing carbon nanotubes. Nanoscale Res. Lett., a Springer Open J. (2014)

10. Sajadi, A.R., Dizaji, A.F.: Investigation of turbulent convective heat transfer and pressure drop of Al_2O_3/water nanofluid in circular tube. Middle-East J. Sci. Res. **12**(11), 1553–1559 (2012). https://doi.org/10.5829/idosi.mejsr.2012.12.11.3977

11. Abdul Hamid, K. Azmi, W.H., Mamat, R., Usri, N. A. Najafi, G.: Effect of temperature on heat transfer coefficient of titanium dioxide in ethylene glycol-based nanofluid. J. Mech. Eng. Sci. (JMES), **8**, 1367–1375 (2015). http://dx.doi.org/10.15282/jmes.8.2015.11.0133

12. Wan, M., Yadav, R.R., Mishra, G., Singthas, D.: Temperature dependent heat transfer performance of multi-walled carbon nanotube-based aqueous nanofluids at very low particle loadings. Johnson Matthey Technol. Rev. **59**(3), 199–206 (2015). https://doi.org/10.1595/205651315x688163

13. Ganesh Kumar, J., Kathirkaman, M.D., Raja, K., Kumaresan, V., Velraj, R.: Experimental study on density, thermal conductivity, specific heat and viscosity of water—ethylene glycol mixture dispersed with carbon nanotubes. Therm. Sci. **21**(1A), 255–265 (2017)

14. Piratheepan, M., Anderson, T.N.: An experimental investigation of turbulent forced convection heat transfer by a multiwalled carbon-nanotube nanofluid. Int. Commun. Heat and Mass Transf. **57**, 286–290 (2014)

15. Ma, J., Xu, Y., Li, W., Zhao, J., Zhang S., Basov, S.: Experimental investigation into the forced convective heat transfer of aqueous Fe_3O_4 nanofluids under transition region. J. Nanopart. **2013**, 5 (2013). https://doi.org/10.1155/2013/601363

16. Balla, H.H., Abdullah, S., Zulkifli, R., Mohd Faizal, W., Sopian, K.: Effect of oxide nanoparticles on the pressure loss and heat transfer of nanofluids in circular pipes. J. Appl. Sci. (2012). https://doi.org/10.3923/jas.2012.13

17. Kalbasi, M., Saeedi, A.: Numerical investigation into the convective heat transfer of CuO nanofluids flowing through a straight tube with uniform heat flux. Indian J. Sci. Technol. **5**(53), 2455–2458 (2012)

18. Hussein, A.M., Sharma, K.V., Bakar, R.A., Kadirgama, K.: The effect of nanofluid volume concentration on heat transfer and friction factor inside a horizontal tube. J. Nanomater. (2013). https://doi.org/10.1155/2013/859563

19. Corcione, M., Cianfrini, M., Quintino, A.: Heat transfer of nanofluids in turbulent pipe flow. Int. J. Therm. Sci. **56**, 58–69 (2012). https://doi.org/10.1016/j.ijthermalsci.2012.01.009

20. Hashemi, S.M., Akhavan-Behabadi, M.A.: An empirical study on heat transfer and pressure drop characteristics of CuO-base oil nanofluid flow in a horizontal helically coiled tube under constant heat flux. Int. Commun. Heat and Mass Transf. **39**, 144–151 (2012). https://doi.org/10.1016/j.icheatmasstransfer.2011.09.002

21. Hasanuzzaman, M., Saidur, R., Rahim, N.A.: Effectiveness enhancement of heat exchanger by using nanofluids. In: IEEE First Conference on Energy and Technology CET 2011, pp. 98–103
22. Sahin, B., Manay, E., Akyurek, E.F.: An experimental study on heat transfer and pressure drop of CuO-water nanofluid. J. Nanomateri. **2015**, 10 (2015). https://doi.org/10.1155/2015/790839
23. Haghighi, E.B., Utomo, A.T., Ghanbarpour, M., Zavareh, A.I.T., Poth, H., Khodabandeh, R., Pacek, A., Palm, B.E.: Experimental study on convective heat transfer of nanofluids in turbulent flow: methods of comparison of their performance. Exp. Therm. Fluid Sci. 1–36 (2014). https://doi.org/10.1016/j.expthermflusci.2014.05.019

Design Analysis of Conventional and Composite Spur Gear Using Finite Element Method

Manjiri S. Gajhas and Ashok J. Keche

Abstract Gears are power transmission element and which are used to change direction, angular speed and variation of torque. The spur gears are applied to transmit the power between two parallel shafts. This present work is based on the finite element analysis to investigate the variation of stresses along pitch line. In industry composite material gears are not used widely and also only theoretical and analytical stress calculations are presented for composite material gear which also lack in experimental and practical results. In this investigation spur gear is taken for actual loading condition that is power and torque transmission. The objective of the present work is to check feasibility of composite material spur gear over conventional material spur gear. The spur gear model is created using CREO and further investigation is done with the help of ANSYS 15.0 software. The experimental results are allowed for comparison of conventional spur gear and composite spur gear.

Keywords FEA · Spur gear · Stress analysis · Ansys 15.0

1 Introduction

The foremost principle of gear mechanisms is to transmit rotation and torque among shaft axes (1). Gears are used for a various and number of types of applications. In this paper spur gear is used for stress analysis. Gears with involute teeth are essentially used in industry for the reason that of the low cost of manufacturing (1). Firstly a 3d model of spur gear of specific dimention is created in CREO and it is imported to ANSYS in IGES form. Further analysis is done in ANSYS by using FEA. The aim of this research is to explore the replacement of conventional spur gear with composite material spur gear as well as it's advantages and future scope.

Hwang [1] presented a contact stress analysis results for a contacting gear pairs in time of rotation. Contact stress analysis for helical as wll as for spur gears are

M. S. Gajhas (✉) · A. J. Keche
Department of Mechanical Engineering, MIT, Aurangabad, India
e-mail: gajhasmanjiri@gmail.com

conducted among respective teeth of a gear at different contact positions in the time of rotation. Two examples of helical and spur gears are accessibled to determine the change in the contact stress in a contacting gear pairs with respect to position of contact. Qin [2] calculated the surface and subsurface stresses of gear teeth and investigated using Hertzian theory and the finite element method. Also states that Friction causes the tangential pressure on the surface and affects the values and distributions of contact stresses. Toni Jabbour et al. [3] a method is used to calculate the distribution of the stress at the tooth root and of the contact stress along each contact line of a pair of spur and helical gears. The stresses results can be used as for preliminary designs of spur and helical gears. the critical load conditions are also considered. Pathan [4] used FEA to predict the dynamical properties of the gear. Experimental modal analysis have been conducted on the gearbox housing to verify the hypothetical predictions of natural frequencies.The paper made use of software in the FEA domain for investigating the effects of the change in the values of the design parameters relative to change in the modal behavior. the contactand bending stresses should be calculated by using ANSYS/NASTRAN.

1.1 Composite Material

Kirupasankar [5] here the efficiency of tansmission of two nanocomposites spur gears are calculated which composites are pristine polyamide 6 (PA6) and polyamide nanocomposite (PNC). To determine the effect of polymeric gear tooth deflection in load sharing, a Finite Element Analysis (FEA) is done with th help of commercial software package ANSYS. a fine mesh is used near the contact region. Linear elastic deformation behavior is assumed for all materials and the investigation is done by rotating the steel gear and holding the polymer gear. The addition of nanoclay reduces the ductility of the polymer but increases the gear efficiency. Prasad Reddy [6] here various the techniques of fabrications are performed and mechanical properties are calculated of Al-MMNCs reinforcing nano SiCp particles. This nano composites gives better results of mechanical properties as compared to other and the unreinforced alloys. This techniques are used in the majority of cases of the production of Al-MMNCs is powder metallurgy. For decidedly sensitive parts the spark plasma sintering and ultrasonic assisted casting method can be used but this leads to more money to spend on. Pawar [7] Silicon carbide particle reinforced aluminium matrix composite (AMCs) were prepared by stir-casting with different particle weight fraction 2.5, 5, 7.5, and 10%. The composite is prepared by stir casting technique. Mechanical tests are conducted like hardness test, microstructure test. It is projected that the use of this material for power transmitting elements like gears which are subjected to continuous loading.

2 Methodology

- For this stress analysis of spur gear first the 3D model of spur gear is created with help of software for present study model is created in CREO.
- After that the created model is imported into analysis software ANSYS it can be imported either STEP or IGES form.
- In ANSYS firstly the material properties are specified and the given model is divided into finite number of elements and nodes.
- After that boundary conditions and load is applied on created model. ANSYS will investigate all conditions and gives result as gear stress distribution, maximum principal stress and shear stress and equivalent stress.

3 3D Modelling of Spur Gear

GEAR SPECIFICATIONS

Module $(m) = 4$ mm
No. of teeth $(N) = 32$
Pitch circle dia $(d) = t * m = 128$ mm
Tooth thickness $(t) = 3.14$ mm
Face width $= 45$ mm
Pressure angle $(\Phi) = 20°$ full depth
Circular Pitch $= \pi * m = 12.56$
The Base Circle Diameter $(DB) = D * Cos (\Phi) = 128 * Cos (20°) = 120.28$ mm
Outside Diameter $= (z + 2) m = 136$ mm
Clearance $=$ circular pitch$/20 = 0.628$ mm
Addendum for $20°$ full depth $= m = 4$
Diametral pitch $=$ no of teeth/p.c.d $= 32/128 = 0.25$ mm.

With the help of above given gear parameter geometry was created in CREO 2.0 Software (Fig. 1).

4 Finite Element Analysis

In FEA, the complex structure is divided to finite number of small region named as elements number of elements are joint together named as nodes. The loading conditions are calculated over the each nodes and elements. Because of these number of dividations results are more accurate.

Steps in ANSYS
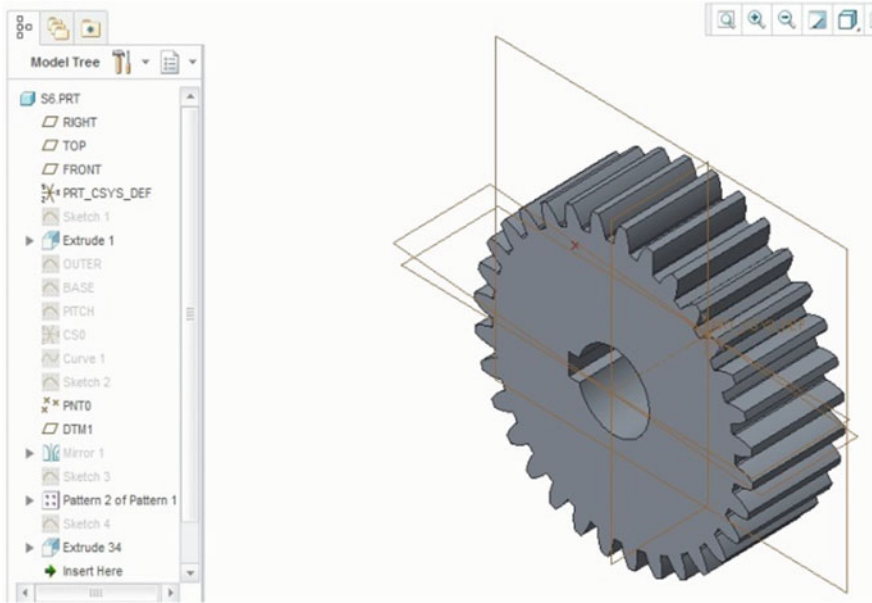
Fig. 1 3D created modal of gear

(1) Define material

Material under consideration was the steel 20MnCr5 which widely used in industry. While the composite material was aluminium silicon carbide. This material can be produced by stir casting and powder metallurgy. in ANSYS number of material and there properties are present in library and new material is also added with providing properties like in this study Al–SiC material properties are added (Table 1).

(2) Geometry

To calculate the stresses coming in 20° full depth involute spur gear was created in CREO 2.0 software. Then the model is imported in ANSYS 15.0 IGES form.

(3) Meshing

Number of nodes are 51467 and number of elements are 10060.

Table 1 Material properties introduced to ANSYS

Material property	Structural steel (20MnCr5)	Aluminium silicon carbide (Al–SiC)
Ultimate tensile strength (MPA)	460	151
Young's modulus (GPA)	210	150
Poisson's ratio	0.3	0.3

(4)   Boundary conditions

The fixed support is applied and shown in blue color in first image and in second image the nodal force is firstly calculated according to loading condition which is 2153 N and applied at pitch line and distributed equally for more accurate result (Figs. 2 and 3).
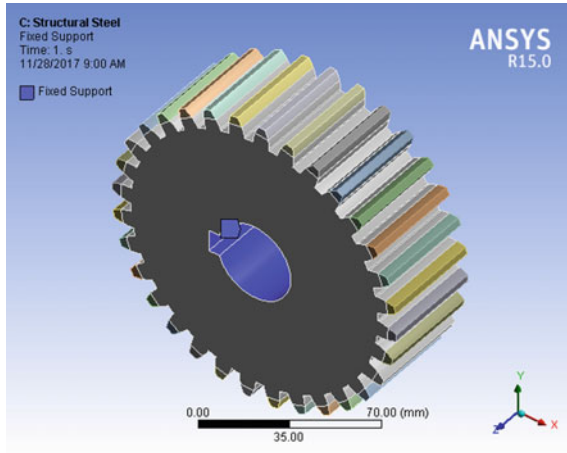
Fig. 2 Fixed force
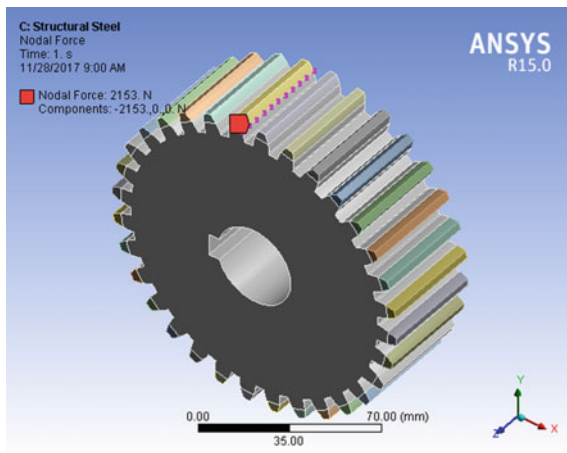
Fig. 3 Nodal force at pitch line

5 Results and Discussion

(1) Figure shows the equivalent stress for 20MnCr5 which gives a stress of 166.04 MPa and for composite gear which gives a stress value of 99.03 MPa (Figs. 4 and 5).

(2) Figure shows the maximum shear 91.73stress for 20MnCr5 which gives a stress of 166.04 MPa and for composite gear which gives a stress value of 55.603 MPa (Figs. 6 and 7).
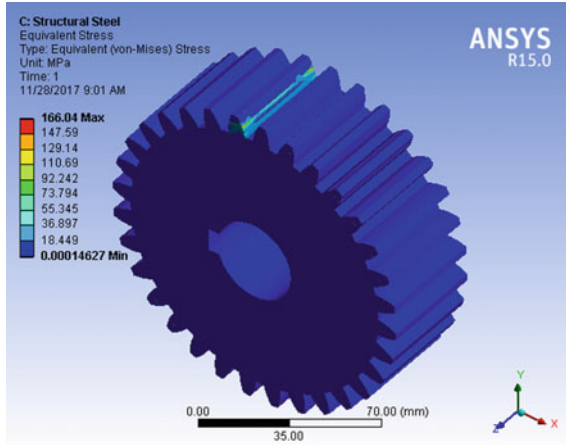
Fig. 4 Equivalent stress for 20MnCr5
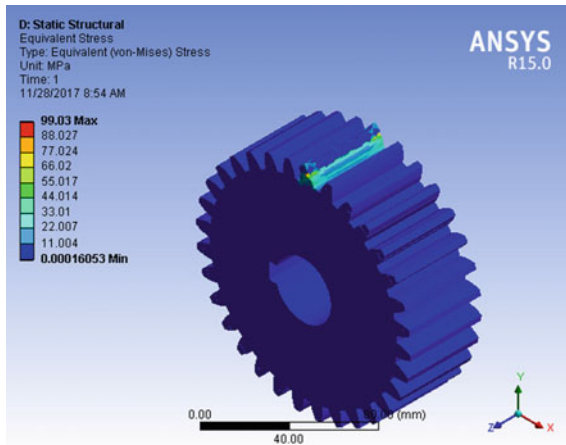
Fig. 5 Equivalent stress for Al–SiC

Fig. 6 Maximum shear stress for 20MnCr5
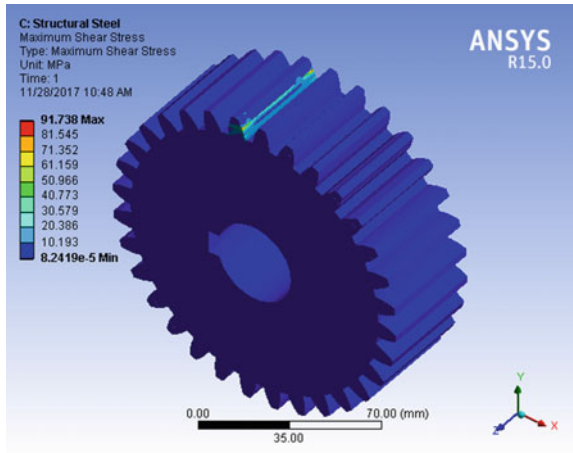
Fig. 7 Maximum shear stress for Al–SiC
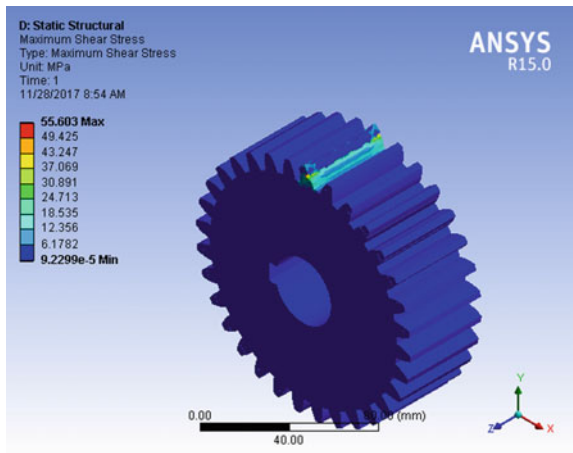
(3) Figure shows the maximum principal stress for 20MnCr5 which gives a stress of 46.12 MPa and for composite gear which gives a stress value of 44.74 MPa (Figs. 8 and 9).

6   Conclusions

From present study following conclusions are arrived as:

1. The stresses coming on Al–SiC spur gear are less than the 20MnCr5 spur gear.
2. It is desirable to replace conventional spur gear with composite spur gear.
3. Nodal force applied at pitch line gives more accurate results in ANSYS.

Fig. 8 Maximum principal stress for 20MnCr5
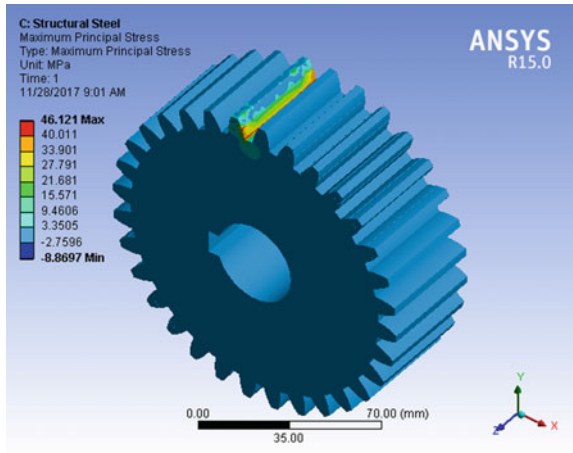
Fig. 9 Maximum principal stress for Al–SiC
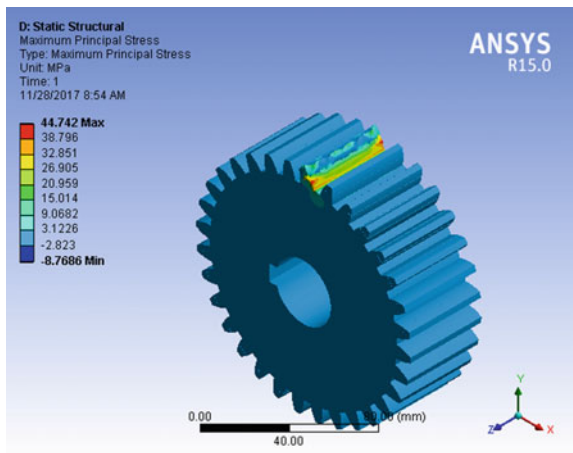
4. Equivalent stress and maximum shear stress are less in Al–SiC spur gear with respect to 20MnCr5 spur gear.
5. Maximum principal stress is slightly more to 20MnCr5 spur gear compared to Al–SiC spur gear.

References

1. Hwang, S.-C., Lee, J.-H., Lee, D.-H., Hana, S.-H., Lee, K.-H.: Transmission efficiency of polyamide nanocomposite spur gears. Math. Comput. Model. **57**, 40–49 (2013)
2. Qin, W.J., Guan, C.Y.: An investigation of contact stresses and crack initiation in spur gears based on finite element dynamics analysis. Int. J. Mech. Sci. **83**, 96–103 (2014)

3. Jabbour, T., Asmar, G.: Tooth stress calculation of metal spur and helical gears. Mech. Mach. Theory **92**, 375–390 (2015)
4. Pathan, N.H., Singh, V.P., Kulkarni, S.S.: Modal analysis of spur gear to determine the natural frequencies and it's effect over the geometry of the gear. Int. J. Adv. Eng. Res. Stud. E-ISSN 2249–8974
5. Kirupasankar, S., Gurunathan, C., Gnanamoorthy, R.: Transmission efficiency of polyamide nanocomposite spur gears. Mater. Des. 39, 338–343 (2012)
6. Prasad Reddya, A., Vamsi Krishna, P., Narasimha Rao, R., Murthy, N.V.: Silicon carbide reinforced aluminium metal matrix nano composites-a review. In: 5th International Conference of Materials Processing and Characterization (ICMPC 2016)
7. Pawar, P.B., Utpat, A.A.: Development of aluminium based silicon carbide particulate metal matrix composite for spur gear. In: 3rd International Conference on Materials Processing and Characterisation (ICMPC 2014)

Automation on Front Fork Assembly Machines Using Vibro-Feeder & Pick and Place Mechanism

Dhananjay Kathar, S. V. Lomte and Dilip Pawar

Abstract The automation on front fork assembly machine is the project design to improve the quality as well as productivity of manual machines. Manual operating process consist of lots of errors like parts missing in assembly, parts fitment in the wrong direction, misalignment during assembly, inconsistency in process, etc. The automated multipurpose machine eliminates the errors generated by a manual operating process. Proposed machine is also focused to reduce operator fatigue & ergonomic improvement during working. Reduction in operator fatigue, improves working efficiency of operator which will result in an increase in productivity. This proposed automation is the combination of four individual process, namely Oil seal pressing, Guide bush pressing, Washer insertion & Oil seal greasing. The machine is controlled by a programmable logical control (PLC). It consist of number of pneumatic cylinders which will apply for pressing, pick & place & clamping of component, etc. The operator function is just to load & unload the component all the rest process is automatically done by the machine itself. This automation is beneficial in quality & productivity of the product; it will also reduce manpower cost as the proposed automation saves nine men per day.

Keywords Pick & place mechanism · Vibro feeder · Automation · Oil seal & guide bush pressing · Front fork assembly

1 Introduction

This automation is designed to improve the quality as well as productivity of the process. This project is going to convert manually operated machines to automated machine. This automation is applicable for front fork assembly line. In front fork

---

D. Kathar (✉) · S. V. Lomte
Department of Mechanical Engineering, MIT, Aurangabad, India
e-mail: kathardhananjay@gmail.com

D. Pawar
Department of Manufacturing Engineering, ETL, Aurangabad, India

assembly line manual process involves Oil seal pressing, Guide bush pressing, Washer insertion & Oil seal greasing. The objective of work is to replace four manual operated processes with the single automation. With the help of this automation the elimination of operator is done by implementing pick & place mechanism for parts insertion. The quality errors like excess or less part quantity & wrong direction of parts can be detected by sensors & vision camera system. In this proposed automation, operator fatigue & ergonomic improvements also can be reduced as an operator is only required to load & unload the components.

2 Gaps in Earlier Studies

Lots of studies are carried out on assembly machine which consist of multi handling pick & place robotic arm. No studies had done for automation of multipurpose assembly machines control using programmable logical control. No study shows the automation on assembly machine using Vibro feeder. Very less research is conducted for programmable logical control based oil seal & guide bush pressing machines. No studies available for automation of assembly machines using greasing unit. There is scope to study the automation of combination of process like pressing, part insertion & greasing.

3 Front Fork Assembly Details

Front fork assembly process starts with fork pipe cleaning and ends to packing & dispatch. In this assembly flow some processes are manually operated like guide bush pressing, oil seal pressing, washer insertion & oil seal greasing. Some of the processes have automation involved like fork pipe caulking, fork bolt tightening, Oil filling etc. (Table 1).

The table shows the individual detail of the assembly process flow. From the table it is clearly seen that in assembly line lots of process are fully operator dependent like center bolt tightening, guide bush pressing, washer insertion, oil seal greasing, oil seal pressing, stopper insertion etc. (Figs. 1 and 2).

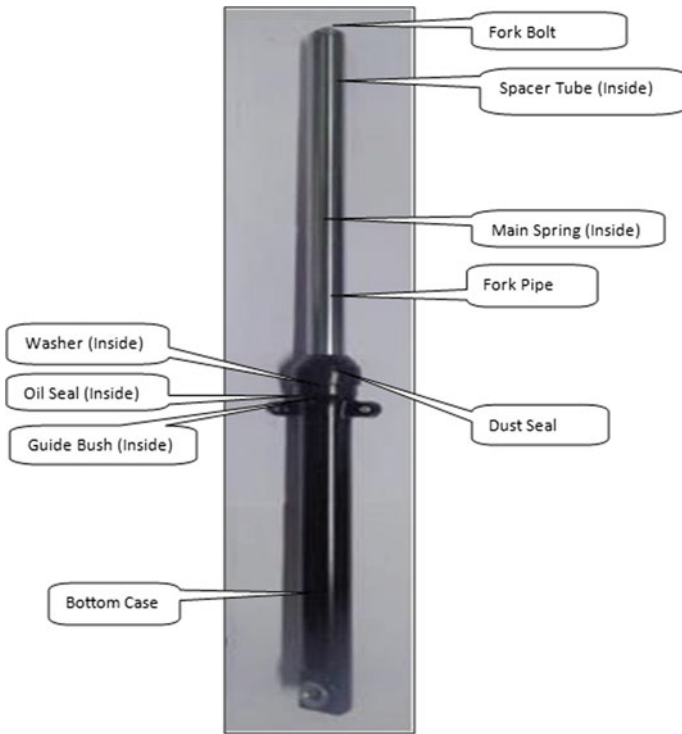Assembly part details & assembly process flow shown above.
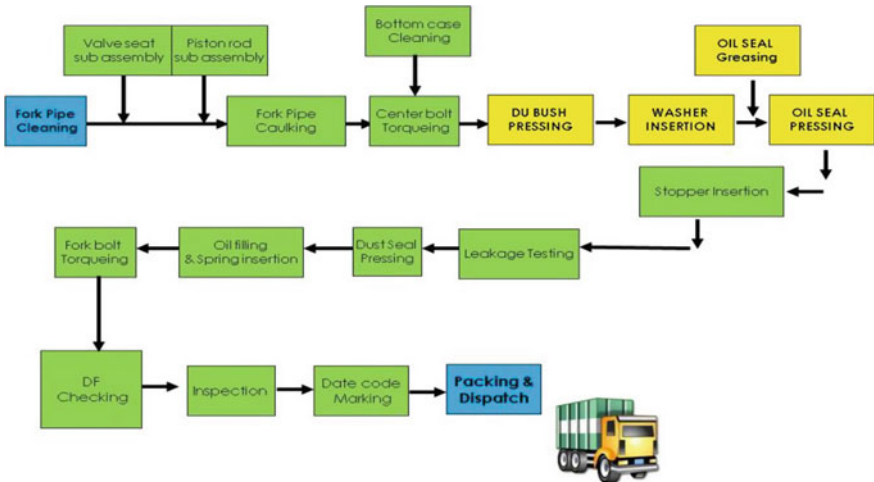
Fig. 1 Part details

Fig. 2 Assembly process

Table 1 Process detail

Sr. no.	Process name	Process type
1	Cleaning process	Semi-automatic
2	Fork pipe caulking	Automatic
3	Center-bolt tightening	Manual
4	Guide bush pressing	Manual
5	Washer insertion	Manual
6	Oil seal greasing	Manual
7	Oil seal pressing	Manual
8	Stopper insertion	Manual
9	Dry leakage testing	Semi-automatic
10	Dust seal pressing	Manual
11	Oil filling	Semi-automatic
12	Fork bolt tightening	Semi-automatic
13	DF checking	Semi-automatic
14	Inspection & date code marking	Semi-automatic

4 Drawbacks in Current Assembly Process

4.1 Rejection Quantity

Rejection & rework quantity is very high for defects oil seal leakage, bottom case dent, improper fitment etc. & all the defects consist manually operated process (Table 2).

4.2 Errors in Existing Process

Parts missing, Parts wrong direction insertion, Double parts insertion, Inconsistency in the process, Parts assembly misalignment, Improper fitment.

Table 2 Rejection data

| Sr. no. | Month | Type of defects in assembly process | | | | | | |
		Oil seal leakage	Bottom case dent	PipeRusty	Assembly hard Jam	Total Rej. Qty.	Production Qty.	PPM
1	Apr-16	8	20	1	2	31	151,720	204
2	May-16	5	15	0	1	21	135,095	155
3	Jun-16	1	21	2	0	30	154,961	193
4	July-16	3	11	2	0	21	164,242	127
5	Aug-16	3	07	1	4	15	142,320	105
6	Sep-16	4	16	0	1	21	160,206	131

Front fork assembly rejection summery—Apr 16 to Sep 16
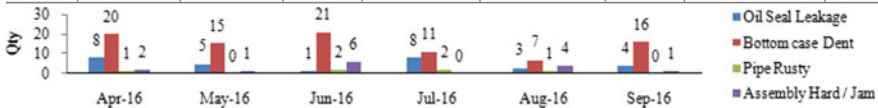
4.3 Manpower

High operator fatigue at manual assembly processes lowers the operational efficiency, which will result in less productivity. Some manpower related drawbacks like operator absenteeism, manpower availability, high manpower cost, skilled manpower, etc. Cycle time of machine depends on operator skill hence always an inconsistency in productivity. While operating manual pressing machine, there is a higher risk to have an accident.

5 Scope of Automation

Considering the above drawbacks, there is scope of automation for the assembly of oil seal, washer & guide bush. There is a scope to eliminate four manual operated processes & replace it with single automation (Fig. 3).

6 Objective of Automation

The main objective is to replace all the four manual operated process with the single automated machine. Eliminate quality errors like excess parts quantity, parts missing & wrong direction of parts with the help of sensors & vision camera. Eliminate operator by implementing pick & place mechanism, Vibro feeder, dispenser for parts insertion.
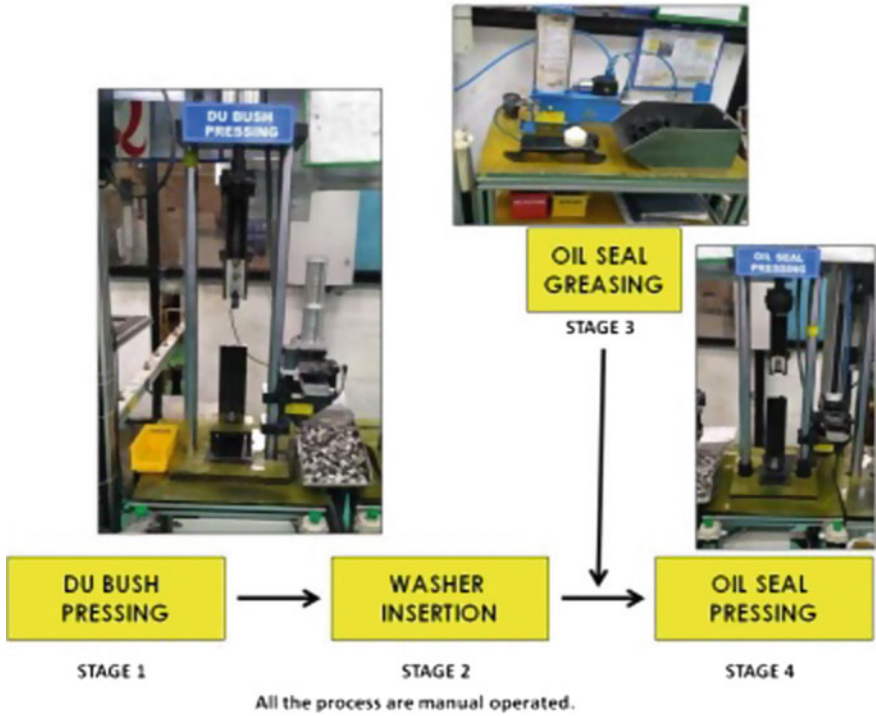
Fig. 3 Manually operated machines

7 Design Consideration in Automation

Several considerations should be taken into account for efficient design. Few considerations are made for designing the new automation (Table 3).

7.1 Recognize and Analyzes the Earlier Defects

To recognize & analyzes the earlier defect the matrix has been prepared. In this matrix all the processes along with their possible & earlier defects has been noted. The study has been done for each & every defect & possible Poka-Yoke to arrest all the process errors in automation. This study has a major role for design purpose.

All the processes which considered for new automation are mentioned here.

Table 3 Possible defects in process

Sr. no.	Process	Defect type
1	Guide bush insertion	Missing
2		Less/more Qty.
3		Wrong part
4	Guide bush pressing	Missing/incomplete
5	Washer insertion	Missing
6		Reverse direction
7	Oil seal insertion	Missing
8		Reverse direction
9		Less/more Qty.
10		Wrong part
11	Oil seal greasing	Missing
12	Oil seal pressing	Less/more Qty.
13		Missing/incomplete

Table 4 Process defects

		AUTO OIL SEAL & GUIDE BUSH PRESSING					
PROCESS →		Guide Bush Insertion	Guide Bush Pressing	Washer Insertion	Oil Seal Insertion	Oil Seal Greasing	Oil Seal Pressing
POKAYOKE POSSIBILITY →	Missing/ Incomplete	🟩	🟩	🟩	🟩	🟩	🟩
	Reverse				🟩		
	Less/more qty	🟩		🟩	🟩	🟩	
	Wrong parts	🟩			🟦		

Identified Defects with Implemented PokaYoke · Identified Defects & PokaYoke at Subsequent Process · Identified Defects Without PokaYoke

7.2 Prevention of Defects

Prevention of defects is very much important consideration from a design point of view. Below approach is used for prevention of defects in front fork assembly. In this approach all the defects are considered along with their Poka-Yoke possibilities. Some of the defects can directly arrest at the same stage & some defects can arrest in their subsequent process. Green highlighted identified defects are having the possibility of Poka-Yoke in the same stage. No single defect is left without Poka-Yoke (Table 4).

7.3 Determine Load Condition

Calculation of pressing force requirement on pressing machine
Guide Bush Pressing Force Calculation
    Firstly calculate the pressure at interference between the guide bush (Shaft) &
Bottom Case (Hub), The pressure p generated at the interface of the interference fit
is given by,

$$p = \frac{\delta}{\frac{d}{E_o}\left(\frac{d_o^2+d^2}{d_o^2-d^2}+v_o\right)+\frac{d}{E_i}\left(\frac{d_o^2+d^2}{d_o^2-d^2}+v_i\right)}$$

where,

$\delta = 0.09$ mm $=$ Diametrical interference
$d = 38.1$ mm $=$ Nominal diameter of hub
$d_o = 52.35$ mm $=$ Outside diameter of hub
$d_i = 35.235$ mm $=$ Inside diameter of shaft
$E_o = 69$ GPa $=$ Young's modulus of hub (aluminum)
$E_i = 200$ GPa $=$ Young's modulus of shaft (steel)
$v_o = 0.32 =$ Poisson's ratio of hub (aluminum)
$v_i = 0.3 =$ Poisson's ratio of shaft (steel).

    Hence,

$$p = \frac{0.09}{\frac{38.1}{69000}\left(\frac{52.35^2+38.1^2}{52.35^2-38.1^2}+0.32\right)+\frac{38.1}{200000}\left(\frac{38.1^2+35.235^2}{38.1^2-35.235^2}-0.3\right)}$$

$$\boxed{p = 20\,\text{N/mm}^2}$$

    The Frictional force F_f is given by,

$$F_f = \mu\,p\,\pi\,d\,l$$

where,

$\mu = 0.15 =$ Coefficient of friction
$p = 20$ N/mm^2 $=$ Pressure of interference
$d = 38.1$ mm $=$ Nominal diameter of hub
$l = 12$ mm $=$ Length of hub.

$$F_f = 0.15 \times 20 \times \pi \times 38.1 \times 12$$
$$F_f = 4306.8\ N$$

$$\boxed{F_f = 439.03\,\text{Kgf}}$$

Pneumatic cylinder pressing force should always higher than the required pressing force. Here required **439.02** KgF of force for pressing, hence Bore Ø 100 pneumatic cylinder has been selected which produces a force of **450** KgF, Our required pressing force is **439.02** KgF. Hence this cylinder is preferred for guide bush pressing operation.

(Note: For oil seal pressing bore Ø 125 mm pneumatic cylinder has been selected which will produce pressing force of 701 KgF as required.)

7.4 Productivity

To have a higher productivity assembly process must have consistent cycle time. In manual operation, it is not possible to get consistent cycle time throughout the shift due to manual operation. So, 85% are the considerable operating efficiency in manual process & it is nothing but the indirect loss of productivity. Hence now days to reduce this loss the processes are going for automation. From design consideration point of view automation should fulfill the requirements of productivity. Automation should contain efficient pick & place mechanism. It should have programmable logic for sequencing of processes. Controllable speed is required to get appropriate flow.

7.5 Optimized Layout

When drawing the preliminary design, engineers should plan layout to reduce waste. Minimum space has to acquire by proposing automation. Material Flow should be uniform not complex in layout. To reduce waste, use of optimum layout is very much essential factor in lean manufacturing.

7.6 Cost

Cost of automation should be low so as to get higher profit. Minimum investment cost has high return on investment. So during the design of automation designer should know what resources or approved budget to be considered. Considering the available resources designer has to proceed for design.

8 Design of Automation

- The design consists of a main base plate which rotates using the rotary indexer.
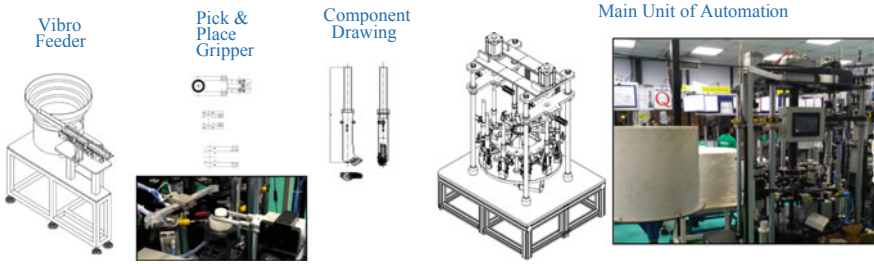- Ten numbers of components can load & unload by operator on the indexer.

Fig. 4 Design of automation

- On the top plate four, individual stations has mounted for oil seal greasing, oil seal pressing, Guide bush pressing, washer insertion etc.
- To dispense the oil seal & guide bush Vibro unit is used.
- Pneumatic cylinders are used for pressing and pick-n-place purpose.
- Parts missing, parts wrong direction, etc. quality errors have eliminated by using sensors & vision camera which is interlocked with PLC.
- Complete automation is controlled by a delta programmable logical control (Fig. 4).

9 Process Sequence in Automation

See Fig. 5.

10 Part List

Refer below table for automation sub assembly fixture details (Table 5).

11 Results and Discussion

11.1 Quality Improvement

See Tables 6 and 7.

From above values it is clearly seen that the defect rate of assembly defect is in reducing trend. Rejection PPM reduced from ~**204** to ~**94** PPM.

Table 5 Sub assembly fixture

Guide bush & oil seal pressing machine—fixture list				
Sr no.	Fixture description	Qty.	Purpose	Remark
1	Guide bush & oil seal pressing main fixture	1	It is main structure of machine which supports all sub units. It is use for the pressing of oil seal & guide bush	–
2	Sub assembly for sensor mounting bracket	1	Job presence sensors are mounted on bracket assembly. It consist of hollow column at the center of machine, inside that all the electrical cables & pneumatics piping are provided. Special pneumatic unit is provided to avoid meshing of pipes	Special unit to avoid pipe meshing is **MQR12-M5**
3	Oil seal dispenser unit	1	This unit mainly serves the purpose of dispensing of oil seal. This is takes place by using three different cylinders namely rotary gripper, rotary cyl. & linear displacment cyl.	Rotary gripper are use to pick up the oil seal & reverse it in case of wrong direction. **(MRIIQ10S-10S)**
4	Washer dispenser unit	1	Washer dispenser unit dispense the washer with the help of vacuum gripper. Same pick & place mechanism is use as used in oil seal	–
5	Guide bush dispenser unit	1	Use lo dispense the guide bush with the help of pick & place mechanism	–
6	Greasing fixture	1	Greasing fixture use to apply grease on oil seal lip ID	–
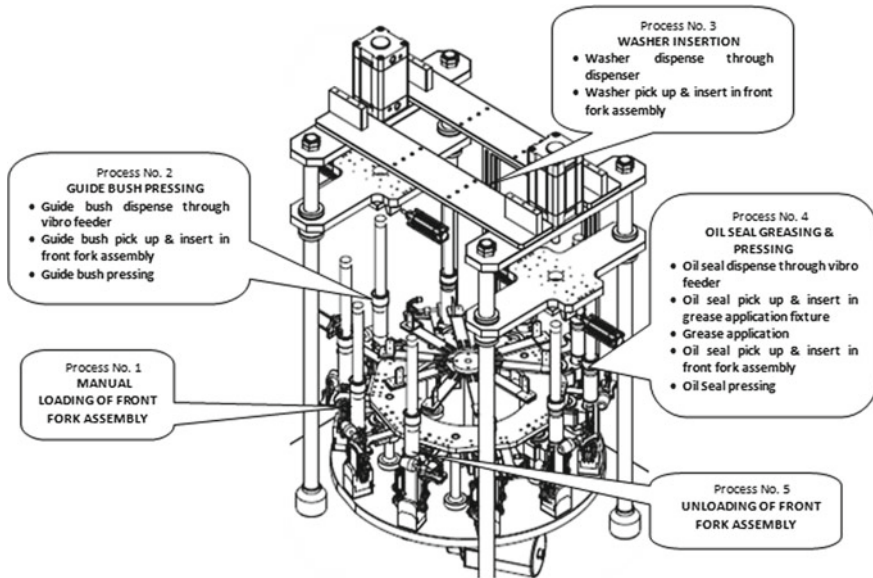
Fig. 5 Process sequence in automation

Table 6 Rejection quantity

		Type of defects in assembly process						
		Front Fork Assembly leakage Testing Rejection Summery – Mar 2017						
Sr. No.	Month	Oil Seal Leakage	Bottom case Dent	Pipe Rusty	Assembly Hard / Jam	Total Rej. Qty	Production Qty	PPM
1	Mar-17	01	07	4	2	14	147560	94

11.2 Optimized Layout

As per layouts the space requirement has been minimized. No material movement takes place in between the processes as all the process has combined. Auto feeding is done by Vibro feeder. Spaced saved from 4 × 4 m to 2.3 × 2.3 m (Fig. 6).

Table 7 Rejection PPM
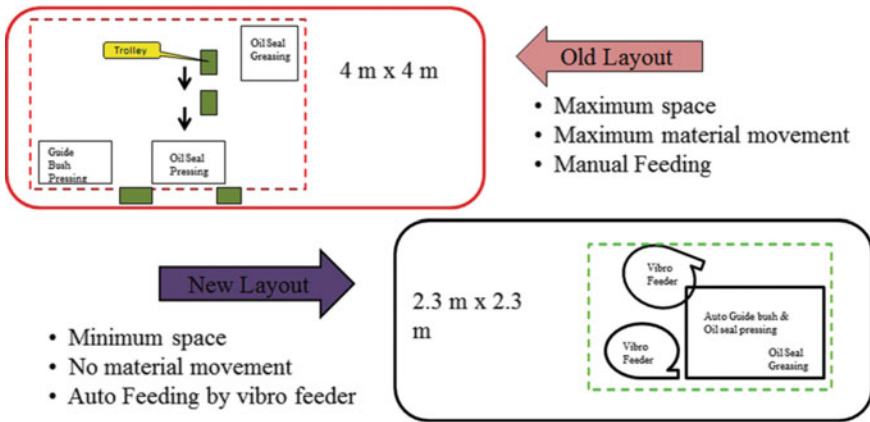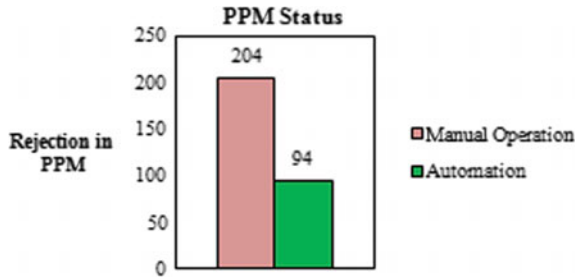
Fig. 6 Optimized layout

11.3 Man-Days Saved

In old manual operation, 4 operators are required, new automation only required single operator for loading & unloading of components. Hence nine Man-days are saved. Cost of nine man-days is approx. **1.08 Lacs Rs**.

11.4 Productivity

In new automation accessories are used to achieve a desire output, i.e. loading, unloading cycle time, Parts insertion position, Parts Qty etc. Automation is equipped with vision camera to get online inspection instead of operator's visual inspection.

Because of automation working efficiency is increased to 100%. Considering 9 s consistent cycle time productivity increased from **6885 to 8100 Nos.**

11.5   Other Benefits

Some other benefits from this automation that are Single Piece Flow of Product, High accuracy in the process, Interlocks for individual processes, Operator Fatigue is reduced, Consistency in the process.

12   Conclusion

It is concluded that the automation on front fork assembly machines using Vibro feeder and pick & place mechanism has been completed successfully as per our objectives oriented in beginning. Thus, this type of automation used to improve our product quality by reducing rejection PPM from 204 to 94 PPM. Nine Man-days have saved and operator only use for loading & unloading of components. Because of automation working efficiency is increased to 100%. Considering 9 s consistent cycle time productivity increased from 6885 to 8100 Nos.

Hydraulic Design of Diffuser of Catalytic Converter

Mihir Joshi, Femina Patel, Sanjay Patel and Niraj Shah

Abstract Air pollution generated from automobile source is playing a vital role in green house effect so it is a problem of general interest. The pollutants like carbon monoxide (CO), unburned hydrocarbons (HC), oxides of nitrogen (NO_x), oxides of sulfur (SO_x), and particulate matters are generated at the end of the combustion in the engine. These pollutants have negative impacts on the environment, air quality, and health. To control these pollutants, various stringent norms of pollutants emission are applicable in various countries. Most promising method of converting these gases into less harmful form is after treatment of it in the catalytic converter. To improve the performance of the catalytic converter, hydraulic phenomenon occurring in it needs to be studied. In present work, a numerical study using finite volume approach is carried out for catalytic converter with conventional diffuser for four diffuser angle. Three-dimensional steady-state analysis of catalytic converter is carried out using Ansys Fluent software. Based on the CFD results, it is found that 20° conventional geometry gives the minimum pressure drop, minimum peak pressure, and better uniformity index.

Keywords Catalytic converter · Diffuser · CFD

1 Introduction

The major air quality problems in rural, urban, and industrialized area are air pollution generated from automobile sources. The emission from vehicles runs on the gasoline and diesel is carbon monoxide (CO), unburned hydrocarbons (HC), oxides

M. Joshi · N. Shah (✉)
Mechanical Engineering Department, Institute of Technology, Nirma University, Ahmedabad 382481, India
e-mail: niraj.shah@nirmauni.ac.in

F. Patel · S. Patel
Chemical Engineering Department, Institute of Technology, Nirma University, Ahmedabad 382481, India

of nitrogen (NO_x), and particulates matters (PM). Carbon monoxide and unburned hydrocarbons occur because the combustion efficiency is less than 100%. The NO_x is formed at very high temperature (>1500 °C) of the combustion process resulting in thermal oxidation of the nitrogen using the oxygen of air. Typical exhaust compositions at normal operating conditions are unburned hydrocarbons (350 ppm), carbon monoxide (0.5 vol.%), oxides of nitrogen (900 ppm), hydrogen (0.17 vol.%), oxygen (0.5%), carbon dioxide (10 vol.%), and water (10 vol.%) [1]. To reduce the effect of toxic substance emission from combustion engine, there are two methods that are primary and secondary measures. Primary approach of reduction in engine emission includes improvement in engine design, fuel pretreatment, use of alternative fuels, and fuel additives. In secondary approach, exhaust gases are reacted with catalyst, in the catalytic converter, after releasing from engine. This method of after treatment of exhaust gases using catalytic converter is one of the most effective way in which harmful exhaust gases are converted into eco-friendly gases such as carbon dioxide (CO_2), nitrogen (N_2), and H_2O.

Catalytic converters are of two types (i) the two-way catalytic converter and (ii) three-way catalytic converter. The two-way catalytic converter is known as the oxidation catalytic converter as oxidization of carbon monoxide and unburnt hydrocarbons takes places in it. These two reactions are mentioned as Eqs. (1) and (2).

$$2CO + O_2 = 2CO_2 \tag{1}$$

$$C_xH_{2x+2} + \left[\frac{3x+1}{2}\right]O_2 = xCO_2 + (x+1)H_2O \tag{2}$$
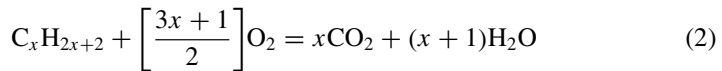
The three-way catalytic converter works same as two-way catalytic converter but additionally it reduces the effect the oxides of nitrogen.

$$2NO_x = xO_2 + N_2 \tag{3}$$

2 Selection of Monolith

The catalytic converter as shown in Fig. 1 consists of inlet pipe, diffuser, monolith, nozzle, and outlet pipe. Out of these monolith is main heart of the catalytic converter as it is the reactor. A monolith is a block consisting of large number of small straight and parallel channels, mat, and housing. On the walls of the honeycomb channels, the active catalyst layer is applied on internal surfaces of channels for effective chemical reactions. Because of large number of parallel channels, the flow will not get obstructed and so that pressure drop across the monolith is uniform.

The basic construction material of monolith substrate is made either of metal (stainless steel, metal, alloys etc.) or ceramic (mainly cordierite). The selection of
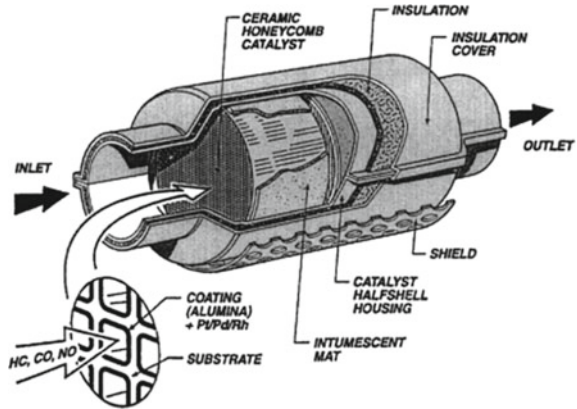
material depends on parameters like pressure drop, wash coat distribution, light off temperature, cost, etc.

There are number of shapes and sizes of monolith available according to application. For automotive purpose, cylindrical shape monolith is preferred because of ease to design, large surface area, and compactness. The major design criteria involved in the design of the substrate are the cell densities, diameter, and channel shape. As a thumb rule, the monolith volume is taken same as the engine capacity (in cc) [2].

There are different types of the cell shapes in the monolith, i.e., square, triangular, circular, hexagonal, and sinusoidal. The most common commercially available cell shape is square. The square cells have better uniform velocity distribution (except in sharp corners) better mass flow distribution and, lower pressure drop [2].

Channel cell density is number of cell per unit of cross-sectional area of substrate. As the cell density increases, the surface area of substrate increases which results in better conversion efficiency and also decreases the minimum light off temperature to maintain the conversion in catalytic converter. The cell density should be optimized to achieve the desired conversion efficiency with minimum light off temperature.

3 Numerical Modeling

The CFD analysis of catalytic converter is carried out using ANSYS Workbench. The flow assumed to be three-dimensional and steady inside the catalytic converter. The working fluid is considered as ideal and compressible. The range of operating velocity of working fluid inside the channel of honeycomb structure is from 0 to 12 m/s.

3.1 Governing Equations

The governing equations solved using finite volume approach for catalytic converters are mass, momentum, energy, and species equation. From the momentum equation, the velocity of fluid can be studied. The species transport equation shows the transport of species such as CO, HC, and NO_x across the geometry.

Overall Mass:

$$\frac{\partial}{\partial t}(\rho) + \nabla(\rho U) = 0 \tag{4}$$

Momentum:

$$\frac{\partial}{\partial t}(\rho U) + \nabla(\rho UU) = -\nabla p + \nabla \tau + \rho B \tag{5}$$

Hexahedral mesh is used to discretize the geometry. The simulation is carried out in Fluent with pressure-based solver. The standard K-ε viscous model is used to model turbulent flow. The boundary conditions are defined as velocity inlet and pressure outlet. The wall of monolith is considered as adiabatic. A SIMPLE method of pressure–velocity coupling is used, the standard discritization scheme for pressure, second-order upwind for momentum and energy. The default values are used for under relaxation factor. The working fluid is composition of five gases, and their mass fractions are C_3H_6 (6.74e-04), CO(0.0142), NO(0.00107), O_2(0.00879), and N_2(0.975266) [3]. Monolith is modeled as porous details of which is as follows.

3.2 Porous Modeling

The ceramic substrate in the catalytic converter is porous and honeycomb type structure having 600 cells per square inch (cpsi). To model the substrate porous in CFD software, inertial resistance and viscous resistance must be calculated using Eqs. (6) and (7) [4].

$$\alpha = \frac{D_p^2}{150} \frac{\varepsilon^2}{(1 - \varepsilon)^2} \tag{6}$$

$$C_2 = \frac{3.5}{D_p} \frac{(1 - \varepsilon)}{\varepsilon^3} \tag{7}$$

3.3 Uniformity Index

In order to design the optimize geometry of catalytic converter, one first needs to predict the fluid flow inside the inlet pipe, inlet cone, and substrate of catalytic converter. The flow uniformity in the catalytic converter is referred here as uniformity index. The uniformity index is a measure of flow uniformity on a plane. It is the root mean square of difference between the local velocity and spatial mean of the velocity integrated over the area of the plane. As the value of uniformity index tends to 1, the flow uniformity increases.

$$\gamma = 1 - \frac{\sum_{i=1}^{n} \frac{\sqrt{(w_i - \bar{w})^2}}{\bar{w}} A_i}{2.n.A} \tag{8}$$

4 Results and Discussion

The diffuser section design is important for flow distribution inside monolith of the catalytic converter. The parametric study is done for four conventional type diffuser having cone angle 20°, 30°, 45°, and 60° (Fig. 2). The angle of nozzle (outlet cone) is fixed at 30° since it gives good results. These geometries have been optimized for minimizing the pressure loss, lower value of maximum pressure, and uniform flow distribution inside the catalytic converter.

4.1 Validation

The present work of numerical modeling is validated with Heibal et al. [5]. Heibel et al. have done numerical modeling of catalytic converter in ANSYS Fluent. The simulation is carried out on axisymmetric geometry of catalytic converter. The geometry parameters are shown in Table 1.

The axisymmetric turbulent flow is simulated using renormalization group k-ε turbulent model with air as a working fluid. The substrate is modeled as laminar and porous medium with finite inertial and viscous resistance in axial direction and zero inertial and viscous resistance in radial direction, i.e., no flow in radial direction. The inlet velocity and pressure outlet is defined as boundary conditions. The boundary condition at wall is chosen as no slip and adiabatic. The plot of velocity in the radial direction is shown in Fig. 3. The experimental, numerical simulation, and present study are in good agreement with each other.
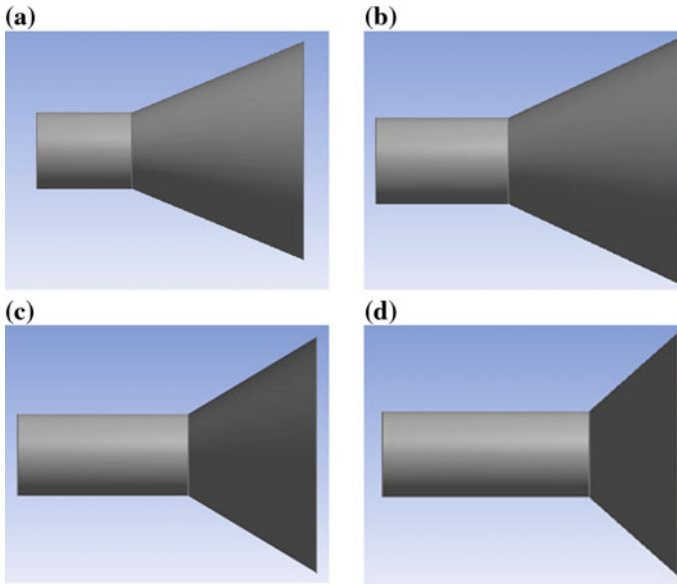
Fig. 2 Conventional diffusers with cone angle **a** 20°, **b** 30°, **c** 45°, **d** 60°

Table 1 Geometrical parameters

Parameters	Values
Cell density	62 cpcm^2
Wall thickness	0.165 mm
Geometrical surface area	2.74 m^2/l
Substrate diameter	118.4 mm
Maximum substrate length	101.6 mm
Substrate volume	1.21
Total surface length	3.07 m^2
Inlet and outlet pipe diameter	47 mm
Inlet and outlet cone angle	70

4.2 Hydraulic Analysis of Diffuser

This section discusses the results of four conventional geometries. The results of pressure contour, pressure drop across the catalytic converter, and velocity vector for four conventional geometries are shown in Fig. 4. The graph of pressure drop shows the high pressure at the diffuser zone since the velocity is decreasing in the diffuser. In the pressure contour, the pressure is uniformly dropping in substrate area since the substrate is modeled as porous media. A high pressure is found at inlet and it uniformly drops once the fluid is entered in the substrate area. The velocity in the substrate region is maximum at the centerline of the substrate. The velocity is low at
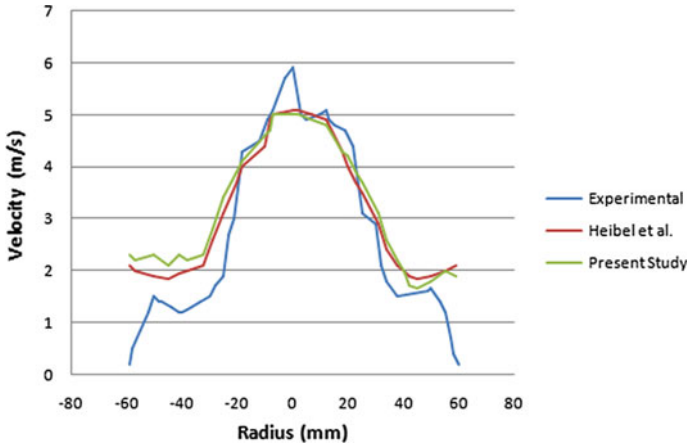
Fig. 3 Velocity profile in the substrate

Table 2 Hydraulic parameters values for various geometries

Geometries	Pressure drop (Pa)	Maximum pressure (Pa)	Uniformity index
Conventional 20°	75	180	0.79
Conventional 30°	102	190	0.82
Conventional 45°	130	192	0.69
Conventional 60°	163	213	0.66

the near wall region because of the resistance from the wall. As pressure variation is found similar in all cases, it is not shown in subsequent figures for other three geometries (Figs. 5, 6 and 7).

The recirculation zone (not shown here) mostly occurred at the diffuser area. The recirculation can be minimized by reducing diffuser angle. Lower the diffuser angle, minimum the recirculation. The pressure at exit is atmospheric as the exhaust gas is then going in the atmosphere. The pressure drop, maximum pressure, and uniformity index of all four conventional geometries are shown in Table 2. It is seen from the data of table that as angle of diffuser increases, the pressure drops and peak pressure increases due to increase in recirculation of fluid. The uniformity index is found to be maximum for conventional 30° diffuser; however, the difference between conventional 20° and 30° found to be less compare to other geometries. Due to more recirculation, uniformity index for diffusers with angle 45° and 60° is found least.
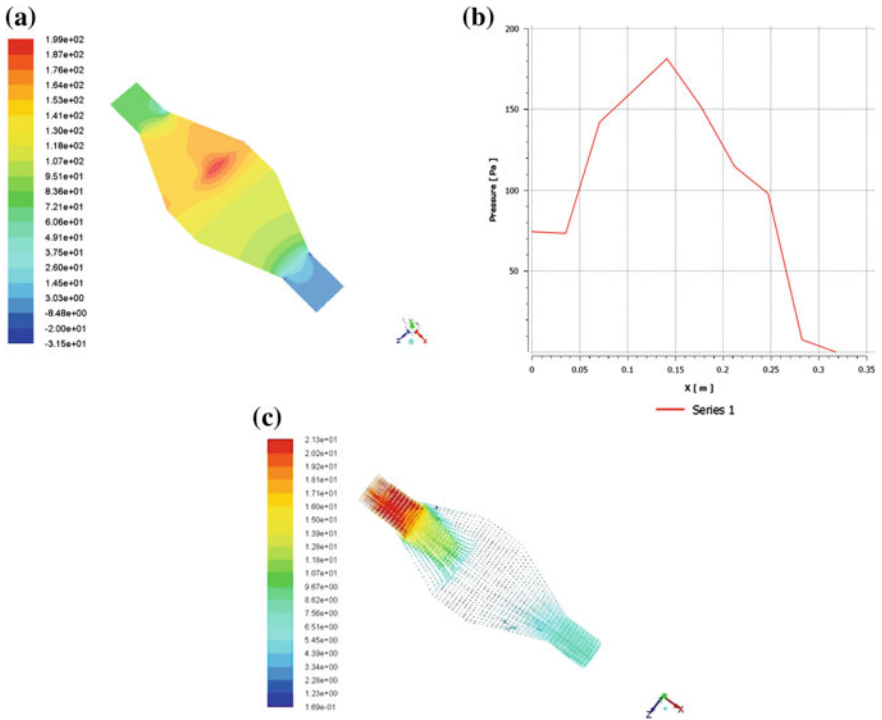
Fig. 4 **a** Pressure contour, **b** pressure across catalytic converter, **c** velocity vector for conventional diffuser geometry with cone angle 20°
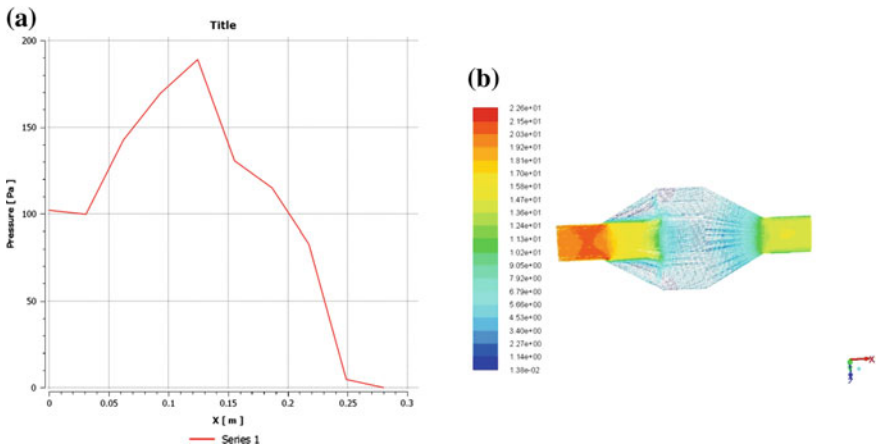

Fig. 5 **a** Pressure across catalytic converter, **b** velocity vector for conventional for diffuser geometry with cone angle 30°
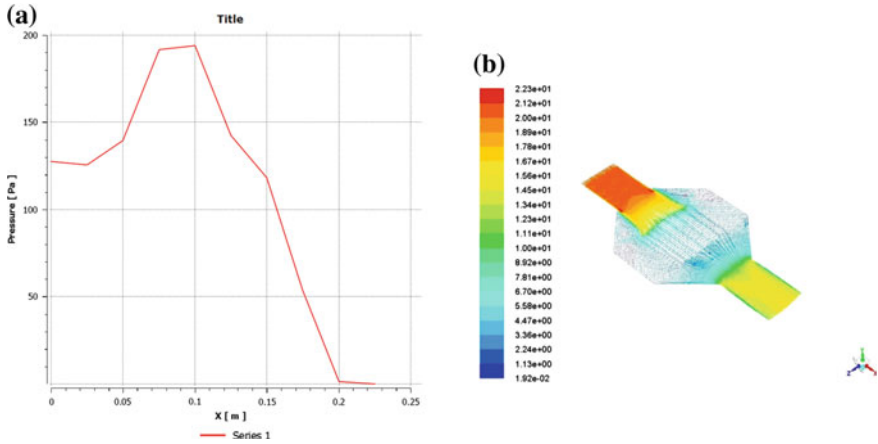
Fig. 6 **a** Pressure across catalytic converter, **b** velocity vector for conventional diffuser geometry with cone angle 45°
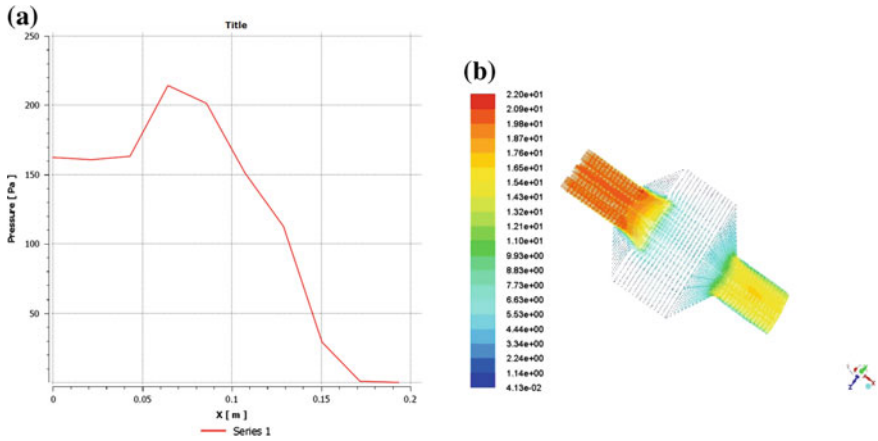

Fig. 7 **a** Pressure across catalytic converter, **b** velocity vector for conventional diffuser geometry with cone angle 60°

5 Conclusions

3D simulation of catalytic converter is carried out using Fluent software. A parametric study on four conventional geometries having diffuser angle 20°, 30°, 45°, and 60° is carried based on pressure and flow distribution. The pressure drop, peak pressure, and uniformity index are the parameters used to design the diffuser of the catalytic converter. Based on these three parameters, conventional diffuser with 20° cone angle geometry is found best among four.

References

1. Pardiwala, J.M., Patel, F., Patel, S.: Review paper on catalytic converter for automotive exhaust emission. In: Nirma University International Conference on Current Trends in Technology Ahmedabad, pp. 08–10 (2011)
2. Williams, J.L.: Monolith structures, material, properties and uses. Catal. Today **69**, 3–9 (2001)
3. Kumar, A., Mazumdar, S.: Towards simulation of full scale monolith catalytic converter with complex heterogeneous chemistry. J. Comput. Chem. Eng. **34**(2), 135–145 (2010)
4. Fluent User Manual: https://www.sharcnet.ca/Software/Ansys/16.2.3/en-us/help/flu_ug/flu_ug.html
5. Achim, H., Michael, A.A.: A new monolith converter concept providing improved flow distribution and space utilization. SAE Technical Paper Series, Advance Catalyst Technology (SP-1409)

Reduction of Warm-Up Time in Light Duty Petrol Engine

Check for updates

Sachin Avghad, Ashok J. Keche and Kishor Kulkarni

Abstract The aim of the present research work is to reduce starting time of engine by utilizing the heat stored in thermal energy storage (TES) system by using different properties of phase change material (PCM) are studied by varying test conditions and based on the performance paraffin wax was selected as best suitable material for experimentation. This paper represents an experimental investigation of thermal energy storage system by light duty petrol engine. The storage system was initially design by considering size of the engine and amount of heat required, thus to reduce exhaust gases emission of engine at starting time and also improve engine performance. The experimental work concludes that reducing the start up time of engine by five minute and also improve warm up time nearly at 45% achieved with TES system.

Keywords Thermal energy storage (TES) · Light duty petrol engine (LDPE) · Phase changing materials (PCM) · Start up process

Nomenclature

C_p	Specific heat (J/Kg K)
LD	Light duty
LH	Latent heat
PCM	Phase change material
POC	Petrol oxidizing catalyst
PPF	Petrol particle filter
SCR	Selective catalytic reduction
TES	Thermal energy storage

S. Avghad (✉) · A. J. Keche · K. Kulkarni
Department of Mechanical Engineering, Maharashtra Institute of Technology, Aurangabad (M.S), India
e-mail: sachinavaghad@gmail.com

1 Introduction

Light duty (LD) petrol engines are commonly used in day to day life such vehicles as cars, mini buses and many other machines, due to their excellent fuel economy, favorable torque output and reliability. In order to control LD petrol engine emission the required engine introduce for both running and rest condition. To meet the latest legislation requirement for LD petrol engine after some treatment is required for system such as selective catalytic reduction (SCR), petrol partial filter (PPF), and petrol oxidation catalyst (POC) have become necessary. At the time of after treatment storage system using catalytic effect to remove harmful emission, therefore at the present temperature becomes effective [1]. Research show that the efficiency of engine is low at temperature becomes low. Farther some application of engine becomes fully warm up become working it properly. At those reasons engine becomes accelerating at the warm up process and also improve the emission and fuel economy of engine. For modern LD petrol engine, overall more than 40% of heat is generated by combustion of fuel. Those heats will exhaust to surrounding environment in the form of wasted heat. Now a day's significant amount of research is aim to recover wastage of heat and improve the overall efficiency of engine [2].

The new technology, including exhaust conditioning devices and design modification, focus on the enhancement of engine efficiency for reduction in greenhouse gas emission and the climb increasing fuel prices so to utilize the different sources of renewable energy. Mostly in the world solar energy considered to one of the most powerful energy source the researchers is search a new technology to eliminating the environmental problem and increasing the efficiency of energy consumption in IC engine [3]. Modern automotive engine are designed for operating over a cretin temperature range. When the ambient temperature is low, it could take substantial length of time for various engine fluid and component to warm up. In the present condition, when the demand is more than available resources, it's our necessary to develop an energy storage device to storage energy at the time of availability and supply it whenever demand is more than supply [4]. In this paper represents a storage system to select best suitable phase change material to storage west heat from engine when engine at running condition and release the storage heat at the time of engine is at rest condition and it also to assist the engine worm up process for reducing start up time of engine [5].

2 Experimental Procedure

The experiment was conducted on three cylinder engine of Maruti 800 car. The specifications of the engine are shown in Table 1. Pilot run was taken to check the performance of the engine. Test Rig was designed to customize different parameters and test were conducted for different PCM. Parameters like heat carrying capacity

Table 1 Specifications of engine used in the present work [6]

Type	Four stroke cycle, water cooled
No. of cylinder	3
Bore	68.5 mm
Stroke	72 mm
Piston displacement volume	796 cm^3
Compression ratio	8.7:1
Maximum RPM	5500
Torque	6 kg m at 3000 rpm
Lubrication system	Wet sump
Ignition timing	7° BTDC, below 900 rpm
I.P/cylinder	3.676 KW
B.P.	8.823 KW
B.P/cylinder	2.941 KW
Mechanical efficiency	80%
Mass of fuel consumed in 3 cylinders	0.00097984 kg/s
Mass of fuel consumed in each cylinder	0.0003266 kg/s
Thermal efficiency	20.46%
Specific fuel consumption	0.39979 kg/KW h

with different temperature of PCM material, charging and discharging by carrying the latent heat and to minimize the time to warm up the engine.

2.1 Testing Facility—Maruti 800 Engine

Figure 2 shows schematically diagram and Fig. 1 photographic view of the experimental setup. It is composed by three main modules; (a) TES device (b) Radiator as cooling component (c) Test Engine as sample module. When the heat absorbs PCM in water circulating engine is charging process (heating) and supplying the heat to the engine is discharging process (cooling).

A schematic representation of thermal energy storage unit in automotive application is shown in Fig. 2. Water is used as a medium for heat transfer in engine & TES unit. The main purpose of TES unit storage heat and used for heating the engine. Water is circulated from engine is also passing throw TES container with melting PCM in different flow rates 0.67 to 1.2 lit/min, and different temperature range. The flow rate is measured by a Rota meter. Thermocouples & multi-meter are used to measure inlet & the outlet temperature of TES unit & Radiator.

An engine block heat-up experiments were performed based on all results the LH storage packed with paraffin and copper radiator, it found to provide the maximum
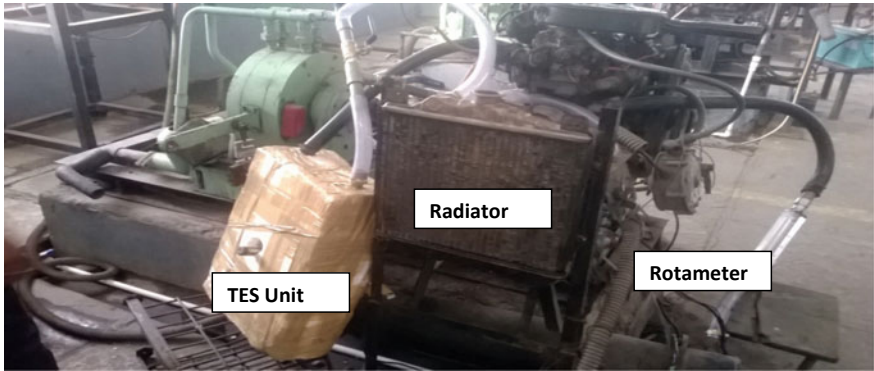
Fig. 1 Photographic view of experimental setup
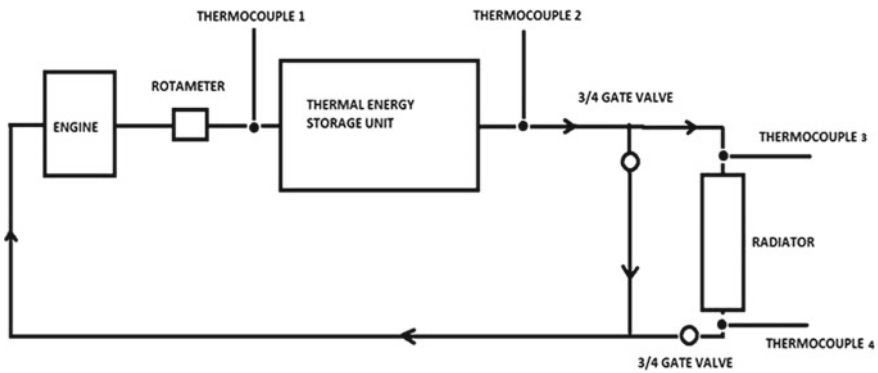

Fig. 2 Schematic representation

amount of heat. Thus, the LH storage device with 3.6 kg of paraffin was used with cooling water rate of flow 1.2 lit/min to heat up engine block. At before the heat up test, the engine block temperature was measured and water from TES was circulated. At the beginning of the heat up process the water temperature entering the engine block was much higher than the initial temperature of engine block and steadily decreased since less and less energy was discharged from the LH storage device over time. Over the 15 min period the water temperature entering the metal block dropped from 74 to 38 °C. Thus heating up the metal block.

TES devices constructed using brass material with inserting copper tubes. Total 8 copper tubes are inserted in box to releasing sensible heat. Pub insulation is provided in the thermal energy storage box in order to reduce heat loss during operation. It has high heat resistance and can sustain a wide temperature range. Hence used for thermal insulation.

Fig. 3 General water
circulation in cars
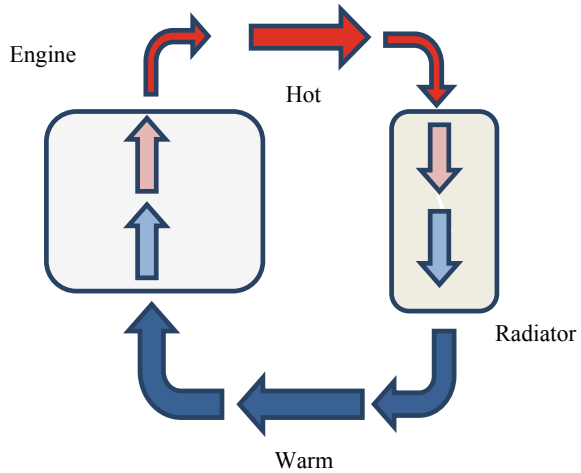
2.2 General Water Circulation Takes Place in Cars

Figure 3 shows the water circulation in the car, how general water circulation takes place. Engine after combustion releases heat. This heat is carried away by water or coolant through water jacket & hoses. This hot water is further circulated through the finned radiator which helps in dissipating the heat at a faster rate and water temperature decreases inside the radiator. The fan is provided in front of the radiator to increase the cooling rate. This cooled water from the exit of the radiator is re-circulated through engine and process is continued [7].

2.3 Actual Working Systems by Using TES System

Figure 4 explains the actual working of system in the car when TES unit is used. Instead, this unit is fitted in between the engine and radiator. The hot water from the engine is directly passing through the storage unit instead of circulating directly through the radiator. Whole day the same cycle is continued. This allows the heat passing throw hot water stored in the storage unit. The warm water from the outlet of the storage unit then circulates through the radiator. This system allows a greater temperature drop of water. The simultaneously overheating problem of the engine is avoided and the engine is kept cold.

Fig. 4 Working of water
with TES unit
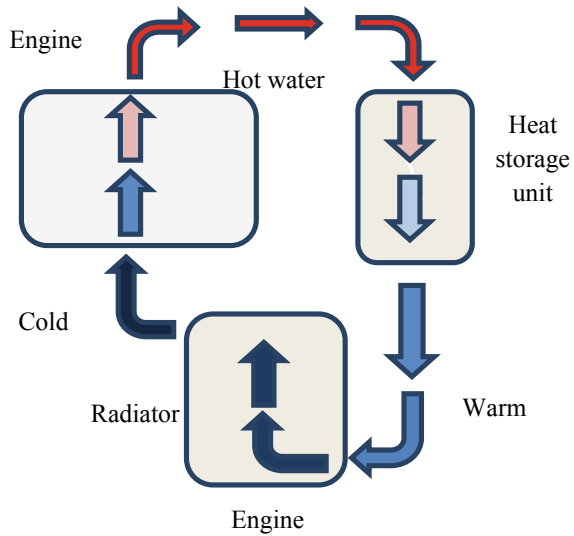
2.4 Storage Design

Assuming a temperature over at night at winter season is at 16 °C, its mean that the block of engine, coolant and PCM will be starting up to 16 °C and also assumed that the energy storage is heated by engine with PCM and coolant at maximum operating temperature 93 °C. When the system is a stable equilibrium condition hence the total heat energy requested in worm-up process is 16–68 °C at melting point for NaOH + H_2O which also calculated by using following equation [8]

$$Q = mc_P(T_f - T_i) \tag{1}$$

For above equitation the total thermal energy required at 61 MJ with including cooling system. With storage of PCM at 10 kg will be needed on experimental work at storage volume 4368 cm^3. Following figure shown Photographic view of storage system [9].

3 Results and Discussion

In present experimental work five thermocouples are used for the face and back side of TES devise to measurement of temperature. The entry and exit temperature increase by increasing the mass of water. The critical temperature of paraffin wax 94 °C above which no phase change takes place if addition of heat taken in the system. This is a temperature up to above paraffin wax absorb the heat of the engine.
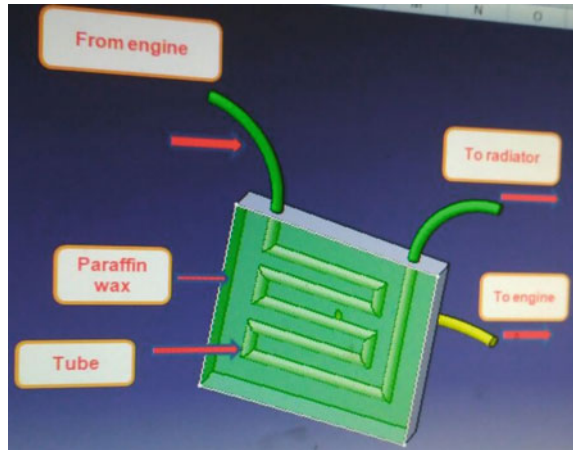
Fig. 5 Actual model TES unit

Figure 5 shows the average temperature measured on the front surface of TES unit and it also measured the temperature on the front surface of the engine. The front side of the TES unit face of heating model and back side face the cooling model. The temperature difference is measured in TES units to determine the efficiency and heat transfer rate of the system. The heat extraction performance test determines the ability of a thermal energy storage unit to absorb or release heat in unit mass as shown in Fig. 5 and it is observed that convection is initially the main mechanism of heat transfer with a liner temperature increase in the time for the temperature on the boat surface of the TES unit with inside PCM.

The heat extraction rate is calculated by determining inlet and outlet temperatures of heat storage unit. Higher heat extraction rate indicates higher heat extraction performance. During the experiment, Hot water is passed through the thermal energy storage unit. A larger drop in outlet temperature indicates the high heat extraction rate with respective time as shown in Fig. 6. The conduction is the effective contrivance of heat transfer therefore no thermal significant thermal stratification is observed due to natural convection.

When the engine is equipped with TES system the worm-up timing of engine 3 min compared to standard condition (without TES system) is 8 min effectively saving 5 min of time. The supplied cooling water at the inlet of the TES was kept at 30 °C during the experiment. This is to measure how well and to what extent the latent heat thermal energy storage device would be able to operate.

Figure 6 shown actual heat transfer and results obtained by the Turbo C++ programming method with respective masses of water. It is observed that if the number of fins is increased then the solidification rate decreases and the time required for solidification of PCM increases as shown mid-plane of TES unit. Moreover, lower the value of the cooled water boundary condition, the higher the rate of heat transferred is achieved. Solidification of PCM time is reduced at the time of discharging process. The simulation based optimization scheme is developed to account for annual
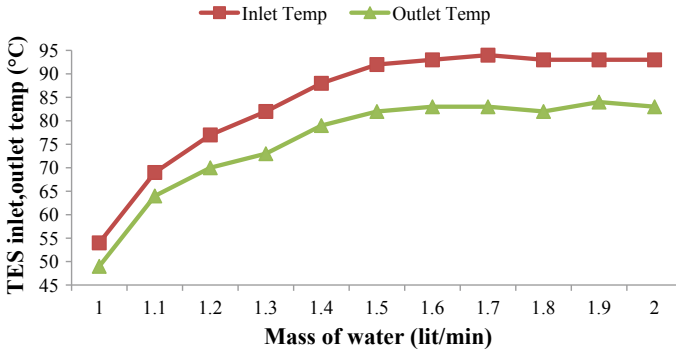
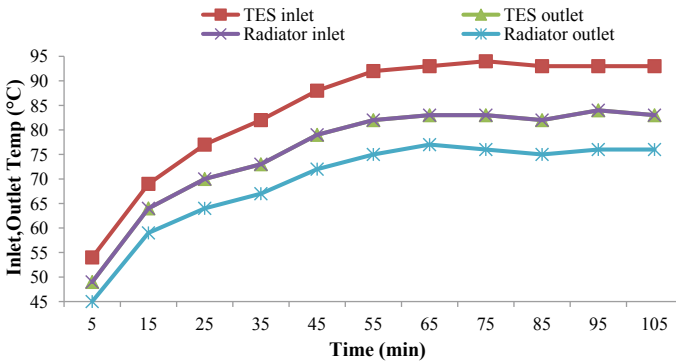**Fig. 6** Mass versus temperature in TES system

Fig. 7 Time versus temperature in TES system

cooling and heating energy. The energy saved due to incorporation of PCM in TES system. This energy is used to warm the engine to enhance the engine performance.

Comparing the start up time of the standard engine with engine fitted with the TES unit it is observed that the warm up time has been reduced by 3 min. The time required by standard engine was 8 min hence effective reduction in engine warm up time by 5 min and also reduces unbent gases during engine start. Figure 7 shows a comparison of experimental results and model predicted results of PCM at various temperature differences and mass of water in TES system. The proposed technique for PCM is implemented by using Turbo C++ programming. It is observing that the model predicted results shown good agreements with experimental results for the difference of temperature in PCM. The maximum error between experimental and model predicted value of various temperature difference is 4.57% (Fig. 8).

For the charging phase changing process finishing after 1 h and the discharging phase changing process finish approximate 11 h. The solidification process gives much more time than the melting. For the low temperature difference between the phase change material and the flow temperature, is nearly at 45 and 93 °C.
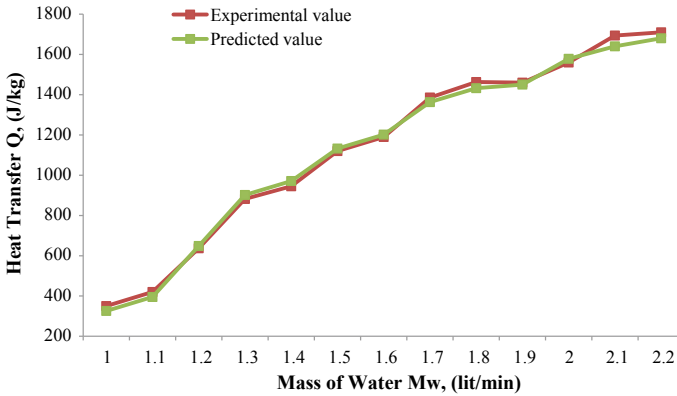
Fig. 8 Mass versus heat transfer in TES system

4 Conclusions

Following conclusions can be drawn from the present study;

- With the implementation system the warm up time of the engine is reduced by 5 min.
- Reduces exhaust gases emission at the time of engine start up.
- Energy extraction depends on the cooling water flow rate. As the flow rate is increased, the heat transfer increases.
- The TES use of paraffin wax to store thermal energy, and it can effectively accelerate the engine worm up process up to 45%.

References

1. Yang, J.: Develop thermoelectric technology for automotive waste heat recovery. In: DOE 2009 Vehicle Technologies Annual Merit Review and Peer Evaluation Meeting (2009)
2. Sharma, A., Tyagi, V.V., Chen, C.R., Buddhi, D.: Review on thermal energy storage with phase change materials and applications. Renew. Sustain. Energy Rev. **13**(2), 318–345 (2009)
3. Sharma, S.D., Sagara, K.: Latent heat storage materials and systems: a review. Int. J. Green Energy **2**(1), 1–56 (2005)
4. Senthilkumar, R., Shankar, N.S.N.: Experimental investigation of solar water heater using phase change material. Int. J. Res. Advent Technol. **2**(7), 79–88 (2014)
5. Wang, T., Zhang, Y., Peng, Z., Shu, G.: A review of researches on thermal exhaust heat recovery with rankine cycle. Renew. Sustain. Energy Rev. **15**(6), 2862–2871 (2011)
6. Hasnain, S.M.: Review on sustainable thermal energy storage technologies, part 1: heat storage material and technologies. Energy Convers. Manag. **39**, 1127–1138 (1998)

7. Abhat, A.: Low temperature latent heat thermal energy storage: heat storage material. Sol. Energy **30**, 313–332 (1983)
8. Sari, A., Kaygusuz, K.: Thermal performance of mystiric acid as a phase change material for energy storage application. Renew. Energy **24**, 303–317 (2001)
9. Bhatt, V.D., Gohil, K., Mishra, A.: Thermal Energy Storage Capacity of Some Phase changing Materials and Ionic Liquids

"Study of Springback Effect in Industrial Grade Materials in Sheet Metal Processing Using FEA"

Akshay P. Thakare and P. T. Borlepwar

Abstract The objective of this paper was parenthetically the numerical resolution of sheet metal forming application using ABAQUS implicit finite part module. Every bending operation involves springback, that is outlined as elastic recovery of the part during unloading. During this study, FEA of springback has done for optimization of sheet metal bending process. In this paper, commercially available finite element analyses (FEA) is used to analyse springback and compensation of it. By increasing downward distance of punch, means that with assistance of the iterations get the optimized geometry of bending profile. Once completion of some iteration of downward distance of punch got optimized, V bending profile comprises of minimum springback as compared to previous profiles. The number of springback, von-mises stress distribution for benchmark and iteration conditions are pictured because of that compensation of springback.

Keywords Springback · Implicit finite element module · Compensation · Benchmark · Iteration

1 Introduction

In sheet metal industry, sheet metal bending is one in every of the foremost widely used produced processes. Sheet metal forming refers to numerous processes used to convert sheet metal in several shapes for specific functions. The demand of sheet metal product increases because its advantages like lightweight, bigger interchange ability, smart surface finish and low cost applications. This is more used in automobile industry, construction of enormous spherical and cylindrical pressure vessels. The bending method involves more deformation of plates either with temperature

A. P. Thakare (✉) · P. T. Borlepwar
Department of Mechanical Engineering, MIT, Aurangabad, Maharashtra, India
e-mail: akshaythakare282@gmail.com

P. T. Borlepwar
e-mail: borlepwarprashant@gmail.com

or without temperature application. However, in every mechanical method, certain defects exist due to the inherent material properties for forming it to the specific form. On alternative aspect, success of bending product depends upon operating parameters, material properties and sort, working condition, clearance and geometry of die, punch, friction condition. Some element on which bending geometry depends are stretching, elongation, anisotropy, grain size, etc. The various modes of failure that occurred throughout sheet metaforming process are wrinkling, puckering and shape distortion factors.

Due to high magnitude relation of surface area to thickness, preceding failure happens through sheet metal bending operation. For achieving correct bending profile, this consists of less springback, stress–strain distribution is incredibly vital. The aluminium alloy 5058 is used for low weight application, whereas the steel and its alloy are being used for high strength purpose. Aluminium alloy materials become favourable as compared to steel, which uses in aerodynamic industry. FEA plays a significant role in conniving springback value and compensation of it for two different types of sheet material like low carbon steel and aluminium alloy 5058. In general, FEA provides data regarding effective and optimized tools and environment to model and stimulate the various operations. FEA additionally provides different kinds of stresses, strains and alternative helpful data that needed in industries.

2 Literature Review on Sheet Metal, that Involves Springback

Bending is a forming process within which shaping of sheet metal is completed while not removing chips around a particular axis with or without application of temperature.

Khamis et al. performed work on study of various drawbeads so as to reduce springback effect in U-bending [1]. For the aim of experiment, mild steel is used as a sheet metal. ABAQUS is used as simulation code, which supplies data regarding every type of drawbead on sheet metal forming process as well as its bending angle value. There are four types of drawbead geometry involved in this study named as without drawbeads, circular drawbeads, rectangular drawbeads and triangular drawbeads. From simulation results, it is concluded that triangular drawbeads reduce springback effectively as compared to opposite varieties of drawbeads.

Gupta et al. provide data on design and analysis of aircraft sheet metal [2]. During this work, spring back effect is calculated on completely different values of thicknesses and angles. It studied spring back effect on varied thickness values of 1.2, 2, 3 mm. The angle of throughout bending operation changes for every thickness. There are three values of bending angles like 60°, 90°, and 120°. It compares the springback result through an experiment and by FEA code LS Dyna. From comparison, it is seen that because the thickness will increase, springback increases.

Panthi et al. have illustrated springback in sheet metal bending by finite element method [3]. For modelling of sheet metal bending process, algorithm rule supported total elastic incremental plastic strain (TEIPS) was used for simulation work because of large rotation and elastic recovery in sheet metal bending process. They represented whole procedure from numerical setup to validation of results. Then, the values of springback evaluate from analysis and are compared to experimental setup for various types of materials named as aluminium, copper, brass and mild steel.

Tisza provides information on numerical modelling as well as simulation of sheet metal forming process [4]. In sheet metal forming process with the assistance of simulation got data regarding material flow, to analyse stress–strain distribution, to determine formability, and varied factors. It gives significant advantages both in the design and in the manufacturing process. Applying these principles got the additional correct output. These kind of works offer correct leads to shorter time with optimum design.

Math et al. studied plate-bending process using finite element analysis [5]. For calculation springback result, steel StE500 is used as per standard of DIN 17102/83. By using MARC II software with nonlinear type, numerical analysis has been performed for bending. During this research, springback values are comparing with experimental value of springback. It provides information about the factors like force, time of indentation, material, which result on mechanical springback. From obtained result, it reduces a springback with the help of some factors like as needed forces and stresses. Thus, FEA helps to reduce springback effect.

3 Experiment of V Bending

Experiments have been conducted to measure spring back angle of bending operation of low carbon steel and aluminium alloy 5058 sheets having thickness of 3 mm. The dimension of this specimen is 100×100 mm. The punch is made of tool steel material and processed under hydraulic press of capacity having 200 KN. Springback angle of the bending profile is calculated by using angle measuring device, and the radius of punch is 1 mm. Bending angle of value $90°$ is used in this sheet metal forming operation. In this bending operation, punch moves 14 mm downward from the upper surface of sheet metal to form bending profile. V-opening distance for the bending operation is 22 mm.

The composition of low carbon steel is carbon (1.47%), manganese (0.25%), iron (98.28%) while aluminium alloy 5058 has manganese (0.25%), aluminium (92.59%), magnesium (0.25%) (Table 1).

Table 1 Experimental value of springback bending

Sheet materials	Angle (°)	Bending angle (°)
Low carbon steel	90	89.50
Aluminium alloy 5058	90	90.57

4 FEA Information

In industries, sheet metal forming simulation performed a very important factor from manufacturing into the product design at an early stage of production. In past years, there has been an ascension in usage of finite element simulations for the sheet metal forming process. The standard implicit statics finite element program still gives information about analysis of sheet metal forming operations.

The major assumptions regarding sheet metal bending process are given as follows.

(1) The materials are isotropic as well as homogenous.
(2) The thermal effects occurred throughout manufacturing process are avoided.
(3) The constant friction is assumed at the die–workpiece interface, and coefficient of friction remains constant during the process.

The elements, which are use in simulation, are CPE4R, which has 4-node bilinear, reduced integration with hourglass control. The bending operations simulated during this study done as per plain strain condition. In simulation, several parameters and influencing factors are considered like material properties and constitutive laws, and others are of significant importance. In sheet metal forming process, modelling and simulation can be used for many purposes, for example, to predict the material flow throughout bending process (Figs. 1 and 2).

The figure shows the setup of FEA model, which is same as experimental setup. The setup consists of die, punch, and sheet metal having a thickness of 3 mm. Die and
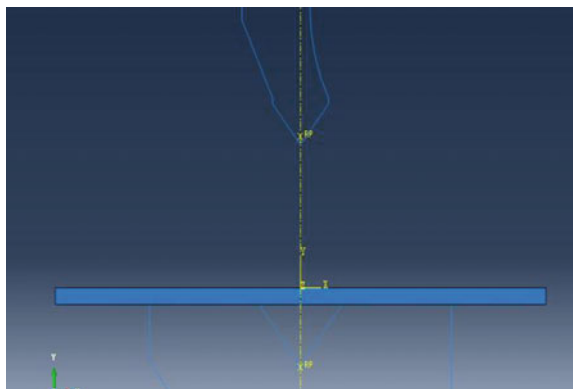
Fig. 1 FEA setup

Fig. 2 Meshing of sheet metal in FEA

Table 2 Mechanical properties of sheet metals

Specification data	Low carbon steel	Aluminium alloy 5058
Young's modulus (GPA)	210	70
Poisson's ratio	0.3	0.3
Density(g/cc)	7.75	2.84
Yield tensile strength (MPA)	140	40
Ultimate tensile strength (MPA)	241	110

punch are taken as discrete rigid body while sheet metal considered as deformable body (Table 2).

5 Springback Analysis

It is vital to calculate the springback in bending process because the formed part is never same as tool geometry. Springback is elastic deformation that perpetually occurs during unloading of punch in sheet metal bending process (Figs. 3 and 4).

Following table provides data of bending angle, when simulation is carried out at an experimental setup. It gives more deviation as compared to experimental values of bending angle (Table 3).
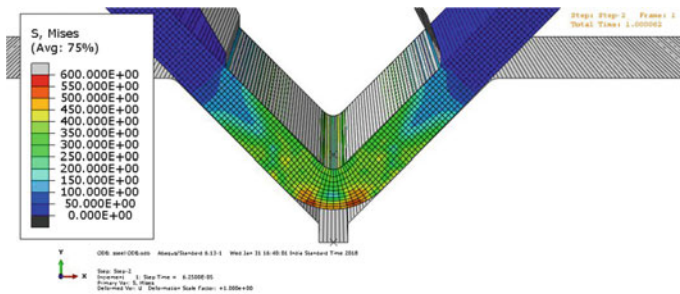

Fig. 3 Von-mises stress distribution for low carbon steel benchmark condition
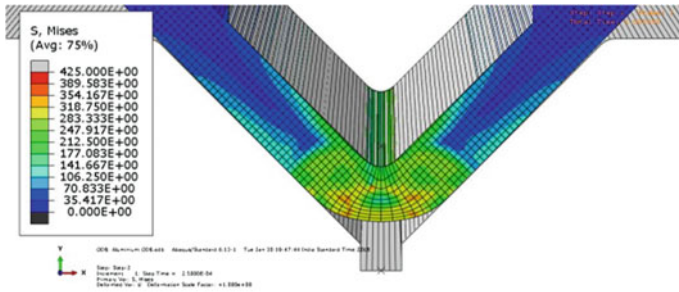
Fig. 4 Von-mises stress distribution for low carbon steel at 0.1 mm iteration

Table 3 FEA on springback bending for sheet metals

Sheet materials	Angle (°)	Bending angle (°)
Low carbon steel	90	90.48
Aluminium alloy 5058	90	90.41

6 Springback Compensation

During sheet metal bending process, springback present in bent sheet metals has great importance because it creates an impact on final geometry of bending profile. In the manufacturing industry, it is still problematic to predict the final geometry of the part after spring back. For compensation of springback, downward distance of punch is to increase or decrease to optimize the springback. However, in most of the cases, these downward distances are increased in downward direction to compensate. In this case, firstly increase the distance of punch by 0.10 mm (Figs. 5 and 6).

Following table gives the value of bending angle, so we calculate springback in bending operation (Table 4).
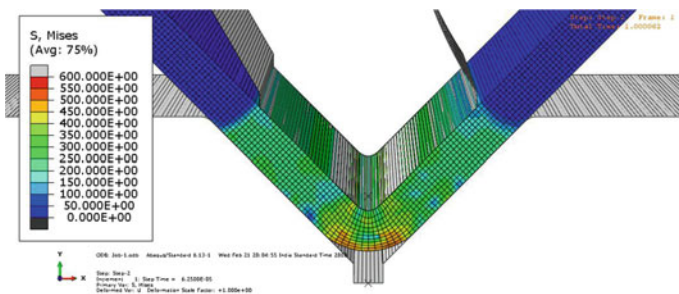

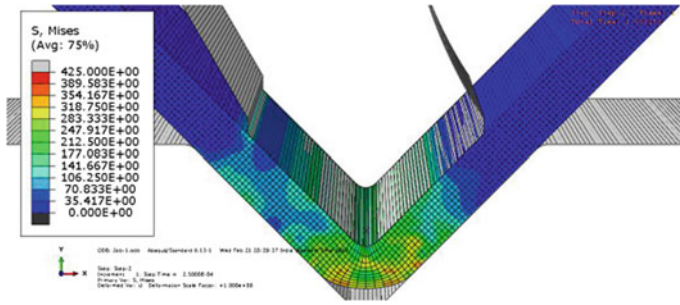**Fig. 5** Von-mises stress distribution aluminium alloy 5058 benchmark condition

Fig. 6 Von-mises stress distribution for aluminium alloy 5058 at 0.1 mm iteration

Table 4 Springback compensation by 0.10 mm	Sheet materials	Angle (°)	Bending angle (°)
	Low carbon steel	90	89.29
	Aluminium alloy 5058	90	89.35

After the completion of compensation of spring back of 0.10 mm, here compensate it by 0.125 mm distance. Reason behind that is to reduce springback by some amount, which is present in 0.10 mm iteration (Figs. 7 and 8).

Following bending angle values are obtained when the punch downward distance is increased by 0.125 mm (Table 5).
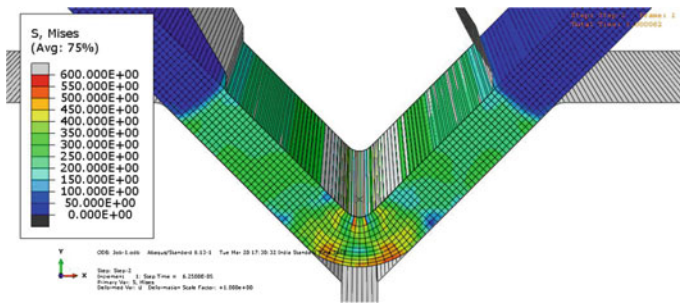

Fig. 7 Von-mises stress distribution for low carbon steel at 0.125 mm iteration

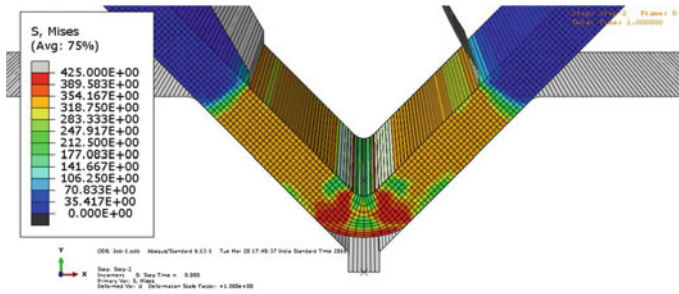| **Table 5** Springback compensation by 0.125 mm	Sheet materials	Angle (°)	Bending angle (°)
	Low carbon steel	90	89.30
	Aluminium alloy 5058	90	89.67

Fig. 8 Von-mises stress distribution for aluminium alloy 5058 at 0.125 mm iteration

From the above value of bending angles, concluded that bending angle values are optimized for bending operation. It shows that springback effect is now minimized to angle of values that consist of less springback as compared to previous values.

7 Conclusions

(1) The recent changes and trends in sheet metal simulations clearly indicate that there is a need of complete, integrated scalable, and optimum solution, covering the whole design process.

(2) The concept provides useful information in both design and manufacturing phase. It helps in getting result that is more accurate. Applying these principles, theoretically more reliable results as compared to benchmark condition, i.e., a more optimum bending profile.

(3) By increasing the punch downward distance, during this case by adding 0.125 mm distance to punch downward brings springback is compensate by 80% as compared to previous iteration.

References

1. Khamis, N.A., Zin, S.M., Bahari, A.R.: Mild steel sheet metal forming using abaqus software: influence of drawbeads in minimize springback. ARPN J. Eng. Appl. Sci. **11**, 11888–11893 (2016)
2. Satyanarayana Gupta, M., Ramana Reddy, D.: Design and analysis of aircraft sheet metal for springback effect. Mater. Today: Proc. **4**, 8287–8295 (2017)
3. Panthi, S.K., Ramakrishnana, N., Pathak, K.K.: An analysis of springback in sheet metal bending using finite element method. J. Mater. Process Technol. 120–124 (2007)
4. Tisza, M.: Numerical modelling and simulation in sheet metal forming. J. Mater. Process Technol. **151**, 58–62 (2004)
5. Math, M., GRizelj, B.: Finite element approach in bending process. J. Mater. Process Technol. 778–784 (2002)

An Experimental Investigation of Thermal Performance of an Octagonal Box Type Solar Cooker

Akshadnya Ukey and V. P. Katekar

Abstract The octagonal box type solar cooker works on the principle of concentrating the solar radiation and converting it into heat. The solar radiations concentrate on the targeted area so that the cooking temperature increases at very fast rate. Modified cooker contain eight reflective inclined sides. The copper plate at the bottom maintains a constant temperature inside the cooker. After rigorous experimentation, modified cooker gives first figure of merit as 0.3027 and second figure of merit as 0.607. Cooking power is 19.767 W. Standard cooking power is 49.639 W. The efficiency of the proposed octagonal solar cooker is 38.36%. As compared to box type solar cooker available in market, modified octagonal cooker has 23.52% more cooking power, 26.55% increase in efficiency. The modified solar cooker comes under the "A grade" class as per guidelines laid down by the Bureau of Indian Standard. This paper describes this work in the concise form.

Keywords Box type solar cooker · Figure of merit · Cooking power · Modified solar cooker · Mathematical modeling of solar cooker

1 Introduction

Solar cooking is the great step toward making environment clean and pollution free. The food usually cooked in various types of solar cooker. Researchers have used various innovative methods to develop energy efficient and cost-effective solar cooker. Coccia et al. [1] have worked on the improved box solar cooker having thermal storage system that has allowed evening cooking. They have reduced cooking time by almost 12% when compared to conventional box type solar cooker. Yettou et al. [2]

A. Ukey · V. P. Katekar (✉)
Department of Mechanical Engineering, S. B. Jain Institute of Technology, Management and Research, Nagpur, India
e-mail: vpkatekar@gmail.com

A. Ukey
e-mail: akshadnyaukey12@gmail.com

experimented a solar box cooker with inclined aperture area. They have got thermal performance parameters, i.e., first figure of merit (F_1) as 0.15 and second figure of merit (F_2) as 0.47. Kesarwani et al. [3] have done a comparative experimental study on finned and un-finned box type solar cookers. They have noticed the improvement in F_1 as 26.89% and in F_2 as 35.5%. Chaudhari et al. (2015) [4], have performed various experiments on a hybrid solar dryer cum cooker. They have claimed F_1 as 0.11 and F_2 as 0.41 with thermal efficiency of 28.93%, average cooking power 84.18 W and standardized cooking power has 63.76 W. Singh et al. [5] have the comparison between un-finned cooking pot and finned cooking pot under the same test conditions in box type solar cooker. They have found that, the temperature of the water in the finned cooking pot is always higher than the temperature of water in the un-finned cooking pot. Kumar et al. [6] have tested solar cooker with finned and un-finned solar absorber plate. The tests have revealed that 5.2 kg of water has got up to 96 °C in 170 min with un-finned and 210 min for finned absorber plate. The time for the boiling of water and cooking power has increased by 19 and 23%, respectively. Pankaj Saini et al. (2014) [7] have tested solar cooker equipped with the thermal storage unit (TSU) with finned cooking pot in place of conventional one. The solar cooker equipped with TSU is able to perform indoor afternoon and evening cooking. The solar cooker efficiency increases by increasing solar energy concentration. From the literature review, it has been learned that, hemispherical solar cooker is the better option for higher efficiency and lower cooking time. But it has fabrication difficulty and high cost of construction. Octagonal shape is a good substitute for hemispherical one. Therefore, we have decided to make an octagonal box type solar cooker.

2 Design

The conventional box type solar cooker had been purchased from market to study its proportions and for experimental assessment. On the basis of it, the size of the top octagon has taken. The size of bottom octagon has been obtained proportionately. The design of reflecting sides has been find out by trial and error method using law of reflection. Finally, the angular position of movable reflector has been decided.

2.1 Design of Top Octagonal Cover

The dimensions of box type solar cooker (purchased from market) are as following: side of bottom square (I) = 34 cm, side of top square (L) = 38 cm, inclination angle (α) of side from horizontal = 75°, the area of bottom square (a) has calculated as 1156 cm². The area of top octagon has calculated as 1156 cm². Hence, the side of the top of the octagon (S) is 15.473 cm as it has octagonal geometry.

2.2 Method for Designing Reflector

For finding the length of the reflector, the single incident ray from any of the angle from horizontal is assumed. For obtaining the high intensity of sun rays up to 3 pm, the angle of the incident rays varied from 45° to 90° with respect to horizontal while facing south direction. From this exercise shown in Fig. 1, it has been originated that, the 60-degree angle is the most accurate angle as it collects maximum amount of sun rays at the collector from morning 10 a.m. to 2 p.m.

2.3 Designs for the Length of Reflecting Side

Length of reflector side has been calculated by using trigonometric computation as specified below. Figure 2 shows an orthographic front view of the cooker.

From trigonometric identities, from Fig. 2, we have got inclined length $I = 8.66$ cm, $x = 4.33$ cm. Figure 3 shows the top view of single vertices of an octagonal box type solar cooker.

From trigonometric identities, Fig. 3, we have got, length (OR) is 18.679 cm, m is 37.358 cm, n is 28.698 cm, y is 1.793, and s $= 11.887$ cm. Therefore, an area of bottom octagon has calculated as 682.26 cm^2.
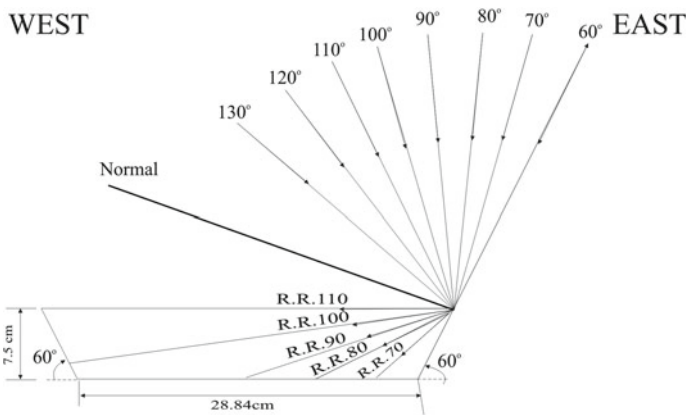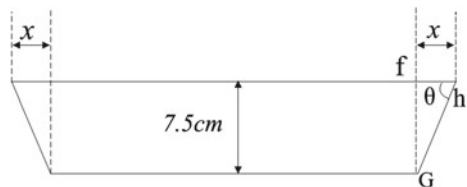

Fig. 1 Side inclined at 60°

Fig. 2 Front view of solar cooker

2.4 Design of Reflector Angle

Reflector is having square geometry and latitude angle for Nagpur city is 21° with minimum and maximum tilt angle as, 0°& 45° facing south. The reflector angle θ = 90° is investigated by trial and error method for maximum energy absorption and focusing to base absorber. Figure 4 shows an optimum position of the reflector.

The layout of the proposed octagonal box type solar cooker is shown in Fig. 5, and the actual fabricated model is shown in Fig. 6. The model is a combination of different components as the wooden box with handle, wooden plates, copper plate,

Fig. 3 Top view of single vertices of octagonal box type solar cooker
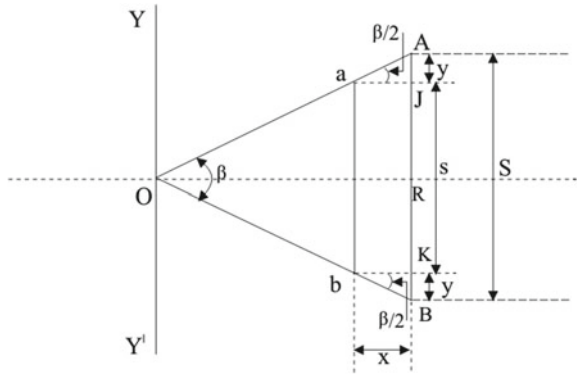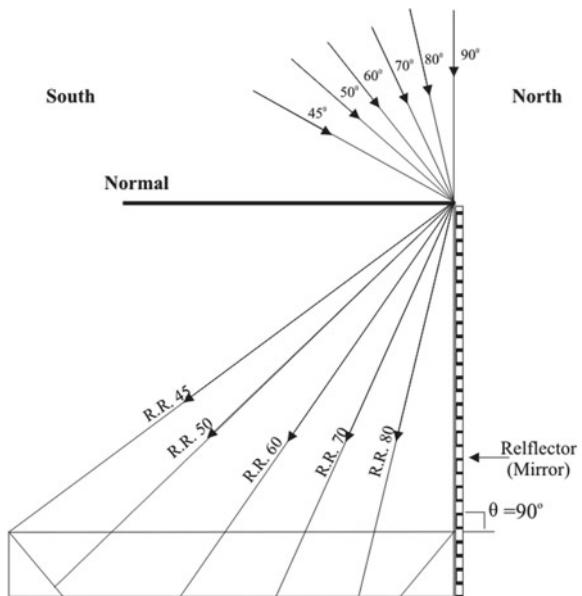

Fig. 4 Reflector inclined

and reflector plates (inner), rubber black (gasket), cover plate with metal frame, booster mirror (outer), and mirror support (Table 1).

3 Thermodynamic Analysis

As per the procedure suggested by Bureau of Indian standard (BIS), the thermal performance of the cooker is evaluated in terms of F_1 and F_2 (first and the second figure of merit), an average cooking power (P) and standard cooking power (P_s). The energy analysis has been performed to evaluate the efficiency of the general box type solar cooker.
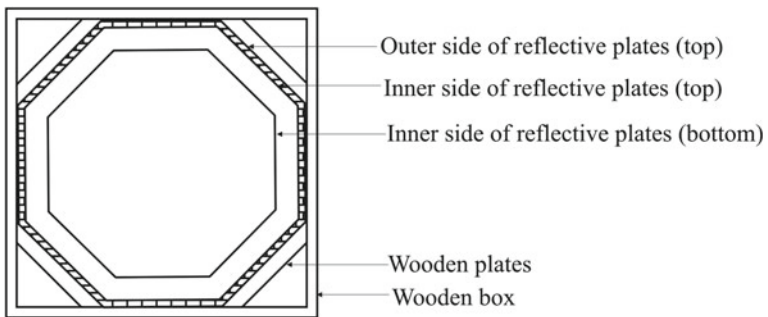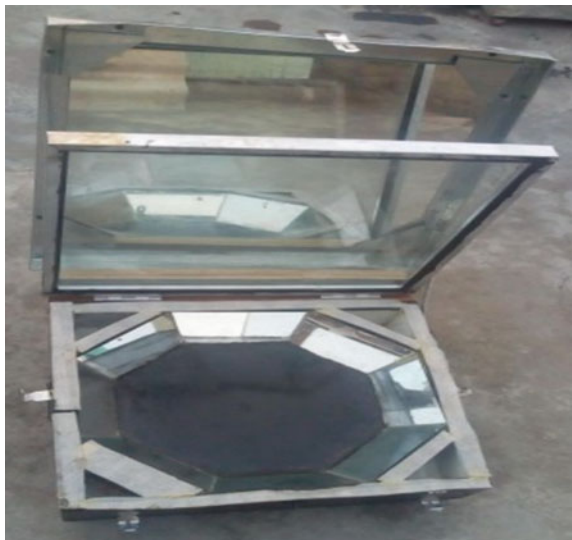

Fig. 5 The top view of proposed solar cooker

Fig. 6 Actual fabricated model

3.1 First Figure of Merit (F_1)

The first figure of merit F_1 is the stagnation test (no load) for box type solar cooker, and it is the ratio of optical efficiency to the overall heat loss coefficient of the cooker. It is mathematically represented as [8]

$$F_1 = \frac{T_{ps} - T_a}{H_s} \qquad (1)$$

where T_{ps} is the stagnant plate temperature in °C, T_a is ambient air temperature in °C, H_s is the solar insolation on horizontal surface at the time of stagnation [8].

3.2 Second Figure of Merit (F_2)

The second figure of merit F_2 is obtained by heating the containers placed on the absorber plate, i.e., under full load condition and is mathematically expressed as [8]:

$$F_2 = \frac{F_1 (MC)_w}{A\tau} \ln \left[\frac{1 - \frac{1}{F_1}\left(\frac{T_1 - T_a}{H}\right)}{1 - \frac{1}{F_1}\left(\frac{T_2 - T_a}{H}\right)} \right] \qquad (2)$$

where F_1 is the first figure of merit, $(MC)_w$ is the product of mass of water and specific heat capacity of water, A is the aperture area of cooker (m^2), τ is the time interval during water temperature rises from T_1 to T_2, T_1 is the initial water temperature in °C, T_2 is the final water temperature in °C, T_a is the average ambient air temperature in °C. H is the average solar insolation W/m^2 [8].

Table 1 Dimension and materials of proposed solar cooker

Overall size	Width	0.42 m
	Length	0.42 m
	Height at front & back	0.093 m
	Top collector aperture area	0.1156 m^2
	Bottom absorber area	0.068226 m^2
Outer box	Wood	Thickness, 18 mm
Inner box	Reflector glass (mirror)	Thickness, 4 mm
	Copper plate	Thickness, 0.5 mm
Upper glazing	Toughened glass	Thickness, 4 mm
	Spacing	10 mm

3.3 Calculating Cooking Power (P)

Cooking power P is defined as rate of useful energy available during heating period. It may be determined by change in water temperature for each interval and mass and specific heat of water contained in the cooking pot.

$$P = \frac{MC_w(T_2 - T_1)}{600} \tag{3}$$

where m is the mass of water (kg), C_w is the specific heat capacity of water, T_2 and T_1 are the final and initial temperature of water in °C, 600(sec) is time interval between 10 min [8].

3.4 Standardize Cooking Power (P_s)

To determine the standardizing cooking power (P_s) from the cooking power (P), each interval has corrected to a standard insolation normalize to 700 W/m² [8].

$$P_s = P \times \frac{700}{H} \tag{4}$$

where P_s is the standard cooking power, H is the interval average solar insolation W/m².

4 Energy Transfer Analysis

Energy analysis of a box type solar cooker has based on the principle of conservation of energy. In this regard, the input energy to the cooker and the output energy of the cooker need to be determined. For the steady-state flow process during time interval Δt, the overall energy balance equation for solar box cooker can be written as [8],

$$[\text{Energy gained by the water}] = [\text{Energy supplied to the water}]$$
$$- [\text{Energy lost from the water}]$$

The energy gained by the water in the vessel kept inside the cooker can be considered as the output energy E_o of the system (in KJ) and is given as,

$$E_o = MC_w(T_2 - T_1) \tag{5}$$

where m is the mass of water (kg), C_w is the specific heat of water (J/Kg °C), T_2 and T_1 are the final of water and ambient temperature (°C) during the full load test. The

energy supplied to water in the vessel kept inside the cooker can be considered as the input energy (E_i) of the system (in KJ) and is written as,

$$E_i = HA\Delta t \tag{6}$$

where H is the solar insolation (W/m^2) recorded over time interval during the test period, A is the aperture area of cooker (m^2), Δt is the time interval.

The energy efficiency (η_E) of the system can be defined as the ratio of the energy gained by the water to the energy supplied to water and is expressed below as,

$$\eta_E = \frac{E_o}{E_i} = \frac{MC_w(T_2 - T_1)}{HA\Delta t} \tag{7}$$

4.1 Observation and Calculation

The thermal performance test for F_1 and F_2 is conducted as per BIS and cooking power evaluated by international standards. Calculating interval averages, the average insolation, average ambient temperature average cooking vessel content temperature have been calculated for each interval. Stagnation temperature test, full load test, and cooking power test have been conducted on the cooker.

4.2 Stagnation Temperature Test

The stagnation temperature test has conducted on 18th of March 2018 on both the solar cookers. The graph, shown in Fig. 7, gives the comparison between the stagnation temperatures of the solar cookers. In the box type solar cooker, initially the temperature rises gradually (up to 11.45 am). It is more than octagonal solar cooker. Then after the temperature of octagonal box type solar cooker rises to 117 °C, which is more than box cooker. It remains at this value for a longer time period (up to 1.50 pm).

4.3 Load Test

The load test has been conducted on 19th of March 2018 on both the solar cookers. The graph, shown in Fig. 8, gives the comparison between the load tests. In the octagonal box type solar cooker, the temperature initially rises gradually as compared to the box type solar cooker (up to 11.15 am). Then, , the temperature of box type solar cooker rises (up to 12.50 pm). But lastly the temperature of octagonal solar

cooker exceeds to the temperature of box type solar cooker and remains at higher value up to 83.2 °C for a longer time period.

4.4 Stagnation Temperature Test

The stagnation temperature test was conducted on 27th of March 2018 on both the solar cookers. The graph shown in Fig. 9 gives the comparison between the stagnation temperatures of both the solar cookers. In the box type solar cooker, the temperature initially rises gradually which is more than octagonal solar cooker. These conditions remain up to 12.15 am. Then, the temperature of octagonal box type solar cooker exceeds to box type cooker and reaches up to maximum value of 125 °C and remains at this value for a longer time period.
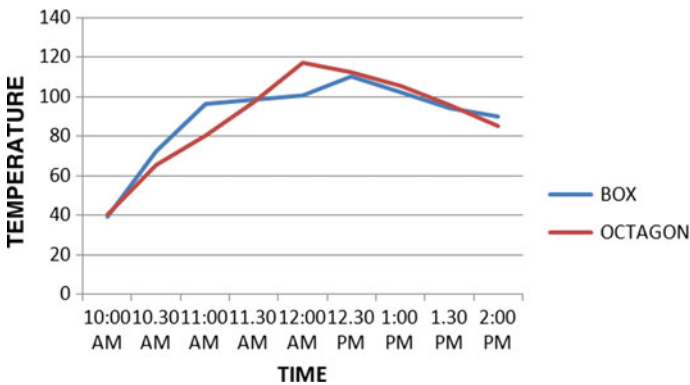

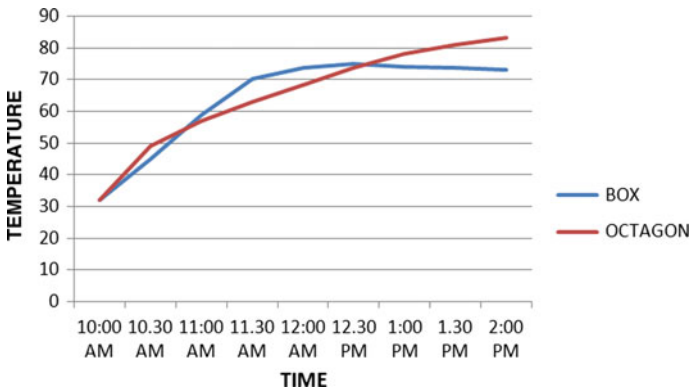**Fig. 7** Result of stagnation temperature test

Fig. 8 Result of load test

Table 2 shows comparative experimental observation of average results of simple box type solar cooker and octagonal box type solar cooker.

5 Conclusion

Octagonal box type solar cooker is new in design and one of its kind. The multiple reflectors inside the cooking area will not affect the incoming sunrays and are able to focus all the incoming sunrays into the area provided for cooking. This cooker comes under the "A grade" class as it satisfies the conditions provided by the BIS for finding figure of merit, designing, and testing of the solar cooker. Standardize cooking power of octagonal box type solar cooker is slight greater than general box type solar cooker. The octagonal box type solar cooker is able to cook variety of food like egg, potato, rise, yellow pigeon peas, etc. efficiently. After rigorous experimentation, modified cooker gives first figure of merit as 0.3027 and second figure of merit as 0.607. Cooking power is 19.767 W. Standard cooking power is 49.639 W. The efficiency of the proposed octagonal solar cooker is 38.36%. As compared to box type solar
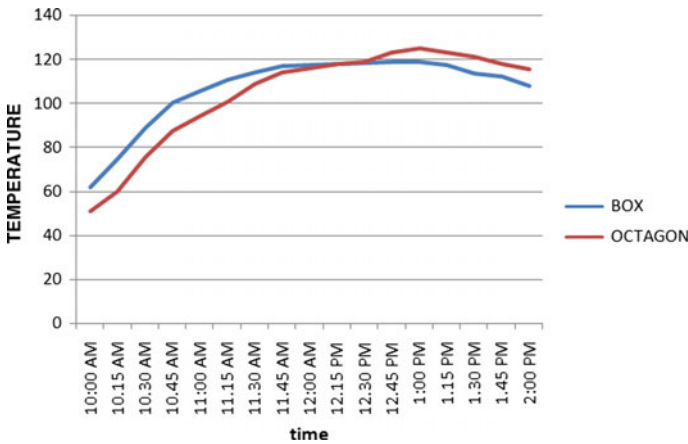

Fig. 9 Result of stagnation temperature test

Table 2 Average experimental results of octagonal and box type solar cooker

Parameters	Symbols	Box type	Octagonal
First figure of merit	F_1	0.2779	0.3027
Second figure of merit	F_2	0.456	0.607
Cooking power	P	15.116 W	19.767 W
Standard cooking power	P_s	37.959 W	49.639 W
Efficiency	η_E	30.31%	38.36%

cooker available in market of same size, octagonal cooker has 23.52% more cooking power, 26.55% increase in efficiency.

References

1. Coccia, G., di Nicola, G., Pierantozzi, M., Tomassetti, S., Aquilanti, A.: Design, manufacturing, and test of a high concentration ratio solar box cooker with multiple reflectors. Sol. Energy **155**, 781–792 (2017)
2. Yettou, F., Gama, A., Panwar, N.L., Malek, A., Azoui, B.: Experimental investigation of thermal performance evaluation and thermodynamic analysis of domestic box type solar cooker with inclined aperture area. Revue des Energies Renouvelables **19**(2), 211–224 (2016)
3. Kesarwani, S., Rai, A.K., Sachann, V.: An experimental study on box-type solar cooker. Int. J. Adv. Res. Eng. Technol. (IJARET) **6**(7), (2015). ISSN 0976-6480 (print) ISSN 0976–6499
4. Chaudhari, R.H., Bhavsar, S.: Hybrid Solar Box Type Dryer Cum Cooker of Chilly Drying for Domestic Usage. Department of Renewable Energy Engineering
5. Singh, S., Singh, N., Uppadhya, W.S.: Analysis of different cooking pots in box type solar cooker with outer reflectors. IJSRD-Int. J. Sci. Res. Dev. **3**(09) (2015). ISSN: 2321-0613
6. Kumar, P., Chourasia', B.K.: Performance B.K. investigation of two reflector box type solar cooker with a finned absorber plate. Int. J. Emerg. Trends Eng. Dev. **4**(4), (2014). ISSN 2249-6149
7. Lecuona, A., Nogueira, J.I., Vereda, C., Ventas, R.: Solar cooking figures of merit extension to heat storage. Sol. Energy **159**, 984–991 (2018)
8. Funk, P.A.: Evaluating the international standard procedure for testing solar cookers and reporting performance. Solar Energy **68**(1), 1–7 (2000)

"Design of Wire Rope Straightener Equipped with Micrometer Screw Gauges"

Avinash T. Panchal, Ajinkya Joshi, Manoj Belokar, Arbaaz Khan and Sankalp Wani

Abstract In wire rope production and processing, the straightening process defines the engineering and business variables which determine success or failure. Straightening is the process of releasing stresses, kinks from the just formed wire, and increasing strength and life of wire ropes. Most of the industries use conventional manual method to apply the forces. It is demand of wire industries from all over the world to replace this time consuming, manual method with standardized equipment that can reduce inaccuracy in application of forces and helps in maintaining a constant and desirable strength to wire rope. After a crucial study of various researches on the wire straightening unit, a model of a straightener has been designed to automate the force on the wire, using latest modeling software. This paper tried to fill up this gap with the well suitable model equipped with a set of digital micrometers.

Keywords Wire rope straightener · Waviness · Micrometer screw gauges · CATIA mode

1 Introduction

Straightening is used to assure you the straightness of a wire rope work piece also to redistribute as well as reduce the induced residual stresses in a just formed wire rope. The quality of finished wire rope is mainly dependent on quality of wire, process sequence, stranding, and straightening. Straightening is one of the most important processes to be executed in every wire rope manufacturing industry. Straightness is one of the most vital quality factors when manufacturing metal wire ropes of a small diameter. The process of wire rope manufacturing mainly includes galvanizing, pre-forming (stranding), and post-forming (straightening) as shown in Fig. 1.

A. T. Panchal (✉) · A. Joshi · M. Belokar · A. Khan · S. Wani
G. H. Raisoni Institute of Engineering and Management, Jalgaon, India
e-mail: avi30panchal@gmail.com

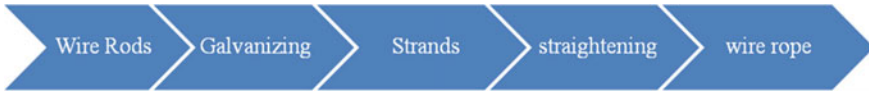M. Belokar
e-mail: manojbelokar1996@gmail.com

Fig. 1 A generalized process of wire rope manufacturing

Fig. 2 Available straightening unit at wire rope industries

During the visit to company, it has been observed that there is a post-forming unit just after the stranding. After observation and analyzing the working of the system, we came to a conclusion that during wire rope formation, this post-forming unit primarily removes the internal residual stresses and kinks, also straighten the wire by removing three-dimensional waviness. This unit was in the form of set of roll type straighteners. Two set of rollers are attached on a vertical plate one is fixed and other is adjustable with screws. In between the two sets of rollers, wire strand is forced to pass (Fig. 2). For various diameters, it has to change the offset distance to have sufficient amount of force to remove residual stresses. Every time for different sizes of strands, a new setting for rollers has to be done. It needs highly skilled technicians to set a good combination of alternating forces on the wire. It is purely a trial and error method which consumes plenty of time for finalization. Also we cannot say that the quality of wire rope is same as that of previous. So we found it as a global need to design a system which can eliminate all these flaws.

After a crucial study of various researches on the wire straightening unit, a model of alternative wire bending roller plates in a straightener has designed to automate force applied on the wire. Analyzing all the related literatures and patents published found a big gap in the research. This paper tried to fill up this gap with a nicely designed, suitable model equipped with a set of digital micrometers.

1.1 The Roll Straightening Process

Straightening is primarily needed to modify or remove curvature in process material. Curvature is the result of mechanical and thermal effects, and it may be desirable or undesirable. As a secondary effect, the straightening process may change the mechanical properties of the process material. A straightener has straightening rolls alternatively arranged in two rows, which can effectively modify or eliminate curvature, waviness, and kinks from a just formed wire rope. The well-positioned adjustable straightening rolls causes' alternate elastic/plastic deformation which forms the basis for changes to the geometric and mechanical properties of the process material.

2 Design of Straightening Unit

The count of rollers is needed in a straightener dependent on the elongation limit R_p and the range of the radius of curvature Δ_r using the maximum (r_{max}) and minimum radius of curvature (r_{min}).

$$\Delta_r = r_{max} - r_{min} \tag{1}$$

Deformation power requirements power is needed to deform process materials using straightening rolls. The amount of power required depends on key variables of the straightening device and the process material as well as the type and speed of roller adjustment. Translation or rotation which is converted to translation can be used to make the best individual roll adjuster.

Adjustment screws or spindles, which act as gear units with good self-locking and convert torque M_{iG} into adjustment force F_{iA}, are well-known solutions. The variables which apply to these gear units are thread flank diameter d_{iF}, mean helix angle α_{im}, and friction angle ρ_i. The angular velocity ϖ_{iG}, respectively, the spindle speed n_{iG} can be used in Eq. 2 to calculate the minimum power P_i which is required to adjust roll i.

$$P_i = F_{iA} \cdot \tan(\alpha_{im} + \rho_i) \cdot (d_{iF}/2) \cdot (\pi \cdot n_{iG}/30) \tag{2}$$

The adjustment force F_{iA} results from the deformation of the process material in the area which is affected by straightening roll i. It is equal to the amount of straightening force $|F_{iR}|$ (Eq. 3), which is applied at the point where process material contacts the straightening roll in correlation with reaction forces. $F_{iA} = |F_{iR}|$ Eq. 3 Analysis of the quasi-static case in the x–y plane (Fig. 1) allows us to ignore external forces and the tangential reaction force fit. The radial reaction force at the straightening roll is equal to the resulting straightening force. If we also ignore the spacing which has changed by ΔT, then the straightening force F_{iR} is only made up of the vertical component of the resulting straightening force F_{iver}.

$$F_{iR} = |F_{iver}| \tag{3}$$

Calculation of the amount of non-dimensional straightening force |F*$_{iR}$| is based on equilibrium analysis which includes the bending moments at the rolls (Fig. 2) and the spacing.

$$\left|F_{iR}^*\right| = \left|M_{(i-1)v}^*\right| + \left|2 + M_{iv}^*\right| + \left|M_{(i+1)v}^*\right| \tag{4}$$

The use of non-dimensional values (indicated by an asterisk) simplifies the calculation [1]. Equation 5 is used to calculate the adjustment force F_{iA} (Eq. 4) or the actual straightening force |F_{iR}|.

$$|F_{iR}| = (R_p \cdot \pi \cdot d^3/16 \cdot T) \cdot \left|F_{iR}^*\right| \tag{5}$$

The analysis presented above shows that calculation of the non-dimensional bending moments $M^*(i-1)v$, M^*iv and $M^*(i+1)v$ is needed to determine the power which is required to achieve deformation. Simulation of the straightening process [2] can be run to generate numeric bending moment/curvature graphs. The analysis uses iteration to calculate the curve for bending moment $M^* = f(x)$, curvature.

$\kappa^* = f(x)$ and the bending line of the process material $y = f(x)$ for a given roll adjustment. With the bending moment curve also the non-dimensional values for the bending moments for calculating the amount of power required are known.

To produce straight process material, the roll adjustments are need to be set based on simulation of the straightening process [2] which is run using SimDATA software. Based on this, a model has developed in a well-known and very popular CATIA v5R19 modeling software.

2.1 Modeling and Operations

According to the design, a model is developed in very popular CAD modeling software CATIA v5 R19. This proposed model has been designed by considering all flaws for removal and found a proof solution. With consideration of existence system, this model not only standardizes the forces to be applied on the wire rope but also it gives user friendliness to the operator. Fixed lower plate has rolls attached along a straight line while the upper rolls to the upper plate. The upper plate has pivoted by constraining it at the center with the help of a set screw. This finds the degree of comparatively higher opposite bending force on the wire rope at the entry of the straightener. Generally, this needs re-adjustment whenever diameter of wire will be changed.

The reverse bending force required for the wire rope can be given by a handle having quick release mechanism, attached with upper plate. The upper plate is secured by two socket head cap screws in the slotted groove.
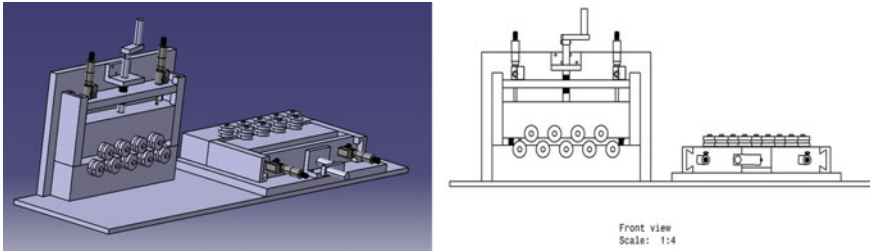
Fig. 3 A 3D model of wire rope straightener with micrometer screw gauges

When the handle is screwed to downward direction, it tilts the upper plate assembly till it restricted by thumb screw setting.

This screw can be adjusted upward and downward so that the wire moving from the wire rope straightener is subjected to very less reverse bending on rolls to attain required straightness. All rolls are positioned in integrated and controlled manner relative to other, with the limiting thumb screw.

With the help of the handle with threaded screw, vertical distance can be adjusted at the nearest. Micrometer screw gauges now play a corrective role in fixing upper plate to the distance exact in microns. Upper plate slides into the slot in such a way that, it will get constrained except required vertical movement. The model is well equipped with micrometer screw gauges and a screw for adjusting vertical distances (Fig. 3).

3 Conclusion

Instead of using simple manually operated tools to adjust straightening rolls, advanced semi-automatic straighteners which are equipped with micrometer screw gauges are used. This type of design leads to the following functional profile:

- Guaranteed accurate application of forces
- Minimizes the time, human resources and achieves the desired product quality
- Minimize operator error.

References

1. Lee, J.-S., et al.: Design optimization of roller straightening process for steel cord using response surface methodology. AIP Conf. Proc. **908**(1). AIP (2007)
2. Schneidereit, H., Schilling, M.: Straightening unit with electronic position control. Wire **47**(2), 34–37 (1997)

Uncertainty of Measurement—An Overview

Shweta V. Matey, Nitin K. Mandavgade and Ramesh R. Lakhe

Abstract In past few years, uncertainty of measurement has grabbed attention of number of researchers, as nowadays there is huge awareness about quality of information, quality of result or a product amongst producers as well as consumers. Measurement of uncertainty plays vital role in quality improvement. It is applicable to various areas like mechanical, chemical and electrical laboratories and testing equipment. The paper gives a brief description about uncertainty, need of uncertainty study, factors responsible for UOM, methods to reduce uncertainty and case studies based on it.

Keywords GUM · Quality improvement · Testing · Uncertainty of measurement (UOM)

1 Introduction

The process of measurement has achieved critical importance globally as measurement provides the information about the unknown quantity—a measurand. Measurement is a process of comparison between measurand and a known standard. Measurand has a true value but it cannot be completely determined. It is important to get the perfect and accurate results from the available resources. As far as accuracy in measurement is concerned, hundred per cent perfection in results is not possi-

S. V. Matey (✉)
Dept. of Mechanical Engg, Lokmanya Tilak College of Engineering,
Mumbai University, Navi Mumbai, India
e-mail: svm4ltjss@gmail.com

N. K. Mandavgade
Dept of Mechanical Engg, Nagpur Institute of Technology, Nagpur, India
e-mail: nkmandavgade@gmail.com

R. R. Lakhe
Shreyas Quality Management System, Nagpur, Maharashtra, India
e-mail: rameshlakhe786@gmail.com

ble and that small amount of imperfection or doubt present in the result is known as uncertainty. Of course it is different from errors in measurements as corrections can be applied to the results when the value of error is known, and when value is unknown, it is considered as uncertainty. Various internal as well as external factors like operator, instruments, method or procedure and environmental conditions are responsible for the presence of uncertainty in measurements.

1.1 What is Uncertainty of Measurement?

Uncertainty of measurement has been interpreted differently by different researchers such as uncertainty of measurement is a doubt about the result of any measurement. Even in the case of careful measurements—there can be a margin of doubt [1, 2]. It is also defined as "a non-negative parameter characterizing the dispersion of quantity values being attributed to a measurand, based on the information used" [3].

1.2 Need of Evaluation of Uncertainty of Measurement

All the accredited calibration laboratories are required to describe the uncertainty linked with the results reported on calibration certificate. Evaluation of uncertainty is recommended for the test laboratories to know and understand which factors of the test procedure have the substantial effects on the results so that such aspects may be closely controlled or monitored.

Importance of evaluation of uncertainty [4].

1. To quantify the quality of a measured value
2. To compare different measured values, e.g., from different measuring systems
3. To compare a measured value with theory
4. To compare a measured value with a tolerance.

1.3 Sources of Errors and Uncertainties

Many things can hamper the quality of measurement. As it is not possible to make actual measurements under perfect conditions, errors and uncertainties may originate from the sources like [1]:

1. The measuring instrument—instruments can give inaccurate results due to bias, ageing, wear, or drift, poor readability, etc.
2. The item being measured—unstable nature of the measurand.
3. The measurement process—The measurement procedure itself may be difficult follow.
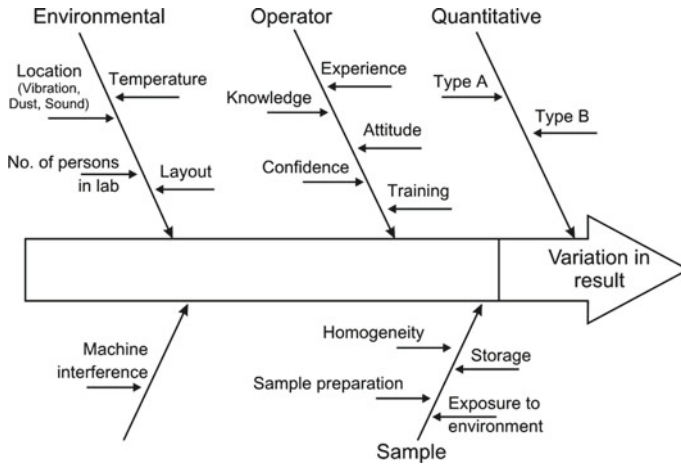
Fig. 1 General Sources of uncertainty [5]

4. Operator's skill—Sometimes quality of the measurements depends on the operator's skill.
5. Sampling issues—The measurements made must be properly representative of the process while choosing samples from a production line.
6. The environment—Environmental conditions like temperature, air pressure, humidity and many can affect the measuring instrument or the object being measured (Fig. 1).

2   Literature Review

Literature has been categorized on the basis of evaluation of uncertainty approach.

Pedro da Silva Hack et al. re-examined 114 papers published between 2004 and 2010 and carried out studies related to measurement uncertainty. Classification of the papers was done according to six different approaches and six different methods used by researchers for calculating uncertainty of measurement. This paper gives a summary of the research status in the field of uncertainty measurement [6]. Mandavgade et al. [7] reviewed literature on measurement of uncertainty and identified how closely the uncertainty is related to measurement and calibration process only. The paper suggested a literature classification scheme.

2.1 UOM Using GUM Approach

Shiv Kumar Jaiswal et al., carried out the calibration study of precision DC high current source, with the help of the case studies of mutual conductance [8]. Luiz Roberto Oliveira da Silva A. developed the methodology to determine the result of measurement associated with the tensile mechanical properties and the uncertainties related to them using advanced metrology concepts in order to implement it in laboratories and research centres. [9]. YadavS. et al. described a new method for evaluating uncertainty in pressure measurement using thorough statistical analysis of errors. [10]. RojoAbollado et al. conducted the research to assess the strain gauge calibration test uncertainty of various aerospace components using guide to the expression of Uncertainty in measurement [11]. CaisucarMahesh et al. identified various factors contributing uncertainty in New Product Development (NPD). Uncertainties associated with the factors were resolved using multiattribute decision making approach [12].

2.2 UOM Using Monte Carlo Technique

Kumar Harish et al. used method based on Law of Propagation of Uncertainty (LPU) described in GUM. In this paper, the procedure of determining uncertainty of measurement of hardness blocks, calibrated by Brinell's Hardness machine, using MCM is discussed. A comparison between LPU and MCM showed a good agreement [13]. Papadopoulos Christos E. concluded that the Monte Carlo simulation method is completely suitable for linear systems and systems with small uncertainties [14]. RadlovackiStrbac B. presented a model for the uncertainty evaluation in the process of flatness measurement of a CMM. The model is used with concrete work piece and concrete measuring machine [15]. Damasceno et al shown that while uncertainty evaluation of Ag/AgCl electrode Monte Carlo and ISO-GUM methods have given similar results [16]. Kosarevsky et al., used Monte Carlo error propagation method to evaluate the uncertainty of a position tolerance using least squares criterion [17].

2.3 UOM Using Analytical Approach

Mandavgade et al. developed a methodology for determining the result of measurement about electrical properties of transformer oil and uncertainties associated with them, by considering factors like repeatability, accuracy of reading, accuracy of test voltage and calibration of capacitor and resistor [18]. Mandavgade et al. carried out uncertainty evaluation with the help of bomb calorimeter, a device used for measuring the performance of coal in terms of heat of combustion [19].

2.4 UOM Using Fuzzy Approach

Mauris Gilles used Fuzzy approach to evaluate uncertainty of measurements as it is compatible with the ISO guide for the expression of uncertainty in measurement [20]. Ferrero, proposed a theory of the evidence and frames the random-fuzzy variables for UOM [21].

3 Evaluation of Measurement Uncertainty

UOM is a generic term which consists of two types of uncertainty: Types A and B.
   Type A evaluations—uncertainty estimates from repeated readings (statistical).
   Type B evaluations—information like previous experience, calibration certificates, specifications, calculations, published information, and common sense estimates *Type B* type uncertainty (qualitative and quantitative parameters).

3.1 Main Steps to Evaluate Uncertainty

1. Specify the measurand.
2. Complete the measurements procedure.
3. Evaluate the uncertainty of the input quantity.
4. Identify the dependency of the errors and input quantities.
5. Find the combined uncertainty.
6. State the confidence level and express the uncertainty in terms of a coverage factor.
7. Declare the measurement uncertainty (Fig. 2).

4 Case Study

Case study was conducted in an oil refinery. Objective of this uncertainty evaluation study is to detect amount of Benzene in Motor Spirit volume (MS/Petrol). Benzene is an aromatic hydrocarbon that is naturally present in crude oil, and hence, it is present in the petrol which is derived from it. Extra amount of benzene is formed in the refining process. Additional amount of benzene is formed in the refining process. The maximum amount of benzene permitted in petrol is 1% in its volume since year 2000. Benzene is also produced during the combustion of petrol in the engines of vehicles [23].
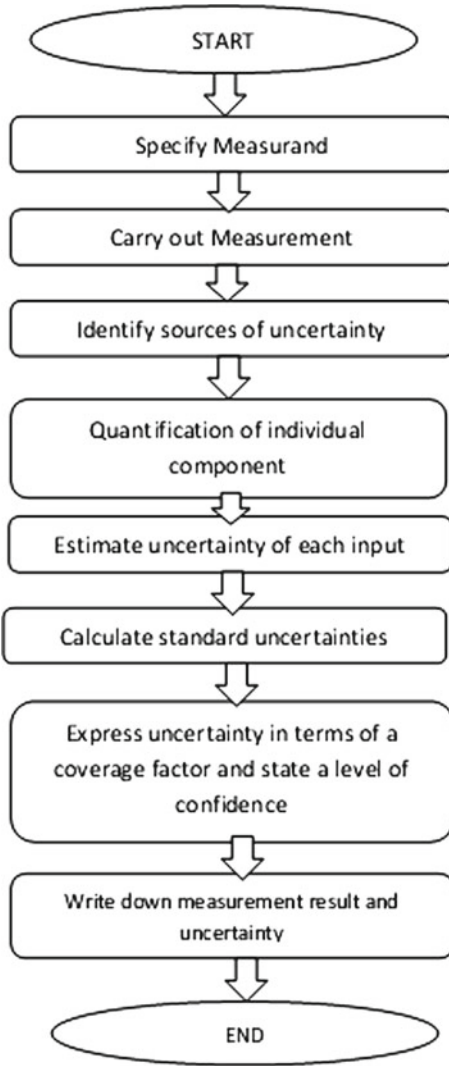
Fig. 2 Steps to Calculate Uncertainty [1, 2, 22]

As it is carcinogenic, excess amount is undesirable. Hence amount of Benzene is determined after refining process and uncertainty analysis is carried out to prevent every sort of doubt. The calculation of uncertainty is shown in tabular format below.

Benzene in MS Vol.%

(1) Sample—Motor Spirit (MS)
(2) Measurand—Benzene (vol.%) in MS
(3) Measurement Procedure—ASTM D-5580
(4) Components Involved in Uncertainty identification

    (a) Human Error
    (b) Uncertainty due to CRM

(5) Mathematical Model.

Uncertainty due to Repeat Observation + Uncertainty due to CRM Accuracy (Table 1, 2 and Fig. 3).

5 How to Reduce Uncertainty of Measurement

With the help of few practices given below. Uncertainty can be reduced [1].

1. Use calibrated instruments and refers calibration corrections given on the certificate.
2. Make corrections to remove error.
3. Make your measurements noticeable to national standards. (UKAS in the UK).
4. Select the best available measuring instruments.
5. Take measurements repeatedly to avoid errors.
6. Check calculations, and record the numbers carefully.

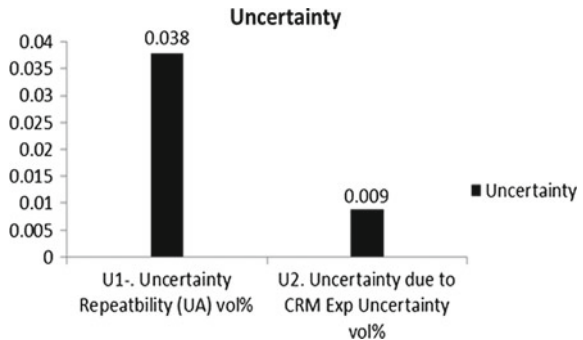**Fig. 3** Uncertainty analysis of Benzene in MS vol.%

Table 1 Uncertainty Analysis

(6) Type a uncertainty repeatability	Benzene in MS vol.%	Results
	1	0.68
	2	0.68
	3	0.72
	4	0.88
	5	0.77
Mean value vol.%	x^-	0.75
Standard deviation vol.%	Std. Deviation $= \sqrt{1/n\text{-}1\{\sum(x-x^-)^2 + \ldots\}}$	0.08
Uncertainty UA vol.%	$UA = STD.\ Deviation/\sqrt{n}$	0.04
Degree of freedom	$n-1$	4
(7) Uncertainty due to CRM D-5580-65-CAL-IS-1		
Uncertainty as per certificate of CRM is + 2.0 vol.%		
Benzene in MS CRM conc. Is 0.9 vol.%, uncertainty is $\pm$ 0.0018	0.018	0.018
Expanded uncertainty (Ucrm) Normal Distribution	$Ucrm = Uncertainty/2$	0.009
Degree of freedom		∞
(8) Components of Uncertainty	Type	
Uncertainty repeatability (UA%)	A	0.037
Uncertainty due to CRM(Ucrm)	B	0.009
(9) Combined Uncertainty %Ucomb% $= \sqrt{\{(Type\ 'A')2 + (Type\ 'B')2\}}$	$ubal = \sqrt{\{(ur)^2 + (uu)^2\}}$	0.038
(10) Effective Degree of Freedom	$V_{eff} = (Ucomb)^4/\{(UA)^4/4 + (Ucm)^4/\infty\}$	4.48
(11) Coverage Factor K-From Student Distribution Table, At confidence level 95% & Veff = 4.48 Coverage Factor K = 2.78	2.78	
(12) Expanded Uncertainty vol.%	Ucomb%*K	0.11
Combined Std Uncertainty vol.%	**= 0.038%**	
Degree of Freedom Veff	**= 4.48**	
Coverage Factor	**= 2.78**	
Expanded Uncertainty vol.% 0.038 × 2.78	**= 0.11 vol.%**	

Result Benzene in MS = 0.75 + 0.11 vol.% at 95% confidence level with coverage factor = 2.78

Table 2 Uncertainty Budget

Source of uncertainty	Value	Probability distribution	Divisor	Uncertainty	Degree of freedom
Uncertainty repeatability (UA) vol.%	0.080	Type A rectangular	$\sqrt{5}$	0.038	4
Uncertainty due to CRM Exp Uncertainty vol.%	0.018	Type B normal	2	0.009	∞

5.1 Some Other Good Measurement Practices [1]

1. Refer the instructions manual for using and maintaining instruments.
2. Use experienced and trained staff.
3. Make sure that software works correctly.
4. Rounding should be done correctly.
5. Keep records of your measurements and calculations immediately after measurements made.
6. Keep a note of any extra information that may be relevant.

6 Conclusion

Measurement of uncertainty is extremely important production sector. It is associated with the quality of measurement and ultimately with the quality of a product to satisfy customers requirements. This article categorized the papers according to the approaches used to estimate the uncertainty, like, GUM methodology, Monte Carlo technique, and fuzzy logic. The UOM techniques are applicable to mechanical, civil, electrical and chemical field. In this case study, uncertainty has been evaluated successfully using GUM approach, and results are within the acceptable limit of uncertainty. The conclusion of the study is that the application of the technique depends upon the source and type of uncertainty. Lot of research work is still required to reduce the amount of uncertainty by a substantial percentage from measurement results.

References

1. Guide to the Expression of Uncertainty in Measurement, ISO/IEC Guide 98: 1993, 1992
2. Bell, S.: A beginner's guide to uncertainty of measurement. Teddington, United Kingdom, TW11 0LW: NPL National Physical Laboratory, 1999
3. International Vocabulary of Metrology.: Basic and General Concepts and Associated Terms (VIM) 3rd edn. Final draft 2006-08-01
4. Ian, S.: An introduction to measurement uncertainty. Data Sci. National Physical Laboratory 25 Jan 2008
5. Birch, K.: Estimating Uncertainties in Testing, Measurement Good Practice Guide No.36. British Measurement and Testing Association. Teddington, Middlesex: HMSO (2001)
6. da Silva Hack, P., ten Caten, C.S.: Measurement uncertainty: literature review and research trends. IEEE Trans. Instrum. Meas. **61**(8) (2012)
7. Mandavgade, N.K., Jaju, S.B., Lakhe, R.R.: Uncertainty of measurement: literature review. Elixir Mech. Engg. **86**, 35078–35085 (2015)
8. Jaiswal, S.K., Ojha, V.N., Singh, A.: Estimation of uncertainty in measurement in precision calibration of DC high current source up to 100. J. Sci. Ind. Res. A JVS & DC Standards, National Physical Laboratory (2005)
9. da Silva A, L.R.O.: Evaluation of the uncertainty of measurement of mechanical properties on the tensile testing. 25 al 27 de OctubreSimposio de Metrología (2004)
10. Yadav, S., Gupta, V.K., Prakash, O., Bandyopadhyay, A. K.: Evaluation of associated uncertainties in calibration of direct pressure indicating electromechanical devices. Meas. Sci. Rev. **5**(3) 2005
11. Abollado, R., Shehab, E., Rose, M., Schröter, T.: Uncertainty assessment for measurement processes in the aerospace manufacturing industry. Procedia CIRP **60** 326–331 (2017)
12. Mahesh, C., Dr. Gaonkar, R.P.: Uncertainty identification in new product development. Ind. Eng. J. **X**(12) (2017)
13. Kumar, H., Moona, G., Arora, P.K., Haleem, A., Singh, J., Kumar, R., Kumar, A.: Monte Carlo method for evaluation of uncertainty of measurement in Brinell hardness scale. Indian J. Pure Appl. Phys. **55**, 445–453 (2017)
14. Papadopoulos, C.E., Yeung, H.: Uncertainty estimation and Monte Carlo Simulation Method. Received 11 December 2000; received in revised form 26 Jan 2001. Accepted 3 April 2001
15. Strbac, B., Radlovacki, V., Acko, B., Spasic, Jokic, V., Zupunski,L.J., Hadzistevic, M.: The use of Monte Carlo simulation in evaluating the uncertainty of flatness measurement on a CMM", JPE **19** (2016)
16. Damasceno, et al.: Evaluation of Ag/AgCl-electrode standard potential uncertainty used in primary pH measurements by Monte Carlo simulation. Meas. Sci. Rev. **5**(2), 49–52 (2005)
17. Kosarevsky, S., Latypov, V.: Practical procedure for position tolerance uncertainty determination via monte-carlo error propagation. Meas. Sci. Rev. **12**(1), 01–07 (2012)
18. Mandavgade, N.K., et al.: Measurement uncertainty evaluation of automatic Tan Delta and resistivity test set for transformer oil. Int. J. Metrol. Qual. Eng. **3**(39–45) (2012)
19. Mandavgade, et al (2011). Determination of uncertainty in gross calorific value of coal using bomb calorimeter. Int. J. Meas. Technol. Instrum. Engineering, **1**(4), 45–52 (2011)
20. Gilles, M., A fuzzy approach for the expression of uncertainty in measurement. Measurement **29**(3), 165–177 (2001)
21. Ferrero, A.: The random-fuzzy variables:a new approach to the expression of uncertainty in measurement. IEEE Trans. Instrum. Measur. **53**(5), 1370–1377 (2004)
22. EURACHEM/ CITAC. 2000. EURACHEM/CITAC Guide CG4 Quantifying Uncertainty in Analytical Measurement. (2000)
23. ISO/IEC 17025.: General Requirements for the Competence of Testing and Calibration Laboratories (2000). https://www.ukpia.com/docs/default-source/publication-files/ukpiabenzenein-petrol.pdf?sfvrsn=0

Arduino-Based Tuned Electromagnetic Shaker Using Relay for MEMS Cantilever Beam

Abhay M. Khalatkar, Ritesh Kumar, Rakesh Haldkar and Durwesh Jhodkar

Abstract These days Micro-Electro-Mechanical Systems (MEMS) is the most interested field like a pie chart of research fields. Many MEMS devices like microsensor, microactuator, and microenergy harvester are the backbone of electronics applications in the form of sensors and actuator. These all are mostly based on the basic concept of deflection of cantilever beam. These all have requirement of vibration testing for their long-life working. This study proposes one method called Arduino-based tuneable electromagnetic shaker using relay for MEMS Cantilever beam. Tuneable means we can tune its frequency according to requirement called Frequency Tuning Concept (FTP). In this paper, we designed and developed electronics shaker controlled by Arduino circuit with 12 V relay which can be controlled by programmable Arduino-Uno board. By this, we can check the resonance frequency modes of the MEMS sensors and actuators, which is the substitute measurement method rather than the frequency measurement of beam by very costly existing vibration shakers.

Keywords Arduino · Vibration shaker · Relay · Frequency tuning · Energy harvesting

A. M. Khalatkar (✉) · R. Haldkar · D. Jhodkar
G H Raisoni College of Engineering, Nagpur 440016, India
e-mail: abhay.khalatkar@raisoni.net

R. Haldkar
e-mail: rakesh.haldkar@raisoni.net

D. Jhodkar
e-mail: durwesh.jhodkar@raisoni.net

R. Kumar
Indian Institute of Technology, Patna 440011, India
e-mail: Riteshshing0206@gmail.com

1   Introduction

Since 2005, the MEMS research gained its peak because of its large area application. The main areas of application are sensor and actuator. Frequency tuning is an important aspect in turns of measurement of vibration response of any rotary or nonrotary elements [1, 2]. In this study of measurement of vibrations, the findings of mode shapes of beams at different frequency are the key factors [3, 4]. These mode shapes of beams in turns of natural frequencies are to be measured by vibration shakers [5]. Most of the researcher focused their study toward the findings of resonant modes for maximum energy harvesting by means of Smart Materials like piezoelectric [6]. Sodano, H. A. et al. formulate the model for energy harvesting based on frequency tuning concept by means of vibration shaker [7]. In our earlier paper [8–10], we have also discussed the geometry optimization piezo patch by means of cantilever beam on charge output by means of frequency tuning concept. Recently Kang et al. [11] and Priya et al. [12] discussed effect of the shape and geometry of a bimorph piezoelectric cantilever beam harvester on the electromechanical efficiency of the system and also developed analytic model using Rayleigh cantilever beam approximations for piezoelectric harvesters with tapered bimorph piezoelectric cantilever beam. Electromagnetic is defined as generation of magnetic field using electricity in coil. This electromagnet is called solenoid. The strength of electromagnet depends on relative permeability of core in the coil, number of turns, and current in the coil. This controls the amplitude of excitation. The frequency of the electromagnet is controlled by the external circuit. In this paper, Programmable Arduino is used to control electromagnet shaker. The objective of this research was to get low-cost electromagnet shaker for vibration analysis. Vibration analysis is used to check long-life feasibility of product under dynamic state. This study focuses on the development of the electromagnet shaker according to personalize research requirement.

2   Concept of Solenoid

A solenoid is a long coil of wire wrapped in many turns. When a current passes through it, it creates a nearly uniform magnetic field inside. Solenoids can convert electric current to mechanical action, and so are very commonly used as switches. The magnetic field within a solenoid depends upon the current and density of turns. The energy density of the magnetic field depends on the strength of the field, squared, and also upon the magnetic permeability of the material it fills. Iron has a much larger permeability than a vacuum. Even small solenoids can exert forces of a few Newtons. The solenoid-based mini electromagnetic shaker is shown in Fig. 1.

The total energy stored in the coil is

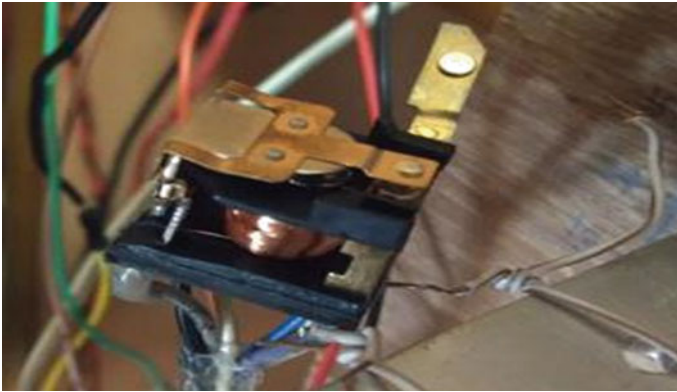$$W = \frac{B^2 A g}{2\mu_0}\left(\frac{\mu_m}{\mu_0}\right)$$

Fig. 1 Solenoid-based mini electromagnetic shaker

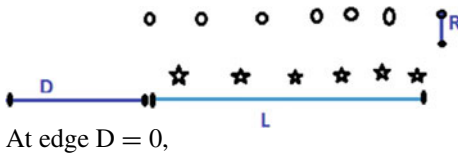$$w = \frac{B^2}{2\mu_0}\left(\frac{\mu_m}{\mu_0}\right)$$

where w is energy density, and W is total stored energy. The force F can be calculated by differentiating energy with respect to gap length, because this is the maximum displacement.

$$F = \frac{dW}{dg}$$

$$F = \frac{B^2 A}{2\mu_0}\left(\frac{\mu_m}{\mu_0} - 1\right)$$

B(total) = Magnetic field intensity

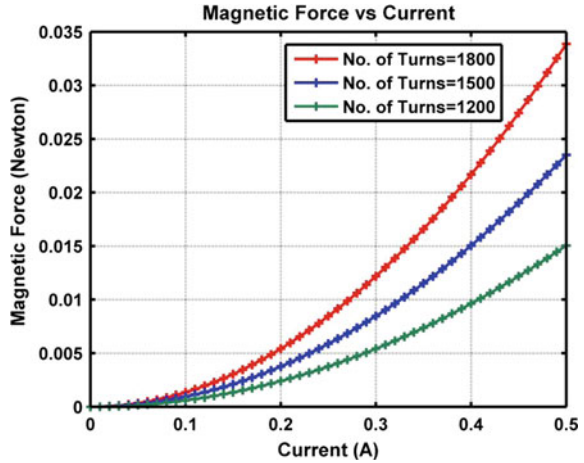$$= \frac{\mu_0 n I}{2}\left[\frac{D+L}{\sqrt{(D+L)^2 + R^2}} - \frac{D}{\sqrt{D^2 + R^2}}\right]$$

At edge $D = 0$,

$$\text{B(total)} = \text{Magnetic field intensity} = \frac{\mu_0 n I}{2}\left[\frac{L}{\sqrt{L^2 + R^2}}\right]$$

$$= \frac{\mu_0 n I}{2} \quad (\text{if } L >> R)$$

Table 1 Parameter for Analytical formulation

Sr. No.	Parameter for Mini Shaker	Value
1	D	0.0005
2	L	0.006
3	R	0.004
4	μ_0	$4\pi * 10^{-7}$

Fig. 2 Magnetic force versus current

$A =$ Crosssection area of core

$\mu_0 = 4\pi * 10^{-7}$

$\mu_m =$ Magnetic permeability

$\mu_m = 10^4 * \mu_0 = 4\pi * 10^{-3}$ (Magnetic permeability is very high for iron, cobalt, and nickel) (Table 1).

Above Fig. 2 shows the response of Magnetic force (Newton) generated at the tip of solenoid. The figure shows the force magnitude goes on increasing with the increase in number of coils. The magnetic force (Newton) generated by the coil also increases nonlinearly with increase in current. The figure shows 0.034 N at 0.5 A current for 1800 turning of the coil.

When the current flows in the coil (Fig. 3), a strong magnetic field is generated along the axis of the coil with a constant slope which measures 4.2e-4 Teslaat 0.5 A ampere current for 1800 turning of coil.

3 Arduino Program

Arduino is an open-source microcontroller-based programming device. This paper is using Arduino-Uno which has Atmega 328 microcontroller. This can be easily pro-

Fig. 3 Magnetic field versus current in coil
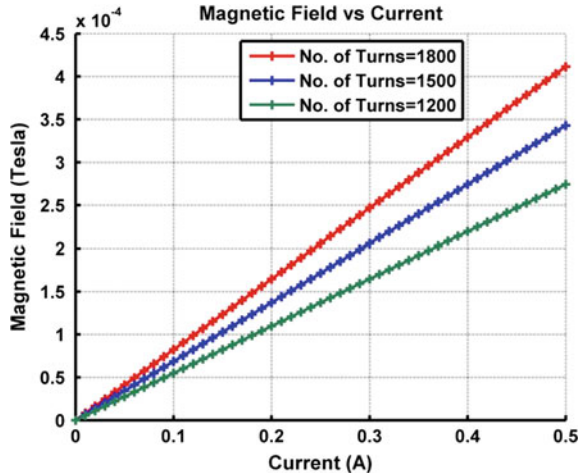
grammed according to research project. Here the frequency is controlled by program using potentiometer. In this, the delay has been used as a variable to vary frequency of shaker. As the delay is reduced, frequency will increase. The code is shown here:

Arduino Code: int led = 3; intanalogPin = 1; intval = 0;
```
Int time = 0; int t = 0;
#include <LiquidCrystal.h> LiquidCrystallcd(4, 7, 10, 11, 12, 13); void setup() {
pinMode(led, OUTPUT); lcd.begin(16,2); Serial.begin(9600);
}
void loop() {
val = analogRead(analogPin); time = val/4;
t = 255-time; analogWrite(led, val/4); digitalWrite(led, HIGH); delay(t); digitalWrite(led, LOW); delay(t); lcd.setCursor(0,0); lcd.print("Delay="); lcd.print(t);
Serial.println(t);
}
```

In circuit shown in Fig. 4, Arduino board, Relay, potentiometer and power MOSFET IRFZ44 is shown. Power MOSFETs (Metal Oxide Semiconductor Field Effect Transistor) are the most commonly used power devices due to their low gate drive power, fast switching speed, and superior paralleling capability. Most power MOSFETs feature a vertical structure with Source and Drain on opposite sides of the wafer in order to support higher current and voltage.

Figure 5 shows the deflection plot of cantilever mounted with the electromagnetic shaker. The various type of micro-beam can be mounted for vibration testing using this setup.
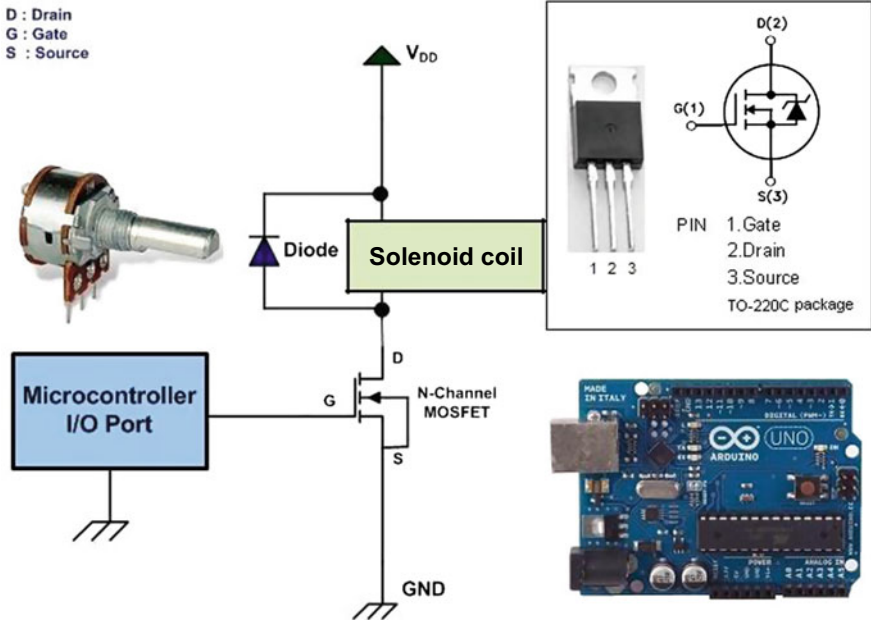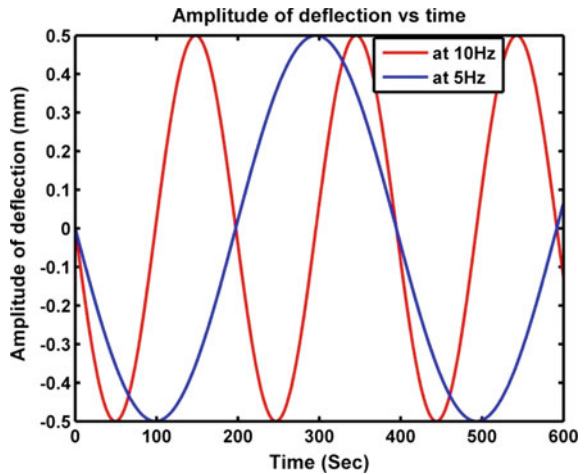
D : Drain
G : Gate
S : Source

Fig. 4 Arduino circuit for frequency controlled shaker

Fig. 5 Mini cantilever tip deflection mounted at the tip of electromagnetic shaker

4 Conclusion

A fully controlled mini electromagnetic exciter has been developed using Arduino as a controller. The frequency has been controlled by writing a controller code. As the analog value changes, the delay will vary that change the digital write frequency. When the delay is 250 milli second, then the time period will be 500 milli second. It means the frequency will be 2 Hz. When the delay is 5 milli second, then the time period will be 10 milli second means frequency will be 100 Hz. So from here the frequency can vary from 2 to 100 Hz. The strength of the force generated by solenoid magnetic field can be enhanced by increasing number of turns and current amplitude. This can be applied for the vibration testing of microsensor and actuator. The controller can be applied for various application based on frequency.

References

1. Ali, W.G., Nagib, G.: Design Consideration for Piezoelectric Energy Harvesting Systems. IEEE 2012
2. Lu, F., Lee, H.P., Lim, S.P.: Modeling and Analysis of Micro Piezoelectric Power Generators for Micro-electromechanical-systems Application. 2004 IOP Publishing
3. Rao, S.S.: Vibration of Continuous Systems
4. Khalatkar, A.M., Gupta, V.K.: Mathematical modeling and validation of piezoelectric energy harvester for low engine vibrations. Am. Inst. Phys. (AIP) J. Renew. Sustain. Energy **2**, (2017)
5. Sodano, H.A., Park, G., Inman, D.J.: Estimation of electric charge output for piezoelectric energy harvesting. J. Strain **40**, 49–58 (2004)
6. Sodano, H.A., Inman, D.J., Park, G.: A review of power harvesting from vibration using piezoelectric materials. Shock Vibr. Digest, **36**(3), 197–205 (2004)
7. Sodano, H.A., Inman, D.J., Park, G.: Generation & storage of electricity from power harvesting devices. J. Intell. Mater. Syst. Struct. **16** (2005)
8. Khalatkar, A.M., Gupta, V.K.: Mathematical modeling and validation of piezoelectric energy harvester for low engine vibrations. Am. Inst.Phys. (AIP) J. Renew. Sustain. Energy (2017)
9. Khalatkar Abhay, M., Gupta, V.K.: Analytical, FEA and experimental comparisons of piezoelectric energy harvesting using engine vibrations. J. Smart Mater. Res. Hindawi Publications USA, Published online on 6th April 2014, Volume 2014, Article ID 741280
10. Abhay, K., Gupta, V.K., Rakesh, H.: Finite element analysis of cantilever beam for optimal placement of piezoelectric actuator. J. Appl. Mech. Mater. **110**, 4212–4219 (2012). (Trans Tech Publications, Switzerland)
11. Kang, M.-G., Jung, W.-S., Kang, C.-Y., Yoon, S.-J.: Recent progress on PZT based piezoelectric energy harvesting technologies. J. Actuators (Licensee MDPI, Basel, Switzerland) (2016)
12. Priya, S., Song, H.-C., Zhou, Y., Varghese, R., Chopra, A., Kim, S.-G., Kanno, I., Wu, L., Sam Ha, D, Ryu, J., Polcawich, R.G: A review on piezoelectric energy harvesting: materials, methods, and circuits. In: Energy Harvesting and Systems 2017